CARDIOVASCULAR RISK FACTORS: RELATED VASCULAR INJURY AND NEW MOLECULAR BIOMARKERS

EDITED BY: Yuli Huang, Zhen Yang and Ji Bihl
PUBLISHED IN: Frontiers in Cardiovascular Medicine

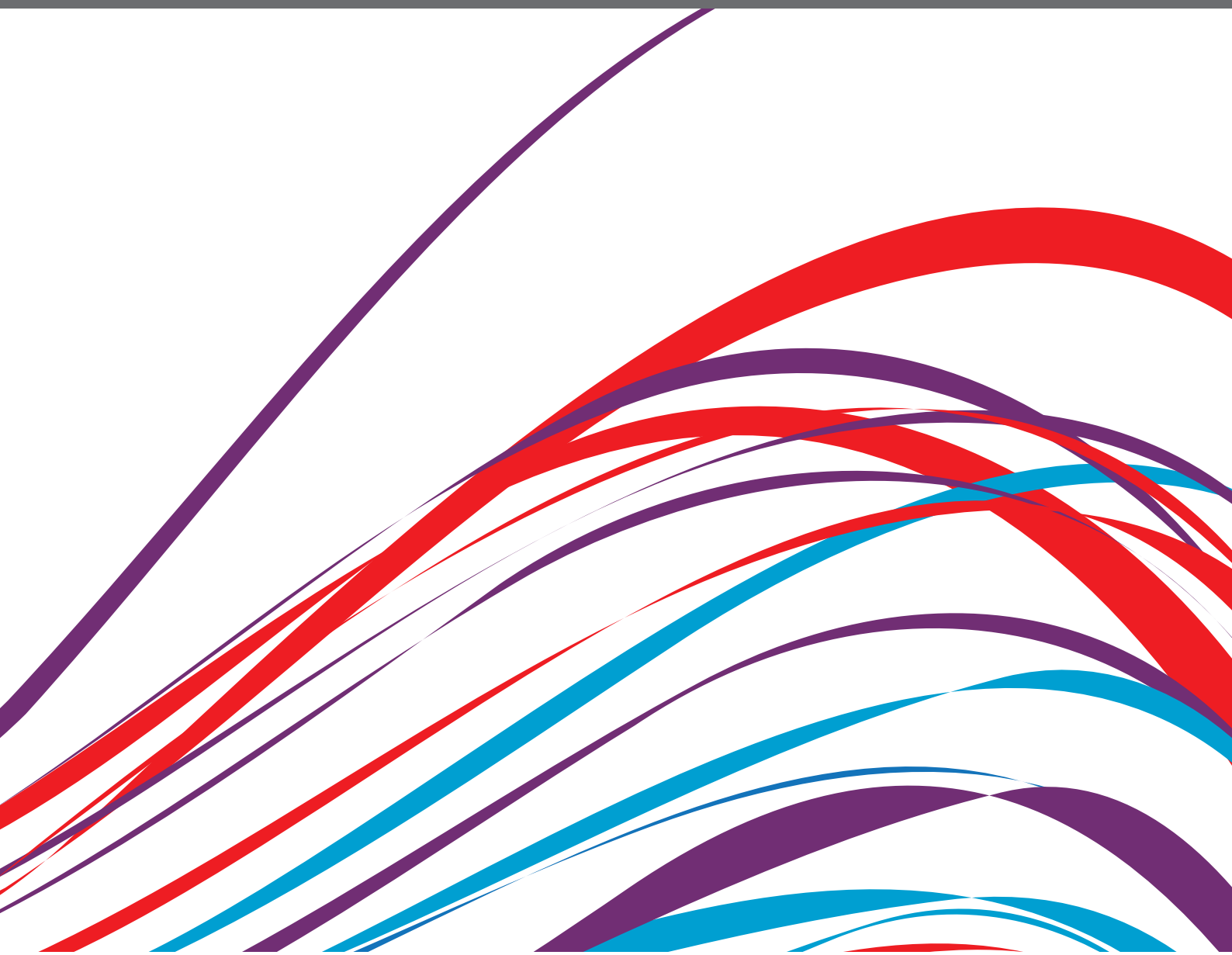

frontiers Research Topics

Frontiers eBook Copyright Statement

The copyright in the text of individual articles in this eBook is the property of their respective authors or their respective institutions or funders. The copyright in graphics and images within each article may be subject to copyright of other parties. In both cases this is subject to a license granted to Frontiers.

The compilation of articles constituting this eBook is the property of Frontiers.

Each article within this eBook, and the eBook itself, are published under the most recent version of the Creative Commons CC-BY licence. The version current at the date of publication of this eBook is CC-BY 4.0. If the CC-BY licence is updated, the licence granted by Frontiers is automatically updated to the new version.

When exercising any right under the CC-BY licence, Frontiers must be attributed as the original publisher of the article or eBook, as applicable.

Authors have the responsibility of ensuring that any graphics or other materials which are the property of others may be included in the CC-BY licence, but this should be checked before relying on the CC-BY licence to reproduce those materials. Any copyright notices relating to those materials must be complied with.

Copyright and source acknowledgement notices may not be removed and must be displayed in any copy, derivative work or partial copy which includes the elements in question.

All copyright, and all rights therein, are protected by national and international copyright laws. The above represents a summary only. For further information please read Frontiers' Conditions for Website Use and Copyright Statement, and the applicable CC-BY licence.

ISSN 1664-8714
ISBN 978-2-83250-313-3
DOI 10.3389/978-2-83250-313-3

About Frontiers

Frontiers is more than just an open-access publisher of scholarly articles: it is a pioneering approach to the world of academia, radically improving the way scholarly research is managed. The grand vision of Frontiers is a world where all people have an equal opportunity to seek, share and generate knowledge. Frontiers provides immediate and permanent online open access to all its publications, but this alone is not enough to realize our grand goals.

Frontiers Journal Series

The Frontiers Journal Series is a multi-tier and interdisciplinary set of open-access, online journals, promising a paradigm shift from the current review, selection and dissemination processes in academic publishing. All Frontiers journals are driven by researchers for researchers; therefore, they constitute a service to the scholarly community. At the same time, the Frontiers Journal Series operates on a revolutionary invention, the tiered publishing system, initially addressing specific communities of scholars, and gradually climbing up to broader public understanding, thus serving the interests of the lay society, too.

Dedication to Quality

Each Frontiers article is a landmark of the highest quality, thanks to genuinely collaborative interactions between authors and review editors, who include some of the world's best academicians. Research must be certified by peers before entering a stream of knowledge that may eventually reach the public - and shape society; therefore, Frontiers only applies the most rigorous and unbiased reviews.
Frontiers revolutionizes research publishing by freely delivering the most outstanding research, evaluated with no bias from both the academic and social point of view. By applying the most advanced information technologies, Frontiers is catapulting scholarly publishing into a new generation.

What are Frontiers Research Topics?

Frontiers Research Topics are very popular trademarks of the Frontiers Journals Series: they are collections of at least ten articles, all centered on a particular subject. With their unique mix of varied contributions from Original Research to Review Articles, Frontiers Research Topics unify the most influential researchers, the latest key findings and historical advances in a hot research area! Find out more on how to host your own Frontiers Research Topic or contribute to one as an author by contacting the Frontiers Editorial Office: frontiersin.org/about/contact

CARDIOVASCULAR RISK FACTORS: RELATED VASCULAR INJURY AND NEW MOLECULAR BIOMARKERS

Topic Editors:
Yuli Huang, Shunde Hospital, Southern Medical University, China
Zhen Yang, The First Affiliated Hospital of Sun Yat-sen University, China
Ji Bihl, Marshall University, United States

Citation: Huang, Y., Yang, Z., Bihl, J., eds. (2022). Cardiovascular Risk Factors: Related Vascular Injury and New Molecular Biomarkers. Lausanne: Frontiers Media SA. doi: 10.3389/978-2-83250-313-3

Table of Contents

frontiers in Cardiovascular Medicine

ORIGINAL RESEARCH
published: 06 July 2021
doi: 10.3389/fcvm.2021.702489

Association Between Dietary Inflammatory Index and Heart Failure: Results From NHANES (1999–2018)

Zuheng Liu[1†], Haiyue Liu[2,3†], Qinsheng Deng[1], Changqing Sun[1], Wangwei He[1], Wuyang Zheng[1], Rong Tang[1], Weihua Li[1] and Qiang Xie[1*]*

[1] Department of Cardiology, The First Affiliated Hospital of Xiamen University, Xiamen, China, [2] Department of Laboratory Medicine, The First Affiliated Hospital of Xiamen University, Xiamen, China, [3] Xiamen Key Laboratory of Genetic Testing, Xiamen, China

OPEN ACCESS

Edited by:
Yuli Huang,
Southern Medical University, China

Reviewed by:
Andre Rodrigues Duraes,
Federal University of Bahia, Brazil
Xuyu He,
Guangdong Academy of Medical Sciences, China

***Correspondence:**
Weihua Li
liweihua@xmu.edu.cn
Qiang Xie
arthur2014@sina.com

[†]These authors have contributed equally to this work and share first authorship

Specialty section:
This article was submitted to General Cardiovascular Medicine, a section of the journal Frontiers in Cardiovascular Medicine

Received: 29 April 2021
Accepted: 02 June 2021
Published: 06 July 2021

Citation:
Liu Z, Liu H, Deng Q, Sun C, He W, Zheng W, Tang R, Li W and Xie Q (2021) Association Between Dietary Inflammatory Index and Heart Failure: Results From NHANES (1999–2018). Front. Cardiovasc. Med. 8:702489. doi: 10.3389/fcvm.2021.702489

Objective: To explore the relationship between dietary inflammatory index (DII) and heart failure (HF) in participants with cardiovascular and cerebrovascular diseases.

Methods: NHANES (1998–2018) data were collected and used to assess the association of HF with DII. Twenty-four-hour dietary consumptions were used to calculate the scores of DII. Demographic characteristics and physical and laboratory examinations were collected for the comparison between HF and non-HF groups. Logistic regression analysis and random forest analysis were performed to calculate the odds rate and determine the potential beneficial dietary components in HF.

Results: A total of 19,067 cardiac-cerebral vascular disease participants were categorized as HF ($n = 1,382$; 7.25%) and non-HF ($n = 17,685$; 92.75%) groups. Heart failure participants had higher levels of DII score compared with those in the non-HF group (0.239 ± 1.702 vs. −0.145 ± 1.704, $p < 0.001$). Compared with individuals with T1 (DII: −3.884 to −0.570) of DII, those in T3 (DII: 1.019 to 4.598) had a higher level of total cholesterol (4.49 ± 1.16 vs. 4.75 ± 1.28 mmol/L, $p < 0.01$), globulin (29.92 ± 5.37 vs. 31.29 ± 5.84 g/L, $p < 0.001$), and pulse rate (69.90 ± 12.22 vs. 72.22 ± 12.77, $p < 0.001$) and lower levels of albumin (40.76 ± 3.52 vs. 39.86 ± 3.83 g/L, $p < 0.001$), hemoglobin (13.76 ± 1.65 vs. 13.46 ± 1.77 g/dl, $p < 0.05$), and hematocrit (40.83 ± 4.69 vs. 40.17 ± 5.01%, $p < 0.05$). The odds rates of HF for DII from the logistic regression were 1.140, 1.158, and 1.110 in models 1, 2, and 3, respectively. In addition, from the results of random forest analysis, dietary magnesium, fiber, and beta carotene may be essential in HF.

Conclusion: Dietary inflammatory index was positively associated with HF in US adults, and dietary intervention might be a promising method in the therapy of HF.

Keywords: heart failure, dietary inflammatory index, nutrition, national health and nutrition examination survey, cardiovascular and cerebrovascular diseases

INTRODUCTION

Chronic heart failure (HF) is a complicated syndrome that occurs with a high probability at the end stage of various cardiovascular diseases (CVDs). Intestinal congestion is a common feature of HF, which is always contributed to anorexia or poor appetite (1). The variety of dietary supplement pattern had been reported to be linked with the progression of HF. A Western dietary pattern with a higher intake of high-fat products is closely associated with the risk of HF (2). On the contrary, a Mediterranean dietary pattern, which contains high consumptions of vegetables or fish, reduces the risk of HF (3).

The connection between dietary consumption and inflammation has been proposed for many years (4). Although sufficient energy or nutrients supply potentially postpones the evolution of cardiac cachexia (5), the diet-related inflammation should not be neglected. The dietary inflammation index (DII), a widely used scoring system in evaluating the levels of inflammation derived from nutrient supplements, was developed by Cavicchia et al. (6) and updated by Shivappa et al. (7).

An inappropriate dietary pattern is closely related with higher inflammatory factors. For example, a Western diet increases the level of CRP and IL-6 (8), while a Mediterranean diet is associated with lower inflammation factors (9).

Previous studies suggested that IL-1, IL-6, TNF-α, and IFN-γ are increased in HF patients (10). Inflammatory factors lead to anorexia and promote protein degradation in skeletal muscles (11). In addition, inflammatory factors increase cardiac apoptosis and impair cardiac function (12). Importantly, evidence from a clinical trial (CANTOS) indicated that the application of IL-1β receptor inhibitor reduced cardiovascular events (13). In addition, anakinra exhibited favorable trends in reducing high-sensitivity CRP and NT-proBNP in HF with a preserved ejection fraction (14).

Since HF is regarded as an inflammatory-related disease (15, 16) and closely linked with nutrient intake, the assessment of diet-related inflammation would be essential. In order to explore the underlying beneficial nutrients and provide some clues in the therapeutics of HF, we investigated the connections between DII score and HF from the NHANES data.

MATERIALS AND METHODS

Study Population and Design

Data from NHANES 1999–2018 were combined to increase the sample sizes. In order to alleviate the effects of confounding factors, participants with a diagnostic history of coronary artery disease, prediabetes, diabetes, hypertension, heart attack, stroke, or angina were regarded as the control group, while participants who were accompanied with at least one of those basic diseases and HF was defined as the HF group. The verification of HF is based on the questionnaire from MCQ by asking "Someone ever told you had congestive heart failure?" The demographic information and characteristics, which consist of the age, gender, BMI, race, education, income, and current smoking status, were obtained by interviewing. The present study is based on a secondary date analysis which lacked personal identifiers and does not need institutional reviewing.

Calculation of the Dietary Inflammation Index

The DII is a scoring system in evaluating the potential inflammatory levels of dietary components, which was developed by Shivappa through literature review (7). DII calculates the inflammation effects of dietary consumption from 45 nutrients. The calculation of DII is based on the addition of each component's score from the diet consumed in 24 h, including the score from the pro-inflammatory and anti-inflammatory diet. Briefly, the Z score is a value obtained by subtracting the Global daily mean intake and divided by the standard deviation, and then, the value is converted to a percentile score, followed by doubling each percentile score and subtracting "1" to achieve a symmetrical distribution. Then, the percentile value is multiplied by the corresponding "overall inflammation effect score." By summing each DII score, we can achieve an individual "overall DII score." In this study, 26 nutrients were used for the calculation of the DII score, which includes alcohol, vitamin B12/B6, β-carotene, caffeine, carbohydrate, cholesterol, energy, total fat, fiber, folic acid, Fe, Mg, MUFA, niacin, n-3 fatty acids, protein, PUFA, riboflavin, saturated fat, Se, thiamin, vitamins A/C/E, and Zn. Importantly, even if the nutrients applied for the calculation of DII is <30, the DII scores are still available (7).

Statistical Analysis

The data were processed by R or SPSS 20.0. Student's *t*-test or one-way ANOVA was performed for the comparison of continuous variables followed by LSD or Dunnett's T3

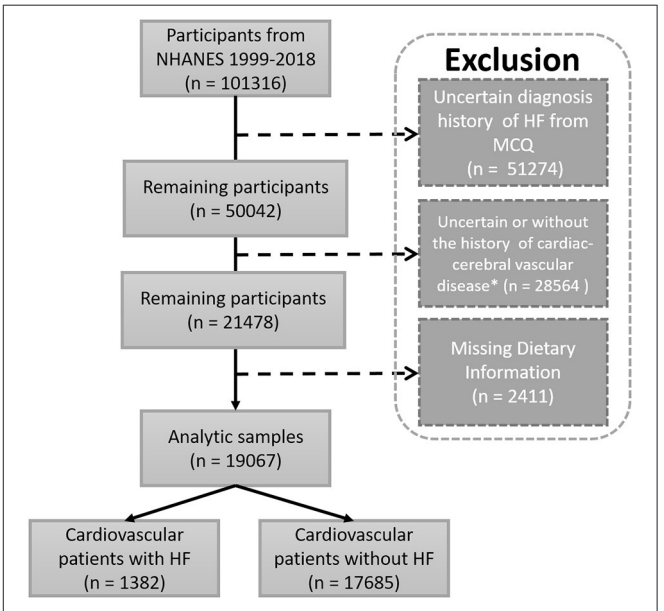

FIGURE 1 | Flow chart of study participants. Sample selection and exclusion criteria for the comparison of HF and non-HF participants, as well as the association between DII and HF. MCQ, the questionnaire of Medical Conditions; NHANES, National Survey of the National Center for Health Statistics; *Including one of the following diagnostic history: hypertension, diabetes, prediabetes, coronary artery disease, heart attack, stroke, angina.

TABLE 1 | Demographics and characteristics of participants, from NHANES 1999–2018.

Characteristic	HF (*N* = 1,382; 7.25%)	Non-HF (*N* = 17,685; 92.75%)	*p*-values
Age, years, Mean ± *SD*	67.82 ± 12.16	58.82 ± 15.55	<0.001
Gender, *N* (%)			
Male	778 (56.30%)	8,472 (47.91%)	<0.001
Female	604 (43.70%)	9,213 (52.10%)	
BMI, kg/m^2, *N* (%)			
<20	34 (2.46%)	412 (2.33%)	0.001
20–25	195 (14.11%)	2,959 (16.73%)	
25–30	386 (27.93%)	5,720 (32.34%)	
≥30	695 (50.29%)	8,225 (46.51%)	
Mean ± *SD*	31.89 ± 8.06	30.74 ± 7.14	<0.001
Missing	72 (5.21%)	369 (2.09%)	
Waist, cm, Mean ± *SD*	108.78 ± 17.01	104.35 ± 15.71	<0.001
Race, *N* (%)			
Mexican American	130 (9.41%)	2,481 (14.03%)	<0.001
Other Hispanic	90 (6.51%)	1,395 (7.89%)	
Non-Hispanic white	748 (54.12%)	8,003 (45.25%)	
Non-Hispanic black	350 (25.33%)	4,388 (24.81%)	
Other race or multi-racial	64 (4.63%)	1,418 (8.02%)	
Education, *N* (%)			
<High school	530 (38.35%)	4,963 (28.06%)	<0.001
High school	344 (24.89%)	4,234 (23.94%)	
>High school	507 (36.69%)	8,463 (47.85%)	
Missing	1 (0.07%)	25 (0.14%)	
Annual family income, *N* (%)			
<20,000 USD	532 (38.50%)	4,793 (27.10%)	<0.001
≥20,000 USD	789 (57.09%)	12,159 (68.75%)	
Missing	61 (4.41%)	733 (4.14%)	
Current smoking status, *N* (%)			
Smoking	266 (19.25%)	3,290 (18.60%)	<0.001
Non-smoking	588 (42.55%)	5,503 (31.12%)	
Missing	528 (38.21%)	8,892 (50.28%)	
Hypertension, *N* (%)	1,156 (83.80%)	14,414 (81.60%)	0.043
Diabetes, *N* (%)	593 (44.40%)	4,848 (28.30%)	<0.001
Prediabetes, *N* (%)	82 (14.50%)	1,925 (19.40%)	0.004
Coronary artery disease, *N* (%)	580 (43.30%)	1,265 (7.20%)	<0.001
Angina, *N* (%)	360 (26.70%)	876 (5.00%)	<0.001
Heart attack, *N* (%)	651 (47.40%)	1,261 (7.10%)	<0.001
Stroke, *N* (%)	301 (21.90%)	1,381 (7.80%)	<0.001

Data are presented as N% (χ^2-test) or Mean ± SD (independent t-test).

for *post-hoc* multiple comparisons, while chi-square test was performed for comparing the constituent ratio of each group. Levene statistic was used for the homogeneity of the variance test. Logistic regression was performed to assess the association between HF and DII after adjusting for covariates. Random forest analysis was performed using the dietary and examination data using R and 10-fold cross-validation. Receiver operative characteristic curve (ROC) were plotted and area under curves (AUCs) were compared using the pROC package in R (17). Random forest model constructed by Machine learning was used to calculate the score of AUC and explore the possibly beneficial nutrients in HF. In all analyses, differences were considered statistically significant at a value of $p < 0.05$.

RESULTS

Demographic Characteristics of Participants

A total of 101,316 participants were included from NHANES 1999–2018. After excluding participants without information

TABLE 2 | Characteristics of HF participants by tertiles of dietary inflammatory index (DII).

Characteristic	Tertiles of dietary inflammatory index			*p*-values
	T1, $n = 460$ (–3.884–0.570)	T2, $n = 461$ (–0.566–1.019)	T3, $n = 461$ (1.019–4.598)	
Age, years, Mean ± *SD*	68.23 ± 11.89	68.57 ± 12.24[b*]	66.67 ± 12.31	0.041
Gender, *N* (%)				
Male	322 (70.00%)	251 (54.45%)	205 (44.47%)	<0.001
Female	138 (30.00%)	210 (45.55%)	256 (55.53%)	
BMI, kg/m^2, *N* (%)				
<20	10 (2.17%)	9 (2.10%)	15 (3.40%)	0.182
20–25	72 (15.65%)	63 (13.67%)	60 (13.02%)	
25–30	144 (31.31%)	123 (26.68%)	119 (25.810%)	
≥30	210 (45.65%)	239 (51.84%)	246 (53.36%)	
Mean ± *SD*	31.01 ± 7.21[a**]	32.58 ± 8.44	32.07 ± 8.41	0.013
Missing	24 (5.22%)	27 (5.86%)	21 (4.56%)	
Waist, cm, Mean ± *SD*	108.25 ± 16.23	110.25 ± 18.17	107.94 ± 16.60	0.119
Race, *N* (%)				
Mexican American	46 (10.00%)	38 (8.24%)	46 (9.98%)	<0.001
Other Hispanic	27 (5.87%)	30 (6.51%)	33 (7.16%)	
Non-Hispanic white	266 (57.83%)	256 (55.53%)	226 (49.02%)	
Non-Hispanic black	87 (18.91%)	121 (26.25%)	142 (30.80%)	
Other race or multi-racial	34 (7.38%)	16 (3.47%)	14 (3.04%)	
Education, *N* (%)				
<High school	141 (30.65%)	173 (37.53%)	216 (46.85%)	<0.001
High school	120 (26.09%)	114 (24.73%)	110 (23.86%)	
>High school	199 (43.26%)	174 (37.74%)	135 (29.28%)	
Annual family income, *N* (%)				
<20,000 USD	146 (31.74%)	184 (39.91%)	202 (43.82%)	0.001
≥20,000 USD	289 (62.83%)	255 (55.31%)	245 (53.15%)	
Missing	25 (5.43%)	22 (4.77%)	14 (3.04%)	
Current smoking status, *N* (%)				
Smoking	68 (14.78%)	79 (17.14%)	119 (25.81%)	<0.001
Non-smoking	232 (50.43%)	189 (41.00%)	167 (36.23%)	
Missing	160 (34.78%)	193 (41.87%)	175 (37.96%)	
Hypertension, *N* (%)	380 (82.61%)	387 (83.95%)	389 (84.38%)	0.280
Diabetes, *N* (%)	191 (41.52%)	202 (43.82%)	200 (43.38%)	0.959
Prediabetes, *N* (%)	32 (6.96%)	27 (5.86%)	23 (4.99%)	0.612
Coronary artery disease, *N* (%)	203 (44.13%)	189 (41.00%)	188 (40.78%)	0.343
Angina, *N* (%)	132 (28.70%)	124 (26.90%)	104 (22.56%)	0.157
Heart attack, *N* (%)	200 (43.48%)	231 (50.11%)	220 (47.72%)	0.016
Stroke, *N* (%)	93 (20.22%)	87 (18.87%)	121 (26.25%)	0.003

*Data are presented as N% (χ^2-test) or Mean ± SD (independent t-test). a, b represents the post hoc between T1 and T2, T1 and T3, respectively. *p < 0.05, **p < 0.01.*

of HF diagnosis, uncertain cardiac-cerebral vascular disease, and missing essential dietary information for the calculation of DII, 19,067 participants were obtained for the statistical analysis. Then, they were divided into two groups including the HF (Cardiovascular patients with HF, $n = 1,382$) and non-HF (Cardiovascular patients without HF, $n = 17,685$) groups (**Figure 1**). The characteristics of analysis samples are shown in **Table 1**. The prevalence of HF in cardiovascular and cerebrovascular diseases participants was 7.25%. The enrolled participants included 778 (56.30%) and 8,472 (47.91%) male participants with mean ages of 67.82 ± 12.16 and 58.82 ± 15.55 years old in the HF and non-HF groups, respectively Heart failure participants had a higher BMI (31.89 ± 8.06 vs. 30.74 ± 7.14 kg/m^2, $p < 0.001$) and waist circumference (108.78 ± 17.01 vs. 104.35 ± 15.71, $p < 0.001$) compared with the non-HF group. In addition, the HF participants had a lower education and annual family income. Moreover, the composition of race is also different between these two groups. It is also not surprising that the prevalence of diabetes, coronary artery disease, angina, heart attack, and stroke was higher in participants in the HF group than

TABLE 3 | Logistic regression analysis of DII on HF in participants with cardiac-cerebral vascular disease in NHANES (1999–2018).

	OR	95% CI	*p*-values
Model 1			
DII score	1.140	1.104–1.177	<0.001
Model 2			
DII score	1.158	1.119–1.199	<0.001
Age, years	1.054	1.048–1.059	<0.001
Gender			
Male	Ref.	Ref.	<0.001
Female	0.606	0.538–0.682	
BMI, kg/m^2	1.049	1.040–1.057	<0.001
Model 3			
DII score	1.110	1.060–1.163	<0.001
Age, years	1.048	1.041–1.056	<0.001
Gender			
Male	Ref.	Ref.	<0.001
Female	0.611	0.518–0.721	
BMI, kg/m^2	1.051	1.040–1.062	<0.001
Race			
Mexican American	0.680	0.434–1.065	0.092
Other Hispanic	0.961	0.594–1.555	0.872
Non-Hispanic white	1.157	0.795–1.683	0.447
Non-Hispanic black	1.056	0.713–1.565	0.785
Other Race or Multi-racial	Ref.	Ref.	
Education			
<High school	1.276	1.056–1.542	0.012
High school	1.185	0.976–1.437	0.086
>High school	Ref.	Ref.	
Annual family income			
<20,000 USD	Ref.	Ref.	
≥20,000 USD	0.696	0.592–0.818	<0.001
Current smoking status			
Smoking	1.305	1.085–1.571	0.005
Non-smoking	Ref.	Ref.	

The cardiac-cerebral vascular disease in the present study including: hypertension, diabetes, prediabetes, coronary artery disease, angina, heart attack, and stroke.

that of the non-HF group, as these basic diseases would increase the incidence of HF.

Physical and Laboratory Examinations of Participants

The results of examinations are shown in **Supplementary Table 1**. The DII scores ranged from −3.884 to 4.598 and −4.949 to 4.422 in the HF and non-HF groups, respectively Heart failure participants showed a slight increasing trend of WBC (7.60 ± 2.66 vs. 7.38 ± 4.00, $p = 0.051$) and had a higher DII score (0.239 ± 1.702 vs. −0.145 ± 1.704, $p < 0.001$) when compared with the non-HF group. Although the average BMI and waist were higher in HF participants, they had an interesting blood lipid profile, which had a lower total cholesterol (4.61 ± 1.20 vs. 5.05 ± 1.14 mmol/L, $p < 0.001$), HDL (1.26 ± 0.41 vs. 1.36 ± 0.42 mmol/L, $p < 0.001$), LDL (2.58 ± 0.99 vs. 2.91 ± 0.93 mmol/L, $p < 0.001$), and a slightly higher triglyceride (1.77 ± 1.92 vs. 1.62 ± 1.34 mmol/L, p = 0.055) when compared with non-HF participants. Additionally, HF groups had lower levels of albumin (40.27 ± 3.66 vs. 41.63 ± 3.42 g/L, $p < 0.001$), while there was no significance in ALT, AST, and blood sodium. BUN (7.43 ± 4.32 vs. 5.41 ± 2.45 mmol/L, $p < 0.001$), Cr (1.30 ± 0.96 vs. 0.97 ± 0.58 mg/dl, $p < 0.001$), and UA (386.22 ± 11.56 vs. 339.32 ± 88.29 μmol/L, $p < 0.001$) were increased in HF patients which indicated their impairment of renal function. In addition, the plus rate in HF and non-HF are similar though they showed a significant difference (70.84 ± 12.46 vs. 72.59 ± 12.79, $p < 0.001$). Moreover, the levels of hemoglobin (13.55 ± 1.72 g/dl vs. 13.98 ± 1.55 g/dl, $p < 0.001$) and hematocrit (40.29 ± 4.90 vs. 41.35 ± 4.38, $p < 0.001$) in HF were slightly lower than in the non-HF groups. Another interesting finding is that, there is no significant difference in the systolic blood pressure, but the HF group had a lower diastolic blood pressure (66.48 ± 16.20 mmHg vs. 71.10 ± 14.97 mmHg, $p < 0.001$).

Characteristics and Examinations of HF Participants by Tertiles of Dietary Inflammatory Index

In order to further investigate the correlation between DII and HF, DII was divided by tertiles (**Table 2**). The DII score ranges from −3.884 to −0.570, −0.566 to 1.019, and 1.019 to 4.598 in tertile 1 (T1), tertile 2 (T2), and tertile 3 (T3), respectively. Individuals in T2 seem to be the oldest, with 54.45% of them males. In addition, individuals in T1 had the lowest BMI, with higher education, more family income, and lowest smoking rate. The prevalence of hypertension, diabetes, prediabetes, coronary artery disease, and angina had no significant difference among T1, T2, and T3, while T3 occupied a highest proportion of stroke (26.25%) and T2 occupied a highest proportion of heart attack (50.11%).

The physical and laboratory examinations in HF participants divided by tertiles are exhibited in **Supplementary Table 2**. Individuals in T1 had the lowest level of cholesterol compared with the T3 individuals (4.49 ± 1.16 vs. 4.75 ± 1.28 mmol/L, $p < 0.01$). In addition, the T1 group had the highest level of albumin (40.76 ± 3.52 g/L), hemoglobin (13.76 ± 1.65 g/dl), and hematocrit (40.83 ± 4.69%) among these groups, which possibly indicates that a lower DII score is correlated with a better cardiac function.

Association Between HF and Dietary Inflammatory Index

The unadjusted and adjusted models are presented in **Table 3**. Model 1 was a crude model which shows that there is a statistically significant difference between increased odds of HF and higher DII score [OR (95% CI) = 1.140 (1.104–1.177), $p < 0.001$]. The odds rate in model 2 was 1.158 after it was adjusted for age, gender, and BMI, while model 3 was

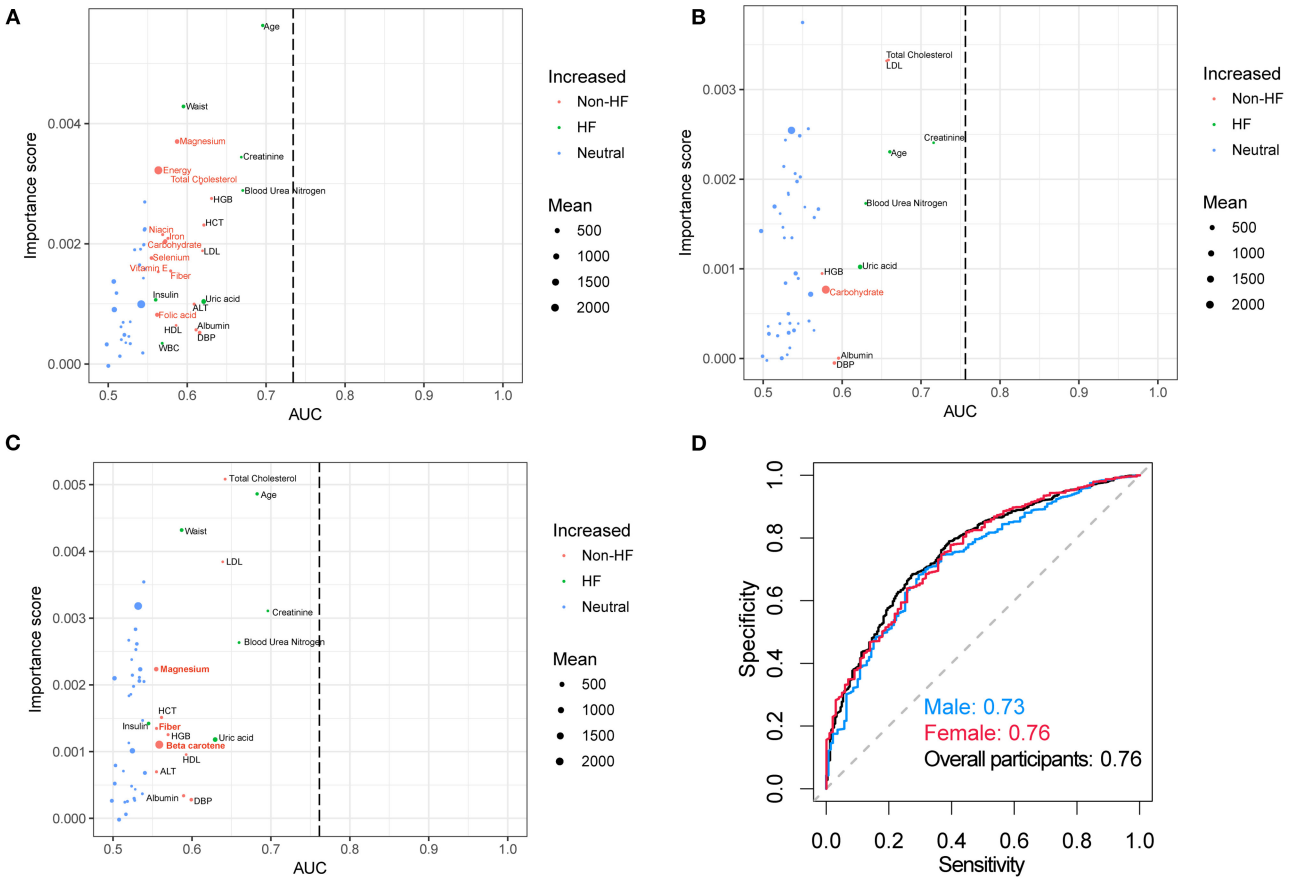

FIGURE 2 | Random forest analysis and AUC curves. Random forest analysis in **(A)** male, **(B)** female, **(C)** overall participants and their corresponding **(D)** AUC curves. The green (HF group) and red (non-HF group) nodes which were significantly different between these two groups denoted the important score in the construction of the random forest model. The AUC curves for the random forest models in separating HF and non-HF groups using the dietary information and laboratory examinations. The red font indicated the dietary indices. AUC, area under the curve.

additionally adjusted for race, education, income, and smoking status. Although the association was slightly weakened, there was still a significant association between higher DII levels and the increase of HF (OR = 1.110, 95 CI% 1.060–1.163, $p < 0.001$) in model 3.

Random Forest Modeling of HF Using Laboratory Examinations and Dietary Data

Random forest analysis discriminated HF participants from non-HF with an area under the curve (AUC) of 0.73, 0.76, and 0.76 using the laboratory examinations and demographic characteristics from male, female, and total individuals, respectively (**Figure 2**). The important dietary indices in constructing a random forest model in the male subgroup include magnesium, energy, total cholesterol, niacin, iron, carbohydrate, selenium, vitamin E, fiber, and folic acid. However, these important dietary indices disappeared in the model of the female subgroup except for carbohydrate, while magnesium, fiber, and beta carotene were important indices in all the participants. These results might suggest that dietary intervention is more essential for male. In addition, supplement with magnesium might be essential for HF.

DISCUSSION

In this study, we provide evidences that HF is closely associated with DII by using the NHANES 1999–2018 data, in which fiber, niacin, iron, selenium, vitamin E, β-carotene, and magnesium might be important dietary factors in HF. Nutrition is a factor that should not be ignored in the progress of HF. Malnutrition or cachexia is an independent risk factor which increases the mortality of HF (18). In fact, the failing heart is regarded as an engine out of fuels (19). Beyond the supply of raw materials for protein synthesis, nutrients also serve as energy sources for the heart. Therefore, supplement with sufficient nutrients is recommended at the end stage of HF, especially those patients who are accompanied with malnutrition (5). Nevertheless, the diet-related inflammation is an indispensable factor that needs to be a concern.

Previous studies have investigated the association between DII and metabolic syndrome or cardiovascular risk factors (20–22). Although HF is the terminal stage of various CVD, their pathological mechanism indeed might be different and fewer studies are concerned about DII and HF. Recently, growing evidences have indicated that the progress and prognosis of HF are influenced by gut microbiota and their metabolites (23). In addition, dietary intakes severely impact the composition of gut microbiota (24). For example, trimethylamine oxide, which is derived from a high choline diet by gut microbiota, is highly associated with HF (25). Focusing on the dietary consumption of HF patients might provide some valuable information.

In the present study, we observed that HF is more prevalent in individuals with a lower family income and lower education. However, a small sample size prospective study indicated that education levels were not associated with readmission or mortality rates (26). This discrepancy might be due to the difference of regions. From a multinational, prospective cohort study, the effect of low education on CVD is stronger in middle-income or low-income countries rather than high-income countries (27). Another interesting finding is that LDL, a traditional risk factor in CVDs, is reduced in HF individuals. The possible explanation is on the poor nutritional intake or appetite of HF patients (28). In addition, individuals in T1 of DII have a slightly increased level of serum albumin, hemoglobin, and hematocrit, which also supported that diet is essential in HF.

Furthermore, from the results of the random forest model, the dietary magnesium, fiber, and beta carotene might be nutritional elements that are beneficial to HF. Emerging evidences suggested that a low dietary magnesium intake is associated with an increased CVDs risk and the beneficial effects of magnesium supplements on the prevention of CVDs (29). However, the impact of magnesium might be more profound in males from our observation. In addition, a high fiber intake has been shown to be closely linked with gut microbiota and ameliorated cardiac function (30). Previous studies have demonstrated that lower concentrations of serum beta carotene may increase the risk of sudden cardiac death (31) and is associated with an increased risk of chronic HF (32). Diet intervention might be an easily modifiable method in the therapy of HF, while further investigation is needed to determine the underlying mechanism.

There are still some limitations that should be mentioned in the present study. First, the design is an observational study, which might lead to bias and lack of evidence of the cause and effect. Second, the diagnosis of HF is acquired by a questionnaire survey, and it is hard to assess the severity of HF. In addition, without the data of ejection fraction, the subtype of HF cannot be categorized.

In summary, we report an association between DII and HF, in which the dietary components should be a concern in the future.

DATA AVAILABILITY STATEMENT

The datasets presented in this study can be found in online repositories. The names of the repository/repositories and accession number(s) can be found at: NHANES 1999-2000 https://wwwn.cdc.gov/nchs/nhanes/continuousnhanes/default.aspx?BeginYear=1999; NHANES 2001-2002 https://wwwn.cdc.gov/nchs/nhanes/continuousnhanes/default.aspx?BeginYear=2001; NHANES 2003-2004 https://wwwn.cdc.gov/nchs/nhanes/continuousnhanes/default.aspx?BeginYear=2003; NHANES 2005-2006 https://wwwn.cdc.gov/nchs/nhanes/continuousnhanes/default.aspx?BeginYear=2005; NHANES 2007-2008 https://wwwn.cdc.gov/nchs/nhanes/continuousnhanes/default.aspx?BeginYear=2007; NHANES 2009-2010 https://wwwn.cdc.gov/nchs/nhanes/continuousnhanes/default.aspx?BeginYear=2009; NHANES 2011-2012 https://wwwn.cdc.gov/nchs/nhanes/continuousnhanes/default.aspx?BeginYear=2011; NHANES 2013-2014 https://wwwn.cdc.gov/nchs/nhanes/continuousnhanes/default.aspx?BeginYear=2013; NHANES 2015-2016 https://wwwn.cdc.gov/nchs/nhanes/continuousnhanes/default.aspx?BeginYear=2015; NHANES 2017-2018 https://wwwn.cdc.gov/nchs/nhanes/continuousnhanes/default.aspx?BeginYear=2017.

ETHICS STATEMENT

Ethical review and approval was not required for the study on human participants in accordance with the local legislation and institutional requirements. Written informed consent for participation was not required for this study in accordance with the national legislation and the institutional requirements.

AUTHOR CONTRIBUTIONS

QX, WL, RT, ZL, and HL conceived the ideas and design of the study. ZL, HL, QD, and CS collected data from NEHANES. ZL, HL, WH, and WZ analyzed the data. ZL, HL, and RT drafted the manuscript. QX and WL revised the final version of the manuscript and supervised the study. All authors have read and approved the final version of the manuscript for publication.

FUNDING

This project was partly supported by the Xiamen Science and Technology project (3502Z20199169), National Natural Science Foundation of China (82070423), Natural Science Foundation of Fujian Province (2019J01578), and Xiamen Science and Technology project (3502Z20209018).

ACKNOWLEDGMENTS

We gratefully acknowledge Dr. Haobin Zhou from Nanfang hospital Southern Medical University for his help in the statistical analysis.

SUPPLEMENTARY MATERIAL

The Supplementary Material for this article can be found online at: https://www.frontiersin.org/articles/10.3389/fcvm.2021.702489/full#supplementary-material

REFERENCES

1. Saitoh M, Dos SM, Emami A, Ishida J, Ebner N, Valentova M, et al. Anorexia, functional capacity, and clinical outcome in patients with chronic heart failure: results from the Studies Investigating Co-morbidities Aggravating Heart Failure (SICA-HF). *ESC Heart Fail.* (2017) 4:448–57. doi: 10.1002/ehf2.12209
2. Olver TD, Edwards JC, Jurrissen TJ, Veteto AB, Jones JL, Gao C, et al. Western diet-fed, aortic-banded Ossabaw swine: a preclinical model of cardio-metabolic heart failure. *JACC Basic Transl Sci.* (2019) 4:404–21. doi: 10.1016/j.jacbts.2019.02.004
3. Sanches MDK, Ronchi SS, Zuchinali P, Corrêa SG. Mediterranean diet and other dietary patterns in primary prevention of heart failure and changes in cardiac function markers: a systematic review. *Nutrients.* (2018) 10:58. doi: 10.3390/nu10010058
4. Kalantar-Zadeh K, Anker SD, Horwich TB, Fonarow GC. Nutritional and anti-inflammatory interventions in chronic heart failure. *Am J Cardiol.* (2008). 101:89E—103E. doi: 10.1016/j.amjcard.2008.03.007
5. Rahman A, Jafry S, Jeejeebhoy K, Nagpal AD, Pisani B, Agarwala R. Malnutrition and cachexia in heart failure. *JPEN J Parenter Enteral Nutr.* (2016) 40:475–86. doi: 10.1177/0148607114566854
6. Cavicchia PP, Steck SE, Hurley TG, Hussey JR, Ma Y, Ockene IS, et al. A new dietary inflammatory index predicts interval changes in serum high-sensitivity C-reactive protein. *J Nutr.* (2009) 139:2365–72. doi: 10.3945/jn.109.114025
7. Shivappa N, Steck SE, Hurley TG, Hussey JR, Hébert JR. Designing and developing a literature-derived, population-based dietary inflammatory index. *Public Health Nutr.* (2014) 17:1689–96. doi: 10.1017/S1368980013002115
8. Naja F, Shivappa N, Nasreddine L, Kharroubi S, Itani L, Hwalla N, et al. Role of inflammation in the association between the western dietary pattern and metabolic syndrome among Lebanese adults. *Int J Food Sci Nutr.* (2017) 68:997–1004. doi: 10.1080/09637486.2017.1312297
9. Bonaccio M, Pounis G, Cerletti C, Donati MB, Iacoviello L, de Gaetano G. Mediterranean diet, dietary polyphenols and low grade inflammation: results from the MOLI-SANI study. *Br J Clin Pharmacol.* (2017) 83:107–13. doi: 10.1111/bcp.12924
10. Abbate A, Toldo S, Marchetti C, Kron J, Van Tassell BW, Dinarello CA. Interleukin-1 and the inflammasome as therapeutic targets in cardiovascular disease. *Circ Res.* (2020) 126:1260–80. doi: 10.1161/CIRCRESAHA.120.315937
11. Seelaender M, Laviano A, Busquets S, Püschel GP, Margaria T, Batista MJ. Inflammation in cachexia. *Mediators Inflamm.* (2015) 2015:536954. doi: 10.1155/2015/536954
12. Wang X, Guo Z, Ding Z, Mehta JL. Inflammation, autophagy, and apoptosis after myocardial infarction. *J Am Heart Assoc.* (2018) 7:e008024. doi: 10.1161/JAHA.117.008024
13. Libby P. Interleukin-1 beta as a target for atherosclerosis therapy: biological basis of CANTOS and beyond. *J Am Coll Cardiol.* (2017) 70:2278–89. doi: 10.1016/j.jacc.2017.09.028
14. Van Tassell BW, Trankle CR, Canada JM, Carbone S, Buckley L, Kadariya D, et al. IL-1 blockade in patients with heart failure with preserved ejection fraction. *Circ Heart Fail.* (2018) 11:e005036. doi: 10.1161/CIRCHEARTFAILURE.118.005036
15. Yang S, Chen H, Tan K, Cai F, Du Y, Lv W, et al. Secreted frizzled-related protein 2 and extracellular volume fraction in patients with heart failure. *Oxid Med Cell Longev.* (2020) 2020:2563508. doi: 10.1155/2020/2563508
16. Wu J, Zheng H, Liu X, Chen P, Zhang Y, Luo J, et al. Prognostic value of secreted frizzled-related protein 5 in heart failure patients with and without type 2 diabetes mellitus. *Circ Heart Fail.* (2020) 13:e007054. doi: 10.1161/CIRCHEARTFAILURE.120.007054
17. Robin X, Turck N, Hainard A, Tiberti N, Lisacek F, Sanchez JC, et al. pROC: an open-source package for R and S+ to analyze and compare ROC curves. *BMC Bioinformatics.* (2011) 12:77. doi: 10.1186/1471-2105-12-77
18. Chien SC, Lo CI, Lin CF, Sung KT, Tsai JP, Huang WH, et al. Malnutrition in acute heart failure with preserved ejection fraction: clinical correlates and prognostic implications. *ESC Heart Fail.* (2019) 6:953–64. doi: 10.1002/ehf2.12501
19. Neubauer S. The failing heart–an engine out of fuel. *N Engl J Med.* (2007) 356:1140–51. doi: 10.1056/NEJMra063052
20. Wirth MD, Shivappa N, Hurley TG, Hébert JR. Association between previously diagnosed circulatory conditions and a dietary inflammatory index. *Nutr Res.* (2016) 36:227–33. doi: 10.1016/j.nutres.2015.11.016
21. Correa-Rodríguez M, González-Jiménez E, Rueda-Medina B, Tovar-Gálvez MI, Ramírez-Vélez R, Correa-Bautista JE, et al. Dietary inflammatory index and cardiovascular risk factors in Spanish children and adolescents. *Res Nurs Health.* (2018) 41:448–58. doi: 10.1002/nur.21904
22. Mazidi M, Shivappa N, Wirth MD, Hebert JR, Mikhailidis DP, Kengne AP, et al. Dietary inflammatory index and cardiometabolic risk in US adults. *Atherosclerosis.* (2018) 276:23–7. doi: 10.1016/j.atherosclerosis.2018.02.020
23. Kitai T, Tang W. Gut microbiota in cardiovascular disease and heart failure. *Clin Sci (Lond).* (2018) 132:85–91. doi: 10.1042/CS20171090
24. Garcia-Mantrana I, Selma-Royo M, Alcantara C, Collado MC. Shifts on gut microbiota associated to mediterranean diet adherence and specific dietary intakes on general adult population. *Front Microbiol.* (2018) 9:890. doi: 10.3389/fmicb.2018.00890
25. Li W, Huang A, Zhu H, Liu X, Huang X, Huang Y, et al. Gut microbiota-derived trimethylamine N-oxide is associated with poor prognosis in patients with heart failure. *Med J Aust.* (2020) 213:374–9. doi: 10.5694/mja2.50781
26. Elkhateeb O, Salem K. Patient and caregiver education levels and readmission and mortality rates of congestive heart failure patients. *East Mediterr Health J.* (2018) 24:345–50. doi: 10.26719/2018.24.4.345
27. Yusuf S, Joseph P, Rangarajan S, Islam S, Mente A, Hystad P, et al. Modifiable risk factors, cardiovascular disease, and mortality in 155 722 individuals from 21 high-income, middle-income, and low-income countries (PURE): a prospective cohort study. *Lancet.* (2020) 395:795–808. doi: 10.1016/S0140-6736(19)32008-2
28. Andreae C, van der Wal M, van Veldhuisen DJ, Yang B, Strömberg A, Jaarsma T. Changes in appetite during the heart failure trajectory and association with fatigue, depressive symptoms, and quality of life. *J Cardiovasc Nurs.* (2020). doi: 10.1097/JCN.0000000000000756. [Epub ahead of print].
29. Tangvoraphonkchai K, Davenport A. Magnesium and cardiovascular disease. *Adv Chronic Kidney Dis.* (2018) 25:251–60. doi: 10.1053/j.ackd.2018.02.010
30. Marques FZ, Nelson E, Chu PY, Horlock D, Fiedler A, Ziemann M, et al. High-fiber diet and acetate supplementation change the gut microbiota and prevent the development of hypertension and heart failure in hypertensive mice. *Circulation.* (2017) 135:964–77. doi: 10.1161/CIRCULATIONAHA.116.024545
31. Karppi J, Laukkanen JA, Mäkikallio TH, Ronkainen K, Kurl S. Serum β-carotene and the risk of sudden cardiac death in men: a population-based follow-up study. *Atherosclerosis.* (2013) 226:172–7. doi: 10.1016/j.atherosclerosis.2012.10.077
32. Karppi J, Kurl S, Mäkikallio TH, Ronkainen K, Laukkanen JA. Serum β-carotene concentrations and the risk of congestive heart failure in men: a population-based study. *Int J Cardiol.* (2013) 168:1841–6. doi: 10.1016/j.ijcard.2012.12.072

Conflict of Interest: The authors declare that the research was conducted in the absence of any commercial or financial relationships that could be construed as a potential conflict of interest.

Copyright © 2021 Liu, Liu, Deng, Sun, He, Zheng, Tang, Li and Xie. This is an open-access article distributed under the terms of the Creative Commons Attribution License (CC BY). The use, distribution or reproduction in other forums is permitted, provided the original author(s) and the copyright owner(s) are credited and that the original publication in this journal is cited, in accordance with accepted academic practice. No use, distribution or reproduction is permitted which does not comply with these terms.

frontiers in Cardiovascular Medicine

ORIGINAL RESEARCH
published: 07 July 2021
doi: 10.3389/fcvm.2021.692856

The Expression Patterns and Roles of Lysyl Oxidases in Aortic Dissection

Xin Yi[1,2,3†], Yi Zhou[1,2,3†], Yue Chen[4], Xin Feng[4], Chang Liu[1,2,3], Ding-Sheng Jiang[4], Jing Geng[1,2,3], Xiaoyan Li[1,2,3], Xuejun Jiang[1,2,3] and Ze-Min Fang[4*]*

[1] Department of Cardiology, Renmin Hospital of Wuhan University, Wuhan, China, [2] Cardiovascular Research Institute, Wuhan University, Wuhan, China, [3] Hubei Key Laboratory of Cardiology, Wuhan, China, [4] Division of Cardiothoracic and Vascular Surgery, Tongji Hospital, Tongji Medical College, Huazhong University of Science and Technology, Wuhan, China

OPEN ACCESS

Edited by:
Yuli Huang,
Southern Medical University, China

Reviewed by:
Fernando Rodriguez-Pascual,
Consejo Superior de Investigaciones Científicas (CSIC), Spain
Hong S. Lu,
University of Kentucky, United States

***Correspondence:**
Xuejun Jiang
xjjiang@whu.edu.cn
Ze-Min Fang
francemine@hotmail.com

[†] These authors have contributed equally to this work

Specialty section:
This article was submitted to General Cardiovascular Medicine, a section of the journal Frontiers in Cardiovascular Medicine

Received: 09 April 2021
Accepted: 11 June 2021
Published: 07 July 2021

Citation:
Yi X, Zhou Y, Chen Y, Feng X, Liu C, Jiang D-S, Geng J, Li X, Jiang X and Fang Z-M (2021) The Expression Patterns and Roles of Lysyl Oxidases in Aortic Dissection. Front. Cardiovasc. Med. 8:692856. doi: 10.3389/fcvm.2021.692856

Background: Lysyl oxidases (LOXs), including LOX, LOXL1, LOXL2, LOXL3, and LOXL4, catalyze the formation of a cross-link between elastin (ELN) and collagen. Multiple LOX mutations have been shown to be associated with the occurrence of aortic dissection (AD) in humans, and LOX-knockout mice died during the perinatal period due to aortic aneurysm and rupture. However, the expression levels and roles of other LOX members in AD remain unknown.

Methods: A total of 33 aorta samples of AD and 15 normal aorta were collected for LOXs mRNA and protein levels detection. We also analyzed the datasets of AD in GEO database through bioinformatics methods. LOXL2 and LOXL3 were knocked down in primary cultured human aortic smooth muscle cells (HASMCs) via lentivirus.

Results: Here, we show that the protein levels of LOXL2 and LOXL3 are upregulated, while LOXL4 is downregulated in AD subjects compared with non-AD subjects, but comparable protein levels of LOX and LOXL1 are detected. Knockdown of LOXL2 suppressed MMP2 expression, the phosphorylation of AKT (p-AKT) and S6 (p-S6), but increased the mono-, di-, tri-methylation of H3K4 (H3K4me1/2/3), H3K9me3, and p-P38 levels in HASMCs. These results indicate that LOXL2 is involved in regulation of the extracellular matrix (ECM) in HASMCs. In contrast, LOXL3 knockdown inhibited PCNA and cyclin D1, suppressing HASMC proliferation. Our results suggest that in addition to LOX, LOXL2 and LOXL3 are involved in the pathological process of AD by regulating ECM and the proliferation of HASMCs, respectively. Furthermore, we found that LOXL2 and LOXL4 was inhibited by metformin and losartan in HASMCs, which indicated that LOXL2 and LOXL4 are the potential targets that involved in the therapeutic effects of metformin and losartan on aortic or aneurysm expansion.

Conclusions: Thus, differential regulation of LOXs might be a novel strategy to prevent or treat AD.

Keywords: lysyl oxidase, aortic dissection, LOX, MMP2, metformin, losartan

BACKGROUND

Aortic dissection (AD) is a life-threatening condition, and the annual incidence of AD is estimated to be 3.8–8.8 per 100,000 persons (1–3). Patients with acute Stanford type A AD (TAAD) who do not receive proper operation have a mortality rate of up to 50% within the first 48 h, and surgery is the main treatment of choice due to the lack of effective conservative treatment strategies (4). Thus, the need to further investigate the pathogenesis of AD is critical. The major pathological features of AD include an enlarged and degenerative medial layer, vascular smooth muscle cell (VSMC) death and loss, and collagen-elastic fiber crosslinking disorder and fragmentation (5–7). Given that elastin (ELN) and collagen are two of the most abundant extracellular matrix (ECM) proteins, their adequate crosslinking is necessary to maintain the vessel's normal function (8). Moreover, mutations in ECM-associated genes [e.g., fibrillin 1 (FBN1) and lysyl oxidase (LOX)] lead to the occurrence of AD (9, 10).

Lysyl oxidase and its family members are the primary enzymes that regulate the crosslinking of ELN and collagen (11). The LOX family, including LOX, LOX-like 1 (LOXL1), LOXL2, LOXL3, and LOXL4, consists of mammalian copper-binding amine oxidases (12). These enzymes oxidize lysine and hydroxylysine ε-amino groups in ELN and collagen into highly reactive aldehydes, which then spontaneously react to form a variety of inter- and intra-chain crosslinks (8, 11). Lysyl oxidase family members (LOXs) play crucial roles in the cardiovascular system. For example, $Lox^{-/-}$ mice died perinatally due to severe vascular abnormalities (e.g., aortic aneurysms and aortic tortuosity) (13); $Loxl1^{-/-}$ mice were also found to have vascular defects (14). More importantly, accumulated evidence suggests that *LOX* mutations, such as p.Met292Arg, p.Met298Arg, p.Ser280Arg, and p.Ser348Arg, are closely associated with aortic dilation, thoracic aortic aneurysm and AD in humans (8, 10, 15). However, conflicting results on the role of LOX in vasculopathy in patients with Marfan syndrome (MFS) have been reported. Some studies reported that LOX expression and activity were reduced in the aortas of MFS patients, while other research demonstrated that comparable LOX mRNA levels and activity were found in the aortas of MFS patients and healthy subjects (11). Intriguingly, O Busnadiego et al. showed that the expression levels of LOX and LOXL1 were increased in the aortas of MFS patients and in a MFS mouse model ($Fbn1^{C1039G/+}$) (11). Thus, the need to clarify the expression pattern of the LOX family, as well as their function in aortic dilation, is urgent. Aortic dilation and MFS are risk factors or etiologies of AD, but the expression patterns and roles of the LOX family in AD, especially non-hereditary AD, remain largely unknown. In addition, recent findings have shown that the functions of LOXs extend beyond their role in stabilization of the ECM and include roles in cell chemotactic responses, cell proliferation, adhesion, migration, and transcriptional regulation (13). Thus, investigating the non-classical functions of the LOX family in VSMCs would be interesting.

Here, we show that the protein levels of LOXL2 and LOXL3 are elevated in the aortas of patients with TAAD, but LOXL2 and LOXL3 play different roles in VSMCs. LOXL2 affects ECM by upregulating MMP2, while LOXL3 facilitates VSMC proliferation. Furthermore, the inhibitory effects of metformin and losartan on aortic dilatation may be partially achieved by suppressing LOXL2 and LOXL4 expression. These results suggest that activating LOXL3 and inhibiting LOXL2 might be a novel therapeutic strategy for the prevention of AD.

METHODS

Human Aorta Samples

The human thoracic aortic tissue samples were collected from Division of Cardiothoracic and Vascular Surgery at Tongji Hospital, Tongji Medical College, Huazhong University of Science and Technology, with approval of Institutional Review Board. Written informed consent was obtained from all subjects. All experiments conducted with human tissue samples were performed in accordance with the relevant guidelines and regulations. Samples were obtained from patients with TAAD and donors for cardiac transplant. We did not conduct genetic testing on all patients, so we were unable to rule out whether these patients had unknown mutations in genes. Detailed patient information is displayed in **Supplementary Table 1**.

Gene Expression Profiles in the Gene Expression Omnibus Database

We used the keywords "aortic dissection" and "Homo sapiens [porgn]" to search datasets in the GEO database (https://www.ncbi.nlm.nih.gov/geo/). To investigate the expression levels of LOXs in patients with AD, we included all microarray and RNA-sequence datasets with both control and AD samples. Thus, four gene expression datasets, "GSE153434," "GSE98770," "GSE52093," and "GSE147026," were included in the present study. The GSE153434 dataset contains data from 10 TAAD samples and 10 control samples and is based on the GPL20795 platform [HiSeq X Ten (*Homo sapiens*)]. The GSE98770 dataset contains data from six TAAD samples and five control samples and is based on the GPL14550 platform [Agilent-028004 SurePrint G3 Human GE 8×60K Microarray (Probe Name Version)]. The GSE52093 dataset contains data from seven TAAD samples and five normal samples and is based on GPL10558 (Illumina HumanHT-12 V4.0 Expression BeadChip). The GSE147026 dataset, which contains four aorta tissue samples from donors and four aorta tissue samples from patients with AD, is based on GPL24676 [Illumina NovaSeq 6000 (*Homo sapiens*)].

Western Blot and Antibodies

Total proteins in human aortic smooth muscle cell (HASMC) and aortic tissues were extracted by RIPA solution with phosphatase inhibitors and protease inhibitors, and western blot was performed as described previously (3, 16, 17). The antibodies

Abbreviations: LOXs, lysyl oxidases; AD, aortic dissection; TAAD, Stanford type A AD; HASMCs, human aortic smooth muscle cells; VSMC, vascular smooth muscle cell; ECM, extracellular matrix; FBN1, fibrillin 1; LOXL1, LOX-like 1; MFS, Marfan syndrome; GEO, gene expression omnibus; PBS, phosphate-buffered saline; DMEM, Dulbecco's modified Eagle's medium; SD, standard deviation; shRNA, short hairpin RNA; ELN, elastin; TGFβ, transforming growth factor-β; ERK1/2, extracellular signal regulated kinases 1/2.

used in this study included α-SMA (ab7817), LOX (ab174316), SM22 (ab14106), H3K4me1 (ab8895), H3K36me3 (ab9050), Bax (ab32503), and Bcl-2 (ab182858) which were bought from Abcam. LOXL1 (A10191) and LOXL4 (A13131) were got from ABclonal. LOXL2 (GTX105085), MMP2 (GTX634832), MMP9 (GTX100458), H3K9me3 (GTX121677), and PCNA (GTX100539) were purchased from GeneTex. LOXL3 (sc-377216) was obtained from Santa Cruz. β-actin (#8457S), Beclin-1 (#3495), S6 (#2317), phosphorylation of S6 (p-S6) (#5364), AKT (#4685), phosphorylation of AKT (p-AKT) (#4060), p38 (#8690), p-p38 (#4511), p-JNK1/2 (#9255), p-ERK1/2 (#4370), p-GSK3 β (#5558), H3K4me2 (#9725), H3K4me3 (#9727), p-p65 (#3033), cyclinD1 (#2978), and LC3 (#12741) were purchased from Cell Signaling Technology.

Real-Time PCR

Total mRNA was extracted from human aorta tissues and HASMCs by using TRI Reagent® solution (AM9738; ThermoFisher Scientific). The precipitated mRNA was dissolved in nuclease-free water, and the RNA concentration was determined by a Nanodrop2000 (ThermoFisher Scientific). Subsequently, mRNA was reverse transcribed into cDNA by using a Transcriptor First Strand cDNA Synthesis Kit (4896866001, Roche). Then, 2 μl of the cDNA solution, primers, DEPC water and Hieff® qPCR SYBR® Green Master Mix (YEASEN, 11201ES08) were added to each well for the real-time PCR assay. Furthermore, the relative mRNA levels were detected by the CFX Connect™ Real-Time PCR Detection System (Bio-Rad). The primers used in this study are listed in **Supplementary Table 2**.

Plasmids

LOXL2 and LOXL3 knockdown plasmids were constructed by cloning double-stranded shRNA oligonucleotides targeting human LOXL2 and LOXL3 into the pLKO.1 plasmid at AgeI and EcoRI restriction enzyme sites. The targeting sequences of shRNA were shLOXL2: CCAGATAGAGAACCTGAATAT; shLOXL3: CATCTTCACTCACTATGATAT.

Primary Human Aorta Smooth Muscle Cell Culture and Treatments

Ascending aortic tissues were taken from patients who underwent heart transplantation. Then, the tissues were placed into culture dishes filled with Dulbecco's modified Eagle's medium (DMEM)/F12 (SH30023.01; HyClone) at 4°C. Intimal and residual adventitial tissues were stripped under a stereomicroscope. Subsequently, the middle layer of the aortic wall was cut into small pieces (1–2 mm) and transferred to cell culture flasks with 5 ml of DMEM/F12 supplemented with 10% fetal bovine serum (SH30084.03; HyClone) and 1% penicillin-streptomycin (15140-122; ThermoFisher Scientific). A few days later, long, spindle-shaped HASMCs were observed and then passaged when the degree of cell fusion reached approximately 80%. Human aortic smooth muscle cells were cultured at 37°C in a humidified incubator with 5% CO_2. Human aortic smooth muscle cells were infected with lentivirus containing shLOXL2 or shLOXL3 to knockdown LOXL2 or LOXL3 according to our previously reported methods (3, 17). Human aortic smooth muscle cells were starved for 12 h and then treated with losartan (10 and 100 μM, S1359; Selleck) and metformin (5 and 10 mM, HY17471A; MedChemExpress) for 48 h, with DMSO treatment serving as a control.

EdU Incorporation Assay

Human aortic smooth muscle cells infected with lenti-PLKO.1 or lenti-shLOXL3 were plated in 24-well plates and incubated with EdU medium (50 μmol/L) for 4 h. After washing with phosphate-buffered saline (PBS) twice, HASMCs were fixed with 4% paraformaldehyde for 30 min. Then, the HASMCs were incubated with glycine (2 mg/ml) to neutralize paraformaldehyde and immersed in 0.5% Triton X-100 for 10 min. The HASMCs were stained with 1× Apollo staining solution, and the nuclei were stained with 1× Hoechst 33342 for 30 min at room temperature. Images were captured with a BX53 Olympus light microscope system.

Statistical Analyses

All the data are represented as the mean ± standard deviation (*SD*) in the present study. For bioinformatics analysis, because different platforms were used for each dataset, we analyzed each dataset separately. We downloaded data from the supplementary file and selected raw data instead of the processed matrix file. To analyze the data, the raw expression values in each dataset were normalized by the R package limma, and $\log_2$ conversion was completed. After processing, we calculated the *p*-value for the difference in expression between AD samples and control samples by Student's *t*-test. Statistical analyses to compare the means of two groups were carried out by using Student's two-tailed *t*-test, while multiple group comparisons were conducted by using one-way ANOVA with least significant difference (equal variances assumed) or the Tamhane T2 (equal variances not assumed) test in SPSS software (version 13.0). $p < 0.05$ was used to indicate a statistically significant difference.

RESULTS

Analysis of LOXs Expression Levels in the Aorta Based on Data From the Gene Expression Omnibus Database

To clarify the role of LOXs in AD, we first analyzed the relative mRNA expression levels of LOXs in aorta samples from patients with TAAD and normal aorta samples from GEO datasets (GSE153434, GSE147026, GSE52093, and GSE98770). These four datasets include a total of 24 normal and 27 TAAD samples. Because different platforms were used to prepare the datasets, the expression levels of LOXs in four datasets are shown individually in **Figure 1**. Specifically, in the GSE153434 and GSE147026 datasets, the mRNA levels of LOXL2 and LOXL3 were significantly increased in the aortas of TAAD patients. In the GSE52093 dataset, elevated LOX mRNA levels were detected in individuals with TAAD, and in the GSE98770 dataset, LOXL2 expression levels were higher in samples from patients with TAAD than in those from their normal counterparts. However, no significant changes in the expression of other LOX family

members were detected (**Figure 1**). These results indicated that the occurrence of TAAD is accompanied by expression changes in specific LOXs, but this finding needs further verification.

Verification of the Expression Levels of LOXs in the Human Aorta

Because the four GEO datasets were collected from a relatively small sample size and no consistent conclusions were drawn, we further verified the protein levels of LOXs in aorta samples from normal controls and TAAD patients in our own center. The detailed demographic and clinical characteristics of the patients are presented in **Supplementary Table 1**. Compared with those in normal controls, the protein levels of LOXL2, and LOXL3 were significantly increased, while LOXL4 protein levels were decreased in patients with TAAD, but comparable protein levels of LOX and LOXL1 was observed between groups (**Figures 2A,B**). We further investigated the relationship between LOXs expression levels and aortic diameter in 33 TAAD patients. The results demonstrated that except for the significant correlation between LOXL1 mRNA expression and the diameter of the aortic arch, other LOXs showed no significant correlation with the diameter of the ascending aorta, aortic arch, descending aorta, or abdominal aorta (**Supplementary Figures 1A–E**).

LOXL2 Regulates ECM in Primary Cultured HASMCs

In human TAAD samples, we found that LOXL2 protein levels were obviously upregulated. Given that LOXL2 is critical for ECM regulation, we first evaluated the impact of LOXL2 knockdown on ECM. We constructed short hairpin RNA (shRNA) targeting LOXL2, which was packaged into lentivirus and then used to infect primary cultured HASMCs to knock down LOXL2. The LOXL2 mRNA and protein levels were verified, the results of which demonstrated that the mRNA and protein levels of LOXL2 were remarkably reduced in HASMCs infected with shLOXL2 (**Figures 3A,B**). More importantly, we found that the protein level of MMP2, but not MMP9, was dramatically reduced after LOXL2 knockdown in HASMCs (**Figure 3C**). Given that MMP2 is the primary matrix metalloproteinase that regulates Col1A1, Col1A2, Col4A1, Col5A1, and ELN (18), our results showed that Col5A1 and ELN were downregulated by LOXL2 knockdown, while Col1A1, Col1A2, and Col4A1 were not affected by LOXL2 deficiency (**Figure 3D**). These results indicates that LOXL2 plays a critical role in ECM regulation by promoting MMP2, Col5A1, and ELN expression.

The phenotypic switching of HASMCs is one of the features of AD (19). However, LOXL2 knockdown did not affect expression of the contractile markers α-SMA or SM22 (**Figure 3C**). Apoptosis and autophagy were reported to affect HASMC loss during AD (3, 17, 20). However, our data showed that LOXL2 knockdown had no impact on the expression of the apoptosis markers Bcl2 or Bax, or the autophagy marker LC3I/II (**Figure 3C**).

LOXL2 Knockdown Inhibited AKT Phosphorylation but Activated p38 in Primary Cultured HASMCs

LOXL2 knockdown was reported to inhibit p38 phosphorylation in MDA-MB-231 cells (21), and LOXL2 accelerates cardiac fibroblast-to-myofibroblast transformation by activating the PI3K/AKT signaling pathway to produce TGFβ2 (22). Thus, we wondered whether the p38 and AKT signaling pathways would be regulated by LOXL2 in HASMCs. Our results demonstrated that knockdown of LOXL2 suppressed AKT and S6 ribosomal protein phosphorylation but facilitated p38 phosphorylation in HASMCs (**Figure 3E**). However, comparable levels of phosphorylated JNK1/2 and ERK1/2 were detected in HASMCs with or without LOXL2 knockdown (**Figure 3E**). In addition, LOXL2 inhibits NF-κBp65 phosphorylation in ATDC5 cells, and NF-κBp65 activation is also involved in AD (23). Unexpectedly, the phosphorylation of NF-κBp65 was not regulated by LOXL2 in HASMCs (**Figure 3E**).

LOXL2 Inhibited H3K4me1/2/3 and H3K9me3 in HASMCs

Our previous data demonstrated that histone methylation is involved in the pathologic process of TAAD in humans (6). Recently, Peiró et al. found that LOXL2 could oxidize histone H3 at lysine 4 (H3K4ox) to prevent the di- and trimethylation in H3K4 but had no effect on H3K9me2 or H3K9me3 (24, 25). Thus, we further detected the levels of H3K4me1/2/3, H3K9me3, and H3K36me3 in HASMCs with LOXL2-knockdown. We found that H3K4me1/2/3 and H3K9me3 were significantly upregulated after LOXL2 knockdown, while H3K36me3 were not affected by LOXL2 (**Figure 3F**).

Knockdown of LOXL3 Inhibited Primary Cultured HASMCs Proliferation

To investigate the role of LOXL3 in HASMCs, we first knocked down LOXL3 in primary cultured HASMCs (**Figures 4A,C**). We subsequently evaluated the impact of LOXL3 on autophagy, apoptosis, and phenotypic switching, and the results indicated that LOXL3 knockdown had no effect on these biological processes, as evidenced by the similar protein levels of Beclin-1, Bax, Bcl2, α-SMA, and SM22 in HASMCs with or without LOXL3 knockdown (**Figure 4A**). Additionally, LOXL3 did not regulate MMP2 expression or H3K4 methylation (**Figure 4A**). Intriguingly, we found that PCNA and cyclin D1 were downregulated by LOXL3 knockdown in HASMCs, indicating that proliferation had been inhibited (**Figures 4B,C**). Furthermore, the EdU incorporation assay indicated that EdU-positive HASMCs were remarkably reduced after LOXL3 knockdown (**Figures 4D,E**). STAT3 is a ground-state transcription factor required for cell proliferation, and LOXL3 deacetylates/deacetyliminates STAT3, disrupting its dimerization, nuclear translocation, and activation to restrict cell proliferation (26). However, we found that LOXL3 knockdown facilitated the phosphorylation of Tyr705 in STAT3, and inhibited the phosphorylation of Ser727 in STAT3 in HASMCs

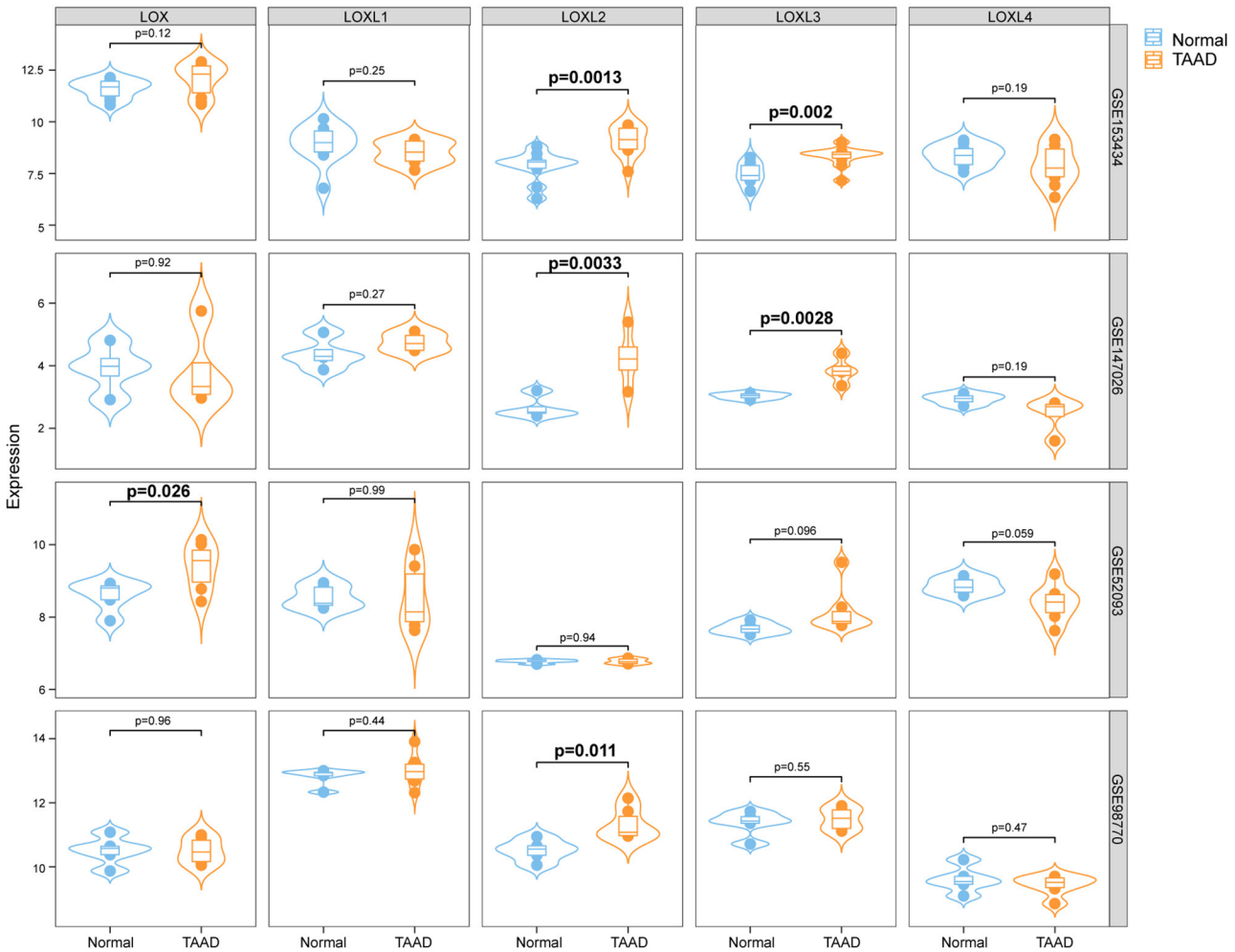

FIGURE 1 | The relative mRNA levels of LOXs in the aortas of individuals with or without AD. We downloaded four datasets from the GEO database, and the relative mRNA levels of LOXs in the GSE153434, GSE147026, GSE52093, and GSE98770 datasets are shown. Normal indicates aorta samples from individuals without aortic dissection, and TAAD indicates aorta samples from individuals with Stanford type A aortic dissection.

(**Figure 4F**). These results indicated that LOXL3 is a positive regulator that accelerates HASMC proliferation.

The Effect of Losartan and Metformin on LOXs Expression

Accumulating evidence has demonstrated that losartan and metformin have the potential to delay expansion of the aortic root or abdominal aorta or even prevent this major life-threatening manifestation in patients with MFS or AAA (27, 28). Thus, we wondered whether LOXs are involved in the effect of losartan and metformin on the aorta. We treated primary cultured HASMCs with metformin (5 and 10 mM) or losartan (10 and 100 μM) for 48 h. Our results showed that the protein levels of LOX (5 mM), LOXL2 and LOXL4 were reduced in HASMCs treated with metformin, while LOXL1 and LOXL3 were not affected by metformin (**Figures 5A,B**). Instead, losartan inhibited LOXL1, LOXL2, and LOXL4 expression at a concentration of 100 mM, but not LOX or LOXL3 expression in HASMCs (**Figures 5C,D**). These results suggest that LOXL2 and LOXL4 may partially mediate the protective roles of both losartan and metformin on aorta dilation and AAA.

DISCUSSION

Lysyl oxidases are well known to be crucial for ECM (13). However, the expression levels of LOXs in the aortas of patients with TAAD and their non-canonical functions in VSMCs are unclear. In the present study, we found that the protein levels of LOXL2 and LOXL3 are upregulated in the aortas of TAAD patients. Knockdown of LOXL2 inhibited MMP2, p-AKT, and p-S6 but promoted H3K4me1/2/3, H3K9me3, and p-P38 in HASMCs, which may be involved in regulating ECM. Instead, LOXL3 knockdown suppressed cyclin D1 and PCNA expression to inhibit HASMC proliferation. Moreover, LOXL2 and LOXL4 may partially mediate the therapeutic effects of losartan and

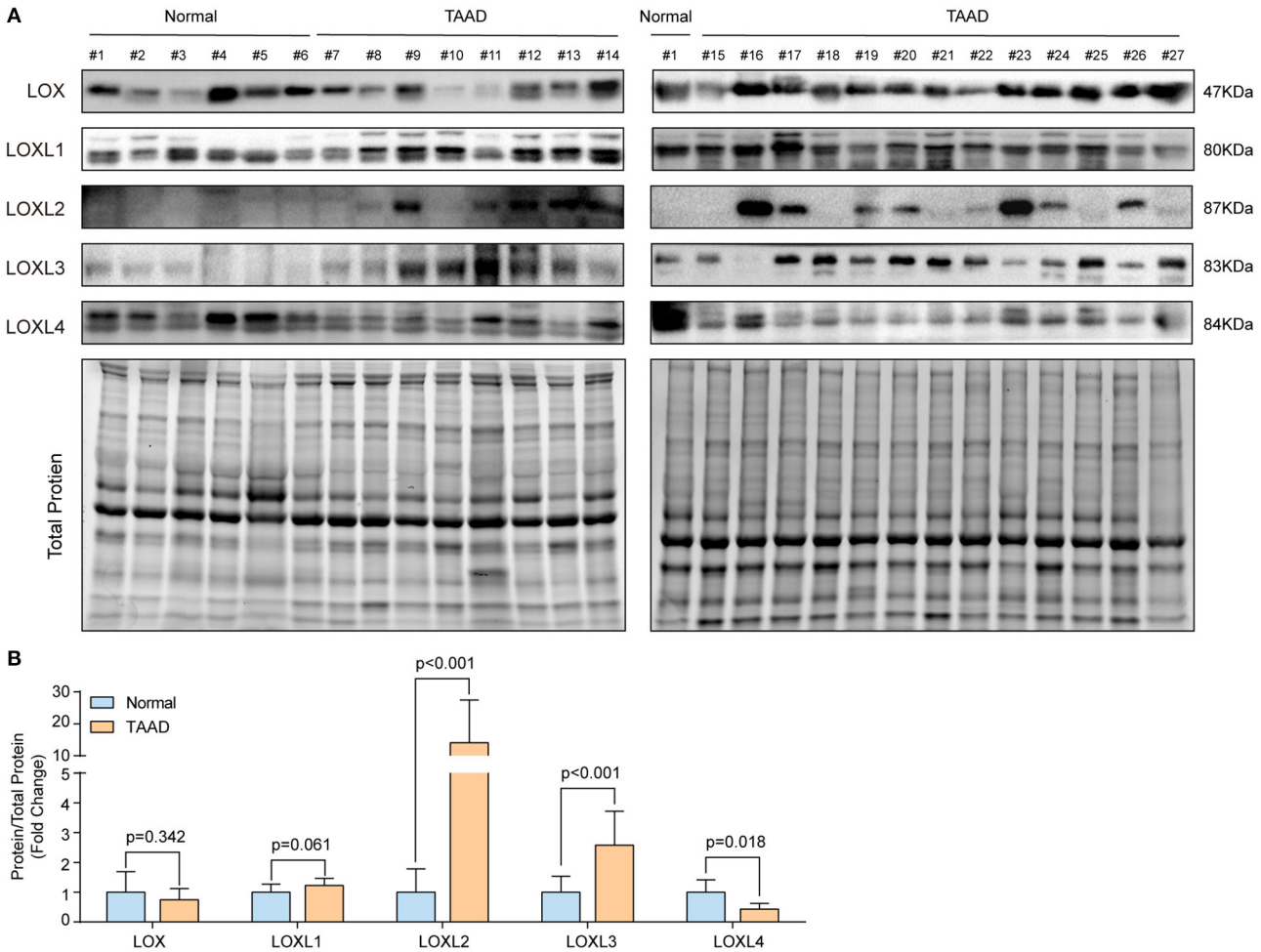

FIGURE 2 | The protein levels of LOXs in the human aorta. **(A)** The protein levels of LOXs were detected in aorta samples from 6 normal controls and 21 TAAD patients by using western blotting. **(B)** Relative quantification of LOXs protein levels in **(A)**. Total protein served as the loading control.

metformin on aortic dilatation. Therefore, our present study not only detected the expression patterns of LOXs in patients with TAAD but also clarified the functions of LOXL2 and LOXL3 in HASMCs.

Lysyl oxidases are the enzymes responsible for the crosslinking between collagen and ELN, which is critical to the structural integrity of the aorta (13). Accumulating evidence has demonstrated that the mutation or downregulation of LOX is closely related to aorta dilation and AD (15), and knockout of LOX in mice resulted in perinatal death due to AD rupture and was accompanied by reductions in ELN- and collagen-specific crosslinks in the aorta by 60 and 40%, respectively (29). BAPN is an irreversible inhibitor of LOX activity that can efficiently induce AD in both young mice and rats, but it is less efficient in adult mice and rats (7). The reason for this phenomenon may partially be because that ELN layers in the aorta are laid down during development and have a long half-life (approximately 40 years) (10, 30). In addition, a high-fat diet induced LOX overexpression in the aortas of rats, and BAPN prevented an increase in circulating leptin levels, reducing fibrosis, in rats fed a high-fat diet (31). Lysyl oxidases was also found to be upregulated in the vitreous of diabetic subjects (32). Given that diabetes mellitus is negatively associated with AD (33), diabetes-induced LOX overexpression in the aorta may mediate this protective effect.

In addition to LOX, the roles of other members of the LOX family in AD have been rarely reported. In the present study, we found that LOXL2 and LOXL3 protein levels are enhanced, while the protein level of LOXL4 is reduced in patients with TAAD compared to normal subjects. Although LOXL2 has been widely studied in cancer and fibrotic diseases such as idiopathic pulmonary fibrosis, liver fibrosis, and cardiac fibrosis (34), its expression and function in AD were unclear. Our results showed that compared with that in non-AD aorta samples, the protein level of LOXL2 in the aortas of patients with TAAD was remarkably increased. Wong et al. reported that chronic inflammation could induce LOXL2 expression and extracellular secretion in the liver (35, 36). The pathological process of AD is

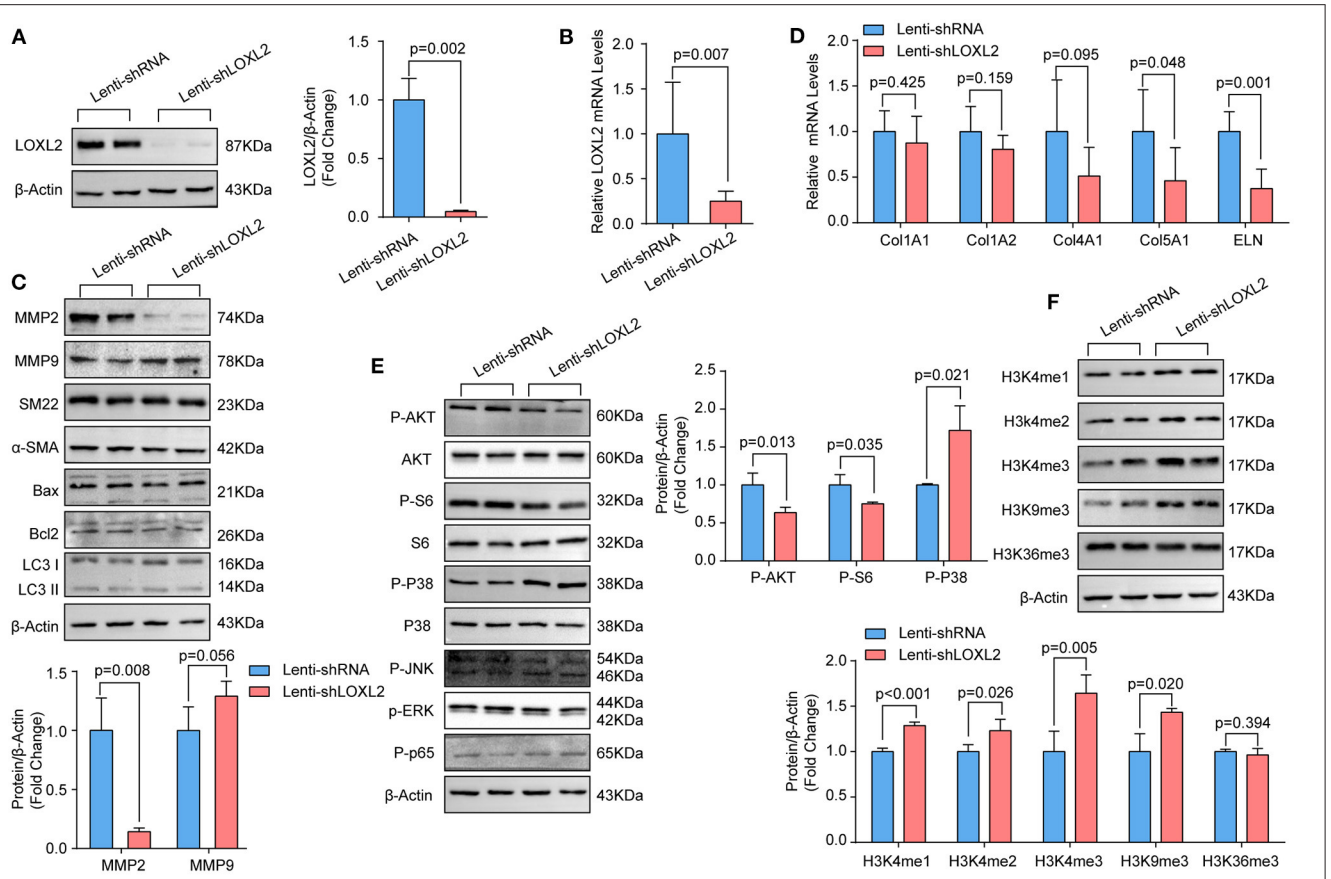

FIGURE 3 | Knockdown of LOXL2 inhibited MMP2 expression and AKT signaling, but facilitated the methylation of H3K4 and H3K9 in primary cultured HASMCs. **(A)** The protein levels of LOXL2 were evaluated by western blotting ($n = 4$). **(B)** The mRNA levels of LOXL2 in HASMCs infected with lenti-shRNA, lenti-shLOXL2 were detected by RT-PCR ($n = 5$). **(C)** The protein levels of MMP2, MMP9, SM22, Bax, Bcl2, and LC3I/II in HASMCs infected with lenti-shRNA or lenti-shLOXL2 ($n = 4$). **(D)** The mRNA levels of Col1A1, Col1A2, Col4A1, Col5A1, and ELN in HASMCs were detected by RT-PCR ($n = 5$). **(E)** The p-AKT, S6, GSK3β, p38, ERK1/2, JNK1/2, and p65 in HASMCs was evaluated by western blotting ($n = 4$). **(F)** Western blotting was used to detect the protein levels of H3K4me1, H3K4me2, H3K4me3, H3K9me3, and H3K36me3 in HASMCs infected with lenti-shRNA or lenti-shLOXL2 ($n = 4$). β-Actin served as the loading control.

accompanied by inflammation, and excessive inflammation is an independent predictor of adverse clinical outcomes (37). Thus, elevated LOXL2 expression levels in the aortas of AD patients may be related to inflammation.

As LOXL2 is critical for ECM regulation (35), we detected the expression levels of MMP2 and MMP9 in primary cultured HASMCs with or without LOXL2 knockdown. Our results demonstrated that LOXL2 knockdown significantly suppressed MMP2 expression but not MMP9 expression. Increased MMP2 expression was also observed in the aorta of patients with AD (38). MMP2 is predominantly derived from VSMCs and fibroblasts, and MMP2 degrades collagen and ELN (38). Moreover, MMP2 deficiency significantly reduced BAPN-induced formation and AD rupture in mice (39). MMP2 deletion inhibited the activation of transforming growth factor-β (TGFβ) and its non-canonical signaling cascade downstream of extracellular signal regulated kinases 1/2 (ERK1/2) in the aortas of mice (40). Atorvastatin and amlodipine were reported to reduce MMP2 activity, and doxycycline inhibited MMP2 expression to delay aorta dilation (38, 40). Thus, LOXL2 may facilitate AD by inducing MMP2 expression. However, the precise effect of LOXL2 on AD and how it regulates the expression of MMP2 require further investigation.

We found that the expression levels of LOXL3 were elevated in the aortas of humans with AD. LOXL3 was initially identified as an amine oxidase, but a variety of novel functions have recently been attributed to LOXL3 (41). In our study, we demonstrated that LOXL3 deficiency in primary cultured HASMCs remarkably suppressed HASMC proliferation. As VSMC loss is one of the major feature of AD, the LOXL3-mediated regulation of VSMC proliferation may be a compensatory effect. In pancreatic ductal adenocarcinoma cells, LOXL3 physically interacted with SNAIL to promote proliferation (41). Another study demonstrated that LOXL3 interacted with proteins involved in DNA stability (e.g., BRCA2 and SMC1A) and mitosis completion to accelerate the proliferation of melanoma cells (42). However, LOXL3 colocalized with STAT3 in the nucleus to deacetylate STAT3, disrupt STAT3 dimerization, and then inhibit the transcriptional

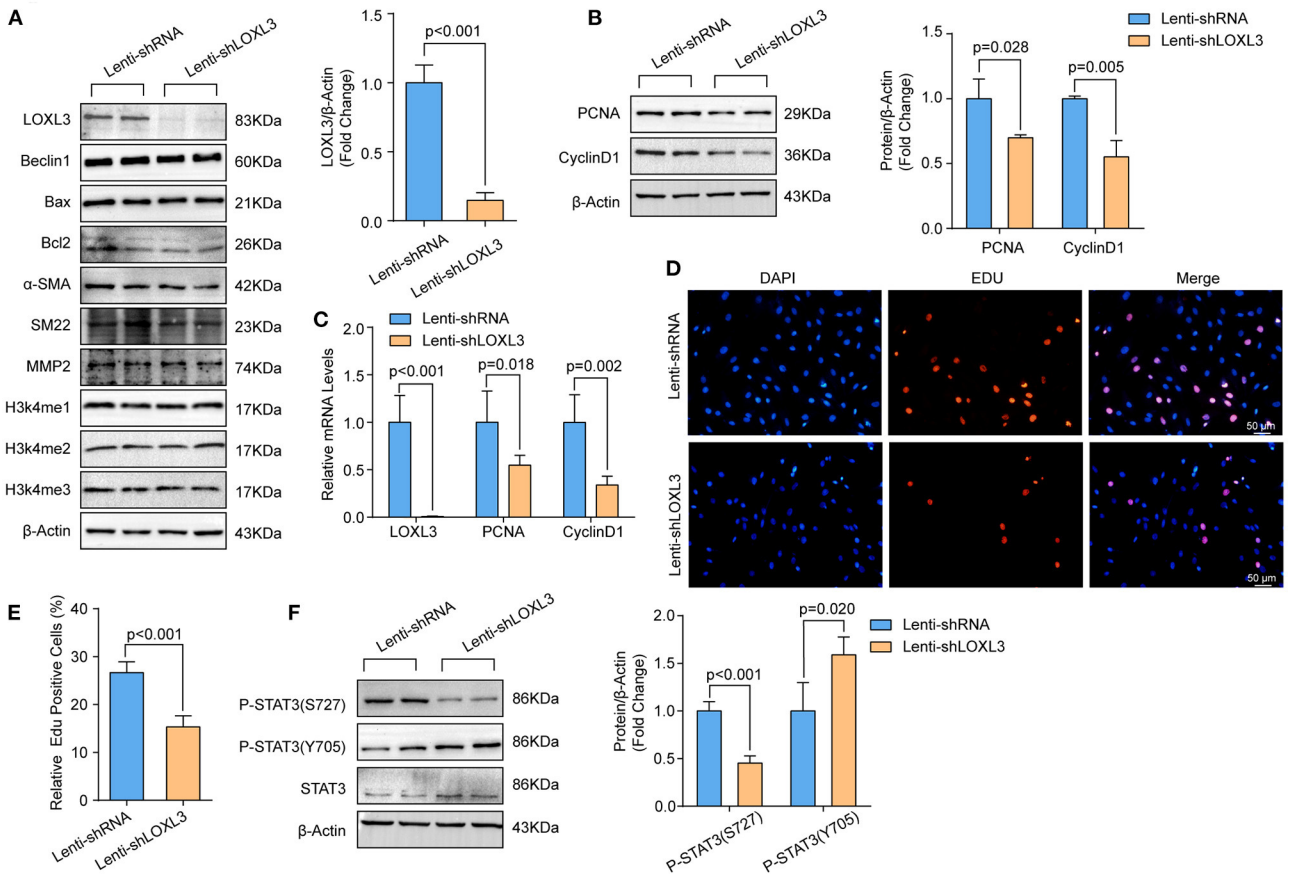

FIGURE 4 | LOXL3 knockdown suppressed the proliferation of primary cultured HASMCs. **(A)** The protein levels of LOXL3, Beclin 1, Bax, Bcl2, α-SMA, SM22, MMP2, H3K4me2, and H3K4me3 in HASMCs infected with lenti-shRNA or lenti-shLOXL3 ($n = 4$). **(B)** The protein levels of the proliferation markers cyclin D1 and PCNA in HASMCs infected with lenti-shRNA or lenti-shLOXL3 ($n = 4$). **(C)** The mRNA levels of LOXL3, cyclin D1, and PCNA in the indicated HASMCs were evaluated by RT-PCR ($n = 5$). **(D,E)** The EdU assay was performed in HASMCs infected with lenti-shRNA or lenti-shLOXL3 **(D)**, and EdU-positive cells were quantified **(E)** ($n = 4$). **(F)** Levels of STAT3 phosphorylated at serine 727 and tyrosine 705 in HASMCs infected with lenti-shRNA or lenti-shLOXL3 ($n = 4$). β-Actin served as the loading control.

activity of STAT3 to restrict Th17 and Treg proliferation and differentiation (26). In our study, the levels of p-STAT3 (Ser727) were decreased, while those of p-STAT3 (Tyr705) were increased in LOXL3-knockdown HASMCs. It has been reported that the phosphorylation of Ser727 in STAT3 inhibits STAT3 dimerization and nuclear translocation by enhancing the dephosphorylation of Tyr705 in STAT3 (43). Thus, the impact of LOXL3 on VSMCs proliferation may not be associated with STAT3 phosphorylation, but whether LOXL3 regulates VSMCs proliferation by interacting with SNAIL, BRCA2 or SMC1A requires further research.

Accumulating evidence indicates that losartan (an AT1 antagonist) and metformin (a hypoglycemic drug) have an inhibitory effect on aortic dilation in MFS patients or AAA patients (27, 28, 44). A recently published long-term clinical study suggested that combined losartan and β-blocker treatment in patients with MFS had a clinical benefit (27). We treated primary cultured human VSMCs with losartan and metformin. Our results showed that both losartan and metformin inhibited LOXL2 and LOXL4 expression. Thus, LOXL2 and LOXL4 may be common targets of losartan and metformin in this condition. Nevertheless, other mechanisms are involved in their protective roles; for example, the PI3K/AKT/mTOR/autophagy pathway was inhibited by metformin to repress the pathophysiology of AAA (45).

Although we have systematically verified the expression of LOXs at the mRNA and protein levels in human clinical samples, we have not clarified the regulatory mechanisms that mediate these changes in LOXs expression. In addition, we studied the role of LOXL2 and LOXL3 at only the cellular level and did not use knockout animal models to reveal their roles in AD *in vivo*. In addition, whether LOXL1 and LOXL4 are also involved in the regulation of AD needs to be further explored.

CONCLUSIONS

In conclusion, the present study demonstrated that increased LOXL2 in patients with TAAD might facilitate

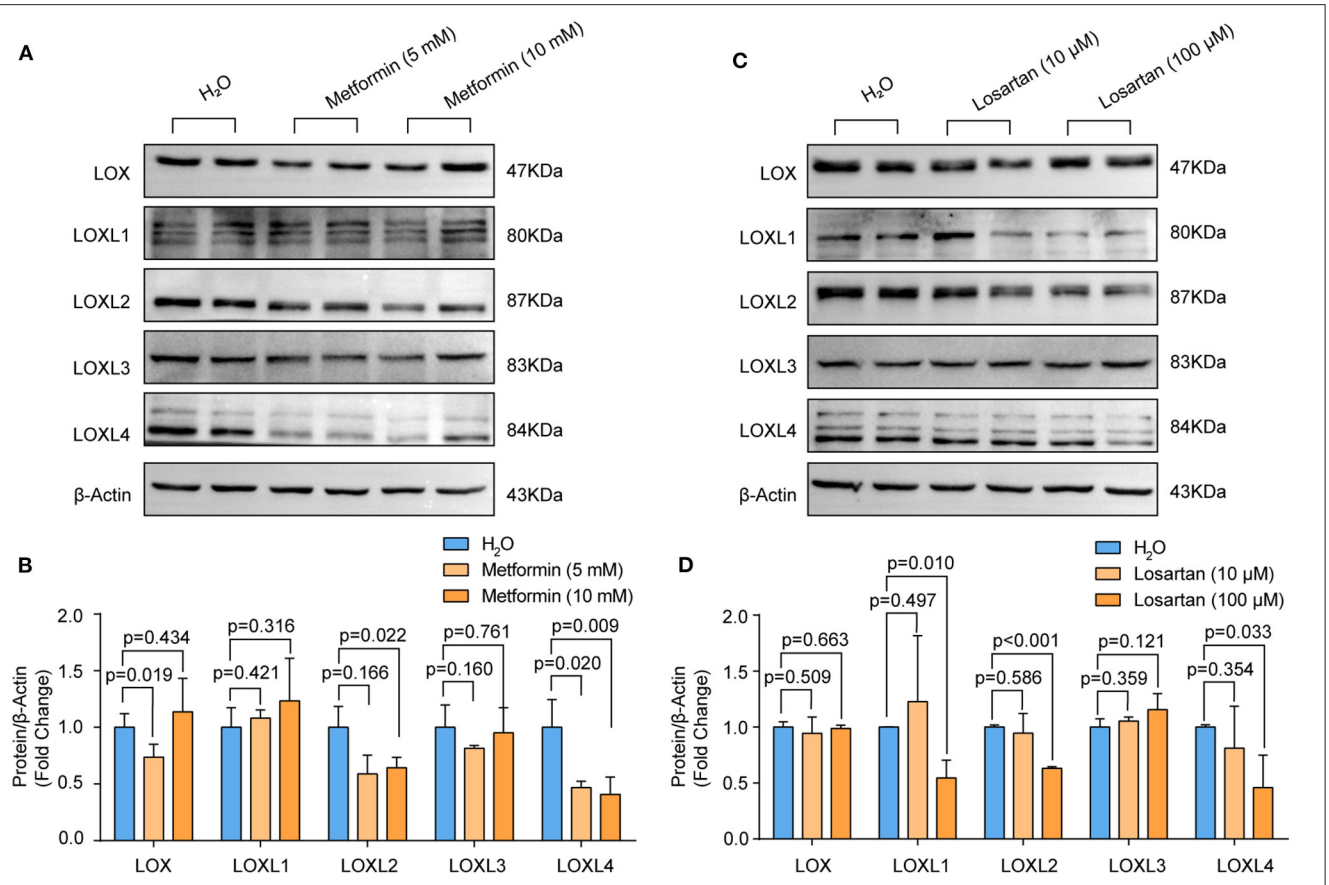

FIGURE 5 | The protein levels of LOXs in primary cultured HASMCs treated with metformin or losartan. **(A,B)** The protein levels of LOX, LOXL1, LOXL2, LOXL3, and LOXL4 in HASMCs stimulated with 5 or 10 mM metformin were evaluated by western blotting ($n = 4$). **(C,D)** LOX, LOXL1, LOXL2, LOXL3, and LOXL4 protein levels in HASMCs treated with 10 or 100 μM losartan were detected by using western blotting ($n = 4$). H_2O-treated HASMCs served as the control group in **(A)** and **(B)**.

MMP2, Col5A1, and ELN expression to affect ECM in aorta. However, as LOXL3 knockdown inhibited VSMC proliferation, elevated LOXL3 seems to be a compensatory effect. Thus, the differential regulation of LOXs may be a novel strategy for the treatment of AD.

DATA AVAILABILITY STATEMENT

The datasets presented in this study can be found in online repositories. The names of the repository/repositories and accession number(s) can be found in the article/**Supplementary Material**.

ETHICS STATEMENT

The studies involving human participants were reviewed and approved by the Human Research Ethics Committees of Tongji Hospital, Tongji Medical College, Huazhong University of Science and Technology. The patients/participants provided their written informed consent to participate in this study. The animal study was reviewed and approved by the Animal Care and Use Committee of Tongji Hospital, Tongji Medical College, Huazhong University of Science and Technology.

AUTHOR CONTRIBUTIONS

YZ, YC, and CL carried out the immunoassays and cell culture. XF, Z-MF, and JG performed the surgery and collected the samples. Z-MF, XY, and XJ participated in the design of the study and performed the statistical analysis. XY drafted the manuscript. XL revised the manuscript. XJ and Z-MF conceived of the study, participated in its design, and coordination and helped to draft the manuscript. XY and Z-MF provided funding support. All authors read and approved the final manuscript.

FUNDING

This work was supported by grants from the National Natural Science Foundation of China

(No. 81700249), the Natural Science Foundation of Hubei Province (No. 2018CFB734), and the Hubei Province health and Family Planning Scientific Research Project (WJ2019Q043 and WJ2021M1).

SUPPLEMENTARY MATERIAL

The Supplementary Material for this article can be found online at: https://www.frontiersin.org/articles/10.3389/fcvm.2021.692856/full#supplementary-material

REFERENCES

1. Dong YH, Chang CH, Wang JL, Wu LC, Lin JW, Toh S. Association of infections and use of fluoroquinolones with the risk of aortic aneurysm or aortic dissection. *JAMA Intern Med*. (2020) 180:1587–95. doi: 10.1001/jamainternmed.2020.4192
2. Chen SW, Kuo CF, Huang YT, Lin WT, Chien-Chia WV, Chou AH, et al. Association of family history with incidence and outcomes of aortic dissection. *J Am Coll Cardiol*. (2020) 76:1181–92. doi: 10.1016/j.jacc.2020.07.028
3. Li R, Yi X, Wei X, Huo B, Guo X, Cheng C, et al. EZH2 inhibits autophagic cell death of aortic vascular smooth muscle cells to affect aortic dissection. *Cell Death Dis*. (2018) 9:180. doi: 10.1038/s41419-017-0213-2
4. Erbel R, Aboyans V, Boileau C, Bossone E, Bartolomeo RD, Eggebrecht H, et al. 2014 ESC Guidelines on the diagnosis and treatment of aortic diseases: document covering acute and chronic aortic diseases of the thoracic and abdominal aorta of the adult. The task force for the diagnosis and treatment of aortic diseases of the European Society of Cardiology (ESC). *Eur Heart J*. (2014) 35:2873–926. doi: 10.1093/eurheartj/ehu281
5. Wei X, Yi X, Zhu XH, Jiang DS. Histone methylation and vascular biology. *Clin Epigenet*. (2020) 12:30. doi: 10.1186/s13148-020-00826-4
6. Guo X, Fang ZM, Wei X, Huo B, Yi X, Cheng C, et al. HDAC6 is associated with the formation of aortic dissection in human. *Mol Med*. (2019) 25:10. doi: 10.1186/s10020-019-0080-7
7. Jiang DS, Yi X, Zhu XH, Wei X. Experimental *in vivo* and *ex vivo* models for the study of human aortic dissection: promises and challenges. *Am J Transl Res*. (2016) 8:5125–40.
8. Lee VS, Halabi CM, Broekelmann TJ, Trackman PC, Stitziel NO, Mecham RP. Intracellular retention of mutant lysyl oxidase leads to aortic dilation in response to increased hemodynamic stress. *JCI Insight*. (2019) 5:e127748. doi: 10.1172/jci.insight.127748
9. Wolford BN, Hornsby WE, Guo D, Zhou W, Lin M, Farhat L, et al. Clinical implications of identifying pathogenic variants in individuals with thoracic aortic dissection. *Circ Genom Precis Med*. (2019) 12:e2476. doi: 10.1161/CIRCGEN.118.002476
10. Guo DC, Regalado ES, Gong L, Duan X, Santos-Cortez RL, Arnaud P, et al. LOX mutations predispose to thoracic aortic aneurysms and dissections. *Circ Res*. (2016) 118:928–34. doi: 10.1161/CIRCRESAHA.115.307130
11. Busnadiego O, Gorbenko DBD, Gonzalez-Santamaria J, Habashi JP, Calderon JF, Sandoval P, et al. Elevated expression levels of lysyl oxidases protect against aortic aneurysm progression in Marfan syndrome. *J Mol Cell Cardiol*. (2015) 85:48–57. doi: 10.1016/j.yjmcc.2015.05.008
12. Al-U'Datt D, Allen BG, Nattel S. Role of the lysyl oxidase enzyme family in cardiac function and disease. *Cardiovasc Res*. (2019) 115:1820–37. doi: 10.1093/cvr/cvz176
13. Martinez-Gonzalez J, Varona S, Canes L, Galan M, Briones AM, Cachofeiro V, et al. Emerging roles of lysyl oxidases in the cardiovascular system: new concepts and therapeutic challenges. *Biomolecules*. (2019) 9:610. doi: 10.3390/biom9100610
14. Liu X, Zhao Y, Gao J, Pawlyk B, Starcher B, Spencer JA, et al. Elastic fiber homeostasis requires lysyl oxidase-like 1 protein. *Nat Genet*. (2004) 36:178–82. doi: 10.1038/ng1297
15. Lee VS, Halabi CM, Hoffman EP, Carmichael N, Leshchiner I, Lian CG, et al. Loss of function mutation in LOX causes thoracic aortic aneurysm and dissection in humans. *Proc Natl Acad Sci USA*. (2016) 113:8759–64. doi: 10.1073/pnas.1601442113
16. Jiang DS, Zeng HL, Li R, Huo B, Su YS, Fang J, et al. Aberrant epicardial adipose tissue extracellular matrix remodeling in patients with severe ischemic cardiomyopathy: insight from comparative quantitative proteomics. *Sci Rep*. (2017) 7:43787. doi: 10.1038/srep43787
17. Chen TQ, Hu N, Huo B, Masau JF, Yi X, Zhong XX, et al. EHMT2/G9a inhibits aortic smooth muscle cell death by suppressing autophagy activation. *Int J Biol Sci*. (2020) 16:1252–63. doi: 10.7150/ijbs.38835
18. Chen Q, Jin M, Yang F, Zhu J, Xiao Q, Zhang L. Matrix metalloproteinases: inflammatory regulators of cell behaviors in vascular formation and remodeling. *Mediators Inflamm*. (2013) 2013:928315. doi: 10.1155/2013/928315
19. Yang K, Ren J, Li X, Wang Z, Xue L, Cui S, et al. Prevention of aortic dissection and aneurysm via an ALDH2-mediated switch in vascular smooth muscle cell phenotype. *Eur Heart J*. (2020) 41:2442–53. doi: 10.1093/eurheartj/ehaa352
20. Grond-Ginsbach C, Pjontek R, Aksay SS, Hyhlik-Durr A, Bockler D, Gross-Weissmann ML. Spontaneous arterial dissection: phenotype and molecular pathogenesis. *Cell Mol Life Sci*. (2010) 67:1799–815. doi: 10.1007/s00018-010-0276-z
21. Brekhman V, Lugassie J, Zaffryar-Eilot S, Sabo E, Kessler O, Smith V, et al. Receptor activity modifying protein-3 mediates the protumorigenic activity of lysyl oxidase-like protein-2. *Faseb J*. (2011) 25:55–65. doi: 10.1096/fj.10-162677
22. Yang J, Savvatis K, Kang JS, Fan P, Zhong H, Schwartz K, et al. Targeting LOXL2 for cardiac interstitial fibrosis and heart failure treatment. *Nat Commun*. (2016) 7:13710. doi: 10.1038/ncomms13710
23. Tashkandi M, Ali F, Alsaqer S, Alhousami T, Cano A, Martin A, et al. Lysyl oxidase-like 2 protects against progressive and aging related knee joint osteoarthritis in mice. *Int J Mol Sci*. (2019) 20:4798. doi: 10.3390/ijms20194798
24. Herranz N, Dave N, Millanes-Romero A, Pascual-Reguant L, Morey L, Diaz VM, et al. Lysyl oxidase-like 2 (LOXL2) oxidizes trimethylated lysine 4 in histone H3. *Febs J*. (2016) 283:4263–73. doi: 10.1111/febs.13922
25. Cebria-Costa JP, Pascual-Reguant L, Gonzalez-Perez A, Serra-Bardenys G, Querol J, Cosin M, et al. LOXL2-mediated H3K4 oxidation reduces chromatin accessibility in triple-negative breast cancer cells. *Oncogene*. (2020) 39:79–121. doi: 10.1038/s41388-019-0969-1
26. Ma L, Huang C, Wang XJ, Xin DE, Wang LS, Zou QC, et al. Lysyl oxidase 3 is a dual-specificity enzyme involved in STAT3 deacetylation and deacetylimination modulation. *Mol Cell*. (2017) 65:296–309. doi: 10.1016/j.molcel.2016.12.002
27. van Andel MM, Indrakusuma R, Jalalzadeh H, Balm R, Timmermans J, Scholte AJ, et al. Long-term clinical outcomes of losartan in patients with Marfan syndrome: follow-up of the multicentre randomized controlled COMPARE trial. *Eur Heart J*. (2020) 41:4181–7. doi: 10.1093/eurheartj/ehaa377
28. Yu X, Jiang D, Wang J, Wang R, Chen T, Wang K, et al. Metformin prescription and aortic aneurysm: systematic review and meta-analysis. *Heart*. (2019) 105:1351–57. doi: 10.1136/heartjnl-2018-314639
29. Staiculescu MC, Kim J, Mecham RP, Wagenseil JE. Mechanical behavior and matrisome gene expression in the aneurysm-prone thoracic aorta of newborn lysyl oxidase knockout mice. *Am J Physiol Heart Circ Physiol*. (2017) 313:H446–56. doi: 10.1152/ajpheart.00712.2016
30. Arribas SM, Hinek A, Gonzalez MC. Elastic fibres and vascular structure in hypertension. *Pharmacol Ther*. (2006) 111:771–91. doi: 10.1016/j.pharmthera.2005.12.003
31. Martinez-Martinez E, Rodriguez C, Galan M, Miana M, Jurado-Lopez R, Bartolome MV, et al. The lysyl oxidase inhibitor (beta-aminopropionitrile) reduces leptin profibrotic effects and ameliorates cardiovascular remodeling in diet-induced obesity in rats. *J Mol Cell Cardiol*. (2016) 92:96–104. doi: 10.1016/j.yjmcc.2016.01.012
32. Subramanian ML, Stein TD, Siegel N, Ness S, Fiorello MG, Kim D, et al. Upregulation of lysyl oxidase expression in vitreous of diabetic subjects: implications for diabetic retinopathy. *Cells Basel*. (2019) 8:1122. doi: 10.3390/cells8101122

33. LeMaire SA, Russell L. Epidemiology of thoracic aortic dissection. *Nat Rev Cardiol.* (2011) 8:103–13. doi: 10.1038/nrcardio.2010.187
34. Erasmus M, Samodien E, Lecour S, Cour M, Lorenzo O, Dludla P, et al. Linking LOXL2 to cardiac interstitial fibrosis. *Int J Mol Sci.* (2020) 21:5913. doi: 10.3390/ijms21165913
35. Puente A, Fortea JI, Cabezas J, Arias LM, Iruzubieta P, Llerena S, et al. LOXL2-a new target in antifibrogenic therapy? *Int J Mol Sci.* (2019) 20:1634. doi: 10.3390/ijms20071634
36. Wong CC, Tse AP, Huang YP, Zhu YT, Chiu DK, Lai RK, et al. Lysyl oxidase-like 2 is critical to tumor microenvironment and metastatic niche formation in hepatocellular carcinoma. *Hepatology.* (2014) 60:1645–58. doi: 10.1002/hep.27320
37. Anzai A, Shimoda M, Endo J, Kohno T, Katsumata Y, Matsuhashi T, et al. Adventitial CXCL1/G-CSF expression in response to acute aortic dissection triggers local neutrophil recruitment and activation leading to aortic rupture. *Circ Res.* (2015) 116:612–23. doi: 10.1161/CIRCRESAHA.116.304918
38. Maguire EM, Pearce S, Xiao R, Oo AY, Xiao Q. Matrix metalloproteinase in abdominal aortic aneurysm and aortic dissection. *Pharmaceuticals (Basel).* (2019) 12:118. doi: 10.3390/ph12030118
39. Ren W, Liu Y, Wang X, Piao C, Ma Y, Qiu S, et al. The complement C3a-C3aR axis promotes development of thoracic aortic dissection via regulation of MMP2 expression. *J Immunol.* (2018) 200:1829–38. doi: 10.4049/jimmunol.1601386
40. Xiong W, Meisinger T, Knispel R, Worth JM, Baxter BT. MMP-2 regulates Erk1/2 phosphorylation and aortic dilatation in Marfan syndrome. *Circ Res.* (2012) 110:e92–101. doi: 10.1161/CIRCRESAHA.112.268268
41. Laurentino TS, Soares R, Marie S, Oba-Shinjo SM. LOXL3 Function beyond amino oxidase and role in pathologies, including cancer. *Int J Mol Sci.* (2019) 20:3587. doi: 10.3390/ijms20143587
42. Santamaria PG, Floristan A, Fontanals-Cirera B, Vazquez-Naharro A, Santos V, Morales S, et al. Lysyl oxidase-like 3 is required for melanoma cell survival by maintaining genomic stability. *Cell Death Differ.* (2018) 25:935–50. doi: 10.1038/s41418-017-0030-2
43. Wakahara R, Kunimoto H, Tanino K, Kojima H, Inoue A, Shintaku H, et al. Phospho-Ser727 of STAT3 regulates STAT3 activity by enhancing dephosphorylation of phospho-Tyr705 largely through TC45. *Genes Cells.* (2012) 17:132–45. doi: 10.1111/j.1365-2443.2011.01575.x
44. Habashi JP, Judge DP, Holm TM, Cohn RD, Loeys BL, Cooper TK, et al. Losartan, an AT1 antagonist, prevents aortic aneurysm in a mouse model of Marfan syndrome. *Science.* (2006) 312:117–21. doi: 10.1126/science.1124287
45. Wang Z, Guo J, Han X, Xue M, Wang W, Mi L, et al. Metformin represses the pathophysiology of AAA by suppressing the activation of PI3K/AKT/mTOR/autophagy pathway in ApoE$^{(-/-)}$ mice. *Cell Biosci.* (2019) 9:68. doi: 10.1186/s13578-019-0332-9

Conflict of Interest: The authors declare that the research was conducted in the absence of any commercial or financial relationships that could be construed as a potential conflict of interest.

Copyright © 2021 Yi, Zhou, Chen, Feng, Liu, Jiang, Geng, Li, Jiang and Fang. This is an open-access article distributed under the terms of the Creative Commons Attribution License (CC BY). The use, distribution or reproduction in other forums is permitted, provided the original author(s) and the copyright owner(s) are credited and that the original publication in this journal is cited, in accordance with accepted academic practice. No use, distribution or reproduction is permitted which does not comply with these terms.

frontiers in Cardiovascular Medicine

ORIGINAL RESEARCH
published: 02 August 2021
doi: 10.3389/fcvm.2021.710425

Association of *IL1R1* Coding Variant With Plasma-Level Soluble ST2 and Risk of Aortic Dissection

*Wenxi Jiang[1,2], Xue Wang[1,2], Pei Gao[3], Fengjuan Li[1,2], Ke Lu[3], Xin Tan[1,2], Shuai Zheng[1,2], Wang Pei[1,2], Meiyu An[1,2], Xi Li[1], Rong Hu[1], Yongliang Zhong[1], Junming Zhu[1], Jie Du[1,2] and Yuan Wang[1,2]**

[1] Key Laboratory of Remodeling-Related Cardiovascular Diseases, Ministry of Education, The Collaborative Innovation Center for Cardiovascular Disorders, Beijing Anzhen Hospital, Capital Medical University, Beijing, China, [2] Department of Vascular Biology, Beijing Institute of Heart, Lung and Blood Vessel Disease, Beijing, China, [3] Department of Epidemiology and Biostatistics, School of Public Health, Peking University, Beijing, China

OPEN ACCESS

Edited by:
Yuli Huang,
Southern Medical University, China

Reviewed by:
Xiangping Chai,
Central South University, China
Dongjin Wang,
Nanjing Drum Tower Hospital, China

***Correspondence:**
Yuan Wang
wangyuan980510@ccmu.edu.cn

Specialty section:
This article was submitted to General Cardiovascular Medicine, a section of the journal Frontiers in Cardiovascular Medicine

Received: 16 May 2021
Accepted: 28 June 2021
Published: 02 August 2021

Citation:
Jiang W, Wang X, Gao P, Li F, Lu K, Tan X, Zheng S, Pei W, An M, Li X, Hu R, Zhong Y, Zhu J, Du J and Wang Y (2021) Association of IL1R1 Coding Variant With Plasma-Level Soluble ST2 and Risk of Aortic Dissection. Front. Cardiovasc. Med. 8:710425. doi: 10.3389/fcvm.2021.710425

Objective: Aortic dissection (AD) is characterized by an acute onset, rapid progress, and high mortality. Levels of soluble ST2 (sST2) on presentation are elevated in patients with acute AD, which can be used to discriminate AD patients from patients with chest pain. sST2 concentrations were found to be highly heritable in the general population. The aim of this study was to investigate the associations of variations in ST2-related gene expression with sST2 concentrations and AD risk.

Methods: This case-control study involving a total of 2,277 participants were conducted, including 435 AD patients and age- and sex-matched 435 controls in the discovery stage, and 464 patients and 943 controls in the validation stage. Eight ST2-related genes were selected by systematic review. Tag single-nucleotide polymorphisms (SNPs) were screened out from the Chinese population of the 1,000 Genomes Database. Twenty-one ST2-related SNPs were genotyped, and plasma sST2 concentrations were measured.

Results: In the discovery stage, rs13019803 located in *IL1R1* was significantly associated with AD after Bonferroni correction ($p = 0.0009$) and was correlated with circulating sST2 levels in patients with type A AD(AAD) [log-sST2 per C allele increased by 0.180 (95%) CI: 0.002 – 0.357] but not in type B. Combining the two stages together, rs13019803C was associated with plasma sST2 level in AAD patients [log-sST2 increased by 0.141 (95% CI: 0.055–0.227) for per C allele]. Odds ratio of rs13019803 on the risk of AAD is 1.67 (95% CI: 1.33–2.09).

Conclusions: The *IL1R1* SNP rs13019803C is associated with higher sST2 levels and increased risk of AAD.

Keywords: *IL1R1* gene, soluble ST2, aortic dissection, ST2-related genes, risk factor

INTRODUCTION

Aortic dissection (AD) is an important cause of cardiovascular death characterized by acute onset and rapid progress with poor prognosis and high mortality (1). Acute AD is a fatal clinical emergency, with an untreated mortality rate of 1–2% per hour after symptom onset and almost 50% in the first week (2). Therefore, identifying those members of the population with higher risk to AD is very important. Contributing factors of AD are diverse, including male sex, advanced age, smoking, hypertension, and genetic factors (3). Although the pathogenesis of AD remains unclear, genetic variation plays a critical role, and the American College of Cardiology Foundation and the American Heart Association recommended that identification of the genetic variations leading to these aortic diseases has the potential for early identification of individuals at risk (4).

AD is a multifactorial disease whose primary pathology is connective tissue degeneration of the medial layer of the aorta. During the early phase of aortic damage, a large number of vascular injury-related proteins are produced in response to injury of vascular smooth muscle and elastic laminae (5–7). Soluble (s)ST2 is also regulated by vascular injury and is rapidly secreted into the circulation after stress and pro-inflammatory stimulation. We have used it to discriminate acute AD from other diseases presenting with acute chest pain (8). In the early stages of AD, sST2 elevated levels reflect the degree of vascular injury (9, 10). sST2 also participates in adverse remodeling of blood vessels by stimulating expression of type I collagen, fibronectin, and profibrotic factors (11).

In previous studies, it was found that the concentration of sST2 varies greatly in AD patients (8). The level of soluble ST2 was affected by age, gender, clinical manifestations, and genetic variation in the general population (12). Despite being correlated with multiple traditional cardiovascular risk factors, soluble ST2 concentrations were found to be highly heritable in the Framingham Heart Study population, in which clinical factors accounted for only 14% of the interindividual variation in soluble ST2 concentrations, and genetic factors accounted for up to 45% of the remaining variation. Therefore, although sST2 is affected by different clinical phenotypes, genetic factors may also play an important role in determining the circulating level of patients.

Variation in genes encoding vascular injury-associated proteins is known to associate increased risk for AD, such as matrix metalloproteinases(MMPs), SMAD4, and interleukin 6 (IL-6) genes (13–15). However, it is unclear whether variation in ST2 gene expression is related to AD risk. Determination of genetic variants that significantly affect sST2 concentrations and AD risk would be helpful in the early identification of high-risk populations to achieve better clinical outcomes.

Abbreviations: AD, aortic dissection; sST2, soluble ST2; SNP, single-nucleotide polymorphism; MAF, minor allele frequency; CI, confidence interval; IQR, interquartile range; CAD, coronary artery heart disease; HBP, high blood pressure; BMI, body mass index.

The aim of this study, therefore, was to investigate whether sST2-related gene polymorphisms are associated with increased sST2 concentrations and higher risk of AD.

MATERIALS AND METHODS

Participants

The overall study design is shown in **Figure 1**. This study included AD patients and controls who had visited Anzhen Hospital, Beijing, China, between January 2017 and January 2019. The study comprised a discovery stage including participants from January 2017 to August 2017 and a validation stage including participants from September 2017 to January 2019. All patients who were referred to the surgical service for the evaluation and management of AD were included. All patients with AD had image information from echocardiograms and computed tomography to confirm the final diagnosis. The diagnosis of AD was based on the detection of intimal flaps in the aorta (16). The Stanford classification was applied to determine the types of AD. With this classification system, type A AD is defined as an intimal tear involving the ascending aorta, whereas type B AD is not (17). Patients were excluded if they met any of the following criteria: (a) received packed red blood cells, whole blood, or platelets fewer than 10 days before the blood sample was taken; (b) aortic trauma; (c)with active cancer; and (d) entered the hospital for checkups after surgery or undergone open or endovascular treatment in temporal proximity fewer than 1 year. A patient's aorta was considered aneurysmal when its diameter was >1.5 times the normal diameter, based on the patient's sex, age, and body size. The acute phase, subacute phase, and chronic phase are defined as occurring within 2 weeks, 2 weeks to 2 months, and more than 2 months after the onset of initial symptoms, respectively. We defined the thoracic aorta as the portion of the vessel located above the diaphragm, including the ascending aorta, the aortic arch, and the descending thoracic aorta, and we defined the abdominal aorta as the portion of the vessel located below the diaphragm, including the suprarenal and infrarenal segments. Malperfusion syndromes were subclassified as (1) coronary: ischemic electrocardiographic changes, elevation of troponin levels, and regional wall motion abnormalities on echocardiography; (2) hepatic: increased liver enzymes; (3) mesenteric: abdominal tenderness, bowel paralysis, lactate acidosis; (4) renal: decreased urine output and increased creatinine; (5) nervous system: transient ischemic attack, stroke, paraplegia/paraparesis, limb (loss of pulses, clinical signs of limb ischemia). The degree of aortic injury was defined based on previous studies, including *in situ* aortic and distal aorta injury. Severely involved aortic root type: (a) the diameter of the aortic sinus was between 35 and 50 mm with severe disruption of the sinotubular junction, (b) the diameter of the aortic sinus was 50 mm or greater, and (c) severe aortic insufficiency. Severely involved in the distal aorta are the following (dependent upon the extent and extension of aortic dissection extending beyond the ascending aorta and arch): (a) the primary tear located in the transverse arch or the descending aorta; (b) aneurysm formation in the aortic arch or the distal aorta (>40 mm); (c) involvement, aneurysm formation, and occlusion of the brachiocephalic artery;

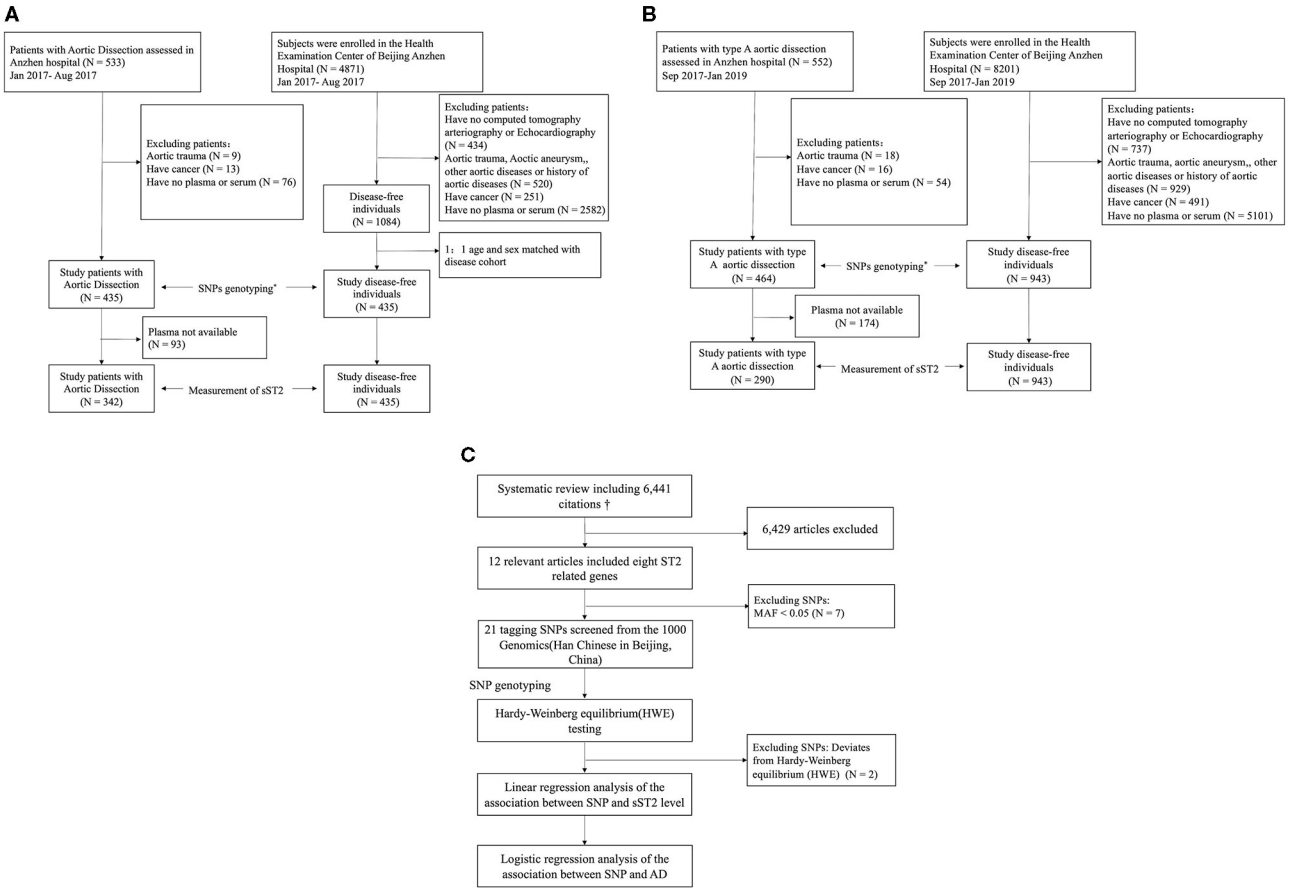

FIGURE 1 | Overall study design. **(A)** Work flow of the selection subjects for the discovery stage. **(B)** Work flow of the selection subjects for the validation stage. **(C)** Selection of tag SNPs. AD, aortic dissection; SNP, single-nucleotide polymorphism. *The SNP screening design is shown in **(C)**. †See **Supplementary Materials** for system review details.

(d) Marfan syndrome; (e) or sleeve-like striping. Mild involved type is when the primary tear was located in the ascending aorta without the above characteristics (18).

Controls were participants without aortic diseases who underwent routine annual health checks and who had a blood sample saved at the hospital. Controls without aortic dissection were selected from potentially eligible subjects who had chest or abdominal images admitted during the same period. They were excluded from the study if they met any of the following criteria: (a) received packed red blood cells, whole blood, or platelets fewer than 10 days before the blood sample was taken; (b) with aortic trauma, aortic aneurysm, other aortic disease or family history of aortic disease; and (c) active cancer. In the discovery stage, a subset of healthy controls was then randomly selected from the database, matched 1:1 with the selected cases by age (3 years), sex, and geographic region.

None of the subjects were related to each other, and all provided written informed consent for study participation. Baseline characteristics of the subjects were collected from medical records and confirmed by the study physicians. The height and weight of the patients were measured directly or self-reported, and body mass index (BMI) was calculated. The study included eligible patients from the DPANDA aortic aneurysm and/or dissection registry study at Anzhen Hospital (NCT03233087 in clinicaltrials.gov). This study was approved by the Beijing Anzhen Hospital Ethics Review Board.

Tag Single-Nucleotide Polymorphisms Selection and Genotyping

All reported genes related to sST2 concentrations were identified from a systematic review (see details in **Supplementary Text 1**; **Supplementary Text 2**; **Supplementary Table 1**; **Supplementary Figure 1**). Polymorphisms around the eight candidate loci (*IL1RL1*, *IL1RL2*, *IL1R1*, *IL18R1*, *IL18RAP*, *SLC9A2*, *SLC9A4*, and *SH3YL1*) drawn from the 1000 Genomes Project (Han Chinese in Beijing, China, https://www.internationalgenome.org) were analyzed with Haploview (v4.1, Broad Institute, Boston, MA, USA). Markers were selected from the genomic region of each locus, including 5 kb up- and downstream of the coding region. Following filtering of the marker set to exclude rare alleles (minor allele frequency <0.05), the tagger algorithm was used to select markers from the 1,000 Genomes Project database. This identified a set of SNPs that efficiently captured genetic variation at each locus

so that all untyped variants had a high correlation ($R^2 > 0.8$) with one member of the typed set. If there is a linkage balance between SNPs in the same gene in the screening process, the reported SNPs will be preferred. Genotyping results were tested for Hardy–Weinberg equilibrium. Nineteen of 21 SNPs did not deviate significantly from the Hardy–Weinberg equilibrium ($p > 0.001$), so they were included in the subsequent analysis (**Supplementary Table 2**).

DNA from whole blood was isolated using a commercial DNA isolation kit (BioTeKe Corporation, Beijing, China). Genotyping was performed by mass spectrometry (Massarray System 4; Agena Inc., San Diego, CA, USA). Polymerase chain reaction (PCR) and detection primers were designed using the MassARRAY Assay Design software (Sequenom). The DNA samples were amplified by multiplex PCR reactions. The terminator nucleotides were desalted and added into a 384-element SpectroCHIP array. Then, allele detection was performed using a time-of-flight (MALDI-TOF) SpectroReader mass spectrometer (Sequenom). Last, the mass spectrograms were analyzed for peak identification using the Typer Analyzer software (Sequenom), and for quality control, the missing genotype rate of each SNP was set to lower than 10%.

sST2 Measurements

Plasma samples were collected from subjects at admission and stored at −80°C. Circulating sST2 was measured using a DuoSet ELISA kit (DY523B-05; R&D Systems, Minneapolis, MN, USA) according to the instructions of the manufacturer (19–21). The limit of detection for sST2 was 0.019 ng/ml, with a mean intra-assay coefficient of variation of <6.0% and mean inter-assay coefficient of variation of <9.5%. Detailed procedures as well as the comparison between assay methods for sST2 are described in **Supplementary Text 3.**

Statistical Analyses

Continuous variables in the patients' information were expressed as mean [standard deviation (SD)] or median (interquartile range) for skewed variables (e.g., sST2). The two-sample *t*-test was used to compare continuous variables (log-transformed where appropriate). Categorical variables were presented as counts and percentages, and differences were assessed using the χ^2 test or Fisher's exact test. Soluble ST2 concentrations were log-transformed because of their right-skewed distribution. Associations of genetic variants and sST2 concentrations were tested using linear regression under an additive genetic model. Bonferroni correction was used for multiple comparison adjustments of the *p*-values. Analyses were performed using Stata version 15.1 (Stata Corp, College Station, TX, USA) and Haploview version 4.2 (Daly Lab, Cambridge, MA, USA) software.

RESULTS

Study Populations

This study included 899 AD patients and 1,378 controls. The discovery stage included 435 AD patients and 435 controls from Anzhen Hospital in China between January 2017 and August 2017, whereas the validation study included 464 type A AD patients and 943 controls recruited between September 2017 and January 2019 (**Figure 1**; **Supplementary Text 4**; **Supplementary Figures 2, 3**). sST2 concentrations were measured in 632 AD patients with plasma available. Baseline characteristics of all participants are shown in **Table 1**. Compared with controls, AD patients had a significantly higher body mass index (BMI; 25.56 ± 3.67 vs. 24.52 ± 3.16 in the discovery stage, and 25.99 ± 3.62 vs. 23.68 ± 3.27 in the validation stage; both $p < 0.05$), significantly more were smokers (42.8 vs. 27.1% in the discovery stage and 44.0 vs. 19.5% in the validation stage; both $p < 0.05$), and had significantly more frequent hypertension (68.7 vs. 21.4% in the discovery stage and 71.6 vs. 18.6% in the validation stage; both $p < 0.05$). sST2 levels were elevated at 34.63 ng/ml (median, IQR: 15.85–74.90) in the patients with AD compared with 8.09 ng/ml in controls (median, IQR: 6.18–10.70) in the discovery stage, and 53.64 ng/ml (median, IQR: 25.03–120.08) in the patients with type A AD compared with 7.98 ng/ml (median, IQR: 5.87–10.16) in controls in the validation stage. No other differences were observed between the two groups. Among the 899 AD patients, there were 652(72.5%) patients with type A aortic dissection and 247 (27.5%) patients with type B.

Selection of Single-Nucleotide Polymorphisms With Soluble ST2 Concentrations in Control and Aortic Dissection

The association of these 19 SNPs with sST2 concentrations was reported in the discovery stage of the study. Of these SNPs, 15 located in seven genes (rs1921622, rs3821204, rs6751967, and rs12712135 in *IL1RL1*; rs887971 and rs1558650 in *IL18RAP*; rs4241211, rs4851608, rs1468788, and rs11692304 in *SLC9A4*; rs3771172 and rs2241116 in *IL18R1*; rs13019803 in *IL1R1*; rs17775170 in *SLC9A2*; and rs2241132 in *IL1RL2*) were shown to be significantly associated with sST2 concentration in controls ($p < 0.0026$; **Supplementary Table 3**).

The genotype distribution of the 19 SNPs and chi-square analysis in the discovery stage is shown in **Table 2**. In controls, the C allele of rs13019803 (located in *IL1R1*) accounted for 82.4%, and the T allele accounted for 17.6%. In patients with AD, the C allele accounted for 88.0% and the T allele for 12.0%. The T allele of rs13019803, referring to the reverse strand, represents the alternative (minor) allele for this SNP. rs13019803 (located in *IL1R1*) was significantly associated with AD ($p = 9.30E{-}04$), even after a conservative Bonferroni adjustment ($p < 0.0026$).

Association of rs13019803 With Soluble ST2 Concentration in Aortic Dissection Patients

In the discovery stage, sST2 concentrations were measured in 173 type A AD patients and 169 type B AD patients. For all AD patients, rs13019803C is related to the sST2 level [beta(95% CI) = 0.106 (−0.006–0.219), $p = 0.064$]. Compared with type A AD, type B AD does not involve the ascending aorta and is less dangerous (22). We separately analyzed type A and type

TABLE 1 | Summary of participant characteristics.

	Discovery stage		Validation stage	
	Controls (*n* = 435)	**AD patients (*n* = 435)**	**Controls (*n* = 943)**	**Type A AD patients (*n* = 464)**
Age	48.88 (11.91)	48.95 (12.01)	42.56 (12.11)	50.03 (11.78)*
Sex (male)	330 (75.9%)	330 (75.9%)	474 (50.3%)	361 (77.8%)*
Smoke (current)	118 (27.1%)	186 (42.8%)*	184 (19.5%)	204 (44.0%)*
Diabetes (yes)	18 (4.1%)	24 (5.5%)	26 (2.8%)	21 (4.5%)
Hypertension (yes)	93 (21.4%)	299 (68.7%)*	175 (18.6%)	332 (71.6%)*
BMI (kg/m^2)	24.52 (3.16)	25.56 (3.67)*	23.68 (3.27)	25.99 (3.62)*
CAD (yes)	26 (6.0%)	34 (7.8%)	33 (3.5%)	38 (8.2%)*
Hyperlipidemia (yes)	88 (20.2%)	77 (17.7%)	204 (21.6%)	90 (19.4%)
sST2 (ng/ml)	8.09 (6.18,10.70)	34.63 (15.85,74.90)*[a]	7.98 (5.87,10.16)	53.64 (25.03, 120.08)*[b]
Log-sST2	0.90 (0.18)	1.55 (0.49)*[a]	0.88 (0.18)	1.73 (0.48)*[b]

*$p < 0.05$.
[a]*Only 342 AD patients in the discovery stage had sST2 concentrations measured with plasma available.*
[b]*Only 290 type A AD patients in the validation stage had sST2 concentrations measured with plasma available.*
AD, aortic dissection; BMI, body mass index; CAD, coronary artery disease.

TABLE 2 | Genotype distribution and chi-square analysis in the discovery stage.

SNP	**Gene**	**Major allele/minor allele**	**Controls (*N* = 435)[a]**	**AD patients (*N* = 435)[a]**	***p*-value***
rs13019803	IL1R1	C/T	0.176	0.120	9.30E−04
rs2241132	IL1RL2	C/A	0.300	0.272	0.200
rs4988958	IL1RL1	T/C	0.131	0.154	0.175
rs11692304	SLC9A4	G/A	0.181	0.203	0.262
rs6751967	IL1RL1	T/C	0.133	0.151	0.283
rs2241116	IL18R1	C/A	0.179	0.174	0.784
rs3917296	IL1R1	A/G	0.152	0.174	0.209
rs3917254	IL1R1	G/A	0.236	0.201	0.077
rs1468788	SLC9A4	C/T	0.223	0.202	0.279
rs887971	IL18RAP	T/C	0.321	0.293	0.222
rs4851608	SLC9A4	C/T	0.320	0.315	0.836
rs4241211	SLC9A4	T/G	0.439	0.445	0.805
rs10167431	IL1RL2	C/T	0.338	0.352	0.565
rs1921622	IL1RL1	G/A	0.366	0.354	0.597
rs17775170	SLC9A2	G/A	0.181	0.174	0.690
rs3771172	IL18R1	C/T	0.306	0.264	0.054
rs3821204	IL1RL1	C/G	0.312	0.275	0.086
rs1558650	IL18RAP	T/A	0.459	0.449	0.703
rs12712135	IL1RL1	A/G	0.456	0.485	0.234

**Significant after Bonferroni correction for 19 tests ($p < 0.0026$).*
[a]*Minor allele frequencies.*
AD, aortic dissection.

B patients. rs13019803 is only related to the level of sST2 in patients with type A [beta(95% CI) = 0.180(0.002–0.357), p = 0.048], but not in type B [beta(95% CI) = −0.033 (−0.160–0.093), p = 0.604]. The correlation between rs13019803 and sST2 concentration in AAD patients remained significant after adjusting for confounders [beta(95% CI) = 0.229(0.066–0.393), p = 0.006] (**Table 3**). Therefore, only patients with type A AD were included in the validation cohort.

Overall, a total of 463 among 652 type A AD (AAD) patients were measured for sST2 concentrations with plasma available. Patients were divided into two groups according to the median level of sST2. Patients with acute onset, severe chest

TABLE 3 | rs13019803 associated with sST2 concentrations in AD patients in the discovery stage.

	Beta (95% CI)[a]	*p*-value[a]
Discovery (*N* = 342)		
Model 1	0.106 (−0.006,0.219)	0.064
Model 2	0.126 (0.016,0.236)	0.025
Model 3	0.132 (0.031,0.234)	0.010
Type A (*N* = 173)		
Model 1	0.180 (0.002,0.357)	0.048
Model 2	0.189 (0.012,0.366)	0.036
Model 3	0.229 (0.066,0.393)	0.006
Type B (*N* = 169)		
Model 1	−0.033 (−0.160, 0.093)	0.604
Model 2	−0.031 (−0.151, 0.089)	0.607
Model 3	−0.020 (−0.130,0.091)	0.725

[a]*Linear regression for log-sST2.*
Model 1: Unadjusted.
Model 2: Adjusted age, sex, BMI, hypertension, hyperlipidemia, diabetes, smoking, and cardiovascular disease.
Model 3: Adjusted age, sex, BMI, hypertension, hyperlipidemia, diabetes, smoking, cardiovascular disease, and acuity.

TABLE 4 | Association rs13019803C between sST2 in type A AD patients (*N* = 463).

	Model	Beta (95% CI)[a]	*p*-value[a]
Validation	Model 1	0.139 (0.022, 0.257)	0.020
	Model 2	0.133 (0.014, 0.252)	0.029
	Model 3	0.113 (0.008, 0.217)	0.035
Combined	Model 1	0.151 (0.054, 0.248)	0.002
	Model 2	0.155 (0.057, 0.252)	0.002
	Model 3	0.141 (0.055, 0.227)	0.001

[a]*Linear regression for log-sST2.*
Model 1: Unadjusted.
Model 2: Adjusted age, sex, BMI, hypertension, hyperlipidemia, diabetes, smoking, and cardiovascular disease.
Model 3: Adjusted age, sex, BMI, hypertension, hyperlipidemia, diabetes, smoking, cardiovascular disease, acute, abrupt onset pain, severely involved distal aorta, and pre-operative presence of malperfusion.

TABLE 5 | Odds ratio of rs13019803 on the risk of type A AD.

	Model	OR (95% CI)*	*p*-value
Discovery[a]	Model 1	2.37 (1.57, 3.59)	3.9E−5
	Model 2	2.37 (1.57, 3.58)	4.2E−5
	Model 3	2.97 (1.82, 4.84)	1.2E−5
Validation	Model 1	1.35 (1.08,1.68)	0.007
	Model 2	1.34 (1.06,1.69)	0.015
	Model 3	1.42 (1.09,1.85)	0.010
Combined	Model 1	1.54 (1.27,1.86)	1.1E−5
	Model 2	1.52 (1.25,1.86)	2.8E−5
	Model 3	1.67 (1.33,2.09)	1.0E−5

**C allele is risk allele.*
[a]*Only type A AD patients included.*
Model 1: Unadjusted.
Model 2: Adjusted age, sex.
Model 3: Adjusted age, sex, BMI, hypertension, hyperlipidemia, diabetes, smoking, and cardiovascular disease.
OR, odds ratio; CI, confidence interval.

and back pain, malperfusion, and severe distal aorta injury have higher sST2 levels ($p < 0.05$; **Supplementary Table 4**). Then, we added the analysis after adjusting the above variables to the discovery stage. In the discovery stage, the correlation between rs13019803 and sST2 concentration in AAD patients remained significant after adjusting for confounders (age, sex, BMI, hypertension, hyperlipidemia, diabetes, smoking, cardiovascular disease, acute, abrupt onset pain, severely involved distal aorta, and pre-operative presence of malperfusion) [beta(95% CI) = 0.198(0.042–0.353), $p = 0.013$] (**Supplementary Table 5**). In the validation stage, for each additional copy of the C-allele, log-sST2 was increased by 0.139 (95% CI: 0.022–0.257) in AAD patients. Overall, for each additional copy of the C-allele, log-sST2 was increased by 0.151 (95% CI: 0.054–0.248) in AAD patients. After adjusting for the confounding factors in AAD patients, the correlation between rs13019803 and sST2 concentration in AAD patients remained significant [0.141 (95% CI: 0.055–0.227), $p = 0.001$] (**Table 4**).

Association of rs13019803 With Type A Aortic Dissection Risk

We investigated the association of the SNPs rs13019803 and risk of AAD according to three regression models (**Table 5**). In the validation stage, for each additional C allele of rs13019803, the odds ratio (OR) of AAD was 1.35 (95% CI: 1.08–1.68; $p = 0.007$). Furthermore, this association remained significant after adjusting for age, sex, BMI, coronary artery disease (CAD), hypertension, diabetes, and hyperlipidemia (OR = 1.42; 95% CI: 1.09–1.85; $p = 0.010$). Overall, the OR of AAD was 1.54 (95% CI: 1.27–1.86; $p = 1.1E{-}5$) for each additional C allele of rs13019803. This association remained significant after adjusting for confounding factors (OR = 1.67; 95% CI: 1.33–2.09; $p = 1.0E{-}5$). The genotype of rs13019803 distribution was not associated with confounding factors of AAD patients ($p > 0.05$), but with sST2 level ($p < 0.05$) (**Supplementary Table 6**). In addition, we performed a subgroup analysis with or without hypertension. The results showed that rs13019803 was associated with the risk of AD in patients with and without hypertension [OR (95% CI) = 1.71 (1.26–2.33), $p = 0.001$ with hypertension; OR (95% CI) = 1.59 (1.13–2.23), $p = 0.007$ without hypertension] (**Supplementary Table 7**).

DISCUSSION

In this study, we analyzed the relationship between ST2-related genes and circulating sST2 concentrations or AD. The C allele of *IL1R1* rs13019803 was associated with increased circulating sST2 concentrations and risk of AAD.

Genetic variation was verified to affect sST2 levels. In five independent GWAS studies, it was found that multiple SNPs in a 1 M area near *IL1RL1* were related to ST2 concentration ($p <$

5×10^{-8}) (23–27). Our results in controls are consistent with those of other studies. In molecular studies, *IL1RL1* missense mutation-induced ST2 expression directly affects the ST2L signal and regulates ST2 promoter activity. Variants of *IL1RL1* can also increase the expression of sST2 by inducing the expression of IL-33 and IL1-β, and enhancing the reactivity of IL-33 (23). In this study, we found that the C allele of rs13019803 is not only associated with sST2 concentration in healthy people but also with high sST2 concentration in patients with aortic dissection. The MAF of rs13019803 is 0.162 in Anzhen hospital population, which is nearly the same with that of the CHB population [$T = 29$ (14.1%) vs. 740 (16.2%), $p = 0.407$] (Han Chinese in Beijing, China, https://www.internationalgenome.org).

We found that rs13019803 was associated with sST2 level in patients, independent of patients characters. Before the onset of AD, ST2-related gene variations may contribute to disease development by increasing ST2 production at transcriptional and translational levels (28, 29). The long-term accumulation of ST2 from genetic variations may induce inflammatory reactions of the aorta and systemic blood vessels, leading to severe vascular injury in patients with high ST2 level (10, 30–32). Soluble ST2 concentration may be affected by the expression of ST2-related genes, which is driven by genetic variation under stress conditions in AD patients and finally leads to the difference of sST2 level in patients (33). There is a significantly positive correlation between rs13019803 and serum sST2 in type A AD; however, it showed no correlation in type B AD. Compared with type A AD, type B AD does not involve the ascending aorta and has less hemodynamic stress (22). This indicates that there may be differences for underlining pathophysiology between type A and type B. The level of sST2 could be differently regulated by hemodynamics between type A and type B. ST2-related genes are attractive candidates for AD risk. Soluble ST2 acts as a decoy receptor for IL-33 and inhibits IL-33/ST2L signaling, thus, blocking its protective effect. sST2 may be involved in the occurrence and expansion of AD through injury and inflammation of smooth muscle cells (34). Variants in these genes are associated with a range of diseases risk (23, 35) and are involved in a variety of progressive diseases including CAD, hypertension, and asthma (28, 36). The long-term accumulation of ST2 from genetic variations may induce inflammatory reactions of the aorta and systemic blood vessels, leading to blood vessel damage in the smooth muscle cells of individuals without AD (10).

This study investigated 21 SNPs in seven ST2-related genes, but only rs13019803 in *IL1R1* was found to be associated with AAD. Rs13019803 is located in the intron region. In the Framingham study, rs13019803 is the top 10 SNP in the GWAS study with the concentration of sST2 and is the most strongly associated with sST2 in *IL1R1* gene (23). In GTEx studies, it is located in the 3′-promoter flaking region of the gene, which may regulate the expression of this gene region. Rs13019803 is not only related to the concentration of sST2 but also to the regulation of *IL1R1* and *IL18* gene expression (37, 38). This SNP was not found to be related to other phenotypes other than sST2 (39, 40). *IL1R1* encodes cytokine receptors belonging to the IL-1 receptor family, including IL-1α, IL-1β, and IL-33 (41). IL-1β is a multifunctional proinflammatory cytokine that binds to the IL1-R receptor on target cells (42). Recent studies reported that sST2 and IL-1β expression is strongly correlated and that both systems are associated with inflammation and vascular smooth muscle cell injury (43–45). Local IL-1β expression may be involved in AD development by upregulating matrix metallopeptidase (MMP)-2 and MMP-9 and increasing elastin fiber breaks (46, 47). IL-18 encoded by *IL18* gene may participate in AD by regulating macrophage differentiation and inducing SMC apoptosis induced by macrophages (48). Therefore, the genetic variation of rs13019803 may affect the whole IL1 axis, not only the role of sST2. Although rs13019803C showed an increased risk of AD accompanied by high levels of sST2 in the AD group, further studies are needed to determine whether IL1β or other factors are involved in the effect of IL1R1 on AD.

Accumulating evidence supports the conclusion that sST2 is a biomarker of vascular health with diagnostic and/or prognostic value in various cardiovascular diseases, including coronary artery disease, myocardial infarction, atherosclerosis, giant-cell arteritis, acute aortic dissection, and ischemic stroke (10). Genetic variations may affect the development and prognosis of cardiovascular diseases by regulating sST2 production. ST2-related genes may have the value of being added to the polygenic detection panel of AD risk. However, these *IL1R1* variants should still be interpreted with caution because recent studies suggest that a small number of potentially causal genetic findings can be selected for return into clinical practice (49). Nonetheless, molecular studies can help clarify the causative role of identified variants (50). Our findings suggest that genetic variations of biomarkers for acute elevation might also have potential value in disease. This finding also provides a possible explanation for patients with similar disease severity, but the level of circulating sST2 is of variety.

This study demonstrates that genetic polymorphisms affect plasma sST2 levels and AD risk. The findings of this study will help to explain the difference in circulating sST2 levels after onset of disease and early identification of high-risk patients. However, this study also has potential limitations. First, it was a single-center study with a relatively small sample size at the discovery stage, so may lack the ability to detect SNPs with small effects and/or low MAF. Second, the mechanisms by which genes affect sST2 concentrations are still not fully understood. Therefore, there is a clear need for further studies to better understand the underlying molecular mechanisms.

In conclusion, *IL1R1* variation is related to sST2 levels and AAD risk. This SNP is located in an intron and, therefore, is unlikely to be functional itself, but it may be in LD with a yet to be identified functional locus. This study supports the notion that ST2-related genes, in particular, the *IL1R1* gene, might play a role in AD etiology and development. Further research is needed to confirm whether it can be used for patient screening and stratification.

DATA AVAILABILITY STATEMENT

The original contributions presented in the study are publicly available. This data can be found here: ClinVar, SCV001652890–SCV001652908.

ETHICS STATEMENT

This study was approved by the Beijing Anzhen Hospital Ethics Review Board. The patients/participants provided their written informed consent to participate in this study.

AUTHOR CONTRIBUTIONS

YW and JD conceived and designed the research. WJ and XW acquired the data. WJ and PG performed the statistical analysis. WJ drafted the manuscript. JD made critical revision of the manuscript for key intellectual content. FL, XT, and SZ collected and subpacked the plasma samples. XL, RH, YZ, and JZ evaluated the participants. KL, WP, and MA consummated the clinical information. All authors contributed to the article and approved the submitted version.

FUNDING

This study was supported by the Ministry of Science and Technology of China (Key Projects of Precision Medicine Program, Grant No. 2017YFC0908400), NSFC (Natural Science Foundation of China, Grant No.81870341, No. 81861128025), and the Beijing Natural Science Foundation (Grant No. 7182084).

SUPPLEMENTARY MATERIAL

The Supplementary Material for this article can be found online at: https://www.frontiersin.org/articles/10.3389/fcvm.2021.710425/full#supplementary-material

REFERENCES

1. Parker FB, Neville JF Jr, Hanson EL, Mohiuddin S, Webb WR. Management of acute aortic dissection. *Ann Thorac Surg.* (1975) 19:436–42. doi: 10.1016/S0003-4975(10)64045-3
2. Hagan PG, Nienaber CA, Isselbacher EM, Bruckman D, Karavite DJ, Russman PL, et al. The International Registry of Acute Aortic Dissection (IRAD): new insights into an old disease. *JAMA.* (2000) 283:897–903. doi: 10.1001/jama.283.7.897
3. Goldfinger JZ, Halperin JL, Marin ML, Stewart AS, Eagle KA, Fuster V. Thoracic aortic aneurysm and dissection. *J Am Coll Cardiol.* (2014) 64:1725–39. doi: 10.1016/j.jacc.2014.08.025
4. Hiratzka LF, Bakris GL, Beckman JA, Bersin RM, Carr VF, Casey DE Jr, et al. 2010 ACCF/AHA/AATS/ACR/ASA/SCA/SCAI/SIR/STS/SVM guidelines for the diagnosis and management of patients with Thoracic Aortic Disease: a report of the American College of Cardiology Foundation/American Heart Association Task Force on Practice Guidelines, American Association for Thoracic Surgery, American College of Radiology, American Stroke Association, Society of Cardiovascular Anesthesiologists, Society for Cardiovascular Angiography and Interventions, Society of Interventional Radiology, Society of Thoracic Surgeons, and Society for Vascular Medicine. *Circulation.* (2010) 121:e266–369. doi: 10.1161/CIR.0b013e3181d4739e
5. Suzuki T, Katoh H, Watanabe M, Kurabayashi M, Hiramori K, Hori S, et al. Novel biochemical diagnostic method for aortic dissection. Results of a prospective study using an immunoassay of smooth muscle myosin heavy chain. *Circulation.* (1996) 93:1244–9. doi: 10.1161/01.CIR.93.6.1244
6. Suzuki T, Trimarchi S, Sawaki D, Grassi V, Costa E, Rampoldi V, et al. Circulating transforming growth factor-beta levels in acute aortic dissection. *J Am Coll Cardiol.* (2011) 58:775. doi: 10.1016/j.jacc.2010.01.079
7. Marshall LM, Carlson EJ, O'Malley J, Snyder CK, Charbonneau NL, Hayflick SJ, et al. Thoracic aortic aneurysm frequency and dissection are associated with fibrillin-1 fragment concentrations in circulation. *Circ Res.* (2013) 113:1159–68. doi: 10.1161/CIRCRESAHA.113.301498
8. Wang Y, Tan X, Gao H, Yuan H, Hu R, Jia L, et al. Magnitude of soluble ST2 as a novel biomarker for acute aortic dissection. *Circulation.* (2018) 137:259–69. doi: 10.1161/CIRCULATIONAHA.117.030469
9. Kakkar R, Lee RT. The IL-33/ST2 pathway: therapeutic target and novel biomarker. *Nat Rev Drug Discov.* (2008) 7:827–40. doi: 10.1038/nrd2660
10. Altara R, Ghali R, Mallat Z, Cataliotti A, Booz GW, Zouein FA. Conflicting vascular and metabolic impact of the IL-33/sST2 axis. *Cardiovasc Res.* (2018) 114:1578–94. doi: 10.1093/cvr/cvy166
11. Ernesto MM, María M, Raquel J-L, Elodie R, Patrick R, Faiez Z, et al. A role for soluble ST2 in vascular remodeling associated with obesity in rats. *PLoS One.* (2013) 8:e79176. doi: 10.1371/journal.pone.0079176
12. Ho JE, Sritara P, deFilippi CR, Wang TJ. Soluble ST2 testing in the general population. *Am J Cardiol.* (2015) 115(7 Suppl):22B—5B. doi: 10.1016/j.amjcard.2015.01.036
13. Pearce WH, Shively VP. Abdominal aortic aneurysm as a complex multifactorial disease: interactions of polymorphisms of inflammatory genes, features of autoimmunity, and current status of MMPs. *Ann N Y Acad Sci.* (2006) 1085:117–32. doi: 10.1196/annals.1383.025
14. Wang Y, Huang HY, Bian GL, Yu YS, Ye WX, Hua F, et al. A functional variant of SMAD4 enhances thoracic aortic aneurysm and dissection risk through promoting smooth muscle cell apoptosis and proteoglycan degradation. *EBioMedicine.* (2017) 21:197–205. doi: 10.1016/j.ebiom.2017.06.022
15. Cai T, Zhang Y, Ho YL, Link N, Sun J, Huang J, et al. Association of interleukin 6 receptor variant with cardiovascular disease effects of interleukin 6 receptor blocking therapy: a phenome-wide association study. *JAMA Cardiol.* (2018) 3:849–57. doi: 10.1001/jamacardio.2018.2287
16. Erbel R, Aboyans V, Boileau C, Bossone E, Bartolomeo RD, Eggebrecht H, et al. 2014 ESC Guidelines on the diagnosis and treatment of aortic diseases: Document covering acute and chronic aortic diseases of the thoracic and abdominal aorta of the adult. The Task Force for the Diagnosis and Treatment of Aortic Diseases of the European Society of Cardiology (ESC). *Eur Heart J.* (2014) 35:2873–926. doi: 10.1093/eurheartj/ehu281
17. Nienaber CA, Clough RE. Management of acute aortic dissection. *Lancet.* (2015) 385:800–11. doi: 10.1016/S0140-6736(14)61005-9
18. Sun L, Qi R, Zhu J, Liu Y, Chang Q, Zheng J. Repair of acute type A dissection: our experiences and results. *Ann Thorac Surg.* (2011) 91:1147–52. doi: 10.1016/j.athoracsur.2010.12.005
19. Weir RA, Miller AM, Murphy GE, Clements S, Steedman T, Connell JM, et al. Serum soluble ST2: a potential novel mediator in left ventricular and infarct remodeling after acute myocardial infarction. *J Am Coll Cardiol.* (2010) 55:243–50. doi: 10.1016/j.jacc.2009.08.047
20. Dworakowski R, Wendler O, Bhan A, Smith L, Pearson P, Alcock E, et al. Successful transcatheter aortic valve implantation (TAVI) is associated with transient left ventricular dysfunction. *Heart (British Cardiac Society).* (2012) 98:1641–6. doi: 10.1136/heartjnl-2012-302505
21. Chida A, Sato H, Shintani M, Nakayama T, Kawamura Y, Furutani Y, et al. Soluble ST2 and N-terminal pro-brain natriuretic peptide combination. Useful biomarker for predicting outcome of childhoodpulmonary arterial hypertension. *Circulation J.* (2014) 78:436–42. doi: 10.1253/circj.CJ-13-1033

22. Parve S, Ziganshin BA, Elefteriades JA. Overview of the current knowledge on etiology, natural history and treatment of aortic dissection. *J Cardiovasc Surg.* (2017) 58:238–51. doi: 10.23736/S0021-9509.17.09883-4
23. Ho JE, Chen WY, Chen MH, Larson MG, McCabe EL, Cheng S, et al. Common genetic variation at the IL1RL1 locus regulates IL-33/ST2 signaling. *J Clin Invest.* (2013) 123:4208–18. doi: 10.1172/JCI67119
24. Yao C, Chen G, Song C, Keefe J, Mendelson M, Huan T, et al. Author Correction: genome-wide mapping of plasma protein QTLs identifies putatively causal genes and pathways for cardiovascular disease. *Nat Commun.* (2018) 9:3853. doi: 10.1038/s41467-018-06231-z
25. Folkersen L, Fauman E, Sabater-Lleal M, Strawbridge RJ, Franberg M, Sennblad B, et al. Mapping of 79 loci for 83 plasma protein biomarkers in cardiovascular disease. *PLoS Genet.* (2017) 13:e1006706. doi: 10.1371/journal.pgen.1006706
26. Suhre K, Arnold M, Bhagwat AM, Cotton RJ, Engelke R, Raffler J, et al. Connecting genetic risk to disease end points through the human blood plasma proteome. *Nature Commun.* (2017) 8:14357. doi: 10.1038/ncomms15345
27. Lourdusamy A, Newhouse S, Lunnon K, Proitsi P, Powell J, Hodges A, et al. Identification of cis-regulatory variation influencing protein abundance levels in human plasma. *Hum Mol Genet.* (2012) 21:3719–26. doi: 10.1093/hmg/dds186
28. Wu F, Li L, Wen Q, Yang J, Chen Z, Wu P, et al. A functional variant in ST2 gene is associated with risk of hypertension *via* interfering MiR-202-3p. *J Cell Mol Med.* (2017) 21:1292–9. doi: 10.1111/jcmm.13058
29. Wei ZH, Li YY, Huang SQ, Tan ZQ. Genetic variants in IL-33/ST2 pathway with the susceptibility to hepatocellular carcinoma in a Chinese population. *Cytokine.* (2019) 118:124–9. doi: 10.1016/j.cyto.2018.03.036
30. Li J, Xia N, Wen S, Li D, Lu Y, Gu M, et al. IL (Interleukin)-33 suppresses abdominal aortic aneurysm by enhancing regulatory T-cell expansion and activity. *Arteriosc Thromb Vasc Biol.* (2019) 39:446–58. doi: 10.1161/ATVBAHA.118.312023
31. Ahsan M, Ek WE, Rask-Andersen M, Karlsson T, Lind-Thomsen A, Enroth S, et al. The relative contribution of DNA methylation and genetic variants on protein biomarkers for human diseases. *PLoS Genet.* (2017) 13:e1007005. doi: 10.1371/journal.pgen.1007005
32. Lam SM, Wang Y, Li B, Du J, Shui G. Metabolomics through the lens of precision cardiovascular medicine. *J Genet Genomics.* (2017) 44:127–38. doi: 10.1016/j.jgg.2017.02.004
33. Ko YA, Yi H, Qiu C, Huang S, Park J, Ledo N, et al. Genetic-variation-driven gene-expression changes highlight genes with important functions for kidney disease. *Am J Hum Genet.* (2017) 100:940–53. doi: 10.1016/j.ajhg.2017.05.004
34. El-Hamamsy I, Yacoub MH. Cellular and molecular mechanisms of thoracic aortic aneurysms. *Nat Rev Cardiol.* (2009) 6:771–86. doi: 10.1038/nrcardio.2009.191
35. Savenije OE, Kerkhof M, Reijmerink NE, Brunekreef B, de Jongste JC, Smit HA, et al. Interleukin-1 receptor-like 1 polymorphisms are associated with serum IL1RL1-a, eosinophils, and asthma in childhood. *J Allergy Clin Immunol.* (2011) 127:750–6.e1–5. doi: 10.1016/j.jaci.2010.12.014
36. Hayakawa H, Hayakawa M, Kume A, Tominaga S. Soluble ST2 blocks interleukin-33 signaling in allergic airway inflammation. *J Biol Chem.* (2007) 282:26369–80. doi: 10.1074/jbc.M704916200
37. Joehanes R, Zhang X, Huan T, Yao C, Ying SX, Nguyen QT, et al. Integrated genome-wide analysis of expression quantitative trait loci aids interpretation of genomic association studies. *Genome Biol.* (2017) 18:16. doi: 10.1186/s13059-016-1142-6
38. Consortium GT. Human genomics. The Genotype-Tissue Expression (GTEx) pilot analysis: multitissue gene regulation in humans. *Science (New York, NY).* (2015) 348:648–60. doi: 10.1126/science.1262110
39. Yang J, Loos RJ, Powell JE, Medland SE, Speliotes EK, Chasman DI, et al. FTO genotype is associated with phenotypic variability of body mass index. *Nature.* (2012) 490:267–72. doi: 10.1038/nature11401
40. Claussnitzer M, Cho JH, Collins R, Cox NJ, Dermitzakis ET, Hurles ME, et al. A brief history of human disease genetics. *Nature.* (2020) 577:179–89. doi: 10.1038/s41586-019-1879-7
41. Sims JE, Smith DE. The IL-1 family: regulators of immunity. *Nat Rev Immunol.* (2010) 10:89–102. doi: 10.1038/nri2691
42. Wilcox RG, von der Lippe G, Olsson CG, Jensen G, Skene AM, Hampton JR. Trial of tissue plasminogen activator for mortality reduction in acute myocardial infarction. Anglo-Scandinavian Study of Early Thrombolysis (ASSET). *Lancet.* (1988) 2:525–30. doi: 10.1016/S0140-6736(88)92656-6
43. Pascual-Figal DA, Bayes-Genis A, Asensio-Lopez MC, Hernandez-Vicente A, Garrido-Bravo I, Pastor-Perez F, et al. The interleukin-1 axis and risk of death in patients with acutely decompensated heart failure. *J Am Coll Cardiol.* (2019) 73:1016–25. doi: 10.1016/j.jacc.2018.11.054
44. Hong YS, Moon SJ, Joo YB, Jeon CH, Cho ML, Ju JH, et al. Measurement of interleukin-33 (IL-33) and IL-33 receptors (sST2 and ST2L) in patients with rheumatoid arthritis. *J Korean Med Sci.* (2011) 26:1132–9. doi: 10.3346/jkms.2011.26.9.1132
45. Lax A, Sanchez-Mas J, Asensio-Lopez MC, Fernandez-Del Palacio MJ, Caballero L, Garrido IP, et al. Mineralocorticoid receptor antagonists modulate galectin-3 and interleukin-33/ST2 signaling in left ventricular systolic dysfunction after acute myocardial infarction. *JACC Heart Failure.* (2015) 3:50–8. doi: 10.1016/j.jchf.2014.07.015
46. Johnston WF, Salmon M, Su G, Lu G, Stone ML, Zhao Y, et al. Genetic and pharmacologic disruption of interleukin-1beta signaling inhibits experimental aortic aneurysm formation. *Arteriosc Thromb Vasc Biol.* (2013) 33:294–304. doi: 10.1161/ATVBAHA.112.300432
47. Wakita D, Kurashima Y, Crother TR, Noval Rivas M, Lee Y, Chen S, et al. Role of interleukin-1 signaling in a mouse model of Kawasaki disease-associated abdominal aortic aneurysm. *Arteriosc Thromb Vasc Biol.* (2016) 36:886–97. doi: 10.1161/ATVBAHA.115.307072
48. Hu H, Zhang G, Hu H, Liu W, Liu J, Xin S, et al. Interleukin-18 expression increases in the aorta and plasma of patients with acute aortic dissection. *Mediat Inflamm.* (2019) 2019:8691294. doi: 10.1155/2019/8691294
49. Olfson E, Cottrell CE, Davidson NO, Gurnett CA, Heusel JW, Stitziel NO, et al. Identification of medically actionable secondary findings in the 1000 genomes. *PLoS One.* (2015) 10:e0135193. doi: 10.1371/journal.pone.0135193
50. Jarvik GP, Browning BL. Consideration of cosegregation in the pathogenicity classification of genomic variants. *Am J Hum Genet.* (2016) 98:1077–81. doi: 10.1016/j.ajhg.2016.04.003

Conflict of Interest: The authors declare that the research was conducted in the absence of any commercial or financial relationships that could be construed as a potential conflict of interest.

Publisher's Note: All claims expressed in this article are solely those of the authors and do not necessarily represent those of their affiliated organizations, or those of the publisher, the editors and the reviewers. Any product that may be evaluated in this article, or claim that may be made by its manufacturer, is not guaranteed or endorsed by the publisher.

Copyright © 2021 Jiang, Wang, Gao, Li, Lu, Tan, Zheng, Pei, An, Li, Hu, Zhong, Zhu, Du and Wang. This is an open-access article distributed under the terms of the Creative Commons Attribution License (CC BY). The use, distribution or reproduction in other forums is permitted, provided the original author(s) and the copyright owner(s) are credited and that the original publication in this journal is cited, in accordance with accepted academic practice. No use, distribution or reproduction is permitted which does not comply with these terms.

frontiers in Cardiovascular Medicine

REVIEW
published: 10 August 2021
doi: 10.3389/fcvm.2021.706490

The Predictive Value of Carotid Ultrasonography With Cardiovascular Risk Factors—A "SPIDER" Promoting Atherosclerosis

Hongwei Li[1,2†], *Xiaolin Xu*[3†], *Baoming Luo*[3] *and Yuling Zhang*[1,2*]

[1] *Department of Cardiology, Sun Yat-sen Memorial Hospital, Sun Yat-sen University, Guangzhou, China,* [2] *Guangdong Province Key Laboratory of Arrhythmia and Electrophysiology, Guangzhou, China,* [3] *Department of Ultrasound, Sun Yat-sen Memorial Hospital, Sun Yat-sen University, Guangzhou, China*

Insufficient recommendations do not support the clinical use of carotid ultrasonography for further risk stratification in moderate-to-high risk patients with cardiovascular disease (CVD). A literature review was performed to assess six aspects of the research progress and limitations of carotid ultrasonography and carotid atherosclerosis-related risk factors: (1) structures of the carotid intima and media; (2) plaques; (3) inflammation; (4) dynamics of carotid blood flow; (5) early detection and intervention; and (6) risk factors for CVD. Although carotid intima-media thickness and carotid plaques are well-acknowledged independent predictors of CVD risk, normative and cut-off values are difficult to define due to the heterogeneous measurements reported in previous studies. Plaque properties, including location, number, density, and size, become more important risk predictors for cardiovascular disease, but a better approach for clinical use needs to be further established. Three-dimensional ultrasound and contrast-enhanced ultrasound are promising for promoting risk stratification with more details on plaque morphology. Moreover, inflammatory diseases and biomarkers should be evaluated for a full assessment of the inflammatory burden for atherosclerosis. Carotid flow velocity is not only an indicator for stenosis but also a potential risk predictor. Carotid atherosclerosis should be detected and treated early, and additional clinical trials are needed to determine the efficacy of these measures in reducing CVD risk. Cardiovascular risk factors tend to affect carotid plaques, and early treat-to-target therapy might yield clinical benefits. Based on the aforementioned six aspects, we consider that these six important factors act like a "SPIDER" spinning the web of atherosclerosis; a timely comprehensive assessment and intervention may halt the progression to CVD. Carotid ultrasound results should be combined with other atherosclerotic factors, and a comprehensive risk assessment may help to guide cardiovascular prevention decisions.

Keywords: carotid ultrasonography, carotid intima-media thickness, carotid plaque, cardiovascular risk prediction, cardiovascular risk factors

Subject terms: ultrasound, atherosclerosis, vascular disease, cardiovascular disease, peripheral vascular disease.

OPEN ACCESS

Edited by:
Yuli Huang,
Southern Medical University, China

Reviewed by:
Miguel Angel González-Gay,
University of Cantabria, Spain
Hang Xi,
Temple University, United States

***Correspondence:**
Yuling Zhang
zhyul@mail.sysu.edu.cn

† These authors have contributed equally to this work

Specialty section:
This article was submitted to General Cardiovascular Medicine, a section of the journal Frontiers in Cardiovascular Medicine

Received: *07 May 2021*
Accepted: *19 July 2021*
Published: *10 August 2021*

Citation:
Li H, Xu X, Luo B and Zhang Y (2021) The Predictive Value of Carotid Ultrasonography With Cardiovascular Risk Factors—A "SPIDER" Promoting Atherosclerosis. Front. Cardiovasc. Med. 8:706490. doi: 10.3389/fcvm.2021.706490

BACKGROUND

Carotid ultrasonography is a non-invasive, non-radioactive and reproducible imaging method used to detect carotid atherosclerosis and screen high-risk patients for cardiovascular disease (CVD). The carotid intima-media thickness (CIMT) is recommended to be measured in asymptomatic patients at intermediate risk for further risk stratification (1). However, the inconsistency in cut-off values and additive values used in cardiovascular risk prediction models limit the clinical application of CIMT (2, 3). Although carotid plaques are independently associated with an increased CVD risk and are recommended to be screened in patients with diabetes for a cardiovascular risk evaluation, the current method used to detect the presence of carotid plaques does not comprehensively consider their morphological properties (4–6). Furthermore, evidence that early carotid atherosclerosis interventions are beneficial is lacking (1). Despite the large body of research, no individual parameters of carotid ultrasonography are sufficient for determining an accurate prediction of the cardiovascular risk in asymptomatic patients. Insufficient recommendations limit the clinical use of carotid ultrasonography for cardiovascular risk evaluations as a primary preventative measure. A recent review focusing on the usefulness of carotid ultrasonography for risk stratification of cerebral and cardiovascular disease suggests the need to consider various aspects of carotid ultrasound imaging (7). In addition to carotid ultrasonography itself, there are other atherosclerotic factors affecting carotid atherosclerosis and cardiovascular events. Hence, we further propose a combination of carotid ultrasound, clinical condition, and laboratory tests to comprehensively evaluate the future risk of CVD.

In this review, we summarize the research progress, predictive value and limitations of carotid ultrasonography in determining the structure of the carotid intima and media, plaques and carotid flow velocity, and discuss other carotid atherosclerotic factors, including inflammation, early detection and intervention, and traditional CVD risk factors. A comprehensive cardiovascular assessment based on carotid ultrasonography with other atherosclerotic factors is important for risk stratification and medical decisions.

DIRECT PARAMETERS OF CAROTID ULTRASONOGRAPHY

Structures of the Carotid Intima and Media

CIMT

An abnormal increase in CIMT reflects the progression of carotid atherosclerosis, which is detected clearly by ultrasound. The CIMT has been suggested to be an independent predictor of the risk of incident CVD in most studies (8–10). Moreover, a slower CIMT progression caused by therapeutic intervention could predict the degree of CVD risk prediction (11). It is measured between the lumen-intima and the media-adventitia interfaces at the far wall of carotid arteries on ultrasound images, which show an obvious "double-line" sign. Changes in the intima and media have been further specified, as the intima layer is thicker and the media layer is thinner in patients with CVD than in healthy subjects (12). There were relatively few small-scale cross-sectional studies calculating the age-specific normal value of CIMT in healthy individuals, but the measurement methods and normative value of CIMT were not identical (13, 14). To date, a stable normative value for CVD risk prediction has not yet been defined (2).

The CIMT measurements, endpoint events and cut-off values for the CIMT used in large population-based prospective studies are summarized in **Table 1**. The discrepancies between studies concern five aspects: (1) the sites of CIMT measurement; (2) the CIMT parameters used for statistical analysis; (3) the endpoints of each study; (4) whether carotid plaques are included; and (5) the cut-off values used for predicting CVD risk.

Most studies measured the CIMT at the far wall of bilateral common carotid arteries (CCAs), but some studies measured the CIMT at both the near and far walls, at the carotid bifurcations (BIFs) and internal carotid arteries (ICAs), or only at the right CCA; measurements were recorded at three different angles or were repeated three times. The maximal CCA-IMT (18); the mean maximal CIMT (5, 9, 15, 20, 24, 26); the mean CIMT normalized by the IMT of the bilateral CCAs, BIFs, and ICAs (8); and the mean CCA-IMT and ICA-IMT of the bilateral carotid arteries (10, 17, 22, 25, 26) have been separately used for establishing distinct risk prediction models. For example, Chambless et al. (8) defined the mean CIMT as the average of the bilateral CCA-IMT, BIF-IMT, and ICA-IMT, while Baldassarre et al. (25) and O'Leary et al. (9) reported different values for the mean CIMT of the bilateral CCAs and ICAs.

Growing evidence suggests that CIMT can predict CVD risk partly because of the inclusion of plaques (22), which might magnify the measurement of the IMT and elicit false positive associations with CVD risk. Studies have reported the mean CCA-IMT, excluding plaques, but did not identify an association between the CCA-IMT and risk of incident CVD (22, 26, 29). Another source of heterogeneity was the arbitrary cut-off value used to predict the risk of the cardiovascular endpoints. For instance, the top quintile of the mean CCA-IMT was 1.18 mm in the Cardiovascular Health Study (9), while the top quintile of the mean CCA-IMT was 0.805 mm in the three-city study (22). Such heterogeneity might affect the comparison and synthesis of CIMT results.

The consensus for the use of carotid ultrasound to evaluate CVD risk and identify subclinical vascular disease issued by the American Society of Echocardiography (ASE) in 2008 established a standard method for CIMT assessment. It is categorized into four parts: (1) a cross-sectional scan for an overview of the arterial wall structure; (2) a Doppler ultrasound scan for identifying significant stenosis; (3) three-angle scans (anterior, lateral, and posterior) for the identification and description of plaques at the near and far walls of bilateral CCAs, bulbs, and ICAs; and (4) three-angle images of the "double line" sign for CIMT measurements, with the distal 1 cm of each CCA gated

TABLE 1 | Prospective studies with a large general population that assessed the association between carotid intima-media thickness (CIMT) and cardiovascular risk.

Study	Year	Sample size	Age (years)	Follow-up	Measurements	Primary endpoints	Hazard ratio* (95% CI)
KIHD (5)	1991	1,288	42–60	1 month−2.5 years	Mean of the maximal CCA-IMT, far wall, bilateral, three repeated measures, mineralized plaque not included	AMI	2.17 (1.08–4.26) per 0.1 mm
ARIC (8)	1997	12,841	45–64	Median 5.2 years	Mean CIMT of CCA + BIF + ICA, far wall, bilateral	MI, CHD death	IMT ≥ 1 mm: women: 5.07 (3.08–8.36), men: 1.85 (1.28–2.69); The third tertile vs. the first tertile: women: 6.69 (3.01–14.89), men: 2.88 (1.91–4.34)
CHS (9)	1999	4,476	72.5 ± 5.5	Median 6.2 years	Mean of the maximal CCA/ICA-IMT and the average CIMT, near and far walls, bilateral, three repeated measures for ICA, focal plaque included	MI, stroke	Relative risk per 1 SD increase: CCA-IMT: 1.27 (1.17–1.38); ICA-IMT: 1.30 (1.20–1.41); average IMT: 1.36 (1.25–1.47); The top quintile vs. the bottom quintile: CCA-IMT: 2.22 (1.58–3.13); ICA-IMT: 2.47 (1.59–3.85); average IMT: 3.15 (2.19–4.52)
Rotterdam study (15)	2004	6,389	69.3 ± 9.2	7–10 years	Mean of the maximal CCA-IMT, near and far walls, bilateral	MI	IMT ≥ 1.12 mm: 1.95 (1.19–3.19)
MDCS (16)	2005	5,163	45–64	Median 7 years	CCA-IMT, far wall, right	MI, IHD	IMT per 1SD increase: 1.23 (1.07–1.41); The top quintile vs. the bottom quintile: 2.76 (1.05–7.25)
CAPS (17)	2006	5,056	50.1 ± 13.1	Mean 4.2 years	Mean CCA/BIF/ICA-IMT, far wall, bilateral	MI, stroke, death	IMT per 1 SD increase: CCA: 1.17 (1.08–1.26); BIF: 1.14 (1.05–1.24); ICA: 1.09 (1.01–1.18); The top quartile vs. the bottom quartile: CCA: 1.85 (1.09–1.35); BIF: 1.27 (0.80–1.99); ICA: 1.25 (0.84–1.86)
EAS (18)	2007	1,007	69.4 ± 5.6	12 years	Maximal CCA -IMT, far wall, bilateral	MI, angina, stroke, IC	Odd ratios for MI/stoke with IMT ≥ 0.9 mm: 1.59 (1.07–2.37)
Tromsø study (19)	2007	6,226	55–74	Mean 5.4 years	Mean CCA-IMT and mean IMT, near and far walls for the CCA and far walls for the carotid bulb, right, plaque included	MI	Relative risk: the top quartile vs. the bottom quartile: 1.73 (0.98–3.06) for men and 2.86 (1.07–7.65) for women
CCCC (20)	2008	2,190	≥35	Median 10.5 years	Mean of the maximal CCA-IMT, far wall, bilateral	MI, CHD death, revascularization	Relative risk for CHD: IMT per 1 SD increase: 1.38 (1.12–1.70)
Cournot et al. (21)	2009	2,561	51.6 ± 10.5	Median 6 years	Mean CCA-IMT, far wall, bilateral, 3 times, plaque not included	AMI, angina, cardiac death, sudden death	IMT > 0.63: 2.26 (1.35–3.79)
Three-city study (22)	2011	5,895	73.3 ± 4.9	Median 5.4 years	Mean CCA-IMT, far wall, bilateral, plaque not included	MI, angina, CHD death, revascularization	IMT per 1SD increase: 0.8–1.1; The top quintile vs. the bottom quintile: 0.8 (0.5–1.2)
Framingham offspring study (23)	2011	2,965	58 ± 10	Average 7.2 years	Mean CCA-IMT and maximal ICA-IMT, far wall, bilateral, end-diastole, plaque not included	MI, angina, HF, CHD death, stroke, IC	IMT per 1 SD increase: CCA: 1.13 (1.02–1.24); ICA: 1.21 (1.13–1.29); IMT per 1 mm increase: CCA: 2.46 (1.18–5.13) ICA: 1.26 (1.16–1.36)
FATE (24)	2011	1,574	49.4 ± 9.9	Mean 7.2 years	Mean of the maximum CCA-IMT, far wall, right, at least 3 repeated measures	MI, RSCA, revascularization, SVD	IMT per 1 SD increase: 1.45 (1.15–1.83)
IMPROVE (25)	2012	3,703	Mean 64.2	Median 36.2 months	Mean and maximal CCA/BIF/ICA-IMT, far wall, bilateral, 3 angles, plaque included	MI, angina, HF, SCD, stroke, IC, revascularization	Mean IMT per 1SD increase: CCA: 1.31 (1.14–1.49); BIF: 1.24 (1.08–1.44); ICA: 1.27 (1.11–1.44); Maximal IMT per 1SD increase: CCA: 1.27 (1.12–1.44); BIF 1.26 (1.08–1.46); ICA: 1.30 (1.14–1.50)
MESA (26)	2012	1,330	63.8 ± 9.5	Median 7.6 years	Mean of the maximal CCA-IMT, far wall, right, plaque excluded	MI, angina, CHD death, RSCA, revascularization	IMT per 1 SD increase: 1.17 (0.95–1.45)

(Continued)

TABLE 1 | Continued

Study	Year	Sample size	Age (years)	Follow-up	Measurements	Primary endpoints	Hazard ratio* (95% CI)
Suzuki et al. (ARIC + CHS) (27)	2020	20,862	ARIC: 54.2 ± 5.8 CHS: 72.8 ± 5.5	23.5 years in ARIC 13.1 years in CHS	ARIC: Mean and maximum CIMT of CCA + BIF + ICA, far wall, bilateral CHS: Mean of the maximal CCA/ICA-IMT and the average CIMT, near and far walls, bilateral	SCD	The fourth quartile vs. the first quartile of maximal CIMT: 1.75 (1.22–2.51)
CIRCS (28)	2020	2,943	40–75	Median 15.1 years	Mean of the maximal CCA/ICA-IMT and the average CIMT, near and far walls, bilateral	CHD and stroke	The highest quartile vs. the lowest quartile of maximal CCA-IMT: 2.11 (1.44–3.11) The highest quartile vs. the lowest quartile of maximal ICA-IMT: 1.78 (1.20–2.62)

The measurements of CIMT are reported in the following order: the parameters, near/far wall, left/right side (if specified), number of repeated measures, systolic/diastolic phase and whether plaque was included.

**Hazard ratios were adjusted by age, sex, other traditional risk factors and medications provided by each study.*

AMI, acute myocardial infarction; ARIC, the Atherosclerosis Risk in Communities Study; BIF, carotid bifurcation; CAPS, the Carotid Atherosclerosis Progression Study; CCA, common carotid artery; CCCC, the Chin-Shan Community Cardiovascular Cohort Study; CHD, coronary heart disease; CHS, the Cardiovascular Health Study; CI, confidence interval; EAS, the Edinburgh Artery Study; FATE, the Firefighters and Their Endothelium Study; HF, heart failure; KIHD, the Kuopio Ischemic Heart Disease Risk Factor Study; IC, intermittent claudication; ICA, internal carotid artery; IHD, ischemic heart disease; IMPROVE, the IMT-Progression as Predictors of Vascular Events in a High-Risk European Population Study; MESA, the Multi-Ethnic Study of Atherosclerosis; MDCS, the Malmo Diet and Cancer Study; MI, myocardial infarction; RSCA, resuscitated cardiac arrest; SCD, sudden cardiac death; SVD, systematic vascular disease; mm, millimeter; SD, standard deviation.

FIGURE 1 | A single-angle cross-sectional scan of the near wall and far wall CIMT of the left CCA. To better show the distinction between the near wall and far wall of common carotid artery, we choose the cross section. The far wall CIMT of a 50-year-old Chinese man is 0.8 mm in **(A)**, while the near wall CIMT of a 41-year-old Chinese man is thicker (1.3 mm) than the far wall CIMT in **(B)**.

by the optimized R-wave (4). The accuracy of far-wall CCA-IMT measurements has been validated by the absence of a significant difference from *in vitro* specimens (30), while the near-wall measurements are less accurate due to liable artifacts. Three-angle scans of the CCAs help prevent an irregular CIMT from being inadequately evaluated without considering the near-wall CIMT. For instance, the far-wall CIMT of a 50-year-old man is clearly measured to be 0.8 millimeters (mm) in **Figure 1A**, while the CIMT of another 41-year-old man was significantly thicker, measuring 1.3 mm at the near wall in **Figure 1B**. In addition to CCA-IMT, significantly thicker CIMT values at carotid bulbs and ICAs should not be neglected, especially in patients with normal CCA-IMT values, to avoid underestimations of cardiovascular risk. The Mannheim CIMT and Plaque Consensus states that CIMT can be assessed at carotid bulbs and ICAs (31). A CIMT ≥75th percentile after adjusting for the patient's age, ethnicity, and sex is recommended as an indication of an increased CVD risk.

A comprehensive meta-analysis of 16 prospective studies performed by the PROG-IMT collaboration revealed a positive association between the mean CCA-CIMT and a 16% increase in cardiovascular risk but no association between CIMT

progression and cardiovascular events (32); moreover, the identification of meaningful normative values is difficult due to the substantial heterogeneity in the percentiles of CIMT reported across studies (2). In addition, another meta-analysis challenged the additive value of CIMT, as it showed only a 0.8% net reclassification improvement (NRI) after it was added to the 10-year Framingham risk score (FRS)-based risk prediction model (3). The challenge to the predictive value of CIMT progression and the additive value of CIMT to the FRS reduce the priority to measure the CIMT in cardiovascular risk assessments (33, 34). Interestingly, recent research using two cohorts with 20,862 participants from the ARIC study and the CHS study revealed a significantly positive association between CIMT and sudden cardiac death (SCD) during at least 13.1 years of follow-up (27). The long-term predictive value of CIMT for SCD may be better than the unsatisfactory predictive ability of 10-year total cardiovascular risk.

In short, far-wall CIMT is a useful independent predictor for CVD risk, with good reproducibility and accuracy. Due to the heterogeneity of CIMT measurements, CIMT results must be combined with other atherosclerotic markers instead of using carotid ultrasound alone (18, 35). Furthermore, the lifetime predictive value of the CIMT in young adults is worth exploring, regardless of whether the 10-year risk predictive value is low.

Carotid Artery Diameters

The CCA diameter, which is affected by the CIMT and carotid plaques, increases in individuals with carotid atherosclerosis and is measured transversely at a plaque-free site (36). An increased carotid lumen diameter was demonstrated to be associated with increased all-cause mortality (37), but its correlation with incident cardiovascular disease was uncertain. The interadventitia CCA diameter (ICCAD) is easier to detect than the lumen diameter, and an increase in the ICCAD exhibits additive predictive value for composite cardiovascular events (25). A meta-analysis of four cohort studies also reported that patients with a CCA diameter >8 mm had a higher risk of total CVD than patients with a diameter <7 mm (38). However, direct evidence that the ICCAD or the CCA diameter predicts the risk of coronary heart disease is unavailable (38). Carotid artery diameters represent the structural and functional changes induced by atherosclerosis and may be associated with an increased cardiovascular risk. Carotid arterial diameters should not be neglected in risk assessments.

Plaques

The Presence of Carotid Plaques

In people aged 30–79 years, the global prevalence of an increased CIMT is estimated to be 27.6% and the global prevalence of the presence of carotid plaques is estimated to be 21.1% in 2020. The percent increase in both an increased CIMT and the presence of carotid plaques is >50% in 2020 (39). The carotid atherosclerotic burden is significantly increased worldwide. Accumulating evidence from prospective studies has identified the presence of carotid plaques as a strong independent CVD risk factor, with significant additive value for risk prediction models (10, 40). Carotid plaques are defined as having a focal thickness that is at least 50% greater than that of the surrounding wall or a focal thickness distinct from the adjacent boundary greater than 1.5 mm, with protrusion into the lumen, which easily occurs at carotid bulbs. Carotid plaques are classified into three grades according to the up-to-date recommendations for the assessment of carotid arterial plaque by ultrasound from ASE: grade I is defined as protuberant plaques with CIMT <1.5 mm, grade II as either protuberant or diffuse plaques with CIMT ≥1.5 mm but <2.5 mm, and grade III as either protuberant or diffuse plaques with CIMT ≥2.5 mm (41). Plaques are recommended to be detected at both the near and far walls of bilateral CCA, carotid bulb and ICA segments, and the presence of carotid plaques after adjustment for the patient's age, sex, and ethnicity implicates an increased CVD risk (4, 42). Carotid atherosclerosis including carotid plaques is a strong cardiovascular predictor, even among patients with previous myocardial infarction or previous stroke (43).

A summary of the large prospective studies on the association between carotid plaques and CVD risk is shown in **Table 2**. Heterogeneity in plaque measurements mainly exists due to heterogeneity in three aspects: (1) the site at which plaques are detected; (2) the parameters of interest for plaques; and (3) the definition of plaques. Most of the studies detected plaques at bilateral CCAs, carotid bulbs, and ICAs (15). A few studies detected carotid plaques in the bilateral CCAs and bulbs (5), bilateral CCAs and ICAs (19, 21), and only the right carotid arteries (16).

The parameters of interest for carotid plaques also varied across studies. Despite the presence of plaques, most studies chose plaque scores to predict the risk (16, 18, 20, 36), while some studies collected data on plaque echogenicity, plaque texture, plaque surface, and plaque area (9, 19, 29). In addition, early studies defined plaques as a focal area with protrusion into the lumen without a cut-off standard for CIMT, which might lead to overestimations of the predictive value of CIMT. The heterogeneity of plaque parameters also increased the difficulty of identifying a stable cut-off value for plaque number or properties to predict the cardiovascular risk. Uniform quantification of carotid plaques may help to better establish the cut-off value for parameters of carotid plaques in cardiovascular risk prediction.

Plaque Scores

Various scoring systems with satisfactory predictive ability have been developed to quantitatively measure carotid plaques (**Table 3**). In the Rotterdam study, the plaque score was computed as the total number of sites where plaques occurred in bilateral CCAs, BIFs, and ICAs, with a total score of 6 points (15). A similar score was calculated for the near and far walls of the bilateral CCAs, BIFs, and ICAs, with a total score of 12 points, in the MESA study (46). Plaque scores reflecting the severity of plaques in carotid arteries also showed a significant association with cardiovascular events (16, 20). Handa et al. (48) reported an algorithm that calculated the sum of the bilateral maximal thickness of each plaque in four segments, which was associated with the severity of coronary artery lesions (50). Prati et al. (49) established a scoring system consisting of four parts: the degree of stenosis, echogenicity, heterogeneity of the texture,

TABLE 2 | Prospective studies with a large general population that assessed the association between carotid plaques and cardiovascular risk.

Study	Year	Sample size	Age (years)	Follow-up	Measurements	Primary endpoints	Hazard ratio*
KIHD (5)	1991	1,288	42–60	1 month−2.5 years	Bilateral CCAs + carotid bulbs, the presence of plaques, a focal area with mineralization or protrusion into the lumen	AMI	Small plaque: 4.15 (1.15–11.47); Stenotic plaque†: 6.71 (1.33–33.91)
Rotterdam study (15)	2004	6,389	69.3 ± 9.2	At least 7 years	Bilateral CCAs + carotid bulbs + ICAs, the presence of plaques and plaque score, a focal area with protrusion into the lumen	MI	Plaque score ≥ 3 points: 1.38 (1.27–2.62)
MDCS (16)	2005	5,163	45–64	Median 7 years	Right CCA + carotid bulb + ICA + ECA, the presence of plaques and plaque score, a focal thickening of IMT > 1.2 mm	MI, IHD	Plaque score per 1 SD increase: 1.39 (1.10–1.78)
CHS (44)	2007	5,020	72.6 ± 5.5	Median 11 years	Bilateral CCAs + ICAs, classification of plaques, the largest focal lesion classified by surface characteristics, echogenicity, and texture	MI, stroke, cardiovascular death, all-cause death	High-risk plaque‡: 1.38 (1.14–1.67)
Tromsø study (19)	2007	6,226	55–74	Mean 5.4 years	Bilateral CCAs + carotid bulbs + ICAs, the presence of plaques + plaque echogenicity (grade 1–4) + plaque area, a focal area with protrusion into the lumen	MI	Relative risk according to plaque area: the top tertile vs. no plaque: 1.56 (1.04–2.36) for men; 3.95 (2.16–7.19) for women; Echogenicity: the bottom tertile vs. no plaque: 1.08 (0.68–1.70) for men; 2.79 (1.45–5.37) for women
NOMAS (45)	2007	1,118	68 ± 8	Mean 2.7 years	Bilateral CCAs + ICAs, the presence of plaques and calcified plaque, a focal area with protrusion 50% greater than the surrounding wall and plaques with acoustic shadowing were calcified	MI, stroke, vascular death	Calcified plaques vs. no plaque: 2.4 (1.0–5.8)
NOMAS (6)	2008	2,189	68 ± 10	Mean 6.9 years	Bilateral CCAs + BIFs + ICAs, MCPT, a focal area with protrusion 50% greater than the surrounding wall	MI, stroke, vascular death	MCPT ≥ 1.9 mm vs. no plaque: 1.48 (1.05–2.10);
CCCC (20)	2008	2,190	≥35	Median 10.5 years	Bilateral CCAs + carotid bulbs + ICAs + ECAs, the severity of plaque score	MI, CHD death, revascularization	Relative risk for CHD: 1.15 (1.07–1.24) per 1 increase in plaque score
Cournot et al. (21)	2009	2,561	51.6 ± 10.5	Median 6 years	Bilateral CCAs + ICAs, the presence of plaques, a focal area with hyperechogenicity or protrusion into the lumen	AMI, angina, cardiac death, sudden death	2.81 (1.84–4.29)
Three-city study (22)	2011	5,895	73.3 ± 4.9	Median 5.4 years	Bilateral CCAs + BIFs + ICAs, the presence of plaques, a focal area with protrusion into the lumen for at least 50% greater than the surrounding vessel wall	MI, angina, CHD death, PCI, CABG	Plaques at ≥ 2 sites vs. no plaque: 2.2 (1.6–3.1)
Framingham offspring study (23)	2011	2,965	58 ± 10	Average 7.2 years	Bilateral ICA, the presence of plaques, an area of IMT ≥ 1.5 mm	MI, angina, CHD death, stroke, IC, HF	1.92 (1.49–2.47)
MESA (10)	2013	6,562	61.1 ± 10.2	Mean 7.8 years	Bilateral CCAs + BIFs + ICAs, the presence of plaques, a focal area with protrusion into the lumen	MI, angina, CHD death, RSCA	1.45 (1.20–1.76)
High-risk plaque BioImage (29)	2017	5,808	Average 69	Median 2.7 years	Bilateral carotid arteries, MCPT and total plaque area (mm^2), a focal protrusion ≥ 0.5 mm or 50% of the surrounding wall; or IMT > 1.5 mm	MI, stroke, cardiovascular death	The top tertile vs. the bottom tertile: MCPT: 1.96 (0.91–4.25); Total plaque area: 2.36 (1.13–4.92)
MESA (46)	2017	4,955	61.6 ± 10.1	Median 11.3 years	Bilateral CCAs + BIFs + ICAs, plaque score, a focal thickness of IMT > 1.5 mm or > 50% of the surrounding wall	MI, angina, CHD death, RSCA, stroke	Plaque score per 1 SD increase: 1.27 (1.16–1.40)
MESA (47)	2018	2,706	65.4 ± 9.6	Mean 13.3 years	Bilateral CCAs + BIFs + ICAs, plaque score and total plaque score and greyscale plaque features	MI, angina, CHD death, RSCA, stroke	Total plaque area per 1 SD increase: 1.23 (1.11, 1.36); carotid plaque score per 1 SD increase: 1.33 (1.18–1.49)

(Continued)

TABLE 2 | Continued

Study	Year	Sample size	Age (years)	Follow-up	Measurements	Primary endpoints	Hazard ratio*
Suzuki et al. (ARIC + CHS) (27)	2020	20,862	ARIC: 54.2 ± 5.8 CHS: 72.8 ± 5.5	23.5 years in ARIC 13.1 years in CHS	ARIC: Bilateral CCAs + BIFs + ICAs, the presence of plaques, two of the following criteria: CIMT > 1.5 mm/a focal protrusion into the lumen/brighter echoes than adjacent boundaries CHS: Bilateral CCAs + ICAs, the presence of high risk and intermediate risk plaques[‡#]	SCD	ARIC: 1.37 (1.13–1.67) CHS: 1.32 (1.04–1.68)
CIRCS (28)	2020	2,943	40–75	Median 15.1 years	Bilateral ICAs, the presence of homogeneous or heterogeneous plaques, a focal thickness of IMT ≥ 1.5 mm	CHD and stroke	1.71 (1.25–2.35)

The measurements of the carotid artery are reported in the following order: the segments, parameters, and definitions of plaques.

**Hazard ratios were adjusted by age, sex, other traditional risk factors and medications provided by each study.*

†A plaque with ≥20% diameter stenosis was classified as stenotic plaque.

‡High-risk plaque was defined as plaques with markedly irregular or ulcerated surfaces or hypodense or heterogeneous plaques that occupied 50% of the total plaque volume.

#Intermediate- risk plaque was defined as hyperdense, calcified, or homogeneous plaque or those with a mildly irregular surface.

AMI, acute myocardial infarction; BIF, carotid bifurcation; CCA, common carotid artery; CCCC, the Chin-Shan Community Cardiovascular Cohort Study; CHD, coronary heart disease; CHS, the Cardiovascular Health Study; CI, confidence interval; CIRCS, the Circulatory Risk in Communities Study; ECA, external carotid artery; KIHD, the Kuopio Ischemic Heart Disease Risk Factor Study; HF, heart failure; IC, intermittent claudication; ICA, internal carotid artery; IHD, ischemic heart disease; mm, millimeter; MESA, the Multi-Ethnic Study of Atherosclerosis; MCPT, the maximum carotid plaque thickness; MDCS, the Malmo Diet and Cancer Study; MI, myocardial infarction; NOMAS, the Northern Manhattan Study; RSCA, resuscitated cardiac arrest; SD, standard deviation.

and surface characteristics of each plaque. These quantitative plaque scoring systems are considered to improve the evaluation of plaque severity and future cardiovascular risk.

Plaque Properties

Plaque properties, including the thickness, area, echogenicity and surface characteristics, have attracted the attention of an increasing number of researchers. Rundek et al. measured the maximal carotid plaque thickness, and values greater than the 75th percentile were associated with a 1.48-fold higher risk of combined vascular events (6). In addition, the plaque area also predicts the risks of myocardial infarction (MI), stroke, and cardiovascular death, which are significantly higher in females than in males (19, 29, 47). Carotid plaques are categorized as hyper-echo, low-echo, mixed-echo, and ulcer plaques based on the level of echogenicity (**Figure 2**). The echogenicity of plaques is positively associated with the density and stability of carotid plaques. Ulcer plaques are more unstable and have a rough surface. Cao et al. (44) defined high-risk plaques as plaques with markedly irregular or ulcerated surfaces or hypodense or heterogeneous plaques that occupy 50% of the total plaque volume, which were related to a 1.38-fold greater risk of composite CVD events. Patients with calcified carotid plaques exhibiting high echogenicity also had a notably higher risk of combined cardiovascular events than patients without plaques (45). In the Circulatory Risk Communities Study, heterogeneous plaques correlated positively with increased risk of total stroke, ischemic stroke, lacunar infarction, coronary artery disease, and total cardiovascular disease. In addition, patients with markedly irregular or ulcerated plaques had a significantly higher risk for coronary artery disease and total cardiovascular disease but not stroke (28). Recording plaque location, thickness, area, and number is recommended for a more precise description of carotid plaques (31). Plaque properties are associated with CVD risk, but additional scientific evidence must be obtained for validation.

Plaque identification by carotid ultrasound is largely based on two-dimensional ultrasound, which cannot display the original three-dimensional structure of carotid plaques. Three-dimensional ultrasound has a wider dynamic scale for measurement of the progression of the plaque area and CIMT (32), which is too small to be detected by a two-dimensional scan. A more accurate measurement of plaque morphology by either single-region or full-vessel protocols by using three-dimensional ultrasound has been recently recommended for the assessment of carotid arterial plaque by ultrasound from ASE. Three-dimensional ultrasound is capable of measuring a specific lesion in all planes, which can avoid missing height or area when it is out of plane by two-dimensional ultrasound imaging (41). A prospective study demonstrated that a three-dimensional plaque volume <0.09 mL can better identify patients with a low risk of coronary artery disease than a two-dimensional plaque thickness <1.35 mm (51). Additionally, 1-year progression of total plaque volume is reported to independently predict cardiovascular events (52). Contrast-enhanced ultrasound is also a novel technology that allows visualization of carotid intraplaque neovascularization and evaluation of carotid plaque vulnerability,

TABLE 3 | Differences between the carotid plaque scoring systems.

Study	Scoring system
Rotterdam study (15) and MESA (46)	The sum of the sites with plaque in (the near and far walls of) the CCA, BIF, and ICA
MDCS (16)	A scale dependent on the severity of BIF: 0 = normal; 1 = one small plaque (<10 mm^2); 2 = small plaques ≥2; 3 = one large plaque (>10 mm^2); 4 = one large plaque plus small plaques; 5 = large plaques ≥2 or one plaque with stenosis >50% or circumferent
CCCC (20)	The total grade of each CCA, carotid bulb, ICA and ECA bilaterally: grade 0 = normal; 1= one small plaque (stenosis: <30%); 2 = one medium plaque (stenosis: 30–49%) or multiple small plaques; 3 = one large plaque (stenosis: 50–99%) or multiple plaques with medium plaque ≥1; 4 = occlusion
Handa et al. (48)	The sum of the bilateral maximal thickness of each plaque in the area from the ICA < 15 mm proximal to the BIF region to the CCA >30 mm proximal to the BIF region.
Prati et al. (49)	The total score of four parameters: (1) stenosis ≥40% = 1; (2) echogenicity from low (1) to high (3); (3) heterogeneous texture with complex echo pattern = 1; and (4) irregular surface = 1. In addition, the plaque with the highest score was analyzed.

BIF, carotid bifurcation; CCA, common carotid artery, CCCC, the Chin-Shan Community Cardiovascular Cohort Study; ECA, external carotid artery; ICA, internal carotid artery; MDCS, the Malmo Diet and Cancer Study; MESA, the Multi-Ethnic Study of Atherosclerosis; mm, millimeter.

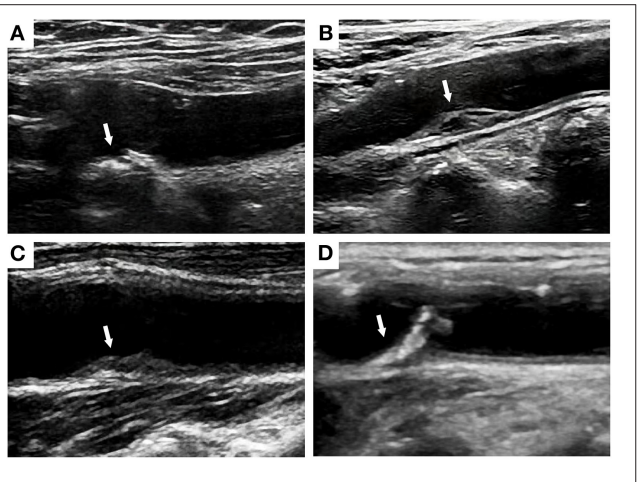

FIGURE 2 | Ultrasound images of hyper-echo **(A)**, low-echo **(B)**, mixed-echo **(C)**, and ulcer plaques **(D)** at the carotid bulbs.

and an increased carotid intraplaque neovascularization score is a strong predictor for significant coronary artery disease, with high sensitivity and specificity (53, 54). Superb microvascular imaging ultrasound without contrast is a novel technology using an algorithm to remove clutter and motion wall artifacts under the condition of low-velocity blood flow, and seems to detect carotid intraplaque neovascularization accurately comparable to contrast-enhanced ultrasound (55). Plaque properties obtained by three-dimensional ultrasound, contrast-enhanced ultrasound, and superb microvascular imaging appear to be powerful tools of cardiovascular risk assessment in clinical use, but further studies are necessary to validate precise and practical parameters.

In summary, carotid plaques are more powerful risk predictors than CIMT and should be reported in combination with CIMT (4). For high-risk patients with diabetes whose stratification of CVD risk may be underestimated by traditional risk assessments, carotid plaques should be measured for risk stratification (34).

Dynamics of Carotid Blood Flow

Carotid Flow Velocity

Carotid flow velocity, specifically peak-systolic velocity (PSV), as measured by gray-scale or Doppler ultrasound, is always used to classify ICA stenosis. For instance, a PSV ≥125 cm/s indicates ICA stenosis rate ≥50%, while a PSV ≥230 cm/s indicates >80% ICA stenosis. When the ICA stenosis rate is >90%, PSV is undetectable (56). However, the predictive ability of carotid flow velocity remains unclear. A large follow-up study measured end diastolic velocity (EDV), which was reported to be associated with ischemic stroke. Patients with a low EDV and high IMT exhibited a 2.10-fold higher risk of ischemic stroke than patients with a high EDV and low IMT. However, the predictive value of a low EDV for coronary events has not been validated (57). Another cohort study of patients with hypertension revealed a higher risk of composite cardiovascular events that was related to a PSV/systolic carotid artery diameter < 85.7 s, which provided additive value for risk prediction models (58). Additional studies should be conducted to confirm the association between carotid flow velocity and the risk of coronary heart disease. Carotid flow velocity should not be merely considered as a stratification standard for diameter stenosis.

Shear Stress of Carotid Artery Wall

The disrupted and turbulent flow at the stenosis location may promote carotid plaque formation. An asymmetrical distribution of CIMT is closely correlated with hemodynamic changes across the carotid artery, and the highest CIMT was reported to be located at the posteromedial wall of the bifurcation and internal carotid segments and the anterolateral wall of the common carotid segment (59). The maximum wall shear stress appears at the peak of carotid plaques, while the minimum wall shear stress was reported to be located at the place after passing of the peak, which was lower than non-stenotic areas (60). The reduction in carotid endothelial shear stress with age was also an independent predictor of carotid plaque development (61). Goudot et al. suggested that a combination of maximal wall shear stress at the peak of carotid plaque and shear wave elastography texture predicted vulnerable carotid plaques with good performance

(62). However, there is no reference value of shear stress for vascular evaluation in clinical practice. Additionally, perivascular adipose tissue also participates in carotid plaque formation induced by disturbed flow in ApoE$^{-/-}$ mice which may be mediated by focal inflammation attenuation (63). Haberka and Gasior provided a novel index of the perivascular adipose index, carotid extra-media thickness (EMT), and found that EMT was positively associated with cardiometabolic risk factors (64). Detection of perivascular adipose tissue by the combination of inflammatory markers and imaging for cardiovascular risk prediction requires further struggles.

EARLY DETECTION AND INTERVENTION

CIMT is recommended to be measured in intermediate-risk adults for additional risk stratification. However, whether the early detection of carotid atherosclerosis is beneficial for improving clinical outcomes remains uncertain. There is no strong evidence that suggests the need for therapies for abnormal CIMT (1). Whether extra measures for the early detection and treatment of carotid atherosclerosis are needed is a key question.

A recent randomized controlled study compared the FRS between patients who were informed of their carotid ultrasound results and patients who did not receive their results, and a significant decrease in the FRS from baseline to the 1-year follow-up was unexpectedly observed in the intervention group. Thus, an awareness of subclinical carotid atherosclerosis is beneficial for reducing cardiovascular risk, which might originate from improved compliance with medication and lifestyle modifications (65). In addition, a treat-to-target approach for CVD risk factors, including lifestyle interventions and medications, contributed to slower CIMT progression and lower morbidity related to cardiovascular events compared to usual care in patients with rheumatoid arthritis who did not present with CVD (66). However, in elderly patients with type 2 diabetes and coronary artery disease, the CIMT of patients without identified carotid plaques was reduced by a 1-year exercise training program (67). These studies stressed the importance of early detection and intervention for subclinical carotid atherosclerosis. Carotid ultrasonography may also help to evaluate cerebrovascular and cardiovascular risk without unnecessary invasive examination in low-risk patients with infectious disease, including human immunodeficiency infection and COVID-19 (68, 69). Hence, an early alarm and intervention based on carotid ultrasound results might prevent irreversible outcomes of carotid plaques or established CVD.

CARDIOVASCULAR RISK FACTORS RELATED TO CAROTID ATHEROSCLEROSIS

Inflammation

Inflammation plays an important role in carotid atherosclerosis. The CIMT and presence of carotid plaques are positively correlated with systematic inflammatory diseases and chronic inflammation (70, 71). Patients with chronic inflammatory disease are at increased risk of cardiovascular events. This is the case for rheumatoid arthritis, the prototype of a chronic inflammatory disease, which is associated with accelerated atherosclerosis (72). Interestingly, several studies have revealed that both CIMT (73) and the presence of carotid plaques (74) are strong predictors of future cardiovascular events in patients with rheumatoid arthritis. Furthermore, carotid ultrasound, as well as other surrogate markers, better identifies rheumatoid arthritis patients with a very high risk of cardiovascular disease than well-defined risk chart algorithms, such as the Systematic Coronary Risk Assessment (SCORE) (75, 76). Moreover, inflammatory intermediate monocytes are reported to correlate strongly with CIMT (77). A proteomic analysis also revealed that CIMT mainly correlates with chemotaxis-related proteins rather than other inflammatory proteins (78). According to the Canakinumab Anti-inflammatory Thrombosis Outcome study (CANTOS), the administration of anti-inflammatory therapy reveals a close association between inflammation and cardiovascular disease (79). An increased inflammatory burden should be carefully considered when carotid ultrasound results are interpreted.

Traditional Inflammatory Markers

High-sensitivity C-reactive protein (hsCRP) and serum amyloid A (SAA) are two of the classic acute-phase proteins that have been proven to be independent cardiovascular risk predictors (26, 35). A large asymptomatic cohort revealed a positive association of hsCRP and SAA with the risk for carotid atherosclerotic progression (80). Interestingly, high hsCRP levels predict CVD mortality only in patients with severe atherosclerosis but not in patients with atherosclerosis (44). In addition to hsCRP, other traditional inflammatory markers including fibrinogen and leukocyte counts were demonstrated to be independently associated with the progression of CIMT (81).

Cytokines, Chemokines, and Other Novel Inflammatory Factors

A recent systematic review provided a summary of high-risk carotid plaque-related inflammatory cytokines (interleukin-6, interleukin-1β, tumor necrosis factor-α, etc.), chemokines (monocyte chemotactic protein-1, MCP-1), endothelial and cell adhesion factors (intracellular adhesion molecule-1, vascular cell adhesion molecules-1, and selectins), proteolysis factors (matrix metalloproteinases), metabolic biomarkers (lipids, adipokines, homocysteine, etc.), angiogenic markers (vascular endothelial growth factor), and thrombotic biomarkers (plasminogen activator inhibitor-1) (82). Among these serum biomarkers, interleukin 6 was also demonstrated to further increase the predictive capacity, accompanied by the presence of carotid plaques, for obstructive coronary artery disease (83). Other serum inflammatory markers play an important role in both carotid and coronary atherosclerosis. Neopterin, an activation biomarker for monocytes/macrophages, is positively associated with both complex carotid plaques and coronary artery disease (84, 85). High lipoprotein-associated phospholipase A2 (Lp-PLA2), correlated with a high risk of coronary artery disease, is significantly associated with the symptomatic status of carotid plaques (86, 87). Fatty acid binding protein 4, an important

inflammatory protein also participating in macrophage cholesterol trafficking, is positively correlated with carotid plaques and stroke symptoms and clearly predicts the risk of cardiovascular mortality (88, 89). Local inflammation of carotid atherosclerosis can be assessed by 2-deoxy-2-[^{18}F]fluoro-D-glucose positron emission tomography/computed tomography (^{18}F-FDG PET/CT) and the expression inflammatory markers at carotid plaque lesions (86). A high level of galectin 3, a novel vascular inflammatory marker, is a strong predictor of heart failure and poor cardiovascular outcome (90). However, a low intraplaque concentration of galectin-3 is associated with symptomatic and unstable carotid plaques, which can be reversed by short-term statin treatment (91). Serum complement complex C5b-C9 was also an independent risk factor for unstable carotid plaques in patients with acute ischemic stroke (92), whereas the relationship between complement C3 and carotid plaques was controversial in patients with systematic lupus erythematosus (93, 94). Some activated T and B cells, including $CD33^+HLA\text{-}DR^+$ T cells, $CD19^+CD86^+$ B cells, $CD20^+CD69^+$ T cells, and $CD16^+$ monocytes, were also found to be associated with CIMT, carotid plaques, and the severity of stenosis (95).

Furthermore, moderate doses of statins have been shown to decrease MCP-1 levels followed by CIMT regression, indicating that anti-inflammatory drugs reverse carotid atherosclerosis (96). Therefore, inflammation should be simultaneously assessed with carotid ultrasound for comprehensive evaluations of cardiovascular risk.

Risk Factors for CVD

High-Density Lipoprotein

A low high-density lipoprotein cholesterol (HDL-C) level is well-acknowledged to be associated with high cardiovascular risk, and is also associated with elevated CIMT and carotid plaque burden (97). An elevation in HDL-C levels was shown to be correlated with a reduction in carotid plaque growth in patients with preexisting carotid plaques (98). With the advancement of HDL quality studies, other HDL-related metrics were also found to be associated with carotid atherosclerosis. El Khoudary et al. reported that higher large HDL particles *via* ion-mobility were associated with higher CIMT close to menopause but with lower CIMT in the postmenopausal period (99). Moreover, HDL2-C was positively associated with carotid plaque thickness, while HDL3-C was inversely associated with carotid plaque area (100). The relationship between protein components in HDL and carotid atherosclerosis was also investigated. Aroner et al. found that HDL containing apoC-III was positively associated with carotid plaque score, while HDL lacking apoC-III was negatively associated with carotid plaque score and CIMT, which supported the role of apoC-III in HDL in carotid atherosclerosis (101). Surprisingly, Shea et al. reported that HDL-mediated cholesterol efflux capacity was positively associated with carotid plaque progression, but negatively associated with incident hard CVD based on cross-sectional analysis (102). The correlation between HDL function and carotid atherosclerosis requires further investigation. Non-HDL-C, calculated as total cholesterol minus HDL-C, and the non-HDL-C/HDL-C ratio were also cardiovascular risk factors positively associated with carotid atherosclerosis (103, 104). In total, HDL-related metrics were important variables for cardiovascular risk prediction and the evaluation of carotid atherosclerosis.

Low-Density Lipoprotein

Low-density lipoprotein cholesterol (LDL-C) is a strong predictor for both cerebrovascular events and cardiovascular events, and the recommended target of LDL-C becomes lower in order to reduce residual risk (105). A greater possibility of a higher carotid plaque score was demonstrated to be related to an increase in LDL-C within 1 year of the final menstrual period, which might be associated with an elevation of cardiovascular risk for postmenopausal women (106). Furthermore, an increased circulating oxidized LDL-C was significantly associated with a higher risk of 10-year progression of subclinical carotid plaques (107). However, a targeted LDL-C level of <70 mg/dL did not reduce the incidence of newly diagnosed carotid plaque compared to a higher LDL-C target in patients with ischemic stroke (108). Therefore, early target control of LDL-C before the incidence of atherosclerotic events is more beneficial in cardiovascular prevention.

Diabetes

Diabetes is one of the strongest risk factors for both carotid atherosclerosis and CVD, and the detection of carotid plaque is recommended in diabetic high-risk patients (39, 109). The presence of echogenic carotid plaques, compared to that of echolucent and heterogeneous plaques, was demonstrated to be a stronger predictor for incident major adverse cardiovascular events in patients with type 2 diabetes (110). Patients with type 1 diabetes also had a higher proportion of echogenic and calcified plaques than subjects without type 1 diabetes (111). Furthermore, the frequency of carotid plaques was increased in patients with latent autoimmune diabetes in adults (LADA) compared to type 1 and type 2 diabetes, which was also increased with increasing diabetes duration in LADA (112). For diabetic complications, obesity, renal function decline, and diabetic retinopathy were investigated to be positively associated with the presence of carotid plaques (113–115). Therefore, carotid ultrasonography is necessary for the evaluation of vascular complications as well as the risk of cardiovascular events.

Hypertension

Hypertension is an important traditional risk factor, and antihypertensive targeted therapy is protective against cardiovascular events (116). Both high systolic and diastolic blood pressure at age 40 were demonstrated to be associated with carotid plaque burden late midlife (117). Additionally, carotid plaque score and CIMT were demonstrated to be potent predictors for stroke, and the former performed more accurately (118). H-type hypertension, characterized by hypertension and hyperhomocysteinemia with high cardio-cerebrovascular risk, was reported to be positively associated with higher presence of carotid plaques than isolated systolic hypertension and simple hypercysteinemia (119). Recently, Ben et al. also found that blood homocysteine levels in hypertensive patients with hyperhomocysteinemia were

positively associated with carotid plaque thickness, stenosis degree, and contrast-enhanced ultrasound quantification, but negatively associated with shear wave velocity (120). Hence, carotid ultrasonography is a useful tool for atherosclerotic evaluation of hypertensive patients.

Unhealthy Lifestyle

An unhealthy lifestyle associated with increased cardiovascular risk can also promote carotid atherosclerosis. Smoking is one of the major atherosclerotic factors, and both current and former smokers were at higher risk of echodense carotid plaques than never smokers (121). Sedentary behavior is another common unhealthy lifestyle. A moderate level of physical activity with a sedentary time ≤3 hours/day was associated with lower odds of the presence of carotid plaques, but no reduction in carotid plaque presence by physical activity combined with a sedentary time >3 hours/day (122). Moreover, a Western dietary pattern, including higher red meat, sugar intake, and deep-fried products, was positively associated with higher CIMT in the common carotid artery, which might contribute to future cardiovascular risk (123). Poor sleep quality and short sleep time, a universal phenomenon of menopause, were found to be associated with higher CIMT and odds of carotid plaques (124). Middle-aged male shift workers also had higher CIMT and carotid plaque presence than fixed daytime workers (125). Additionally, sleep apnea, defined as an apnea-hypopnea index of 15 events per hour, was associated with an increased presence of carotid plaque in subjects aged <68 years but not in older adults. Greater hypoxemia was also associated with increasing carotid intima-media thickness in younger subjects but not in older adults (126). Patients with chronic obstructive pulmonary disease had higher CIMT (127), and lower pulmonary function was associated with an increased risk of carotid atherosclerosis compared to higher pulmonary function (128).

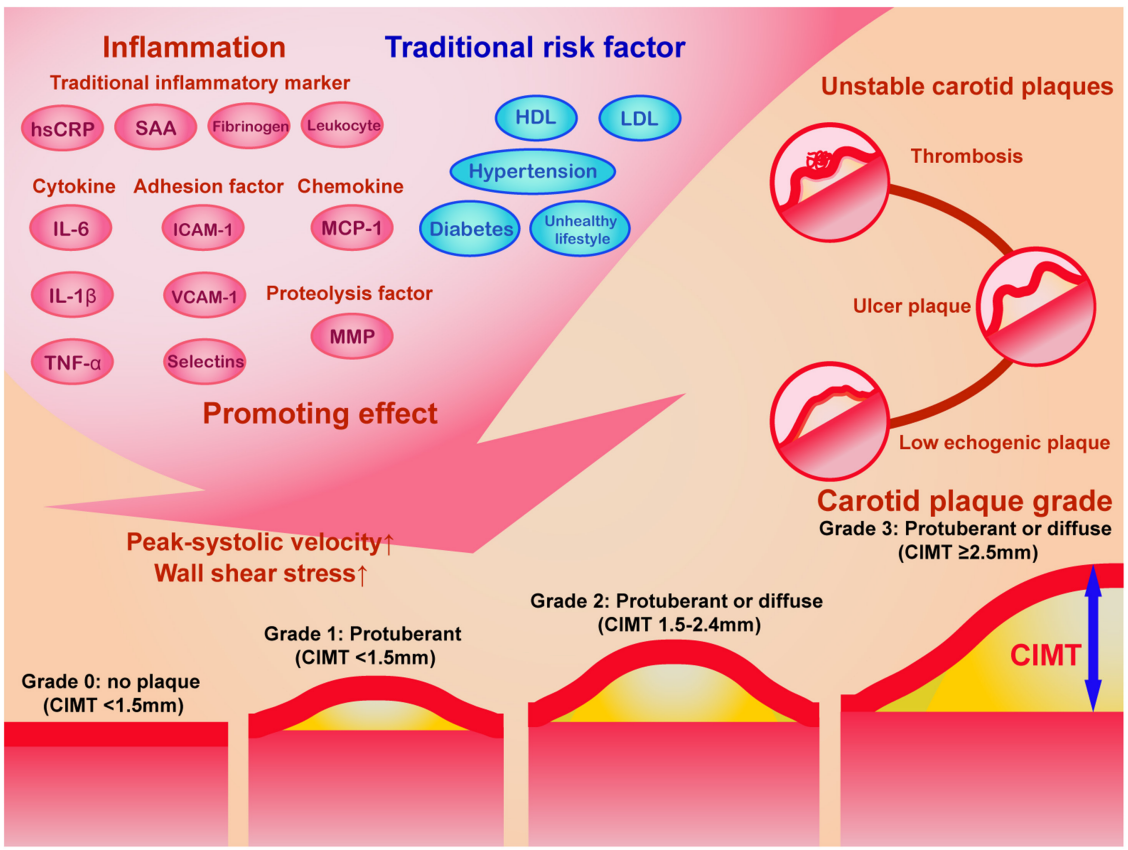

FIGURE 3 | The schematic diagram of the impact of inflammation and traditional risk factor on carotid plaque progression and the grading system of carotid plaques. Traditional inflammatory markers, cytokines, chemokines, adhesion factors, proteolysis factors, and other novel inflammatory factors, in combination with traditional risk factors promotes elevated carotid plaque grade and unstable carotid plaques. According to Recommendations for the Assessment of Carotid Arterial Plaque by Ultrasound from the American Society of Echocardiography in 2020 (41), the carotid plaque grade was classified into 4 levels: grade 0 (no plaques with CIMT <1.5 mm), grade 1 (protuberant CIMT < 1.5 mm), grade 2 (protuberant or diffuse CIMT between 1.5 and 2.4 mm), and grade 3 (protuberant or diffuse CIMT ≥2.5 mm). The ultrasound characteristics of unstable carotid plaques includes low echogenic plaques, ulcer plaques, and thrombosis. CIMT, carotid intima-media thickness; HDL, high-density lipoprotein; hsCRP, hypersensitive C reactive protein; ICAM-1, intercellular cell adhesion molecule-1; IL-6, interleukin-6; IL-1β, interleukin-1 beta; LDL, low-density lipoprotein; MCP, monocyte chemotactic protein-1; MMP, matrix metallopeptidase; TNF-α, tumor necrosis factor-alpha; VCAM-1, vascular cell adhesion molecule-1.

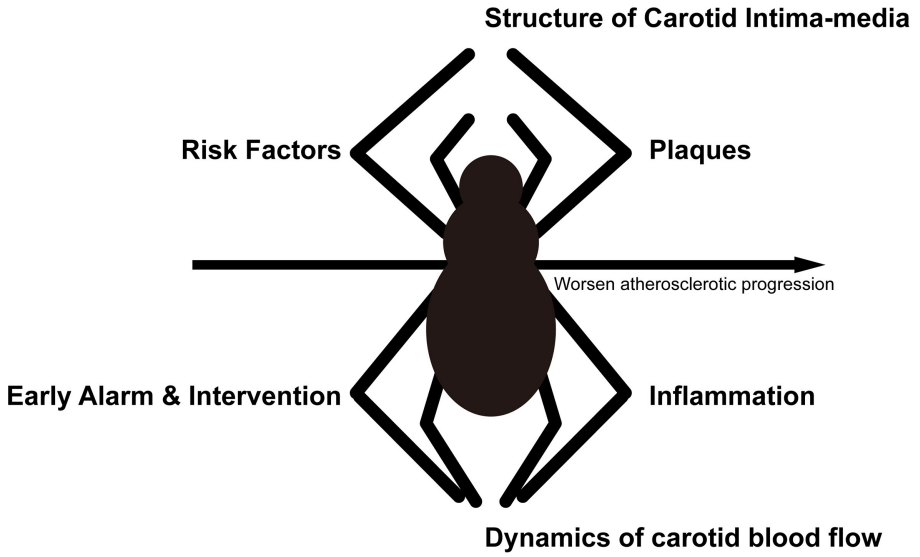

FIGURE 4 | Schematic diagram of the "SPIDER" proposal. The progression of atherosclerosis is similar to a spider spinning a web, and a full consideration of these 6 aspects may help to prevent the progression of atherosclerosis.

Intervention for Traditional Risk Factors

Traditional cardiovascular risk factors, including age, sex, blood pressure, smoking history, lipid levels, and diabetes, are independent determinants of the presence of carotid atherosclerosis (129–131). Previous evidence has shown that traditional risk factors do not largely contribute to the variance in CIMT and carotid plaque burden (132, 133). CVD risk factors have also been reported to partly account for of the total carotid plaque area and three-dimensional carotid plaque volume (129, 134). However, an improvement in CVD risk factors may not reduce carotid plaque progression to a greater extent than an early increase in the CIMT. As mentioned above, an early treat-to-target approach for CVD risk factors has been shown to slow down CIMT progression and reduce the risk of incident cardiovascular events in a high CIMT population without prior CVD (66). However, no benefits of exercise training in terms of CIMT reduction were observed in patients with established CVD (67). Moreover, in the Study of Women's Health Across the Nation, a healthier diet score was associated with a smaller CCA-IMT and CCA adventitial diameter, but it was not significantly correlated with the presence of carotid plaques (135). Our previous network meta-analysis also demonstrated that high-intensity statins and the combination therapy of statins and ezetimibe were associated with larger CIMT reduction compared to moderate/low-intensity statins and no statins, but the evidence for the association between statins and carotid plaque changes remained insufficient (136). Another population-based observational study did not observe a correlation between omega-3 fatty acid consumption and the presence of carotid plaques (137).

Hence, CVD risk factors interact with carotid atherosclerosis, and treatments targeting CVD factors may possibly reverse carotid atherosclerosis in the early phase, but multidisciplinary efforts are needed for the early prevention of carotid atherosclerosis progression.

EVALUATION OF CAROTID ULTRASONOGRAPHY COMBINED WITH CARDIOVASCULAR RISK FACTORS

The prevalence of carotid atherosclerosis increases with age (39, 138); thus middle-aged and elderly individuals are at higher risk of carotid atherosclerosis and CVD than young adults and may benefit from carotid ultrasound detection. Inflammatory factors and traditional risk factors have integral effect on the hemodynamics and vessel dysfunction of carotid artery, which causes carotid plaque progression and instability (**Figure 3**). Additionally, high-risk plaque is not clearly defined, and lacks evidences for intervention, although it is largely correlated with cerebrovascular and cardiovascular disease. Several serum atherosclerotic biomarkers combined with carotid ultrasonography may assist clinicians in identifying high cardiovascular risk patients who need intervention (82). When evaluating the risk of CVD using carotid ultrasonography, the major problem is the lack of normative values of carotid ultrasound parameters and the weak combination of carotid ultrasound results with cardiovascular risk factors in clinical practice. Based on the comprehensive literature review and within the context of international guidelines (1, 33, 34, 139), we propose that atherosclerosis, like a web, is promoted and alarmed by the "SPIDER" (**Figure 4**), the name of which originated from the first letter of the 6 abovementioned aspects. A comprehensive assessment of combining carotid ultrasonography and other atherosclerotic factors may halt the progression of atherosclerosis for cardiovascular prevention.

CONCLUSION

Carotid ultrasound results should be combined with other important atherosclerotic factors, and a comprehensive cardiovascular assessment can better predict CVD risk and guide primary preventative measures.

AUTHOR CONTRIBUTIONS

HL and XX contributed to literature review and manuscript drafting. BL contributed to providing image. YZ contributed to the conception of the work and assessed the quality of evidence and suggestions. All authors contributed to the article and approved the submitted version.

FUNDING

This study was supported by the National Natural Science Foundation of China (NSFC) (Nos. 81970388 and 81801719), the Natural Science Foundation of Guangdong (No. 2019A1515011682), and the Development Funding of the International Science and Technology Innovation Center in the Greater Bay Area of the 2020–2022 Science and Technology Project of Guangdong Province (No. 2021A0505030021).

REFERENCES

1. Greenland P, Alpert JS, Beller GA, Benjamin EJ, Budoff MJ, Fayad ZA, et al. 2010 ACCF/AHA guideline for assessment of cardiovascular risk in asymptomatic adults: a report of the American college of cardiology foundation/American heart association task force on practice guidelines. *J Am Coll Cardiol.* (2010) 56:e50–103. doi: 10.1016/j.jacc.2010.09.001
2. Liao X, Norata GD, Polak JF, Stehouwer CD, Catapano A, Rundek T, et al. Normative values for carotid intima media thickness and its progression: are they transferrable outside of their cohort of origin? *Eur J Prev Cardiol.* (2016) 23:1165–73. doi: 10.1177/2047487315625543
3. Den Ruijter HM, Peters SAE, Anderson TJ, Britton AR, Dekker JM, Eijkemans MJ, et al. Common carotid intima-media thickness measurements in cardiovascular risk prediction: a meta-analysis. *JAMA.* (2012) 308:796–803. doi: 10.1001/jama.2012.9630
4. Stein JH, Korcarz CE, Hurst RT, Lonn E, Kendall CB, Mohler ER, et al. Use of carotid ultrasound to identify subclinical vascular disease and evaluate cardiovascular disease risk: a consensus statement from the American society of echocardiography carotid intima-media thickness task force. Endorsed by the society for vascular medicine. *J Am Soc Echocardiogr.* (2008) 21:93–111; quiz: 189–90. doi: 10.1016/j.echo.2007.11.011
5. Salonen JT, Salonen R. Ultrasonographically assessed carotid morphology and the risk of coronary heart disease. *Arterioscler Thromb.* (1991) 11:1245–9. doi: 10.1161/01.ATV.11.5.1245
6. Rundek T, Arif H, Boden-Albala B, Elkind MS, Paik MC, Sacco RL. Carotid plaque, a subclinical precursor of vascular events: the Northern Manhattan Study. *Neurology.* (2008) 70:1200–7. doi: 10.1212/01.wnl.0000303969.63165.34
7. Nezu T, Hosomi N. Usefulness of carotid ultrasonography for risk stratification of cerebral and cardiovascular disease. *J Atheroscler Thromb.* (2020) 27:1023–35. doi: 10.5551/jat.RV17044
8. Chambless LE, Heiss G, Folsom AR, Rosamond W, Szklo M, Sharrett AR, et al. Association of coronary artery disease incidence with carotid arterial wall thickness and major risk factors: the atherosclerosis risk in communities (ARIC) study, 1987-1993. *Atherosclerosis.* (1997) 146:489–94. doi: 10.1093/oxfordjournals.aje.a009302
9. O'Leary DH, Polak JF, Kronmal RA, Manolio TA, Burke GL, Wolfson SK. Carotid-artery intima and media thickness as a risk factor for myocardial infarction and stroke in older adults. Cardiovascular Health Study Collaborative Research Group. *N Engl J Med.* (1999) 340:14–22. doi: 10.1056/NEJM199901073400103
10. Polak JF, Szklo M, Kronmal RA, Burke GL, Shea S, Zavodni AE, et al. The value of carotid artery plaque and intima-media thickness for incident cardiovascular disease: the multi-ethnic study of atherosclerosis. *J Am Heart Assoc.* (2013) 2:e000087. doi: 10.1161/JAHA.113.000087
11. Willeit P, Tschiderer L, Allara E, Reuber K, Seekircher L, Gao L, et al. Carotid intima-media thickness progression as surrogate marker for cardiovascular risk: meta-analysis of 119 clinical trials involving 100 667 patients. *Circulation.* (2020) 142:621–42. doi: 10.1161/CIRCULATIONAHA.120.046361
12. Rodriguez-Macias KA, Lind L, Naessen T. Thicker carotid intima layer and thinner media layer in subjects with cardiovascular diseases. An investigation using noninvasive high-frequency ultrasound. *Atherosclerosis.* (2006) 189:393–400. doi: 10.1016/j.atherosclerosis.2006.02.020
13. Lim TK, Lim E, Dwivedi G, Kooner J, Senior R. Normal value of carotid intima-media thickness–a surrogate marker of atherosclerosis: quantitative assessment by B-mode carotid ultrasound. *J Am Soc Echocardiogr.* (2008) 21:112–6. doi: 10.1016/j.echo.2007.05.002
14. Pastorius CA, Medina-Lezama J, Corrales-Medina F, Bernabe-Ortiz A, Paz-Manrique R, Salinas-Najarro B, et al. Normative values and correlates of carotid artery intima-media thickness and carotid atherosclerosis in Andean-Hispanics: the Prevencion Study. *Atherosclerosis.* (2010) 211:499–505. doi: 10.1016/j.atherosclerosis.2010.04.009
15. van der Meer IM, Bots ML, Hofman A, del Sol AI, van der Kuip DA, Witteman JC. Predictive value of noninvasive measures of atherosclerosis for incident myocardial infarction: the Rotterdam Study. *Circulation.* (2004) 109:1089–94. doi: 10.1161/01.CIR.0000120708.59903.1B
16. Rosvall M, Janzon L, Berglund G, Engström G, Hedblad B. Incident coronary events and case fatality in relation to common carotid intima-media thickness. *J Intern Med.* (2005) 257:430–7. doi: 10.1111/j.1365-2796.2005.01485.x
17. Lorenz MW, von Kegler S, Steinmetz H, Markus HS, Sitzer M. Carotid intima-media thickening indicates a higher vascular risk across a wide age range: prospective data from the Carotid Atherosclerosis Progression Study (CAPS). *Stroke.* (2006) 37:87–92. doi: 10.1161/01.STR.0000196964.24024.ea
18. Price JF, Tzoulaki I, Lee AJ, Fowkes FG. Ankle brachial index and intima media thickness predict cardiovascular events similarly and increased prediction when combined. *J Clin Epidemiol.* (2007) 60:1067–75. doi: 10.1016/j.jclinepi.2007.01.011
19. Johnsen SH, Mathiesen EB, Joakimsen O, Stensland E, Wilsgaard T, Lochen ML, et al. Carotid atherosclerosis is a stronger predictor of myocardial infarction in women than in men: a 6-year follow-up study of 6226 persons: the Tromso Study. *Stroke.* (2007) 38:2873–80. doi: 10.1161/STROKEAHA.107.487264
20. Chien KL, Su TC, Jeng JS, Hsu HC, Chang WT, Chen MF, et al. Carotid artery intima-media thickness, carotid plaque and coronary heart disease and stroke in Chinese. *PLoS ONE.* (2008) 3:e3435. doi: 10.1371/journal.pone.0003435
21. Cournot M, Taraszkiewicz D, Cambou JP, Galinier M, Boccalon H, Hanaire-Broutin H, et al. Additional prognostic value of physical examination, exercise testing, and arterial ultrasonography for coronary risk assessment in primary prevention. *Am Heart J.* (2009) 158:845–51. doi: 10.1016/j.ahj.2009.08.017
22. Plichart M, Celermajer DS, Zureik M, Helmer C, Jouven X, Ritchie K, et al. Carotid intima-media thickness in plaque-free site, carotid plaques and coronary heart disease risk prediction in older adults. The Three-City Study. *Atherosclerosis.* (2011) 219:917–24. doi: 10.1016/j.atherosclerosis.2011.09.024

23. Polak JF, Pencina MJ, Pencina KM, O'Donnell CJ, Wolf PA, D'Agostino RB Sr. Carotid-wall intima-media thickness and cardiovascular events. *N Engl J Med*. (2011) 365:213–21. doi: 10.1056/NEJMoa1012592
24. Anderson TJ, Charbonneau F, Title LM, Buithieu J, Rose MS, Conradson H, et al. Microvascular function predicts cardiovascular events in primary prevention: long-term results from the Firefighters and Their Endothelium (FATE) study. *Circulation.* (2011) 123:163–9. doi: 10.1161/CIRCULATIONAHA.110.953653
25. Baldassarre D, Hamsten A, Veglia F, de Faire U, Humphries SE, Smit AJ, et al. Measurements of carotid intima-media thickness and of interadventitia common carotid diameter improve prediction of cardiovascular events: results of the IMPROVE (Carotid Intima Media Thickness [IMT] and IMT-Progression as Predictors of Vascular Events in a High Risk European Population) study. *J Am Coll Cardiol.* (2012) 60:1489–99. doi: 10.1016/j.jacc.2012.06.034
26. Yeboah J, McClelland RL, Polonsky TS, Burke GL, Sibley CT, O'Leary D, et al. Comparison of novel risk markers for improvement in cardiovascular risk assessment in intermediate-risk individuals. *JAMA*. (2012) 308:788–95. doi: 10.1001/jama.2012.9624
27. Suzuki T, Wang W, Wilsdon A, Butler KR, Adabag S, Griswold ME, et al. Carotid intima-media thickness and the risk of sudden cardiac death: the ARIC study and the CHS. *J Am Heart Assoc.* (2020) 9:e016981. doi: 10.1161/JAHA.120.016981
28. Shimoda S, Kitamura A, Imano H, Cui R, Muraki I, Yamagishi K, et al. Associations of carotid intima-media thickness and plaque heterogeneity with the risks of stroke subtypes and coronary artery disease in the japanese general population: the circulatory risk in communities study. *J Am Heart Assoc.* (2020) 9:e017020. doi: 10.1161/JAHA.120.017020
29. Sillesen H, Sartori S, Sandholt B, Baber U, Mehran R, Fuster V. Carotid plaque thickness and carotid plaque burden predict future cardiovascular events in asymptomatic adult Americans. *Eur Heart J Cardiovasc Imaging.* (2018) 19:1042–50. doi: 10.1093/ehjci/jex239
30. Pignoli P, Tremoli E, Poli A, Oreste P, Paoletti R. Intimal plus medial thickness of the arterial wall: a direct measurement with ultrasound imaging. *Circulation.* (1986) 74:1399–406. doi: 10.1161/01.CIR.74.6.1399
31. Touboul PJ, Hennerici MG, Meairs S, Adams H, Amarenco P, Bornstein N, et al. Mannheim carotid intima-media thickness and plaque consensus (2004-2006-2011). *Cerebrovasc Dis*. (2012) 34:290–6. doi: 10.1159/000343145
32. Lorenz MW, Polak JF, Kavousi M, Mathiesen EB, Völzke H, Tuomainen TP, et al. Carotid intima-media thickness progression to predict cardiovascular events in the general population (the PROG-IMT collaborative project): a meta-analysis of individual participant data. *Lancet.* (2012) 379:2053–62. doi: 10.1016/S0140-6736(12)60441-3
33. Piepoli MF, Hoes AW, Agewall S, Albus C, Brotons C, Catapano AL, et al. 2016 European guidelines on cardiovascular disease prevention in clinical practice: the sixth joint task force of the European society of cardiology and other societies on cardiovascular disease prevention in clinical practice (constituted by representatives of 10 societies and by invited experts) developed with the special contribution of the European association for cardiovascular prevention & rehabilitation (EACPR). *Eur Heart J*. (2016) 37:2315–81. doi: 10.1093/eurheartj/ehw106
34. Cosentino F, Grant PJ, Aboyans V, Bailey CJ, Ceriello A, Delgado V, et al. 2019 ESC guidelines on diabetes, pre-diabetes, cardiovascular diseases developed in collaboration with the EASD. *Eur Heart J*. (2020) 41:255–323. doi: 10.1093/eurheartj/ehz486
35. Ridker PM, Hennekens CH, Buring JE, Rifai N. C-reactive protein and other markers of inflammation in the prediction of cardiovascular disease in women. *N Engl J Med.* (2000) 342:836–43. doi: 10.1056/NEJM200003233421202
36. Bonithon-Kopp C, Touboul PJ, Berr C, Magne C, Ducimetiere P. Factors of carotid arterial enlargement in a population aged 59 to 71 years: the EVA study. *Stroke.* (1996) 27:654–60. doi: 10.1161/01.STR.27.4.654
37. Fritze F, Groß S, Ittermann T, Völzke H, Felix SB, Schminke U, et al. Carotid lumen diameter is associated with all-cause mortality in the general population. *J Am Heart Assoc.* (2020) 9:e015630. doi: 10.1161/JAHA.119.015630
38. Sedaghat S, van Sloten TT, Laurent S, London GM, Pannier B, Kavousi M, et al. Common carotid artery diameter and risk of cardiovascular events and mortality: pooled analyses of four cohort studies. *Hypertension.* (2018) 72:85–92. doi: 10.1161/HYPERTENSIONAHA.118.11253
39. Song P, Fang Z, Wang H, Cai Y, Rahimi K, Zhu Y, et al. Global and regional prevalence, burden, and risk factors for carotid atherosclerosis: a systematic review, meta-analysis, and modelling study. *Lancet Glob Health.* (2020) 8:e721–9. doi: 10.1016/S2214-109X(20)30117-0
40. Inaba Y, Chen JA, Bergmann SR. Carotid plaque, compared with carotid intima-media thickness, more accurately predicts coronary artery disease events: a meta-analysis. *Atherosclerosis.* (2012) 220:128–33. doi: 10.1016/j.atherosclerosis.2011.06.044
41. Johri AM, Nambi V, Naqvi TZ, Feinstein SB, Kim ESH, Park MM, et al. Recommendations for the assessment of carotid arterial plaque by ultrasound for the characterization of atherosclerosis and evaluation of cardiovascular risk: from the American society of echocardiography. *J Am Soc Echocardiogr.* (2020) 33:917–33. doi: 10.1016/j.echo.2020.04.021
42. Gregg S, Li TY, Hetu MF, Pang SC, Ewart P, Johri AM. Relationship between carotid artery atherosclerosis and bulb geometry. *Int J Cardiovasc Imaging.* (2018) 34:1081–90. doi: 10.1007/s10554-018-1319-z
43. Sirimarco G, Amarenco P, Labreuche J, Touboul PJ, Alberts M, Goto S, et al. Carotid atherosclerosis and risk of subsequent coronary event in outpatients with atherothrombosis. *Stroke.* (2013) 44:373–9. doi: 10.1161/STROKEAHA.112.673129
44. Cao JJ, Arnold AM, Manolio TA, Polak JF, Psaty BM, Hirsch CH, et al. Association of carotid artery intima-media thickness, plaques, and c-reactive protein with future cardiovascular disease and all-cause mortality. *Circulation.* (2007) 116:32–8. doi: 10.1161/CIRCULATIONAHA.106.645606
45. Prabhakaran S, Singh R, Zhou X, Ramas R, Sacco RL, Rundek T. Presence of calcified carotid plaque predicts vascular events: the Northern Manhattan Study. *Atherosclerosis.* (2007) 195:e197–201. doi: 10.1016/j.atherosclerosis.2007.03.044
46. Gepner AD, Young R, Delaney JA, Budoff MJ, Polak JF, Blaha MJ, et al. Comparison of carotid plaque score and coronary artery calcium score for predicting cardiovascular disease events: the multi-ethnic study of atherosclerosis. *J Am Heart Assoc.* (2017) 6:e005179. doi: 10.1161/JAHA.116.005179
47. Mitchell C, Korcarz CE, Gepner AD, Kaufman JD, Post W, Tracy R, et al. Ultrasound carotid plaque features, cardiovascular disease risk factors and events: the Multi-Ethnic Study of Atherosclerosis. *Atherosclerosis.* (2018) 276:195–202. doi: 10.1016/j.atherosclerosis.2018.06.005
48. Handa N, Matsumoto M, Maeda H, Hougaku H, Ogawa S, Fukunaga R, et al. Ultrasonic evaluation of early carotid atherosclerosis. *Stroke.* (1990) 21:1567–72. doi: 10.1161/01.STR.21.11.1567
49. Prati P, Tosetto A, Casaroli M, Bignamini A, Canciani L, Bornstein N, et al. Carotid plaque morphology improves stroke risk prediction: usefulness of a new ultrasonographic score. *Cerebrovasc Dis.* (2011) 31:300–4. doi: 10.1159/000320852
50. Ikeda N, Kogame N, Iijima R, Nakamura M, Sugi K. Carotid artery intima-media thickness and plaque score can predict the SYNTAX score. *Eur Heart J.* (2012) 33:113–9. doi: 10.1093/eurheartj/ehr399
51. Johri AM, Chitty DW, Matangi M, Malik P, Mousavi P, Day A, et al. Can carotid bulb plaque assessment rule out significant coronary artery disease? A comparison of plaque quantification by two- and three-dimensional ultrasound. *J Am Soc Echocardiogr.* (2013) 26:86–95. doi: 10.1016/j.echo.2012.09.005
52. Wannarong T, Parraga G, Buchanan D, Fenster A, House AA, Hackam DG, et al. Progression of carotid plaque volume predicts cardiovascular events. *Stroke.* (2013) 44:1859–65. doi: 10.1161/STROKEAHA.113.001461
53. Mantella LE, Colledanchise KN, Hetu MF, Feinstein SB, Abunassar J, Johri AM. Carotid intraplaque neovascularization predicts coronary artery disease and cardiovascular events. *Eur Heart J Cardiovasc Imaging.* (2019) 20:1239–47. doi: 10.1093/ehjci/jez070
54. Toutouzas K, Drakopoulou M, Aggeli C, Nikolaou C, Felekos I, Grassos H, et al. *In vivo* measurement of plaque neovascularisation and thermal heterogeneity in intermediate lesions of human carotid arteries. *Heart.* (2012) 98:1716–21. doi: 10.1136/heartjnl-2012-302507
55. Zamani M, Skagen K, Scott H, Lindberg B, Russell D, Skjelland M. Carotid plaque neovascularization detected with superb microvascular

imaging ultrasound without using contrast media. *Stroke.* (2019) 50:3121–7. doi: 10.1161/STROKEAHA.119.025496
56. von Reutern GM, Goertler MW, Bornstein NM, Del Sette M, Evans DH, Hetzel A, et al. Grading carotid stenosis using ultrasonic methods. *Stroke.* (2012) 43:916–21. doi: 10.1161/STROKEAHA.111.636084
57. Chuang SY, Bai CH, Chen JR, Yeh WT, Chen HJ, Chiu HC, et al. Common carotid end-diastolic velocity and intima-media thickness jointly predict ischemic stroke in Taiwan. *Stroke.* (2011) 42:1338–44. doi: 10.1161/STROKEAHA.110.605477
58. Bellinazzi VR, Cipolli JA, Pimenta MV, Guimaraes PV, Pio-Magalhaes JA, Coelho-Filho OR, et al. Carotid flow velocity/diameter ratio is a predictor of cardiovascular events in hypertensive patients. *J Hypertens*. (2015) 33:2054–60. doi: 10.1097/HJH.0000000000000688
59. Tajik P, Meijer R, Duivenvoorden R, Peters SA, Kastelein JJ, Visseren FJ, et al. Asymmetrical distribution of atherosclerosis in the carotid artery: identical patterns across age, race, and gender. *Eur J Prev Cardiol.* (2012) 19:687–97. doi: 10.1177/1741826711410821
60. Goudot G, Poree J, Pedreira O, Khider L, Julia P, Alsac JM, et al. Wall shear stress measurement by ultrafast vector flow imaging for atherosclerotic carotid stenosis. *Ultraschall Med.* (2021) 42:297–305. doi: 10.1055/a-1060-0529
61. Carallo C, Tripolino C, De Franceschi MS, Irace C, Xu XY, Gnasso A. Carotid endothelial shear stress reduction with aging is associated with plaque development in twelve years. *Atherosclerosis.* (2016) 251:63–9. doi: 10.1016/j.atherosclerosis.2016.05.048
62. Goudot G, Sitruk J, Jimenez A, Julia P, Khider L, Alsac JM, et al. Carotid plaque vulnerability assessed by combined shear wave elastography and ultrafast doppler compared to histology. *Transl Stroke Res.* (2021). doi: 10.1007/s12975-021-00920-6
63. Ren L, Wang L, You T, Liu Y, Wu F, Zhu L, et al. Perivascular adipose tissue modulates carotid plaque formation induced by disturbed flow in mice. *J Vasc Surg.* (2019) 70:927–36 e4. doi: 10.1016/j.jvs.2018.09.064
64. Haberka M, Gasior Z. Carotid extra-media thickness in obesity and metabolic syndrome: a novel index of perivascular adipose tissue: extra-media thickness in obesity and metabolic syndrome. *Atherosclerosis.* (2015) 239:169–77. doi: 10.1016/j.atherosclerosis.2014.12.058
65. Näslund U, Ng N, Lundgren A, Fhärm E, Grönlund C, Johansson H, et al. Visualization of asymptomatic atherosclerotic disease for optimum cardiovascular prevention (VIPVIZA): a pragmatic, open-label, randomised controlled trial. *Lancet.* (2019) 393:133–42. doi: 10.1016/S0140-6736(18)32818-6
66. Burggraaf B, van Breukelen-van der Stoep DF, de Vries MA, Klop B, Liem AH, van de Geijn GM, et al. Effect of a treat-to-target intervention of cardiovascular risk factors on subclinical and clinical atherosclerosis in rheumatoid arthritis: a randomised clinical trial. *Ann Rheum Dis.* (2019) 78:335–41. doi: 10.1136/annrheumdis-2018-214075
67. Byrkjeland R, Stensaeth KH, Anderssen S, Njerve IU, Arnesen H, Seljeflot I, et al. Effects of exercise training on carotid intima-media thickness in patients with type 2 diabetes and coronary artery disease. Influence of carotid plaques. *Cardiovasc Diabetol.* (2016) 15:13. doi: 10.1186/s12933-016-0336-2
68. Janjua SA, Staziaki PV, Szilveszter B, Takx RAP, Mayrhofer T, Hennessy O, et al. Presence, characteristics, and prognostic associations of carotid plaque among People living with HIV. *Circ Cardiovasc Imaging.* (2017) 10:e005777. doi: 10.1161/CIRCIMAGING.116.005777
69. Jud P, Kessler HH, Brodmann M. Case report: changes of vascular reactivity and arterial stiffness in a patient with Covid-19 infection. *Front Cardiovasc Med.* (2021) 8:671669. doi: 10.3389/fcvm.2021.671669
70. Wu GC, Liu HR, Leng RX, Li XP, Li XM, Pan HF, et al. Subclinical atherosclerosis in patients with systemic lupus erythematosus: a systemic review and meta-analysis. *Autoimmun Rev.* (2016) 15:22–37. doi: 10.1016/j.autrev.2015.10.002
71. Kiechl S, Egger G, Mayr M, Wiedermann CJ, Bonora E, Oberhollenzer F, et al. Chronic infections and the risk of carotid atherosclerosis: prospective results from a large population study. *Circulation.* (2001) 103:1064–70. doi: 10.1161/01.CIR.103.8.1064
72. Gonzalez-Gay MA, Gonzalez-Juanatey C, Vazquez-Rodriguez TR, Martin J, Llorca J. Endothelial dysfunction, carotid intima-media thickness, and accelerated atherosclerosis in rheumatoid arthritis. *Semin Arthritis Rheum.* (2008) 38:67–70. doi: 10.1016/j.semarthrit.2008.02.001
73. Gonzalez-Juanatey C, Llorca J, Martin J, Gonzalez-Gay MA. Carotid intima-media thickness predicts the development of cardiovascular events in patients with rheumatoid arthritis. *Semin Arthritis Rheum.* (2009) 38:366–71. doi: 10.1016/j.semarthrit.2008.01.012
74. Corrales A, Vegas-Revenga N, Rueda-Gotor J, Portilla V, Atienza-Mateo B, Blanco R, et al. Carotid plaques as predictors of cardiovascular events in patients with Rheumatoid Arthritis. Results from a 5-year-prospective follow-up study. *Semin Arthritis Rheum.* (2020) 50:1333–8. doi: 10.1016/j.semarthrit.2020.03.011
75. Corrales A, Gonzalez-Juanatey C, Peiro ME, Blanco R, Llorca J, Gonzalez-Gay MA. Carotid ultrasound is useful for the cardiovascular risk stratification of patients with rheumatoid arthritis: results of a population-based study. *Ann Rheum Dis.* (2014) 73:722–7. doi: 10.1136/annrheumdis-2012-203101
76. Corrales A, Parra JA, Gonzalez-Juanatey C, Rueda-Gotor J, Blanco R, Llorca J, et al. Cardiovascular risk stratification in rheumatic diseases: carotid ultrasound is more sensitive than Coronary Artery Calcification Score to detect subclinical atherosclerosis in patients with rheumatoid arthritis. *Ann Rheum Dis.* (2013) 72:1764–70. doi: 10.1136/annrheumdis-2013-203688
77. SahBandar IN, Ndhlovu LC, Saiki K, Kohorn LB, Peterson MM, D'Antoni ML, et al. Relationship between circulating inflammatory monocytes and cardiovascular disease measures of carotid intimal thickness. *J Atheroscler Thromb.* (2020) 27:441–8. doi: 10.5551/jat.49791
78. Pettersson-Pablo P, Cao Y, Breimer LH, Nilsson TK, Hurtig-Wennlof A. Pulse wave velocity, augmentation index, and carotid intima-media thickness are each associated with different inflammatory protein signatures in young healthy adults: the lifestyle, biomarkers and atherosclerosis study. *Atherosclerosis.* (2020) 313:150–5. doi: 10.1016/j.atherosclerosis.2020.09.027
79. Ridker PM, Everett BM, Thuren T, MacFadyen JG, Chang WH, Ballantyne C, et al. Antiinflammatory therapy with canakinumab for atherosclerotic disease. *N Engl J Med.* (2017) 377:1119–31. doi: 10.1056/NEJMoa1707914
80. Schillinger M, Exner M, Mlekusch W, Sabeti S, Amighi J, Nikowitsch R, et al. Inflammation and carotid artery–risk for atherosclerosis study (ICARAS). *Circulation.* (2005) 111:2203–9. doi: 10.1161/01.CIR.0000163569.97918.C0
81. Willeit P, Thompson SG, Agewall S, Bergstrom G, Bickel H, Catapano AL, et al. Inflammatory markers and extent and progression of early atherosclerosis: meta-analysis of individual-participant-data from 20 prospective studies of the PROG-IMT collaboration. *Eur J Prev Cardiol.* (2016) 23:194–205. doi: 10.1177/2047487314560664
82. Martinez E, Martorell J, Riambau V. Review of serum biomarkers in carotid atherosclerosis. *J Vasc Surg.* (2020) 71:329–41. doi: 10.1016/j.jvs.2019.04.488
83. Guaricci AI, Pontone G, Fusini L, De Luca M, Cafarelli FP, Guglielmo M, et al. Additional value of inflammatory biomarkers and carotid artery disease in prediction of significant coronary artery disease as assessed by coronary computed tomography angiography. *Eur Heart J Cardiovasc Imaging.* (2017) 18:1049–56. doi: 10.1093/ehjci/jew173
84. Sugioka K, Naruko T, Hozumi T, Nakagawa M, Kitabayashi C, Ikura Y, et al. Elevated levels of neopterin are associated with carotid plaques with complex morphology in patients with stable angina pectoris. *Atherosclerosis.* (2010) 208:524–30. doi: 10.1016/j.atherosclerosis.2009.07.054
85. Firoz CK, Jabir NR, Kamal MA, Alama MN, Damanhouri GA, Khan W, et al. Neopterin: An immune biomarker of coronary artery disease and its association with other CAD markers. *IUBMB Life.* (2015) 67:453–9. doi: 10.1002/iub.1390
86. Bueno A, March JR, Garcia P, Canibano C, Ferruelo A, Fernandez-Casado JL. Carotid plaque inflammation assessed by (18)F-FDG PET/CT and Lp-PLA2 is higher in symptomatic patients. *Angiology.* (2021) 72:260–7. doi: 10.1177/0003319720965419
87. Khuseyinova N, Imhof A, Rothenbacher D, Trischler G, Kuelb S, Scharnagl H, et al. Association between Lp-PLA2 and coronary artery disease: focus on its relationship with lipoproteins and markers of inflammation and hemostasis. *Atherosclerosis.* (2005) 182:181–8. doi: 10.1016/j.atherosclerosis.2004.10.046
88. Holm S, Ueland T, Dahl TB, Michelsen AE, Skjelland M, Russell D, et al. Fatty acid binding protein 4 is associated with carotid atherosclerosis and

outcome in patients with acute ischemic stroke. *PLoS ONE.* (2011) 6:e28785. doi: 10.1371/journal.pone.0028785
89. Egbuche O, Biggs ML, Ix JH, Kizer JR, Lyles MF, Siscovick DS, et al. Fatty acid binding protein-4 and risk of cardiovascular disease: the cardiovascular health study. *J Am Heart Assoc.* (2020) 9:e014070. doi: 10.1161/JAHA.119.014070
90. Ghorbani A, Bhambhani V, Christenson RH, Meijers WC, de Boer RA, Levy D, et al. Longitudinal change in galectin-3 and incident cardiovascular outcomes. *J Am Coll Cardiol.* (2018) 72:3246–54. doi: 10.1016/j.jacc.2018.09.076
91. Kadoglou NP, Sfyroeras GS, Spathis A, Gkekas C, Gastounioti A, Mantas G, et al. Galectin-3, carotid plaque vulnerability, and potential effects of statin therapy. *Eur J Vasc Endovasc Surg.* (2015) 49:4–9. doi: 10.1016/j.ejvs.2014.10.009
92. Si W, He P, Wang Y, Fu Y, Li X, Lin X, et al. Complement complex C5b-9 levels are associated with the clinical outcomes of acute ischemic stroke and carotid plaque stability. *Transl Stroke Res.* (2019) 10:279–86. doi: 10.1007/s12975-018-0658-3
93. Maksimowicz-McKinnon K, Magder LS, Petri M. Predictors of carotid atherosclerosis in systemic lupus erythematosus. *J Rheumatol.* (2006) 33:2458–63.
94. Reynolds HR, Buyon J, Kim M, Rivera TL, Izmirly P, Tunick P, et al. Association of plasma soluble E-selectin and adiponectin with carotid plaque in patients with systemic lupus erythematosus. *Atherosclerosis.* (2010) 210:569–74. doi: 10.1016/j.atherosclerosis.2009.12.007
95. Ammirati E, Moroni F, Norata GD, Magnoni M, Camici PG. Markers of inflammation associated with plaque progression and instability in patients with carotid atherosclerosis. *Mediators Inflamm.* (2015) 2015:718329. doi: 10.1155/2015/718329
96. Nakagomi A, Shibui T, Kohashi K, Kosugi M, Kusama Y, Atarashi H, et al. Differential effects of atorvastatin and pitavastatin on inflammation, insulin resistance, and the carotid intima-media thickness in patients with dyslipidemia. *J Atheroscler Thromb.* (2015) 22:1158–71. doi: 10.5551/jat.29520
97. Bian L, Xia L, Wang Y, Jiang J, Zhang Y, Li D, et al. Risk factors of subclinical atherosclerosis and plaque burden in high risk individuals: results from a community-based study. *Front Physiol.* (2018) 9:739. doi: 10.3389/fphys.2018.00739
98. Johnsen SH, Mathiesen EB, Fosse E, Joakimsen O, Stensland-Bugge E, Njolstad I, et al. Elevated high-density lipoprotein cholesterol levels are protective against plaque progression: a follow-up study of 1952 persons with carotid atherosclerosis the Tromso study. *Circulation.* (2005) 112:498–504. doi: 10.1161/CIRCULATIONAHA.104.522706
99. El Khoudary SR, Ceponiene I, Samargandy S, Stein JH, Li D, Tattersall MC, et al. HDL (high-density lipoprotein) metrics and atherosclerotic risk in women. *Arterioscler Thromb Vasc Biol.* (2018) 38:2236–44. doi: 10.1161/ATVBAHA.118.311017
100. Tiozzo E, Gardener H, Hudson BI, Dong C, Della-Morte D, Crisby M, et al. High-density lipoprotein subfractions and carotid plaque: the Northern Manhattan Study. *Atherosclerosis.* (2014) 237:163–8. doi: 10.1016/j.atherosclerosis.2014.09.002
101. Aroner SA, Koch M, Mukamal KJ, Furtado JD, Stein JH, Tattersall MC, et al. High-density lipoprotein subspecies defined by apolipoprotein C-III and subclinical atherosclerosis measures: MESA (the multi-ethnic study of atherosclerosis). *J Am Heart Assoc.* (2018) 7:e007824. doi: 10.1161/JAHA.117.007824
102. Shea S, Stein JH, Jorgensen NW, McClelland RL, Tascau L, Shrager S, et al. Cholesterol mass efflux capacity, incident cardiovascular disease, and progression of carotid plaque. *Arterioscler Thromb Vasc Biol.* (2019) 39:89–96. doi: 10.1161/ATVBAHA.118.311366
103. Ma H, Lin H, Hu Y, Li X, He W, Jin X, et al. Relationship between non-high-density lipoprotein cholesterol and carotid atherosclerosis in normotensive and euglycemic Chinese middle-aged and elderly adults. *Lipids Health Dis.* (2017) 16:55. doi: 10.1186/s12944-017-0451-4
104. Liu Y, Zhang Z, Xia B, Wang L, Zhang H, Zhu Y, et al. Relationship between the non-HDLc-to-HDLc ratio and carotid plaques in a high stroke risk population: a cross-sectional study in China. *Lipids Health Dis.* (2020) 19:168. doi: 10.1186/s12944-020-01344-1
105. Mach F, Baigent C, Catapano AL, Koskinas KC, Casula M, Badimon L, et al. 2019 ESC/EAS guidelines for the management of dyslipidaemias: lipid modification to reduce cardiovascular risk. *Eur Heart J.* (2020) 41:111–88. doi: 10.15829/1560-4071-2020-3826
106. Matthews KA, El Khoudary SR, Brooks MM, Derby CA, Harlow SD, Barinas-Mitchell EJ, et al. Lipid changes around the final menstrual period predict carotid subclinical disease in postmenopausal women. *Stroke.* (2017) 48:70–6. doi: 10.1161/STROKEAHA.116.014743
107. Gao S, Zhao D, Qi Y, Wang W, Wang M, Sun J, et al. Circulating oxidized low-density lipoprotein levels independently predict 10-year progression of subclinical carotid atherosclerosis: a community-based cohort study. *J Atheroscler Thromb.* (2018) 25:1032–43. doi: 10.5551/jat.43299
108. Amarenco P, Hobeanu C, Labreuche J, Charles H, Giroud M, Meseguer E, et al. Carotid atherosclerosis evolution when targeting a low-density lipoprotein cholesterol concentration <70 mg/dL after an ischemic stroke of atherosclerotic origin. *Circulation.* (2020) 142:748–57. doi: 10.1161/CIRCULATIONAHA.120.046774
109. Cosentino F, Grant PJ, Aboyans V, Bailey CJ, Ceriello A, Delgado V, et al. 2019 ESC Guidelines on diabetes, pre-diabetes, cardiovascular diseases developed in collaboration with the EASD. *Eur Heart J.* (2020) 41:255–323.
110. Vigili de Kreutzenberg S, Fadini GP, Guzzinati S, Mazzucato M, Volpi A, Coracina A, et al. Carotid plaque calcification predicts future cardiovascular events in type 2 diabetes. *Diabetes Care.* (2015) 38:1937–44. doi: 10.2337/dc15-0327
111. Castelblanco E, Betriu A, Hernandez M, Granado-Casas M, Ortega E, Soldevila B, et al. Ultrasound tissue characterization of carotid plaques differs between patients with type 1 diabetes and subjects without diabetes. *J Clin Med.* (2019) 8:424. doi: 10.3390/jcm8040424
112. Hernandez M, Lopez C, Real J, Valls J, Ortega-Martinez de Victoria E, Vazquez F, et al. Preclinical carotid atherosclerosis in patients with latent autoimmune diabetes in adults (LADA), type 2 diabetes and classical type 1 diabetes. *Cardiovasc Diabetol.* (2017) 16:94. doi: 10.1186/s12933-017-0576-9
113. Botvin Moshe C, Haratz S, Ravona-Springer R, Heymann A, Hung-Mo L, Schnaider Beeri M, et al. Long-term trajectories of BMI predict carotid stiffness and plaque volume in type 2 diabetes older adults: a cohort study. *Cardiovasc Diabetol.* (2020) 19:138. doi: 10.1186/s12933-020-01104-6
114. Seo DH, Kim SH, Song JH, Hong S, Suh YJ, Ahn SH, et al. Presence of carotid plaque is associated with rapid renal function decline in patients with type 2 diabetes mellitus and normal renal function. *Diabetes Metab J.* (2019) 43:840–53. doi: 10.4093/dmj.2018.0186
115. Alonso N, Traveset A, Rubinat E, Ortega E, Alcubierre N, Sanahuja J, et al. Type 2 diabetes-associated carotid plaque burden is increased in patients with retinopathy compared to those without retinopathy. *Cardiovasc Diabetol.* (2015) 14:33. doi: 10.1186/s12933-015-0196-1
116. Whelton PK, Carey RM, Aronow WS, Casey DE Jr, Collins KJ, Dennison Himmelfarb C, et al. 2017 ACC/AHA/AAPA/ABC/ACPM/AGS/APhA/ASH/ASPC/NMA/PCNA guideline for the prevention, detection, evaluation, and management of high blood pressure in adults: executive summary: a report of the American College of Cardiology/American Heart Association Task Force on Clinical Practice Guidelines. *Hypertension.* (2018) 71:1269–324. doi: 10.1161/HYP.0000000000000065
117. Vigen T, Ihle-Hansen H, Lyngbakken MN, Berge T, Thommessen B, Ihle-Hansen H, et al. Blood pressure at age 40 predicts carotid atherosclerosis two decades later: data from the Akershus Cardiac Examination 1950 Study. *J Hypertens.* (2019) 37:1982–90. doi: 10.1097/HJH.0000000000002131
118. Kawai T, Ohishi M, Takeya Y, Onishi M, Ito N, Oguro R, et al. Carotid plaque score and intima media thickness as predictors of stroke and mortality in hypertensive patients. *Hypertens Res.* (2013) 36:902–9. doi: 10.1038/hr.2013.61
119. Chen Z, Wang F, Zheng Y, Zeng Q, Liu H. H-type hypertension is an important risk factor of carotid atherosclerotic plaques. *Clin Exp Hypertens.* (2016) 38:424–8. doi: 10.3109/10641963.2015.1116547
120. Ben Z, Wang J, Zhan J, Li X, Ruan H, Chen S. Characteristics of the carotid plaque in hypertensive patients with hyperhomocysteinemia using multimode ultrasound. *J Stroke Cerebrovasc Dis.* (2020) 29:104925. doi: 10.1016/j.jstrokecerebrovasdis.2020.104925

121. Yang D, Iyer S, Gardener H, Della-Morte D, Crisby M, Dong C, et al. Cigarette smoking and carotid plaque echodensity in the Northern Manhattan study. *Cerebrovasc Dis.* (2015) 40:136–43. doi: 10.1159/000434761
122. Walker TJ, Heredia NI, Lee M, Laing ST, Fisher-Hoch SP, McCormick JB, et al. The combined effect of physical activity and sedentary behavior on subclinical atherosclerosis: a cross-sectional study among Mexican Americans. *BMC Public Health.* (2019) 19:161. doi: 10.1186/s12889-019-6439-4
123. Wang D, Karvonen-Gutierrez CA, Jackson EA, Elliott MR, Appelhans BM, Barinas-Mitchell E, et al. Western dietary pattern derived by multiple statistical methods is prospectively associated with subclinical carotid atherosclerosis in midlife women. *J Nutr.* (2020) 150:579–91. doi: 10.1093/jn/nxz270
124. Thurston RC, Chang Y, von Kanel R, Barinas-Mitchell E, Jennings JR, Hall MH, et al. Sleep characteristics and carotid atherosclerosis among midlife women. *Sleep.* (2017) 40:zsw052. doi: 10.1093/sleep/zsw052
125. Sugiura T, Dohi Y, Takagi Y, Yoshikane N, Ito M, Suzuki K, et al. Impacts of lifestyle behavior and shift work on visceral fat accumulation and the presence of atherosclerosis in middle-aged male workers. *Hypertens Res.* (2020) 43:235–45. doi: 10.1038/s41440-019-0362-z
126. Zhao YY, Javaheri S, Wang R, Guo N, Koo BB, Stein JH, et al. Associations between sleep apnea and subclinical carotid atherosclerosis: the multi-ethnic study of atherosclerosis. *Stroke.* (2019) 50:3340–6. doi: 10.1161/STROKEAHA.118.022184
127. Wang LY, Zhu YN, Cui JJ, Yin KQ, Liu SX, Gao YH. Subclinical atherosclerosis risk markers in patients with chronic obstructive pulmonary disease: a systematic review and meta-analysis. *Respir Med.* (2017) 123:18–27. doi: 10.1016/j.rmed.2016.12.004
128. Pan J, Xu L, Cai SX, Jiang CQ, Cheng KK, Zhao HJ, et al. The association of pulmonary function with carotid atherosclerosis in older Chinese: Guangzhou Biobank Cohort Study-CVD Subcohort. *Atherosclerosis.* (2015) 243:469–76. doi: 10.1016/j.atherosclerosis.2015.09.036
129. Spence JD, Barnett PA, Bulman DE, Hegele RA. An approach to ascertain probands with a non-traditional risk factor for carotid atherosclerosis. *Atherosclerosis.* (1999) 144:429–34. doi: 10.1016/S0021-9150(99)00003-9
130. Salonen R, Seppänen K, Rauramaa R, Salonen JT. Prevalence of carotid atherosclerosis and serum cholesterol levels in eastern Finland. *Arteriosclerosis.* (1988) 8:788–92. doi: 10.1161/01.ATV.8.6.788
131. Mannami T, Konishi M, Baba S, Nishi N, Terao A. Prevalence of asymptomatic carotid atherosclerotic lesions detected by high-resolution ultrasonography and its relation to cardiovascular risk factors in the general population of a Japanese city: the Suita study. *Stroke.* (1997) 28:518–25. doi: 10.1161/01.STR.28.3.518
132. Rundek T, Blanton SH, Bartels S, Dong C, Raval A, Demmer RT, et al. Traditional risk factors are not major contributors to the variance in carotid intima-media thickness. *Stroke.* (2013) 44:2101–8. doi: 10.1161/STROKEAHA.111.000745
133. Kuo F, Gardener H, Dong C, Cabral D, Della-Morte D, Blanton SH, et al. Traditional cardiovascular risk factors explain the minority of the variability in carotid plaque. *Stroke.* (2012) 43:1755–60. doi: 10.1161/STROKEAHA.112.651059
134. Noflatscher M, Schreinlechner M, Sommer P, Kerschbaum J, Berggren K, Theurl M, et al. Influence of traditional cardiovascular risk factors on carotid and femoral atherosclerotic plaque volume as measured by three-dimensional ultrasound. *J Clin Med.* (2018) 8:32. doi: 10.3390/jcm8010032
135. Wang D, Jackson EA, Karvonen-Gutierrez CA, Elliott MR, Harlow SD, Hood MM, et al. Healthy lifestyle during the midlife is prospectively associated with less subclinical carotid atherosclerosis: the study of women's health across the nation. *J Am Heart Assoc.* (2018) 7:e010405. doi: 10.1161/JAHA.118.010405
136. Li H, Xu X, Lu L, Sun R, Guo Q, Chen Q, et al. The comparative impact among different intensive statins and combination therapies with niacin/ezetimibe on carotid intima-media thickness: a systematic review, traditional meta-analysis, and network meta-analysis of randomized controlled trials. *Eur J Clin Pharmacol.* (2021) 77:1133–45. doi: 10.1007/s00228-021-03113-0
137. Ebbesson SO, Roman MJ, Devereux RB, Kaufman D, Fabsitz RR, Maccluer JW, et al. Consumption of omega-3 fatty acids is not associated with a reduction in carotid atherosclerosis: the Genetics of Coronary Artery Disease in Alaska Natives study. *Atherosclerosis.* (2008) 199:346–53. doi: 10.1016/j.atherosclerosis.2007.10.020
138. Joakimsen O, Bonaa KH, Stensland-Bugge E, Jacobsen BK. Age and sex differences in the distribution and ultrasound morphology of carotid atherosclerosis: the Tromsø Study. *Arteriosclerosis Thromb Vasc Biol.* (1999) 19:3007–13. doi: 10.1161/01.ATV.19.12.3007
139. Goff DC Jr, Lloyd-Jones DM, Bennett G, Coady S, D'Agostino RB, Gibbons R, et al. 2013 ACC/AHA guideline on the assessment of cardiovascular risk: a report of the American college of cardiology/American heart association task force on practice guidelines. *Circulation.* (2014) 129:S49–73. doi: 10.1161/01.cir.0000437741.48606.98

Conflict of Interest: The authors declare that the research was conducted in the absence of any commercial or financial relationships that could be construed as a potential conflict of interest.

Publisher's Note: All claims expressed in this article are solely those of the authors and do not necessarily represent those of their affiliated organizations, or those of the publisher, the editors and the reviewers. Any product that may be evaluated in this article, or claim that may be made by its manufacturer, is not guaranteed or endorsed by the publisher.

Copyright © 2021 Li, Xu, Luo and Zhang. This is an open-access article distributed under the terms of the Creative Commons Attribution License (CC BY). The use, distribution or reproduction in other forums is permitted, provided the original author(s) and the copyright owner(s) are credited and that the original publication in this journal is cited, in accordance with accepted academic practice. No use, distribution or reproduction is permitted which does not comply with these terms.

frontiers in Cardiovascular Medicine

ORIGINAL RESEARCH
published: 07 September 2021
doi: 10.3389/fcvm.2021.731730

Development and Validation of a Nomogram to Predict the 180-Day Readmission Risk for Chronic Heart Failure: A Multicenter Prospective Study

*Shanshan Gao[1], Gang Yin[2], Qing Xia[2], Guihai Wu[1], Jinxiu Zhu[1], Nan Lu[1], Jingyi Yan[1] and Xuerui Tan[1]**

[1] Clinical Research Center, The First Affiliated Hospital of Shantou University Medical College (SUMC), Cardiology, Shantou, China, [2] Heart Failure center, Qingdao Central Hospital, Cardiology, Qingdao, China

Background: The existing prediction models lack the generalized applicability for chronic heart failure (CHF) readmission. We aimed to develop and validate a widely applicable nomogram for the prediction of 180-day readmission to the patients.

Methods: We prospectively enrolled 2,980 consecutive patients with CHF from two hospitals. A nomogram was created to predict 180-day readmission based on the selected variables. The patients were divided into three datasets for development, internal validation, and external validation (mean age: 74.2 ± 14.1, 73.8 ± 14.2, and 71.0 ± 11.7 years, respectively; sex: 50.2, 48.8, and 55.2% male, respectively). At baseline, 102 variables were submitted to the least absolute shrinkage and selection operator (Lasso) regression algorithm for variable selection. The selected variables were processed by the multivariable Cox proportional hazards regression modeling combined with univariate analysis and stepwise regression. The model was evaluated by the concordance index (C-index) and calibration plot. Finally, the nomogram was provided to visualize the results. The improvement in the regression model was calculated by the net reclassification index (NRI) (with tenfold cross-validation and 200 bootstraps).

Results: Among the selected 2,980 patients, 1,696 (56.9%) were readmitted within 180 days, and 1,502 (50.4%) were men. A nomogram was established by the results of Lasso regression, univariate analysis, stepwise regression and multivariate Cox regression, as well as variables with clinical significance. The values of the C-index were 0.75 [95% confidence interval (CI): 0.72–0.79], 0.75 [95% CI: 0.69–0.81], and 0.73 [95% CI: 0.64–0.83] for the development, internal validation, and external validation datasets, respectively. Calibration plots were provided for both the internal and external validation sets. Five variables including history of acute heart failure, emergency department visit, age, blood urea nitrogen level, and beta blocker usage were considered in the final prediction model. When adding variables involving hospital discharge way, alcohol taken and left bundle branch block, the calculated values of NRI demonstrated no significant improvements.

OPEN ACCESS

Edited by:
Yuli Huang,
Southern Medical University, China

Reviewed by:
Enfa Zhao,
The First Affiliated Hospital of Xi'an Jiaotong University, China
Ruisheng Liu,
University of South Florida, United States

***Correspondence:**
Xuerui Tan
doctortxr@126.com

Specialty section:
This article was submitted to General Cardiovascular Medicine, a section of the journal Frontiers in Cardiovascular Medicine

Received: *28 June 2021*
Accepted: *09 August 2021*
Published: *07 September 2021*

Citation:
Gao S, Yin G, Xia Q, Wu G, Zhu J, Lu N, Yan J and Tan X (2021) Development and Validation of a Nomogram to Predict the 180-Day Readmission Risk for Chronic Heart Failure: A Multicenter Prospective Study. Front. Cardiovasc. Med. 8:731730. doi: 10.3389/fcvm.2021.731730

Conclusions: A nomogram for the prediction of 180-day readmission of patients with CHF was developed and validated based on five variables. The proposed methodology can improve the accurate prediction of patient readmission and have the wide applications for CHF.

Keywords: chronic heart failure, readmission, hospitalization, nomogram, prediction model

INTRODUCTION

It is well-known that chronic heart failure (CHF) is a systemic clinical syndrome as well as an endpoint stage of various cardiovascular diseases with typical symptoms of systolic and/or diastolic dysfunction. In recent years, existing treatments are effective in reversing the progression to end-stage disease among patients diagnosed with CHF; however, the mortality and readmission rates are still high (1). To better address these issues, many experts and clinical physicians have committed to identifying a prognostic model of CHF in its early stages (2).

In developed countries, some physicians in the United States focus on the 30-day readmission rate (3, 4), thus leading to the investigation on the readmission rate in patients with CHF (5), which usually reflects the 30-day all-cause readmission or cardiovascular outcomes (6). However, the focus varies in developing countries (7). The existing readmission models of heart failure (HF) have been established and widely used in different regions of China, including the standard model developed by Tan et al. (8) and two models restricted to the northern cities of China (9, 10). Given the delay in the treatment of patients, the 180-day readmission time seems more suitable for patients in developing countries (11, 12). Based on these studies, we can conclude that readmission rates vary from 34.9 to 56.4%, and most of the state-of-the-art models are derived from single-center studies consisting of a large sample of patients admitted in the hospital, which usually lack general applicability in real-world clinical diagnoses. The objective of this study is to establish a widely applicable 180-day readmission nomogram for patients with CHF in North and South China.

MATERIALS AND METHODS

The flowchart of the selection of patients for the multicenter prospective cohort study is depicted in **Figure 1**. First, the collected samples from a medical center of North China were divided into development and internal validation databases, and then a nomogram was proposed for the research works. Second, the models were evaluated by using an interval validation set. Third, the data provided by a medical center in South China were used for external validation. Following the steps mentioned above, it is natural for us to develop effective methods.

Study Population

We selected patients hospitalized for CHF between January 2019 and June 2019 at two centers, where one was a North China center of HF (Qingdao Central Hospital) and the other was a South China center of HF (The First Affiliated Hospital of Shantou University Medical College). The patients would be enrolled if they met the following criteria: patients with CHF and diagnosed with various etiologies, New York Heart Association (NYHA) class II–IV, and age >18 years. Moreover, the exclusion criteria were as follows: planned HF readmission within 6 months (patients who had hospitalization plan within 6 months were excluded), missing data for the essential variables and outcomes (patients missing 30% or more variables will be excluded), severe patients with liver and kidney dysfunction and/or malignant tumors, and poorer treatment compliance (i.e., difficult to follow up). Severe liver dysfunction is defined as an alanine aminotransferase level more than twice that of normal or Budd–Chiari grade C. Severe renal dysfunction is defined as chronic kidney disease stage V. As per the above indicators, the definitions are provided in further studies.

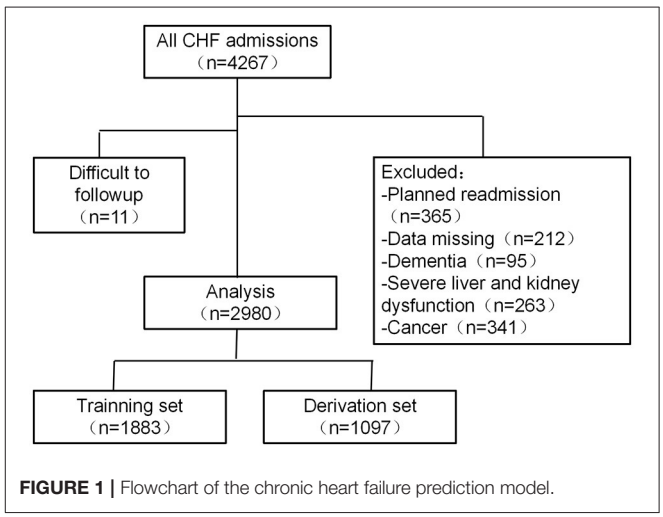

FIGURE 1 | Flowchart of the chronic heart failure prediction model.

It should be stressed that this study was approved by the ethics committee (KY-2018046, No. 2019129) of each chosen hospital and was also conducted in accordance with the Declaration of Helsinki (ChiCTR1800019869). Furthermore, the participants from both hospitals provided informed written consent for supporting the clinical research studies.

Predictors

In this study, the main predictors include sociodemographics, clinical characteristics, comorbidities, results of laboratory tests (blood sample assay), other relevant physical examinations, medication usages in the hospital and at discharge, and other treatment measures. In detail, the sociodemographics contain basic information, such as age, sex, the distance between

the hospital and residence, length of hospital stay, medical social insurance status, and other variables associated with readmission. In addition, we collected some samples in the progress of treatments, as detailed as possible, and selected the features that corresponded to the prognosis of the disease. Among these predictors, comorbidities, complications, and Charlson comorbidity index (CCI) (13) were recorded for each patient.

Definitions

The diagnosis of CHF is based on the 2016 ESC Guideline for HF management, and patients were diagnosed by two experienced cardiologists in each HF center (1). The 180-day cardiovascular readmission is defined as 180-day unplanned readmission, registered in the same HF center as the index hospitalization (when HF worsens, the patients will be transferred from the community hospital to the nearest HF center). It should be mentioned that estimated glomerular filtration rate (eGFR), as a baseline indicator, reflects the filtration function of the kidney and mortality due to heart failure with preserved ejection fraction (HFpEF) (14). In the numerical results, eGFR is calculated by the Chronic Kidney Disease Epidemiology Collaboration formulas shown below:

$$\text{eGFR} = 141 \times \min(Cr/k,1)^{\alpha} \times \max(Cr/k,1)^{-1.209} \times 0.993^{\text{Age}} \times 1.018(\text{Female}) \times 1.159\ (\text{Black}),$$

where k = 0.7 (Female) or 0.9 (Male), α= -0.329(Female) or -0.411 (Male), Cr = plasma creatinine

(mg/dl)

1 mg/dl = 88.4 μmol/l (15).

Model Development Cohorts

The prediction model for CHF can be established according to the statements in the transparent reporting of a multivariable prediction model for individual prognosis (TRIPOD) guidelines (16), where we use the data samples from a prospective cohort study at the HF center of Qingdao Central Hospital. To satisfy the study requirements, we identified 2,687 consecutive patients with HF and then randomly divided them into development and validation cohorts by virtue of a ratio of 7:3. The development cohort (comprising 1,883 patients, i.e., 70% of the Qingdao Central Hospital cohort) was used for the model development.

Model Validation Cohorts

In addition to the internal validation cohorts (comprising 804 patients, i.e., 30% of the Qingdao Central Hospital cohort), an external validation cohort (comprising 293 patients) was developed from a prospective study at the First Affiliated Hospital of Medical College in Shantou University. Based on the development and validation cohorts, numerical comparisons will be provided by the proposed methodology.

Outcome

The primary outcome is unplanned HF readmission within 180 days after the first admission for the referred patients. They are collected from both centers mentioned above, and they are followed up for 180 days after discharge from the index admissions. To better track the patients, we adopted the way by telephoning the interviews and further verified their conditions by virtue of the hospital system.

Statistical Analysis

We provide the numerical comparisons for the continuous variables, which are described as the mean ± standard deviation. Meanwhile, categorical variables are described as percentages or frequencies. Continuous variables are divided into categorical variables based on the results of restricted cubic spline according to data distribution and its clinical implications and boundaries (**Figures 2A–D**). Hazard ratios (HRs) are expressed as 95% confidence interval (CI). The least absolute shrinkage and selection operator (Lasso) regression-based mathematical model would be considered to screen the variables, and the multivariate Cox regression analysis is presented to generate a prediction model for patients with CHF. Meanwhile, taking the results of univariate Cox and stepwise regression into consideration, they are combined with clinical significance. The improvement of the model is evaluated by net reclassification improvement (NRI) (17) when adding variables to the model. The involved variables with missing values are <30% of the development population, and they are selected to enter into the Lasso and Cox regression models for further analysis. To make comparisons, 10-fold cross-validation operations are presented in the model development set. Finally, the missing values are imputed through multiple imputation in the statistical analysis.

In the numerical verification, both internal and external comparisons are conducted for the desired expectations. The concordance index (C-index), with 200 bootstrap samples, and the calibration plot are considered to evaluate the prediction accuracy as well as test the consistency of the prediction model, respectively. Besides this, the NRI is provided to compare the different models in the numerical experiments. All of the statistical analyses are conducted using SPSS version 25.0 (IBM Corp., Armonk, NY) and the R Project package for statistical computing (www.cran.r-project.org/version 3.6.1) on a personal computer.

RESULTS

Baseline Characteristics

A total of 2,980 patients were enrolled between January 2019 and June 2019. The baseline characteristics of the patients are shown in **Table 1**. In the entire cohort, 1,696 (56.9%) patients were readmitted within 180 days. The 180-day readmission rates were 59.0% (1,112 patients), 54.1% (435 patients), and 51.2% (150 patients) in the development, internal validation, and external validation cohorts, respectively. The mean ages were 74.2 ± 14.1 years in the development cohort, 73.8 ± 14.2 years in

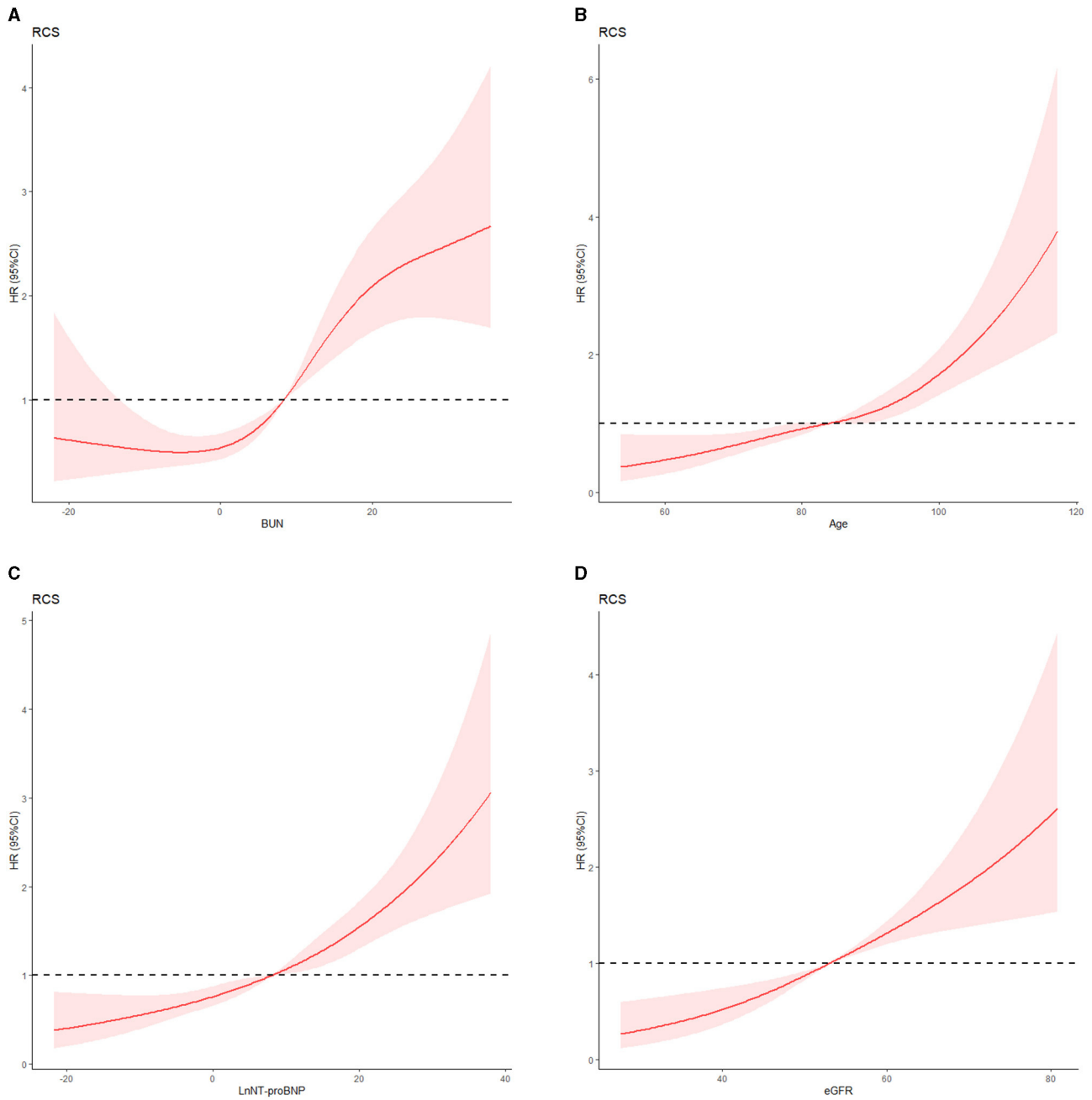

FIGURE 2 | (A) Blood urea nitrogen level and 180-day heart failure readmission risk. **(B)** Age and 180-day heart failure readmission risk. **(C)** Natural logarithm of plasma N-terminal pro-B-type natriuretic peptide (LnNT-proBNP) and 180-day heart failure readmission risk. **(D)** Estimated glomerular filtration rate and 180-day heart failure readmission risk. We used a three-level classification of BUN, eGFR, and LnNT-proBNP and five-level classification of age according to the results of restricted cubic spline and clinical meanings.

the internal validation cohort, and 71.0 ± 11.7 years in the external validation cohort. Male patients accounted for 50.4% (1,502) of the patients in the entire cohort; 1,345 (45.1%) had coronary heart disease and 1,795 (60.2%) had a history of acute heart failure (AHF). The proportion of HFrEF is 31.3%, both in the development set and internal validation set. In the external validation set, the rate is 12.9%. Based on previously published data, patients with HFpEF and patients with HFrEF often have similar predictors (18). Consequently, they are all included in our study. We made a collinearity diagnosis of prediction variables at baseline and excluded the variables with no clinical significance and correlation coefficient >0.7.

TABLE 1 | Baseline characteristics of the enrolled patients with CHF.

Characteristic	Development set (*n* = 1,883)	Internal vad (*n* = 804)	External vad (*n* = 293)	*P*-Value
Age, years (mean ± SD)	74.2 ± 14.1	73.8 ± 14.2	71.0 ± 11.7	0.089
Gender: Male, *n* (%)	947 (50.2%)	393 (48.8%)	162 (55.2%)	0.169
HFrEF, *n* (%)	590 (31.3%)	252 (31.3%)	38 (12.9%)	<0.01
SBP (mmHg), mean ± SD	148 ± 17	132 ± 7	147 ± 33	<0.01
DBP (mmHg), mean ± SD	81 ± 8	76 ± 2	89 ± 13	<0.01
Remoteness (<5 km), *n* (%)	1,653 (87.8%)	713 (88.6%)	142 (48.4%)	<0.01
Hospital stay (day), mean ± SD	15 ± 5	12 ± 2	5 ± 2	<0.01
CHD, *n* (%)	898 (47.6%)	376 (46.7%)	71 (24.2%)	<0.01
AHF, *n* (%)	1,204 (63.9%)	484 (60.1%)	107 (36.5%)	<0.01
Hypertension, *n* (%)	1,547 (82.1%)	658 (81.8%)	256 (87.3%)	0.07
Diabetes, *n* (%)	716 (38.0%)	310 (38.5%)	115 (39.2%)	<0.01
Alcohol consumption, *n* (%)	354 (18.7%)	150 (18.6%)	18 (6.1%)	<0.01
Smoker, *n* (%)	363 (19.2%)	157 (19.5%)	64 (21.8%)	0.433
COPD, *n* (%)	179 (9.5%)	60 (7.4%)	32 (10.9%)	0.146
Pulmonary infection (not COVID-19), *n* (%)	220 (11.6%)	81 (10%)	67 (22.8%)	<0.01
AF, *n* (%)	709 (37.6%)	275 (34.2%)	73 (24.9%)	<0.01
CCI, mean ± SD	4.0 ± 0.5	4.5 ± 1.5	4.5 ± 0.5	<0.01
Stroke, *n* (%)	200 (10.6%)	118 (14.6%)	47 (16.0%)	0.076
Hypertensive heart disease, *n* (%)	805 (42.7%)	318 (39.5%)	85 (29.0%)	<0.01
Hyperthyroidism, *n* (%)	56 (2.9%)	23 (2.8%)	6 (2.0%)	0.07
Hyperkalemia, *n* (%)	105 (5.5%)	35 (4.3%)	9 (3.0%)	0.292
WBC (*10∧9/L), mean ± SD	6.0 ± 1.02	6.7 ± 0.5	4.2 ± 2.73	0.012
RBC (*10∧12/L), mean ± SD	4.0 ± 0.5	5.2 ± 0.7	4.1 ± 0.2	<0.01
Hemoglobin (g/L), mean ± SD	144 ± 4	127 ± 6	119 ± 19	<0.01
RDW-CV (%)	13.6 ± 1.1	9.9 ± 1.0	16.7 ± 0.8	<0.01
Glucose (mmol/L), mean ± SD	9.6 ± 0.5	4.7 ± 0.1	8.7 ± 3.6	<0.01
Serum sodium (mmol/L), mean ± SD	140 ± 4	142 ± 3	135 ± 7.9	<0.01
Serum potassium (mmol/L), mean ± SD	3.9 ± 0.8	4.3 ± 0.1	4.1 ± 0.1	<0.01
TC (mmol/L), mean ± SD	4.52 ± 1.51	3.75 ± 0.54	1.5 ± 0.3	<0.01
NTproBNP (pg/mL), mean ± SD	8,720 ± 4,914	9,669 ± 9,479	500	<0.01
eGFR (mL/min/1.73 m^2), mean ± SD	34 ± 9	57 ± 31	46 ± 3	<0.01
Creatinine (μmol/L), mean ± SD	82 ± 3	203 ± 74	109 ± 4	<0.01
BUN (mmol/L), mean ± SD	12.9 ± 5.5	8.0 ± 0.8	7.2 ± 0.6	<0.01
CysC (mg/L), mean ± SD	0.8 ± 0.1	1.1 ± 0.3	1.31	0.037
UA (μmol/L), mean ± SD	330 ± 117	323 ± 167	382 ± 66	<0.01
Albumin (g/L), mean ± SD	44 ± 7	37 ± 9	32.8 ± 6.9	<0.01
ACEI, *n* (%)	336 (17.8%)	157 (19.5%)	76 (25.9%)	<0.01
ARB, *n* (%)	962 (51.0%)	403 (50.1%)	106 (36.1%)	<0.01
Beta-blocker, *n* (%)	1,216 (64.5%)	531 (66%)	134 (45.7%)	<0.01
Diuretic, *n* (%)	1,362 (72.3%)	572 (71.1%)	148 (50.5%)	<0.01
MRA, *n* (%)	1,605 (85.2)	683 (84.9%)	127 (43.3%)	<0.01
ARNI, *n* (%)	585 (31%)	244 (30.3%)	12 (4.0%)	<0.01
Anti-PLT medication, *n* (%)	1,193 (63.3%)	537 (66.7%)	77 (26.2%)	<0.01
CCB, *n* (%)	587 (31.1%)	257 (31.9%)	169 (57.6%)	<0.01
Antidiabetic drugs, *n* (%)	578 (30.6%)	243 (30.2%)	88 (30.0%)	0.955
Statin, *n* (%)	602 (31.9%)	271 (33.7%)	153 (52.2%)	<0.01
QRS duration, mean ± SD	97.2 ± 29.1	118.6 ± 17.0	73 ± 7	0.292
LVEDD (mm), mean ± SD	45 ± 5	58 ± 5	53 ± 7	<0.01

ACEI, angiotensin-converting enzyme inhibitor; AF, atrial fibrillation; AHF, acute heart failure; ARB, angiotensin receptor blocker; ARNI, angiotensin receptor enkephalinase inhibitor; BUN, blood urea nitrogen; CCB, calcium channel blockers; CCI, Charlson comorbidity index; CHD, coronary heart disease; COPD, chronic obstructive pulmonary disease; CysC, Cystatin C; DBP, diastolic blood pressure; eGFR, estimated glomerular filtration rate; External Vad, external validation set; Glu, fasting glucose; HFrEF, heart failure with reduced ejection fraction; Hospital stay, length of hospital stay; Internal Vad, internal validation set; LVEDD, Left ventricular end diastolic diameter; MRA, mineralocorticoid receptor antagonist; NT-proBNP, N-terminal pro brain natriuretic peptide; SBP, systolic blood pressure; RDW-CV, coefficient of variation in red blood cell distribution width; Remoteness, distance of residence from hospital; TC, total cholesterol; UA, uric acid.

Lasso and Cox Regression for Model Development

The model is developed from 102 variables by screening with the Lasso–Cox regression algorithm. The most prominent advantage of Lasso regression is that it penalizes the coefficients of all variables by regression and makes the relatively unimportant independent variable coefficients zero by the regularization technique. Therefore, when we use Lasso regression, we have retained the punitive and inhibited the collinearity. Results of Lasso regression are shown in **Figure 3** [Lasso regression (**A**) and cross-validation (**B**) results].

The five selected variables consisted of AHF, emergency department visit (emergency), eGFR, N-terminal pro-B-type natriuretic peptide (NT-proBNP) and blood urea nitrogen (BUN) level. It supported the proportional risk hypothesis ($p > 0.05$): the p-values for AHF, BUN, emergency, eGFR, and NT-proBNP were 0.77, 0.27, 0.38, 0.79, and 0.88, respectively. They were identified as independently associated with the 180-day HF readmission. The results of collinearity diagnosis of the five selected variables are shown in the **Table 2**. The variance inflation factors are all <10, and the five selected factors preserved very weak multicollinearity.

At the same time, we combined the results with univariate Cox analysis and stepwise regression to avoid missing variables that were clinically significant. According to the results of univariate analysis and stepwise regression, 24 variables were selected from 102 baseline variables, and 24 variables were allocated to five groups (the group was divided into five groups according to the Lasso–Cox result) according to the model inclusion principle of clinical significance (16). In each group, we identified variables with low correlation. They were age ($r = 0.137$), β-blocker usage ($r = -0.141$), hospital discharge way ($r = 0.136$), alcohol taken ($r = 0.131$), and left bundle branch block ($r = 0.097$).

NRI (17) was assessed to evaluate the value of adding the additional clinical variables to the model. NRI showed a significant improvement: 18.5% (95% CI 10.3% to 24.4%) in the development set, 8.2% (95% CI 4.2% to 10.9%) in the internal validation set, and 6.3% (95% CI 2.2% to 7.8%) in the external validation set when adding variables of age and β-blocker. The new model (AHF + emergency + BUN + NT-proBNP + eGFR + age + β-blocker) showed a positive improvement compared with the old model (AHF + emergency + BUN + NT-proBNP + eGFR). However, when adding variables of hospital discharge way, LBBB, and alcohol taken, the model suggested a poor improvement: 2.7 (95% CI 0.5% to 3.6%), 2.6 (95% CI 1.8% to 3.8%), and 0.2 (95% CI −0.2% to 0.5%) (**Table 3**). It means that some CHF patients cannot be correctly classified.

Considering the Akaike information criterion (19) and convenience of clinical practice, we finally applied five variables related to HF readmission. The HRs of age, AHF, emergency, β-blocker, and BUN are 1.247 (1.180–1.317, $p < 0.01$), 3.342 (2.632–4.773, $p < 0.01$), 1.201 (1.086–1.329, $p < 0.01$), 0.722 (0.549–0.950, $p = 0.02$), and 1.132 (1.045–1.225, $p < 0.01$), respectively (depicted in **Table 4**). The C-index in the development set is 0.75 (95% CI: 0.72–0.79; $p < 0.001$).

A nomogram is built to visualize the risk of readmission by using the selected predictors according to the probability values obtained by Cox regression modeling in the development set (**Figure 4**). Firstly, the values of the predictive factors at baseline were recorded using standard criteria for each patient. Secondly, the score of the patient for each variable is determined by drawing a line perpendicular to the top line. Finally, we add the scores of all selected variables, and the total score is determined by drawing a corresponding line perpendicular to the bottom line to obtain the 180-day HF readmission risk. For example, a patient with a history of emergency admission, with a total of 60 points, has an 80% risk of 180-day readmission according to the nomogram of the study. Meanwhile, we developed an interactively dynamic nomogram online (https://youyueer.shinyapps.io/dynnomapp/).

The validation of the prediction model in the internal validation set is evaluated by discrimination and calibration. A calibration plot further shows good fitness with the actual readmission rates (Supporting Information, **Supplementary Figure 1**).

Internal Validation

In order to verify the effectiveness of the nomogram, it is necessary to predict the 180-day readmission of patients with CHF. Besides this, we conducted a comprehensive validation using the internal validation set. The C-index of the internal validation model is 0.75 (95% CI: 0.69–0.81). It should be specially noted that the calibration plot can show good consistency in predicting the 180-day readmission risk for patients with CHF (Supporting Information, **Supplementary Figure 1**).

External Validation

We found that AHF, emergency, eGFR, BUN, and NT-proBNP were independently associated with the 180-day readmission of patients with CHF. In order to establish an optimal nomogram model, the C-index is used to validate the model using the external validation set. The C-index is 0.73 (95% CI: 0.64–0.83), indicating that the nomogram could correctly predict individuals with a 180-day unplanned readmission in the external validation set.

DISCUSSION

For patients with CHF, an accurate prediction of the readmission rate will aid in clinical stratification and treatment decision-making for the development of appropriate diagnosis and treatment programs and the development of healthcare and management guidelines for HF. In this study, we established an easy-to-use nomogram based on easy-to-get clinical variables and validated in patients in a second hospital (>1,000 km away from the first hospital). This ensured wide applicability of the prediction model. This is the first 180-day CHF readmission model based on data of hospitals in North and South China. Compared with previous HF readmission models (8–11), we considered that the lateness of hospitalization in patients with CHF after discharge and the 180-day readmission are more in line with the actual situation.

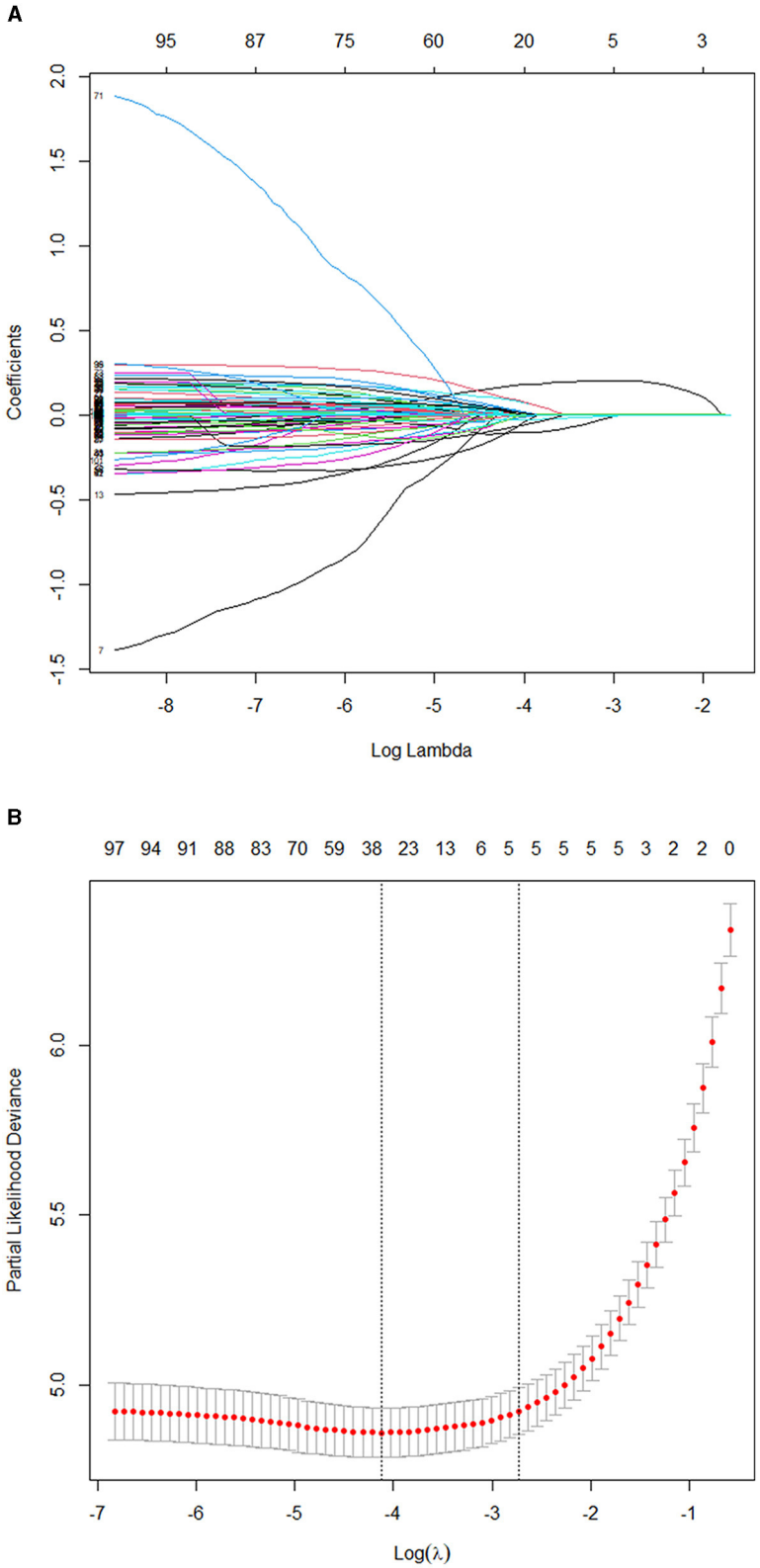

FIGURE 3 | (A) Results of the Lasso regression. **(B)** Results of the 10-fold cross-validation. Consequently, five variables were selected for inclusion in the more concise prediction model within one standard error.

TABLE 2 | Collinearity diagnosis results of five selected variables.

Variable	Tolerance	VIF	*P*-Value
AHF	0.395	2.532	<0.01*
BUN	0.726	1.377	<0.01*
Emergency	0.683	1.464	<0.01*
eGFR	0.394	2.538	<0.01*
NT-proBNP	0.505	1.980	<0.01*

AHF, acute heart failure; BUN, blood urea nitrogen; eGFR, estimated glomerular filtration rate; Emergency, emergency department visit; N-terminal-pro B-type natriuretic peptide; VIF, variance inflation factor.
**P < 0.01.*

TABLE 3 | Net reclassification improvement in CHF patients who had unplanned readmission in the three patient sets.

Net reclassification improvement in CHF patients		
	NRI (%) (AHF +Emergency + BUN + NT-proBNP + eGFR + Age + β-blocker)	NRI (%) (AHF +Emergency + BUN + NT-proBNP + eGFR + Hospital discharge way + LBBB + Alcohol taken)
Training set (AHF + Emergency + BUN + NTproBNP + eGFR)	18.5	2.7
Internal Vad (AHF + Emergency + BUN + NTproBNP + eGFR)	8.2	2.6
External Vad (AHF + Emergency + BUN + NTproBNP + eGFR)	6.3	0.2

External Vad, external validation set; Internal Vad, internal validation set; NRI, net reclassification improvement.

TABLE 4 | Multivariate Cox regression of 180-day unplanned readmission in patients with CHF.

Variable	Hazard ratio (HR)	Lower 95%	Upper 95%	*P*-Value
Age	1.247	1.180	1.317	<0.01*
AHF	3.342	2.632	4.773	<0.01*
Emergency	1.201	1.086	1.329	<0.01*
β-blocker	0.722	0.549	0.950	0.02*
BUN	1.132	1.045	1.225	<0.01*

AHF, acute heart failure; β-blocker, beta-blocker usage; BUN, blood urea nitrogen; Emergency, emergency department visit.
**P < 0.05.*

A 90-day readmission model of HF is developed by Tan et al. from the South China. The C-statistic of the model of Tan is 0.732. The model shows a moderate predictive accuracy; however, 95% CI and validation are not given. Another HF model is developed by Yang et al. and they estimate 30-day (C-index: 0.778, 95% CI: 0.693–0.862) and 1-year readmission rates (C-index: 0.738, 95% CI: 0.640–0.836). The model is developed in North China and lacks external validation. Our nomogram shows a similar accuracy (C-index: 0.752, 95% CI: 0.720–0.790) and we validate it in internal and external sets. However, more mental variables (such as depression, anxiety) and social support should be taken into account in further studies. Han's model (C-index: 0.737, 95% CI: 0.673–0.800) enrolls mental variables, but the common variables of HF and the lack of internal and external validation are neglected. Hughes' analysis of 30- and 180-day readmission showed a lower accuracy (**Supplementary Table 1** shows details in the **Supplementary Materials**).

In terms of validation, our model is validated by cross-validation, internal validation, and external validation. We used 10-fold cross-validation (20), that is, the original samples are divided into 10 groups, each group has several samples, each time a different group is selected for validation, and another nine groups are used to train the model. After the model is trained, the selected group is used to verify the model, and the deviation between the predictive value and the real value of each sample in the group is obtained, and then the average deviation is obtained. According to the above process, the parameter value of the simulation process is the target parameter value when the average deviation is the smallest for 10 cycles. At the same time, the sample is split 7:3 to complete the internal verification. Finally, the validity and consistency of the model are verified in the external set.

In terms of applicability, we used two CHF prospective study cohorts from HF centers in both North and South China, an optimal prognostic prediction model for 180-day readmission, including age, AHF, β-blocker, BUN, and emergency. Different data sources ensure the general applicability of the model. Besides, Lasso regression made the coefficients of some useless variable features penalized and even made some coefficients with smaller absolute values directly forced to zero. Finally, the penalty condition was satisfied and the sum of residual squares was minimized so as to enhance the generalization ability of the model.

Lasso regression used the following formula (21):

$$\hat{\beta}^{Lasso} = \sum_{i=1}^{n} (y_i - \sum_{j=1}^{p} x_{ij}\beta_j)^2 + \lambda \sum_{j=1}^{p} |\beta_j|$$

Penalty condition: $\sum_{j=1}^{p} |\beta_j| \leq \lambda$; the penalty function is to punish the absolute value of the regression coefficient, which requires that the sum of the absolute values of all regression coefficients is less than or equal to the penalty coefficient lambda; p refers to the number of the variable; n refers to the number of samples. Satisfactory consistency with good calibration was observed in the independent external validation set. The developed nomogram robustly quantified the risk of readmission of an individual within 180 days of discharge. The intuitive features easily allowed the clinical staffs to predict the readmission and prognosis of patients with CHF using several important symptoms and clinical indicators.

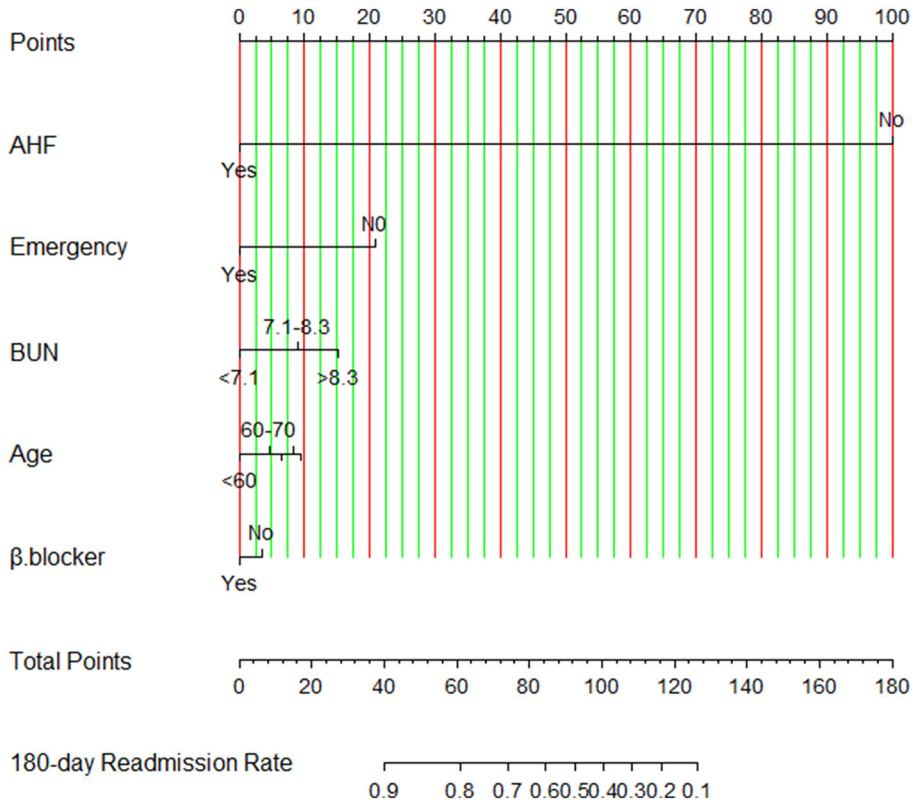

FIGURE 4 | Nomogram for risk of readmission constructed using the selected predictors. Using this nomogram, the individualized 180-day readmission risk for patients with chronic heart failure is easy to calculate. AHF, history of acute heart failure; BUN, blood urea nitrogen level; β-blocker, beta-blocker usage; emergency, emergency department visit.

History of CHF

Prediction variables independently associated with readmission are included in our model. Two predictors (AHF and emergency) are associated with the medical history of the patients. AHF (22) is common in the natural history of HF, and it is associated with high in-hospital mortality (23). The occurrence of AHF will lead patients to enter a state of stress. The state of stress will aggravate AHF and atrial fibrillation (24). AHF attack is caused by amplified leukocytes/neutrophils and monocytes/macrophages (25). Neutrophilic leukocytosis (neutrophilia) and continuous activation of neutrophils are the main factors determining the overactive inflammation of AHF and the prognosis of long-term CHF. This keeps patients with CHF in a state of persistent inflammation. A history of AHF suggests that it usually occurred within the past 3 months. Generally speaking, early AHF is an independent risk factor for acute exacerbation in patients with CHF and this is consistent with a previous study of AHF (26), which suggests that the prognosis of patients with CHF is poor at some degree. A Denmark nationwide study showed that patients with acute attack of CHF have higher all-cause mortality and readmission rates than patients with new-onset AHF (27). This may because CHF patients with AHF attack often have more comorbidities. However, AHF recurrence may be reduced if given early and timely attention, and technical clinicians are able to provide too much comprehensive and effective treatment measures.

The emergency treatments are important indicators in the 180-day readmission model for CHF. The emergency department is the key point of initial treatment for patients with AHF attack. The emergency department plays an important role in the management and treatment of AHF patients (28). Therefore, whether CHF patients have AHF attacks and whether they have been to the emergency department are closely related to readmission, as we found in our studies (22).

Age and NT-proBNP

With the aging process, the number of CHF patients is increasing. In developed countries, the incidence rate of HF is about 1–2% in adults, while in elderly people over 70, the figure rises to nearly 10% (29). The prevalence of HF over 35 years old is 1.3% in China (7), and considering the population base, there are about 13.7 million patients with HF. In addition to aging combined with various diseases, we cannot ignore the problem of frailty. The FRAIL-HF study has shown that patients with frailty had a higher risk of 30-day dysfunction and0 higher 1-year readmission rate and 1-year all-cause mortality (30). This is one of the reasons for CHF readmission. In addition, the elderly have higher levels of plasma natriuretic peptide. NT-proBNP varies with age and

cardiac dysfunction. It follows from previous studies that plasma NT-proBNP level is an important biomarker in predicting the prognosis of patients with CHF, especially for patients with diabetes (31), where NT-proBNP is closely related to the left ventricular reconstruction in CHF. However, the NT-proBNP level varies greatly after finishing the HF therapy, accompanied with apparent individualization. In our study, we regard the elevated NT-proBNP level as a baseline predictor, which seems not appropriate at some degree. We should regard the NT-proBNP level as an independent, dynamic biomarker. Only in this way can we get a more accurate readmission rate. ΔNT-proBNP or the ratio of BNP/NT-proBNP could be observed and calculated in the future prediction model.

Renal Dysfunction and CHF

In the present study, we mainly consider plasma BUN level. The level of BUN reflects the protein metabolism, indicating the renal function, which is independently associated with the prognosis of patients with CHF. Moreover, they are also selected for model inclusion. Fluid overload is a common pathophysiological mechanism of CHF as well as renal disorders. There exist complex neurohormonal interactions between the heart and kidney for patients with CHF. Patients with CHF have a higher incidence of renal dysfunction due to several shared pathophysiological pathways and mutual risk factors (32). The existing results suggest that renal dysfunction progression is closely related to readmission rate and clinical prognosis. For patients with CHF, the hemodynamic perturbations would lead to sodium and water retention and worsening of renal function. In addition, the cardiorenal syndrome further highlights the concept of bidirectional interaction, such that CHF has several negative effects on kidney function, while renal dysfunction significantly influences cardiac function. As the course of CHF progresses, blood flow will decrease through tissues and organs. It should be noted that the kidney is sensitive to ischemia, resulting in significant decreases in eGFR, as well as glomerular and secondary tubular injuries, activation of the neuroendocrine system (renin–angiotensin–aldosterone system and sympathetic nervous system), congestion of the venous system, and increased central venous pressure. In recent years, studies have shown that an increase of central venous pressure is associated with a poor prognosis for patients with CHF, potentially because a disproportionately higher central venous pressure effectively contributes to elevated left-sided filling pressure (14).

In order to design new strategies to improve clinical outcomes, a better understanding of the mechanisms has to be achieved, and the experimental results for the hemodynamic changes affecting the lungs and kidneys in HF need to be validated further.

eGFR is another factor to be analyzed; however, it is a sensitive factor together with the change of blood creatinine. Improvement is not obvious when we add eGFR to our prediction model. This is similar to the conclusion of an HFpEF study (26). This may because of the fluctuation of eGFR, which leads to inaccurate results. Compared with this study, our present study included a small number of ultrasound variables and future research should be evaluated in detail.

Usage of β-Blocker and CHF

From the analysis, we observed the benefits of β-blocker usage in CHF patients. In future studies, we would consider the dosage of β-blockers in detail, as well as the individual differences when choosing the requirements of drug use. The elderly aged ≥75 years who received a β-blocker hold a lower 90-day mortality rate and lower readmission rate (33). Consequently, β-blocker therapy is closely related to the prognosis of patients with HF.

Finally, the five variables associated with CHF readmission entered into the model were as follows: AHF, emergency, age, BUN, and β-blocker usage. This fits with the AIC principle. When the predictive effect is similar, we tend to choose fewer variables for clinical applicability.

STUDY STRENGTHS AND LIMITATIONS

Several studies focused on the enhancement of the accuracy of the models (34) but ignored their wide clinical applications. Our study was conducted in a real-world situation. By conducting a rigorous multicenter prospective study, this work focuses on developing a prediction model for a 180-day CHF readmission using standard and easily collected clinical variables. The prediction model can be well-validated in an external database from a second HF center. As a result, the proposed predictor model will play a key role for effective verification. Nevertheless, this study has several potential limitations. Firstly, we did not take into account the all-cause mortality endpoint completely. Because of the influence of COVID-19, accurate mortality might not have been observed at some degree. In a future study, we will take into account heart injury as a result of the new coronavirus (35–37). Secondly, the model does not consider some novel biomarker phenotypes associated with CHF. We are considering whether adding some novel biomarker phenotypes can increase the accuracy of model prediction.

CONCLUSIONS

This work mainly provides a simple model, which can address data collected for clinical practice to predict the 180-day readmission of patients with CHF. Both internal and external validations further suggest a broad applicability of the given model. From the results, the prediction model can show a reference value for a meaningful prognosis to stratify patients with CHF and then aid in timely clinical decision-making.

DATA AVAILABILITY STATEMENT

The raw data supporting the conclusions of this article will be made available by the authors, without undue reservation.

ETHICS STATEMENT

The studies involving human participants were reviewed and approved by Qingdao Central Hospital Ethics Committee, The Ethics Committee of the First Affiliated Hospital of Shantou

University Medical College. The patients/participants provided their written informed consent to participate in this study.

AUTHOR CONTRIBUTIONS

SG: conception and methodology, project administration, and writing of the original draft. GY: conception and methodology and data curation (from the North China Heart Failure Center). QX: conception and methodology and data curation (from the North China Heart Failure Center). GW: conception and methodology and data curation (from the South China Heart Failure Center). XT: conception and methodology and data curation (from the South China Heart Failure Center). JZ: writing, review, and editing. NL: writing, review, and editing. All authors contributed to the article and approved the submitted version.

FUNDING

This study was supported by the Guangdong High-Level University Development Program Research Fund (2020) and Innovation Team Project of Guangdong Universities, China (Natural, No. 2019KCXTD003).

ACKNOWLEDGMENTS

The authors thank the staff of the Heart Failure Centers in both Qingdao Central Hospital and the First Affiliated Hospital of Shantou University for their co-operation. The clinical diagnosis and data collection progress were shared by each center. The authors thank Dr. Stanley Li Lin, Department of Cell Biology and Genetics, Shantou University Medical College, for his helpful comments and English language editing and Yi Li, School of Mathematics and Statistics, Nanjing Audit University, for his statistical analysis assistance.

SUPPLEMENTARY MATERIAL

The Supplementary Material for this article can be found online at: https://www.frontiersin.org/articles/10.3389/fcvm.2021.731730/full#supplementary-material

REFERENCES

1. Ponikowski P, Voors AA, Anker SD, Bueno H, Cleland JGF, Coats AJS, et al. 2016 ESC Guidelines for the diagnosis and treatment of acute and chronic heart failure: the Task Force for the diagnosis and treatment of acute and chronic heart failure of the European Society of Cardiology (ESC) Developed with the special contribution of the Heart Failure Association (HFA) of the ESC. *Eur Heart J.* (2016) 37:2129–200. doi: 10.1093/eurheartj/ehw128
2. Zhang J, Goode KM, Rigby A, Balk AH, Cleland JG. Identifying patients at risk of death or hospitalisation due to worsening heart failure using decision tree analysis: evidence from the Trans-European Network-Home-Care Management System (TEN-HMS) study. *Int J Cardiol.* (2013) 163:149–56. doi: 10.1016/j.ijcard.2011.06.009
3. Wallmann R., Llorca J, Gómez-Acebo I, Ortega AC, Roldan FR, Dierssen-Sotos T, et al. Prediction of 30-day cardiac-related-emergency-readmissions using simple administrative hospital data. *Int J Cardiol.* (2013) 164:193–200. doi: 10.1016/j.ijcard.2011.06.119
4. Leong K, Wong LY, Aung KC, Macdonald M, Cao Y, Lee S, et al. Risk stratification model for 30-day heart failure readmission in a multiethnic South East Asian community. *Am J Cardiol.* (2017) 119:1428–32. doi: 10.1016/j.amjcard.2017.01.026
5. Goyal P, Loop M, Chen L, Brown TM, Durant RW, Safford MM, et al. Causes and temporal patterns of 30-day readmission among older adults hospitalized with heart failure with preserved or reduced ejection fraction. *J Am Heart Assoc.* (2018) 7:e007785. doi: 10.1161/JAHA.117.007785
6. Frizzell J, Liang L, Schulte PJ, Yancy CW, Heidenreich PA, Hernandez AF et al. Prediction of 30-day all-cause readmissions in patients hospitalized for heart failure: comparison of machine learning and other statistical approaches. *JAMA Cardiol.* (2017) 2:204–09. doi: 10.1001/jamacardio.2016.3956
7. Hao G, Wang X, Chen Z, Zhang L, Zhang Y, Wei B, et al. Prevalence of heart failure and left ventricular dysfunction in China: the China Hypertension Survey, 2012–2015. *Eur J Heart Fail.* (2019) 21:1329–37. doi: 10.1002/ejhf.1629
8. Tan B, Gu JY, Wei HY, Chen L, Yan SL, Deng N, et al. Electronic medical record-based model to predict the risk of 90-day readmission for patients with heart failure. *BMC Med Inform Decis.* (2019) 19:193. doi: 10.1186/s12911-019-0915-8
9. Yang M, Tao L, An H, Liu G, Tu Q, Zhang H, et al. A novel nomogram to predict all-cause readmission or death risk in Chinese elderly patients with heart failure. *ESC Heart Fail.* (2020) 7:1015–24. doi: 10.1002/ehf2.12703
10. Han Q, Ren J, Tian J, Yang H, Zhang Q, Wang R, et al. A nomogram based on a patient-reported outcomes measure: predicting the risk of readmission for patients with chronic heart failure. *Health Qual Life Out.* (2020) 18:290. doi: 10.1186/s12955-020-01534-6
11. Hughes LD, Witham MD. Causes and correlates of 30 day and 180 day readmission following discharge from a Medicine for the Elderly Rehabilitation unit. *BMC Geriatr.* (2018) 18:197. doi: 10.1186/s12877-018-0883-3
12. O'Connor M, Murtaugh CM, Shah S, Barrón-Vaya Y, Bowles KH, Peng TR, et al. Patient characteristics predicting readmission among individuals hospitalized for heart failure. *Med Care Res Rev.* (2016) 73:3–40. doi: 10.1177/1077558715595156
13. Charlson ME, Pompei P, Ales KL, Mackenzie CR. A new method of classifying prognostic comorbidity in longitudinal studies: development and validation. *J Chronic Dis.* (1987) 40:373–83. doi: 10.1016/0021-9681(87)90171-8
14. Verbrugge F, Guazzi M, Testani JM, Borlaug BA. Altered hemodynamics and end-organ damage in heart failure: impact on the lung and kidney. *Circulation.* (2020) 142:998–1012. doi: 10.1161/CIRCULATIONAHA.119.045409
15. Yue L, Pan B, Shi X, Du X. Comparison between the beta-2 Microglobulin-based equation and the CKD-EPI equation for estimating GFR in CKD patients in China: ES-CKD study. *Kidney Dis.* (2020) 6:204–14. doi: 10.1159/000505850
16. Heus P, Damen JAAG, Pajouheshnia R, Scholten RJPM, Reitsma JB, Collins GS, et al. Poor reporting of multivariable prediction model studies: towards a targeted implementation strategy of the TRIPOD statement. *BMC Med.* (2018) 16:120. doi: 10.1186/s12916-018-1099-2
17. Pencina M, D'Agostino RB, Demler OV. Novel metrics for evaluating improvement in discrimination: net reclassification and integrated discrimination improvement for normal variables and nested models. *Stat Med.* (2012) 31:101–13. doi: 10.1002/sim.4348
18. Loop M, Van Dyke MK, Chen L, Brown TM, Durant RW, Safford MM, et al. Comparison of length of stay, 30-day mortality, and 30-day readmission rates in medicare patients with heart failure and with reduced versus preserved ejection fraction. *Am J Cardiol.* (2016) 118:79–85. doi: 10.1016/j.amjcard.2016.04.015

19. Glatting G, Kletting P, Reske SN, Hohl K, Ring C. Choosing the optimal fit function: comparison of the Akaike information criterion and the F-test. *Med Phys.* (2007) 34:4285–92. doi: 10.1118/1.2794176
20. Rodriguez JD, Perez A, Lozano JA. Sensitivity analysis of k-fold cross validation in prediction error estimation. *IEEE T Patterrn Anal.* (2010) 32:569–75. doi: 10.1109/TPAMI.2009.187
21. Tibshirani R. The LASSO method for variable selection in the Cox Model. *Stat Med.* (1997) 16:385–95.doi: 10.1002/(sici)1097-0258(19970228)16:4<385::aid-sim380>3.0.co;2-3
22. Miró Ò, García Sarasola A, Fuenzalida C, Calderón S, Jacob J, Aguirre A, et al. Departments involved during the first episode of acute heart failure and subsequent emergency department revisits and rehospitalisations: an outlook through the NOVICA cohort. *Eur J Heart Fail.* (2019) 21:1231–44. doi: 10.1002/ejhf.1567
23. Vader JM, LaRue SJ, Stevens SR, Mentz RJ, DeVore AD, Lalau A, et al. Timing and causes of readmission after acute heart failure hospitalization-insights from the heart failure network trials. *J Card Fail.* (2016) 22:875–83. doi: 10.1016/j.cardfail.2016.04.014
24. Ivanovic B, Tadic M. Emotional stress-induced takotsubo cardiomyopathy, acute heart failure, and atrial fibrillation in the same patient. *Heart Mind.* (2019) 3:70–2. doi: 10.4103/hm.hm_41_19
25. Kain V, Halade GV. Role of neutrophils in ischemic heart failure. *Pharmacology.* (2020) 205:107424. doi: 10.1016/j.pharmthera.2019.107424
26. Zamfirescu M, Ghilencea LN, Popescu MR, Bejan GC, Ghiordanescu IM, Popescu AC, et al. A practical risk score for prediction of early readmission after a first episode of acute heart failure with preserved ejection fraction. *Diagnostics.* (2021) 11:198. doi: 10.3390/diagnostics11020198
27. Butt JH, Fosbøl EL, Gerds TA, Andersson C, McMurray JJV, Petrie MC, et al. Readmission and death in patients admitted with new-onset versus worsening of chronic heart failure: insights from a nationwide cohort. *Eur J Heart Fail.* (2020) 22:1777–85. doi: 10.1002/ejhf.1800
28. Pang P, Collins SP, Miró Ò, Bueno H, Diercks DB, Di Somma S, et al. Editor's choice-the role of the emergency department in the management of acute heart failure: an international perspective on education and research. *Eur Heart J Acute Ca.* (2017) 6:421–9. doi: 10.1177/2048872615600096
29. Ceia F, Fonseca C, Mota T, Morais H, Matias F, de Sousa A, et al. Prevalence of chronic heart failure in Southwestern Europe: the EPICA study. *Eur J Heart Fail.* (2002) 4:531–9. doi: 10.1016/S1388-9842(02)00034-X
30. Vidán MT, Blaya-Novakova V, Sánchez E, Ortiz J, Serra-Rexach JA, Bueno H, et al. Prevalence and prognostic impact of frailty and its components in non-dependent elderly patients with heart failure. *Eur J Heart Fail.* (2016) 18:869–75. doi: 10.1002/ejhf.518
31. Berezin AE, Berezin AA. Emerging role of natriuretic peptides in diabetes mellitus: new approaches for risk stratification. *Heart Mind.* (2020) 4:100–8. doi: 10.4103/hm.hm_3_20
32. Ter Maaten JM, Damman K, Verhaar MC, Paulus WJ, Duncker DJ, Cheng C, et al. Connecting heart failure with preserved ejection fraction and renal dysfunction: the role of endothelial dysfunction and inflammation. *Eur J Heart Fail.* (2016) 18:588–98. doi: 10.1002/ejhf.497
33. Gilstrap L, Austin AM, O'Malley AJ, Gladders B, Barnato AE, Tosteson A, et al. Association between beta-blockers and mortality and readmission in older patients with heart failure: an instrumental variable analysis. *J Gen Intern Med.* (2021) 36:2361–9. doi: 10.1007/s11606-021-06901-7
34. Chu J, Dong W, Huang Z. Endpoint prediction of heart failure using electronic health records. *J Biomed Inform.* (2020) 109:103518. doi: 10.1016/j.jbi.2020.103518
35. Brito J, Silva BV, da Silva PA, Cortez-Dias N, Silva D, Agostinho JR, et al. Cardiovascular complications of COVID-19. *Heart Mind.* (2020) 4:67–74. doi: 10.4103/hm.hm_28_20
36. Allam HH, Kinsara AJ, A Alrajawi AA, Tuiama T. Concomitant acute aortic thrombosis and pulmonary embolism complicating COVID-19 pneumonia. *Heart Mind.* (2020) 4:123–5. doi: 10.4103/hm.hm_34_20
37. Cereda A, Toselli M, Laricchia A, Mangieri A, Ruggiero R, Gallo F, et al. Stress-induced cardiomyopathy related to SARS-CoV-2. *Heart Mind.* (2020) 4:57–8. doi: 10.4103/hm.hm_10_20

Conflict of Interest: The authors declare that the research was conducted in the absence of any commercial or financial relationships that could be construed as a potential conflict of interest.

Publisher's Note: All claims expressed in this article are solely those of the authors and do not necessarily represent those of their affiliated organizations, or those of the publisher, the editors and the reviewers. Any product that may be evaluated in this article, or claim that may be made by its manufacturer, is not guaranteed or endorsed by the publisher.

Copyright © 2021 Gao, Yin, Xia, Wu, Zhu, Lu, Yan and Tan. This is an open-access article distributed under the terms of the Creative Commons Attribution License (CC BY). The use, distribution or reproduction in other forums is permitted, provided the original author(s) and the copyright owner(s) are credited and that the original publication in this journal is cited, in accordance with accepted academic practice. No use, distribution or reproduction is permitted which does not comply with these terms.

frontiers in Cardiovascular Medicine

ORIGINAL RESEARCH
published: 10 September 2021
doi: 10.3389/fcvm.2021.710090

Olanzapine: Association Between a Typical Antipsychotic Drug and Aortic Calcification

Chao Zhang[1†], Dongdong Zheng[2†], Weijing Feng[1†], Huanji Zhang[3†], Feng Han[4], Wanbing He[1], Aiting Liu[3], Hui Huang[3] and Jie Chen[5*]*

[1] Department of Cardiology, Sun Yat-sen Memorial Hospital, Sun Yat-sen University, Guangzhou, China, [2] Department of Psychiatry, Psychiatric Hospital of Guangzhou Civil Affairs Bureau, Guangzhou, China, [3] Cardiovascular Department, The Eighth Affiliated Hospital, Sun Yat-sen University, Shenzhen, China, [4] Department of Ultrasound, Cancer Center, Sun Yat-sen University, Guangzhou, China, [5] Department of Radiation Oncology, Sun Yat-sen Memorial Hospital, Sun Yat-sen University, Guangzhou, China

OPEN ACCESS

Edited by:
Yuli Huang,
Southern Medical University, China

Reviewed by:
Jijin Lin,
Guangdong Academy of Medical Sciences, China
Wusheng Zhu,
Nanjing University, China

***Correspondence:**
Hui Huang
huangh8@mail.sysu.edu.cn
Jie Chen
1450517759@qq.com

[†] These authors have contributed equally to this work and share first authorship

Specialty section:
This article was submitted to General Cardiovascular Medicine, a section of the journal Frontiers in Cardiovascular Medicine

Received: 15 May 2021
Accepted: 14 July 2021
Published: 10 September 2021

Citation:
Zhang C, Zheng D, Feng W, Zhang H, Han F, He W, Liu A, Huang H and Chen J (2021) Olanzapine: Association Between a Typical Antipsychotic Drug and Aortic Calcification. Front. Cardiovasc. Med. 8:710090. doi: 10.3389/fcvm.2021.710090

Aims: This study concentrates on the relationship between antipsychotic drugs (APDs) and aortic calcification.

Methods: All 56 patients with schizophrenia were divided into two groups according to aortic calcification index. APD equivalent dose was calculated via defined daily doses method.

Results: In schizophrenia patients with higher aortic calcification index scores, APD equivalent doses were lower. APD equivalent dose was negatively related to aortic calcification index. Although equivalent APD dose in patients without olanzapine treatment was negatively related to aortic calcification index, it seems that equivalent APD dose did not associate with aortic calcification.

Conclusion: Aortic calcification is negatively associated with APD dose in schizophrenia patients. Olanzapine seems to be vital to the relationship between aortic calcification and APD treatment.

Keywords: aortic calcification, mental illness, schizophrenia, olanzapine, antipsychotic drugs

INTRODUCTION

Severe mental illness has persistent procession, and schizophrenia causes serious disabilities to individuals worldwide (1). Antipsychotic drugs (APDs) are essential in providing recovery opportunities for schizophrenia patients (2, 3). However, besides alleviating symptoms, APDs also lead to adverse effects, especially elevating cardiovascular risks (4).

Several APDs have been proven to have metabolic effects, which would cause cardiovascular diseases (5). Jess Fiedorowicz et al. reported that vasculopathy is related to psychosis and arterial stiffness is also enhanced in patients with conventional APD exposure (6). Different APDs exert adverse side effects on the vascular system, based on their metabolic effects (7). Olanzapine has been confirmed to result in metabolic syndromes and exert several adverse cardiovascular effects (8, 9). Olanzapine has also been widely used in cancer patients to avoid chemotherapy-caused nausea and vomiting (10). Of note, the dose of APD is especially vital for all patients who underwent such a medication process (10).

Emerging evidence suggests that APD dose should be personalized and cardiovascular risk must be taken into consideration (11). Aortic calcification is acknowledged as a vital predictor of cardiovascular risk (12). Moreover, olanzapine could reduce blood pressure and cardiac contractile function *in vivo* (8). However, the relationship between aortic calcification and APD treatment, especially olanzapine, was not clear. In this study, we investigated schizophrenia patients to explore the relationship between APD treatment and aortic calcification.

METHODS

Study Subjects and Clinical Information Extraction

Between December 2016 and August 2017, 79 patients diagnosed with schizophrenia were enrolled in this study. All these patients sought routine follow-ups at the Psychiatric Hospital of Guangzhou Civil Affairs Bureau. We enrolled patients of both sexes, and both the patients and their relatives consented to our accessing their medical records. The study was approved by the Ethics Committee of Psychiatric Hospital of Guangzhou Civil Affairs Bureau. The methods complied with the ethical guidelines of the 1975 Declaration of Helsinki. All the subjects, or their agents, provided their written informed consent.

Diagnosis of schizophrenia was conducted according to Chinese Classification and Diagnosis of Mental Diseases and confirmed by at least two different independent psychiatrists (13). All the subjects enrolled in this study underwent a continuous oral APD treatment for at least 1 year. Patients who received more than one kind of APD treatment or who were admitted to a hospital for further treatment were excluded. The patients' APD doses were unchanged for at least 6 months. In total, 56 patients with schizophrenia were enrolled in this study. Clinical information including blood sample measurements was obtained in the medical records, and individual histories were provided by patients or their relatives. In addition, no interference is present in this manuscript, and written informed consent was provided by the patients or their guardians.

Collection of Blood Samples and Baseline Diameters Measurement

Blood samples were collected and sent to the clinical laboratory of the Psychiatric Hospital of Guangzhou Civil Affairs Bureau. Some biochemical characteristics including lipoprotein metabolism, hepatic function, and blood routines were measured by a standardized procedure.

Blood pressure and body mass index (BMI) were measured and calculated by at least 2 nurses from the clinic department and confirmed by their relatives. ECGs were conducted and diagnosed by the ECG section and confirmed by physicians.

Aortic Calcification Index Calculation

Aortic calcification (AoAC) indices were obtained via chest X-rays. The chest radiology information was obtained from the medical imaging department of Psychiatric Hospital of Guangzhou Civil Affairs Bureau. The aortic calcification index was calculated by experienced radiologists using established methods (14). Briefly, each plain chest radiography was divided into 16 sections according to the aortic arch and assigned a calcification index present as a percentage in our study. The aortic calcification indices were graded on a scale from 0 to 3, as in previous studies (15, 16).

APD Equivalent Dose Calculation

According to the defined method for minimum effective dose, APD doses were standardized into equivalent doses for further analysis (17). APD equivalent dose was calculated by the defined daily doses (DDD) method (18). The standardization process was based on chlorpromazine, and the duration of APD treatment was recorded in years. The accumulated APD treatment was calculated by multiplying the standardized daily dose by the duration of the treatment. Accumulated APD treatment was tested for the normal distribution. Log transformation was conducted if necessary.

Statistical Analysis

All such data extracted from medical records are presented in this article, with continuous data as mean values with a standard deviation (SD) and categorical data as frequencies with percentages. Before comparison, all continuous data underwent non-parametric tests to confirm normal distribution. For those normal distribution values, comparisons were conducted by Student's *t*-test and multiple regression analysis. Some of the non-normal data were transformed, which was further confirmed by nonparametric tests, (specific details are included in the results section). Nonparametric comparisons were conducted on the data that could not be transformed. Furthermore, Pearson's correlations were conducted for parametric data and Spearman's correlations were conducted for non-parametric data, referred to as r or r_S. To reveal the independent factors, multiple regression analysis was used. All statistical analysis was performed using the software SPSS 20.0. For all statistical tests, two-tailed p-values < 0.05 was the threshold of statistical significance.

RESULTS

Comparison of Aortic Calcification, Accumulated APD Treatment, and Clinical Characteristics in Schizophrenia Patients Receiving APDs

All schizophrenia patients included in this project were divided into two groups according to their AoAC score. The comparison of clinical characteristics and kinds of ADP treatment are shown in **Table 1**. It is shown that patients with higher AoAC scores were older, male, and inclined to develop smoking habits. Comparison of APD profiles indicated that in the high AoAC score group, APD equivalent doses were lower, with no difference in the duration of APD treatment (**Figure 1**).

Relationship Between Aortic Calcification Index, APD Treatment, and Clinical Characteristics

To further investigate the relationship between the aortic calcification index and other potential factors, Spearman's correlation analysis was conducted. As shown in **Table 2**, aortic calcification index was related to age, sex, and smoking ($r = 0.536$, $P < 0.001$; $r = 0.332$, $P = 0.012$; $r = 0.349$, $P = 0.008$). In addition, APD equivalent dose was negatively related to aortic calcification index ($r = -0.413$, $P = 0.002$). It is indicated that APD equivalent dose would be the one of factors for aortic calcification.

TABLE 1 | Comparation between patients with different severities of aortic calcification.

	AoAC < 2	AoAC ≥ 2	*P*
Age (years)	56.09 ± 12.35	65.08 ± 8.00	0.001*
Gender (Male%)	3 (13.6%)	16 (47.1%)	0.010*
Smoking (*n*%)	0 (0%)	9 (26.5%)	0.008*
Hypertension (*n*%)	6 (27.3%)	11 (32.4%)	0.686
DM (*n*%)	4 (18.2%)	11 (32.4)	0.242
CAD (*n*%)	1 (4.5%)	7 (20.6%)	0.130
Stroke (*n*%)	2 (9.1%)	2 (5.9%)	0.642
BMI (kg/m^2)	22.74 ± 3.48	21.40 ± 3.12	0.146
WBC (10^9/L)	7.41 ± 1.80	7.17 ± 1.73	0.605
RBC (10^9/L)	4.04 ± 0.48	3.92 ± 0.66	0.467
PLT (10^9/L)	267.36 ± 90.97	251.71 ± 93.42	0.539
ALT (U/L)	18.05 ± 6.90	20.29 ± 9.01	0.324
AST (U/L)	20.05 ± 6.86	21.56 ± 5.94	0.385
γ-GGT (U/L)	22.23 ± 14.65	21.18 ± 10.54	0.756
TG (mmol/L)	1.54 ± 0.94	1.49 ± 0.87	0.845
TC (mmol/L)	4.70 ± 0.90	4.79 ± 1.06	0.765
Glucose (mmol/L)	5.39 ± 0.99	5.78 ± 2.33	0.395

ALT, alanine aminotransferase; APD, antipsychotic drugs; AST, aspartate aminotransferase; BMI, body mass index; CAD, coronary artery disease; DM, diabetes mellitus; TC, total cholesterol; TG, triglyceride; γ-GGT, γ glutamyl transferase.
**P < 0.05.*

Olanzapine Treatment and Aortic Calcification in Schizophrenia Patients

Patients were divided into four groups, based on which APD was used in their treatment. It is shown in **Figure 2** that the aortic calcification indices in these groups (clozapine, olanzapine, quetiapine, and risperidone) did not differ. However, the duration and equivalent dose were quite different between groups, and olanzapine treated patients seemed to have higher APD equivalent doses compared to the clozapine and quetiapine groups (**Figure 2B**). Although clozapine-treated patients had

TABLE 2 | Relationship between aortic calcification index and clinical characteristics.

	r_s	*P*
Age	0.536	<0.001*
Gender	0.332	0.012*
Smoking	0.349	0.008*
Hypertension	0.148	0.276
DM	0.102	0.454
CAD	0.207	0.125
Stroke	0.035	0.800
BMI	−0.235	0.082
WBC	−0.017	0.900
RBC	−0.202	0.136
PLT	0.036	0.794
ALT	0.175	0.197
AST	0.140	0.304
γ-GGT	0.033	0.811
TG	−0.039	0.773
TC	−0.122	0.368
Glucose	−0.159	0.243
APD equivalent dose	−0.413	0.002*
Duration of APD treatment	−0.151	0.266

ALT, alanine aminotransferase; APD, antipsychotic drugs; AST, aspartate aminotransferase; BMI, body mass index; CAD, coronary artery disease; DM, diabetes mellitus; TC, total cholesterol; TG, triglyceride; γ-GGT, γ glutamyl transferase.
**P < 0.05.*

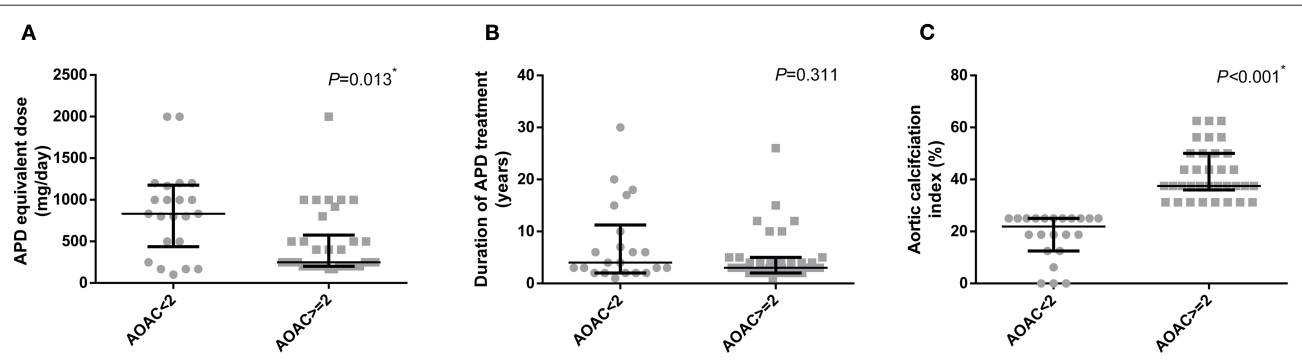

FIGURE 1 | Comparison of APD medication profiles in patients according to their AoAC index. **(A)** APD equivalent dose, **(B)** duration of APD treatment, **(C)** Aortic calcification index. *$p < 0.05$. APD, antipsychotic drug.

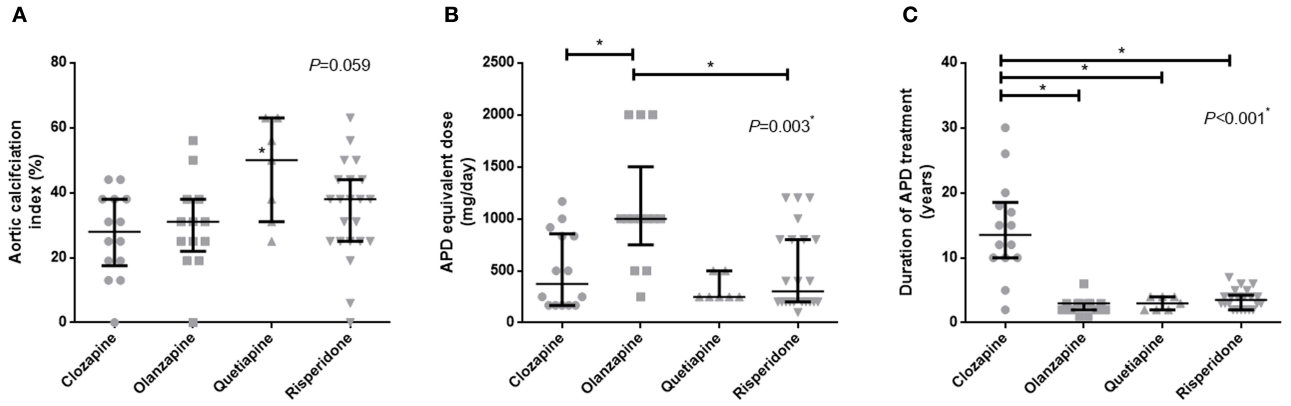

FIGURE 2 | Comparison of aortic calcification index and APD treatment in patients with different kinds of APDs. **(A)** APD equivalent dose, **(B)** duration of APD treatment, **(C)** Aortic calcification index. *$p < 0.05$. APD, antipsychotic drugs.

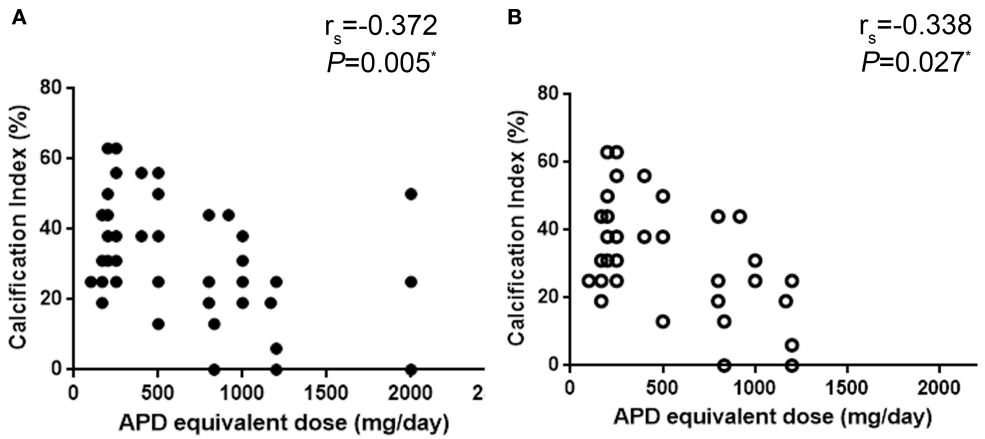

FIGURE 3 | Correlation analysis of equivalent APD dose and aortic calcification index. **(A)** all patient, **(B)** patients without olanzapine treatment. APD, antipsychotic drugs.

longer durations of APD treatment, it seems that the duration of APD treatment was not related to aortic calcification, as shown in **Table 2**.

Correlation analysis showed that in patients who were not treated with olanzapine, the aortic calcification index was associated with APD equivalent dose ($r = -0.338$, $P = 0.027$, **Figure 3**). Considering the limited number of patients in each group, and that age is a major factor in the development of aortic calcification, age should be ruled out while comparing equivalent APD dose and aortic calcification index. Ordinal regression analysis indicated that in all patients age and equivalent APD dose are vital factors associated with aggravation of aortic calcification (age: OR = 1.122, $P < 0.001$; equivalent APD dose: OR = 0.999, $P = 0.021$). However, in patients without olanzapine treatment, only age is associated with aggravation of aortic calcification (OR = 1.126, $P = 0.001$) (**Table 3**). Such results indicated that olanzapine would be a vital factor related to aortic calcification, regardless of age.

DISCUSSION

Using an aortic calcification indices from chest X-rays is believed to be one most available and effective methods to predict cardiovascular events (19). To describe the severity of aortic calcification degree, AoAC score was used to predict the cardiovascular risks (15). Although calcification evaluation from chest X-ray might not be as accurate as from CT (20), long-term APD treatment for schizophrenia patients tend to suffer more from financial burdens (21), and it is quite hard for patients or caregivers to arrange such examinations. In our study, schizophrenia patients were enrolled and APD equivalent dose was higher in the group with AoAC ≥ 2, indicating that some potential relationship between aortic calcification and APD treatment. Some recent studies revealed that besides some potential benefits, long-term APD treatment did indeed lead to several adverse results in patients' cardiovascular and metabolic systems, including disrupting lipid and glucose metabolism (22).

TABLE 3 | Ordinal regression analysis between AoAC grade and potential factors in patients with APD treatment or without olanzapine treatment.

All patients	**OR**	**95% CI**	***P***
Age	1.122	(1.054, 1.194)	<0.001*
APD equivalent dose	0.999	(0.997, 1.000)	0.021*
Gender (Female)	0.404	(0.096, 1.700)	0.216
Gender (Male)	1	–	–
Smoking	0.586	(0.091, 3.759)	0.573
Non-smoking	1	–	–
Not Olanzapine	**OR**	**95% CI**	***P***
Age	1.126	(1.048, 1.210)	0.001*
APD equivalent dose	0.998	(0.996, 1.000)	0.087
Gender (Female)	0.312	(0.045, 2.147)	0.237
Gender (Male)	1	–	–
Smoking	1.668	(0.156, 17.880)	0.673
Non-smoking	1	–	–

APD, antipsychotic drugs. $^{*}P < 0.05$.

Presently, APD treatment is still a major beneficial treatment for schizophrenia patients that decreases the risk of relapse and reduces all-cause mortality (23). Emerging evidence indicated that APDs could also contribute to overall 5-year diabetes occurrence (24). Some pharmacological research also emphasized that long-term use of APD treatment would leave schizophrenia patients suffering from adverse effects, including cardiovascular risks and brain structure changes (25). As one efficient method to evaluate cardiovascular risk, aortic calcification was proven to be negatively related to equivalent APD dose, suggesting that APD exerts some potential effects on patients (**Table 2**). Despite this, schizophrenia patients with olanzapine treatment suffered more from cardiovascular risk, and the major disturbance from olanzapine is based on metabolic abnormalities (26).

Due to the high heterogeneity of atypical APDs, different kinds of APDs exert various effects, especially on the cardiovascular system (27). Of note, olanzapine seems to dramatically enhance cardiovascular risk compared to all other atypical APDs, including risperidone, clozapine, and quetiapine (22). Surprisingly, this study showed that the aortic calcification index is negatively associated with APD dose increment. Olanzapine has a higher equivalent dose among patients, and in patients without olanzapine treatment the relationship between equivalent APD dose and aortic calcification index vanishes. Although olanzapine is proven to induce some metabolic disorders (9), it is reported recently that olanzapine might have some extra protective effects such as reducing reactive oxygen species induced cell death (28). Therefore, the exact mechanism of olanzapine in the pathological process of aortic calcification needs further investigation.

Our study had several limitations. Firstly, the number of patients involved in our study was relatively small. Due to the poor management of schizophrenia patients in China, long-term APD treatments and monitoring were not satisfying, and some schizophrenia patients and their guardians or relatives refused to do further tests in clinics. Secondly, the present work is based on one sectional study and we could only reveal the relationship between aortic calcification and APD equivalent dose. We could not rule out the possibility that patients with lower aortic calcification could tolerate higher doses of APD. Thus, further studies with larger sample sizes and cohort studies are needed to confirm our findings.

CONCLUSIONS

It is shown in this study that aortic calcification was negatively correlated with APD equivalent dose in schizophrenia patients, and that olanzapine plays a role in aortic calcification. The marked effects of APD treatment on aortic calcification should not be ignored when choosing different kinds of APDs.

DATA AVAILABILITY STATEMENT

The raw data supporting the conclusions of this article will be made available by the authors, without undue reservation.

ETHICS STATEMENT

Written informed consent was obtained from the individual(s) for the publication of any potentially identifiable images or data included in this article.

AUTHOR CONTRIBUTIONS

CZ, DZ, WF, and HH were responsible for study design, statistical analysis, and manuscript preparation. CZ, DZ, WF, FH, WH, HZ, AL, JC, and HH were responsible for subjects recruitment and clinical data collecting. CZ, WF, JC, and HH were involved in writing the protocol and providing the funding for this study. All authors contributed to and have approved the final manuscript.

FUNDING

This work was supported in part by National Natural Science Foundation of China (NSFC) (82073408 and 81500563) to JC, Funds for International Cooperation and Exchange of NSFC, NSFC-FDCT (8201101103), NSFC (81870506 and 81670676), Guangzhou Science and Technology Plan Project (201607010075) and Futian District Public Health Scientific Research Project of Shenzhen (FTWS2019003) to HH.

REFERENCES

1. Murray CJ, Vos T, Lozano R, Naghavi M, Flaxman AD, Michaud C, et al. Disability-adjusted life years (DALYs) for 291 diseases and injuries in 21 regions, 1990-2010: a systematic analysis for the Global Burden of Disease Study 2010. *Lancet.* (2012) 380:2197–223. doi: 10.1016/S0140-6736(12)61689-4
2. Bilder RM, Goldman RS, Volavka J, Czobor P, Hoptman M, Sheitman B, et al. Neurocognitive effects of clozapine, olanzapine, risperidone, and haloperidol in patients with chronic schizophrenia or schizoaffective disorder. *Am J Psychiatry.* (2002) 159:1018–28. doi: 10.1176/appi.ajp.159.6.1018
3. Grunder G, Heinze M, Cordes J, Muhlbauer B, Juckel G, Schulz C, et al. Effects of first-generation antipsychotics versus second-generation antipsychotics on quality of life in schizophrenia: a double-blind, randomised study. *Lancet Psychiatry.* (2016) 3:717–29. doi: 10.1016/S2215-0366(16)00085-7
4. Stroup TS, Gray N. Management of common adverse effects of antipsychotic medications. *World Psychiatry.* (2018) 17:341–56. doi: 10.1002/wps.20567
5. Mangurian C, Newcomer JW, Modlin C, Schillinger D. Diabetes and cardiovascular care among people with severe mental illness: a literature review. *J Gen Intern Med.* (2016) 31:1083–91. doi: 10.1007/s11606-016-3712-4
6. Fiedorowicz JG, Coryell WH, Rice JP, Warren LL, Haynes WG. Vasculopathy related to manic/hypomanic symptom burden and first-generation antipsychotics in a sub-sample from the collaborative depression study. *Psychother Psychosom.* (2012) 81:235–43. doi: 10.1159/000334779
7. Kahl KG, Westhoff-Bleck M, Kruger THC. Effects of psychopharmacological treatment with antipsychotic drugs on the vascular system. *Vascul Pharmacol.* (2018) 100:20–5. doi: 10.1016/j.vph.2017.09.001
8. Leung JY, Pang CC, Procyshyn RM, Barr AM. Cardiovascular effects of acute treatment with the antipsychotic drug olanzapine in rats. *Vascul Pharmacol.* (2014) 62:143–9. doi: 10.1016/j.vph.2014.06.003
9. Ranchoux B, Nadeau V, Bourgeois A, Provencher S, Tremblay E, Omura J, et al. Metabolic syndrome exacerbates pulmonary hypertension due to left heart disease. *Circ Res.* (2019) 125:449–66. doi: 10.1161/CIRCRESAHA.118.314555
10. Molassiotis A. Time to re-think the olanzapine dose. *Lancet Oncol.* (2019) 21:189–90. doi: 10.1016/S1470-2045(19)30791-0
11. de Leon J. Personalizing dosing of risperidone, paliperidone and clozapine using therapeutic drug monitoring and pharmacogenetics. *Neuropharmacology.* (2019) 168:107656. doi: 10.1016/j.neuropharm.2019.05.033
12. Raggi P, Bellasi A, Bushinsky D, Bover J, Rodriguez M, Ketteler M, et al. Slowing progression of cardiovascular calcification with SNF472 in patients on hemodialysis: results of a randomized, phase 2b study. *Circulation.* (2019) 141:728–39. doi: 10.1161/CIRCULATIONAHA.119.044195
13. Chen YF. Chinese classification of mental disorders (CCMD-3): towards integration in international classification. *Psychopathology.* (2002) 35:171–5. doi: 10.1159/000065140
14. Ogawa T, Ishida H, Matsuda N, Fujiu A, Matsuda A, Ito K, et al. Simple evaluation of aortic arch calcification by chest radiography in hemodialysis patients. *Hemodial Int.* (2009) 13:301–6. doi: 10.1111/j.1542-4758.2009.00366.x
15. Woo JS, Kim W, Kwon SH, Youn HC, Kim HS, Kim JB, et al. Aortic arch calcification on chest X-ray combined with coronary calcium score show additional benefit for diagnosis and outcome in patients with angina. *J Geriatr Cardiol.* (2016) 13:218–25. doi: 10.11909/j.issn.1671-5411.2016.03.006
16. Yamaguchi Y, Tanaka T, Yoshimura S, Koga M, Nagatsuka K, Toyoda K. A novel evaluation for predicting aortic complicated lesions using calcification on chest X-ray. *Cerebrovasc Dis.* (2017) 44:169–78. doi: 10.1159/000479117
17. Woods SW. Chlorpromazine equivalent doses for the newer atypical antipsychotics. *J Clin Psychiatry.* (2003) 64:663–7. doi: 10.4088/JCP.v64n0607
18. Leucht S, Samara M, Heres S, Davis JM. Dose equivalents for antipsychotic drugs: the DDD method. *Schizophr Bull.* (2016) 42 (Suppl 1) S90–94. doi: 10.1093/schbul/sbv167
19. Iijima K, Hashimoto H, Hashimoto M, Son BK, Ota H, Ogawa S, et al. Aortic arch calcification detectable on chest X-ray is a strong independent predictor of cardiovascular events beyond traditional risk factors. *Atherosclerosis.* (2010) 210:137–44. doi: 10.1016/j.atherosclerosis.2009.11.012
20. Demer LL, Tintut Y, Nguyen KL, Hsiai T, Lee JT. Rigor and reproducibility in analysis of vascular calcification. *Circ Res.* (2017) 120:1240–2. doi: 10.1161/CIRCRESAHA.116.310326
21. Zhou Y, Ning Y, Rosenheck R, Sun B, Zhang J, Ou Y, et al. Effect of living with patients on caregiver burden of individual with schizophrenia in China. *Psychiatry Res.* (2016) 245:230–7. doi: 10.1016/j.psychres.2016.08.046
22. De Hert M, Detraux J, van Winkel R, Yu W, Correll CU. Metabolic and cardiovascular adverse effects associated with antipsychotic drugs. *Nat Rev Endocrinol.* (2011) 8:114–26. doi: 10.1038/nrendo.2011.156
23. Kahn RS. On the continued benefit of antipsychotics after the first episode of schizophrenia. *Am J Psychiatry.* (2018) 175:712–3. doi: 10.1176/appi.ajp.2018.18060639
24. Henderson DC, Cagliero E, Gray C, Nasrallah RA, Hayden DL, Schoenfeld DA, et al. Clozapine, diabetes mellitus, weight gain, and lipid abnormalities: a five-year naturalistic study. *Am J Psychiatry.* (2000) 157:975–81. doi: 10.1176/appi.ajp.157.6.975
25. Murray RM, Quattrone D, Natesan S, van Os J, Nordentoft M, Howes O, et al. Should psychiatrists be more cautious about the long-term prophylactic use of antipsychotics? *Br J Psychiatry.* (2016) 209:361–5. doi: 10.1192/bjp.bp.116.182683
26. Larsen JR, Svensson CK, Vedtofte L, Jakobsen ML, Jespersen HS, Jakobsen MI, et al. High prevalence of prediabetes and metabolic abnormalities in overweight or obese schizophrenia patients treated with clozapine or olanzapine. *CNS Spectr.* (2018) 24:441–52. doi: 10.1017/S1092852918001311
27. Emul M, Kalelioglu T. Etiology of cardiovascular disease in patients with schizophrenia: current perspectives. *Neuropsychiatr Dis Treat.* (2015) 11:2493–503. doi: 10.2147/NDT.S50006
28. Miyauchi A, Kouga T, Jimbo EF, Matsuhashi T, Abe T, Yamagata T, et al. Apomorphine rescues reactive oxygen species-induced apoptosis of fibroblasts with mitochondrial disease. *Mitochondrion.* (2019) 49:111–20. doi: 10.1016/j.mito.2019.07.006

Conflict of Interest: The authors declare that the research was conducted in the absence of any commercial or financial relationships that could be construed as a potential conflict of interest.

Publisher's Note: All claims expressed in this article are solely those of the authors and do not necessarily represent those of their affiliated organizations, or those of the publisher, the editors and the reviewers. Any product that may be evaluated in this article, or claim that may be made by its manufacturer, is not guaranteed or endorsed by the publisher.

Copyright © 2021 Zhang, Zheng, Feng, Zhang, Han, He, Liu, Huang and Chen. This is an open-access article distributed under the terms of the Creative Commons Attribution License (CC BY). The use, distribution or reproduction in other forums is permitted, provided the original author(s) and the copyright owner(s) are credited and that the original publication in this journal is cited, in accordance with accepted academic practice. No use, distribution or reproduction is permitted which does not comply with these terms.

frontiers in Cardiovascular Medicine

ORIGINAL RESEARCH
published: 21 September 2021
doi: 10.3389/fcvm.2021.707008

Association of the Monocyte–to–High-Density Lipoprotein Cholesterol Ratio With Diabetic Retinopathy

Xixiang Tang[1,2†], Ying Tan[1†], Yi Yang[1], Mei Li[1,2], Xuemin He[1], Yan Lu[3], Guojun Shi[1], Yanhua Zhu[1], Yuanpeng Nie[1], Haicheng Li[1], Panwei Mu[1] and Yanming Chen[1*]*

[1] Department of Endocrinology & Metabolism, The Third Affiliated Hospital of Sun Yat-sen University, Guangdong Provincial Key Laboratory of Diabetology, Guangzhou, China, [2] VIP Medical Service Center, The Third Affiliated Hospital of Sun Yat-sen University, Guangzhou, China, [3] Department of Clinical Immunology, The Third Affiliated Hospital of Sun Yat-sen University, Guangzhou, China

OPEN ACCESS

Edited by:
Yuli Huang,
Southern Medical University, China

Reviewed by:
C. Roger White,
University of Alabama at Birmingham, United States
Jingming Li,
The First Affiliated Hospital of Xi'an Jiaotong University, China

***Correspondence:**
Yanming Chen
chyanm@mail.sysu.edu.cn
Yanhua Zhu
zhuyanh2@mail.sysu.edu.cn

[†]These authors have contributed equally to this work and share first authorship

Specialty section:
This article was submitted to General Cardiovascular Medicine, a section of the journal Frontiers in Cardiovascular Medicine

Received: 08 May 2021
Accepted: 27 August 2021
Published: 21 September 2021

Citation:
Tang X, Tan Y, Yang Y, Li M, He X, Lu Y, Shi G, Zhu Y, Nie Y, Li H, Mu P and Chen Y (2021) Association of the Monocyte–to–High-Density Lipoprotein Cholesterol Ratio With Diabetic Retinopathy. Front. Cardiovasc. Med. 8:707008. doi: 10.3389/fcvm.2021.707008

Background: Chronic inflammation in type 2 diabetes mellitus (T2DM) is an essential contributor to the development of diabetic retinopathy (DR). The monocyte–to–high-density lipoprotein cholesterol (HDL-C) ratio (MHR) is a novel and simple measure related to inflammatory and oxidative stress status. However, little is known regarding the role of the MHR in evaluating the development of DR.

Methods: A total of 771 patients with T2DM and 607 healthy controls were enrolled in this cross-sectional study. MHR determination and eye examination were performed. The association of MHR with the prevalence of DR in T2DM patients was analyzed.

Results: The MHR in patients with DR was significantly higher than that in both non-DR diabetic patients ($P < 0.05$) and healthy controls ($P < 0.01$). No significance was observed in the MHR of different DR severity grades. Moreover, the MHR was similar between patients with non-macular oedema and those with macular oedema. Logistic regression analysis demonstrated that MHR was independently associated with the prevalence of DR in diabetic patients [odds ratio (OR) = 1.438, 95% confidence interval (CI): 1.249–1.655, $P < 0.01$]. After additional stratification by HbA1c level and diabetic duration, the MHR was still independently associated with the prevalence of DR.

Conclusions: Our study suggests that the MHR can be used as a marker to indicate the prevalence of DR in patients with T2DM.

Keywords: monocyte to high-density lipoprotein cholesterol ratio, type 2 diabetes, diabetic retinopathy, biomarker, inflammation

INTRODUCTION

Type 2 diabetes mellitus (T2DM) is a highly and rapidly evolving global health issue (1, 2), even in patients with prediabetes, the risk of macrovascular and microvascular disease were increased (3–5). Diabetic retinopathy (DR) is one of the most important diabetic microvascular complications and a leading cause of irreversible blindness among the working-age population around the world (6). Although the underlying molecular mechanisms of DR are not yet fully understood, abundant

evidence indicates that inflammation plays a key role in the pathophysiology of DR (7). Various inflammatory cytokines and chemokines, such as ICAM-1, IL-1β, IL-6, IL-8, TNF-α, and MCP-1, have been reported to be elevated in the serum and vitreous and aqueous humor from diabetic patients with DR (8).

Monocytes are released from their precursors in bone marrow into the circulation and migrate to tissues and release proinflammatory cytokines at sites of inflammation, thereby affecting the severity of inflammation, which is considered an inflammatory biomarker (9). Additionally, plasma high-density lipoprotein cholesterol (HDL-C) has an inverse relationship with DR risk (10, 11). In addition, HDL-C has antioxidant efficacy to protect endothelial functions (12, 13). Therefore, the monocyte count–to–HDL-C ratio (MHR) can reflect the inflammatory status and is related to the development of disease associated with chronic inflammation. The MHR has been found to be associated with the occurrence and prognosis of cardiovascular diseases (CVDs), diabetic nephropathy and diabetic peripheral neuropathy (14–17). However, to the best of our knowledge, there are a few studies with small sample size that evaluated the associations of the MHR with DR and got contradictory conclusion (18, 19). Further studies investigating the relationship between MHR and DR in larger patient groups are needed. Thus, in the present study, we aimed to investigate the associations between the MHR and the prevalence of DR in adults with T2DM.

METHODS

Study Population

A total of 1,378 subjects between the ages of 18 and 70 years, including 771 patients with T2DM and 607 healthy individuals, were included consecutively in this observational cross-sectional study between January 2016 and December 2018. T2DM patients were diagnosed based on the 1999 criteria of the World Health Organization (WHO) (20). The exclusion criteria were as follows: active or chronic inflammation, active infection, autoimmune diseases, hematological disorder, recent blood transfusion before enrolment, malignancy, acute or chronic renal/hepatic diseases, or coronary artery disease. Ethics approval was obtained from the Third Affiliated Hospital of Sun Yat-sen University Network Ethics Committee.

Data Collection and Laboratory Analysis

Baseline information, including age, sex, comorbidities, smoking status, alcohol intake, medications, body height, weight, and blood pressure, was collected from medical records. Laboratory assessments consisted of fasting blood glucose, liver and renal function, uric acid, total cholesterol, triglycerides, low-density lipoprotein cholesterol (LDL-C), and high-density lipoprotein cholesterol (HDL-C), which were examined by a HITACHI (Tokyo, Japan) 7180 Automatic Analyser using 8-h overnight fasting blood samples. HbA1c was measured by high-performance liquid chromatography (HPLC) with a D-10 hemoglobin testing program (Bio-Rad). White blood cell measurement was performed with an automated hematology analyser XE-1200 (Sysmex, Kobe, Japan). The MHR ratio was calculated by dividing the monocyte count by HDL-C.

Eye Examination

Eye examinations were performed on all participants according to standard operation procedures by trained ophthalmologists. The eye examinations included visual acuity measurements, tonometry, intraocular pressure, an anterior ocular structure, and fundus examination using a standard protocol. The external and anterior ocular segments were examined by slit lamp biomicroscopy (BQ900; Haag-Streit, Bern, Switzerland). Two 45° field digital, color, non-stereoscopic fundal photographs of each eye were taken in the macula-centered and posterior pole by a non-mydriatic auto-fundus camera (TRC-NW400 Non-Mydriatic Retinal Camera, Topcon, Tokyo, Japan).

Assessment of DR

Two physicians made the assessment of DR independently (Kappa index = 0.919, $P < 0.0001$, indicating an excellent agreement between two physician). DR was diagnosed if any characteristic lesions existed as defined by the Early Treatment Diabetic Retinopathy Study (ETDRS). DR severity was further categorized into mild, moderate and severe non-proliferative DR (NPDR) and proliferative DR (PDR). Another important additional categorization in DR was diabetic macular oedema (DME) and non-DME (21).

Statistical Analyses

Database management and statistical analysis were performed using PASW 22.0 for Windows (IBM Inc., Armonk, USA). Continuous variables are presented as the means ± standard deviation or median (interquartile range), while categorical variables are expressed as numbers (percentages). One-way ANOVA was applied for the comparison of continuous variables among groups, and a *post-hoc* test using Fisher's least significant difference (LSD) was used to determine which means differed following ANOVA. Differences in categorical variables were evaluated by Pearson's chi-square test. Univariate logistic regression analysis was performed to assess the non-adjusted relationships between 10*MHR and the prevalence of DR. Odds ratios (ORs) and 95% confidence intervals (CIs) were estimated for the association between DR and 10*MHR. Then, two multivariate logistic regression models were performed to adjust for confounding factors. Model 1 was adjusted for age, sex. Model 2 was additionally adjusted for body mass index, diabetes duration, smoking status, SBP, DBP, triglyceride, LDL-C, Cr, UA, FBG, HbA1c, and medications. To determine whether the duration of diabetes and glucose control status affect the relationship between MHR and the prevalence of DR, subgroup analyses were performed based on the duration of diabetes (<10 and ≥10 years) and HbA1c levels (<7.0 and ≥7.0%). A two-tailed $P < 0.05$ was considered statistically significant.

RESULTS

The Clinical Characteristics of the Participants

Of 771 patients with T2DM, 164 (21%) were DR patients. The clinical characteristics of all participants are summarized in **Table 1**. No significant differences were observed in terms of age, sex, smoking status, or alcohol intake among all groups. Body mass index (BMI), blood pressure, monocyte counts, TGs, fasting blood glucose, HbA1c, and BUN in the healthy control group were lower than those in T2DM patients, while HDL-C and LDL-C were higher (all $P < 0.05$). Among all subjects with T2DM, the diabetic duration in the subjects with DR was much longer than that in the subjects with non-DR ($P < 0.01$). Higher neutrophil counts, monocyte counts, TGs, Cr, BUN, UA, and insulin use and lower levels of HDL-C were observed in patients with DR (all $P < 0.05$). However, no significant differences were observed in hyperlipidemia, blood pressure, fasting blood glucose, HbA1c, UACR, antiplatelet use, or statin use between subjects with DR and non-DR.

The Association Between MHR and DR

Compared to that in the healthy controls, the level of MHR was remarkably increased in patients with T2DM ($P < 0.01$), as shown in **Figure 1A**. The MHR in patients with DR was significantly higher than that of both the diabetic patients without DR and the healthy controls ($P < 0.01$). No significant difference was observed in DR subjects with different severity or between subjects with DME and non-DME subjects (**Figures 1B,C**).

Univariate and Multivariate Logistic Regression Analysis

Univariate logistic regression analysis demonstrated that 10*MHR was associated with the development of DR [OR (95% CI) = 1.435 (1.277–1.614), $P < 0.001$] (**Table 2**). After adjusting for age and sex, 10*MHR was still independently related to the development of DR [OR (95% CI) = 1.424 (1.263–1.605), $P < 0.001$]. When further adjusting for BMI, diabetes duration, smoking status, SBP, DBP, triglyceride, LDL-C, Cr, UA, FBG, HbA1c, and medications, 10*MHR remained independently associated with the prevalence of DR [OR (95% CI) = 1.438 (1.249–1.655), $P < 0.001$].

Subgroup Analysis

The most consistent risk factors for the development of DR are long duration of diabetes and hyperglycemia (6, 22, 23). A reasonable HbA1c level is below or around 7% and longer duration of diabetes was 8–11 years according to the American Diabetes Association (ADA) and the European Association for the Study of Diabetes (EASD) (24, 25). To preclude the influence of the duration of diabetes and glucose control status, which were introduced in the subgroup analysis, as shown in **Table 2**, we further performed a subgroup regression analysis stratified by HbA1c levels (<7 vs. ≥7%) and the duration of diabetes (<10 vs. ≥10 years). In multivariate logistic regression Model 2, the 10*MHR group had a significantly higher prevalence of DR regardless of the level of HbA1c ($P < 0.05$) and diabetic duration ($P < 0.01$).

DISCUSSION

In the present study, the results provide evidence about the unique association between the MHR and DR. Elevated MHR levels were associated with increased odds of DR, independent of a variety of conventional DR risk factors. However, we did not detect a significant association between the MHR level and DR severity or macular edema in patients with T2DM.

Inflammation markers and monocytes play an important role in the development of diabetic complications (16, 26, 27). Retinal chronic inflammation plays a pivotal role in the development of DR (6, 7). The levels of monocytes are increased in the retinal vessels and differentiate into macrophages that secrete inflammatory cytokines and growth factors adhering to the outer surface of retinal capillaries, leading to the breakdown of the blood retinal barrier, increased retinal vascular permeability and capillary non-perfusion, which are considered characteristic pathologic features in early DR (28, 29). In the present study, neutrophil and monocyte counts were remarkably increased in patients with DR compared to healthy controls or patients without DR, which is consistent with the findings in previous studies. Hyperglycemia enhances the inflammatory status to release more neutrophils and monocytes from bone marrow and then recruit them into the retinal vessels, causing damage to these vessels (30).

Lipid disorders seem to contribute to the development and progression of DR (31, 32). Accumulated evidence indicates that poor control of triglycerides and LDL is associated with the incidence and progression of DR, while higher HDL-C levels and the use of lipid-lowering medication significantly reduce the risk of DR (33–35). Our results also showed higher levels of triglycerides and lower HDL in DR individuals.

Recently, the MHR has emerged as a novel and convenient marker with the integration of proinflammatory and anti-inflammatory factors (14–19). Emerging data suggest that higher MHR values are associated with various diseases or organ dysfunctions, such as endothelial dysfunction in Behçet disease, the presence and severity of metabolic syndrome, polycystic ovary syndrome, cardiac syndrome X, serum albumin level saphenous vein graft disease in coronary bypass, the high SYNTAX score in patients with stable coronary artery disease, asymptomatic organ damage in patients with primary hypertension, left atrial remodeling in atrial fibrillation, abdominal aortic aneurysm size, myocardial infarction, and CVD in patients with obstructive sleep apnea syndrome (14, 15, 36–43). It has also been shown that MHR is an independent predictor of in-hospital and long-term mortality and major adverse cardiac events in patients with acute coronary syndromes or a post-PCI status (44). Therefore, the MHR is a new prognostic marker in several CVDs, which are associated with inflammation. In addition, accumulated evidence has shown that the MHR is related to diabetes and diabetic complications (16, 45) and

TABLE 1 | Baseline characteristics.

Variables	Health control ($n = 607$)	NDR ($n = 607$)	DR ($n = 164$)
Age, years	56.7 ± 8.6	57.1 ± 10.5	57.4 ± 9.8
Male, *n* (%)	286 (47.1)	294 (48.4)	93 (56.7)
BMI, kg/m2	23.0 ± 3.3	24.4 ± 3.4**	24.3 ± 3.8**
Diabetes duration, years	–	6.0 (2.0–11.0)	10.0 (5.0–15)##
Smoking, *n* (%)	140 (23.1)	143 (23.6)	47 (28.7)
Alcohol, *n* (%)	98 (16.1)	96 (15.9)	32 (19.5)
Hyperlipidemia, *n* (%)	–	38 (6.3)	8 (4.9)
Hypertension, *n* (%)	–	191 (31.5)	65 (39.6)
SBP, mmHg	117.4 ± 14.1	132.1 ± 18.7**	131.9 ± 18.6**
DBP, mmHg	75.1 ± 9.7	80.7 ± 11.0**	80.1 ± 10.9**
Laboratory tests			
White blood cells, 10^9/L	6.22 ± 1.43	6.38 ± 1.61	6.99 ± 2.26
Neutrophils, 10^9/L	3.62 ± 1.16	3.65 ± 1.21	4.28 ± 2.04**#
Lymphocytes, 10^9/L	2.16 ± 0.55	2.11 ± 0.70	2.04 ± 0.59
Monocytes, 10^9/L	0.43 ± 0.13	0.42 ± 0.12	0.47 ± 0.18*#
TC, mmol/L	5.00 ± 0.95	4.81 ± 1.20*	4.88 ± 1.49
TG, mmol/L	1.01 (0.75–1.47)	1.31 (0.92–1.87)**	1.32 (1.00–2.11)**#
HDL-C, mmol/L	1.30 ± 0.29	1.18 ± 0.28**	1.10 ± 0.28**#
LDL-C, mmol/L	3.34 ± 0.92	3.00 ± 1.01**	2.98 ± 1.05**
MHR, 10^9/mmol	0.351 ± 0.147	0.370 ± 0.119*	0.458 ± 0.224**##
FBG, mmol/L	5.18 ± 0.68	9.51 ± 5.88**	9.92 ± 6.43**
HbA1c, %	5.3 ± 0.4	8.9 ± 2.5**	8.9 ± 2.3**
UACR, mg/g	–	0.99 (0.65–2.39)	1.25 (0.78–3.40)
Cr, umol/l	71.97 ± 15.55	71.32 ± 52.77	90.21 ± 52.05**##
BUN, umol/l	4.62 ± 1.13	5.71 ± 1.91**	6.35 ± 3.23**##
UA, umol/l	375.8 ± 101.9	352.7 ± 100.6**	375.3 ±106.1#
Medications			
Insulin, n (%)	–	189 (31.1)	75 (45.7)#
Metformin, *n* (%)	–	399 (65.7)	103 (62.8)
Glucosidase inhibitor, *n* (%)	–	185 (30.5)	52 (31.7)
Sulfonylureas, *n* (%)	–	169 (27.8)	55 (33.5)
DPP-4 inhibitors, *n* (%)	–	152 (25.0)	39 (23.8)
GLP-1R, *n* (%)	–	11 (1.8)	4 (2.4)
SGLT2 inhibitor, *n* (%)	–	13 (2.1)	4 (2.8)
Glinides, *n* (%)	–	19 (3.1)	5 (3.0)
Anti-platelet, *n* (%)	–	273 (45.0)	84 (51.2)
Statin, *n* (%)	–	431 (71.0)	112 (68.3)
ACEI/ARB, *n* (%)	–	151 (24.9)	49 (29.9)
β-blocker, *n* (%)	–	61 (10.0)	28 (17.1)#
CCB, *n* (%)	–	87 (14.3)	32 (19.5)
Diuretic, *n* (%)	–	10 (1.6)	6 (3.7)

Data are mean (SD), median (25th to 75th percentile) or n (%).

BMI, body mass index; SBP, systolic blood pressure; DBP, diastolic blood pressure; FBG, Fasting blood glucose; UACR, urine albumin to creatinine rate; Cr, plasma creatinine; BUN, blood urea nitrogen; UA, uric acid; TC, total cholesterol; TG, triglycerides; HDL-C, high density lipoprotein cholesterol; LDL-C, low density lipoprotein cholesterol; ACEI/ARB, angiotensin converting enzyme inhibitor/angiotensin receptor blocker; CCB, calcium channel blockers.

$^*P < 0.05$ vs. Health control, $^{**}P < 0.01$ vs. Health control, $^{\#}P < 0.05$ vs. NDR, $^{\#\#}P < 0.01$ vs. NDR.

ocular disorders, including pseudoexfoliation syndrome (46), glaucoma, branch retinal vein occlusion (47), and central serous retinopathy (48). MHR values are increased in patients with diabetes compared to healthy controls, and an elevated MHR can predict diabetic nephropathy and diabetic axonal polyneuropathy (49). Moreover, there are a few studies with

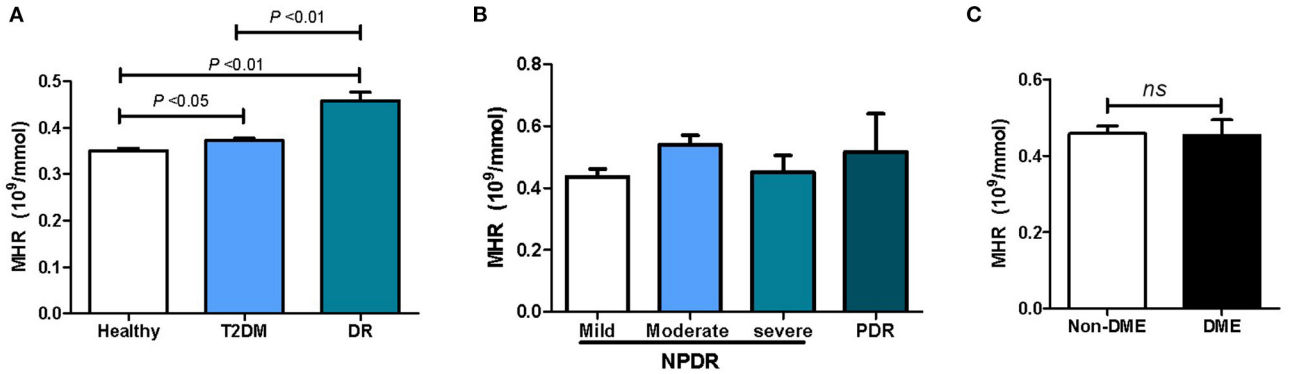

FIGURE 1 | The association between the MHR and patients with DR. **(A)** MHR levels in healthy controls, diabetic patients with and without DR; **(B)** MHR levels in DR subjects with different severity; **(C)** MHR levels between subjects with DME and non-DME.

TABLE 2 | Logistic regression analysis assessing the association of the MHR with diabetic retinopathy.

Variables	Univariate			Model 1*			Model 2*		
	OR	95%CI	*P*-value	OR	95%CI	*P*-value	OR	95%CI	*P*-value
*10*MHR, 10^8/mmol*									
Overall	1.435	1.277–1.614	<0.001	1.424	1.263–1.605	<0.001	1.438	1.249–1.655	<0.001
Stratified by HbA1c									
<7.0	1.440	1.156–1.793	0.001	1.519	1.195–1.931	0.001	1.739	1.232–2.455	0.002
≥7.0	1.433	1.248–1.646	<0.001	1.411	1.226–1.623	<0.001	1.432	1.206–1.699	<0.001
Stratified by diabetic duration									
<10	1.375	1.168–1.618	<0.001	1.373	1.157–1.628	<0.001	1.304	1.070–1.589	0.008
≥10	1.500	1.263–1.781	<0.001	1.465	1.233–1.740	<0.001	1.724	1.354–2.195	<0.001

**Model 1 was adjusted for age, sex.*
Multivariate regression analysis model 2 was adjusted for age, sex, BMI, diabetes duration, smoking status, SBP, DBP, triglyceride, LDL-C, Cr, UA, FBG, HbA1c, and medications.

small sample size that evaluated the associations of the MHR with DR and got contradictory conclusions. Işil Çakir et al.' study showed that MHR was significantly higher in DR group than T2DM without DR group and found that specificity and sensitivity of MHR in detecting DR were relatively low (18); while it can be inferred that MHR is not affected by diabetes, but only by the proliferation process in Inhsan Solmaz et al.' study (19). Then, in the present study with larger sample size showed that diabetes, a chronic inflammatory disease, yields an elevated MHR level, and an elevated MHR can be an useful biomarker for DR independent of conventional risk factors, but not predict the severity stage of DR, which is not consistent with the previous study (18, 19). To date, several studies in addition to our study have consistently demonstrated that the MHR is a reliable factor for inflammation and is associated with diabetic micro- and macrovascular complications.

Furthermore, compared to other expensive inflammatory markers, such as interleukin factor (IL)-1, IL-6, tumor necrosis factor-α, and monocyte chemo-attractant protein-1, the MHR can be easily calculated from a simple blood analysis, making the use of this index more practical, cost-effective, and useful to predict DR (8).

It is important to note the limitations of our investigation. First, it was a single-center cross-sectional study; thus, causal relationships between MHR and DR cannot be confirmed. These findings should be cautiously interpreted, and further prospective studies are needed. Second, we did not exclude subjects with macrovascular complications, such as coronary artery disease, because the percentage of subjects with these complications did not vary significantly between the DR and non-DR groups. Finally, additional inflammation markers, such as CRP, interleukin factor (IL)-6, and tumor necrosis factor-α, were not evaluated herein.

In summary, the present study suggests that elevated MHR is a convenient and effective measurement for predicting the presence of DR in patients with T2DM.

DATA AVAILABILITY STATEMENT

The raw data supporting the conclusions of this article will be made available by the authors, without undue reservation.

ETHICS STATEMENT

The studies involving human participants were reviewed and approved by Ethics approval was obtained from the Third Affiliated Hospital of Sun Yat-sen University Network Ethics

Committee. Written informed consent for participation was not required for this study in accordance with the national legislation and the institutional requirements.

AUTHOR CONTRIBUTIONS

XT, YT, and YC contributed to the study design, formal analysis, and writing—original draft. XT, YT, YY, XH, ML, and HL contributed to the data acquisition and curation. YZ and YN contributed to the literature research. YL, GS, and PM revised the manuscript. All authors contributed to the article and approved the submitted version.

FUNDING

This study was funded by National Key R&D Program of China (2017YFA0105803), the National Natural Science Foundation of China (81770826, 82000278), the 5010 Clinical Research Projects of Sun Yat-sen University (2015015), the Key Area R&D Program of Guangdong Province (2019B020227003), the Science and Technology Plan Project of Guangzhou City (202007040003), the Guangdong Basic and Applied Basic Research Foundation (2020A1515010599), and the fostering special funding projects of the National Natural Science Foundation of China in the third affiliated hospital of SYSU (2020GZRPYQN04).

REFERENCES

1. Magliano DJ, Sacre JW, Harding JL, Gregg EW, Zimmet PZ, Shaw JE. Young-onset type 2 diabetes mellitus - implications for morbidity and mortality. *Nat Rev Endocrinol.* (2020) 16:321–31. doi: 10.1038/s41574-020-0334-z
2. Wang L, Gao P, Zhang M, Huang Z, Zhang D, Deng Q, et al. Prevalence and ethnic pattern of diabetes and prediabetes in China in 2013. *JAMA.* (2017) 317:2515–23. doi: 10.1001/jama.2017.7596
3. Mai L, Wen W, Qiu M, Liu X, Sun L, Zheng H, et al. Association between prediabetes and adverse outcomes in heart failure. *Diabetes Obes Metab.* (2021) 1–8. doi: 10.1111/dom.14490
4. Cai X, Liu X, Sun L, He Y, Zheng S, Zhang Y, et al. Prediabetes and the risk of heart failure: a meta-analysis. *Diabetes Obes Metab.* (2021) 23:1746–53. doi: 10.1111/dom.14388
5. Cai X, Zhang Y, Li M, Wu JH, Mai L, Li J, et al. Association between prediabetes and risk of all cause mortality and cardiovascular disease: updated meta-analysis. *BMJ.* (2020) 370:m2297. doi: 10.1136/bmj.m2297
6. Cheung N, Mitchell P, Wong TY. Diabetic retinopathy. *Lancet.* (2010) 376:124–36. doi: 10.1016/S0140-6736(09)62124-3
7. Rübsam A, Parikh S, Fort PE. Role of inflammation in diabetic retinopathy. *Int J Mol Sci.* (2018) 19:942. doi: 10.3390/ijms19040942
8. Sasongko MB, Wong TY, Jenkins AJ, Nguyen TT, Shaw JE, Wang JJ. Circulating markers of inflammation and endothelial function, and their relationship to diabetic retinopathy. *Diabet Med.* (2015) 32:686–91. doi: 10.1111/dme.12640
9. Yona S, Jung S. Monocytes: subsets, origins, fates and functions. *Curr Opin Hematol.* (2010) 17:53–9. doi: 10.1097/MOH.0b013e3283324f80
10. Klein BE, Myers CE, Howard KP, Klein R. Serum lipids and proliferative diabetic retinopathy and macular edema in persons with long-term type 1 diabetes mellitus: the wisconsin epidemiologic study of diabetic retinopathy. *JAMA Ophthalmol.* (2015) 133:503–10. doi: 10.1001/jamaophthalmol.2014.5108
11. Sasso FC, Pafundi PC, Gelso A, Bono V, Costagliola C, Marfella R, et al. High HDL cholesterol: a risk factor for diabetic retinopathy? Findings from NO BLIND study. *Diabetes Res Clin Pract.* (2019) 150:236–44. doi: 10.1016/j.diabres.2019.03.028
12. Sugano M, Tsuchida K, Makino N. High-density lipoproteins protect endothelial cells from tumor necrosis factor-alpha-induced apoptosis. *Biochem Biophys Res Commun.* (2000) 272:872–6. doi: 10.1006/bbrc.2000.2877
13. Takaeko Y, Matsui S, Kajikawa M, Maruhashi T, Kishimoto S, Hashimoto H, et al. Association of extremely high levels of high-density lipoprotein cholesterol with endothelial dysfunction in men. *J Clin Lipidol.* (2019) 13:664–72.e1. doi: 10.1016/j.jacl.2019.06.004
14. Ganjali S, Gotto AM Jr, Ruscica M, Atkin SL, Butler AE, Banach M, et al. Monocyte-to-HDL-cholesterol ratio as a prognostic marker in cardiovascular diseases. *J Cell Physiol.* (2018) 233:9237–46. doi: 10.1002/jcp.27028
15. Zhang Y, Li S, Guo YL, Wu NQ, Zhu CG, Gao Y, et al. Is monocyte to HDL ratio superior to monocyte count in predicting the cardiovascular outcomes: evidence from a large cohort of Chinese patients undergoing coronary angiography. *Ann Med.* (2016) 48:305–12. doi: 10.3109/07853890.2016.1168935
16. Karatas A, Turkmen E, Erdem E, Dugeroglu H, Kaya Y. Monocyte to high-density lipoprotein cholesterol ratio in patients with diabetes mellitus and diabetic nephropathy. *Biomarkers Med.* (2018) 12:953–9. doi: 10.2217/bmm-2018-0048
17. Gökçay Canpolat A, Emral R, Keskin Ç, Canlar S, Sahin M, Çorapçioglu D. Association of monocyte-to-high density lipoprotein-cholesterol ratio with peripheral neuropathy in patients with Type II diabetes mellitus. *Biomarkers Med.* (2019) 13:907–15. doi: 10.2217/bmm-2018-0451
18. Işil Ç, Hasan Basri A, Nahide Ekici G, Emine P, Derya S, Gökçen Alici S, et al. Monocyte to high-density lipoprotein ratio: a novel inflammation marker related to diabetic retinopathy. *Erciyes Med J.* (2020) 42:190–4. doi: 10.14744/etd.2020.32549
19. Ihsan S, Mine K. Monocyte count / HDL cholesterol ratio: A new marker in diabetic retinopathy. *Ann Med Res.* (2021) 28:258–60. doi: 10.5455/annalsmedres.2020.02.173
20. Alberti KG, Zimmet PZ. Definition, diagnosis and classification of diabetes mellitus and its complications. Part 1: diagnosis and classification of diabetes mellitus provisional report of a WHO consultation. *Diabet Med.* (1998) 15:539–53.
21. Wilkinson CP, Ferris FL III, Klein RE, Lee PP, Agardh CD, Davis M, et al. Proposed international clinical diabetic retinopathy and diabetic macular edema disease severity scales. *Ophthalmology.* (2003) 110:1677–82. doi: 10.1016/S0161-6420(03)00475-5
22. Thomas RL, Dunstan F, Luzio SD, Roy Chowdury S, Hale SL, North RV, et al. Incidence of diabetic retinopathy in people with type 2 diabetes mellitus attending the Diabetic Retinopathy Screening Service for Wales: retrospective analysis. *BMJ.* (2012) 344:e874. doi: 10.1136/bmj.e874
23. Klein BE. Reduction in risk of progression of diabetic retinopathy. *N Engl J Med.* (2010) 363:287–8. doi: 10.1056/NEJMe1005667
24. Glycemic Targets: Standards of Medical Care in Diabetes-2021. *Diabetes Care.* (2021) 44(Suppl. 1):S73–84. doi: 10.2337/dc21-S006
25. Davies MJ, D'Alessio DA, Fradkin J, Kernan WN, Mathieu C, Mingrone G, et al. Management of hyperglycemia in type 2 diabetes, 2018. A consensus report by the American Diabetes Association (ADA) and the European Association for the Study of Diabetes (EASD). *Diabetes Care.* (2018) 41:2669–701. doi: 10.2337/dci18-0033
26. Wu J, Zheng H, Liu X, Chen P, Zhang Y, Luo J, et al. Prognostic value of secreted frizzled-related protein 5 in heart failure patients with and without type 2 diabetes mellitus. *Circ Heart Fail.* (2020) 13:e007054. doi: 10.1161/CIRCHEARTFAILURE.120.007054
27. Kanbay M, Solak Y, Unal HU, Kurt YG, Gok M, Cetinkaya H, et al. Monocyte count/HDL cholesterol ratio and cardiovascular events in patients with chronic kidney disease. *Int Urol Nephrol.* (2014) 46:1619–25. doi: 10.1007/s11255-014-0730-1
28. Schröder S, Palinski W, Schmid-Schönbein GW. Activated monocytes and granulocytes, capillary nonperfusion, and neovascularization in diabetic retinopathy. *Am J Pathol.* (1991) 139:81–100. PubMed PMID: 1713023

29. Benhar I, Reemst K, Kalchenko V, Schwartz M. The retinal pigment epithelium as a gateway for monocyte trafficking into the eye. *EMBO J.* (2016) 35:1219–35. doi: 10.15252/embj.201694202
30. Kaplar M, Kappelmayer J, Veszpremi A, Szabo K, Udvardy M. The possible association of *in vivo* leukocyte-platelet heterophilic aggregate formation and the development of diabetic angiopathy. *Platelets.* (2001) 12:419–22. doi: 10.1080/09537100120078368
31. van Leiden HA, Dekker JM, Moll AC, Nijpels G, Heine RJ, Bouter LM, et al. Blood pressure, lipids, and obesity are associated with retinopathy: the hoorn study. *Diabetes Care.* (2002) 25:1320–5. doi: 10.2337/diacare.25.8.1320
32. Miljanovic B, Glynn RJ, Nathan DM, Manson JE, Schaumberg DA. A prospective study of serum lipids and risk of diabetic macular edema in type 1 diabetes. *Diabetes.* (2004) 53:2883–92. doi: 10.2337/diabetes.53.11.2883
33. Sen K, Misra A, Kumar A, Pandey RM. Simvastatin retards progression of retinopathy in diabetic patients with hypercholesterolemia. *Diabetes Res Clin Pract.* (2002) 56:1–11. doi: 10.1016/S0168-8227(01)00341-2
34. Chew EY, Ambrosius WT, Davis MD, Danis RP, Gangaputra S, Greven CM, et al. Effects of medical therapies on retinopathy progression in type 2 diabetes. *N Engl J Med.* (2010) 363:233–44. doi: 10.1056/NEJMoa1001288
35. Keech AC, Mitchell P, Summanen PA, O'Day J, Davis TM, Moffitt MS, et al. Effect of fenofibrate on the need for laser treatment for diabetic retinopathy (FIELD study): a randomised controlled trial. *Lancet.* (2007) 370:1687–97. doi: 10.1016/S0140-6736(07)61607-9
36. Acikgoz N, Kurtoglu E, Yagmur J, Kapicioglu Y, Cansel M, Ermis N. Elevated monocyte to high-density lipoprotein cholesterol ratio and endothelial dysfunction in Behçet disease. *Angiology.* (2018) 69:65–70. doi: 10.1177/0003319717704748
37. Uslu AU, Sekin Y, Tarhan G, Canakci N, Gunduz M, Karagulle M. Evaluation of monocyte to high-density lipoprotein cholesterol ratio in the presence and severity of metabolic syndrome. *Clin Appl Thromb Hemost.* (2018) 24:828–33. doi: 10.1177/1076029617741362
38. Akboga MK, Balci KG, Maden O, Ertem AG, Kirbas O, Yayla C, et al. Usefulness of monocyte to HDL-cholesterol ratio to predict high SYNTAX score in patients with stable coronary artery disease. *Biomarkers Med.* (2016) 10:375–83. doi: 10.2217/bmm-2015-0050
39. Li N, Ren L, Wang JH, Yan YR, Lin YN, Li QY. Relationship between monocyte to HDL cholesterol ratio and concomitant cardiovascular disease in Chinese Han patients with obstructive sleep apnea. *Cardiovasc Diagn Ther.* (2019) 9:362–70. doi: 10.21037/cdt.2019.08.02
40. Yayla KG, Canpolat U, Yayla Ç, Akboga MK, Akyel A, Akdi A, et al. A novel marker of impaired aortic elasticity in never treated hypertensive patients: monocyte/high-density lipoprotein cholesterol ratio. *Acta Cardiol Sin.* (2017) 33:41–9. doi: 10.6515/ACS20160427A
41. Akboga MK, Yayla C, Balci KG, Ozeke O, Maden O, Kisacik H, et al. Relationship between serum albumin level and monocyte-to-high-density lipoprotein cholesterol ratio with saphenous vein graft disease in coronary bypass. *Thor Cardiovasc Surg.* (2017) 65:315–21. doi: 10.1055/s-0036-1582260
42. Sercelik A, Besnili AF. Increased monocyte to high-density lipoprotein cholesterol ratio is associated with TIMI risk score in patients with ST-segment elevation myocardial infarction. *Rev Port Cardiol.* (2018) 37:217–23. doi: 10.1016/j.repc.2017.06.021
43. Saskin H, Serhan Ozcan K, Yilmaz S. High preoperative monocyte count/high-density lipoprotein ratio is associated with postoperative atrial fibrillation and mortality in coronary artery bypass grafting. *Interact Cardiovasc Thorac Surg.* (2017) 24:395–401. doi: 10.1093/icvts/ivw376
44. Zhang DP, Baituola G, Wu TT, Chen Y, Hou XG, Yang Y, et al. An elevated monocyte-to-high-density lipoprotein-cholesterol ratio is associated with mortality in patients with coronary artery disease who have undergone PCI. *Biosci Rep.* (2020) 40:BSR20201108. doi: 10.1042/BSR20201108
45. Ekizler FA, Cay S, Açar B, Tak BT, Kafes H, Ozeke O, et al. Monocyte to high-density lipoprotein cholesterol ratio predicts adverse cardiac events in patients with hypertrophic cardiomyopathy. *Biomarkers Med.* (2019) 13:1175–86. doi: 10.2217/bmm-2019-0089
46. Mirza E, Oltulu R, Katipoglu Z, Mirza GD, Özkagnici A. Monocyte/HDL ratio and lymphocyte/monocyte ratio in patients with pseudoexfoliation syndrome. *Ocular Immunol Inflamm.* (2020) 28:142–6. doi: 10.1080/09273948.2018.1545913
47. Satirtav G, Mirza E, Oltulu R, Mirza GD, Kerimoglu H. Assessment of monocyte/HDL ratio in branch retinal vein occlusion. *Ocular Immunol Inflamma.* (2020) 28:463–7. doi: 10.1080/09273948.2019.1569244
48. Sirakaya E, Duru Z, Kuçuk B, Duru N. Monocyte to high-density lipoprotein and neutrophil-to-lymphocyte ratios in patients with acute central serous chorioretinopathy. *Indian J Ophthalmol.* (2020) 68:854–8. doi: 10.4103/ijo.IJO_1327_19
49. Vural G, Gümüsyayla S. Monocyte-to-high density lipoprotein ratio is associated with a decreased compound muscle action potential amplitude in patients with diabetic axonal polyneuropathy. *Medicine.* (2018) 97:e12857. doi: 10.1097/MD.0000000000012857

Conflict of Interest: The authors declare that the research was conducted in the absence of any commercial or financial relationships that could be construed as a potential conflict of interest.

Publisher's Note: All claims expressed in this article are solely those of the authors and do not necessarily represent those of their affiliated organizations, or those of the publisher, the editors and the reviewers. Any product that may be evaluated in this article, or claim that may be made by its manufacturer, is not guaranteed or endorsed by the publisher.

Copyright © 2021 Tang, Tan, Yang, Li, He, Lu, Shi, Zhu, Nie, Li, Mu and Chen. This is an open-access article distributed under the terms of the Creative Commons Attribution License (CC BY). The use, distribution or reproduction in other forums is permitted, provided the original author(s) and the copyright owner(s) are credited and that the original publication in this journal is cited, in accordance with accepted academic practice. No use, distribution or reproduction is permitted which does not comply with these terms.

frontiers in Cardiovascular Medicine

REVIEW
published: 01 October 2021
doi: 10.3389/fcvm.2021.713191

Circulating Biomarkers for Cardiovascular Disease Risk Prediction in Patients With Cardiovascular Disease

Yuen-Kwun Wong[1] *and Hung-Fat Tse*[1,2,3,4]*

[1] Department of Medicine, The University of Hong Kong, Queen Mary Hospital, Hong Kong, China, [2] Department of Medicine, Shenzhen Hong Kong University Hospital, Shenzhen, China, [3] Hong Kong-Guangdong Joint Laboratory on Stem Cell and Regenerative Medicine, The University of Hong Kong, Hong Kong, China, [4] Shenzhen Institutes of Research and Innovation, The University of Hong Kong, Hong Kong, China

Cardiovascular disease (CVD) is the leading cause of death globally. Risk assessment is crucial for identifying at-risk individuals who require immediate attention as well as to guide the intensity of medical therapy to reduce subsequent risk of CVD. In the past decade, many risk prediction models have been proposed to estimate the risk of developing CVD. However, in patients with a history of CVD, the current models that based on traditional risk factors provide limited power in predicting recurrent cardiovascular events. Several biomarkers from different pathophysiological pathways have been identified to predict cardiovascular events, and the incorporation of biomarkers into risk assessment may contribute to enhance risk stratification in secondary prevention. This review focuses on biomarkers related to cardiovascular and metabolic diseases, including B-type natriuretic peptide, high-sensitivity cardiac troponin I, adiponectin, adipocyte fatty acid-binding protein, heart-type fatty acid-binding protein, lipocalin-2, fibroblast growth factor 19 and 21, retinol-binding protein 4, plasminogen activator inhibitor-1, 25-hydroxyvitamin D, and proprotein convertase subtilisin/kexin type 9, and discusses the potential utility of these biomarkers in cardiovascular risk prediction among patients with CVD. Many of these biomarkers have shown promise in improving risk prediction of CVD. Further research is needed to assess the validity of biomarker and whether the strategy for incorporating biomarker into clinical practice may help to optimize decision-making and therapeutic management.

Keywords: adipocyte, B-type natriuretic peptide, cardiac troponin, coronary artery disease, fibroblast growth factor, lipocalin, plasminogen activator inhibitor, risk prediction

OPEN ACCESS

Edited by:
Zhen Yang,
The First Affiliated Hospital of Sun Yat-sen University, China

Reviewed by:
Alexander E. Berezin,
Zaporizhia State Medical University, Ukraine
Paulo M. Dourado,
University of São Paulo, Brazil

***Correspondence:**
Hung-Fat Tse
hftse@hku.hk

Specialty section:
This article was submitted to General Cardiovascular Medicine, a section of the journal Frontiers in Cardiovascular Medicine

Received: *22 May 2021*
Accepted: *08 September 2021*
Published: *01 October 2021*

Citation:
Wong Y-K and Tse H-F (2021) Circulating Biomarkers for Cardiovascular Disease Risk Prediction in Patients With Cardiovascular Disease. Front. Cardiovasc. Med. 8:713191. doi: 10.3389/fcvm.2021.713191

INTRODUCTION

Individuals with stable coronary artery disease (CAD) are at higher risk of recurrent cardiovascular event and mortality than the general population. Preventive strategies and intensive management of cardiovascular risk factors are much needed to improve the prognosis of these patients. Although conventional risk prediction models such as Framingham Risk Score have been developed and widely used to estimate individual's risk for primary prevention of cardiovascular disease (CVD) (1), effective tools for risk assessment

in secondary prevention are still missing. The mechanisms underlying the increased risk of recurrent CVD are not fully understood. Existing prediction models that based on traditional risk factors such as age, gender, diabetes status, blood pressure, cholesterol levels, and smoking status may have limited value to risk stratify patients with stable CAD (2).

Circulating biomarkers such as high sensitivity C-reactive protein and cardiac troponin have been playing a crucial role in the diagnosis, risk stratification, and management of patients with several disease conditions including heart failure (HF) and acute coronary syndrome (ACS) (3, 4). Recently, numerous novel biomarkers from different pathophysiological pathways have been found to be associated with cardiovascular risk and may provide important prognostic information (5–7). The combined use of multiple biomarkers has also proven to be useful in the risk stratification of CVD (8). In this review, we focus on the potential utility of various biomarkers from cardiac- and metabolic-related pathways for predicting cardiovascular risk in secondary prevention setting. The reviewed biomarkers include: (i) cardiac-related biomarkers [B-type natriuretic peptide (BNP), N-terminal pro-B-type natriuretic peptide (NT-proBNP), and cardiac troponin I (cTnI)]; and (ii) metabolic-related biomarkers [adiponectin, adipocyte fatty acid-binding protein (A-FABP), heart-type fatty acid binding protein (H-FABP), lipocalin-2, fibroblast growth factor (FGF) 19 and 21, retinol-binding protein 4 (RBP4), plasminogen activator inhibitor-1 (PAI-1), 25-hydroxyvitamin D, and proprotein convertase subtilisin/kexin type 9 (PCSK9)]. These biomarkers are of special interest as they are thought to provide sufficient information for improving cardiovascular risk stratification. Evolving biomarkers such as non-coding RNAs are beyond the scope of this review, although they have shown a potential in this field (9). The potential mechanistic link between biomarkers and CVD are summarized in **Table 1**.

TABLE 1 | Potential mechanistic link between CVD and biomarkers.

Biomarker	Potential link with CVD	References
Cardiac troponin I	Myocardial injury	(10)
BNP/NT-proBNP	Myocardial stretch	(11)
Adiponectin	Insulin resistance Altered lipid metabolism Endothelial dysfunction Atherosclerosis Inflammation	(12, 13)
A-FABP	Insulin resistance Altered lipid metabolism Endothelial dysfunction Atherosclerosis Inflammation	(14, 15)
H-FABP	Altered lipid metabolism Myocardial injury	(16)
Lipocalin-2	Atherosclerosis Plaque instability Vascular remodelling Insulin resistance Inflammation	(17, 18)
FGF-19	Altered lipid metabolism Altered glucose metabolism Insulin resistance	(19, 20)
FGF-21	Altered lipid metabolism Altered glucose metabolism Insulin resistance	(19, 21)
RBP4	Insulin resistance Atherosclerosis Inflammation	(22, 23)
PAI-1	Thrombus formation Impaired fibrinolysis Insulin resistance Inflammation	(24)
25-hydroxyvitamin D	Insulin resistance Endothelial dysfunction Atherosclerosis Inflammation	(25)
PCSK9	Altered lipid metabolism Atherosclerosis	(26)

A-FABP, adipocyte fatty acid-binding protein; BNP, B-type natriuretic peptide; FGF, fibroblast growth factor; H-FABP, heart-type fatty acid-binding protein; NT-proBNP, N-terminal pro-B-type natriuretic peptide; PAI, plasminogen activator inhibitor; PCSK9, proprotein convertase subtilisin/kexin type 9; RBP, retinol-binding protein.

CHARACTERISTICS OF BIOMARKER

A biomarker, or biological marker, is broadly defined as a "characteristic that is objectively measured and evaluated as an indicator of normal biological processes, pathogenic processes, or pharmacologic responses to a therapeutic intervention" (27). Biomarkers can be classified into four types: diagnostic biomarkers are expected to facilitate the early detection of disease; prognostic biomarkers are used for estimating the likely course of the disease; predictive biomarkers are used to predict patient's response to a particular therapy; therapeutic biomarkers help to identify new therapeutic targets (28). Biomarkers can also be used as a substitute for a clinical endpoint in clinical trials. The desired characteristics of biomarkers vary based on their intended use. For instance, high specificity is required if a biomarker is used for screening purpose. As stated by Morrow and de Lemos, biomarker should fulfill a set of criteria to be clinically useful: (1) it must be accurate, reproducible, easy to obtain and inexpensive; (2) it must provide added value over existing measures; (3) it must aid in clinical decision-making (29).

STATISTICAL ASSESSMENTS FOR THE EVALUATION OF BIOMARKER PERFORMANCE

Several statistical measures have been proposed for evaluating the utility of a new biomarker. The statistical association between

Abbreviations: ACS, acute coronary syndrome; A-FABP, adipocyte fatty acid-binding protein; AUC, area under the curve; CAD, coronary artery disease; hs-cTnI, high-sensitivity cardiac troponin I; CVD, cardiovascular disease; BNP, B-type natriuretic peptide; FGF, fibroblast growth factor; HF, heart failure; H-FABP, heart-type fatty acid-binding protein; IDI, integrated discrimination improvement; IMT, intima-media thickness; NT-proBNP, N-terminal pro-B-type natriuretic peptide; NRI, net reclassification index; PAI, plasminogen activator inhibitor; PCSK9, proprotein convertase subtilisin/kexin type 9; RBP, retinol-binding protein; T2DM, type 2 diabetes mellitus.

a biomarker and the outcome can be assessed using metrics such as odds ratio, relative risk or hazard ratio. Statistical significance of an association is necessary but insufficient to provide information regarding the clinical contribution or usefulness of a new biomarker (30). Other measures including discrimination, calibration and reclassification are recommended for assessing the incremental contribution of a new biomarker to a conventional risk prediction model.

Discrimination refers to the ability of a biomarker to distinguish individuals who develop a disease from those who do not (31). The area under the receiver operating characteristic (AUC), which is equivalent to the c statistic, is the most used measure of model discrimination (32). The AUC is the probability that a randomly chosen individual with the disease has a higher predicted risk than a randomly chosen individual without the disease. Values for AUC range from 0.5 (no discrimination) to 1.0 (perfect discrimination). In general, the AUC $>$ 0.7 indicates a good model. The increase in AUC can also be used to quantify the added predictive value offered by the new biomarker. However, the AUC is relatively insensitive to small improvements in model performance when the AUC of the baseline model is well-discriminated (33).

Calibration is also an important measure of model accuracy. It measures the ability of the model to accurately predict the proportion of individuals in a group who will develop the disease events. A risk prediction model is well-calibrated when the predicted probabilities agree with the observed frequencies of an event. Statistical metric of Hosmer-Lemeshow χ^2 test is commonly used for assessing the calibration of a risk prediction model (34). A $P < 0.05$ for Hosmer-Lemeshow test indicates poor calibration of the model.

Reclassification refers to the ability to reclassify individuals into different risk categories. The reclassification measures including net reclassification index (NRI) and integrated discrimination improvement (IDI) have been proposed to quantify how well a new biomarker improves risk classification and as alternatives to the AUC (35). NRI is the net proportion of individuals with the event correctly reclassified "upward" (i.e., moving up to higher risk category) and the net proportion of individuals without the event correctly reclassified "downward" (i.e., moving down to lower risk category). This category-based NRI is highly sensitive to the number of risk categories and the choice of risk thresholds. Pencina et al., therefore, proposed a category-free version of the NRI to overcome the problem of selecting categories (36). Positive values of NRI indicate improved reclassification and negative values indicate worsened reclassification. On the other hand, IDI is independent of risk category and defined as the difference in discrimination slopes between models with and without the new marker (35). Discrimination slope is calculated as the difference between the average predicted probabilities for events and non-events.

In summary, there is no single statistical method can be used for evaluating the incremental value of a new biomarker. The metrics that used should be depending on the needs and objectives.

METHODS

Search Strategy

A literature search was conducted using PubMed to identify all relevant studies. Research articles were also selected manually from the reference lists of articles. The search strategy used the terms "biomarker," "coronary artery disease," "cardiovascular disease," "metabolic disease," "cardiac troponin," "natriuretic peptide," "heart-type fatty acid-binding protein," "adipokines," "adiponectin," "fibroblast growth factor," "fatty acid binding protein," "lipocalin 2," "neutrophil gelatinase-associated lipocalin," "retinol binding protein," "plasminogen activator inhibitor," "vitamin D," "PCSK9," and "risk prediction" in several combinations. Duplicated studies were identified and removed using Endnote duplicate function. The abstracts and titles of article retrieved were screened to exclude the irrelevant studies. Full-text articles were then examined to determine whether they met the inclusion criteria.

Inclusion and Exclusion Criteria

Inclusion criteria were: (1) studies investigating the association of a biomarker with metabolic and cardiovascular diseases, and adverse clinical outcomes such as cardiovascular events and death; (2) studies using blood serum or plasma for biomarker analysis; and (3) peer-reviewed articles and all types of reviews published in English between January 1980 and November 2020. Unpublished theses, reports, and conference proceedings were excluded. Animal studies were also excluded.

Data Extraction and Quality Assessment

Due to the heterogeneity of focus and results from the refined studies, we did not perform a meta-analysis as part of the review process. Data were extracted using a standardized form by one reviewer and verified by a second reviewer. The following data were extracted from eligible studies: first author, year of publication, country, study design, population characteristics and sample size, specimen type, follow-up duration, and main findings. The Newcastle-Ottawa Scale was used to assess the quality of the selected cohort and case-control studies, with a maximum score of nine points (37). The quality of the cross-sectional studies was assessed using the adapted version of the Newcastle-Ottawa Scale that awards a maximum score of 10 points (38). The Newcastle-Ottawa Scale assesses three main domains: selection, comparability, and outcome assessment. The AMSTAR-2 (A Measurement Tool to Assess Systematic Reviews-2) was used to evaluate the methodological quality of systematic reviews (39).

RESULTS

Study Identification

The study selection process is summarized in **Figure 1**. A total of 1,423 records were identified through the initial literature search. After removing 554 duplicates, the remaining 869 articles were screened, and 643 articles were excluded. The remaining 226 full-text articles were retrieved for detailed assessment. Ninety-one

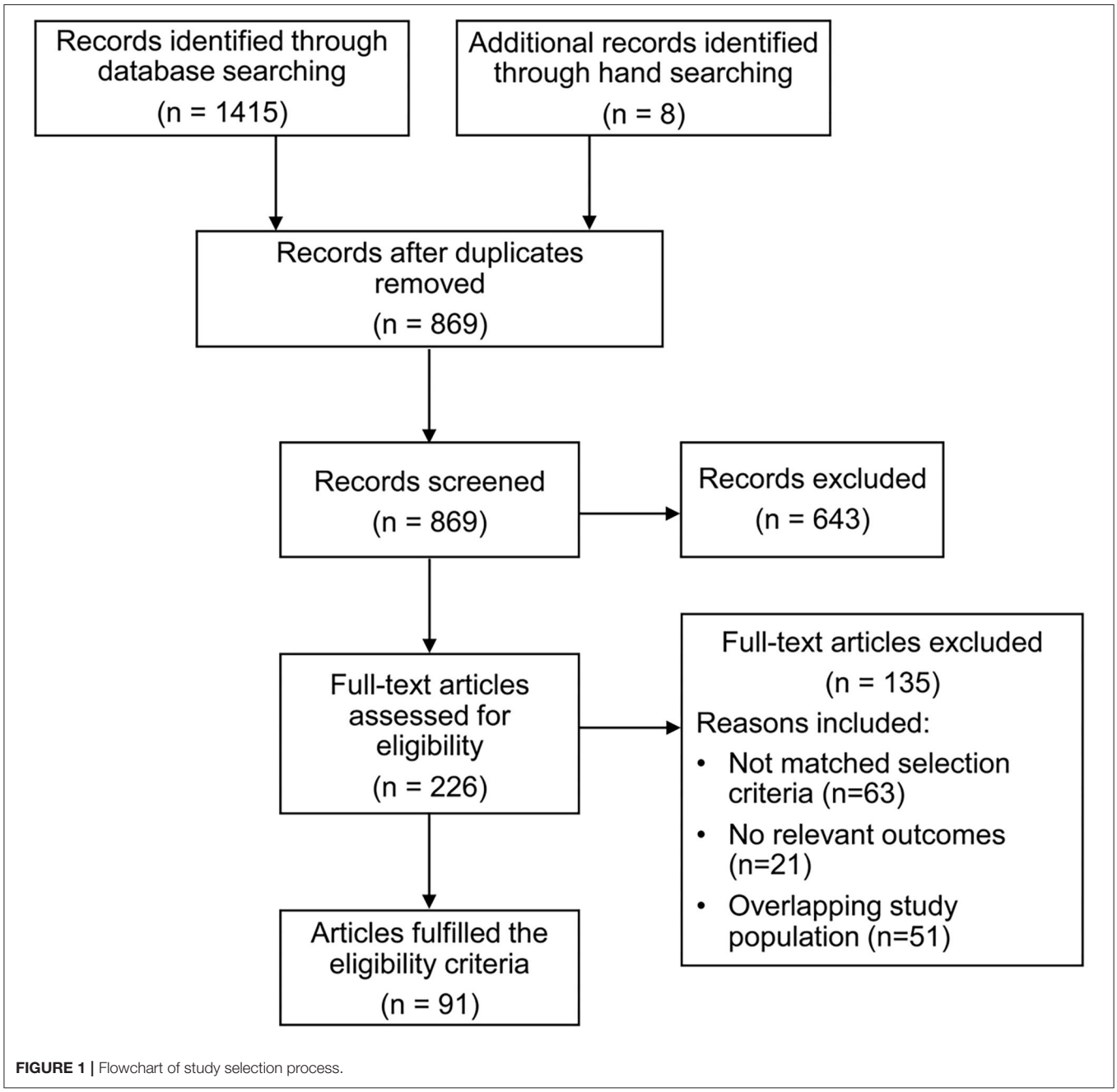

FIGURE 1 | Flowchart of study selection process.

articles were identified to fulfill the eligibility criteria and were included in the final analysis.

Study Characteristics

The 91 included studies were conducted in 24 countries and were published from 1986 to 2020. There were 43 cohort studies, 36 cross-sectional studies, 7 case-control studies, and 5 meta-analyses. The sample size of these observational studies ranged from 22 to 41,504, with a total of 135,811 participants. The following biomarkers were studies: 6 studies investigated cardiac troponin I, 10 investigated BNP or NT-proBNP, 9 reported on adiponectin, 8 reported on A-FABP, 5 reported on H-FABP, 12 on lipocalin-2, 12 on FGF-19 and/or FGF-21, 7 assessed RBP4, 7 assessed PAI-1, 8 reported on vitamin D, and 7 on PCSK9.

Quality Assessment

The results of study quality assessment are presented in **Supplementary Table 1** for the cohort studies, in **Supplementary Table 2** for the case-control studies, in **Supplementary Table 3** for the cross-sectional studies, and in **Supplementary Table 4** for the meta-analyses. According to the Newcastle-Ottawa Scale, 84 studies scored 7 or more points

(good quality) and 2 studies scored 6 points (fair quality). Of the five included reviews, according to the AMSTAR-2 rating, three were rated as moderate or high quality and two were rated as low or critically low quality.

ROLE OF BIOMARKERS IN CARDIOVASCULAR RISK ASSESSMENT

Cardiac Troponin I

cTnI is one of the subunits of troponin regulatory complex that exclusively expressed in cardiac muscle, and released into the bloodstream after cardiac injury. cTnI is an established biomarker and clinically used as gold standard for the detection of myocardial injury (10). Increased levels of cTnI can be found in a variety of cardiac and non-cardiac conditions, including myocardial infarction, HF, pulmonary embolism, myocarditis, sepsis, and renal failure (40). Several studies have demonstrated that elevated high-sensitivity cardiac troponin I (hs-cTnI) levels in patients with HF were associated with poor prognosis and increased risk of mortality (41, 42). The addition of hs-cTnI to a traditional risk factor model improved the AUC by 0.05 for subsequent HF and cardiac death (43). Moreover, levels of hs-cTnI independently predicted adverse cardiovascular events in type 2 diabetes mellitus (T2DM) patients with ACS. Patients with hs-cTnI levels >99th percentile demonstrated a 4-fold higher risk of major cardiovascular events (44). Among patients with stable CAD, hs-cTnI has been shown to predict subsequent myocardial infarction and cardiovascular death during a median follow-up of 6 years (45). In a prospective study of patients with CAD, elevated hs-cTnI levels were higher in patients with more severe CAD, and were independently associated with adverse cardiovascular events and mortality. Addition of hs-cTnI improved the AUC by 0.03 and an NRI of 25% (46). These findings showed that hs-cTnI levels had an additive prognostic value for future cardiovascular outcomes over a conventional model with clinical risk factors. **Supplementary Table 5** summarizes the studies on the predictive value of cTnI.

B-Type Natriuretic Peptide

BNP is a protein secreted by the cardiac ventricles in response to increased ventricular stretch or wall stress. It is also involved in regulating volume homeostasis and cardiovascular remodeling (47). BNP is synthesized as proBNP and is cleaved into active BNP and more stable NT-proBNP within cardiomyocytes. NT-proBNP has a longer half-life and lower variation than BNP. The clinical utility of BNP and NT-proBNP is largely similar (11). BNP and NT-proBNP are widely used for the diagnosis and risk stratification in patients with HF (48). Circulating BNP levels are lower in obese than in non-obese patients, and inversely correlated with body mass index (49). Higher levels of BNP have been found in patients with left ventricular hypertrophy and myocardial infarction (50). It has been proven that BNP level provides important prognostic information in patients with CAD, T2DM, and hypertension (51–53). Among patients with ACS and T2DM, BNP has been shown to be a powerful predictor of cardiovascular death, regardless of prior history or HF or any prior CVD (54). Another study has demonstrated that HF patients with elevated levels of BNP and cardiac troponin were at particularly high risk for mortality (55). Previous studies have also found that elevated BNP levels were associated with increased risk of adverse cardiovascular events and mortality in patients with CAD. The addition of BNP to a traditional risk factor model improved the AUC by 0.02 for prediction of adverse cardiovascular events (51, 56). Multi-marker approach based on NT-proBNP and cardiac troponin was associated with adverse events after adjustment for cardiovascular risk factors. The model incorporating a combination of NT-proBNP and cardiac troponin resulted in increases in the AUC, NRI, and IDI, suggesting that these biomarkers may serve as independent prognostic markers for CVD risk prediction (57). **Supplementary Table 6** summarizes the studies on the predictive value of BNP/NT-proBNP.

Adiponectin

Adiponectin is an adipokine secreted by adipose tissues and exhibits anti-inflammatory, anti-atherogenic, and cardioprotective effects (12, 13). Adiponectin expression is reduced in obesity, insulin resistance, and T2DM, and the plasma level is inversely related to body mass index and components of metabolic syndrome such as triglycerides and insulin levels (58, 59). Lower adiponectin levels are associated with endothelial dysfunction, increased carotid intima-media thickness (IMT) and severity of CAD (60–62). Several studies have demonstrated that adiponectin could serve as a risk factor for CVD and had moderate accuracy for the identification of metabolic syndrome, with AUC ranged from 0.67 to 0.89 (63). Circulating adiponectin has also been shown to predict cardiovascular and all-cause mortality risk in patients with prevalent CVD (64). In patients with ACS, adiponectin was associated with higher risk of adverse cardiovascular outcomes (65). Another prospective study of patients with stable CAD also reported that higher level of adiponectin was associated with a 6-fold increased risk of all-cause mortality, with good discrimination ability (AUC, 0.78) (66). **Supplementary Table 7** summarizes the studies on the predictive value of adiponectin.

Adipocyte Fatty Acid-Binding Protein

A-FABP is mainly expressed in adipocytes and macrophages, and has an important role in regulating glucose and lipid metabolism (14). Circulating A-FABP levels are closely linked to the development of obesity, insulin resistance, diabetes, hypertension, cardiac dysfunction, and atherosclerosis (15, 67). Elevated A-FABP levels are found in patients with CAD, and are positively correlated with metabolic syndrome and severity of coronary atherosclerosis (68, 69). Recent studies have shown that increased A-FABP concentrations were independently associated with increased risk of adverse cardiovascular events and cardiovascular mortality in patients with CAD (70–72). The association between A-FABP levels and cardiovascular events has also been observed in a prospective study with median follow-up of 9.4 years (73). Subjects with elevated A-FABP levels showed a 1.6-fold increased risk of cardiovascular events. The NRI and IDI were significantly improved by adding A-FABP to a traditional risk factor model (NRI, 18.6%; IDI,

0.25%). In another prospective study of patients with ACS, A-FABP was associated with a higher risk of adverse events, and demonstrated that the model with a combination of A-FABP and NT-proBNP may provide a better predictive performance than A-FABP alone, with the AUC increased from 0.65 to 0.68 (74). **Supplementary Table 8** summarizes the studies on the predictive value of A-FABP.

Heart-Type Fatty Acid-Binding Protein

H-FABP is a low molecular-weight cytoplasmic protein that is abundant in the myocardium. H-FABP is released rapidly into the circulation in response to myocardial injury, and is therefore used as an early and sensitive diagnostic marker for myocardial infarction (16). It has been reported that serum H-FABP levels are elevated in patients with metabolic syndrome and pre-diabetic patients, and positively correlated with carotid IMT (75, 76). Circulating H-FABP level has also been shown to be a strong predictor of major cardiac events and mortality in patients with ACS, suggesting that H-FABP may provide incremental information for cardiovascular risk stratification that was independent of traditional risk factors, troponin I, and BNP (77). In patients with chronic heart failure, high H-FABP was associated with 5.4-fold higher risk cardiac events, and had a higher predictive value than BNP (AUC, 0.79 vs. 0.67) (78). A recent prospective study comprising of 4,594 patients with stable CAD showed that high levels of H-FABP were associated with increased risk of adverse cardiovascular events, and found a greater risk in CAD patients with impaired glucose metabolism (79). **Supplementary Table 9** summarizes the studies on the predictive value of H-FABP.

Lipocalin-2

Lipocalin-2, also known as neutrophil gelatinase-associated lipocalin, belongs to the lipocalin superfamily, and was first identified in the specific granules of neutrophils (80). Lipocalin-2 is expressed in a various tissues including liver, kidney, lung, adipose tissue, stomach, and small intestine (81). There is also evidence to suggest that lipocalin-2 may play a role in vascular remodeling and plaque instability in atherosclerosis (17). Circulating lipocalin-2 levels are elevated in obese patients and patients with T2DM, and positively correlated with insulin resistance index and inflammatory markers (18, 82, 83). It has been reported that high levels of lipocalin-2 are associated with markers of atherosclerosis, presence and severity of CAD (84–86). In a population-based cohort study, lipocalin-2 level was an independent predictor of cardiovascular events in male subjects. The addition of lipocalin-2 to traditional risk factors improved the AUC from 0.77 to 0.81 (87). Serum lipocalin-2 levels were higher in patients with CAD or chronic HF compared with the healthy individuals (88, 89). Several studies have reported that elevated lipocalin-2 level was associated with increased risk of cardiovascular and all-cause mortality in patients with ST-segment elevation myocardial infarction after adjustment for conventional risk factors, with AUC ranging from 0.76 to 0.85, indicating a good predictive ability for prediction of mortality in these patients (90, 91). Elevated level of lipocalin-2 has also been found to be associated with a 4-fold higher risk of mortality in a 2-year follow-up study of patients with HF (92). **Supplementary Table 10** summarizes the studies on the predictive value of lipocalin-2.

Fibroblast Growth Factor 19 and 21

FGF-19 and FGF-21 belong to the same subfamily of endocrine FGFs. The FGF family comprises of 22 members, which are classified into seven subfamilies based on the structural characteristics and mechanisms of action (93). FGF-19 is primarily secreted by the small intestine during feeding, and FGF-21 is secreted by the liver during fasting, with both FGF-19 and FGF-21 share similar functions in regulating lipid, glucose and energy metabolism (19). It has been shown that circulating levels of FGF-19 are decreased in obese patients and T2DM patients with metabolic syndrome, and are inversely correlated with fasting glucose levels (20, 21, 94). In a study of 315 patients, serum FGF-19 levels were significantly lower in patients with CAD than those in the control group, and were independently associated with severity of CAD (95). On the other hand, levels of FGF-21 are elevated in patients with T2DM and those with established CAD, and are strongly associated with body mass index, triglycerides, insulin resistance, and serum A-FABP levels (96, 97). High FGF-21 level has also been reported to be an independent predictor of the development of T2DM and metabolic syndrome (98, 99). A prior study recruited individuals who underwent carotid IMT assessment demonstrated that elevated FGF-21 levels were associated with the presence of carotid atherosclerosis (100). Serum FGF-21 level was increased in patients with acute myocardial infarction compared to the control group, and associated with a higher risk of adverse cardiovascular event after follow-up of 24 months. The predictive performance of FGF-21 level was modest with an AUC of 0.67 (101). In patients with CAD, elevated FGF-21 level was associated with increased risk of cardiovascular events and mortality after adjustment for traditional cardiovascular risk factors (102, 103). **Supplementary Table 11** summarizes the studies on the predictive value of FGF-19 and FGF-21.

Retinol-Binding Protein 4

RBP4 is a member of the lipocalin family and the sole retinol transporter in blood. It is mainly secreted by the human liver and adipose tissue (104). Previous studies have revealed that RBP4 concentrations were elevated in patients with obesity and T2DM, and were associated with insulin resistance (105). Other studies have also demonstrated strong correlations of increased RBP4 levels with carotid IMT and components of the metabolic syndrome including hypertension, hypertriglyceridemia, and waist circumference, suggesting that RBP4 may serve as a marker of metabolic complications and atherosclerosis (22, 23, 106). Moreover, circulating RBP4 levels have been shown to be correlated with CVD. A recent study reported that RBP4 levels were higher in patients with CAD than those in control subjects, and were positively correlated with the prevalent and severity of CAD (107). Elevated RBP4 level was associated with an increased risk of CAD in a 16-year follow-up study of women subjects (108). It has also been reported that serum RBP4 level is an independent predictor of adverse cardiovascular events in

patients with chronic HF after adjustment for cardiovascular risk factors, and shows good prognostic performance with an AUC of 0.74 (109). **Supplementary Table 12** summarizes the studies on the predictive value of RBP4.

Plasminogen Activator Inhibitor-1

PAI-1, a member of the serine protease inhibitor (serpin) family, is the primary inhibitor of both the tissue-type and the urinary-type plasminogen activator (110). PAI-1 is mainly secreted by endothelial cells and various tissue types such as liver and adipose tissue. It is also involved in various physiological and pathological processes including fibrinolysis, tissue modeling, cancer, inflammation and CVD (24, 111, 112). Circulating levels of PAI-1 are increased in obesity, insulin resistance, and T2DM (113, 114). Elevated plasma PAI-1 levels have been reported to be an independent predictor of CVD in patients with myocardial infarction (115). Recently, a study revealed that elevated PAI-1 level was causally associated with incident CAD, suggesting that PAI-1 may have a role in the pathogenesis of CAD (116). Several studies have also demonstrated that elevated PAI-1 levels were associated with adverse cardiovascular events in patients with established CAD (117). In a prospective study of patients with ST-elevation myocardial infarction, high PAI-1 level was associated with a 5.5-fold increased risk of 5-year mortality, with an AUC of 0.75 (118). Furthermore, in the study of the Framingham Offspring study, Tofler et al. showed that both baseline and serial changes in PAI-1 levels were associated with subsequent risk of CVD, but only modest improvement in the AUCs were observed when adding PAI-1 to the traditional risk factor model (119). **Supplementary Table 13** summarizes the studies on the predictive value of PAI-1.

Vitamin D

Vitamin D is a secosteroid hormone that involves in maintaining calcium and phosphorus homeostasis, and promoting bone mineralization. 25-hydroxyvitamin D concentrations is the best indicator of vitamin D status (120). Vitamin D deficiency is often associated with bone disorders such as rickets and osteoporosis. Vitamin D has also been linked to non-skeletal diseases, including cancer, CVDs, obesity, diabetes and hypertension (25). Low vitamin D level has been found to be independently associated with increased carotid IMT and presence of carotid plaque, suggesting a potential role of vitamin D in the development of atherosclerosis (121). In addition, vitamin D deficiency was found to be associated with the prevalence and severity of CAD (122). Several studies have demonstrated that low vitamin D level was associated with increased risk of cardiovascular events including myocardial infarction (123–125). In a prospective study of 41,504 individuals, vitamin D deficiency was associated with higher prevalence of diabetes, hypertension, hyperlipidemia, and peripheral vascular disease. Patients with vitamin D level below 15 ng/mL demonstrated a 2-fold higher risk of adverse outcomes than those with normal level (126). Another large prospective study also reported that low vitamin D levels were associated with increased risk of ischemic heart disease, myocardial infarction and early death (127). More recently, a study showed that serum vitamin D levels on admission were associated with in-hospital mortality in patients with acute pulmonary embolism. A cut-off level of vitamin D $\leq$6.47 ng/mL was optimum for the prediction of in-hospital mortality with an AUC of 0.81, suggesting that vitamin D may be a potential prognostic biomarker for pulmonary embolism (128). **Supplementary Table 14** summarizes the studies on the predictive value of 25-hydroxyvitamin D.

Proprotein Convertase Subtilisin/Kexin Type 9

PCSK9, a member of the proprotein convertase family, is predominantly produced in the liver and plays a key role in cholesterol homeostasis. It reduces the low-density lipoprotein intake from circulation by enhancing the degradation of hepatic low-density lipoprotein receptor (26). Circulating PCSK9 concentrations are elevated in patients with metabolic syndrome, T2DM, and obesity (129–131). In a study of 126 with hypertensive patients, serum PCSK9 was associated with carotid IMT (132). Several studies have reported that PCSK9 levels were associated with the severity of coronary stenosis in patients with ACS, after adjustment for established risk factors (133). In a prospective study of 1,225 patients with stable CAD, elevated PCSK9 levels were related to cardiovascular metabolic markers such as total cholesterol and hemoglobin A1c, and independently associated with increased risk of adverse cardiovascular events. Patients with T2DM and high PCSK9 levels demonstrated a 5-fold increased risk of adverse cardiovascular events compared with non-diabetic patients with low PCSK9 levels (134). The association of PCSK9 levels with cardiovascular events was also observed in patients with CAD on statin treatment (135). **Supplementary Table 15** summarizes the studies on the predictive value of PCSK9.

DISCUSSION

Accurate risk stratification tools are important for clinical risk prediction and treatment strategy, particularly for individuals in higher risk groups. The selected biomarkers in this review are closely linked with CVD and have shown promise in improving the prediction of adverse cardiovascular events for primary and secondary prevention. However, validation of potential biomarkers on a larger scale remains challenging and their clinical utility in stable CAD patients is still to be determined. There is some controversy regarding which biomarker is more suitable for the prognosis of CAD. The multi-biomarker approach may help overcome some of the limitations of individual markers and improve the prognostic accuracy. It has been suggested that the strategy of combining biomarkers from different pathways is more likely to be clinically useful than biomarkers in the same pathway, and may provide greater discriminative ability than individual biomarker. For example, Hillis et al. demonstrated that the combined model of NT-proBNP and cardiac troponin provided better prognostic information with regard to the risk for future cardiovascular events than the use of a single biomarker (57). Reiser et al. also reported that the combination of NT-proBNP and A-FABP

yielded a more accurate predictive value for adverse outcomes in patients with ACS (74). These findings provide new insights into the potential use of multiple biomarkers related to cardiovascular and metabolic pathways to improve strategies for secondary prevention of CVD.

Cost is also an important consideration when selecting biomarkers for risk prediction models. Some biomarkers can be expensive to measure and other practical issues such as collection, storage and handling of samples may affect the cost of a biomarker model. Moreover, the economic burden on healthcare system after implementation of biomarker prediction tools may include the costs of: (i) additional biomarker tests; (ii) detailed assessments for risk estimation; and (iii) new therapies or interventions for treating high-risk patients to reduce risk. Although the overall costs may be increased, it may be cost-effective if health outcomes are improved sufficiently. Further evaluation of the cost-effectiveness of using biomarker prediction tools is needed to inform health policy as well as to guide clinical decisions.

In conclusion, our study revealed that these biomarkers representing different pathophysiological pathways could help to improve risk stratification for CVD. Further work is warranted to identify optimal combination of biomarkers for risk stratification of secondary prevention patients. In addition, validation studies are still required to confirm the applicability of these biomarkers in CVD risk prediction.

AUTHOR CONTRIBUTIONS

Y-KW wrote the manuscript. H-FT reviewed the manuscript. Both authors read and approved the final version.

SUPPLEMENTARY MATERIAL

The Supplementary Material for this article can be found online at: https://www.frontiersin.org/articles/10.3389/fcvm.2021.713191/full#supplementary-material

REFERENCES

1. D'Agostino RB. Sr., Vasan RS, Pencina MJ, Wolf PA, Cobain M, Massaro JM, et al. General cardiovascular risk profile for use in primary care: the Framingham Heart study. *Circulation.* (2008) 117:743–53. doi: 10.1161/CIRCULATIONAHA.107.699579
2. Omland T, White HD. State of the art: blood biomarkers for risk stratification in patients with stable ischemic heart disease. *Clin Chem.* (2017) 63:165–76. doi: 10.1373/clinchem.2016.255190
3. Nadar SK, Shaikh MM. Biomarkers in routine heart failure clinical care. *Card Fail Rev.* (2019) 5:50–6. doi: 10.15420/cfr.2018.27.2
4. Salvagno GL, Pavan C. Prognostic biomarkers in acute coronary syndrome. *Ann Transl Med.* (2016) 4:258. doi: 10.21037/atm.2016.06.36
5. Lindholm D, Lindback J, Armstrong PW, Budaj A, Cannon CP, Granger CB, et al. Biomarker-based risk model to predict cardiovascular mortality in patients with stable coronary disease. *J Am Coll Cardiol.* (2017) 70:813–26. doi: 10.1016/j.jacc.2017.06.030
6. Kleber ME, Goliasch G, Grammer TB, Pilz S, Tomaschitz A, Silbernagel G, et al. Evolving biomarkers improve prediction of long-term mortality in patients with stable coronary artery disease: the BIO-VILCAD score. *J Intern Med.* (2014) 276:184–94. doi: 10.1111/joim.12189
7. Rusnak J, Fastner C, Behnes M, Mashayekhi K, Borggrefe M, Akin I. Biomarkers in stable coronary artery disease. *Curr Pharm Biotechnol.* (2017) 18:456–71. doi: 10.2174/1389201018666170630120805
8. Onda T, Inoue K, Suwa S, Nishizaki Y, Kasai T, Kimura Y, et al. Reevaluation of cardiac risk scores and multiple biomarkers for the prediction of first major cardiovascular events and death in the drug-eluting stent era. *Int J Cardiol.* (2016) 219:180–5. doi: 10.1016/j.ijcard.2016.06.014
9. Busch A, Eken SM, Maegdefessel L. Prospective and therapeutic screening value of non-coding RNA as biomarkers in cardiovascular disease. *Ann Transl Med.* (2016) 4:236. doi: 10.21037/atm.2016.06.06
10. Hasic S, Kiseljakovic E, Jadric R, Radovanovic J, Winterhalter-Jadric M. Cardiac troponin I: the gold standard in acute myocardial infarction diagnosis. *Bosn J Basic Med Sci.* (2003) 3:41–4. doi: 10.17305/bjbms.2003.3527
11. Weber M, Hamm C. Role of B-type natriuretic peptide (BNP) and NT-proBNP in clinical routine. *Heart.* (2006) 92:843–9. doi: 10.1136/hrt.2005.071233
12. Nanayakkara G, Kariharan T, Wang L, Zhong J, Amin R. The cardio-protective signaling and mechanisms of adiponectin. *Am J Cardiovasc Dis.* (2012) 2:253–66.
13. Ouchi N, Walsh K. Adiponectin as an anti-inflammatory factor. *Clin Chim Acta.* (2007) 380:24–30. doi: 10.1016/j.cca.2007.01.026
14. Cao H, Sekiya M, Ertunc ME, Burak MF, Mayers JR, White A, et al. Adipocyte lipid chaperone AP2 is a secreted adipokine regulating hepatic glucose production. *Cell Metab.* (2013) 17:768–78. doi: 10.1016/j.cmet.2013.04.012
15. Furuhashi M, Saitoh S, Shimamoto K, Miura T. Fatty Acid-Binding Protein 4 (FABP4): pathophysiological insights and potent clinical biomarker of metabolic and cardiovascular diseases. *Clin Med Insights Cardiol.* (2014) 8:23–33. doi: 10.4137/CMC.S17067
16. Glatz JF, van der Vusse GJ, Simoons ML, Kragten JA, van Dieijen-Visser MP, Hermens WT. Fatty acid-binding protein and the early detection of acute myocardial infarction. *Clin Chim Acta.* (1998) 272:87–92. doi: 10.1016/s0009-8981(97)00255-6
17. Hemdahl AL, Gabrielsen A, Zhu C, Eriksson P, Hedin U, Kastrup J, et al. Expression of neutrophil gelatinase-associated lipocalin in atherosclerosis and myocardial infarction. *Arterioscler Thromb Vasc Biol.* (2006) 26:136–42. doi: 10.1161/01.ATV.0000193567.88685.f4
18. Wang Y, Lam KS, Kraegen EW, Sweeney G, Zhang J, Tso AW, et al. Lipocalin-2 is an inflammatory marker closely associated with obesity, insulin resistance, and hyperglycemia in humans. *Clin Chem.* (2007) 53:34–41. doi: 10.1373/clinchem.2006.075614
19. Zhang F, Yu L, Lin X, Cheng P, He L, Li X, et al. Minireview: roles of fibroblast growth factors 19 and 21 in metabolic regulation and chronic diseases. *Mol Endocrinol.* (2015) 29:1400–13. doi: 10.1210/me.2015-1155
20. Barutcuoglu B, Basol G, Cakir Y, Cetinkalp S, Parildar Z, Kabaroglu C, et al. Fibroblast growth factor-19 levels in type 2 diabetic patients with metabolic syndrome. *Ann Clin Lab Sci.* (2011) 41:390–6.
21. Wang D, Zhu W, Li J, An C, Wang Z. Serum concentrations of fibroblast growth factors 19 and 21 in women with gestational diabetes mellitus: association with insulin resistance, adiponectin, and polycystic ovary syndrome history. *PLoS ONE.* (2013) 8:e81190. doi: 10.1371/journal.pone.0081190
22. Bobbert T, Raila J, Schwarz F, Mai K, Henze A, Pfeiffer AF, et al. Relation between retinol, retinol-binding protein 4, transthyretin and carotid intima media thickness. *Atherosclerosis.* (2010) 213:549–51. doi: 10.1016/j.atherosclerosis.2010.07.063
23. Liu Y, Wang D, Li D, Sun R, Xia M. Associations of retinol-binding protein 4 with oxidative stress, inflammatory markers, and metabolic syndrome in a middle-aged and elderly Chinese population. *Diabetol Metab Syndr.* (2014) 6:25. doi: 10.1186/1758-5996-6-25
24. Cesari M, Pahor M, Incalzi RA. Plasminogen activator inhibitor-1 (PAI-1): a key factor linking fibrinolysis and age-related subclinical

and clinical conditions. *Cardiovasc Ther.* (2010) 28:e72–91. doi: 10.1111/j.1755-5922.2010.00171.x
25. Kheiri B, Abdalla A, Osman M, Ahmed S, Hassan M, Bachuwa G. Vitamin D deficiency and risk of cardiovascular diseases: a narrative review. *Clin Hypertens.* (2018) 24:9. doi: 10.1186/s40885-018-0094-4
26. Seidah NG, Benjannet S, Wickham L, Marcinkiewicz J, Jasmin SB, Stifani S, et al. The secretory proprotein convertase neural apoptosis-regulated convertase 1 (NARC-1): liver regeneration and neuronal differentiation. *Proc Natl Acad Sci USA.* (2003) 100:928–33. doi: 10.1073/pnas.0335507100
27. Biomarkers Definitions Working G. Biomarkers and surrogate endpoints: preferred definitions and conceptual framework. *Clin Pharmacol Ther.* (2001) 69:89–95. doi: 10.1067/mcp.2001.113989
28. Carlomagno N, Incollingo P, Tammaro V, Peluso G, Rupealta N, Chiacchio G, et al. Diagnostic, predictive, prognostic, and therapeutic molecular biomarkers in third millennium: a breakthrough in gastric cancer. *Biomed Res Int.* (2017) 2017:7869802. doi: 10.1155/2017/7869802
29. Morrow DA, de Lemos JA. Benchmarks for the assessment of novel cardiovascular biomarkers. *Circulation.* (2007) 115:949–52. doi: 10.1161/CIRCULATIONAHA.106.683110
30. Koenig W. Cardiovascular biomarkers: added value with an integrated approach? *Circulation.* (2007) 116:3–5. doi: 10.1161/CIRCULATIONAHA.107.707984
31. Hlatky MA, Greenland P, Arnett DK, Ballantyne CM, Criqui MH, Elkind MS, et al. Criteria for evaluation of novel markers of cardiovascular risk: a scientific statement from the American Heart Association. *Circulation.* (2009) 119:2408–16. doi: 10.1161/CIRCULATIONAHA.109.192278
32. Hanley JA, McNeil BJ. The meaning and use of the area under a receiver operating characteristic (ROC) curve. *Radiology.* (1982) 143:29–36. doi: 10.1148/radiology.143.1.7063747
33. Cook NR. Use and misuse of the receiver operating characteristic curve in risk prediction. *Circulation.* (2007) 115:928–35. doi: 10.1161/CIRCULATIONAHA.106.672402
34. Hosmer DW, Hosmer T, Le Cessie S, Lemeshow S, A. comparison of goodness-of-fit tests for the logistic regression model. *Stat Med.* (1997) 16:965–80. doi: 10.1002/(sici)1097-0258(19970515)16:9<965::aid-sim509>3.0.co;2-o
35. Pencina MJ, D'Agostino RB, Sr., D'Agostino RB, Jr., Vasan RS. Evaluating the added predictive ability of a new marker: from area under the ROC curve to reclassification and beyond. *Stat Med.* (2008) 27:157–72; discussion 207–12. doi: 10.1002/sim.2929
36. Pencina MJ, D'Agostino RB. Sr., Steyerberg EW. Extensions of net reclassification improvement calculations to measure usefulness of new biomarkers. *Stat Med.* (2011) 30:11–21. doi: 10.1002/sim.4085
37. Wells GA, Shea B, O'Connell D, Peterson J, Welch V, Losos M, et al. *The Newcastle-Ottawa Scale (NOS) for Assessing the Quality of Nonrandomised Studies in Meta-Analyses*. Available online at: http://www.ohri.ca/programs/clinical_epidemiology/oxford.asp (accessed July 15, 2021).
38. Herzog R, Alvarez-Pasquin MJ, Diaz C, Del Barrio JL, Estrada JM, Gil A. Are healthcare workers' intentions to vaccinate related to their knowledge, beliefs and attitudes? A systematic review. *BMC Public Health.* (2013) 13:154. doi: 10.1186/1471-2458-13-154
39. Shea BJ, Reeves BC, Wells G, Thuku M, Hamel C, Moran J, et al. AMSTAR 2: a critical appraisal tool for systematic reviews that include randomised or non-randomised studies of healthcare interventions, or both. *BMJ.* (2017) 358:j4008. doi: 10.1136/bmj.j4008
40. Roongsritong C, Warraich I, Bradley C. Common causes of troponin elevations in the absence of acute myocardial infarction: incidence and clinical significance. *Chest.* (2004) 125:1877–84. doi: 10.1378/chest.125.5.1877
41. You JJ, Austin PC, Alter DA, Ko DT, Tu JV. Relation between cardiac troponin I and mortality in acute decompensated heart failure. *Am Heart J.* (2007) 153:462–70. doi: 10.1016/j.ahj.2007.01.027
42. Myhre PL, O'Meara E, Claggett BL, de Denus S, Jarolim P, Anand IS, et al. Cardiac troponin I and risk of cardiac events in patients with heart failure and preserved ejection fraction. *Circ Heart Fail.* (2018) 11:e005312. doi: 10.1161/CIRCHEARTFAILURE.118.005312
43. Stelzle D, Shah ASV, Anand A, Strachan FE, Chapman AR, Denvir MA, et al. High-sensitivity cardiac troponin I and risk of heart failure in patients with suspected acute coronary syndrome: a cohort study. *Eur Heart J Qual Care Clin Outcomes.* (2018) 4:36–42. doi: 10.1093/ehjqcco/qcx022
44. Cavender MA, White WB, Jarolim P, Bakris GL, Cushman WC, Kupfer S, et al. Serial measurement of high-sensitivity troponin I and cardiovascular outcomes in patients with type 2 diabetes mellitus in the EXAMINE trial (Examination of Cardiovascular Outcomes With Alogliptin Versus Standard of Care). *Circulation.* (2017) 135:1911–21. doi: 10.1161/CIRCULATIONAHA.116.024632
45. White HD, Tonkin A, Simes J, Stewart R, Mann K, Thompson P, et al. Association of contemporary sensitive troponin I levels at baseline and change at 1 year with long-term coronary events following myocardial infarction or unstable angina: results from the LIPID Study (Long-Term Intervention With Pravastatin in Ischaemic Disease). *J Am Coll Cardiol.* (2014) 63:345–54. doi: 10.1016/j.jacc.2013.08.1643
46. Samman Tahhan A, Sandesara P, Hayek SS, Hammadah M, Alkhoder A, Kelli HM, et al. High-sensitivity troponin i levels and coronary artery disease severity, progression, and long-term outcomes. *J Am Heart Assoc.* (2018) 7:e007914. doi: 10.1161/JAHA.117.007914
47. Nishikimi T, Maeda N, Matsuoka H. The role of natriuretic peptides in cardioprotection. *Cardiovasc Res.* (2006) 69:318–28. doi: 10.1016/j.cardiores.2005.10.001
48. Masson S, Latini R, Anand IS, Barlera S, Angelici L, Vago T, et al. Prognostic value of changes in N-terminal pro-brain natriuretic peptide in Val-HeFT (Valsartan Heart Failure Trial). *J Am Coll Cardiol.* (2008) 52:997–1003. doi: 10.1016/j.jacc.2008.04.069
49. Wang TJ, Larson MG, Levy D, Benjamin EJ, Leip EP, Wilson PW, et al. Impact of obesity on plasma natriuretic peptide levels. *Circulation.* (2004) 109:594–600. doi: 10.1161/01.CIR.0000112582.16683.EA
50. Morita E, Yasue H, Yoshimura M, Ogawa H, Jougasaki M, Matsumura T, et al. Increased plasma levels of brain natriuretic peptide in patients with acute myocardial infarction. *Circulation.* (1993) 88:82–91.
51. Omland T, Sabatine MS, Jablonski KA, Rice MM, Hsia J, Wergeland R, et al. Prognostic value of B-Type natriuretic peptides in patients with stable coronary artery disease: the PEACE trial. *J Am Coll Cardiol.* (2007) 50:205–14. doi: 10.1016/j.jacc.2007.03.038
52. Bhalla MA, Chiang A, Epshteyn VA, Kazanegra R, Bhalla V, Clopton P, et al. Prognostic role of B-type natriuretic peptide levels in patients with type 2 diabetes mellitus. *J Am Coll Cardiol.* (2004) 44:1047–52. doi: 10.1016/j.jacc.2004.05.071
53. Paget V, Legedz L, Gaudebout N, Girerd N, Bricca G, Milon H, et al. N-terminal pro-brain natriuretic peptide: a powerful predictor of mortality in hypertension. *Hypertension.* (2011) 57:702–9. doi: 10.1161/HYPERTENSIONAHA.110.163550
54. Wolsk E, Claggett B, Pfeffer MA, Diaz R, Dickstein K, Gerstein HC, et al. Role of B-type natriuretic peptide and N-terminal prohormone BNP as predictors of cardiovascular morbidity and mortality in patients with a recent coronary event and type 2 diabetes mellitus. *J Am Heart Assoc.* (2017) 6:e004743. doi: 10.1161/JAHA.116.004743
55. Fonarow GC, Peacock WF, Horwich TB, Phillips CO, Givertz MM, Lopatin M, et al. Usefulness of B-type natriuretic peptide and cardiac troponin levels to predict in-hospital mortality from ADHERE. *Am J Cardiol.* (2008) 101:231–7. doi: 10.1016/j.amjcard.2007.07.066
56. Mishra RK, Beatty AL, Jaganath R, Regan M, Wu AH, Whooley MA. B-type natriuretic peptides for the prediction of cardiovascular events in patients with stable coronary heart disease: the Heart and Soul Study. *J Am Heart Assoc.* (2014) 3:e000907. doi: 10.1161/JAHA.114.000907
57. Hillis GS, Welsh P, Chalmers J, Perkovic V, Chow CK, Li Q, et al. The relative and combined ability of high-sensitivity cardiac troponin T and N-terminal pro-B-type natriuretic peptide to predict cardiovascular events and death in patients with type 2 diabetes. *Diabetes Care.* (2014) 37:295–303. doi: 10.2337/dc13-1165
58. Hotta K, Funahashi T, Arita Y, Takahashi M, Matsuda M, Okamoto Y, et al. Plasma concentrations of a novel, adipose-specific protein, adiponectin, in type 2 diabetic patients. *Arterioscler Thromb Vasc Biol.* (2000) 20:1595–9. doi: 10.1161/01.atv.20.6.1595
59. Ng TW, Watts GF, Farvid MS, Chan DC, Barrett PH. Adipocytokines and VLDL metabolism: independent regulatory effects of adiponectin, insulin

resistance, and fat compartments on VLDL apolipoprotein B-100 kinetics? *Diabetes.* (2005) 54:795–802. doi: 10.2337/diabetes.54.3.795
60. Inoue T, Kotooka N, Morooka T, Komoda H, Uchida T, Aso Y, et al. High molecular weight adiponectin as a predictor of long-term clinical outcome in patients with coronary artery disease. *Am J Cardiol.* (2007) 100:569–74. doi: 10.1016/j.amjcard.2007.03.062
61. Gardener H, Sjoberg C, Crisby M, Goldberg R, Mendez A, Wright CB, et al. Adiponectin and carotid intima-media thickness in the northern Manhattan study. *Stroke.* (2012) 43:1123–5. doi: 10.1161/STROKEAHA.111.641761
62. Shimabukuro M, Higa N, Asahi T, Oshiro Y, Takasu N, Tagawa T, et al. Hypoadiponectinemia is closely linked to endothelial dysfunction in man. *J Clin Endocrinol Metab.* (2003) 88:3236–40. doi: 10.1210/jc.2002-021883
63. Liu Z, Liang S, Que S, Zhou L, Zheng S, Mardinoglu A. Meta-analysis of adiponectin as a biomarker for the detection of metabolic syndrome. *Front Physiol.* (2018) 9:1238. doi: 10.3389/fphys.2018.01238
64. Yang L, Li B, Zhao Y, Zhang Z. Prognostic value of adiponectin level in patients with coronary artery disease: a systematic review and meta-analysis. *Lipids Health Dis.* (2019) 18:227. doi: 10.1186/s12944-019-1168-3
65. Oliveira GB, Franca JI, Piegas LS. Serum adiponectin and cardiometabolic risk in patients with acute coronary syndromes. *Arq Bras Cardiol.* (2013) 101:399–409. doi: 10.5935/abc.20130186
66. Pratesi A, Di Serio C, Orso F, Foschini A, Bartoli N, Marella A, et al. Prognostic value of adiponectin in coronary artery disease: role of diabetes and left ventricular systolic dysfunction. *Diabetes Res Clin Pract.* (2016) 118:58–66. doi: 10.1016/j.diabres.2016.04.003
67. Xu A, Wang Y, Xu JY, Stejskal D, Tam S, Zhang J, et al. Adipocyte fatty acid-binding protein is a plasma biomarker closely associated with obesity and metabolic syndrome. *Clin Chem.* (2006) 52:405–13. doi: 10.1373/clinchem.2005.062463
68. Bao Y, Lu Z, Zhou M, Li H, Wang Y, Gao M, et al. Serum levels of adipocyte fatty acid-binding protein are associated with the severity of coronary artery disease in Chinese women. *PLoS ONE.* (2011) 6:e19115. doi: 10.1371/journal.pone.0019115
69. Hsu BG, Chen YC, Lee RP, Lee CC, Lee CJ, Wang JH. Fasting serum level of fatty-acid-binding protein 4 positively correlates with metabolic syndrome in patients with coronary artery disease. *Circ J.* (2010) 74:327–31. doi: 10.1253/circj.cj-09-0568
70. Huang IC, Hsu BG, Chang CC, Lee CJ, Wang JH. High levels of serum adipocyte fatty acid-binding protein predict cardiovascular events in coronary artery disease patients. *Int J Med Sci.* (2018) 15:1268–74. doi: 10.7150/ijms.25588
71. Takagi W, Miyoshi T, Doi M, Okawa K, Nosaka K, Nishibe T, et al. Circulating adipocyte fatty acid-binding protein is a predictor of cardiovascular events in patients with stable angina undergoing percutaneous coronary intervention. *BMC Cardiovasc Disord.* (2017) 17:258. doi: 10.1186/s12872-017-0691-2
72. von Eynatten M, Breitling LP, Roos M, Baumann M, Rothenbacher D, Brenner H. Circulating adipocyte fatty acid-binding protein levels and cardiovascular morbidity and mortality in patients with coronary heart disease: a 10-year prospective study. *Arterioscler Thromb Vasc Biol.* (2012) 32:2327–35. doi: 10.1161/ATVBAHA.112.248609
73. Chow WS, Tso AWK, Xu AM, Yuen MMA, Fong CHY, Lam TH, et al. Elevated circulating adipocyte-fatty acid binding protein levels predict incident cardiovascular events in a community-based cohort: a 12-year prospective study. *J Am Heart Assoc.* (2013) 2:e004176. doi: 10.1161/JAHA.112.004176
74. Reiser H, Klingenberg R, Hof D, Cooksley-Decasper S, Fuchs N, Akhmedov A, et al. Circulating FABP4 is a prognostic biomarker in patients with acute coronary syndrome but not in asymptomatic individuals. *Arterioscler Thromb Vasc Biol.* (2015) 35:1872–9. doi: 10.1161/ATVBAHA.115.305365
75. Akbal E, Ozbek M, Gunes F, Akyurek O, Ureten K, Delibasi T. Serum heart type fatty acid binding protein levels in metabolic syndrome. *Endocrine.* (2009) 36:433–7. doi: 10.1007/s12020-009-9243-6
76. Ramesh P, Chauhan A, Goyal P, Singh A, H-FABP. A beacon of hope for prediabetic heart disease. *J Family Med Prim Care.* (2020) 9:3421–28. doi: 10.4103/jfmpc.jfmpc_296_20
77. O'Donoghue M, de Lemos JA, Morrow DA, Murphy SA, Buros JL, Cannon CP, et al. Prognostic utility of heart-type fatty acid binding protein in patients with acute coronary syndromes. *Circulation.* (2006) 114:550–7. doi: 10.1161/CIRCULATIONAHA.106.641936
78. Niizeki T, Takeishi Y, Arimoto T, Takahashi T, Okuyama H, Takabatake N, et al. Combination of heart-type fatty acid binding protein and brain natriuretic peptide can reliably risk stratify patients hospitalized for chronic heart failure. *Circ J.* (2005) 69:922–7. doi: 10.1253/circj.69.922
79. Zhang HW, Jin JL, Cao YX, Liu HH, Zhang Y, Guo YL, et al. Prognostic utility of heart-type fatty acid-binding protein in patients with stable coronary artery disease and impaired glucose metabolism: a cohort study. *Cardiovasc Diabetol.* (2020) 19:15. doi: 10.1186/s12933-020-0992-0
80. Kjeldsen L, Bainton DF, Sengelov H, Borregaard N. Identification of neutrophil gelatinase-associated lipocalin as a novel matrix protein of specific granules in human neutrophils. *Blood.* (1994) 83:799–807.
81. Cowland JB, Borregaard N. Molecular characterization and pattern of tissue expression of the gene for neutrophil gelatinase-associated lipocalin from humans. *Genomics.* (1997) 45:17–23. doi: 10.1006/geno.1997.4896
82. De la Chesnaye E, Manuel-Apolinar L, Oviedo-de Anda N, Revilla-Monsalve MC, Islas-Andrade S. Gender differences in lipocalin 2 plasmatic levels are correlated with age and the triglyceride/high-density lipoprotein ratio in healthy individuals. *Gac Med Mex.* (2016) 152:612-17.
83. Elkhidir AE, Eltaher HB, Mohamed AO. Association of lipocalin-2 level, glycemic status and obesity in type 2 diabetes mellitus. *BMC Res Notes.* (2017) 10:285. doi: 10.1186/s13104-017-2604-y
84. Zografos T, Haliassos A, Korovesis S, Giazitzoglou E, Voridis E, Katritsis D. Association of neutrophil gelatinase-associated lipocalin with the severity of coronary artery disease. *Am J Cardiol.* (2009) 104:917–20. doi: 10.1016/j.amjcard.2009.05.023
85. Ni J, Ma X, Zhou M, Pan X, Tang J, Hao Y, et al. Serum lipocalin-2 levels positively correlate with coronary artery disease and metabolic syndrome. *Cardiovasc Diabetol.* (2013) 12:176. doi: 10.1186/1475-2840-12-176
86. Xiao Y, Xu A, Hui X, Zhou P, Li X, Zhong H, et al. Circulating lipocalin-2 and retinol-binding protein 4 are associated with intima-media thickness and subclinical atherosclerosis in patients with type 2 diabetes. *PLoS ONE.* (2013) 8:e66607. doi: 10.1371/journal.pone.0066607
87. Wu G, Li H, Fang Q, Jiang S, Zhang L, Zhang J, et al. Elevated circulating lipocalin-2 levels independently predict incident cardiovascular events in men in a population-based cohort. *Arterioscler Thromb Vasc Biol.* (2014) 34:2457–64. doi: 10.1161/ATVBAHA.114.303718
88. Choi KM, Lee JS, Kim EJ, Baik SH, Seo HS, Choi DS, et al. Implication of lipocalin-2 and visfatin levels in patients with coronary heart disease. *Eur J Endocrinol.* (2008) 158:203–7. doi: 10.1530/EJE-07-0633
89. Yndestad A, Landro L, Ueland T, Dahl CP, Flo TH, Vinge LE, et al. Increased systemic and myocardial expression of neutrophil gelatinase-associated lipocalin in clinical and experimental heart failure. *Eur Heart J.* (2009) 30:1229–36. doi: 10.1093/eurheartj/ehp088
90. Akcay AB, Ozlu MF, Sen N, Cay S, Ozturk OH, Yalcn F, et al. Prognostic significance of neutrophil gelatinase-associated lipocalin in ST-segment elevation myocardial infarction. *J Investig Med.* (2012) 60:508–13. doi: 10.2310/JIM.0b013e31823e9d86
91. Avci A, Ozturk B, Demir K, Akyurek F, Altunkeser BB. The prognostic utility of plasma NGAL levels in ST segment elevation in myocardial infarction patients. *Adv Prev Med.* (2020) 2020:4637043. doi: 10.1155/2020/4637043
92. Bolignano D, Basile G, Parisi P, Coppolino G, Nicocia G, Buemi M. Increased plasma neutrophil gelatinase-associated lipocalin levels predict mortality in elderly patients with chronic heart failure. *Rejuvenation Res.* (2009) 12:7–14. doi: 10.1089/rej.2008.0803
93. Itoh N, Ornitz DM. Evolution of the Fgf and Fgfr gene families. *Trends Genet.* (2004) 20:563–9. doi: 10.1016/j.tig.2004.08.007
94. Fang Q, Li H, Song Q, Yang W, Hou X, Ma X, et al. Serum fibroblast growth factor 19 levels are decreased in Chinese subjects with impaired fasting glucose and inversely associated with fasting plasma glucose levels. *Diabetes Care.* (2013) 36:2810–4. doi: 10.2337/dc12-1766
95. Hao YP, Zhou J, Zhou M, Ma XJ, Lu ZG, Gao MF, et al. Serum levels of fibroblast growth factor 19 are inversely associated with coronary artery disease in chinese individuals. *PLoS ONE.* (2013) 8:e72345. doi: 10.1371/journal.pone.0072345

96. Zhang X, Yeung DC, Karpisek M, Stejskal D, Zhou ZG, Liu F, et al. Serum FGF21 levels are increased in obesity and are independently associated with the metabolic syndrome in humans. *Diabetes.* (2008) 57:1246–53. doi: 10.2337/db07-1476
97. Lin Z, Wu Z, Yin X, Liu Y, Yan X, Lin S, et al. Serum levels of FGF-21 are increased in coronary heart disease patients and are independently associated with adverse lipid profile. *PLoS ONE.* (2010) 5:e15534. doi: 10.1371/journal.pone.0015534
98. Bobbert T, Schwarz F, Fischer-Rosinsky A, Pfeiffer AF, Mohlig M, Mai K, et al. Fibroblast growth factor 21 predicts the metabolic syndrome and type 2 diabetes in Caucasians. *Diabetes Care.* (2013) 36:145–9. doi: 10.2337/dc12-0703
99. Chen C, Cheung BM, Tso AW, Wang Y, Law LS, Ong KL, et al. High plasma level of fibroblast growth factor 21 is an Independent predictor of type 2 diabetes: a 54-year population-based prospective study in Chinese subjects. *Diabetes Care.* (2011) 34:2113–5. doi: 10.2337/dc11-0294
100. Chow WS, Xu A, Woo YC, Tso AW, Cheung SC, Fong CH, et al. Serum fibroblast growth factor-21 levels are associated with carotid atherosclerosis independent of established cardiovascular risk factors. *Arterioscler Thromb Vasc Biol.* (2013) 33:2454–9. doi: 10.1161/ATVBAHA.113.301599
101. Chen H, Lu N, Zheng M. A high circulating FGF21 level as a prognostic marker in patients with acute myocardial infarction. *Am J Transl Res.* (2018) 10:2958–66.
102. Shen Y, Zhang X, Xu Y, Xiong Q, Lu Z, Ma X, et al. Serum FGF21 is associated with future cardiovascular events in patients with coronary artery disease. *Cardiology.* (2018) 139:212–18. doi: 10.1159/000486127
103. Li Q, Zhang Y, Ding D, Yang YN, Chen Q, Su DF, et al. Association between serum fibroblast growth factor 21 and mortality among patients with coronary artery disease. *J Clin Endocr Metab.* (2016) 101:4886–94. doi: 10.1210/jc.2016-2308
104. Kotnik P, Fischer-Posovszky P, Wabitsch M. RBP4: a controversial adipokine. *Eur J Endocrinol.* (2011) 165:703–11. doi: 10.1530/EJE-11-0431
105. Yang Q, Graham TE, Mody N, Preitner F, Peroni OD, Zabolotny JM, et al. Serum retinol binding protein 4 contributes to insulin resistance in obesity and type 2 diabetes. *Nature.* (2005) 436:356–62. doi: 10.1038/nature03711
106. Majerczyk M, Kocelak P, Choreza P, Arabzada H, Owczarek AJ, Bozentowicz-Wikarek M, et al. Components of metabolic syndrome in relation to plasma levels of retinol binding protein 4 (RBP4) in a cohort of people aged 65 years and older. *J Endocrinol Invest.* (2018) 41:1211–19. doi: 10.1007/s40618-018-0856-6
107. Lambadiari V, Kadoglou NP, Stasinos V, Maratou E, Antoniadis A, Kolokathis F, et al. Serum levels of retinol-binding protein-4 are associated with the presence and severity of coronary artery disease. *Cardiovasc Diabetol.* (2014) 13:121. doi: 10.1186/s12933-014-0121-z
108. Sun Q, Kiernan UA, Shi L, Phillips DA, Kahn BB, Hu FB, et al. Plasma retinol-binding protein 4 (RBP4) levels and risk of coronary heart disease: a prospective analysis among women in the nurses' health study. *Circulation.* (2013) 127:1938–47. doi: 10.1161/CIRCULATIONAHA.113.002073
109. Li XZ, Zhang KZ, Yan JJ, Wang L, Wang Y, Shen XY, et al. Serum retinol-binding protein 4 as a predictor of cardiovascular events in elderly patients with chronic heart failure. *ESC Heart Fail.* (2020) 7(2):542–50. doi: 10.1002/ehf2.12591
110. Sui GC, Mangs H, Wiman B. The role of His(143) for the pH-dependent stability of plasminogen activator inhibitor-1. *Biochim Biophys Acta.* (1999) 1434:58–63. doi: 10.1016/s0167-4838(99)00157-0
111. Gils A, Declerck PJ. The structural basis for the pathophysiological relevance of PAI-I in cardiovascular diseases and the development of potential PAI-I inhibitors. *Thromb Haemost.* (2004) 91:425–37. doi: 10.1160/TH03-12-0764
112. Zorio E, Gilabert-Estelles J, Espana F, Ramon LA, Cosin R, Estelles A. Fibrinolysis: the key to new pathogenetic mechanisms. *Curr Med Chem.* (2008) 15:923–9. doi: 10.2174/092986708783955455
113. Vague P, Juhan-Vague I, Aillaud MF, Badier C, Viard R, Alessi MC, et al. Correlation between blood fibrinolytic activity, plasminogen activator inhibitor level, plasma insulin level, and relative body weight in normal and obese subjects. *Metabolism.* (1986) 35:250–3. doi: 10.1016/0026-0495(86)90209-x
114. Yarmolinsky J, Bordin Barbieri N, Weinmann T, Ziegelmann PK, Duncan BB, Ines Schmidt M. Plasminogen activator inhibitor-1 and type 2 diabetes: a systematic review and meta-analysis of observational studies. *Sci Rep.* (2016) 6:17714. doi: 10.1038/srep17714
115. Hamsten A, de Faire U, Walldius G, Dahlen G, Szamosi A, Landou C, et al. Plasminogen activator inhibitor in plasma: risk factor for recurrent myocardial infarction. *Lancet.* (1987) 2:3–9. doi: 10.1016/s0140-6736(87)93050-9
116. Song C, Burgess S, Eicher JD, O'Donnell CJ, Johnson AD. Causal effect of plasminogen activator inhibitor type 1 on coronary heart disease. *J Am Heart Assoc.* (2017) 6:e004918. doi: 10.1161/JAHA.116.004918
117. Jung RG, Motazedian P, Ramirez FD, Simard T, Di Santo P, Visintini S, et al. Association between plasminogen activator inhibitor-1 and cardiovascular events: a systematic review and meta-analysis. *Thromb J.* (2018) 16:12. doi: 10.1186/s12959-018-0166-4
118. Pavlov M, Nikolic-Heitzler V, Babic Z, Milosevic M, Kordic K, Celap I, et al. Plasminogen activator inhibitor-1 activity and long-term outcome in patients with ST-elevation myocardial infarction treated with primary percutaneous coronary intervention: a prospective cohort study. *Croat Med J.* (2018) 59:108–17. doi: 10.3325/cmj.2018.59.108
119. Tofler GH, Massaro J, O'Donnell CJ, Wilson PWF, Vasan RS, Sutherland PA, et al. Plasminogen activator inhibitor and the risk of cardiovascular disease: the Framingham Heart Study. *Thromb Res.* (2016) 140:30–5. doi: 10.1016/j.thromres.2016.02.002
120. Holick MF. Vitamin D deficiency. *N Engl J Med.* (2007) 357:266–81. doi: 10.1056/NEJMra070553
121. Wang Y, Zhang H. Serum 25-hydroxyvitamin D3 levels are associated with carotid intima-media thickness and carotid atherosclerotic plaque in type 2 diabetic patients. *J Diabetes Res.* (2017) 2017:3510275. doi: 10.1155/2017/3510275
122. Verdoia M, Schaffer A, Sartori C, Barbieri L, Cassetti E, Marino P, et al. Vitamin D deficiency is independently associated with the extent of coronary artery disease. *Eur J Clin Invest.* (2014) 44:634–42. doi: 10.1111/eci.12281
123. Roy A, Lakshmy R, Tarik M, Tandon N, Reddy KS, Prabhakaran D. Independent association of severe vitamin D deficiency as a risk of acute myocardial infarction in Indians. *Indian Heart J.* (2015) 67:27–32. doi: 10.1016/j.ihj.2015.02.002
124. Giovannucci E, Liu Y, Hollis BW, Rimm EB. 25-hydroxyvitamin D and risk of myocardial infarction in men: a prospective study. *Arch Intern Med.* (2008) 168:1174–80. doi: 10.1001/archinte.168.11.1174
125. Wang TJ, Pencina MJ, Booth SL, Jacques PF, Ingelsson E, Lanier K, et al. Vitamin D deficiency and risk of cardiovascular disease. *Circulation.* (2008) 117:503–11. doi: 10.1161/CIRCULATIONAHA.107.706127
126. Anderson JL, May HT, Horne BD, Bair TL, Hall NL, Carlquist JF, et al. Relation of vitamin D deficiency to cardiovascular risk factors, disease status, and incident events in a general healthcare population. *Am J Cardiol.* (2010) 106:963–8. doi: 10.1016/j.amjcard.2010.05.027
127. Brondum-Jacobsen P, Benn M, Jensen GB, Nordestgaard BG. 25-hydroxyvitamin d levels and risk of ischemic heart disease, myocardial infarction, and early death: population-based study and meta-analyses of 18 and 17 studies. *Arterioscler Thromb Vasc Biol.* (2012) 32:2794–802. doi: 10.1161/ATVBAHA.112.248039
128. Tanik VO, Cinar T, Simsek B. The prognostic value of vitamin D level for in-hospital mortality in patients with acute pulmonary embolism. *Turk Kardiyol Dern Ars.* (2020) 48:20–5. doi: 10.5543/tkda.2019.69256
129. Paquette M, Luna Saavedra YG, Chamberland A, Prat A, Christensen DL, Lajeunesse-Trempe F, et al. Association between plasma proprotein convertase subtilisin/kexin type 9 and the presence of metabolic syndrome in a predominantly rural-based Sub-Saharan African population. *Metab Syndr Relat Disord.* (2017) 15:423–29. doi: 10.1089/met.2017.0027
130. Mba CM, Mbacham W, Sobngwi E, Mbanya JC. Is PCSK9 associated with plasma lipid levels in a Sub-Saharan African population of patients with obesity and type 2 diabetes? *Diabetes Metab Syndr Obes.* (2019) 12:2791–97. doi: 10.2147/DMSO.S234243
131. Toth S, Fedacko J, Pekarova T, Hertelyova Z, Katz M, Mughees A, et al. Elevated circulating PCSK9 concentrations predict subclinical atherosclerotic changes in low risk obese and non-obese patients. *Cardiol Ther.* (2017) 6:281–89. doi: 10.1007/s40119-017-0092-8

132. Lee CJ, Lee YH, Park SW, Kim KJ, Park S, Youn JC, et al. Association of serum proprotein convertase subtilisin/kexin type 9 with carotid intima media thickness in hypertensive subjects. *Metabolism*. (2013) 62:845–50. doi: 10.1016/j.metabol.2013.01.005
133. Bae KH, Kim SW, Choi YK, Seo JB, Kim N, Kim CY, et al. Serum levels of PCSK9 are associated with coronary angiographic severity in patients with acute coronary syndrome. *Diabetes Metab J*. (2018) 42:207–14. doi: 10.4093/dmj.2017.0081
134. Peng J, Liu MM, Jin JL, Cao YX, Guo YL, Wu NQ, et al. Association of circulating PCSK9 concentration with cardiovascular metabolic markers and outcomes in stable coronary artery disease patients with or without diabetes: a prospective, observational cohort study. *Cardiovasc Diabetol*. (2020) 19:167. doi: 10.1186/s12933-020-01142-0
135. Werner C, Hoffmann MM, Winkler K, Bohm M, Laufs U. Risk prediction with proprotein convertase subtilisin/kexin type 9 (PCSK9) in patients with stable coronary disease on statin treatment. *Vascul Pharmacol*. (2014) 62:94–102. doi: 10.1016/j.vph.2014.03.004

Conflict of Interest: The authors declare that the research was conducted in the absence of any commercial or financial relationships that could be construed as a potential conflict of interest.

Publisher's Note: All claims expressed in this article are solely those of the authors and do not necessarily represent those of their affiliated organizations, or those of the publisher, the editors and the reviewers. Any product that may be evaluated in this article, or claim that may be made by its manufacturer, is not guaranteed or endorsed by the publisher.

Copyright © 2021 Wong and Tse. This is an open-access article distributed under the terms of the Creative Commons Attribution License (CC BY). The use, distribution or reproduction in other forums is permitted, provided the original author(s) and the copyright owner(s) are credited and that the original publication in this journal is cited, in accordance with accepted academic practice. No use, distribution or reproduction is permitted which does not comply with these terms.

frontiers in Cardiovascular Medicine

CLINICAL TRIAL
published: 01 October 2021
doi: 10.3389/fcvm.2021.707328

Folic Acid Attenuates Contrast-Induced Nephropathy in Patients With Hyperhomocysteinemia Undergoing Coronary Catheterization: A Randomized Controlled Trial

Long Peng[1†], Xing Shui[1†], Fang Tan[2,3†], Zexiong Li[1,4], Yesheng Ling[1], Bingyuan Wu[1], Lin Chen[1], Suhua Li[1*] and Hui Peng[5*]*

[1] Department of Cardiovascular Medicine, The Third Affiliated Hospital, Sun Yat-sen University, Guangzhou, China, [2] Department of Anaesthesiology, The Seventh Affiliated Hospital of Sun Yat-sen University, Shenzhen, China, [3] Department of Anaesthesiology, The Third Affiliated Hospital, Sun Yat-sen University, Guangzhou, China, [4] Department of Cardiovascular Medicine, Jieyang People's Hospital, Jieyang, China, [5] Nephrology Division, The Third Affiliated Hospital, Sun Yat-sen University, Guangzhou, China

OPEN ACCESS

Edited by:
Yuli Huang,
Southern Medical University, China

Reviewed by:
Chongyang Duan,
Southern Medical University, China
Yiwei Liu,
Shanghai Children's Medical Center, China

***Correspondence:**
Lin Chen
cl1833@21cn.com
Suhua Li
lisuhua3@mail.sysu.edu.cn
Hui Peng
pengh@mail.sysu.edu.cn

[†] These authors have contributed equally to this work

Specialty section:
This article was submitted to General Cardiovascular Medicine, a section of the journal Frontiers in Cardiovascular Medicine

Received: 09 May 2021
Accepted: 06 September 2021
Published: 01 October 2021

Citation:
Peng L, Shui X, Tan F, Li Z, Ling Y, Wu B, Chen L, Li S and Peng H (2021) Folic Acid Attenuates Contrast-Induced Nephropathy in Patients With Hyperhomocysteinemia Undergoing Coronary Catheterization: A Randomized Controlled Trial. Front. Cardiovasc. Med. 8:707328. doi: 10.3389/fcvm.2021.707328

Background: Hyperhomocysteinemia is a risk factor for contrast-induced nephropathy. Folic acid can attenuate such nephropathies in rats. The protective effect of folic acid against contrast-induced nephropathy has not been studied in humans. We aimed to investigate the effect of folic acid on the incidence of contrast-induced nephropathy (CIN) after coronary catheterization in patients with hyperhomocysteinemia.

Methods: This was a single-center, prospective, double-blind, randomized controlled trial (ClinicalTrials.gov, NCT02444013). In total, 412 patients (mean age: 65 ± 12 years, 268 male) with plasma homocysteine ≥15 μM, who underwent coronary arteriography (CAG) or percutaneous coronary intervention (PCI) from May 2015 to August 2018, were enrolled. Patients were randomly assigned to two groups: a treatment group ($n = 203$), taking 5 mg of folic acid (orally, three times/day) immediately after enrollment and for 72 h after operation, and a control group ($n = 209$), taking placebo. Contrast-induced nephropathy was defined as an increase in serum creatinine of >25% or 44 μM within 48 or 72 h after contrast medium administration.

Results: In total, 50 (12%) patients developed CIN after 48 h after catheterization, including 16 (8%) in the treatment group and 34 (16%) in the control group ($P = 0.009$). Meanwhile, 53 (13%) patients developed CIN after 72 h of CAG/PCI, including 18 (9%) in the treatment group and 35 (17%) in the control group ($P = 0.017$). The incidence of contrast-induced nephropathy in the treatment group was lower than that in the control group ($P = 0.017$). Logistic regression analysis confirmed that administration of folic acid was a protective factor against contrast-induced nephropathy (RD = 0.0788, 95%CI: 0.0105–0.1469, $P = 0.019$). We found no serious adverse events associated with folic acid. No death or hemodialysis occurred in either group.

Conclusions: Perioperative administration of folic acid attenuates the incidence of contrast-induced nephropathy after coronary catheterization in patients with hyperhomocysteinemia.

Clinical Trial Registration: ClinicalTrials.gov, identifier [NCT02444013].

Keywords: contrast-induced nephropathy, folic acid, hyperhomocysteinemia, coronary catheterization, acute kidney injury

INTRODUCTION

Contrast-induced nephropathy (CIN) is a common complication when using intravenous iodinated contrast. It is the third most common cause of hospital-acquired acute kidney injury, accounting for 11% of cases (1), second only to decreased renal perfusion and nephrotoxic medication (2). The overall incidence of CIN ranges from 3 to 7% but can be as high as 50% in patients with moderate to advanced chronic kidney disease (CKD) (3). CIN is associated with prolonged hospital stays, as well as an increased risk of CKD, cardiovascular events, and death (4). It has been reported that 49% of CINs occur after either coronary arteriography (CAG) or percutaneous coronary intervention (PCI) (5). Therefore, investigating the potential means to reduce the risk of CIN in patients undergoing CAG or PCI is warranted.

The pathogenesis of CIN has been explained by combinations of various mechanisms, such as renal vasoconstriction, increased oxidative stress, and impaired endothelial function, as well as renal tubular-cell cytotoxicity and apoptosis (6, 7). Homocysteine (Hcy), a sulfhydryl-containing amino acid, is closely associated with a risk of renal and cardiovascular diseases (8–10); hyperhomocysteinemia (HHcy) is known to induce oxidative stress, endothelial dysfunction, apoptosis, and thrombosis (9, 11). From previous studies, including our own (12), HHcy is a known independent risk factor for CIN (13).

Folic acid, an important dietary determinant of Hcy, exerts antioxidative and anti-apoptotic effects, and improves endothelial function; therefore, it plays a vital role in the management of cardiovascular diseases associated with HHcy (14, 15). A previous study revealed that folic acid could attenuate CIN in rats (16). However, the protective effect of folic acid against CIN has not been studied in humans. In this study, we aimed to investigate the effect of folic acid on the incidence of CIN after CAG or PCI in patients with HHcy.

MATERIALS AND METHODS

Study Population

This was a single-center, prospective, double-blind, randomized controlled trial, registered on May 14, 2015 (ClinicalTrials.gov, NCT02444013). Patients with HHcy, scheduled to undergo CAG or PCI, were prospectively enrolled, after screening for eligibility, from May 2015 to August 2018, at the Department of Cardiovascular Medicine, the Third Affiliated Hospital, Sun Yat-sen University. The inclusion criteria were an age $\geq$18 years and a fasting plasma Hcy concentration $\geq$15 μM. The exclusion criteria were as follows: pregnancy; use of folic acid, vitamin B12, contrast agent, or nephrotoxic drugs within 14 days before enrollment; allergy to iodine-containing contrast medium; and end-stage renal failure. All procedures were conducted in accordance with the tenets of the Declaration of Helsinki, and all participants provided written informed consent before being enrolled in the study. This study was approved by the institutional review board of the Third Affiliated Hospital, Sun Yat-sen University (IRB: 20150216).

Randomization and Masking

Patients were randomly assigned (1:1) to the group receiving oral 5-mg folic acid or the group receiving matching placebo three times/day. Patients were allocated to the two treatment arms by central computer allocation using simple randomization with no stratification factors. A random number table was generated by one researcher, and another researcher put the random number and group number into opaque envelopes of the same size and color. Randomization was performed by a third investigator. Random generation, concealment, and assignment were performed by three different investigators, none of whom participated in the subsequent part of the intervention program. All doctors and subjects were blinded to the allocation of drug administration, as a double-blinding method was used for the allocation.

Procedures

As protection against the intravenous contrast medium, all patients received prophylactic hydration with 0.9% NaCl solution (1–2 mL/kg/h, intravenous), 6 h before and 6 h after contrast administration. Random number tables were used to assign patients to two groups: a treatment group, taking 5 mg of folic acid (orally, three times a day) immediately after enrollment, and a control group, taking a placebo at the same intervals.

Blood samples were collected at baseline and analyzed on a Hitachi 7180 clinical analyzer (Hitachi High-Tech Corp, Japan) for the evaluation of blood urea nitrogen, uric acid, blood lipids, cystatin C, and fasting glucose. Hemoglobin was measured using the cyanmethemoglobin method. Hemoglobin A1C was measured, *via* the D-10 Hemoglobin Testing System (Bio-Rad Laboratories, Inc., Hercules, CA, USA), using high-performance liquid chromatography. Plasma Hcy was measured on the ADVIA Centaur (Siemens Healthineers AG, Erlangen, Germany) at baseline, as well as the day before and 72 h after

Abbreviations: CAG, coronary arteriography; CIN, contrast-induced nephropathy; eGFR, estimated glomerular filtration rate; Hcy, homocysteine; HHcy, hyperhomocysteinemia; ICU, intensive care unit; PCI, percutaneous coronary intervention; Scr, serum creatinine.

CAG/PCI. Serum creatinine (Scr) concentration was estimated using the sarcosine oxidase enzymatic method at baseline, the day before CAG/PCI, as well as at 24, 48, and 72 h after CAG/PCI. The estimated glomerular filtration rate (eGFR) was calculated using the equation developed by the Modification of Diet in Renal Disease study group (17).

Cardiac catheterization was performed in accordance with standard clinical practice, *via* a femoral or radial approach. Coronary angiography was routinely performed using the Judkins technique. Significant coronary artery disease was defined as >50% coronary stenosis in at least one vessel. The contrast type and dose were decided by two experienced interventional cardiologists based on operative requirements.

The primary outcome measure was the rate of occurrence of CIN. According to previous studies, CIN can be defined as either 48 or 72 h (18, 19). Therefore, in order to reduce the risk of obtaining different results due to the different criteria, we revised the registration scheme at the beginning of study, and used both CIN criteria for analysis. Thus, CIN was considered as an increase in Scr concentration of more than 25% or 44 μM within 48 and 72 h after contrast medium administration, without evidence of other causes. The secondary outcome measures were major in-hospital clinical events with 72 h, including: (1) bleeding, defined as a reduced hemoglobin level ≥20 g/L; (2) all-cause death; (3) dialysis or hemofiltration due to symptoms or signs of uremic syndrome or management of refractory hypervolemia, hyperkalemia, or acidosis; (4) worsening heart failure, defined as a deteriorated NYHA functional class; and (5) intensive care unit (ICU) admission. The safety outcome was measured by assessment of adverse reactions, such as nausea, decreased appetite, insomnia, and allergic reaction. In addition, we assessed the serial changes in serum creatinine and Hcy concentration.

Statistical Analysis

Statistical analysis was performed using IBM SPSS Statistics for Windows version 22.0 (IBM Corp., Armonk, NY, USA).

We designed this study to assess the superiority of folic acid over the standard approach to reduce CIN in patients with hyperhomocysteinemia undergoing coronary catheterization. We calculated the necessary sample size on the basis of previous trial data suggesting that 15.4% of the control group and 6.34% of folic acid treatment group would develop CIN. We also estimated that 10% of patients would be lost to follow-up, based on previous CIN prevention trials enrolling patients undergoing cardiac procedures (20). On the basis of these assumptions, a chi-squared analysis suggested that 404 patients would be needed to

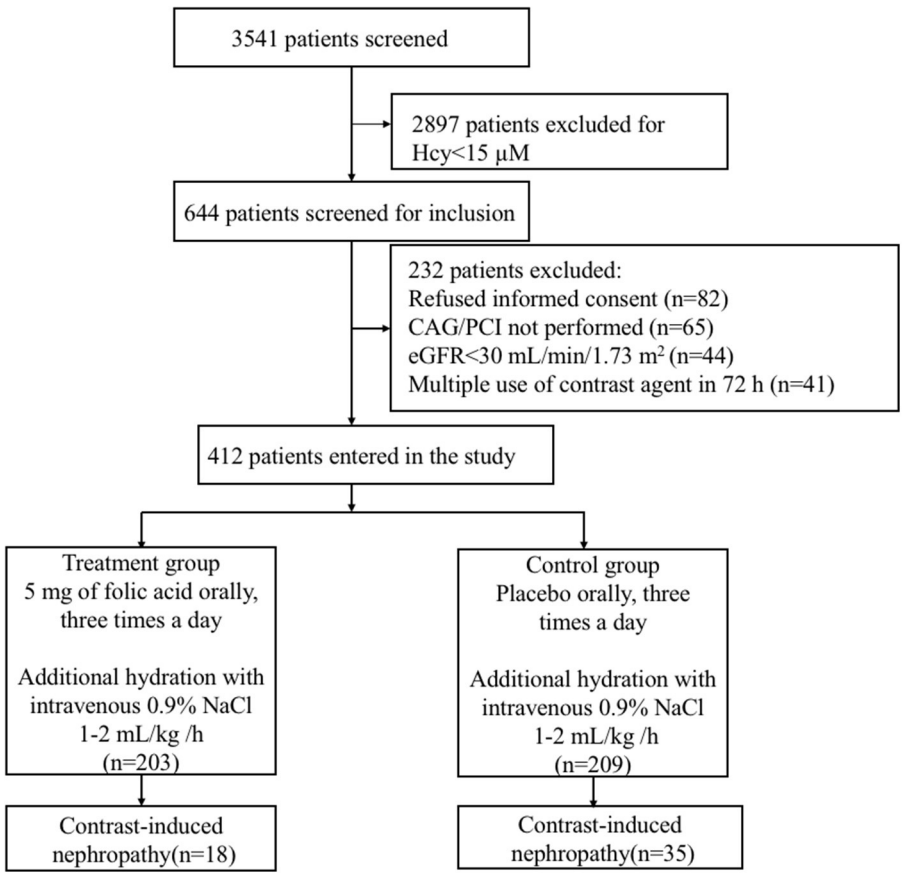

FIGURE 1 | Flowchart of the study population of patients with hyperhomocysteinemia receiving folic acid and the control group. CAG, coronary arteriography; PCI, percutaneous coronary intervention; eGFR, estimated glomerular filtration rate.

TABLE 1 | Baseline characteristics of patients with hyperhomocysteinemia receiving folic acid vs. a control group.

	Treatment group ($n = 203$)	Control group ($n = 209$)	*P*-value
Age, years	66 ± 12	65 ± 12	0.293
Male, *n* (%)	138 (68)	130 (62)	0.219
BMI, kg/m^2	24.9 ± 3.5	24.7 ± 3.2	0.378
Systolic blood pressure, mmHg	139.27 ± 20.21	138.46 ± 22.72	0.396
Diastolic blood pressure, mmHg	81.71 ± 13.31	79.58 ± 12.38	0.149
Heart rate, bpm	75.31 ± 12.25	74.82 ± 12.76	0.350
Hypertension, *n* (%)	158 (78)	152 (73)	0.153
Diabetes mellitus, *n* (%)	70 (34)	78 (37)	0.548
Hyperlipidemia, *n* (%)	72 (35)	69 (33)	0.600
CHF, *n* (%)	24 (12)	25 (12)	0.965
Anemia, *n* (%)	32 (16)	36 (17)	0.690
Current smoker, *n* (%)	86 (42)	86 (41)	0.802
Hemoglobin, g/L	131.7 ± 18.7	130.9 ± 18.7	0.588
Total cholesterol, mM	4.47 ± 1.17	4.53 ± 1.30	0.792
Triglyceride, mM	1.79 ± 1.59	1.56 ± 1.19	0.089
HDL-C, mM	1.02 ± 0.28	1.11 ± 0.28	0.001
LDL-C, mM	2.83 ± 1.03	2.88 ± 1.11	0.748
Fasting glucose, mM	5.81 ± 1.64	5.70 ± 1.61	0.390
HbA1C, %	6.11 ± 0.95	6.27 ± 1.30	0.708
BUN, μM	5.77 ± 1.96	5.41 ± 1.81	0.842
Scr, μM	99.02 ± 27.61	97.14 ± 21.78	0.441
eGFR, mL/min/1.73 m^2	59 ± 19	60 ± 19	0.285
LVEF, %	55.17 ± 9.40	56.13 ± 7.34	0.271
ACEI/ARB, *n* (%)	115 (57)	114 (55)	0.667
Statins, *n* (%)	183 (90)	197 (94)	0.119
Diuretic, *n* (%)	86 (42)	86 (41)	0.802
Aspirin, *n* (%)	139 (68%)	150 (72%)	0.465
Clopidogrel, *n* (%)	94 (46%)	114 (55%)	0.094
Ticagrelor, *n* (%)	26 (13%)	28 (13%)	0.859
Clinical diagnosis			
ACS	56 (28%)	58 (28%)	0.970
CAD	76 (37%)	79 (28%)	0.940
NCHD	71 (35%)	72 (34%)	0.911
Procedure, *n* (%)			0.797
CAG	122 (60)	123 (59)	
PCI	81 (40)	86 (41)	
Duration of procedure, min	77.9 ± 52.2	83.6 ± 55.4	0.282
Contrast volume, mL	102.5 ± 48.2	109.7 ± 51.1	0.150
Prehydration, mL	672.9 ± 89.4	672.0 ± 86.0	0.512
Post-hydration, mL	760.1 ± 132.3	744.7 ± 101.8	0.368
Length of stay, day	9.76 ± 1.6	10.0 ± 2.0	0.133
Hospitalization cost,¥	27,464.9 ± 21,638.3	22,857 ± 22,083.9	0.033

Categorical variables are presented as n (%). Continuous variables are presented as mean ± SD. BMI, body mass index; CHF, congestive heart failure; HDL-C, high-density lipoprotein cholesterol; LDL-C, low-density lipoprotein cholesterol; HbA1C, hemoglobin A1C; BUN, blood urea nitrogen; Scr, serum creatinine; eGFR, estimated glomerular filtration rate; LVEF, left ventricular ejection fraction; ACEI, angiotensin converting enzyme inhibitor; ARB, angiotensin receptor blocker; ACS, acute coronary syndrome; CAD, Chronic coronary artery disease; NCHD, Non-coronary heart disease; CAG, coronary arteriography; PCI, percutaneous coronary intervention.

detect a statistically significant difference, with 80% power and a two-sided α of 0.05.

Intention-to-treat (ITT) analysis was primarily used for this trial including all participants who received folic acid or placebo and underwent coronary angiography. Continuous variables are presented as mean ± standard deviation values, whereas categorical variables are presented as frequencies and percentages. Continuous variables were tested for a normal distribution using the Shapiro–Wilk test. Normally distributed variables were compared using two-tailed, independent *t*-tests. Non-normally distributed variables were compared using the two-tailed Mann–Whitney *U*-test. Repeated measures variables were analyzed using two-way repeated measures ANOVA and a linear mixed model to analyze changes. Categorical data were compared between the groups using Pearson's chi-square and Fisher's exact tests. Univariate logistic regression analyses were used to determine independent predictors of CIN. We used logistic regression with interaction testing and Chi-square test to assess whether the treatment effect was consistent across *post-hoc* subgroups. *P*-values of $\leq$0.05 were considered to indicate statistical significance. One-way ANOVA was used to analyze intergroup differences with a Bonferroni multiple comparison post-test. *P*-values $<$0.0167 were considered statistically significant.

RESULTS

Baseline Characteristics

Among the 3,541 consecutive patients who underwent CAG or PCI, the plasma Hcy concentration was $\geq$15 μM in 644 patients screened for inclusion (**Figure 1**). Ultimately, 412 patients (mean age: 65 ± 12 years, 268 male and 144 female) participated in the study, with 203 in the treatment group and 209 in the control group. All randomized patients who provided consent, constituting the full analysis set, were included according to ITT principles for the efficacy analyses. Baseline characteristics of the study population are presented in **Table 1**. The mean eGFR of all patients was 61 ± 19 mL/min/1.73 m^2. There were similar distributions of clinical diagnosis in two groups. In terms of operations, 245 (59%) patients received CAG and 167 (41%) received PCI, with a mean contrast-material volume of 106.1 ± 49.8 mL. The mean pre- and post-operative intravenous hydration volumes were 672.4 ± 87.7 and 752.3 ± 116.8 mL, respectively. All stents are drug eluting stent. All randomly assigned patients received their allocated treatment (**Figure 1**).

Outcomes

Primary Endpoint

In total, 50 (12%) patients developed CIN after 48 h of CAG/PCI, including 16 (8%) in the treatment group and 34 (16%) in the control group ($P = 0.009$). Meanwhile, 53 (13%) patients developed CIN after 72 h of CAG/PCI, including 18 (9%) in the treatment group and 35 (17%) in the control group ($P = 0.017$). Regardless of the adopted standard, the incidence of CIN was significantly lower in the treatment group than in the control group.

TABLE 2 | Change in serum creatinine concentration from pre-PCI baseline to 48 h and 72 h after the initiation of PCI in two groups.

	Treatment group (n = 203)	Control group (n = 209)	P-value
Baseline Scr, μM	99.02 ± 27.61	97.14 ± 21.78	0.441
48 h max Scr, μM[a]	107.42 ± 30.33	107.66 ± 24.56	0.928
ΔScr (48 h max – baseline), μM	8.39 ± 13.72	10.52 ± 13.12	0.108
72 h max Scr, μM[a]	108.74 ± 30.60	110.86 ± 23.83	0.432
ΔScr (72 h max – baseline), μM	9.71 ± 13.77	13.73 ± 12.08	0.002

[a]*Highest serum creatinine (Scr) concentration within 48 or 72 h; ΔScr, change in serum creatinine concentration. All values are presented as mean ± SD.*

As indicated in **Table 2**, the highest Scr concentrations were significantly higher within 48 h after the initiation of PCI than those at baseline in the two groups (treatment group: 107.42 ± 30.33 vs. 99.02 ± 27.61 μM, $P = 0.0037$; control group: 107.66 ± 24.56 vs. 97.14 ± 21.78 μM, $P < 0.001$). Otherwise, the highest Scr concentrations were significantly higher within 72 h after the initiation of PCI than those at baseline in the two groups (treatment group: 108.74 ± 30.60 vs. 99.02 ± 27.61 μM, $P = 0.0009$; control group: 110.86 ± 23.83 vs. 97.14 ± 21.78 μM, $P < 0.001$). The change in Scr concentration (Δ Scr) from pre-PCI baseline (0 h) to 72 h after PCI in the folic acid group was significantly lower than that in the control group (9.71 ± 13.77 vs. 13.73 ± 12.08 μM, $P = 0.002$). However, there was no significant difference in the Δ Scr within 48 h between two groups (8.39 ± 13.72 vs. 10.52 ± 13.12 μM, $P = 0.108$). The linear mixed model showed that folic acid decreased the Scr concentration ($P < 0.0001$ for group and group-time interaction).

In the treatment group, the baseline concentration of plasma Hcy was 23.99 ± 8.24 μM. After taking folic acid for a median duration of 6.0 (range, 5.0–8.0) days, the concentration of plasma Hcy decreased significantly to 16.94 ± 8.26 μM by the day before CAG/PCI ($P < 0.001$ vs. baseline). At 72 h after CAG/PCI, the concentration of plasma Hcy had further reduced to 13.41 ± 6.01 μM ($P < 0.001$ vs. baseline and vs. the day before CAG/PCI). In the control group, the baseline concentration of plasma Hcy (23.16 ± 3.30 μM) was similar to that of the treatment group ($P = 0.19$). Furthermore, the concentrations of plasma Hcy in the control group did not change significantly during the study ($P > 0.05$; **Figure 2**). The linear mixed model showed significant differences in change in the Hcy concentration between the two groups, due to the interaction between the groups and time, with the folic acid group showing a faster decline.

Secondary Outcomes

Table 3 shows the major adverse clinical events. There were no serious adverse events related to study treatment, and no death or hemodialysis occurred in either group. The rate of worsening heart failure events was lower, although not significantly so, in the treatment group (relative difference [RD] = 0.0138, 95% confidence interval [CI]: −0.0244 to −0.0532, $P = 0.54$). There was no statistical difference in the occurrence of bleeding and ICU admission rate between the two groups. No safety signal related to folic acid administration emerged during the study.

Univariate logistic regression analysis indicated that treatment with folic acid could lower the risk of CIN significantly (RD = 0.0788, 95%CI: 0.0105–0.1469, and $P = 0.019$). We further performed *post-hoc* subgroup analyses stratified by hypertension, diabetes mellitus, heart failure, age, sex, eGFR, and anemia with 72 h (**Table 4**). Administration of folic acid was a protective factor against CIN in patients with hypertension, diabetes mellitus, no heart failure, age>65 years, eGFR > 60 ml/min/1.73 m^2, and no anemia, and those who were male ($P < 0.05$), except in patients with congestive heart failure ($P = 0.299$) or anemia ($P = 0.34$). The P-value of interaction testing for logistic regression in *post-hoc* subgroups was >0.05, except for sex.

DISCUSSION

Intravenous iodinated contrast is associated with a high risk for CIN, which may lead to increased morbidity, prolonged hospitalization, an increased risk of complications, a potential need for dialysis, and an increased mortality rate (5). Therefore, it is crucial to consider strategies for the prevention of CIN. Previous studies indicated HHcy as a risk factor for CIN (12, 13), and that folic acid can attenuate CIN in rats (16). In the present study, of 412 consecutive patients with HHcy undergoing coronary catheterization, we confirmed that perioperative treatment with folic acid could lead to a statistically significant reduction of plasma Hcy concentration and was associated with a lower incidence of CIN compared to those in patients treated with placebo. Logistic regression analysis demonstrated that folic acid was a protective factor against CIN. At the same time, 50 and 53 patients developed CIN within 48 and 72 h, respectively; thus it is necessary to extend the time of creatinine detection in clinical practice.

Many clinical trials have been conducted to test the abilities of various substances to reduce the incidence of CIN, such as acetylcysteine, sodium bicarbonate, statins, and furosemide. However, such attempts have yielded contradictory results (21–25), and the best strategy remains unclear. KDIGO (Kidney Disease: Improving Global Outcomes) published the first international and interdisciplinary clinical practice guideline on acute kidney injury, recommending intravenous prehydration with 0.9% NaCl as the basic strategy in patients at an increased risk for CIN (26). Therefore, in the present study, all participants received prophylactic hydration with intravenous 0.9% NaCl (1–2 mL/kg/h) at 6 h before and after contrast administration. Nonetheless, >12% of patients still developed CIN after catheterization. According to previous reports, the incidence of CIN is ∼2% in patients with normal renal function and without

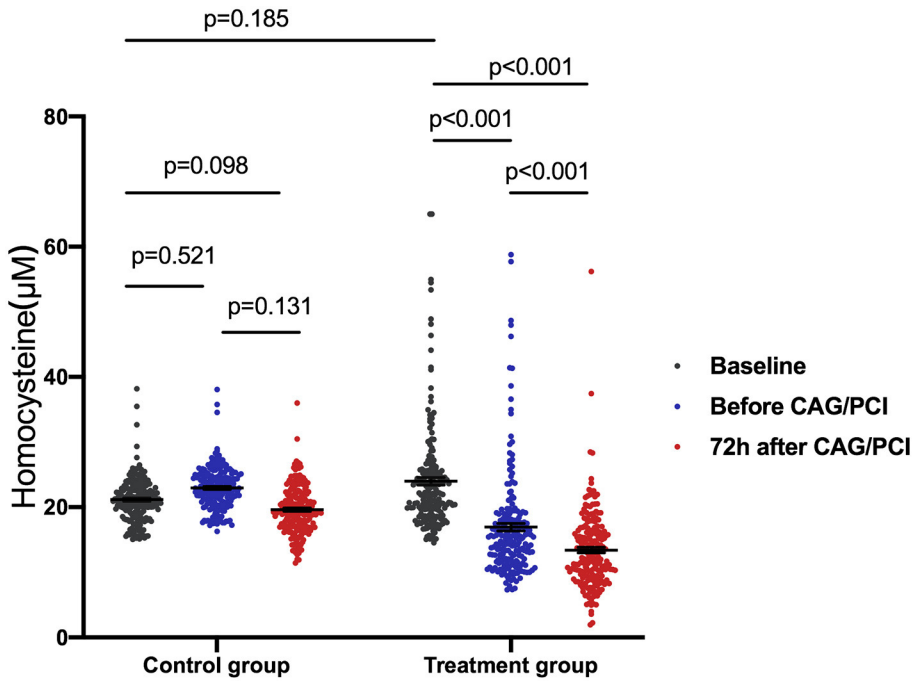

FIGURE 2 | Homocysteine (Hcy) change over time in patients with hyperhomocysteinemia receiving folic acid and the control group. One-way ANOVA was used to analyze intergroup differences with a Bonferroni multiple comparison post-test. $P < 0.0167$ were considered statistically significant. The linear mixed model showed significant differences in the change in Hcy concentration between the two groups due to the interaction between the groups and time ($P < 0.001$). The folic acid group showed a faster decline. The average of the control group was 0.81 lower than that of the folic acid group at baseline, 6.02 higher than that of the folic acid group before procedure, and 9.05 higher than that at 72 h after procedure. ANOVA, analysis of variance; CAG, coronary arteriography; PCI, percutaneous coronary intervention.

TABLE 3 | Incidence of contrast-induced nephropathy and major adverse events in 72 h.

	Treatment group ($n = 203$)	Control group ($n = 209$)	Risk difference (95% CI)	*P*-value
CIN-48 h	16/203 (8.9%)	34/209 (16.7%)	0.0839 (0.0172 to 0.1505)	0.009
CIN-72 h	18/203 (8.9%)	35/209 (16.7%)	0.0788 (0.0105 to 0.1469)	0.017
Bleed	5/203 (2.5%)	5/209 (2.4%)	0.0007 (−0.0367 to −0.0389)	1.00
Worsening heart failure	4/203 (2%)	7/209 (3.3%)	0.0138 (−0.0244 to −0.0532)	0.54
All-cause mortality	0/203	0/209	–	1.00
Dialysis	0/203	0/209	–	1.00
Intensive care admission	2/203 (1.0%)	3/209 (1.4%)	0.0045 (−0.0265 to 0.036)	1.00

other risk factors; however, the incidence can increase to 9–40% in high-risk patients (27). The most important risk factor for CIN is pre-existing renal insufficiency (28). The mean eGFR in the present study was <60 mL/min/1.73 m^2, indicating that many participants had pre-existing renal insufficiency. Besides, many patients had other risk factors for CIN, such as old age, anemia, diabetes, and heart failure. This may explain why the incidence of CIN in the present study was relatively high, despite adequate perioperative hydration. Severe CIN may require hemodialysis to remove the contrast media from the blood (29), which is why we excluded patients with eGFR < 30 mL/min/1.73 m^2. Perhaps we excluded patients who used contrast agents multiple times in a short period of time, which means that some patients with complex conditions were not included. This may explain why there were less serious complications occur serious complications in the present study.

In order to reduce the risk of CIN, it is extremely important to identify patients at a high risk of CIN and to develop new pretreatment strategies. The pathogenesis of CIN is closely related to endothelial dysfunction and cellular toxicity induced by the contrast agent, as well as to tubular apoptosis resulting from hypoxic damage and reactive oxygen species (26). As elevated Hcy concentrations can induce endothelial dysfunction, apoptosis, oxidative stress, and thrombosis (9, 11), it follows that there is a potential link between Hcy and the risk of CIN; however, such a hypothesis has not been extensively evaluated.

TABLE 4 | Occurrence of contrast-induced acute kidney injury in *post-hoc* subgroups.

	Treatment group	Control group	Risk difference (95% CI)	*P*-value	*P*-value for intervention
Hypertension					0.712
Yes ($n = 310$)	15/158	26/126	0.1114 (0.0234 to 0.2033)	0.048	
No ($n = 102$)	3/45	9/57	0.0912 (−0.0578 to 0.2263)	0.156	
Diabetes mellitus					0.35
Yes ($n = 148$)	5/70	15/78	0.1209 (−0.001 to 0.238)	0.032	
No ($n = 264$)	13/123	20/131	0.047 (−0.0431 to 0.1355)	0.177	
CHF					0.927
Yes ($n = 49$)	3/24	6/25	0.115 (−0.1362 to 0.3491)	0.299	
No ($n = 363$)	15/179	29/184	0.0738 (0.0023 to 0.1453)	0.031	
Age					0.632
>65 years ($n = 190$)	10/123	12/67	0.0978 (−0.0059 to 0.221)	0.044	
≤65 ($n = 222$)	8/80	23/142	0.062 (−0.0455 to 0.1523)	0.201	
Sex					0.046
Male ($n = 268$)	8/138	23/130	0.119 (0.0369 to 0.2036)	0.201	
Female ($n = 198$)	10/65	12/79	0.0019 (−0.1242 to 0.1358)	0.754	
eGFR					0.967
>60 ml/min/1.73 m^2 ($n = 214$)	9/104	20/110	0.0953 (−0.0042 to 0.193)	0.042	
≤60 ml/min/1.73 m^2 ($n = 198$)	9/99	15/99	0.0606 (−0.0395 to 0.161)	0.191	
Anemia					0.804
Yes ($n = 68$)	5/32	9/26	0.1899 (−0.0549 to 0.4215)	0.34	
No ($n = 344$)	13/171	26/173	0.0743 (0.0026 to 0.1464)	0.03	

CHF, chronic heart failure; eGFR, estimated glomerular filtration rate.

As we have previously demonstrated (12) that plasma Hcy concentration is an independent biomarker for predicting CIN, and as Barbieri et al. (13) demonstrated a statistically significant relationship between plasma Hcy concentration and the risk of CIN, reduction of the plasma Hcy concentration may reduce the risk of CIN.

Folic acid is an essential co-factor in Hcy metabolism (30); it exerts antioxidative and anti-apoptotic effects and improves endothelial functional properties (31). The administration of folic acid attenuated CIN statistically significantly in diabetic rats, the mechanism of which may be related to the inhibition of oxidative stress (16, 32). In clinical practice, folic acid is used in the management of many diseases, including diabetes mellitus, hypertension, and cardiovascular disorders (14, 15, 31). A meta-analysis of the efficacy of folic acid supplementation in stroke prevention demonstrated that folic acid supplementation can effectively reduce the risk of stroke in primary prevention (33). Xu et al. (34) found that enalapril-folic acid therapy, compared with enalapril alone, can significantly delay the progression of CKD among patients with mild-to-moderate disease.

In the present study, folic acid administration was first demonstrated to reduce both the plasma Hcy level and incidence of CIN statistically significantly after coronary catheterization. Subgroup analyses further confirmed that administration of folic acid was an independent protective factor against CIN, except in patients with congestive heart failure or anemia. However, as the number of participants with congestive heart failure ($n = 49$) or anemia ($n = 68$) was relatively small in our study, the effectiveness of folic acid in protecting such patients against CIN needs to be verified. Based on its potential benefits and few side effects, we recommend perioperative administration of folic acid to attenuate CIN in patients with HHcy undergoing coronary catheterization.

Several limitations of the present study should be noted. First, this was a single-center study. Analyses involving different surgeons and using therapeutic strategies may lead to different results. Second, the overall sample size was relatively small; clinical trials with larger samples should be conducted for verification of our results. Third, this study included only HHcy patients. Potential preventive effects of folic acid on CIN may arise not only from a reduction in Hcy concentration, but also because of its antioxidative and anti-apoptotic properties. Therefore, research into the effect of folic acid in non-HHcy patients is also warranted. Finally, as the pathophysiological link between folic acid and CIN remains unclear, further studies will be required to elucidate the potential molecular mechanism underlying its action.

In conclusion, results from the current study suggest that perioperative administration of folic acid is associated with a statistically significant reduction in the incidence of CIN after coronary catheterization in patients with HHcy. More studies on the potential molecular mechanism should be conducted to uncover the exact role of folic acid in the protection against CIN.

DATA AVAILABILITY STATEMENT

The raw data supporting the conclusions of this article will be made available by the authors, without undue reservation.

ETHICS STATEMENT

The studies involving human participants were reviewed and approved by the Third Affiliated Hospital, Sun Yat-sen University. The patients/participants provided their written informed consent to participate in this study.

AUTHOR CONTRIBUTIONS

SL and HP contributed to the study concepts, study design, and supervision. LP and XS drafted the manuscript and contributed to patient enrollment and follow-up. FT and ZL participated in the interpretation of data and statistical analyses. YL and BW were responsible for data collection. LC helped in revising the manuscript. All authors were involved in reporting the results of this study and approved the final version of the submitted manuscript.

FUNDING

This work was supported by the National Natural Science Foundation of China (Grant Numbers 81900320 and 81470955), the Medical Science and Technology Research Project of Guangdong Province (Grant Number C2019107), the basic research funding of Sun Yat-sen University (Grant Number 19ykpy40), the Guangzhou Science and Technology Project (Grant Number 201807010037), and the National Natural Science Foundation of Guangdong Province (Grant Number 2017A030313714).

SUPPLEMENTARY MATERIAL

The Supplementary Material for this article can be found online at: https://www.frontiersin.org/articles/10.3389/fcvm.2021.707328/full#supplementary-material

REFERENCES

1. Aguiar-Souto P, Ferrante G, Del Furia F, Barlis P, Khurana R, Di Mario C. Frequency and predictors of contrast-induced nephropathy after angioplasty for chronic total occlusions. *Int J Cardiol.* (2010) 139:68–74. doi: 10.1016/j.ijcard.2008.10.006
2. Nash K, Hafeez A, Hou S. Hospital-acquired renal insufficiency. *Am J Kidney Dis.* (2002) 39:930–6. doi: 10.1053/ajkd.2002.32766
3. Luk L, Steinman J, Newhouse JH. Intravenous contrast-induced nephropathy-the rise and fall of a threatening idea. *Adv Chronic Kidney Dis.* (2017) 24:169–75. doi: 10.1053/j.ackd.2017.03.001
4. Mitchell AM, Jones AE, Tumlin JA, Kline JA. Incidence of contrast-induced nephropathy after contrast-enhanced computed tomography in the outpatient setting. *Clin J Am Soc Nephrol.* (2010) 5:4–9. doi: 10.2215/CJN.05200709
5. Lindsay J, Canos DA, Apple S, Pinnow E, Aggrey GK, Pichard AD. Causes of acute renal dysfunction after percutaneous coronary intervention and comparison of late mortality rates with postprocedure rise of creatine kinase-MB versus rise of serum creatinine. *Am J Cardiol.* (2004) 94:786–9. doi: 10.1016/j.amjcard.2004.06.007
6. Zhao Q, Yin J, Lu Z, Kong Y, Zhang G, Zhao B, et al. Sulodexide protects contrast-induced nephropathy in Sprague-Dawley rats. *Cell Physiol Biochem.* (2016) 40:621–32. doi: 10.1159/000452575
7. McCullough PA, Choi JP, Feghali GA, Schussler JM, Stoler RM, Vallabahn RC, et al. Contrast-induced acute kidney injury. *J Am Coll Cardiol.* (2016) 68:1465–73. doi: 10.1016/j.jacc.2016.05.099
8. Faeh D, Chiolero A, Paccaud F. Homocysteine as a risk factor for cardiovascular disease: should we (still) worry about? *Swiss Med Wkly.* (2006) 136:745–56. doi: 10.4414/smw.2006.11283
9. Spence JD. Homocysteine-lowering therapy: a role in stroke prevention? *Lancet Neurol.* (2007) 6:830–8. doi: 10.1016/S1474-4422(07)70219-3
10. Wu Y, Huang Y, Hu Y, Zhong J, He Z, Li W, et al. Hyperhomocysteinemia is an independent risk factor in young patients with coronary artery disease in southern China. *Herz.* (2013) 38:779–84. doi: 10.1007/s00059-013-3761-y
11. Dong F, Zhang X, Li SY, Zhang Z, Ren Q, Culver, et al. Possible involvement of NADPH oxidase and JNK in homocysteine-induced oxidative stress and apoptosis in human umbilical vein endothelial cells. *Cardiovasc Toxicol.* (2005) 5:9–20. doi: 10.1385/CT:5:1:009
12. Li S, Tang X, Peng L, Luo Y, Zhao Y, Chen L, et al. A head-to-head comparison of homocysteine and cystatin C as pre-procedure predictors for contrast-induced nephropathy in patients undergoing coronary computed tomography angiography. *Clin Chim Acta.* (2015) 444:86–91. doi: 10.1016/j.cca.2015.02.019
13. Barbieri L, Verdoia M, Schaffer A, Niccoli G, Perrone-Filardi P, Bellomo G, et al. Elevated homocysteine and the risk of contrast-induced nephropathy. *Angiology.* (2014) 66:333–38. doi: 10.1177/0003319714533401
14. Lonn E, Yusuf S, Arnold MJO, Sheridan P, McQueen MJ, Pogue J, et al. Homocysteine lowering with folic acid and B vitamins in vascular disease. *N Engl J Med.* (2006) 354:1567–77. doi: 10.1056/NEJMoa060900
15. Mao X, Xing X, Xu R, Gong Q, He Y, Li S, et al. Folic acid and vitamins D and B12 correlate with homocysteine in Chinese patients with type-2 diabetes mellitus, hypertension, or cardiovascular disease. *Medicine (Baltimore).* (2016) 95:e2652. doi: 10.1097/MD.0000000000002652
16. Hou J, Yan G, Liu B, Zhu B, Qiao Y, Wang D, et al. The protective effects of enalapril maleate and folic acid tablets against contrast-induced nephropathy in diabetic rats. *Biomed Res Int.* (2018) 2018:4609750. doi: 10.1155/2018/4609750
17. Pottel H, Björk J, Courbebaisse M, Couzi L, Ebert N, Eriksen BO, et al. Development and validation of a modified full age spectrum creatinine-based equation to estimate glomerular filtration rate: a cross-sectional analysis of pooled data. *Ann Intern Med.* (2021) 174:183–91. doi: 10.7326/L21-0248
18. Stacul F, van der Molen AJ, Reimer P, Webb JAW, Thomsen HS, Morcos SK, et al. Contrast induced nephropathy: updated ESUR Contrast Media Safety Committee guidelines. *Eur Radiol.* (2011) 21:2527–41. doi: 10.1007/s00330-011-2225-0
19. Narula A, Mehran R, Weisz G, Dangas GD, Yu J, Genereux P, et al. Contrast-induced acute kidney injury after primary percutaneous coronary intervention: results from the HORIZONS-AMI substudy. *Eur Heart J.* (2014) 35:1533–40. doi: 10.1093/eurheartj/ehu063
20. Brar SS, Aharonian V, Mansukhani P, Moore N, Shen AY, Jorgensen M, et al. Haemodynamic-guided fluid administration for the prevention of contrast-induced acute kidney injury: the POSEIDON randomised controlled trial. *Lancet.* (2014) 383:1814–23. doi: 10.1016/S0140-6736(14)60689-9
21. Duan N, Zhao J, Li Z, Dong P, Wang S, Zhao Y, et al. Furosemide with saline hydration for prevention of contrast-induced nephropathy in patients undergoing coronary angiography: a meta-analysis of randomized controlled trials. *Med Sci Monit.* (2015) 21:292–7. doi: 10.12659/MSM.892446
22. Gonzales DA, Norsworthy KJ, Kern SJ, Banks S, Sieving PC, Star RA, et al. A meta-analysis of N-acetylcysteine in contrast-induced nephrotoxicity: unsupervised clustering to resolve heterogeneity. *BMC Med.* (2007) 5:32. doi: 10.1186/1741-7015-5-32

23. Maioli M, Toso A, Leoncini M, Gallopin M, Tedeschi D, Micheletti C, et al. Sodium bicarbonate versus saline for the prevention of contrast-induced nephropathy in patients with renal dysfunction undergoing coronary angiography or intervention. *J Am Coll Cardiol.* (2008) 52:599–604. doi: 10.1016/j.jacc.2008.05.026
24. Quintavalle C, Fiore D, De Micco F, Visconti G, Focaccio A, Golia B, et al. Impact of a high loading dose of atorvastatin on contrast-induced acute kidney injury. *Circulation.* (2012) 126:3008–16. doi: 10.1161/CIRCULATIONAHA.112.103317
25. Kay JCW, Chan TM, Lo SK, Kwok OH, Yip A, Fan K, et al. Acetylcysteine for prevention of acute deterioration of renal function following elective coronary angiography and intervention- a randomized controlled trial. *JAMA.* (2003) 289:553–8. doi: 10.1001/jama.289.5.553
26. Lameire N, Kellum JA, KDIGO AKI Guideline Work Group. Contrast-induced acute kidney injury and renal support for acute kidney injury- a KDIGO summary (Part 2). *Crit Care.* (2013) 17:205. doi: 10.1186/cc11455
27. Faucon AL, Bobrie G, Clement O. Nephrotoxicity of iodinated contrast media: from pathophysiology to prevention strategies. *Eur J Radiol.* (2019) 116:231–41. doi: 10.1016/j.ejrad.2019.03.008
28. Mehran R, Aymong ED, Nikolsky E, Lasic Z, Iakovou I, Fahy M, et al. A simple risk score for prediction of contrast-induced nephropathy after percutaneous coronary intervention: development and initial validation. *J Am Coll Cardiol.* (2004) 44:1393–9. doi: 10.1016/S0735-1097(04)01445-7
29. Deray G. Dialysis and iodinated contrast media. *Kidney Int Suppl.* (2006) 69(Suppl. 100):S25–S9. doi: 10.1038/sj.ki.5000371
30. Refsum H, Smith AD, Ueland PM, Nexo E, Clarke R, McPartlin J, et al. Facts and recommendations about total homocysteine determinations: an expert opinion. *Clin Chem.* (2004) 50:3–32. doi: 10.1373/clinchem.2003.021634
31. Zhang T, Lin T, Wang Y, Wang B, Qin X, Xie F, et al. Estimated stroke-free survival of folic acid therapy for hypertensive adults: projection based on the CSPPT. *Hypertension.* (2020) 75:339–46. doi: 10.1161/HYPERTENSIONAHA.119.14102
32. Ebaid H, Bashandy SAE, Abdel-Mageed AM, Al-Tamimi J, Hassan I, Alhazza IM. Folic acid and melatonin mitigate diabetic nephropathy in rats *via* inhibition of oxidative stress. *Nutr Metab (Lond).* (2020) 17:6. doi: 10.1186/s12986-019-0419-7
33. Wang X, Qin X, Demirtas H, Li J, Mao G, Huo Y, et al. Efficacy of folic acid supplementation in stroke prevention: a meta-analysis. *Lancet.* (2007) 369:1876–82. doi: 10.1016/S0140-6736(07)60854-X
34. Xu X, Qin X, Li Y, Sun D, Wang J, Liang M, et al. Efficacy of folic acid therapy on the progression of chronic kidney disease: the renal substudy of the China stroke primary prevention trial. *JAMA Intern Med.* (2016) 176:1443–50. doi: 10.1001/jamainternmed.2016.4687

Conflict of Interest: The authors declare that the research was conducted in the absence of any commercial or financial relationships that could be construed as a potential conflict of interest.

Publisher's Note: All claims expressed in this article are solely those of the authors and do not necessarily represent those of their affiliated organizations, or those of the publisher, the editors and the reviewers. Any product that may be evaluated in this article, or claim that may be made by its manufacturer, is not guaranteed or endorsed by the publisher.

Copyright © 2021 Peng, Shui, Tan, Li, Ling, Wu, Chen, Li and Peng. This is an open-access article distributed under the terms of the Creative Commons Attribution License (CC BY). The use, distribution or reproduction in other forums is permitted, provided the original author(s) and the copyright owner(s) are credited and that the original publication in this journal is cited, in accordance with accepted academic practice. No use, distribution or reproduction is permitted which does not comply with these terms.

frontiers in Cardiovascular Medicine

ORIGINAL RESEARCH
published: 15 October 2021
doi: 10.3389/fcvm.2021.756140

Increased Uric Acid, Gamma-Glutamyl Transpeptidase and Alkaline Phosphatase in Early-Pregnancy Associated With the Development of Gestational Hypertension and Preeclampsia

Yequn Chen[1†], Weichao Ou[1,2†], Dong Lin[1], Mengyue Lin[1,2], Xiru Huang[1,2], Shuhua Ni[1], Shaoxing Chen[1], Jian Yong[1], Mary Clare O'Gara[2], Xuerui Tan[1,2] and Ruisheng Liu[3]*

[1] First Affiliated Hospital of Shantou University Medical College, Shantou, China, [2] Shantou University Medical College, Shantou, China, [3] Morsani College of Medicine, University of South Florida, Tampa, FL, United States

OPEN ACCESS

Edited by:
Zhen Yang,
The First Affiliated Hospital of Sun Yat-Sen University, China

Reviewed by:
Lingfang Zeng,
King's College London, United Kingdom
Wanling Xuan,
Augusta University, United States

***Correspondence:**
Xuerui Tan
doctortxr@126.com

[†]These authors have contributed equally to this work and share first authorship

Specialty section:
This article was submitted to General Cardiovascular Medicine, a section of the journal Frontiers in Cardiovascular Medicine

Received: 10 August 2021
Accepted: 21 September 2021
Published: 15 October 2021

Citation:
Chen Y, Ou W, Lin D, Lin M, Huang X, Ni S, Chen S, Yong J, O'Gara MC, Tan X and Liu R (2021) Increased Uric Acid, Gamma-Glutamyl Transpeptidase and Alkaline Phosphatase in Early-Pregnancy Associated With the Development of Gestational Hypertension and Preeclampsia. Front. Cardiovasc. Med. 8:756140. doi: 10.3389/fcvm.2021.756140

Background: Previous studies have reported that biomarkers of liver injury and renal dysfunction were associated with hypertensive disorders of pregnancy (HDP). However, the associations of these biomarkers in early pregnancy with the risk of HDP and longitudinal blood pressure pattern during pregnancy were rarely investigated in prospective cohort studies.

Methods: A total of 1,041 pregnant women were enrolled in this prospective cohort study. BP was assessed in four stages throughout pregnancy. The following biomarkers were measured at early pregnancy before 18 weeks gestation: lactate dehydrogenase (LDH), aspartate aminotransferase to alanine aminotransferase ratio (AST/ALT), gamma-glutamyl transpeptidase (GGT), alkaline phosphatase (ALP), uric acid (UA), and estimated glomerular filtration rate (eGFR). Linear mixed-effects and logistic regression models were used to examine the associations of these biomarkers with longitudinal BP pattern during pregnancy and HDP incidence, respectively.

Results: In unadjusted models, higher serum UA, GGT, ALP, and LDH levels, as well as lower eGFR and AST/ALT, were associated with higher BP levels during pregnancy and an increased risk of HDP. After adjustment for maternal age, pre-pregnancy BMI and other potential confounders, UA, GGT, ALP, and LDH remained positively associated with both BP and HDP. However, eGFR and AST/ALT were not associated with HDP after adjusting for potential confounders. When including all 6 biomarkers simultaneously in multivariable analyses, increased UA, GGT, and ALP significantly associated with gestational hypertension and preeclampsia.

Conclusion: This study suggests that increased UA, GGT, and ALP in early-pregnancy are independent risk factors of gestational hypertension and preeclampsia.

Keywords: biomarker, blood pressure, hypertensive disorders of pregnancy, longitudinal cohort study, pregnancy

INTRODUCTION

Hypertensive disorders of pregnancy (HDP) affect up to 10% of pregnant women and remain major causes of maternal and perinatal morbidity and mortality worldwide (1–5). Identifying women at risk early in the course of such disorders, especially gestational hypertension and preeclampsia would facilitate intensive monitoring and intervention. Serum gamma-glutamyl transpeptidase (GGT), alkaline phosphatase (ALP), lactate dehydrogenase (LDH), aspartate aminotransferase to alanine aminotransferase ratio (AST/ALT) are common biomarkers of liver injury (6–8). Plasma creatinine (Cr), uric acid (UA), and estimated glomerular filtration rate (eGFR) are widely used as indicators for renal dysfunction (9, 10). Previous case-control studies have found that serum GGT, ALP, LDH, and UA levels are increased in women diagnosed with HDP (11–17). Recently, several studies have reported that lower AST/ALT was associated with insulin resistance, metabolic syndrome and cardiovascular disease (18–20). However, the associations of these biomarkers in early pregnancy with the risk of HDP were rarely investigated in prospective cohort studies.

Blood pressure (BP) changes progressively during pregnancy (21). In normal pregnancy, BP initially decreases until mid-pregnancy, and subsequently increases until delivery (21–23). A longitudinal study by Kac and colleagues recently reported that elevation of ALP, ALT, and Cr levels in the first trimester were associated with increased BP levels during pregnancy (24). As noted by the authors, the study involved a relatively small sample size and the study itself pertained to normotensive pregnant women. The associations reported prompt further investigation in large prospective cohort studies and the general population.

Accordingly, we investigated the associations of 6 hepatic and renal function biomarkers (GGT, ALP, AST/ALT, LDH, UA, and eGFR) in early pregnancy with longitudinal BP pattern during pregnancy and the risk of HDP in a large prospective cohort.

MATERIALS AND METHODS

Study Population

This study was embedded in a population-based prospective cohort of pregnant women who received antenatal care in the First Affiliated Hospital of Shantou University Medical College in Shantou, China. Clinical characteristics of participants were assessed by questionnaire and physical examination at 7th−18th, 19th−27th, 28th−34th, and 35th−39th gestational weeks. Subjects were scheduled at enrollment for clinic visits during follow-up. Patients who missed their scheduled visits would be contacted for clinic visits, whereupon the patient's information would be collected. For patients who could not attend clinical visits, patients' information would be collected by telephone interviews with their families and electronic medical records. If patients could not be followed up through in-clinic visits, telephone interviews, or electronic medical records, such patients were recorded as a loss to follow-up. A total of 2,206 pregnant women were accumulatively recruited from March 2014 to April 2016 inclusive. Included were women who had baseline measurement of hepatic and renal biochemical function before 18 weeks gestation (N = 1,371). Exclusion criteria included *in vitro* fertilization or twin pregnancies (N = 16), miscarriage (N = 9), loss to follow-up (N = 221), or having been diagnosed with chronic hepatitis B (N = 74), chronic nephritis (N = 5), rheumatoid arthritis (N = 3), or systemic lupus erythematosus (N = 2). After exclusion, 1,041 participants were enrolled.

Blood Pressure Measurements

BP was assessed in four stages during pregnancy (7th−18th, 19th−27th, 28th−34th, and 35th−39th gestational weeks). At each visit, BP was measured thrice in the morning by qualified nurses using an Omron HEM-7052 automatic blood pressure monitor (Omron Healthcare Ltd., Dalian, China) according to the standard measurement procedure recommended by the American Heart Association (25). The mean of 3 readings was used in the analysis. Some subjects had missing BP measurements

TABLE 1 | Baseline characteristics of the study population.

Characteristics	Total (N = 1,041)
Age, y	29.5 ± 4.3
Pre-pregnancy BMI, kg/m^2	20.5 ± 2.9
Monthly per capita income	
<3,000 RMB	392 (37.7)
3,000–5,000 RMB	355 (34.1)
>5,000 RMB	294 (28.2)
Education level	
Below high school	226 (21.7)
High school	223 (21.4)
Beyond high school	592 (56.9)
Nulliparous	461 (44.3)
Folic acid supplement	761 (73.1)
Family history of hypertension	208 (19.9)
Family history of diabetes mellitus	138 (13.3)
Smoking	25 (2.4)
Alcohol consumption	300 (28.8)
HDP	60 (5.8)
Gestational age at sampling, weeks	13.7 ± 3.1
UA, μmol/L	241.8 ± 50.1
eGFR, mL/min/1.73 m^2	112.2 ± 10.8
GGT, U/L	15.1 ± 8.8
ALP, U/L	49.7 ± 13.7
LDH, U/L	150.8 ± 21.9
AST/ALT	1.19 ± 0.42

Data are presented as means ± standard deviation or n (%). BMI, body mass index; HDP, hypertensive disorders of pregnancy; UA, uric acid; eGFR, estimated glomerular filtration rate; GGT, gamma–glutamyl transpeptidase; ALP, alkaline phosphatase; LDH, lactate dehydrogenase; AST/ALT, aspartate aminotransferase to alanine aminotransferase ratio.

Abbreviations: BP, blood pressure; HDP, hypertensive disorders of pregnancy; LDH, lactate dehydrogenase; AST/ALT, aspartate aminotransferase to alanine aminotransferase ratio; GGT, gamma-glutamyl transpeptidase; ALP, alkaline phosphatase; UA, uric acid; eGFR, estimated glomerular filtration rate; BMI, body mass index; T, tertile.

due to missed visits. In total, 3,274 blood pressure measurements were available for analysis, of which 31 subjects had one measurement, 225 subjects had two measurements, 347 subjects had 3 measurements, and 438 subjects had 4 measurements.

Hypertensive Disorders of Pregnancy

Maternal outcomes were obtained from medical records. A total of 60 pregnant women met the criteria of HDP, including 7 with chronic hypertension, 22 with gestational hypertension, and 31 experienced preeclampsia.

Chronic hypertension was defined as SBP $\geq$ 140 mmHg and/or DBP $\geq$ 90 mmHg before 20 weeks gestation. Gestational hypertension was defined as SBP $\geq$ 140 mmHg and/or DBP $\geq$ 90 mmHg without proteinuria, which had developed for the first time after 20 weeks gestation (26). Preeclampsia was defined as SBP $\geq$ 140 mmHg and/or DBP $\geq$ 90 mmHg with proteinuria (defined as $\geq$300 mg of protein in a 24-h urine specimen or $\geq$1+ in two random urine samples collected at least 4 h apart) (26).

Laboratory Analysis

Hepatic and renal function biochemical testing (comprising LDH, AST, ALT, ALP, GGT, UA, and Cr) was performed in the Department of Clinical Laboratory of the First Affiliated Hospital of Shantou University Medical College, using an automatic biochemical analyzer (Beckman counter AU5800, USA). Maternal overnight fasting blood samples were collected in the morning during early pregnancy (median 13.4 weeks, 95% range 7.1–18.0). The eGFR was calculated using the Chronic Kidney Disease Epidemiology Collaboration (CKD-EPI) formula (27).

Covariates

Maternal age, monthly per capita income, education level, nulliparous (yes or no), folic acid supplement intake during pregnancy (yes or no), family history of hypertension (yes or no), family history of diabetes mellitus (yes or no), smoking habit (yes or no), alcohol consumption (yes or no), pre-pregnancy weight

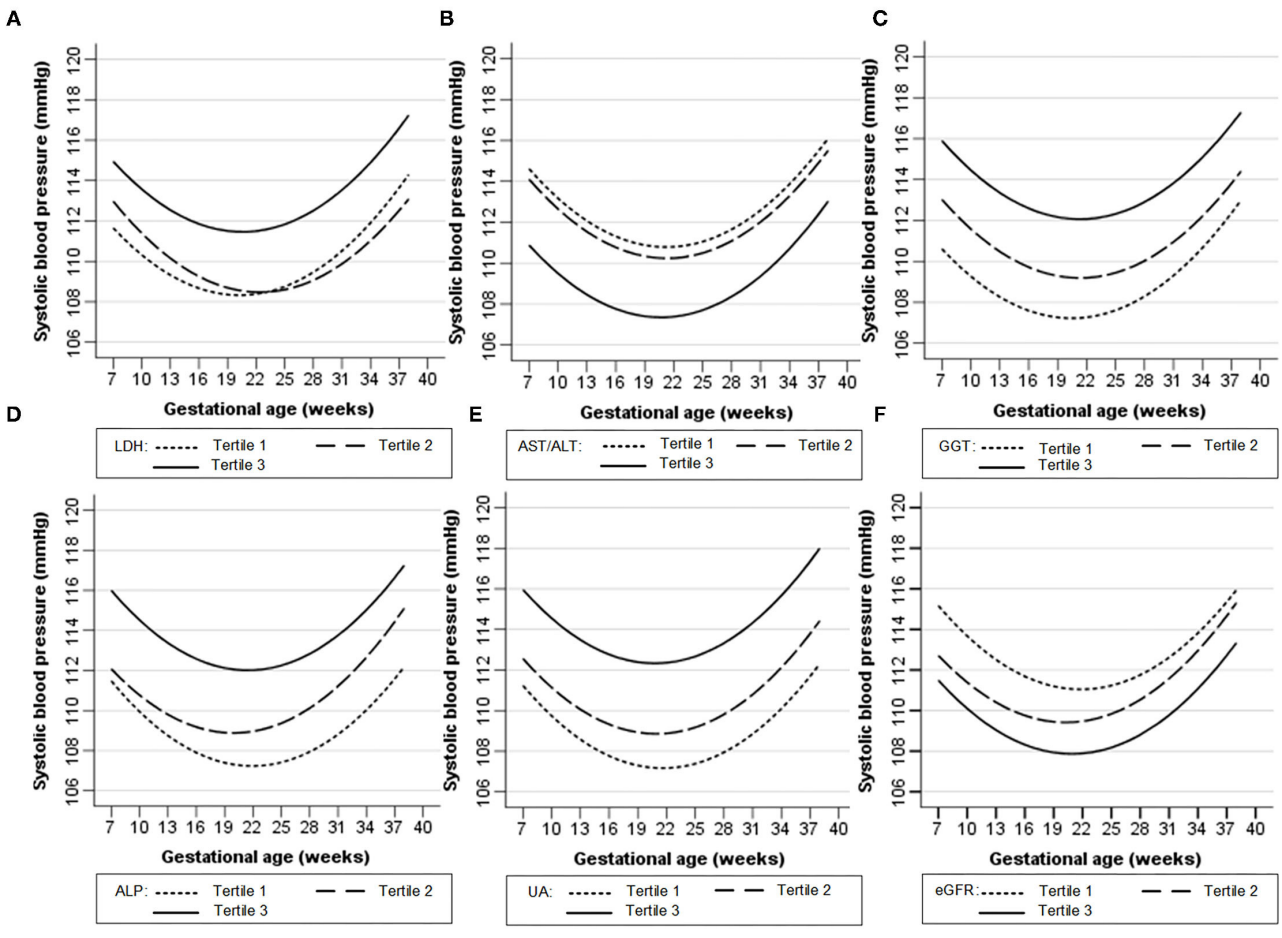

FIGURE 1 | Longitudinal trend of systolic blood pressure change with gestational age vs. early-pregnancy biomarkers levels, predicted by linear mixed-effects regression models. **(A)** lactate dehydrogenase (LDH); **(B)** aspartate aminotransferase to alanine aminotransferase ratio (AST/ALT); **(C)** gamma-glutamyl transpeptidase (GGT); **(D)** alkaline phosphatase (ALP); **(E)** uric acid (UA); **(F)** estimated glomerular filtration rate (eGFR).

and height were obtained by questionnaire on enrolment. Pre-pregnancy BMI was calculated as pre-pregnancy weight/height^2 (kg/m^2) (28).

Statistical Analysis

The hepatic and renal function biomarkers were categorized into tertiles and were analyzed as categorical variables (24). Linear mixed-effects regression models were used to evaluate the association of biomarkers with SBP and DBP change during pregnancy (22). This regression technique considers the correlation of repeated measurements in the same individual and allows incomplete outcome data, commonly applied to the analysis of repeated measurement data (29). Gestational age (linear and quadratic terms) was included in the linear mixed-effects regression models to fit the quadratic function of the association of blood pressure with time (24). Gestational age was included in the models as both random and fixed effects, whereas biomarkers and other covariates were analyzed as fixed effects. Maternal age, BMI, income, education, folic acid supplementation, family history of hypertension, family history of diabetes mellitus, as well as smoking and alcohol consumption have been reported to be associated with HDP (30–32). In order to adjust for these potential confounders, we applied 3 models: Model 1 was adjusted for gestational age (linear and quadratic terms); Model 2 was further adjusted for pre-pregnancy BMI, maternal age, monthly per capita income, education level, parity, folic acid supplementation during pregnancy, family history of hypertension, family history of diabetes mellitus, and smoking and alcohol consumption; Model 3 included all six biomarkers simultaneously and was adjusted for covariates as in Model 2. To further assess whether similar associations were also present in a normotensive population, we repeated the analyses in women who remained normotensive throughout pregnancy. The curve of longitudinal blood pressure change with gestational age was estimated using a crude linear mixed-effects regression model.

The associations of 6 early-pregnancy biomarkers with the risk of HDP were analyzed using three logistic regression models:

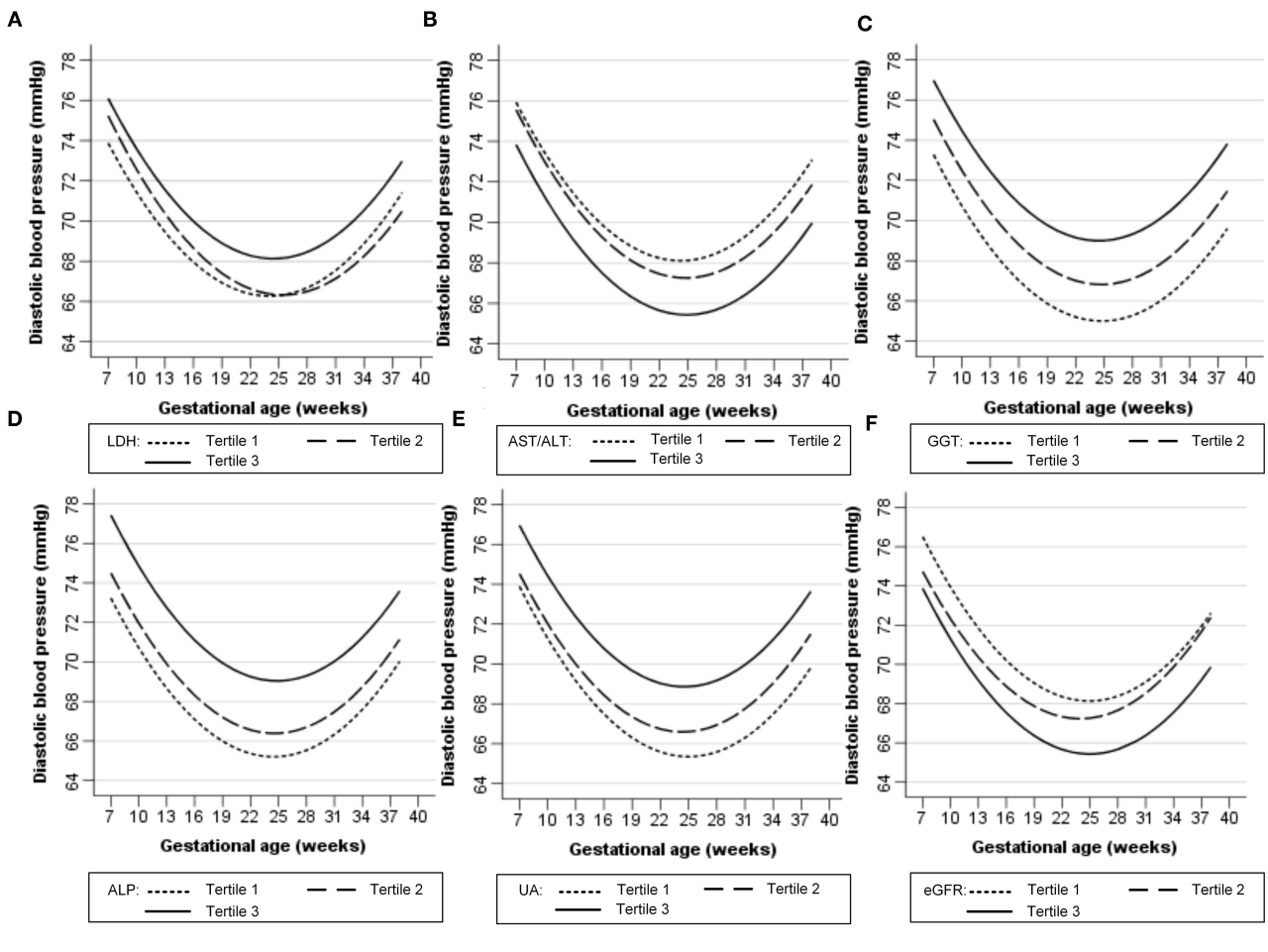

FIGURE 2 | Longitudinal trend of diastolic blood pressure change with gestational age vs. early-pregnancy biomarkers levels, predicted by linear mixed-effects regression models. **(A)** lactate dehydrogenase (LDH); **(B)** aspartate aminotransferase to alanine aminotransferase ratio (AST/ALT); **(C)** gamma-glutamyl transpeptidase (GGT); **(D)** alkaline phosphatase (ALP); **(E)** uric acid (UA); **(F)** estimated glomerular filtration rate (eGFR).

Model 1 was unadjusted; Model 2 was adjusted for pre-pregnancy BMI, maternal age, monthly per capita income, education level, parity, folic acid supplement intake during pregnancy, family history of hypertension, family history of diabetes mellitus, smoking, alcohol consumption, and gestational age at sampling; Model 3 included all six biomarkers simultaneously and was adjusted for covariates as in Model 2.

In addition, among normal pregnancy, gestation hypertension, and preeclampsia, one way ANOVA was performed to analyze the difference of maternal age, pre-pregnancy BMI, gestational age at sampling weeks, UA, eGFR, GGT, ALP, and LDH. Chi-square was used to analyze the difference of monthly per capita income, education level, nulliparous, folic acid supplement intake during pregnancy, family history of hypertension, family history of diabetes mellitus, smoking habit, and alcohol consumption.

All statistical analyses were performed using SPSS version 19.0 (SPSS Inc., Chicago, Illinois, USA). Two-tailed P-values < 0.05 were considered statistically significant.

RESULTS

Participant Characteristics

Baseline characteristics of the study population are shown in **Table 1**. Mean maternal age and pre-pregnancy BMI were 29.5 $\pm$ 4.3 years and 20.5 $\pm$ 2.9 kg/m^2, respectively. Of all women included in the study, 44.3% was nulliparous and 19.9% had a family history of hypertension. At follow-up, 60 (5.8%) pregnant women had developed HDP.

Serum Biomarkers and Blood Pressure Pattern During Pregnancy

Figures 1, **2** show the longitudinal patterns of SBP and DBP change and early pregnancy biomarker level during different tertiles of pregnancy. The distribution of maternal blood pressure throughout pregnancy was shown in **Supplementary Figures S1**, **S2**. Women in the third tertile of LDH, GGT, ALP, and UA levels had higher SBP and DBP than those in the first tertile, whereas

TABLE 2 | Longitudinal associations of early-pregnancy biomarkers levels with systolic blood pressure levels during pregnancy.

Biomarkers	*N*	Model 1*	Model 2†	Model 3‡
UA, μmol/L				
T1 (125–218)	349	Reference	Reference	Reference
T2 (219–256)	347	1.81 (0.31, 3.31)§	1.54 (0.06, 3.03)§	1.22 (-0.27, 2.71)
T3 (257–430)	345	5.29 (3.78, 6.80)‖	3.75 (2.24, 5.27)‖	3.15 (1.63, 4.68)‖
eGFR, mL/min/1.73 m^2				
T1 (68–109)	366	3.07 (1.5, 4.64)‖	0.87 (−0.75, 2.49)	0.25 (−1.35, 1.86)
T2 (110–118)	321	1.65 (0.02, 3.28)§	0.29 (−1.31, 1.89)	−0.08 (−1.66, 1.51)
T3 (119–137)	354	Reference	Reference	Reference
GGT, U/L				
T1 (4–10)	336	Reference	Reference	Reference
T2 (11–15)	375	1.85 (0.27, 3.42)§	1.15 (−0.35, 2.66)	0.69 (−0.84, 2.22)
T3 (16–68)	330	4.72 (3.10, 6.34)‖	3.11 (1.56, 4.67)‖	2.04 (0.31, 3.76)§
ALP, U/L				
T1 (18–43)	341	Reference	Reference	Reference
T2 (44–52)	332	1.92 (0.31, 3.53)§	1.57 (0.06, 3.08)§	1.16 (−0.34, 2.67)
T3 (53–193)	368	4.83 (3.26, 6.40)‖	3.2 (1.69, 4.71)‖	2.32 (0.78, 3.86)‖
LDH, U/L				
T1 (97–139)	333	Reference	Reference	Reference
T2 (140–157)	353	−0.13 (−1.74, 1.48)	−0.02 (−1.52, 1.48)	−0.38 (−1.87, 1.10)
T3 (158–273)	355	3.08 (1.47, 4.69)‖	2.44 (0.94, 3.94)‖	1.48 (−0.08, 3.27)
AST/ALT				
T1 (0.38–0.97)	340	3.36 (1.75, 4.97)‖	1.68 (0.11, 3.25)§	0.09 (−1.62, 1.79)
T2 (1.00–1.29)	355	2.80 (1.21, 4.39)‖	1.49 (−0.03, 3.00)	0.76 (−0.78, 2.30)
T3 (1.30–3.40)	346	Reference	Reference	Reference

Results were regression coefficients (95% confidence interval) of linear mixed-effects regression models. UA, uric acid; eGFR, estimated glomerular filtration rate; GGT, gamma–glutamyl transpeptidase; ALP, alkaline phosphatase; LDH, lactate dehydrogenase; AST/ALT, aspartate aminotransferase to alanine aminotransferase ratio; T, tertile.

**Model 1 was adjusted for gestational age (linear and quadratic terms).*

† Model 2 was adjusted for gestational age (linear and quadratic terms), pre-pregnancy BMI, maternal age, monthly per capita income, education level, nulliparous, folic acid supplement intake during pregnancy, family history of hypertension, family history of diabetes mellitus, smoking and alcohol consumption.

‡ Model 3 included all six biomarkers simultaneously and was adjusted for gestational age (linear and quadratic terms), pre-pregnancy BMI, maternal age, monthly per capita income, education level, nulliparous, folic acid supplement intake during pregnancy, family history of hypertension, family history of diabetes mellitus, smoking and alcohol consumption.

§ $P < 0.05$.

‖ $P < 0.01$.

TABLE 3 | Longitudinal associations of early-pregnancy biomarkers levels with diastolic blood pressure levels during pregnancy.

Biomarkers	*N*	Model 1*	Model 2†	Model 3‡
UA, μmol/L				
T1 (125–218)	349	Reference	Reference	Reference
T2 (219–256)	347	1.27 (0.07, 2.47)§	1.12 (−0.01, 2.25)	0.96 (−0.17, 2.09)
T3 (257–430)	345	3.52 (2.32, 4.73)‖	2.37 (1.21, 3.52)‖	1.88 (0.73, 3.04)‖
eGFR, mL/min/1.73 m²				
T1 (68–109)	366	2.70 (1.51, 3.88)‖	1.28 (0.09, 2.46)§	0.88 (−0.33, 2.10)
T2 (110–118)	321	1.85 (0.62, 3.08)‖	1.02 (−0.15, 2.19)	0.73 (−0.47, 1.93)
T3 (119–137)	354	Reference	Reference	Reference
GGT, U/L				
T1 (4–10)	336	Reference	Reference	Reference
T2 (11–15)	375	1.82 (0.64, 3.01)‖	1.27 (0.13, 2.40)§	0.99 (−0.17, 2.15)
T3 (16–68)	330	4.01 (2.79, 5.23)‖	2.80 (1.63, 3.98)‖	1.93 (0.63, 3.24)‖
ALP, U/L				
T1 (18–43)	341	Reference	Reference	Reference
T2 (44–52)	332	1.18 (−0.04, 2.39)	0.95 (−0.20, 2.09)	0.62 (−0.52, 1.76)
T3 (53–193)	368	3.82 (2.64, 5.01)‖	2.62 (1.47, 3.76)‖	1.98 (0.81, 3.14)‖
LDH, U/L				
T1 (97–139)	333	Reference	Reference	Reference
T2 (140–157)	353	0.01 (−1.22, 1.22)	0.12 (−1.02, 1.26)	−0.18 (−1.3, 0.95)
T3 (158–273)	355	1.83 (0.61, 3.05)‖	1.37 (0.23, 2.51)§	0.76 (−0.38, 1.90)
AST/ALT				
T1 (0.38–0.97)	340	2.70 (1.48, 3.92)‖	1.45 (0.26, 2.64)§	0.18 (−1.11, 1.47)
T2 (1.00–1.29)	355	1.82 (0.62, 3.02)‖	0.87 (−0.28, 2.02)	0.25 (−0.91, 1.42)
T3 (1.30–3.40)	346	Reference	Reference	Reference

Results were regression coefficients (95% confidence interval) of linear mixed-effects regression models. UA, uric acid; eGFR, estimated glomerular filtration rate; GGT, gamma–glutamyl transpeptidase; ALP, alkaline phosphatase; LDH, lactate dehydrogenase; AST/ALT, aspartate aminotransferase to alanine aminotransferase ratio; T, tertile.

**Model 1 was adjusted for gestational age (linear and quadratic terms).*

† Model 2 was adjusted for gestational age (linear and quadratic terms), pre-pregnancy BMI, maternal age, monthly per capita income, education level, nulliparous, folic acid supplement intake during pregnancy, family history of hypertension, family history of diabetes mellitus, smoking and alcohol consumption.

‡ Model 3 included all six biomarkers simultaneously and was adjusted for gestational age (linear and quadratic terms), pre-pregnancy BMI, maternal age, monthly per capita income, education level, nulliparous, folic acid supplement intake during pregnancy, family history of hypertension, family history of diabetes mellitus, smoking and alcohol consumption.

§ $P < 0.05$.

‖ $P < 0.01$.

women in the third tertile of AST/ALT and eGFR had lower SBP and DBP during pregnancy than those in the first tertile.

Tables 2, **3** show the longitudinal associations of early-pregnancy biomarkers with SBP and DBP levels during pregnancy, respectively. In crude analyses (Model 1), higher UA, GGT, ALP, and LDH levels, as well as lower eGFR and AST/ALT, were associated with higher SBP and DBP levels during pregnancy. After adjustment for maternal age, pre-pregnancy BMI and other potential confounders (Model 2), higher UA, GGT, ALP, LDH, and AST/ALT remained associated with both increased SBP and DBP, whereas lower eGFR was only associated with increased DBP. When all 6 biomarkers were simultaneously included in multivariable analyses (Model 3), only increased UA, GGT, and ALP remained associated with increased BP. Similar results were found in pregnant women without HDP (**Supplementary Tables S1**, **S2**).

Serum Biomarkers and HDP

Table 4 presents the association of early-pregnancy biomarkers with the risk of HDP, using multivariable logistic regression models. In unadjusted analyses (Model 1), higher UA, GGT, ALP, and LDH levels, as well as lower eGFR and AST/ALT, were associated with increased risk of HDP. After adjustment for maternal age, pre-pregnancy BMI and other potential confounders (Model 2), only increased UA, GGT, ALP, and LDH remained associated with the risk of HDP. When all 6 biomarkers were simultaneously included in multivariable analyses (Model 3), the highest tertile of UA, GGT, and ALP were associated with a higher risk of HDP (odds ratio, 3.57 [95% confidence interval, 1.36–9.39]; odds ratio, 2.61 [95% confidence interval, 1.05–6.83]; odds ratio, 2.12 [95% confidence interval, 1.01–4.90], respectively). The associations of LDH, eGFR and AST/ALT with HDP were no longer statistically significant following multivariate adjustment for UA, GGT, and ALP (Model 3).

UA, GGT, and ALP Levels in Normal Pregnancy and HDP

Table 5 presents baseline characteristics of normal pregnancy (group 1), chronic hypertension (group 2), gestation

TABLE 4 | Associations of early-pregnancy biomarkers levels with risk of hypertensive disorders of pregnancy.

Biomarkers	*N*	Model 1*	Model 2†	Model 3‡
UA, μmol/L				
T1 (125–218)	349	Reference	Reference	Reference
T2 (219–256)	347	3.50 (1.39, 8.82)‖	3.25 (1.24, 8.53)§	2.91 (1.09, 7.82)§
T3 (257–430)	345	6.25 (2.59, 15.09)‖	4.48 (1.76, 11.41)‖	3.57 (1.36, 9.39)‖
eGFR, mL/min/1.73 m²				
T1 (68–109)	366	3.09 (1.54, 6.22)‖	1.56 (0.67, 3.63)	1.14 (0.48, 2.75)
T2 (110–118)	321	1.64 (0.75, 3.58)	0.97 (0.40, 2.33)	0.75 (0.3, 1.87)
T3 (119–137)	354	Reference	Reference	Reference
GGT, U/L				
T1 (4–10)	336	Reference	Reference	Reference
T2 (11–15)	375	1.83 (0.77, 4.33)	1.29 (0.52, 3.19)	1.17 (0.45, 3.05)
T3 (16–68)	330	5.02 (2.3, 10.97)‖	3.39 (1.46, 7.85)‖	2.61 (1.05, 6.83)§
ALP, U/L				
T1 (18–43)	341	Reference	Reference	Reference
T2 (44–52)	332	1.75 (0.75, 4.05)	1.42 (0.58, 3.46)	1.13 (0.45, 2.87)
T3 (53–193)	368	4.00 (1.9, 8.44)‖	2.83 (1.27, 6.3)§	2.12 (1.01, 4.90)§
LDH, U/L				
T1 (97–139)	333	Reference	Reference	Reference
T2 (140–157)	353	1.17 (0.55, 2.47)	1.3 (0.59, 2.88)	1.14 (0.49, 2.63)
T3 (158–273)	355	2.36 (1.21, 4.58)§	2.1 (1.02, 4.3)§	1.66 (0.78, 3.54)
AST/ALT				
T1 (0.38–0.97)	340	2.40 (1.20, 4.82)§	1.71 (0.79, 3.68)	0.93 (0.38, 2.24)
T2 (1.00–1.29)	355	1.75 (0.85, 3.61)	1.15 (0.52, 2.52)	0.84 (0.36, 1.96)
T3 (1.30–3.40)	346	Reference	Reference	Reference

Results were odds ratio (95% confidence interval) derived from logistic regression models. UA, uric acid; eGFR, estimated glomerular filtration rate; GGT, gamma–glutamyl transpeptidase; ALP, alkaline phosphatase; LDH, lactate dehydrogenase; AST/ALT, aspartate aminotransferase to alanine aminotransferase ratio; T, tertile.

**Model 1 was unadjusted.*

†Model 2 was adjusted for pre-pregnancy BMI, maternal age, monthly per capita income, education level, nulliparous, folic acid supplement intake during pregnancy, family history of hypertension, family history of diabetes mellitus, smoking, alcohol consumption and gestational age at sampling.

‡Model 3 including all six biomarkers simultaneously and was adjusted for pre-pregnancy BMI, maternal age, monthly per capita income, education level, nulliparous, folic acid supplement intake during pregnancy, family history of hypertension, family history of diabetes mellitus, smoking, alcohol consumption and gestational age at sampling.

§$P < 0.05$.

‖$P < 0.01$.

hypertension (group 3), and preeclampsia (group 4). Since the sample size of chronic hypertension is too small, statistical analysis was only performed in groups 1, 3, and 4 and presented in **Figure 3**. UA and ALP levels were significantly higher in gestational hypertension and preeclampsia as compared to normal pregnancy.

DISCUSSION

In this population-based prospective cohort study, we demonstrate that higher serum UA, GGT, ALP, and LDH levels in early pregnancy, as well as lower eGFR and AST/ALT, are associated with higher BP levels during pregnancy and an increased risk of HDP. When including all 6 biomarkers simultaneously in multivariable analyses adjusted for potential confounders, increased levels of UA, GGT, and ALP were significantly associated with gestational hypertension and preeclampsia. Our study suggests that elevated UA, GGT, and ALP in early pregnancy are independent risk factors for the development of gestational hypertension and preeclampsia.

UA

For UA, our results are consistent with previous cross-sectional and prospective studies demonstrating the positive association between UA and HDP (15, 33, 34). Furthermore, we find that increased serum UA in early pregnancy is independent factor associated with higher longitudinal BP progression during pregnancy. In contrast to our findings, Kac et al. reported UA in the first trimester was not associated with BP levels during pregnancy following adjustment for maternal BMI (24). This inconsistency may be due to differences in sample size and participant characteristics. The study, as stated by the authors, investigated a relatively small sample size of 225 and specifically studied normotensive pregnant women (24). However, when we repeated the analysis in pregnant women without HDP, increased UA remained associated with both higher SBP and DBP levels during pregnancy following adjustment for maternal BMI and other confounders (**Supplementary Tables S1**, **S2**).

TABLE 5 | Baseline characteristics of normal pregnancy (group 1), chronic hypertension (group 2), gestation hypertension (group 3), and preeclampsia (group 4).

Characteristics	Group 1	Group 2	Group 3	Group 4	*P*-value**
	(*n* = 981)	(*n* = 7)	(*n* = 22)	(*n* = 31)	
Age, *y*	29.33 ± 4.20	35.86 ± 4.22	32.86 ± 5.66	32.06 ± 4.79	0.000*
Pre-pregnancy BMI, kg/m^2	20.33 ± 2.76	25.33 ± 2.76	23.51 ± 3.59	22.15 ± 4.67	0.000*
Monthly per capita income					0.702&
<3,000 RMB	283 (28.8%)	–	4 (18.2%)	7 (22.6%)	
3,000–5,000 RMB	335 (34.1%)	1 (14.3%)	9 (40.9%)	10 (32.3%)	
>5,000 RMB	363 (37.0%)	6 (85.7%)	9 (40.9%)	14 (45.2%)	
Education level					0.378&
Below high school	565 (57.6%)	3 (42.9%)	10 (45.5%)	14 (45.2%)	
High school	209 (21.3%)		7 (31.8%)	7 (22.6%)	
Beyond high school	207 (21.1%)	4 (57.1%)	5 (22.7%)	10 (32.2%)	
Nulliparous	442 (45.1%)	1 (14.3%)	6 (27.3%)	12 (38.7%)	0.203&
Folic acid supplement	726 (74.0%)	5 (71.4%)	15 (68.2%)	15 (48.4%)	0.006&
Family history of hypertension	185 (18.9%)	5 (71.4%)	7 (31.8%)	11 (35.5%)	0.025&
Family history of diabetes mellitus	125 (12.7%)	1 (14.3%)	5 (22.7%)	7 (22.6%)	0.117&
Smoking	20 (2.0%)	–	2 (9.1%)	3 (9.7%)	0.003&
Alcohol consumption	287 (29.3%)	–	4 (18.2%)	9 (29.0%)	0.527&
Gestational age at sampling, weeks	13.67 ± 3.04	12.39 ± 3.92	13.88 ± 3.57	14.70 ± 3.01	0.172*
eGFR, mL/min/1.73 m^2	112.59 ± 10.46	105.71 ± 7.84	104.11 ± 11.57	106.06 ± 15.87	0.000*
UA, μmol/L	239.96 ± 49.34	258.43 ± 48.86	275.43 ± 56.03	273.81 ± 52.54	0.000*
GGT, U/L	14.80 ± 8.63	23.71 ± 9.79	22.23 ± 11.28	17.77 ± 7.67	0.000*
ALP, U/L	49.02 ± 12.29	67.14 ± 21.10	55.95 ± 17.73	64.68 ± 30.19	0.000*
LDH, U/L	150.03 ± 21.11	162.57 ± 25.11	166.73 ± 30.31	159.90 ± 31.13	0.000*
AST/ALT	1.19 ± 0.42	0.86 ± 0.30	1.06 ± 0.27	1.10 ± 0.42	0.147*

Data are presented as means ± standard deviation or n (%). BMI, body mass index; UA, uric acid; eGFR, estimated glomerular filtration rate; GGT, gamma–glutamyl transpeptidase; ALP, alkaline phosphatase; LDH, lactate dehydrogenase; AST/ALT, aspartate aminotransferase to alanine aminotransferase ratio.
**Analysis with one way ANOVA, & Analysis with Chi-square. **All statistical analysis was not included group 2 due to small sample size.*

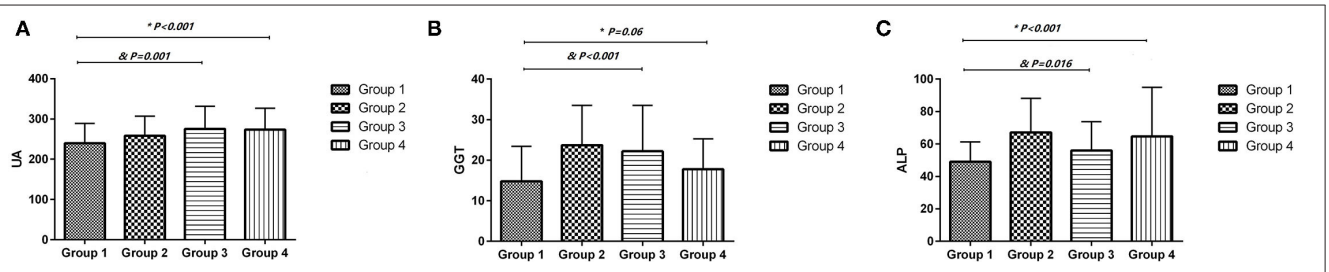

FIGURE 3 | The uric acid, gamma-glutamyl transpeptidase and alkaline phosphatase levels were compared in normal pregnancy (group 1), gestation hypertension (group 3), and preeclampsia (group 4) by One way ANOVA. **(A)** uric acid (UA); **(B)** gamma-glutamyl transpeptidase (GGT); **(C)** alkaline phosphatase (ALP). Chronic hypertension (group 2) was not included for analysis due to small sample size. *Preeclampsia (group 4) compare to normal pregnancy (group1) by One way ANOVA. & Gestation hypertension (group 3) compare to normal pregnancy (group1) by One way ANOVA.

Many experimental studies suggest that UA may play a casual role in the development of hypertension (14, 15). Hyperuricemia induced hypertension, which can be prevented by UA-lowering treatment (35). Hyperuricemia has been shown to stimulate the renin-angiotensin system, inhibit neuronal nitric oxide synthase and induce endothelial dysfunction (35, 36). In addition, UA has been reported to induce trophoblastic production of pro-inflammatory interleukin-1β through activation of inflammatory pathways (37). These underlying mechanisms may partly explain the role of UA in BP progression and the development of HDP.

GGT

Serum GGT is a known biomarker for liver injury and alcohol consumption (38). Several longitudinal studies have reported GGT as positively associated with BP progression and the risk of hypertension in non- pregnant persons (39–41). A study of almost 12,000 hypertensive adults found that higher

baseline GGT levels were associated with higher follow-up BP and an increased risk of cardiovascular mortality (42). However, no prior longitudinal study has investigated the associations of serum GGT in early pregnancy with longitudinal BP during pregnancy and the risk of HDP. In this present study, serum GGT in early pregnancy is positively associated with BP levels during pregnancy and a risk for HDP having adjusted for various confounders. Although exact mechanisms that link GGT with BP progression and HDP are not fully elucidated, several possible explanations are posited: GGT plays a role in the generation of free radical species through its interaction with iron and other transition metals (43). Serum GGT has been positively associated with inflammatory markers such as fibrinogen, C-reactive protein (CRP), and F2-isoprostanes. Thus, elevated GGT could potentially act as an additional marker for oxidative stress and inflammation, which are, as demonstrated by Palei et al., important features of HDP (44).

ALP

In the current study, higher serum ALP in early pregnancy is also independently associated with elevated BP during pregnancy and increased HDP incidence. This finding confirms and extends the result of a previous study that has reported a positive association of ALP with BP during normal pregnancy (24). The relationship of ALP with BP and HDP may be partly explained by its correlation with vascular calcification. ALP is a hydrolase enzyme that catalyzes the hydrolysis of inorganic pyrophosphate, an inhibitor of vascular calcification (45). Increased levels of ALP have been found in vessels with medial calcification (46), and have been positively associated with higher risk of hypertension, peripheral arterial disease and cardiovascular diseases (47–49). In addition, many studies have reported that serum ALP positively correlated with the inflammatory marker, CRP (20, 50–52). High serum ALP levels may partially reflect the inflammatory process, which has been associated with the pathology of HDP (44). We further compared the levels of UA, GGT, and ALP between normal pregnancy and gestational hypertension and preeclampsia. UA, GGT, and ALP were associated preeclampsia (**Figure 3**).

In conclusion, our study provided evidence that higher UA, GGT, and ALP levels in early pregnancy are independent risk factors of gestational hypertension and preeclampsia. These findings suggest that UA, GGT, and ALP could be markers for the development of gestational hypertension and preeclampsia. However, it is not clear the elevations of UA, GGT, and ALP in early pregnancy is a casual factor or consequence of the development of gestational hypertension and preeclampsia. This would be an open and essential question for future studies that could provide new targets for treatment of gestational hypertension and preeclampsia. Our findings warrant further both clinical and experimental studies to identify the underlying mechanisms and clinical value in the early diagnosis, prevention and management of HDP.

Study Strengths and Limitations

The strengths of our study include the large prospective population-based cohort from early pregnancy onwards, standardized measurement of BP, the ability to adjust for multiple traditional confounders and the ability to simultaneously assess multiple biomarkers. However, our study has some limitations. First, this was a single-center study with a small number of HDP events. Second, the serum concentrations of hepatic and renal biomarkers were assayed solely in early pregnancy. Thus, the correlation of blood pressure and HDP with these biomarkers measured before pregnancy and after delivery cannot be evaluated. Third, since BP varies during the day according to a circadian rhythm (53) and our study did not include ambulatory blood pressure measurements, this may introduce some random measurement error in the analysis. Finally, the sample size of chronic hypertension in pregnancy was too small to perform statistical analysis.

DATA AVAILABILITY STATEMENT

The raw data supporting the conclusions of this article will be made available by the authors, without undue reservation.

ETHICS STATEMENT

The studies involving human participants were reviewed and approved by Research and Ethics Committee of First Affiliated Hospital of Shantou University Medical College. The patients/participants provided their written informed consent to participate in this study.

AUTHOR CONTRIBUTIONS

XT, RL, and YC conceived and designed the study. WO, DL, SN, SC, and ML acquired the data. WO, XH, and JY analyzed the data. YC, WO, and MO'G prepared the manuscript. XT and YC reviewed and edited the manuscript. All authors contributed to the article and approved the submitted version.

FUNDING

This work was supported by projects from Grant for Key Disciplinary Project of Clinical Medicine under the High-level University Development Program (2020), Innovation Team Project of Guangdong Universities (2019KCXTD003), Li Ka Shing Foundation Cross-Disciplinary Research Grant (2020LKSFG19B), Funding for Guangdong Medical Leading Talent (2019–2022), National Natural Science Foundation of China (82073659), and Dengfeng Project for the construction of high-level hospitals in Guangdong Province—the First Affiliated Hospital of Shantou University Medical College (202003-2).

ACKNOWLEDGMENTS

The authors thank the staffs and participants for their critical contributions to this study.

SUPPLEMENTARY MATERIAL

The Supplementary Material for this article can be found online at: https://www.frontiersin.org/articles/10.3389/fcvm.2021.756140/full#supplementary-material

REFERENCES

1. Say L, Chou D, Gemmill A, Tunçalp Ö, Moller AB, Daniels J, et al. Global causes of maternal death: a WHO systematic analysis. *Lancet Glob Health.* (2014) 2:e323–33. doi: 10.1016/S2214-109X(14)70227-X
2. Chappell LC, Cluver CA, Kingdom J, Tong S. Pre-eclampsia. *Lancet.* (2021) 398:341–54. doi: 10.1016/S0140-6736(20)32335-7
3. Liu M. Spotlight on the relationship between heart disease and mental stress. *Heart and Mind.* (2021) 5:1–3. doi: 10.4103/hm.hm_12_21
4. Jiang W. Neuropsychocardiology-Evolution and advancement of the heart-mind field. *Heart and Mind.* (2017) 1:59–64. doi: 10.4103/hm.hm_13_17
5. Eizaguirre N, Rementeria GP, González-Torrez MÁ, Gaviria M. Updates in vascular dementia. *Heart and Mind.* (2017) 1:22–35. doi: 10.4103/hm.hm_4_16
6. Mutanen A, Lohi J, Merras-Salmio L, Koivusalo A, Pakarinen MP. Prediction, identification and progression of histopathological liver disease activity in children with intestinal failure. *J Hepatol.* (2021) 74:593–602. doi: 10.1016/j.jhep.2020.09.023
7. Li MX, Zhao H, Bi XY, Li ZY, Yao XS, Li H, et al. Lactate dehydrogenase is a prognostic indicator in patients with hepatocellular carcinoma treated by sorafenib: results from the real life practice in HBV endemic area. *Oncotarget.* (2016) 7:86630–47. doi: 10.18632/oncotarget.13428
8. Su CW, Chan CC, Hung HH, Huo TI, Huang YH, Li CP, et al. Predictive value of aspartate aminotransferase to alanine aminotransferase ratio for hepatic fibrosis and clinical adverse outcomes in patients with primary biliary cirrhosis. *J Clin Gastroenterol.* (2009) 43:876–83. doi: 10.1097/MCG.0b013e31818980ac
9. Takae K, Nagata M, Hata J, Mukai N, Hirakawa Y, Yoshida D, et al. Serum uric acid as a risk factor for chronic kidney disease in a japanese community- the hisayama study. *Circ J.* (2016) 80:1857–62. doi: 10.1253/circj.CJ-16-0030
10. Webster AC, Nagler EV, Morton RL, Masson P. Chronic kidney disease. *Lancet.* (2017) 389:1238–52. doi: 10.1016/S0140-6736(16)32064-5
11. Wu J, Zhou W, Li Q, Yuan R, Li H, Cui S. Combined use of serum gamma glutamyl transferase level and ultrasonography improves prediction of perinatal outcomes associated with preeclamptic pregnancy. *Clin Chim Acta.* (2017) 475:97–101. doi: 10.1016/j.cca.2017.09.018
12. Portelinha A, Cerdeira AS, Belo L, Tejera E, Pinto F, Pinto A, et al. Altered alanine aminotransferase and gamma-glutamyl transpeptidase in women with history of preeclampsia: association with waist-to-hip ratio and body mass index. *Eur J Gastroenterol Hepatol.* (2009) 21:196–200. doi: 10.1097/MEG.0b013e32831d81a7
13. Dacaj R, Izetbegovic S, Stojkanovic G, Dreshaj S. Elevated liver enzymes in cases of preeclampsia and intrauterine growth restriction. *Med Arch.* (2016) 70:44–7. doi: 10.5455/medarh.2016.70.44-47
14. Makuyana D, Mahomed K, Shukusho FD, Majoko F. Liver and kidney function tests in normal and pre-eclamptic gestation–a comparison with non-gestational reference values. *Cent Afr J Med.* (2002) 48:55–9.
15. Padma Y, Aparna VB, Kalpana B, Ritika V, Sudhakar PR. Renal markers in normal and hypertensive disorders of pregnancy in Indian women: a pilot study. *Int J Reprod Contracept Obstet Gynecol.* (2013) 2:514–20. doi: 10.5455/2320-1770.ijrcog20131205
16. Udenze I, Amadi C, Awolola N, Makwe CC. The role of cytokines as inflammatory mediators in preeclampsia. *Pan Afr Med J.* (2015) 20:219. doi: 10.11604/pamj.2015.20.219.5317
17. Hunter RJ, Pinkerton JH, Johnston H. Serum placental alkaline phosphatase in normal pregnancy and preeclampsia. *Obstet Gynecol.* (1970) 36:536–46.
18. Kawamoto R, Kohara K, Kusunoki T, Tabara Y, Abe M, Miki T. Alanine aminotransferase/aspartate aminotransferase ratio is the best surrogate marker for insulin resistance in non-obese Japanese adults. *Cardiovasc Diabetol.* (2012) 11:117. doi: 10.1186/1475-2840-11-117
19. Labayen I, Ruiz JR, Ortega FB, Davis CL, Rodriguez G, Gonzalez-Gross M, et al. Liver enzymes and clustering cardiometabolic risk factors in European adolescents: the HELENA study. *Pediatr Obes.* (2015) 10:361–70. doi: 10.1111/ijpo.273
20. Hanley AJ, Williams K, Festa A, Wagenknecht LE, D'Agostino RB, Haffner SM. Liver markers and development of the metabolic syndrome: the insulin resistance atherosclerosis study. *Diabetes.* (2005) 54:3140–7. doi: 10.2337/diabetes.54.11.3140
21. Grindheim G, Estensen ME, Langesaeter E, Rosseland LA, Toska K. Changes in blood pressure during healthy pregnancy: a longitudinal cohort study. *J Hypertens.* (2012) 30:342–50. doi: 10.1097/HJH.0b013e32834f0b1c
22. Farias DR, Franco-Sena AB, Rebelo F, Schlussel MM, Salles GF, Kac G. Total cholesterol and leptin concentrations are associated with prospective changes in systemic blood pressure in healthy pregnant women. *J Hypertens.* (2014) 32:127–34. doi: 10.1097/HJH.0000000000000037
23. Macdonald-Wallis C, Tilling K, Fraser A, Nelson SM, Lawlor DA. Established preeclampsia risk factors are related to patterns of blood pressure change in normal term pregnancy: findings from the Avon Longitudinal Study of Parents and Children. *J Hypertens.* (2011) 29:1703–11. doi: 10.1097/HJH.0b013e328349eec6
24. Kac G, Mendes RH, Farias DR, Eshriqui I, Rebelo F, Benaim C, et al. Hepatic, renal and inflammatory biomarkers are positively associated with blood pressure changes in healthy pregnant women: a prospective cohort. *Medicine.* (2015) 94:e683. doi: 10.1097/MD.0000000000000683
25. Palatini P, Asmar R, O'Brien E, Padwal R, Parati G, Sarkis J, et al. Recommendations for blood pressure measurement in large arms in research and clinical practice: position paper of the European society of hypertension working group on blood pressure monitoring and cardiovascular variability. *J Hypertens.* (2020) 38:1244–50. doi: 10.1097/HJH.0000000000002399
26. American College of Obstetricians and Gynecologists. Hypertension in pregnancy. Report of the American College of Obstetricians and Gynecologists' Task Force on Hypertension in Pregnancy. *Obstet Gynecol.* (2013) 122:1122–31. doi: 10.1097/01.AOG.0000437382.03963.88
27. Levey AS, Stevens LA, Schmid CH, Zhang YL, Castro AF, 3rd, Feldman HI, et al. A new equation to estimate glomerular filtration rate. *Ann Intern Med.* (2009) 150:604–12. doi: 10.7326/0003-4819-150-9-200905050-00006
28. Hales CM, Fryar CD, Carroll MD, Freedman DS, Aoki Y, Ogden CL. Differences in obesity prevalence by demographic characteristics and urbanization level among adults in the United States, 2013-2016. *JAMA.* (2018) 319:2419–29. doi: 10.1001/jama.2018.7270
29. Quene H, van den Bergh H. Examples of mixed-effects modeling with crossed random effects and with binomial data. *J Memory Lang.* (2008) 59:413–25. doi: 10.1016/j.jml.2008.02.002
30. Ye C, Ruan Y, Zou L, Li G, Li C, Chen Y, et al. The 2011 survey on hypertensive disorders of pregnancy (HDP) in China: prevalence, risk factors, complications, pregnancy and perinatal outcomes. *PLoS ONE.* (2014) 9:e100180. doi: 10.1371/journal.pone.0100180
31. Li Z, Ye R, Zhang L, Li H, Liu J, Ren A. Folic acid supplementation during early pregnancy and the risk of gestational hypertension and preeclampsia. *Hypertension.* (2013) 61:873–9. doi: 10.1161/HYPERTENSIONAHA.111.00230
32. Engel SM, Scher E, Wallenstein S, Savitz DA, Alsaker ER, Trogstad L, et al. Maternal active and passive smoking and hypertensive disorders of pregnancy: risk with trimester-specific exposures. *Epidemiology.* (2013) 24:379–86. doi: 10.1097/EDE.0b013e3182873a73
33. Vyakaranam S, Bhongir AV, Patlolla D, Chintapally R. Study of serum uric acid and creatinine in hypertensive disorders of pregnancy. *Int J Med Sci Public Health.* (2015) 4:1424–8. doi: 10.5455/ijmsph.2015.15042015294

34. Wolak T, Sergienko R, Wiznitzer A, Paran E, Sheiner E. High uric acid level during the first 20 weeks of pregnancy is associated with higher risk for gestational diabetes mellitus and mild preeclampsia. *Hypertens Pregnancy.* (2012) 31:307–15. doi: 10.3109/10641955.2010.507848
35. Liu CW, Ke SR, Tseng GS, Wu YW, Hwang JJ. Elevated serum uric acid is associated with incident hypertension in the health according to various contemporary blood pressure guidelines. *Nutr Metab Cardiovasc Dis.* (2021) 31:1209–18. doi: 10.1016/j.numecd.2021.01.003
36. Ponticelli C, Podesta MA, Moroni G. Hyperuricemia as a trigger of immune response in hypertension and chronic kidney disease. *Kidney Int.* (2020) 98:1149–59. doi: 10.1016/j.kint.2020.05.056
37. Mulla MJ, Myrtolli K, Potter J, Boeras C, Kavathas PB, Sfakianaki AK, et al. Uric acid induces trophoblast IL-1beta production via the inflammasome: implications for the pathogenesis of preeclampsia. *Am J Reprod Immunol.* (2011) 65:542–8. doi: 10.1111/j.1600-0897.2010.00960.x
38. Whitfield JB. Gamma glutamyl transferase. *Crit Rev Clin Lab Sci.* (2001) 38:263–355. doi: 10.1080/20014091084227
39. Cheung BM, Ong KL, Tso AW, Cherny SS, Sham PC, Lam TH, et al. Gamma-glutamyl transferase level predicts the development of hypertension in Hong Kong Chinese. *Clin Chim Acta.* (2011) 412:1326–31. doi: 10.1016/j.cca.2011.03.030
40. Onat A, Can G, Örnek E, Çiçek G, Ayhan E, Dogan Y. Serum γ-glutamyltransferase: independent predictor of risk of diabetes, hypertension, metabolic syndrome, and coronary disease. *Obesity.* (2012) 20:842–8. doi: 10.1038/oby.2011.136
41. Zatu MC, Van Rooyen JM, Kruger A, Schutte AE. Alcohol intake, hypertension development and mortality in black South Africans. *Eur J Prev Cardiol.* (2016) 23:308–15. doi: 10.1177/2047487314563447
42. McCallum L, Panniyammakal J, Hastie CE, Hewitt J, Patel R, Jones GC, et al. Longitudinal blood pressure control, long-term mortality, and predictive utility of serum liver enzymes and bilirubin in hypertensive patients. *Hypertension.* (2015) 66:37–43. doi: 10.1161/HYPERTENSIONAHA.114.04915
43. Lee DH, Blomhoff R, Jacobs DR Jr. Is serum gamma glutamyltransferase a marker of oxidative stress? *Free Radic Res.* (2004) 38:535–9. doi: 10.1080/10715760410001694026
44. Palei AC, Spradley FT, Warrington JP, George EM, Granger JP. Pathophysiology of hypertension in pre-eclampsia: a lesson in integrative physiology. *Acta Physiol (Oxf).* (2013) 208:224–33. doi: 10.1111/apha.12106
45. Schoppet M, Shanahan CM. Role for alkaline phosphatase as an inducer of vascular calcification in renal failure? *Kidney Int.* (2008) 73:989–91. doi: 10.1038/ki.2008.104
46. Shanahan CM, Cary NR, Salisbury JR, Proudfoot D, Weissberg PL, Edmonds ME. Medial localization of mineralization-regulating proteins in association with Monckeberg's sclerosis: evidence for smooth muscle cell-mediated vascular calcification. *Circulation.* (1999) 100:2168–76. doi: 10.1161/01.CIR.100.21.2168
47. Webber M, Krishnan A, Thomas NG, Cheung BM. Association between serum alkaline phosphatase and C-reactive protein in the United States National Health and Nutrition Examination Survey 2005-2006. *Clin Chem Lab Med.* (2010) 48:167–73. doi: 10.1515/CCLM.2010.052
48. Cheung BM, Ong KL, Wong LY. Elevated serum alkaline phosphatase and peripheral arterial disease in the United States National Health and Nutrition Examination Survey 1999-2004. *Int J Cardiol.* (2009) 135:156–61. doi: 10.1016/j.ijcard.2008.03.039
49. Tonelli M, Curhan G, Pfeffer M, Sacks F, Thadhani R, Melamed ML, et al. Relation between alkaline phosphatase, serum phosphate, and all-cause or cardiovascular mortality. *Circulation.* (2009) 120:1784–92. doi: 10.1161/CIRCULATIONAHA.109.851873
50. Cheung BM, Ong KL, Cheung RV, Wong LY, Wat NM, Tam S, et al. Association between plasma alkaline phosphatase and C-reactive protein in Hong Kong Chinese. *Clin Chem Lab Med.* (2008) 46:523–7. doi: 10.1515/CCLM.2008.111
51. Kunutsor SK, Bakker SJ, Kootstra-Ros JE, Gansevoort RT, Gregson J, Dullaart RP. Serum alkaline phosphatase and risk of incident cardiovascular disease: interrelationship with high sensitivity c-reactive protein. *PLoS ONE.* (2015) 10:e0132822. doi: 10.1371/journal.pone.0132822
52. Kuroda R, Nogawa K, Watanabe Y, Morimoto H, Sakata K, Suwazono Y. Association between high-sensitive c-reactive protein and the development of liver damage in japanese male workers. *Int J Environ Res Public Health.* (2021) 18:2985–96. doi: 10.3390/ijerph18062985
53. Zhang J, Sun R, Jiang T, Yang G, Chen L. Circadian blood pressure rhythm in cardiovascular and renal health and disease. *Biomolecules.* (2021) 11:868–82. doi: 10.3390/biom11060868

Conflict of Interest: The authors declare that the research was conducted in the absence of any commercial or financial relationships that could be construed as a potential conflict of interest.

Publisher's Note: All claims expressed in this article are solely those of the authors and do not necessarily represent those of their affiliated organizations, or those of the publisher, the editors and the reviewers. Any product that may be evaluated in this article, or claim that may be made by its manufacturer, is not guaranteed or endorsed by the publisher.

Copyright © 2021 Chen, Ou, Lin, Lin, Huang, Ni, Chen, Yong, O'Gara, Tan and Liu. This is an open-access article distributed under the terms of the Creative Commons Attribution License (CC BY). The use, distribution or reproduction in other forums is permitted, provided the original author(s) and the copyright owner(s) are credited and that the original publication in this journal is cited, in accordance with accepted academic practice. No use, distribution or reproduction is permitted which does not comply with these terms.

frontiers in Cardiovascular Medicine

ORIGINAL RESEARCH
published: 25 October 2021
doi: 10.3389/fcvm.2021.750926

Plasma Hydrogen Sulfide Is Positively Associated With Post-operative Survival in Patients Undergoing Surgical Revascularization

Alban Longchamp[1,2†], Michael R. MacArthur[3†], Kaspar Trocha[4], Janine Ganahl[5], Charlotte G. Mann[3], Peter Kip[4], William W. King[4], Gaurav Sharma[4], Ming Tao[4], Sarah J. Mitchell[3], Tamás Ditrói[6], Jie Yang[7], Péter Nagy[6,8], C. Keith Ozaki[4], Christopher Hine[7] and James R. Mitchell[3]*

[1] Department of Vascular Surgery, Centre Hospitalier Universitaire Vaudois and University of Lausanne, Lausanne, Switzerland, [2] Department of Biomedical Sciences, University of Lausanne, Lausanne, Switzerland, [3] Department of Health Sciences and Technology, Eidgenössische Technische Hochschule (ETH) Zürich, Zurich, Switzerland, [4] Department of Surgery and the Heart and Vascular Center, Brigham and Women's Hospital and Harvard Medical School, Boston, MA, United States, [5] Department of Molecular Metabolism, Harvard T. H. Chan School of Public Health, Boston, MA, United States, [6] Department of Molecular Immunology and Toxicology, National Institute of Oncology, Budapest, Hungary, [7] Department of Cardiovascular and Metabolic Sciences, Cleveland Clinic Lerner Research Institute, Cleveland, OH, United States, [8] Department of Anatomy and Histology, University of Veterinary Medicine, Budapest, Hungary

Objective: Hydrogen sulfide (H_2S) is a gaseous signaling molecule and redox factor important for cardiovascular function. Deficiencies in its production or bioavailability are implicated in atherosclerotic disease. However, it is unknown if circulating H_2S levels differ between vasculopaths and healthy individuals, and if so, whether H_2S measurements can be used to predict surgical outcomes. Here, we examined: (1) Plasma H_2S levels in patients undergoing vascular surgery and compared these to healthy controls, and (2) the association between H_2S levels and mortality in a cohort of patients undergoing surgical revascularization.

Methods: One hundred and fifteen patients undergoing carotid endarterectomy, open lower extremity revascularization or lower leg amputation were enrolled at a single institution. Peripheral blood was also collected from a matched control cohort of 20 patients without peripheral or coronary artery disease. Plasma H_2S production capacity and sulfide concentration were measured using the lead acetate and monobromobimane methods, respectively.

Results: Plasma H_2S production capacity and plasma sulfide concentrations were reduced in patients with PAD ($p < 0.001$, $p = 0.013$, respectively). Patients that underwent surgical revascularization were divided into high vs. low H_2S production capacity groups by median split. Patients in the low H_2S production group had increased

OPEN ACCESS

Edited by:
Yuli Huang,
Shunde Hospital, Southern Medical University, China

Reviewed by:
Nazareno Paolocci,
Johns Hopkins University, United States
Cui Li,
University of Nebraska Medical Center, United States

***Correspondence:**
Alban Longchamp
alban.longchamp@chuv.ch

[†]These authors have contributed equally to this work

Specialty section:
This article was submitted to General Cardiovascular Medicine, a section of the journal Frontiers in Cardiovascular Medicine

Received: *31 July 2021*
Accepted: *13 September 2021*
Published: *25 October 2021*

Citation:
Longchamp A, MacArthur MR, Trocha K, Ganahl J, Mann CG, Kip P, King WW, Sharma G, Tao M, Mitchell SJ, Ditrói T, Yang J, Nagy P, Ozaki CK, Hine C and Mitchell JR (2021) Plasma Hydrogen Sulfide Is Positively Associated With Post-operative Survival in Patients Undergoing Surgical Revascularization. Front. Cardiovasc. Med. 8:750926. doi: 10.3389/fcvm.2021.750926

probability of mortality ($p = 0.003$). This association was robust to correction for potentially confounding variables using Cox proportional hazard models.

Conclusion: Circulating H_2S levels were lower in patients with atherosclerotic disease. Patients undergoing surgical revascularization with lower H_2S production capacity, but not sulfide concentrations, had increased probability of mortality within 36 months post-surgery. This work provides insight on the role H_2S plays as a diagnostic and potential therapeutic for cardiovascular disease.

Keywords: hydrogen sulfide, peripheral artery disease (PAD), limb ischemia, biomarker, surgery

INTRODUCTION

Hydrogen sulfide (H_2S) is a redox modifying and diffusible gasotransmitter that plays numerous physiologic roles across various organ systems including the cardiovascular system (1). While high levels of exogenous H_2S are toxic, increased levels within a supraphysiologic range have been shown to mediate many beneficial effects ranging from stress resistance to longevity (2–4). Exogenous H_2S has been shown to extend lifespan and increase stress resistance in *Caenorhabditis elegans (C. elegans)* and *Drosophila melanogaster (D. melanogaster)*, and to protect mice from lethal levels of hypoxia, although effects on human lifespan and survival remain to be determined (2, 5). H_2S has also emerged as a critical mediator of vascular homeostasis (6) in preclinical models through its functions as a vasodilator (7), antioxidant (8), oxygen sensor (9, 10), immunomodulator (11), and anti-inflammatory gas (12). Individuals with diabetes-related vascular inflammation had decreased circulating sulfide levels (13). As atherosclerosis is a chronic inflammatory disease, it is important to note H_2S is shown to regulate several atherosclerotic cellular and inflammatory processes (14–17).

While H_2S has been implicated in the pathogenesis of multiple cardiovascular disease processes, the measurement of H_2S is arduous and often relies on indirect measures and surrogates (18–23). Nevertheless, further characterizing the role of H_2S in systemic disease states such as peripheral arterial disease (PAD) may yield important insights on potential diagnostic and therapeutic applications.

Thus, our objective was to assess the clinical relevance of plasma H_2S levels in patients suffering from vascular disease. Individuals included in this study were diagnosed with either carotid artery stenosis requiring carotid endarterectomy (CEA), or peripheral artery disease (PAD) necessitating revascularization or amputation secondary to unsalvageable critical limb ischemia. Patients were followed for 36 months post-surgery with clinical outcomes and mortality measured. A baseline control cohort of patients matched for age, sex, and hypertension (7), but with no history of PAD, prior MI, coronary interventions, heart failure, or stroke were included for comparing H_2S levels in the diseased vs. healthy state. Our study provides new insight into the relevance of circulating H_2S levels in patients suffering from atherosclerosis, and during surgical revascularization.

MATERIALS AND METHODS

Study Design and Demographic Data Collection

The study followed the principles of the Declaration of Helsinki and was approved by the Partners Human Research Committee institutional review board (IRB). Informed consent was obtained for prospective collection of demographic and clinical data. All consecutive patients, at a single institution undergoing elective vascular surgery from 2012 to 2015, scheduled for carotid endarterectomy, open lower extremity revascularization, and major lower extremity amputation (secondary to critical limb ischemia) were enrolled. None of the amputations were traumatic. Patients were excluded if they were <18 years, had an emergent indication for the operation or if they were involved in another clinical research study. The cohort baseline risk factors and demographics were collected including age, race, history of PAD, history of stroke or myocardial infarction as well as history of coronary intervention (**Supplemental Table 1**). To compare levels of H_2S between patients with vascular disease vs. healthy patients, an additional group of 20 control subjects were enrolled without documented or diagnosed PAD or CAD. This control cohort was matched for age, sex and hypertension, and was randomly extracted from the Brigham and Women's biobank. No additional clinical information was provided for this control cohort.

Hydrogen Sulfide Measurements

On the day of surgery, but prior to surgical intervention, peripheral venous blood was collected into ethylenediaminetetraacetic acid (EDTA) collection tubes at the time of peripheral intravenous line placement. The tube was inverted several times to ensure mixing with the anticoagulant and then transferred to the lab for processing. To obtain plasma all samples were centrifuged at room temperature for 15 min at 2,000 g, plasma was then stored at −80°C for future analysis. All samples were then thawed and processed for H_2S production capacity at once to ensure uniformity.

Hydrogen sulfide production capacity was measured using the lead acetate method (24). In brief, plasma was mixed with 150 µl freshly prepared reaction mixture, containing 100 mM L-cysteine and 0.5 mM pyridoxal 5'-phosphate (PLP, aka Vitamin B6) in Phosphate buffered saline (PBS) in a plastic 96-well plate. The plate was then incubated at 37°C with lead acetate embedded

filter paper on top. Upon the reaction of H_2S with the lead acetate paper, a dark lead sulfide precipitate is produced. The paper was incubated for 6 h, until a detectable, but non-saturated signal was seen.

In vitro H_2S production assays to demonstrate sensitivity and validity of the lead acetate assay to detect iron-catalyzed H_2S production were similarly performed as previously described (25). Briefly, 150 μL reactions in PBS were set up in 96-well plates. Each reaction contained 10 mM L-cysteine, and according to the respective conditions as indicated in the figures, 0–50 μM $FeCl_3$, 0–50 μM hemin, 0–1,000 μM PLP, and/or 0 to 50 mM homocysteine. The lead acetate filter paper was then placed on top of the reaction plates with a weight on top and incubated at 37°C for 1.5–2 h.

The amount of lead sulfide captured on the paper was quantitated by using the IntDen measurement function in ImageJ software and normalized to the respective control group after subtracting the background. An empty well without plasma, was used as blank value was used for background measurement. These measurements were assessed by 2 independent investigators blinded to group assignment.

Hydrogen sulfide concentration determination using the MBB method was conducted as described previously (26). Briefly: In almost complete darkness due to the light sensitivity of the MBB reagent, 20 μl of 50 mM HEPES (pH = 8.0) buffer and 20 μl of 10 mM monobromo-bimane (Sigma Aldrich) was added to 20 μl of plasma sample. After 10 min in the dark at room temperature, the product sulfide-dibimane was extracted with 200 μl of pure ethyl acetate. The organic supernatant was collected and evaporated to dryness and stored at −20°C until measurement. The solid samples were redissolved prior to HPLC measurements in acetonitrile. Ten microliter was injected and separated on an Agilent Eclipse XDB-C18 (4.6 × 250 mm, 5 μm) using a Merck Hitachi L7000 HPLC instrument with a Thermo UltiMate 3000 fluorescent detector. The elution method employed a 28 min long gradient using water and acetonitrile both containing 0.1% TFA. The detection of the product was carried out using UV-absorbance measurement at 254 nm and fluorescent measurement with extinction at 390 nm and detection at 480 nm. Quantitation was done using a standard calibration curve in aqueous buffered solutions, where H_2S concentrations were verified by the DTNB assays. It should be noted that the MBB method measures endogenous sulfide levels that are easily liberated from the bound plasma sulfide pool and hence absolute values largely depend on the applied conditions (temperature, alkylation time, concentration conditions etc). This is the reason why absolute sulfide values obtained here should not be compared with values reported in other studies (23).

The enzymatic activity of CBS in blood samples was measured by an HPLC-MS/MS protocol previously published (27). Briefly, 20 μL of plasma sample was added to 25 μL of solution containing 200 mmol/L Tris-HCl (pH 8.6), 1 mmol/L pyridoxal 5′-phosphate, 1 mmol/L SAM and 40 mmol/L 2,3,3-2H-labeled serine (Cambridge Isotope Laboratories, Inc). Five microliter of starting solution containing 280 mmol/L homocysteine thiolactone in 100 mmol/L Tris-HCl (pH 8.6), 10 mmol/L DTT, 1.225 mol/L NaOH was incubated for 5 min at 37°C to produce homocysteine by thiolactone cleavage, pH was adjusted to 8.6 with 1:1 HCl solution and the solution was added to the plasma mixture. After 4 h of incubation at 37°C, the reaction was quenched by acidification of the mixture with 100 μL of EZ:faast Internal Standard Solution (Phenomenex) containing 3.3 μmol/L of internal standard 3,3,4,4-2H-labeled cystathionine. Sample preparation was carried out using EZ:faast kit (Phenomenex) kit, that included a solid phase extraction step, derivatization with propyl chloroformate, and an extraction into an organic solvent. The prepared samples were separated on an EZ:faast AAA-MS column (250 × 2.0 mm, Phenomenex) using LC and MS settings described in the EZ:faast user manual using a Thermo Scientific UltiMate 3000 HPLC connected to a Thermo Scientific LTQ-XL MS instrument. Concentrations (and enzyme activities) were calculated using the internal standard.

Statistical Analysis

Plasma H_2S production capacity and sulfide concentration in vascular surgery patients and healthy controls were compared using Student's *t*-test. Pearson correlation coefficient was calculated to assess the association between plasma H_2S production capacity and plasma sulfide concentration. High low H_2S production capacity/free sulfide groups and groups were divided by median split, which was arbitrary. The Kaplan-Meier method was used to estimate survival in high and low H_2S production capacity/free sulfide groups and groups were compared using log-rank test. Cox proportional hazard models were fit to estimate mortality hazard ratios between high and low H_2S producing groups, corrected for potentially confounding variables (age, gender, BMI). Both unadjusted and adjusted Cox proportional hazard models met assumptions of proportional hazard. To assess the odds of post-surgical complication in high vs. low H_2S producing individuals, Fisher's exact test was used. Statistical tests were performed using Graphpad Prism 7 and R version 3.3.2. Kaplan-Meier curves and Cox proportional hazard models were fit in R using the Survival package and Kaplan-Meier curves were visualized using the Survminer package. All reported *P* values are based on 2-sided tests and *P* values of <0.05 were considered statistically significant.

RESULTS

H_2S Levels Are Reduced in Patients With Vascular Disease Compared to Patients With No Documented Atherosclerosis

The characteristics of the control and the vascular cohort are summarized in **Table 1**. Mean (SD) age of the control and vascular patients was 68 (2.3) and 69 (9), respectively. These patients only differed in the prevalence of PAD, prior MI/coronary revascularization, and hyperlipidemia (**Table 1**). The control cohort included a group of 20 subjects, matched for age, sex and hypertension, but with no documented atherosclerotic cardiovascular disease. The vascular cohort included a heterogenous group of 115 patients. Forty nine underwent carotid endarterectomy (asymptomatic $n = 34$,

TABLE 1 | Baseline study population characteristics.

Variable	Control cohort $n = 20$	Vascular cohort $n = 115$	*P*
Age (SD)	68 (2.3)	69 (9)	0.62
Male (%)	13 (65)	73 (63)	0.89
Ethnicity (%)			
White	18 (90)	97 (84)	0.51
Hispanic	0	10 (9)	
Black	0	4 (3.5)	
Other	2 (10)	4 (3.5)	
BMI (SD)	28.7 (7.2)	28.3 (5.3)	0.76
Comorbidities (%)			
Heart failure	0	19 (17)	0.16
History of stroke	0	24 (21)	0.08
PAD	0	75 (65)	<0.01
Prior coronary intervention	0	44 (38)	<0.01
Prior MI	0	30 (26)	0.03
Hypertension	19 (95)	106 (92)	0.65
Hyperlipidemia	6 (30)	98 (85)	<0.01
COPD	0	7 (6)	0.81
Renal dysfunction	1 (5)	16 (14)	0.24
Diabetes mellitus	2 (10)	45 (39)	0.01
Smoking status (%)			
Never	9 (45)	25 (22)	0.03
Former	11 (55)	60 (52)	0.81
Current	0	30 (26)	0.03
Procedure type (%)			
Carotid endarterectomy	0	49 (43)	
Asymptomatic	0	34 (69)	
Symtomatic	0	15 (31)	
Infra-inguinal revascularization	0	44 (38)	
Claudication	0	21 (48)	
Resting pain	0	15 (34)	
Tissue loss	0	13 (30)	
Lower extremity amputation	0	22 (19)	
Medications			
Aspirin		102 (89)	
ACE inhibitor		49 (43)	
Beta blocker		89 (78)	
Coumadin		11 (10)	
Ca^{2+} channel blocker		37 (32)	
Statin		99 (86)	
Fibrate		3 (3)	
Metformin		8 (7)	

SD, standard deviation; BMI, body mass index; MI, myocardial infarct; HTN, hypertension; COPD, chronic obstructive pulmonary disease.

symptomatic $n = 15$), 44 infra-inguinal revascularization (claudication $n = 21$, resting pain $n = 15$, tissue loss $n = 13$), and 22 amputation.

Analysis of the baseline blood sample (pre-operative) H_2S production capacity assay using the lead acetate-based method, showed that controls had significantly higher H_2S production capacity compared to vascular disease patients (**Figure 1A**; **Supplementary Figure 1A**; 80.8±12.9 vs. 57.0 ± 8.4 arbitrary units, $p < 0.001$). Importantly, H_2S levels was similarly reduced in patient that underwent carotid endarterectomy (CEA, 58.6 ± 5.79), infra-inguinal revascularization (IGR, 57.1 ± 10.1) and amputation (Amp, 53.3 ± 8.97). Results using the MBB method also showed that healthy controls had significantly greater plasma sulfide levels (**Figure 1B**; 0.95 ± 0.30 vs. 0.58 ± 0.16 μM, $p < 0.05$), and was consistent across the underlying vascular surgeries (CEA 0.59 ± 0.17, IGR 0.59 ± 0.17, Amp 0.52 ±0.13; **Figure 1B**). Although both of these sulfide-based measurements were significantly higher in healthy controls, there was no observable correlation between the measurements (**Figure 1C**; $r_s = -0.12$, $p = 0.34$), suggesting that the two methods measure fundamentally different phenomena and/or sulfide pools.

H_2S Levels Correlate With Post-operative Survival

To assess the associations of these H_2S measurements with clinical outcomes after surgical procedures, the vascular surgery patients were divided by median split into patients with high and low pre-operative H_2S production capacity (**Supplementary Figure 1B**). Over 36 months of follow up, patients with low H_2S production capacity had significantly decreased probability of survival compared to patients with high H_2S production capacity (**Figure 1D**; 54 vs. 82% survival probability, log-rank test $p = 0.0029$). However, when patients were divided by median split into high and low MBB-measured sulfide measurements, there was no significant association with survival and the trend was reversed such that those with higher sulfide tended to have lower probability of survival (**Figure 1E**; 71 vs. 52% survival probability, log-rank test = 0.15).

To further assess the robustness of H_2S production capacity as a predictor of mortality after a vascular surgery intervention, we generated Cox proportional hazard models to adjust for potential confounding variables. A univariate unadjusted model showed that individuals in the high H_2S production capacity group had significantly reduced risk of death during follow up (HR(95% CI) = 0.31(0.11–0.87), coefficient $p = 0.025$, model Wald $p = 0.025$). In a Cox proportional hazard model adjusted for age, BMI, gender, smoking history, race, procedure type, diabetes, hyperlipidemia, and renal function, H_2S production capacity was significantly associated with survival (HR = 0.95, CI = 0.90–1, coefficient $p = 0.07$, model Wald $p < 0.001$; **Figure 2**).

H_2S Production Reflects a Non-enzymatic Process

Finally, to characterize the biochemical nature of the plasma H_2S production capacity measurement, we investigated whether it might be generated by enzymatic or non-enzymatic production. It has been proposed that the H_2S generating enzyme cystathionine beta synthase (CBS) is present in human plasma. We measured plasma CBS activities, but found no observable association between plasma CBS activity and H_2S production capacity (**Figure 3A**; $r = -0.07$, $p = 0.71$). We

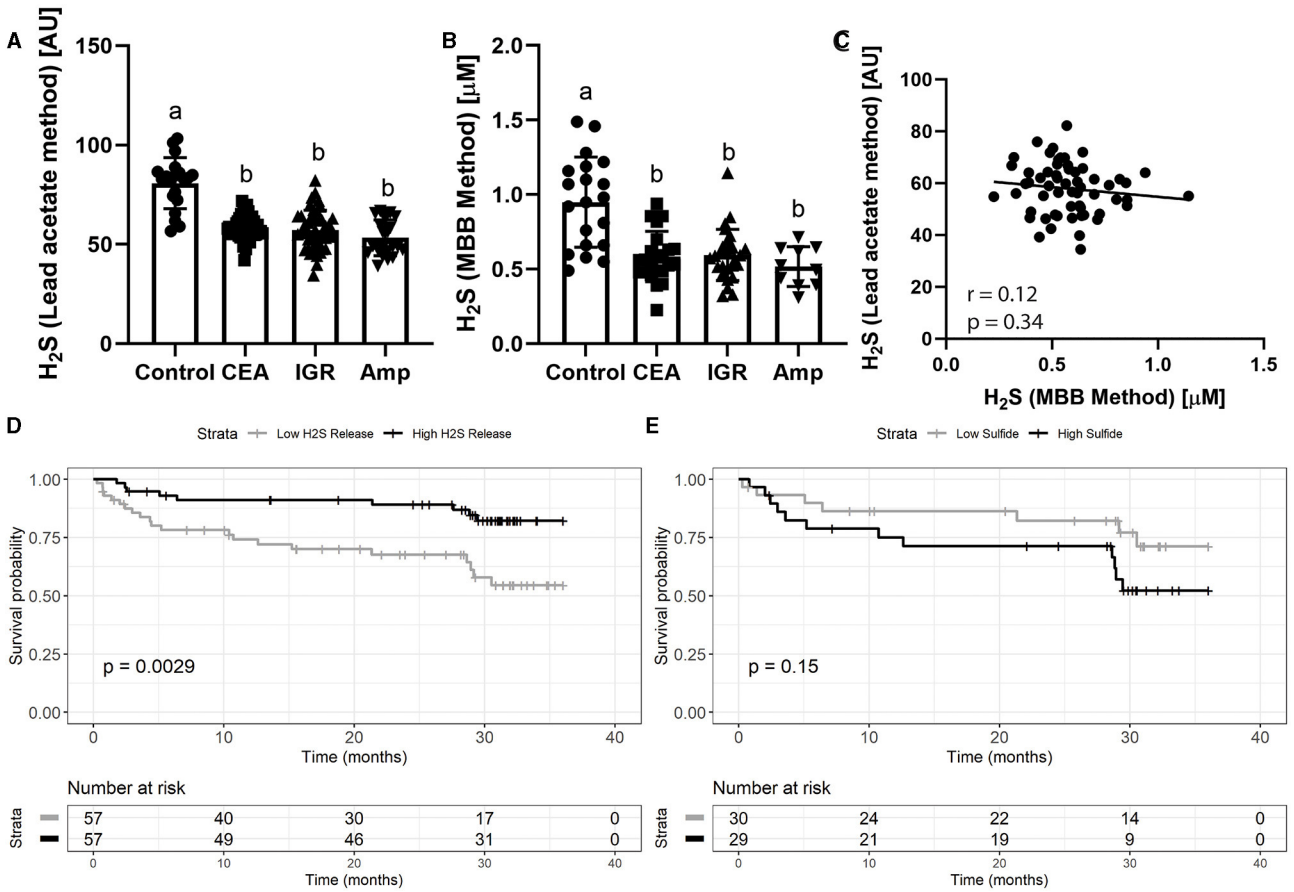

FIGURE 1 | Plasma H_2S production capacity and sulfide levels are reduced in patients with vascular disease, with production capacity predicting mortality. **(A)** Plasma H2S production capacity and **(B)** plasma sulfide measured by the MBB method from human patients suffering vascular occlusive disease including 115 patients undergoing carotid endarterectomy (CEA), infra-inguinal revascularization (IGR) and amputation (Amp), as well as age-matched individuals ($n = 20$). Error bars indicate SD; different letters indicate difference $p < 0.05$ in One Way ANOVA Tukey *post-hoc* test. **(C)** Correlation between H_2S production capacity and sulfide measured by the MBB method in vascular disease patients. **(D)** Probability of survival for vascular disease patients during follow up after intervention with low ($n = 57$) vs. high ($n = 57$) H_2S production capacity and **(E)** low and high plasma sulfide measurements. High vs. low was determined by median split. P value calculated from log-rank test.

next performed the assay under protein denaturing conditions by heating and adding DTT, and found a highly correlated pattern of signals compared to when the assay was performed under non-denaturing conditions (**Figure 3B**; $r = 0.34$, $p = 0.0002$). These results suggest a non-enzymatic process for H_2S production in the plasma. Finally, we added chelators and found that EDTA was able to almost completely ablate the H_2S release, while EGTA was not (**Figure 3C**). On the other hand, EDTA had a reverse effect on measured sulfide concentrations by the MBB method (23) corroborating that the two methods measure sulfide released from fundamentally different endogenous pools and/or production mechanisms. This suggests a vital role for free and bound iron as a catalyst in H_2S release. In combination with PLP and the substrate L-cysteine, H_2S release is ultimately dampened by increasing homocysteine concentrations (**Figures 3D–F**; **Supplementary Figures 1C–E**). These results on the likely non-enzymatic nature of the signal are in agreement with the recent thorough characterization of mechanisms of H_2S release in blood by Hine et al. (25).

DISCUSSION

Pre-clinical studies have suggested that decreased levels of H_2S accelerate the development of atherosclerosis (14), and are reduced in the skeletal muscle of CLI patients (1). Here we show that patients with vascular disease have significantly decreased circulating H_2S production capacity and sulfide concentrations, compared to subjects with no clinical evidence of coronary or peripheral artery disease. Together, these results suggest that patients with atherosclerotic vascular disease have a decreased capability to generate H_2S. Furthermore, patients with higher H_2S production capacity measured prior to vascular surgery had reduced post-operative mortality at 36 months follow-up compared to those with lower H_2S production. It also suggests

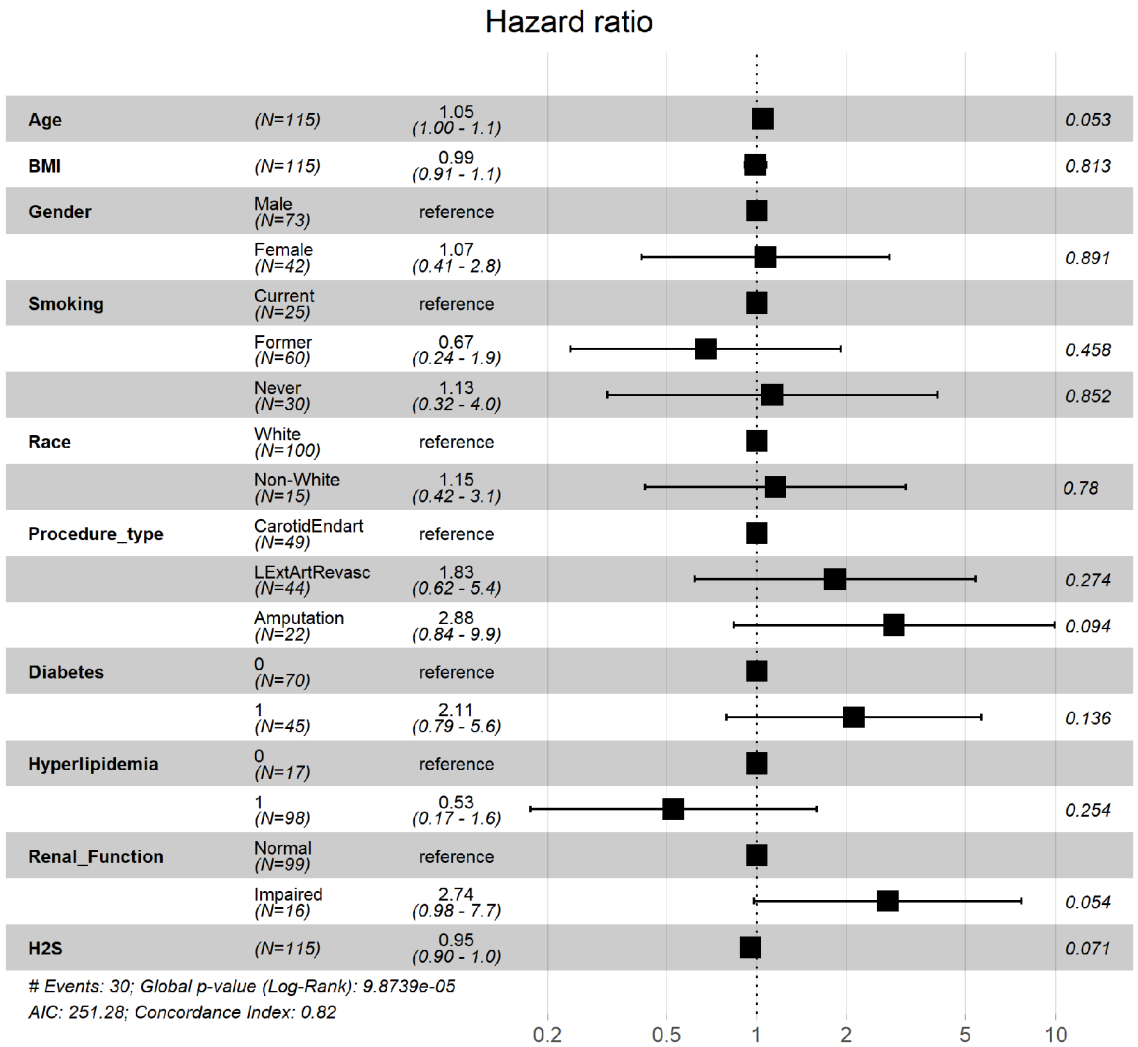

FIGURE 2 | Hazard ratios of death during follow up period. Hazard ratio estimates and 95% confidence intervals for clinically relevant parameters and plasma H_2S production capacity as measured by the lead acetate release method.

possible therapeutic application of H_2S donors, to restore or increase H_2S levels in humans. Indeed, the administration of exogenous H_2S (NaHS, SG1002) protected against ischemia-induced heart failure, and improved overall survival in rodents (28, 29). Such an H_2S donor is being tested in clinical trials (NCT01989208). Similarly, exogenous administration of H_2S in preclinical models protects from ischemic injury to the liver (2), the brain (30), and the kidney (31), which could have therapeutic benefits in the context or solid organ transplantation, myocardial infarction or stroke. Interestingly, some FDA approved drug, with H_2S-releasring properties, such as the ACE inhibitor Zofenopril or sodium thiosulfate, improve vascular function, and limit intimal hyperplasia (unpublished data).

Interestingly, this association was not observed with sulfide levels that were measured by the MBB-method. While this suggest that although both measures are related to sulfide release from bound sulfide reserves, they specifically capture distinct biological phenomena with clinical relevance. Hine and colleagues have recently performed a thorough chemical characterization of the mechanisms of non-enzymatic H_2S production in blood, demonstrating that it is catalyzed by iron and vitamin B_6 (PLP) with cysteine serving as optimum substrate (25). Although this work gives us many clues, important questions remain about what specific components of the plasma determine and regulate H_2S production capacity. One theory revolves around the sulfur containing amino acid homocysteine, which in itself has been long associated with cardiovascular disease risk, but its mechanism of pathology is not well-understood (32). As reported by Nakano et al. (33) and measured via the quantitative analysis of reactive sulfur species using MBB-method similar to our present study, homocysteine captures H_2S and/or HS^- to form a homocysteine persulfide in cardiac tissue, which could potentially interfere with H_2S-related cardiovascular protection (33). Thus, if surgical patients with

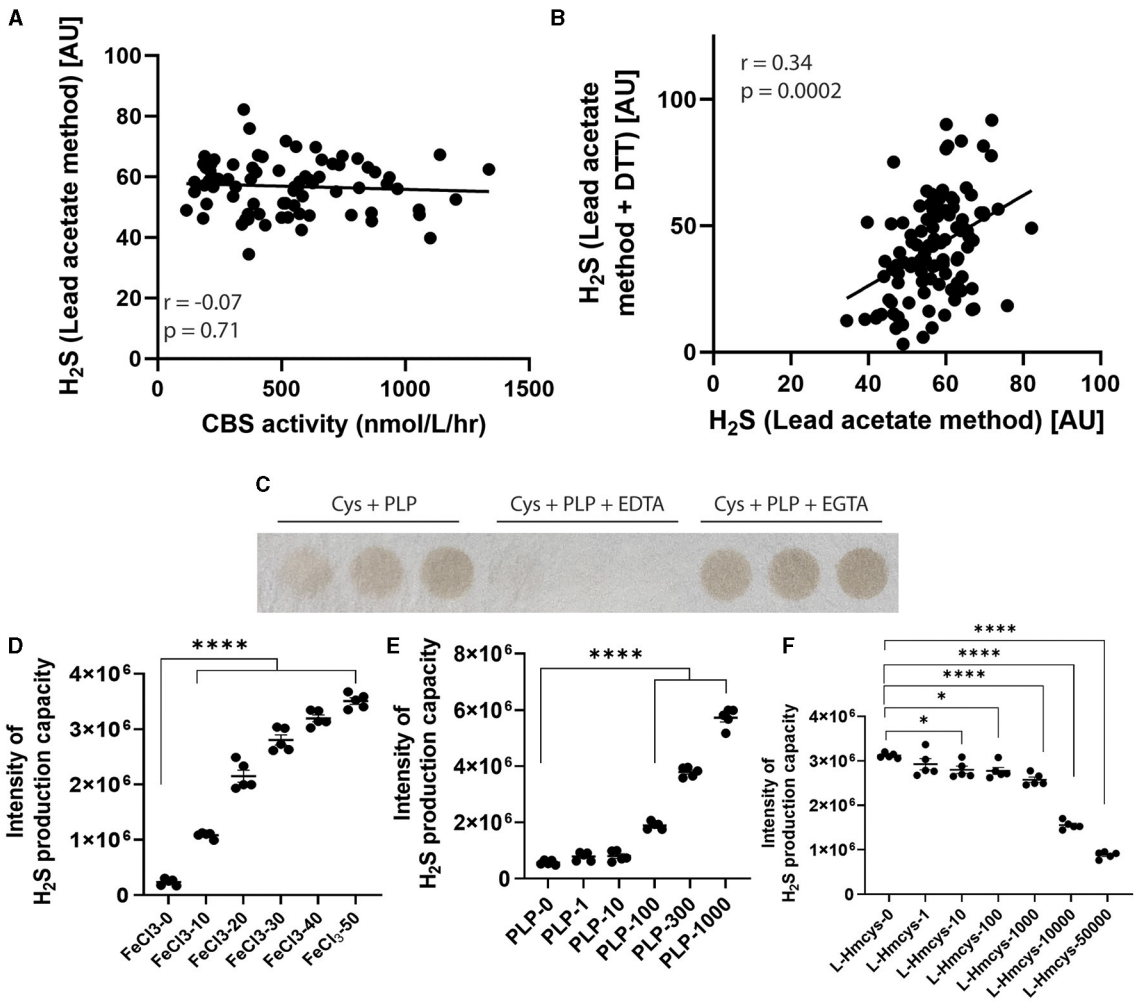

FIGURE 3 | Mechanisms of H_2S release from plasma. **(A)** Correlation between plasma cystathionine-beta synthase activity and plasma H_2S release. **(B)** Correlation between plasma H_2S release performed under protein non-denaturing (x-axis) and protein denaturing (y-axis) conditions. **(C)** H_2S release from plasma when incubated with PLP, PLP + EDTA or PLP + EGTA. **(D)** *In vitro* H_2S release performed using cysteine and increasing concentration of $FeCl_3$, **(E)** PLP or **(F)** homocysteine ($n = 5$ reactions per condition). $^*p < 0.05$, $^{****}p < 0.0001$ vs. respective 0uM control.

decreased survival showed an increase in plasma homocysteine levels, then this could explain the dichotomy in H_2S release in these patients using the two different methods (lead acetate vs. MBB). Furthermore, in the non-enzymatic production of H_2S in plasma catalyzed by iron described previously (25) and confirmed here, PLP still acts as an important co-factor by the formation of a Schiff base and subsequent cysteine-aldimine and thiazolidine five-member ring intermediates prior to iron rapidly catalyzing the release of the sulfide. Importantly, homocysteine itself can also form a Schiff base with PLP, except it will result in a more thermodynamically stable six-member tetrahydrothiazine ring (34). The formation of the stable tetrahydrothiazine ring poses two complications for H_2S production in circulation: the first being sequestration of valuable PLP co-factor from both enzymatic and non-enzymatic H_2S production where cysteine serves as substrate; and the second being slow H_2S production kinetics when iron serves as a catalyst (25), which we demonstrate here. Thus, the suppression of H_2S release by increased circulating homocysteine may represent a mechanism explaining the robust association between homocysteine levels and cardiovascular disease.

In addition to addressing the issues brought up in the discussion, the results reported here will aid in the development of specific H_2S assays for diagnostic purposes. Further, they will guide therapeutic interventions if these specific determinants are shown to be causal to the disease process. Despite these remaining questions, we demonstrate that the lead acetate assay represents a simple, rapid and very low-cost method which appears to capture substantial information on clinical risk in this population.

Limitations of our study include the quantification of H_2S using the lead acetate method measures only relative differences in H_2S between individuals and groups, and not absolute differences. Likewise, it primarily serves as a surrogate for the actual amount of H_2S produced from available substrates in plasma. It is also important to note that mortality outcomes in this study encompassed two uniquely different patient populations, patients with carotid stenosis and patients with PAD necessitating surgical revascularization or amputation. These differences may influence disparities in mortality outcomes and future work will need to validate these findings in larger cohorts with more homogenous interventions. In addition, we previously demonstrated that dietary restriction (2, 35) or the hypothalamic-pituitary axis (36) were important regulators of endogenous H_2S production and downstream signaling (37, 38). These factors, including circulating homocysteine levels, were not specifically assessed here, however, they do illuminate the possibilities that patients with increased survival post-surgery having an H_2S production promoting diet and/or endocrine makeup in the days/hours leading to surgery. Nevertheless, we highlight our important results showing that both H_2S production capacity and MBB-method-measured sulfide levels in vascular patients were significantly reduced compared to healthy subjects, indicating a potential correlation between H_2S and the progression of cardiovascular pathology.

CONCLUSION

This study shows that patients with vascular disease have significantly decreased circulating H_2S production capacity and sulfide concentrations, compared to subjects with no clinical evidence of coronary or peripheral artery disease. In addition, the lead acetate H_2S detection represents a simple, rapid and low-cost method to capture clinical risk in patients undergoing vascular surgery. Altogether, results provide further insights into the role of H_2S biology in surgical patients and open an avenue for the use of H_2S for diagnostics and therapeutics in those with dysfunction of their vascular system.

DATA AVAILABILITY STATEMENT

The original contributions presented in the study are included in the article/**Supplementary Material**, further inquiries can be directed to the corresponding author/s.

ETHICS STATEMENT

The studies involving human participants were reviewed and approved by Partners Human Research Committee institutional review board. The patients/participants provided their written informed consent to participate in this study.

AUTHOR CONTRIBUTIONS

AL, MM, and KT: participated in the conception, design of the work and the acquisition, and analysis and interpretation of data for the work. JG, CM, PK, WK, GS, MT, SM, TD, JY, and PN: participated in the acquisition and analysis and interpretation of data for the work. CO, CH, and JM: participated in the conception, design of the work, and analysis and interpretation of data for the work. All authors contributed to the article and approved the submitted version.

FUNDING

The Swiss National Science Foundation (PZ00P3-185927) to AL, the National Institutes of Health (R01HL148352) to CH, the Hungarian Thematic Excellence Program, the Hungarian National Research, Development and Innovation Office to PN (TKP2020-NKA-26, KH_126766, and K_129286), and the National Institutes of Health (1P01AG055369-01A1) to JM and SM.

SUPPLEMENTARY MATERIAL

The Supplementary Material for this article can be found online at: https://www.frontiersin.org/articles/10.3389/fcvm.2021.750926/full#supplementary-material

REFERENCES

1. Islam KN, Polhemus DJ, Donnarumma E, Brewster LP, Lefer DJ. Hydrogen sulfide levels and nuclear factor-erythroid 2-related factor 2 (NRF2) activity are attenuated in the setting of Critical Limb Ischemia (CLI). *J Am Heart Assoc*. (2015) 4:e001986. doi: 10.1161/JAHA.115.001986
2. Hine C, Harputlugil E, Zhang Y, Ruckenstuhl C, Lee BC, Brace L, et al. Endogenous hydrogen sulfide production is essential for dietary restriction benefits. *Cell*. (2015) 160:132–44. doi: 10.1016/j.cell.2014.11.048
3. Kip P, Tao M, Trocha KM, MacArthur MR, Peters HAB, Mitchell SJ, et al. Periprocedural hydrogen sulfide therapy improves vascular remodeling and attenuates vein graft disease. *J Am Heart Assoc.* (2020) 9:e016391. doi: 10.1161/JAHA.120.016391
4. Longchamp A, Mirabella T, Arduini A, MacArthur MR, Das A, Treviño-Villarreal JH, et al. Amino acid restriction triggers angiogenesis via GCN2/ATF4 regulation of VEGF and H(2)S production. *Cell*. (2018) 173:117–29.e14. doi: 10.1016/j.cell.2018.03.001
5. Blackstone E, Roth MB. Suspended animation-like state protects mice from lethal hypoxia. *Shock*. (2007) 27:370–2. doi: 10.1097/SHK.0b013e31802e27a0
6. Kanagy NL, Szabo C, Papapetropoulos A. Vascular biology of hydrogen sulfide. *Am J Physiol Cell Physiol*. (2017) 312:C537–49. doi: 10.1152/ajpcell.00329.2016
7. Yang G, Wu L, Jiang B, Yang W, Qi J, Cao K, et al. H2S as a physiologic vasorelaxant: hypertension in mice with deletion of cystathionine gamma-lyase. *Science*. (2008) 322:587–90. doi: 10.1126/science.1162667
8. Ahmad A, Olah G, Szczesny B, Wood ME, Whiteman M, Szabo C. AP39, a mitochondrially targeted hydrogen sulfide donor, exerts protective effects in renal epithelial cells subjected to oxidative stress *in vitro* and in acute renal injury *in vivo*. *Shock*. (2016) 45:88–97. doi: 10.1097/SHK.0000000000000478

9. Olson KR, Whitfield NL, Bearden SE, St Leger J, Nilson E, Gao Y, et al. Hypoxic pulmonary vasodilation: a paradigm shift with a hydrogen sulfide mechanism. *Am J Physiol Regul Integr Comp Physiol.* (2010) 298:R51–60. doi: 10.1152/ajpregu.00576.2009
10. Olson KR, Whitfield NL. Hydrogen sulfide and oxygen sensing in the cardiovascular system. *Antioxid Redox Signal.* (2010) 12:1219–34. doi: 10.1089/ars.2009.2921
11. Zanardo RC, Brancaleone V, Distrutti E, Fiorucci S, Cirino G, Wallace JL. Hydrogen sulfide is an endogenous modulator of leukocyte-mediated inflammation. *FASEB J.* (2006) 20:2118–20. doi: 10.1096/fj.06-6270fje
12. Szabo C. Hydrogen sulphide and its therapeutic potential. *Nat Rev Drug Discov.* (2007) 6:917–35. doi: 10.1038/nrd2425
13. Jain SK, Bull R, Rains JL, Bass PF, Levine SN, Reddy S, et al. Low levels of hydrogen sulfide in the blood of diabetes patients and streptozotocin-treated rats causes vascular inflammation? *Antioxid Redox Signal.* (2010) 12:1333–7. doi: 10.1089/ars.2009.2956
14. Mani S, Li H, Untereiner A, Wu L, Yang G, Austin RC, et al. Decreased endogenous production of hydrogen sulfide accelerates atherosclerosis. *Circulation.* (2013) 127:2523–34. doi: 10.1161/CIRCULATIONAHA.113.002208
15. Zhao ZZ, Wang Z, Li GH, Wang R, Tan JM, Cao X, et al. Hydrogen sulfide inhibits macrophage-derived foam cell formation. *Exp Biol Med.* (2011) 236:169–76. doi: 10.1258/ebm.2010.010308
16. Wang Y, Zhao X, Jin H, Wei H, Li W, Bu D, et al. Role of hydrogen sulfide in the development of atherosclerotic lesions in apolipoprotein E knockout mice. *Arterioscler Thromb Vasc Biol.* (2009) 29:173–9. doi: 10.1161/ATVBAHA.108.179333
17. Potor L, Nagy P, Méhes G, Hendrik Z, Jeney V, Petho D, et al. Hydrogen sulfide abrogates hemoglobin-lipid interaction in atherosclerotic lesion. *Oxidative Med Cell Longevity.* (2018) 2018:3812568. doi: 10.1155/2018/3812568
18. Kondo K, Bhushan S, King AL, Prabhu SD, Hamid T, Koenig S, et al. H(2)S protects against pressure overload-induced heart failure via upregulation of endothelial nitric oxide synthase. *Circulation.* (2013) 127:1116–27. doi: 10.1161/CIRCULATIONAHA.112.000855
19. Wang K, Ahmad S, Cai M, Rennie J, Fujisawa T, Crispi F, et al. Dysregulation of hydrogen sulfide producing enzyme cystathionine gamma-lyase contributes to maternal hypertension and placental abnormalities in preeclampsia. *Circulation.* (2013) 127:2514–22. doi: 10.1161/CIRCULATIONAHA.113.001631
20. Fiorucci S, Antonelli E, Mencarelli A, Orlandi S, Renga B, Rizzo G, et al. The third gas: H2S regulates perfusion pressure in both the isolated and perfused normal rat liver and in cirrhosis. *Hepatology.* (2005) 42:539–48. doi: 10.1002/hep.20817
21. Candela J, Wang R, White C. Microvascular endothelial dysfunction in obesity is driven by macrophage-dependent hydrogen sulfide depletion. *Arterioscler Thromb Vasc Biol.* (2017) 37:889–99. doi: 10.1161/ATVBAHA.117.309138
22. Nagy P, Palinkas Z, Nagy A, Budai B, Toth I, Vasas A. Chemical aspects of hydrogen sulfide measurements in physiological samples. *Biochim Biophys Acta.* (2014) 1840:876–91. doi: 10.1016/j.bbagen.2013.05.037
23. Ditrói T, Nagy A, Martinelli D, Rosta A, KoŽich V, Nagy P. Comprehensive analysis of how experimental parameters affect H(2)S measurements by the monobromobimane method. *Free Radical Biol Med.* (2019) 136:146–58. doi: 10.1016/j.freeradbiomed.2019.04.006
24. Hine C, Mitchell JR. Endpoint or kinetic measurement of hydrogen sulfide production capacity in tissue extracts. *Bio Protoc.* (2017) 7:e2382. doi: 10.21769/BioProtoc.2382
25. Yang J, Minkler P, Grove D, Wang R, Willard B, Dweik R, et al. Non-enzymatic hydrogen sulfide production from cysteine in blood is catalyzed by iron and vitamin B6. *Commun Biol.* (2019) 2:194. doi: 10.1038/s42003-019-0431-5
26. KoŽich V, Ditrói T, Sokolová J, KríŽková M, Krijt J, Ješina P, et al. Metabolism of sulfur compounds in homocystinurias. *Br J Pharmacol.* (2019) 176:594–606. doi: 10.1111/bph.14523
27. Krijt J, Kopecká J, Hnízda A, Moat S, Kluijtmans LA, Mayne P, et al. Determination of cystathionine beta-synthase activity in human plasma by LC-MS/MS: potential use in diagnosis of CBS deficiency. *J Inherited Metabolic Dis.* (2011) 34:49–55. doi: 10.1007/s10545-010-9178-3
28. Polhemus DJ, Kondo K, Bhushan S, Bir SC, Kevil CG, Murohara T, et al. Hydrogen sulfide attenuates cardiac dysfunction after heart failure via induction of angiogenesis. *Circ Heart Fail.* (2013) 6:1077–86. doi: 10.1161/CIRCHEARTFAILURE.113.000299
29. Calvert JW, Elston M, Nicholson CK, Gundewar S, Jha S, Elrod JW, et al. Genetic and pharmacologic hydrogen sulfide therapy attenuates ischemia-induced heart failure in mice. *Circulation.* (2010) 122:11–9. doi: 10.1161/CIRCULATIONAHA.109.920991
30. Wei X, Zhang B, Cheng L, Chi M, Deng L, Pan H, et al. Hydrogen sulfide induces neuroprotection against experimental stroke in rats by down-regulation of AQP4 via activating PKC. *Brain Res.* (2015) 1622:292–9. doi: 10.1016/j.brainres.2015.07.001
31. Han SJ, Kim JI, Park JW, Park KM. Hydrogen sulfide accelerates the recovery of kidney tubules after renal ischemia/reperfusion injury. *Nephrol Dial Transplant.* (2015) 30:1497–506. doi: 10.1093/ndt/gfv226
32. Beard RS Jr, Bearden SE. Vascular complications of cystathionine beta-synthase deficiency: future directions for homocysteine-to-hydrogen sulfide research. *Am J Physiol Heart Circ Physiol.* (2011) 300:H13–26. doi: 10.1152/ajpheart.00598.2010
33. Nakano S, Ishii I, Shinmura K, Tamaki K, Hishiki T, Akahoshi N, et al. Hyperhomocysteinemia abrogates fasting-induced cardioprotection against ischemia/reperfusion by limiting bioavailability of hydrogen sulfide anions. *J Mol Med.* (2015) 93:879–89. doi: 10.1007/s00109-015-1271-5
34. Glowacki R, Stachniuk J, Borowczyk K, Jakubowski H. Quantification of homocysteine and cysteine by derivatization with pyridoxal 5'-phosphate and hydrophilic interaction liquid chromatography. *Anal Bioanal Chem.* (2016) 408:1935–41. doi: 10.1007/s00216-016-9308-3
35. Mitchell SJ, Madrigal-Matute J, Scheibye-Knudsen M, Fang E, Aon M, Gonzalez-Reyes JA, et al. Effects of sex, strain, and energy intake on hallmarks of aging in mice. *Cell Metab.* (2016) 23:1093–112. doi: 10.1016/j.cmet.2016.05.027
36. Hine C, Kim HJ, Zhu Y, Harputlugil E, Longchamp A, Matos MS, et al. Hypothalamic-pituitary axis regulates hydrogen sulfide production. *Cell Metab.* (2017) 25:1320–33.e5. doi: 10.1016/j.cmet.2017.05.003
37. Bithi N, Link C, Henderson YO, Kim S, Yang J, Li L, et al. Dietary restriction transforms the mammalian protein persulfidome in a tissue-specific and cystathionine gamma-lyase-dependent manner. *Nat Commun.* (2021) 12:1745. doi: 10.1038/s41467-021-22001-w
38. Zivanovic J, Kouroussis E, Kohl JB, Adhikari B, Bursac B, Schott-Roux S, et al. Selective persulfide detection reveals evolutionarily conserved antiaging effects of S-Sulfhydration. *Cell Metab.* (2020) 31:207. doi: 10.1016/j.cmet.2019.12.001

Conflict of Interest: The authors declare that the research was conducted in the absence of any commercial or financial relationships that could be construed as a potential conflict of interest.

Publisher's Note: All claims expressed in this article are solely those of the authors and do not necessarily represent those of their affiliated organizations, or those of the publisher, the editors and the reviewers. Any product that may be evaluated in this article, or claim that may be made by its manufacturer, is not guaranteed or endorsed by the publisher.

Copyright © 2021 Longchamp, MacArthur, Trocha, Ganahl, Mann, Kip, King, Sharma, Tao, Mitchell, Ditrói, Yang, Nagy, Ozaki, Hine and Mitchell. This is an open-access article distributed under the terms of the Creative Commons Attribution License (CC BY). The use, distribution or reproduction in other forums is permitted, provided the original author(s) and the copyright owner(s) are credited and that the original publication in this journal is cited, in accordance with accepted academic practice. No use, distribution or reproduction is permitted which does not comply with these terms.

frontiers in Cardiovascular Medicine

ORIGINAL RESEARCH
published: 25 November 2021
doi: 10.3389/fcvm.2021.768730

Does Warfarin or Rivaroxaban at Low Anticoagulation Intensity Provide a Survival Benefit to Asian Patients With Atrial Fibrillation?

Dong Lin[1,2†], *Yequn Chen*[1,3,4†], *Jian Yong*[1], *Shiwan Wu*[1], *Yan Zhou*[1], *Weiping Li*[1,3], *Xuerui Tan*[1,3,4*] *and Ruisheng Liu*[5]

[1] Department of Cardiology, The First Affiliated Hospital of Shantou University Medical College, Shantou, China, [2] School of Medical and Health Sciences, Edith Cowan University, Perth, WA, Australia, [3] Clinical Cohort Research Center, The First Affiliated Hospital of Shantou University Medical College, Shantou, China, [4] Clinical Research Center, The First Affiliated Hospital of Shantou University Medical College, Shantou, China, [5] Morsani College of Medicine, University of South Florida, Tampa, FL, United States

OPEN ACCESS

Edited by:
Yuli Huang,
Southern Medical University, China

Reviewed by:
Wanling Xuan,
Augusta University, United States
Jianqing She,
The First Affiliated Hospital of Xi'an Jiaotong University, China
Xina Xie,
Shenzhen Second People's Hospital, China

***Correspondence:**
Xuerui Tan
doctortxr@126.com

[†]These authors have contributed equally to this work and share first authorship

Specialty section:
This article was submitted to General Cardiovascular Medicine, a section of the journal Frontiers in Cardiovascular Medicine

Received: 01 September 2021
Accepted: 03 November 2021
Published: 25 November 2021

Citation:
Lin D, Chen Y, Yong J, Wu S, Zhou Y, Li W, Tan X and Liu R (2021) Does Warfarin or Rivaroxaban at Low Anticoagulation Intensity Provide a Survival Benefit to Asian Patients With Atrial Fibrillation? Front. Cardiovasc. Med. 8:768730. doi: 10.3389/fcvm.2021.768730

Background: Low-dose rivaroxaban and low-intensity warfarin are widely used in Asia for patients with atrial fibrillation (AF). However, in Asians, it is unclear whether low-dose rivaroxaban and low-intensity warfarin can improve the prognosis of AF. In this study, we investigate the survival benefits of low-dose rivaroxaban and low-intensity warfarin in Asian patients with AF in clinical practice.

Methods: This cohort study used medical records in a single tertiary hospital in China, between 2019 and 2020, to identify patients with AF who used rivaroxaban or warfarin, or had no anticoagulant therapy. Follow-ups were performed through telephone contact or medical record review. Cox proportional hazards models were used to compare the risk of mortality of patients in the anticoagulant-untreated group vs. warfarin-treated groups and rivaroxaban-treated groups.

Results: A total of 1727 AF patients, discharged between 2019 and 2020, were enrolled in this cohort, of which 873 patients did not use any anticoagulant, 457 patients received warfarin and 397 patients used rivaroxaban. Multivariable analysis showed that, of all the warfarin groups, patients with an international normalized ratio (INR) below 2, good INR control, or poor INR control had a significantly lower risk of mortality compared with that of patients without anticoagulants (HR 0.309, $p = 0.0001$; HR 0.387, $p = 0.0238$; HR 0.363, $p < 0.0001$). Multivariable Cox proportional hazard analyses also demonstrated that, compared with the no anticoagulant group, all rivaroxaban dosage groups (≤10 mg, HR 0.456, $p = 0.0129$; 15 mg, HR 0.246, $p = 0.0003$; 20 mg, HR 0.264, $p = 0.0237$) were significantly associated with a lower risk of mortality.

Conclusion: Despite effects being smaller than observed with recommended optimal anticoagulation, the use of warfarin with an INR below 2, poor INR control and the use of low-dose rivaroxaban may still provide survival benefits, suggesting viable alternatives that enable physicians to better resolve decisional conflicts concerning the risks and

benefits of anticoagulant therapies, as well as for patients in need of but unable to receive standard anticoagulant therapy due to bleeding risk or other factors, such as financial burden, concerns of adverse outcomes, as well as low treatment compliance and persistence.

Keywords: atrial fibrillation, warfarin, rivaroxaban, mortality, anticoagulant

INTRODUCTION

Atrial fibrillation (AF) has a prevalence of 2–3% worldwide (1, 2), with a recent meta-analysis estimating over 7 million adults in China alone having AF (3). AF significantly increases the risk of thromboembolic events, congestive heart failure, and mortality (2, 4). Vitamin K antagonists (primarily warfarin) have been effective antithrombotic therapies for inexpensive prevention of ischemic stroke in AF patients (5). However, warfarin has many issues that limit its use, such as multiple food, drug, and pharmacogenomic interactions, which result in unpredictable pharmacokinetics and pharmacodynamics (5, 6). Since warfarin is associated with risk of bleeding and thromboembolism, warfarin dosing for maintaining anticoagulation therapy must be monitored using the international normalized ratio (INR). As a result, regular coagulation monitoring and dose adjustments are continually required (7). The European Society of Cardiology (ESC) and American Heart Association (AHA) recommend an INR in the range of 2.0–3.0 as a target for the prevention of thromboembolism and hemorrhage in patients with non-valvular AF (8, 9). However, several studies have shown that Asians are more susceptible to warfarin-induced bleeding than non-Asians (10, 11). Previous meta-analyses have shown that in Asian non-valvular AF patients taking warfarin, patients within INR target values of 1.5–2.5 have a reduced risk of bleeding without increases in thromboembolism (12–15). Several studies have found a high proportion of low INR intensity warfarin use in Asians (16), but the efficacy and safety of low INR intensity warfarin use in Asian populations in clinical practice remain unclear.

Direct oral anticoagulants (DOACs), including dabigatran, apixaban, edoxaban, and rivaroxaban (17), are effective and safe alternatives to warfarin for stroke prevention in patients with non-valvular AF (NVAF) (18, 19). Since DOACs do not require routine monitoring of drug concentrations, it is important to select the appropriate dose of DOACs based on the dosing criteria defined in randomized controlled trials. Results from non-Asian and Japanese clinical trials have shown that the efficacy of rivaroxaban is not inferior to warfarin (19, 20). However, populations from randomized controlled trials are usually selected based on strict eligibility criteria and under careful protocol-based follow-up. Therefore, the results of randomized controlled trials may not apply to all patients with AF in clinical settings. Previous studies found that low-dose rivaroxaban (10 mg/day) is widely used in actual clinical practice in Asian countries (21–23). Since Asian populations are associated with a higher risk of bleeding, such as intracranial hemorrhaging (24), physicians tend to prescribe low-dose DOACs for Asian patients with AF in daily clinical practice. However, there is a paucity of evidence on the effects of low-dose rivaroxaban in Asian populations. In this study, we plan to investigate the survival benefits of low-dose rivaroxaban and low-intensity INR warfarin in Asian patients with AF in a clinical setting.

METHODS

Patients and Data Collection

This was a prospective observational study using data from AF patients who were admitted to the First Affiliated Hospital of Shantou University Medical College from 2019 to 2020. The inclusion criteria were above 18 years of age, had medical conditions that required anticoagulation, received either rivaroxaban, warfarin, or no anticoagulation therapy, and consented to follow-up after the index discharge date. AF patients with the following characteristics were excluded: (1) pregnant; (2) used warfarin with no INR values; (3) used rivaroxaban with missing dosing information; (4) were missing baseline risk factors or demographic information. Patients with evidence of AF from electronic health records or electrophysiologic evaluations were considered as having AF. AF was defined as a supraventricular tachyarrhythmia with uncoordinated atrial electrical activation and consequent ineffective atrial contraction. The electrocardiographic characteristics of AF include irregular R-R intervals (when atrioventricular conduction is not impaired), absence of distinct repeating P-waves, and irregular atrial activations (25). This study was approved by the Ethics Committee of the First Affiliated Hospital of Shantou University Medical College, and all participants provided written informed consent before inclusion in this study.

Subject characteristics at baseline, including medical histories, prior and concomitant medications, demographic characteristics, alcohol, smoking, CHA_2DS_2-VASc score, HAS-BLED score, and other clinical characteristics, as well as the usage of treatments and baseline INR, were collected from the medical records. Follow-up INR records, and anticoagulant treatments were procured from telephone visits and the hospital system's outpatient-based electronic medical records. The baseline comorbidities were rheumatic heart disease (RHD), malignancy, chronic kidney disease (CKD), chronic obstructive pulmonary disease diastolic (COPD), thyroid disease, congestive heart failure (CHF), gastrointestinal (GI) bleeding, hypertension, diabetes mellitus, coronary disease, and ischemic stroke. Other clinical characteristics were systolic blood pressure (SBP), diastolic blood pressure (DBP), creatinine (Cr), prothrombin time-international normalized ratio (PT-INR), and ejection fraction (EF). Prior medications were aspirin, clopidogrel, and statin. For quantifying thromboembolic risk, we combined comorbidity information

into the CHA_2DS_2-VASc score (26), consisting of congestive heart failure, hypertension, age (65–74 years, ≥75 years), diabetes, transient ischemic attack (TIA)/stroke attack, vascular disease, and gender. To assess the risk of bleeding, we calculated the HAS-BLED score (27), which includes hypertension, age > 65, stroke history, renal disease, liver disease, prior major bleeding or predisposition to bleeding, labile INR, medication usage predisposing to bleeding, and alcohol consumption.

Follow-ups were carried out by medical record review and/or telephone interviews at 30, 90, 180, and 365 days after discharge. The follow-up period for patients using rivaroxaban started from the index date of rivaroxaban prescription. The follow-up period of patients without anticoagulants started from the index date of hospital discharge. The follow-up period of patients receiving warfarin began from the last discharge date with warfarin prescription. Patient information, including survival status, INR, and anticoagulant treatment was collected during follow-up through electronic medical records. All INR values were collected during follow-up, independent of the follow-up visits. Patients with missing medical records were contacted via telephone interviews with patients or their family members to collect their information. If patients could not be followed up through electronic medical records or telephone interview, such patients were recorded as lost to follow-up. All patients were followed up to the occurrence of death, switching of treatment (i.e., received OAC for the anticoagulant-untreated group; received an alternative OAC, including dabigatran and apixaban, for the warfarin group and rivaroxaban group), were lost to follow-up, and the end of the study period, whichever came first. For patients who switched anticoagulant treatments during follow-up, only information collected from study enrollment to the day of switching anticoagulant treatments was used for the analysis.

Study Outcomes

The primary outcome of this study was all-cause mortality, collected using telephone visits and medical records of subjects.

Statistical Analysis

The warfarin treatment groups were categorized based on the PT-INR (PT-INR < 2, 2 ≤ PT-INR ≤ 3, PT-INR>3) collected at the last hospital discharge before the occurrence of death or last contact date. The warfarin treatment groups were also categorized based on the percentage of INR measurements in the therapeutic range (PINRR), with a PINRR ≤ 56.1% regarded as poor INR control and a PINRR > 56.1% regarded as good INR control. PINRR was the number of INR values of 2.0–3.0 of the total number of INR values measured. A cut-off value of PINRR ≤ 56.1% was shown to be a good discriminator of a time to therapeutic range (TTR) <65% (28). Patients using rivaroxaban were categorized into ≤10 mg, 15 mg, and 20 mg groups. In all analyses that used comparisons with the rivaroxaban group, subjects who had moderate to severe mitral stenosis, a bioprosthetic or mechanical prosthetic valve, or end-stage chronic kidney disease with or without dialysis or hypertrophic cardiomyopathy were excluded from the anticoagulant-untreated group.

For continuous variables, data are shown as mean ± standard deviation or median with interquartile ranges. For categorical variables, data are shown as counts with percentages. The baseline characteristics of the anticoagulant-untreated groups were compared with warfarin groups and rivaroxaban groups using the Kruskal-Wallis test for continuous variables and chi-square tests for categorical variables.

Cumulative incidence of mortality was estimated using the Kaplan-Meier method and compared using the log-rank test. Univariable and multivariable Cox proportional hazards models were used to compare the risk of mortality of patients without anticoagulants to patients using warfarin, as well as patients receiving rivaroxaban. Hazard ratios (HRs) with 95% confidence intervals (CIs) are presented. Multivariable models for the comparison of patients using warfarin and patients without anticoagulant medication was adjusted for gender, age, TIA/stroke, malignancy, CKD, and GI bleeding. Multivariable models for the comparison of patients receiving rivaroxaban and patients without anticoagulants were adjusted for gender, age, coronary disease, TIA/stroke, aspirin, CHF, malignancy, CKD, and statin. Statistical analyses were performed using SPSS version 22.0 (SPSS Inc., Chicago, Illinois, USA), and figures were constructed using R software version 3.6.1 (R Foundation for Statistical Computing, Vienna, Austria). Two-tailed $p < 0.05$ were considered statistically significant.

RESULTS

Baseline Characteristics

A total of 2092 patients with AF, who were discharged between 2019 and 2020, were enrolled in this cohort. Among the 2092 participants, 204 patients were excluded because of lack of follow-up data, 49 patients in the warfarin-treated group were excluded because of missing INR values, 86 patients in the rivaroxaban-treated group were excluded because of missing dosing information, and 26 patients were excluded owing to lack of baseline risk factors or demographic information. The final analysis included 1,727 patients with diagnosed AF, of which 873 patients did not use any anticoagulant, 457 patients received warfarin and 397 patients used rivaroxaban. Baseline characteristics of patients without anticoagulants, patients using warfarin (PT-INR < 2, 2 ≤ PT-INR ≤ 3, PT-INR > 3, PINRR > 56.1%, PINRR ≤ 56.1%), and NVAF patients receiving rivaroxaban (≤10, 15, 20 mg) are shown in **Tables 1A,B**, respectively. In addition to age, CHA_2DS_2-VASc score, and HAS-BLED score, comorbidities (congestive heart failure, hypertension, coronary disease), smoking, biomarkers (systolic blood pressure, creatinine, and PT-INR), use of other medications (statin, aspirin, or clopidogrel) were significantly different between patients not using anticoagulants and either patients using warfarin or patients receiving rivaroxaban. Gender was significantly different in the comparison of patients without anticoagulants with patients receiving warfarin but not with patients using rivaroxaban. Chronic kidney disease, diabetes, GI bleeding, and ischemic stroke were significantly different in the comparison of patients without anticoagulants with patients receiving rivaroxaban.

TABLE 1 | Baseline characteristics of enrolled patients (A) warfarin and (B) rivaroxaban.

Characteristics	No anticoagulant ($n = 873$)	PT-INR				PINRR		
		PT-INR < 2 ($n = 330$)	PT-INR 2–3 ($n = 93$)	PT-INR > 3 ($n = 34$)	*P*	≤56.1% ($n = 354$)	>56.1% ($n = 103$)	*P*
(A) WARFARIN								
Gender (female)	345 (39.5%)	179 (54.2%)	41 (44.1%)	19 (55.9%)	<0.001	187 (52.8%)	52 (50.5%)	<0.001
Age (years)	70.45 ± 12.61	64.16 ± 11.45	64.75 ± 10.56	67.15 ± 7.97	<0.001	64.42±11.30	64.51 ± 9.87	<0.001
CHA_2DS_2-VASc score	3.48 ± 1.85	3.06 ± 1.68	2.95 ± 1.39	3.24 ± 1.5	<0.001	2.85 ± 1.64	2.92 ± 1.49	<0.001
HAS-BLED score	2.7 ± 1.19	2.34 ± 1.19	2.36 ± 1.14	2.61 ± 1.14	<0.001	2.28 ± 1.08	2.45 ± 1.20	<0.001
RHD	34 (3.95%)	100 (30.9%)	38 (41.3%)	11 (34.4%)	<0.001	105 (29.7%)	44 (42.7%)	<0.001
CKD	122 (14.2%)	33 (10.2%)	10 (10.9%)	7 (21.9%)	0.11	39 (11.0%)	11 (10.7%)	0.49
COPD	64 (7.4%)	10 (3.1%)	4 (4.4%)	1 (3.1%)	0.031	11 (3.1%)	4 (3.9%)	0.0358
CHF	401 (45.9%)	225 (68.2%)	70 (75.3%)	24 (70.6%)	<0.001	245 (6.9%)	74 (7.2%)	<0.001
GI bleeding	32 (3.7%)	4 (1.2%)	1 (1.1%)	2 (6.3%)	0.06	6 (1.7%)	1 (1.0%)	0.14
Hypertension	541 (62.9%)	149 (46.0%)	37 (40.2%)	13 (40.6%)	<0.001	157 (44.4%)	42 (40.8%)	<0.001
Diabetes mellitus	238 (27.7%)	79 (24.9%)	24 (26.1%)	12 (37.5%)	0.37	89 (25.1%)	26 (25.2%)	0.75
Coronary disease	326 (37.9%)	77 (23.8%)	20 (21.7%)	4 (12.5%)	<0.001	84 (23.7%)	17 (16.5%)	<0.001
Ischemic stroke	228 (26.5%)	72 (22.2%)	16 (17.4%)	4 (12.5%)	0.05	74 (20.9%)	18 (17.5%)	0.095
Smoking	270 (30.9%)	70 (21.2%)	23 (24.7%)	5 (14.7%)	0.002	76 (21.5%)	22 (21.4%)	0.0173
SBP (mmHg)	139.6 ± 47.0	131.6 (23.1)	128.5 ± 24.8	130.4 ± 24.2	0.032	131.8 ± 22.7	129.3 ± 22.0	<0.001
DBP (mmHg)	86.29 ± 41.0	84 ± 18.1	79.45 ± 15.2	84.17 ± 12.7	0.53	83. 5 ± 17.1	81.1 ± 14.2	0.17
Cr (μmol/L)	126.96 ± 91.1	118.07 ± 98.0	115.36 ± 57.1	127.42 ± 42.6	<0.001	116.4 ± 81.3	116.6 ± 52.0	0.23
PT-INR	1.16 ± 0.54	1.5 ± 1.31	2.22 ± 0.95	3.79 ± 0.95	0.013	1.61 ± 1.46	2.11 ± 0.94	<0.001
EF (%)	58.01 ± 12.2	57.71 ± 12.6	58.17 ± 12.6	59.31 ± 11.8	0.19	57.84 ± 11.07	57.47 ± 9.84	0.61
Aspirin-clopidogrel	467(53.5%)	95(28.8%)	13(14.0%)	4 (11.8%)	<0.001	98 (27.7%)	14 (13.6%)	<0.001
Statin	489 (56.0%)	158 (47.9%)	39 (41.9%)	10 (29.4%)	<0.001	166 (46.9%)	41 (39.8%)	0.0021

Characteristics	No anticoagulant ($n = 813$)	Rivaroxaban			*P*
		≤10 mg ($n = 131$)	15 mg ($n = 169$)	20 mg ($n = 97$)	
(B) RIVAROXABAN					
Sex (Female)	316 (38.9%)	58 (42.3%)	82 (42.9%)	30 (28.0%)	0.0276
Age (years)	70.70 ± 12.41	74.74 ± 9.0	71.12 ± 9.80	62.06 ± 10.30	<0.001
CHA2DS2-VASc score	3.43 ± 1.83	4.22 ± 1.50	3.35 ± 1.64	2.09 ± 1.60	<0.001
HAS-BLED score	2.66 ± 1.16	2.91 ± 1.12	2.45 ± 1.05	1.8 ± 1.11	<0.001
RHD	8 (0.98%)	3 (2.2%)	5 (2.6%)	2 (1.9%)	0.37
CKD	98 (12.05%)	21 (15.7%)	16 (8.4%)	7 (6.7%)	0.0302
COPD	56 (6.89%)	11 (8.2%)	18 (9.4%)	3 (2.9%)	0.20
CHF	308 (37.9%)	81 (59.1%)	99 (51.8%)	26 (24.3%)	0.0017
GI bleeding	25 (3.08%)	6 (4.5%)	1 (0.5%)	0 (0)	0.081
Hypertension	505 (62.1%)	100 (74.6%)	125 (65.5%)	55 (52.4%)	<0.001
Diabetes mellitus	230 (28.3%)	46 (34.3%)	43 (22.5%)	20 (19.1%)	0.0076
Coronary disease	308 (37.9%)	65 (48.5%)	84 (44.0%)	36 (34.3%)	0.0017
Ischemic stroke	219 (26.9%)	44 (32.8%)	38 (19.9%)	17 (16.2%)	<0.001
Smoking	257 (31.6%)	29 (21.2%)	45 (23.6%)	37 (34.6%)	0.0084
SBP (mmHg)	138.86 ± 46.3	139.6 ± 21.1	138.1 ± 24.0	130.7 ± 20.6	<0.001
DBP (mmHg)	85.97 ± 39.95	84.3 ± 14.4	87.0 ± 16.5	83.2 ± 12.1	0.25
Cr (μmol/L)	118.89 ± 61.56	119.2 ± 43.3	105.4 ± 28.3	104.2 ± 25.1	0.072
PT-INR	1.18 ± 0.46	1.13 ± 0.31	1.14 ± 0.71	1.07 ± 0.24	0.41
EF (%)	58.1 ± 9.98	57.51 ± 13.2%	58.36 ± 12.28	61.46 ± 10.14	0.27
Aspirin-clopidogrel	444 (54.6%)	72 (52.6%)	80 (41.9%)	31 (29.0%)	<0.001
Beta-blocker	484 (59.5%)	73 (54.9%)	106 (64.5%)	66 (70.2%)	0.097
Statin	476 (58.6%)	101 (73.7%)	110 (57.6%)	54 (50.5%)	<0.001

Data are number (%), median (interquartile 1, interquartile 3) or mean ± SD; PT-INR, prothrombin time international normalized ratio; PINRR, the percentage of INR measurements in range; CHA_2DS_2-VASc score includes congestive heart failure, hypertension, age (65–74 years, ≥75 years), diabetes, stroke/transient ischemic attack, vascular disease, sex; HAS-BLED, hypertension, abnormal liver/renal function, stroke history, bleeding history or predisposition, labile INR, elderly, drug/alcohol usage; RHD, rheumatic heart disease; COPD, chronic obstructive pulmonary disease; CHF, congestive heart failure; GI, gastrointestinal; ICH, intracranial hemorrhage; SBP, systolic blood pressure; DBP, diastolic blood pressure; Cr, creatinine; EF, ejection fraction.

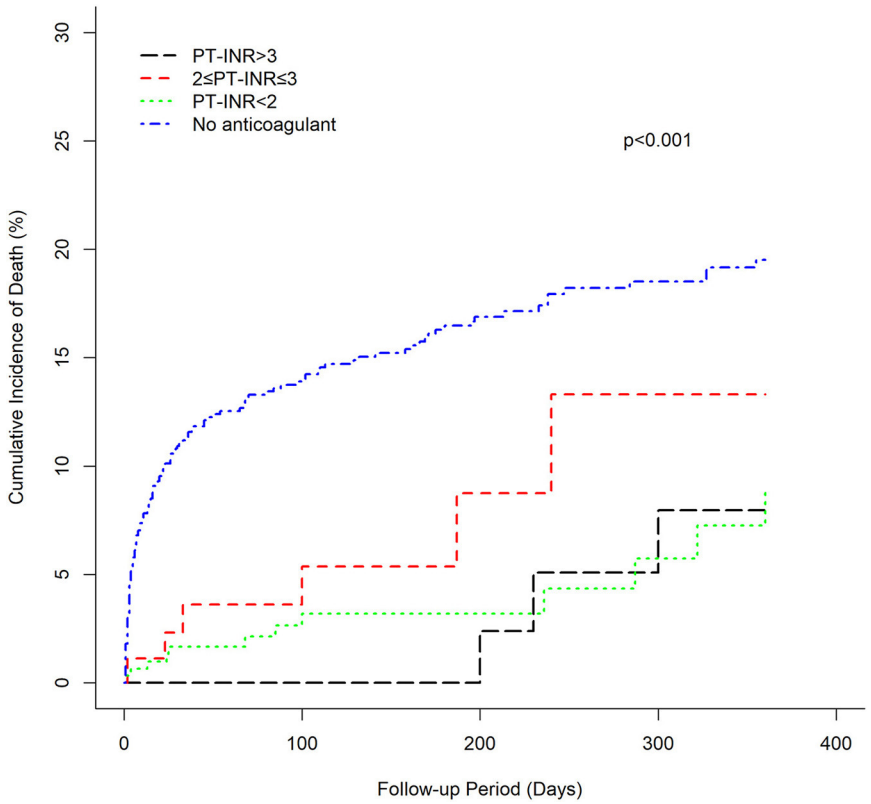

FIGURE 1 | Cumulative mortality of warfarin groups and the anticoagulant-untreated group (PT-INR).

Comparison Between Warfarin- vs. Anticoagulant-Untreated Groups for Mortality

The cumulative incidence of mortality in patients using warfarin (PT-INR < 2, $2 \leq$ PT-INR ≤ 3, PT-INR > 3), as well as PINRR ($>56.1\%$, $\leq 56.1\%$), was lower than that of patients not using anticoagulants (log-rank $p < 0.001$) (**Figures 1**, **2**). To delineate the associations between warfarin usage and the risk of mortality, Cox proportional hazards models were constructed (**Table 2**). Univariate analysis revealed that patients with a PT-INR <2 had only 0.274 times the risk of mortality compared with patients not using anticoagulants. After adjustment for gender, age, TIA/stroke, malignancy, chronic kidney disease, and GI bleeding, patients with a PT-INR < 2 were significantly associated with a lower risk of mortality (HR 0.309, 95%CI 0.170–0.56, $p = 0.0001$) (**Table 2**). Compared with the no anticoagulant group, both PINRR $\leq 56.1\%$ and PINRR $> 56.1\%$ groups had significantly lower risk of mortality in univariate and multivariable analysis (**Table 2**).

Comparison Between Rivaroxaban- vs. Anticoagulant-Untreated Groups for Mortality

There was a clear trend showing that NVAF patients using rivaroxaban ($\leq$10, 15, 20 mg) had a significantly lower incidence of mortality than patients without anticoagulant treatment (log-rank test $p < 0.001$) (**Figure 3**). Similarly, univariate and multivariable Cox proportional hazard model analyses also demonstrated that, compared with the anticoagulant-untreated group, rivaroxaban treatment at all dosages ($\leq$10 mg, HR 0.454, 95%CI 0.256–0.804, $p = 0.0068$; 15 mg, HR 0.139, 95%CI 0.051–0.376, $p = 0.0001$; 20 mg, HR 0.276, 95%CI 0.087–0.874, $p = 0.0286$) was significantly associated with lower risk of mortality in NVAF patients (**Table 3**).

DISCUSSION

In this study, we investigated the risk of mortality in Asians with AF who received warfarin, rivaroxaban, or no anticoagulant therapy. The main findings of this study are as follows: (1) among patients taking warfarin, patients with an INR lower than 2, as well as PINRR $\leq 56.1\%$ and PINRR $> 56.1\%$, had a significantly lower risk of mortality than that of patients without anticoagulant therapy, suggesting that warfarin still noticeably reduces the risk of mortality in Asians despite not achieving a target standard-intensity INR of 2–3; (2) low-dose rivaroxaban treatment (10 mg/day) is associated with a significantly lower risk of mortality than in patients not treated with anticoagulants, indicating that low-dose rivaroxaban may have survival benefits for Asians.

Previous studies have found a high percentage of AF patients do not follow the practice guidelines, especially in

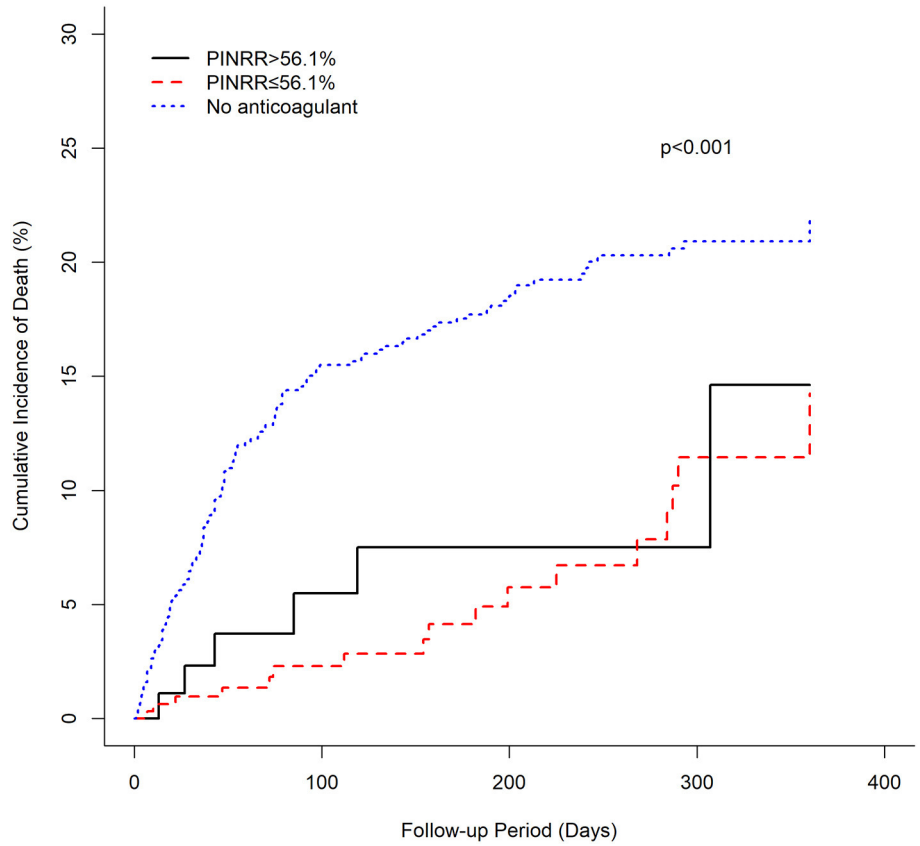

FIGURE 2 | Cumulative mortality of warfarin groups and the anticoagulant-untreated group (PINRR).

TABLE 2 | Univariate and multivariable analysis comparing the mortality of patients receiving warfarin vs. no anticoagulant treatment.

	Unadjusted		Adjusted	
	HR (95% CI)	***P***	**HR (95% CI)**	***P***
No anticoagulant	Reference		Reference	
PT-INR				
<2	0.274 (0.158, 0.475)	<0.0001	0.309 (0.170, 0.560)	0.0001
2–3	0.444 (0.196, 1.007)	0.052	0.539 (0.236, 1.229)	0.14
>3	0.571 (0.182, 1.794)	0.34	0.652 (0.207, 2.052)	0.46
PINRR*				
≤56.1%	0.345 (0.211, 0.562)	<0.0001	0.363 (0.220, 0.599)	<0.0001
>56.1%	0.428 (0.189, 0.969)	0.0418	0.387 (0.170, 0.882)	0.0238

HR, hazard ratio; CI, confidence interval; PT-INR, prothrombin time international normalized ratio; PINRR, the percentage of INR measurements in range; p<0.05 statistically significant; PT-INR vs. no anticoagulant was adjusted for gender, age, TIA/stroke, malignancy, CKD, and GI bleeding.

**PINRR vs. no anticoagulant was adjusted for age, coronary disease, left ventricular heart failure, malignancy, and aspirin.*

the Asian population (2, 3). Compared with Caucasians, Asians have a higher incidence of massive hemorrhaging, including intracranial hemorrhaging (10, 29, 30). Therefore, many physicians and patients in Asia are concerned about warfarin-induced bleeding and thrombosis, resulting in low-intensity INR warfarin becoming common in Asia (31–33). Our study shows that low-intensity INR warfarin substantially reduces mortality. A recent meta-analysis of 32 randomized controlled trials in East Asia showed no significant differences in the mortality of AF patients using warfarin with lower INR and that of AF patients using warfarin with standard INR. These findings show that the use of warfarin provides a survival benefit even in cases with a low INR target, suggesting that the use of warfarin with a low INR target might be beneficial

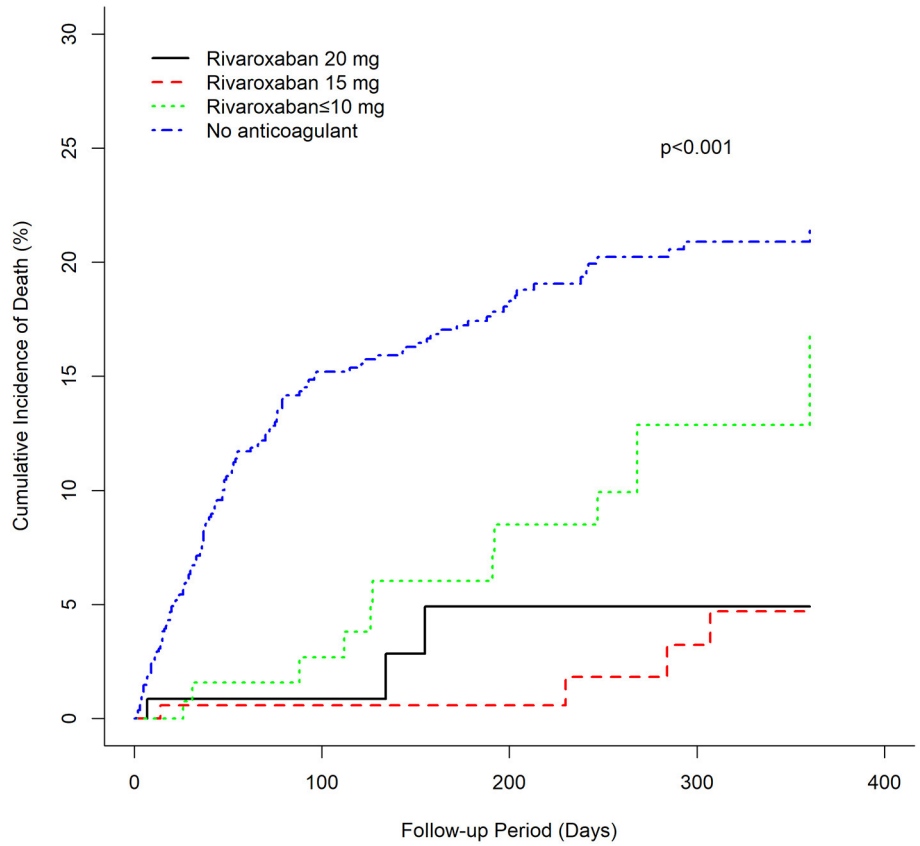

FIGURE 3 | Cumulative mortality of rivaroxaban groups and the anticoagulant-untreated group.

TABLE 3 | Univariate and multivariable analysis comparing the mortality of patients receiving rivaroxaban vs. no anticoagulant treatment.

	Unadjusted		Adjusted	
	HR (95% CI)	***P***	**HR (95% CI)**	***P***
No anticoagulant	Reference		Reference	
Rivaroxaban ≤ 10 mg	0.529 (0.300, 0.935)	0.0285	0.454 (0.256, 0.804)	0.0068
Rivaroxaban 15 mg	0.136 (0.050, 0.368)	<0.0001	0.139 (0.051, 0.376)	0.0001
Rivaroxaban 20 mg	0.171 (0.055, 0.538)	0.0025	0.276 (0.087, 0.874)	0.0286

HR, hazard ratio; CI, confidence interval; p<0.05 statistically significant; Adjusted for age, gender, coronary disease, TIA/stroke, CHF, CKD, aspirin, and statin.

to Asian patients who prefer warfarin but cannot have their anticoagulation intensity frequently monitored.

Intake of direct oral anticoagulants for the prevention of stroke in patients with AF is increasing rapidly worldwide, but varies widely, depending mainly but not exclusively on the socioeconomic status of the country under consideration (34, 35). Since DOACs do not require routine monitoring of drug concentrations, it is important to use an appropriate dose of DOAC based on the dosing criteria defined in a randomized controlled trial. However, the prescription of off-label DOACs remains a major problem in daily practice (36). One of the possible reasons is the concern of drug-induced adverse outcomes. Our study shows that various dosages of rivaroxaban, including 10 mg or less, can substantially reduce mortality, providing evidence of benefits associated with low-dose rivaroxaban use. This finding suggests that the use of low-dose rivaroxaban may be considered as an alternative, or in preference to no anticoagulant therapy, especially in situations where physicians have decisional conflicts with the risks and benefits of rivaroxaban.

Furthermore, several studies have shown that DOACs are more commonly studied in low-risk populations (37). Advanced age, frailty, and co-morbidities are common characteristics of the elderly population, making them less likely to be

treated with DOACs (38). In our study, the mean age of the low-dose rivaroxaban group (74.7 years old) was ∼4 years older than that of the anticoagulant-untreated group (70.7 years old). Although there were larger proportions of comorbidities and higher CHA_2DS_2-VASc and HAS-BLED scores in the low-dose rivaroxaban group compared to that of the anticoagulant-untreated therapy group, the risk of mortality was still significantly lower in the low-dose rivaroxaban group. This result indicates that rivaroxaban may substantially reduce the risk of mortality in Asian patients with AF, suggesting that the use of low-dose rivaroxaban may be an alternative for patients, especially elderly patients, who have concerns about the adverse effects and costs of standard-dose rivaroxaban.

Strengths and Limitations

Due to the complex clinical profile of patients with AF, certain patients were usually excluded from previous randomized controlled trials, making it challenging for physicians to prescribe anticoagulation therapy in clinical practice. On the one hand, our study includes a wide range of AF patients encountered in clinical practice. Therefore, our study could, to some extent, reflect the treatment patterns and associated risks of mortality in the Chinese population. On the other hand, our study observes treatment patterns and outcomes after discharge, and as such, it examines the associations of post-hospitalization anticoagulant dosage use patterns and death. The drug dose of OACs was as per the attending physician's discretion based on the patients' conditions and was collected from the medical records. Non-compliance with guidelines for warfarin and rivaroxaban use may be influenced by many factors. First, the perceived risks of bleeding impeded clinicians from prescribing anticoagulants and patients to adhere to therapy. Second, some patients with low body weight and/or renal impairment were underdosed because of a fear of toxicity. Finally, the high cost of rivaroxaban limited the options for some patients in the cohort. Nevertheless, there are limitations to this study. First, our patients are from a hospital that may have introduced selection bias. Second, our study does not include clinical information, such as bleeding events, thrombosis events, and BMI because of unclear or incomplete data. Third, although TTR has been recommended by the main international guidelines (39, 40) as a measure of the quality of anticoagulation control, it has not gained much popularity in clinical practice due to its tedious calculation; PINNR is much easier to obtain and simpler to calculate in everyday clinical practice, and was shown to have a good correlation with TTR (28). Finally, our sample size is relatively small, and is especially small for subjects with INR 2–3, so this study might have insufficient power to achieve statistical significance in the analyses for subjects with INR 2–3.

CONCLUSION

In Asian patients with AF, the risk of death is significantly lower in both patients receiving rivaroxaban and patients using warfarin with an INR below 2 in comparison with patients without anticoagulant therapy. These findings show that, despite effects being smaller than obtained with recommended doses, the use of warfarin below the standard INR target and the use of low-dose rivaroxaban still provide survival benefits, suggesting viable alternatives to physicians to better resolve decisional conflicts with the risks and benefits of anticoagulant therapy, as well as to patients in need of anticoagulant therapy but are not receiving it due to bleeding risk or other factors, such as financial burden, concerns of adverse outcomes, as well as low treatment compliance and persistence.

DATA AVAILABILITY STATEMENT

The raw data supporting the conclusions of this article will be made available by the authors, without undue reservation.

ETHICS STATEMENT

The studies involving human participants were reviewed and approved by Ethics Committee of the First Affiliated Hospital of Shantou University Medical College. The patients/participants provided their written informed consent to participate in this study.

AUTHOR CONTRIBUTIONS

XT and YC: contributed to the conception and design of the work. DL, JY, SW, YZ, and WL: contributed to the data collection and data management. YC and DL: contributed to the analysis, interpretation of data, and drafted the manuscript. XT, RL, and YC: reviewed and edited the manuscript. All authors contributed to the article and approved the submitted version.

FUNDING

This study was supported by projects from Grant for Key Disciplinary Project of Clinical Medicine under the High-level University Development Program (2020), Innovation Team Project of Guangdong Universities (2019KCXTD003), Li Ka Shing Foundation Cross-Disciplinary Research Grant (2020LKSFG19B), Funding for Guangdong Medical Leading Talent (2019–2022), National Natural Science Foundation of China (82073659), and Dengfeng Project for the construction of high-level hospitals in Guangdong Province—the First Affiliated Hospital of Shantou University Medical College (202003-2).

ACKNOWLEDGMENTS

The authors would like to express their appreciation to the staffs of the First Affiliated Hospital of Shantou University Medical College for their assistance.

REFERENCES

1. Morin DP, Bernard ML, Madias C, Rogers PA, Thihalolipavan S, Estes 3rd NA. The state of the art: atrial fibrillation epidemiology, prevention, and treatment. *Mayo Clin Proc.* (2016) 91:1778–810. doi: 10.1016/j.mayocp.2016.08.022
2. Chao TF, Liu CJ, Tuan TC, Chen TJ, Hsieh MH, Lip GYH, et al. Lifetime risks, projected numbers, and adverse outcomes in Asian patients with atrial fibrillation: a report from the Taiwan Nationwide AF cohort study. *Chest.* (2018) 153:453–66. doi: 10.1016/j.chest.2017.10.001
3. Du X, Guo L, Xia S, Du J, Anderson C, Arima H, et al. Atrial fibrillation prevalence, awareness and management in a nationwide survey of adults in China. *Heart.* (2021) 107:535–41. doi: 10.1136/heartjnl-2020-317915
4. Balsam P, Lodziński P, Gawałko M, Kraj L, Sliwczyński A, Maciejewski C, et al. Antithrombotic management and long-term outcomes of patients with atrial fibrillation. Insights from CRAFT trial. *J Clin Med.* (2021) 10:1780. doi: 10.3390/jcm10081780
5. Ansell J, Hirsh J, Hylek E, Jacobson A, Crowther M, Palareti G. Pharmacology and management of the vitamin K antagonists: American College of Chest Physicians Evidence-Based Clinical Practice Guidelines (8th Edition). *Chest.* (2008) 133(6 Suppl):160s−98s. doi: 10.1378/chest.08-0670
6. Jelavic M, Krstacic G, Pintaric H. Usage and safety of direct oral anticoagulants at patients with atrial fibrillation and planned diagnostic procedures, interventions, and surgery. *Heart Mind.* (2019) 3:1–6. doi: 10.4103/hm.hm_61_19
7. Fuster V, Rydén LE, Cannom DS, Crijns HJ, Curtis AB, Ellenbogen KA, et al. ACC/AHA/ESC 2006 guidelines for the management of patients with atrial fibrillation-executive summary: a report of the American College of Cardiology/American Heart Association Task Force on Practice Guidelines and the European Society of Cardiology Committee for Practice Guidelines (Writing Committee to Revise the 2001 Guidelines for the Management of Patients With Atrial Fibrillation). *J Am Coll Cardiol.* (2006) 48:854–906. doi: 10.1093/eurheartj/ehl176
8. Kirchhof P, Benussi S, Kotecha D, Ahlsson A, Atar D, Casadei B, et al. 2016 ESC Guidelines for the management of atrial fibrillation developed in collaboration with EACTS. *Eur Heart J.* (2016) 37:2893–962. doi: 10.1093/eurheartj/ehw210
9. January CT, Wann LS, Alpert JS, Calkins H, Cigarroa JE, Cleveland JC, Jr., et al. 2014 AHA/ACC/HRS guideline for the management of patients with atrial fibrillation: a report of the American College of Cardiology/American Heart Association Task Force on Practice Guidelines and the Heart Rhythm Society. *J Am Coll Cardiol.* (2014) 64:e1–76. doi: 10.1016/j.jacc.2014.03.022
10. Shen AY, Yao JF, Brar SS, Jorgensen MB, Chen W. Racial/ethnic differences in the risk of intracranial hemorrhage among patients with atrial fibrillation. *J Am Coll Cardiol.* (2007) 50:309–15. doi: 10.1016/j.jacc.2007.01.098
11. van Asch CJ, Luitse MJ, Rinkel GJ, van der Tweel I, Algra A, Klijn CJ. Incidence, case fatality, and functional outcome of intracerebral haemorrhage over time, according to age, sex, and ethnic origin: a systematic review and meta-analysis. *Lancet Neurol.* (2010) 9:167–76. doi: 10.1016/S1474-4422(09)70340-0
12. You JH, Chan FW, Wong RS. Cheng G. Is INR between 20 and 30 the optimal level for Chinese patients on warfarin therapy for moderate-intensity anticoagulation? *Br J Clin Pharmacol.* (2005) 59:582–7. doi: 10.1111/j.1365-2125.2005.02361.x
13. Inoue H, Okumura K, Atarashi H, Yamashita T, Origasa H, Kumagai N, et al. Target international normalized ratio values for preventing thromboembolic and hemorrhagic events in Japanese patients with non-valvular atrial fibrillation: results of the J-RHYTHM Registry. *Circ J.* (2013) 77:2264–70. doi: 10.1253/circj.CJ-13-0290
14. Cheung CM, Tsoi TH, Huang CY. The lowest effective intensity of prophylactic anticoagulation for patients with atrial fibrillation. *Cerebrovasc Dis.* (2005) 20:114–9. doi: 10.1159/000086801
15. Liu T, Hui J, Hou YY, Zou Y, Jiang WP, Yang XJ, et al. Meta-analysis of efficacy and safety of low-intensity warfarin therapy for East Asian patients with nonvalvular atrial fibrillation. *Am J Cardiol.* (2017) 120:1562–7. doi: 10.1016/j.amjcard.2017.07.050
16. Alamneh EA, Chalmers L, Bereznicki LR. Suboptimal use of oral anticoagulants in atrial fibrillation: has the introduction of direct oral anticoagulants improved prescribing practices? *Am J Cardiovasc Drugs.* (2016) 16:183–200. doi: 10.1007/s40256-016-0161-8
17. Lane DA, Wood K. Cardiology patient page. Patient guide for taking the non-vitamin K antagonist oral anticoagulants for atrial fibrillation. *Circulation.* (2015) 131:e412–5. doi: 10.1161/CIRCULATIONAHA.114.012808
18. Connolly SJ, Ezekowitz MD, Yusuf S, Eikelboom J, Oldgren J, Parekh A, et al. Dabigatran versus warfarin in patients with atrial fibrillation. *N Engl J Med.* (2009) 361:1139–51. doi: 10.1056/NEJMoa0905561
19. Patel MR, Mahaffey KW, Garg J, Pan G, Singer DE, Hacke W, et al. Rivaroxaban versus warfarin in nonvalvular atrial fibrillation. *N Engl J Med.* (2011) 365:883–91. doi: 10.1056/NEJMoa1009638
20. Hori M, Matsumoto M, Tanahashi N, Momomura S, Uchiyama S, Goto S, et al. Rivaroxaban vs. warfarin in Japanese patients with atrial fibrillation—the J-ROCKET AF study. *Circ J.* (2012) 76:2104–11. doi: 10.1253/circj.CJ-12-0454
21. Chan YH, Kuo CT, Yeh YH, Chang SH, Wu LS, Lee HF, et al. Thromboembolic, bleeding, and mortality risks of rivaroxaban and dabigatran in asians with nonvalvular atrial fibrillation. *J Am Coll Cardiol.* (2016) 68:1389–401. doi: 10.1016/j.jacc.2016.06.062
22. Ogawa S, Ikeda T, Kitazono T, Nakagawara J, Minematsu K, Miyamoto S, et al. Present profiles of novel anticoagulant use in Japanese patients with atrial fibrillation: insights from the Rivaroxaban Postmarketing Surveillance Registry. *J Stroke Cerebrovasc Dis.* (2014) 23:2520–6. doi: 10.1016/j.jstrokecerebrovasdis.2014.03.006
23. Kohsaka S, Murata T, Izumi N, Katada J, Wang F, Terayama Y. Bleeding risk of apixaban, dabigatran, and low-dose rivaroxaban compared with warfarin in Japanese patients with non-valvular atrial fibrillation: a propensity matched analysis of administrative claims data. *Curr Med Res Opin.* (2017) 33:1955–63. doi: 10.1080/03007995.2017.1374935
24. Chao TF, Chen SA, Ruff CT, Hamershock RA, Mercuri MF, Antman EM, et al. Clinical outcomes, edoxaban concentration, and anti-factor Xa activity of Asian patients with atrial fibrillation compared with non-Asians in the ENGAGE AF-TIMI 48 trial. *Eur Heart J.* (2019) 40:1518–27. doi: 10.1093/eurheartj/ehy807
25. Hindricks G, Potpara T, Dagres N, Arbelo E, Bax JJ, Blomstrom-Lundqvist C, et al. 2020 ESC Guidelines for the diagnosis and management of atrial fibrillation developed in collaboration with the European Association for Cardio-Thoracic Surgery (EACTS). *Eur Heart J.* (2021) 42:373–498.
26. Olesen JB, Torp-Pedersen C, Hansen ML, Lip GY. The value of the CHA_2DS_2-VASc score for refining stroke risk stratification in patients with atrial fibrillation with a $CHADS_2$ score 0–1: a nationwide cohort study. *Thromb Haemost.* (2012) 107:1172–9. doi: 10.1160/TH12-03-0175
27. Pisters R, Lane DA, Nieuwlaat R, de Vos CB, Crijns HJ, Lip GY, et al. novel user-friendly score (HAS-BLED) to assess 1-year risk of major bleeding in patients with atrial fibrillation: the Euro Heart Survey. *Chest.* (2010) 138:1093–100. doi: 10.1378/chest.10-0134
28. Chan PH, Li WH, Hai JJ, Chan EW, Wong IC, Tse HF, et al. Time in therapeutic range and percentage of international normalized ratio in the therapeutic range as a measure of quality of anticoagulation control in patients with atrial fibrillation. *Can J Cardiol.* (2016) 32:1247e23–28. doi: 10.1016/j.cjca.2015.10.029
29. Lip GY, Wang KL, Chiang CE. Non-vitamin K antagonist oral anticoagulants (NOACs) for stroke prevention in Asian patients with atrial fibrillation: time for a reappraisal. *Int J Cardiol.* (2015) 180:246–54. doi: 10.1016/j.ijcard.2014.11.182
30. Lopes RD, Guimarães PO, Kolls BJ, Wojdyla DM, Bushnell CD, Hanna M, et al. Intracranial hemorrhage in patients with atrial fibrillation receiving anticoagulation therapy. *Blood.* (2017) 129:2980–7. doi: 10.1182/blood-2016-08-731638
31. Liu M. Spotlight on the relationship between heart disease and mental stress. *Heart Mind.* (2021) 5:1–3. doi: 10.4103/hm.hm_12_21
32. Chen Y, Huang QF, Sheng CS, Zhang W, Shao S, Wang D, et al. Detection rate and treatment gap for atrial fibrillation identified through screening in community health centers in China (AF-CATCH): A prospective multicenter study. *PLoS Med.* (2020) 17:e1003146. doi: 10.1371/journal.pmed.1003146
33. Mai L, Wu Y, Luo J, Liu X, Zhu H, Zheng H, et al. A retrospective cohort study of oral anticoagulant treatment in patients with acute coronary syndrome and atrial fibrillation. *BMJ Open.* (2019) 9:e031180. doi: 10.1136/bmjopen-2019-031180

34. Camm AJ, Accetta G, Ambrosio G, Atar D, Bassand JP, Berge E, et al. Evolving antithrombotic treatment patterns for patients with newly diagnosed atrial fibrillation. *Heart*. (2017) 103:307–14. doi: 10.1136/heartjnl-2016-309832
35. Huisman MV, Rothman KJ, Paquette M, Teutsch C, Diener HC, Dubner SJ, et al. The changing landscape for stroke prevention in AF: findings from the GLORIA-AF registry phase 2. *J Am Coll Cardiol.* (2017) 69:777–85.
36. Steinberg BA, Shrader P, Thomas L, Ansell J, Fonarow GC, Gersh BJ, et al. Off-label dosing of non-vitamin k antagonist oral anticoagulants and adverse outcomes: the ORBIT-AF II registry. *J Am Coll Cardiol.* (2016) 68:2597–604. doi: 10.1016/j.jacc.2016.09.966
37. Deitelzweig S, Keshishian A, Li X, Kang A, Dhamane AD, Luo X, et al. Comparisons between oral anticoagulants among older nonvalvular atrial fibrillation patients. *J Am Geriatr Soc.* (2019) 67:1662–71. doi: 10.1111/jgs.15956
38. Haas S, Camm AJ, Bassand JP, Angchaisuksiri P, Cools F, Corbalan R, et al. Predictors of NOAC versus VKA use for stroke prevention in patients with newly diagnosed atrial fibrillation: results from GARFIELD-AF. *Am Heart J.* (2019) 213:35–46. doi: 10.1016/j.ahj.2019.03.013
39. Jones C, Pollit V, Fitzmaurice D, Cowan C. The management of atrial fibrillation: summary of updated NICE guidance. *BMJ*. (2014) 348:g3655. doi: 10.1136/bmj.g3655
40. January CT, Wann LS, Alpert JS, Calkins H, Cigarroa JE, Cleveland JC, Jr., et al. 2014 AHA/ACC/HRS guideline for the management of patients with atrial fibrillation: executive summary: a report of the American College of Cardiology/American Heart Association Task Force on practice guidelines and the Heart Rhythm Society. *Circulation*. (2014) 130:2071–104. doi: 10.1161/CIR.0000000000000040

Conflict of Interest: The authors declare that the research was conducted in the absence of any commercial or financial relationships that could be construed as a potential conflict of interest.

Publisher's Note: All claims expressed in this article are solely those of the authors and do not necessarily represent those of their affiliated organizations, or those of the publisher, the editors and the reviewers. Any product that may be evaluated in this article, or claim that may be made by its manufacturer, is not guaranteed or endorsed by the publisher.

Copyright © 2021 Lin, Chen, Yong, Wu, Zhou, Li, Tan and Liu. This is an open-access article distributed under the terms of the Creative Commons Attribution License (CC BY). The use, distribution or reproduction in other forums is permitted, provided the original author(s) and the copyright owner(s) are credited and that the original publication in this journal is cited, in accordance with accepted academic practice. No use, distribution or reproduction is permitted which does not comply with these terms.

frontiers in Cardiovascular Medicine

ORIGINAL RESEARCH
published: 25 November 2021
doi: 10.3389/fcvm.2021.724233

IL-18 Mediates Vascular Calcification Induced by High-Fat Diet in Rats With Chronic Renal Failure

Yinyin Zhang[1], Kun Zhang[1], Yuling Zhang[1], Lingqu Zhou[1], Hui Huang[2] and Jingfeng Wang[1]**

[1] Cardiology, Sun Yat-sen Memorial Hospital, Guangzhou, China, [2] Cardiology, The Eighth Affilliated Hospital, Sun Yat-sen University, Shenzhen, China

Objective: Vascular calcification (VC) is an important predictor of cardiovascular morbidity and mortality in patients with chronic renal failure (CRF). It is well-known that obesity and metabolic syndrome (OB/MS) predicts poor prognosis of CRF patients. However, the influence of OB/MS on VC in CRF patients isn't clear. IL-18 mediates OB/MS-related inflammation, but whether IL-18 is involved in OB/MS -mediated VC in CRF patients hasn't been studied. In this study, it was explored that whether OB/MS caused by high-fat diet (HFD) can affect the level of serum IL-18 and aggravate the degree of VC in CRF rats. Furthermore, it was studied that whether IL-18 induces rat vascular smooth muscle cells (VSMCs) calcification by activating the MAPK pathways.

Approach: The rats were randomly assigned to the sham-operated, CRF and CRF + HFD groups. CRF was induced by 5/6 nephrectomy. Serum IL-18 levels and aortic calcification indicators were compared in each group. Primary rat VSMCs calcification were induced by β-glycerophosphate and exposed to IL-18. VSMCs were also treated with MAPK inhibitors.

Results: The weight, serum levels of hsCRP, TG and LDL-C in CRF + HFD group were significantly higher than those in sham-operated and CRF groups ($p < 0.05$). Compared with the sham-operated group, the calcium content and the expression of BMP-2 of aorta in CRF and CRF + HFD groups were significantly increased ($p < 0.05$). Moreover, the calcium content and the expression of BMP-2 of aorta in CRF + HFD group was significantly higher than those in CRF group ($p < 0.05$). And the serum IL-18 level was positively correlated with aortic calcium content. It was also found that p38 inhibitor SB203580 can suppress the VSMCs calcification and osteoblast phenotype differentiation induced by IL-18. But the JNK inhibitor SP600125 can't suppress the VSMCs calcification and osteoblast phenotype differentiation induced by IL-18.

Conclusions: These findings suggest that obesity-related inflammation induced by high-fat diet could exacerbate VC in CRF rats. Furthermore, serum IL-18 level had a positive correlation with the degree of VC. It is also found that IL-18 promoted osteogenic differentiation and calcification of rat VSMCs via p38 pathway activation.

Keywords: IL-18, vascular calcification, chronic renal failure, high-fat diet, MAPK

OPEN ACCESS

Edited by:
Yuli Huang,
Southern Medical University, China

Reviewed by:
Jijin Lin,
Guangdong Academy of Medical Sciences, China
Zhongqun Wang,
Jiangsu University, China
Belinda Di Bartolo,
The University of Sydney, Australia

***Correspondence:**
Hui Huang
huangh8@mail.sysu.edu.cn
Jingfeng Wang
wjingf@mail.sysiu.edu.cn

Specialty section:
This article was submitted to General Cardiovascular Medicine, a section of the journal Frontiers in Cardiovascular Medicine

Received: *12 June 2021*
Accepted: *28 October 2021*
Published: *25 November 2021*

Citation:
Zhang Y, Zhang K, Zhang Y, Zhou L, Huang H and Wang J (2021) IL-18 Mediates Vascular Calcification Induced by High-Fat Diet in Rats With Chronic Renal Failure. Front. Cardiovasc. Med. 8:724233. doi: 10.3389/fcvm.2021.724233

Vascular calcification (VC) is a pathological process which is increased by age and aggravated in chronic diseases including chronic kidney disease (CKD), hypertension, diabetes mellitus and bone-mineral disorders (1, 2). VC is a common vascular complication in patients with chronic renal failure (CRF), which induce a series of adverse effects on hemodynamics, and is an important factor responsible for the increase in the morbidity and mortality of cardiovascular diseases in patients with CRF (3, 4). VC is believed to be an actively regulated process which is similar with bone formation and is initiated by phenotype change of vascular smooth muscle cells (VSMCs) to osteoblast-like cells (5).

Inflammation is known to be a key factor in promoting the formation of VC, but the exact pathological mechanism of inflammation-mediated VC is not yet fully understood (6, 7). IL-18 (interleukin-18) is a proinflammatory cytokine that belongs to the IL-1 superfamily and is produced by macrophages and other cells, including VSMCs (8). Our previous study had found that IL-18 is an important inflammatory factor that induces VSMCs calcification (7). Many studies have found that serum IL-18 levels in patients with CRF are significantly higher than those with normal renal function (9, 10). It is well-known that VC is the most common vascular complication in patients with CRF, but whether IL-18 is involved in the development of VC in patients with CRF is not clear.

Energy-dense food with a high fat content is identified to implicated in the pathogenesis of obesity and metabolic syndrome (OB/MS) (11). It is well-known that obesity can cause kidney damage, and its mechanism is more complicated. Current research believes that obesity damages the kidneys through four ways: hypertension, hyperglycemia, hyperlipidemia, and hyperuricemia. And at the same time, the four factors affect each other, forming a vicious circle (12, 13). Adipose tissue is also an important endocrine system of the body. It can produce a variety of adipokines, including leptin, adipocytokines, adiponectin, etc., as well as tumor necrosis factor-α, monocyte chemotactic factor and angiotensin II. These substances may have a direct effect on the occurrence and development of CRF (14). VC is an important vascular complication in patients with CRF, which indicates increased cardiovascular and death risk. Our previous research suggested that in subjects without CRF, those with OB/MS had higher incidence VC and the OB/MS-related inflammation might be involved in regulating the formation of VC (15, 16). However, the influence of OB/MS on VC in patients with CRF has not been studied in detail. A large amount of research evidence confirms that IL-18 mediates OB/MS-related inflammation (17). However, whether IL-18 is involved in the pathogenic mechanism of OB/MS -mediated VC in patients with CRF has not yet been studied.

The mitogen-activated protein kinase (MAPK) pathway is responsible for conveying information about the extracellular environment to the cell nucleus and is known to play a critical role in osteoblast differentiation and mineralization (18). JNK and p38 are the main MAPK signaling pathways. At present, studies suggest that the MAPK pathway is involved in the development of VC (19, 20). Studies have also proved that IL-18 can cause biological effects by activating MAPK pathway (21, 22). Therefore, we speculate that IL-18 may promote VSMCs calcification and osteoblast phenotype differentiation by activating the MAPK signaling pathway.

This study was based on a rat model of CRF to observe whether OB/MS caused by high-fat dietary (HFD) can affect the level of serum IL-18 in rats, aggravate the degree of VC, and initially reveal the relationship between IL-18 and OB/MS-related VC in CRF rats. Furthermore, we explore whether IL-18 induces rat VSMCs calcification and osteoblast phenotype differentiation by activating the MAPK pathways, so as to further clarify the mechanism of IL-18 inducing VC.

Abbreviations: ALP, alkaline phosphatase; Apo, apolipoprotein; BMI, body mass index; BMP-2, bone morphogenetic protein-2; BSA, bovine serum albumin; Ca, calcium; CHE, cholinesterase; Cr, creatinine; CRF:chronic renal failure; CVD, cardiovascular disease; HDL-C, high-density lipoprotein cholesterol; LDL-C, low-density lipoprotein cholesterol; hsCRP, high-sensitivity C-reactive protein; MAC, medial arterial calcification; MAP, mean arterial pressure; MetS, metabolic syndrome; OB/MS, obesity and metabolic syndrome; OR, odds ratio; P, phosphate; PVDF, polyvinylidene difluoride; SBP, systolic pressure; SD, standard deviation; SOD, superoxide dismutase; TC, total cholesterol; TG, triglycerides; UA, uric acid; VC, vascular calcification; VSMCs, vascular smooth muscle cells.

MATERIALS AND METHODS

Animal Model and Grouping

The animal experiments were approved by the Committee on Ethics of Animal Experiments and conducted in accordance with the Guidelines for Animal Experiments, Sun Yat-sen University and the Guide for the Care and Use of Laboratory Animals published by the US National Institutes of Health (NIH Publication No. 85-23, revised 1996).

Male Sprague-Dawley rats with an average body weight of 200–250 g were used in this study. All the animals were housed in an environmentally controlled room at 24 ± 1°C with a 12 h light/dark cycle and fed with tap water. The rats were randomly assigned to the CRF and sham-operated groups. CRF was induced by 5/6 nephrectomy (5/6 Nx) with surgical excision of two-thirds of the left kidney, followed by the complete right nephrectomy 1 week later. Sham-operated group underwent similar surgical procedures but with only removal of the renal envelope. The operations were carried out under general anesthesia (pentobarbital sodium, 50 mg/kg ip) using strict hemostasis and aseptic techniques. The 5/6 Nx rats were randomly divided into CRF and CRF + high fat diet (HFD) groups. The sham-operated and CRF groups were fed a standard laboratory diet with a total fat content of 4.3%. The CRF + HFD group were fed a HFD with a total fat content of 34.9%. Six animals were included in each group. Six months later, rats were sacrificed and serum levels of IL-18 were measured with commercially available kits (Ab Frontier). The aortas were dissected for calcium deposition assay, von Kossa and Alizarin red S staining, RNA and protein extraction.

Cell Culture

Primary aortic VSMCs of 2-month-old male Sprague–Dawley rats were obtained as described previously (7) and maintained in the high glucose (4.5 g/L) Dulbecco's modified Eagle's medium

(DMEM, Gibco) containing 10% fetal bovine serum (FBS), 100 U/ml penicillin and 100 mg/ml streptomycin at 37°C in a humidified atmosphere containing 5% CO_2. The cells at passages 4–8 were used for the experiments. Each experiment was repeated for at least three times. VSMCs calcification was induced by calcifying medium, DMEM containing 10% FBS, 10 mM sodium pyruvate, 100 U/ml penicillin, 100 mg/ml streptomycin and 10 mM β-glycerophosphate (β-GP, Sigma) for 14 days with medium changes every 2 days 4. After using IL-18 (R&D) to interfere with rat VSMCs for 2, 5, 10, 15, and 30 min, the phosphorylation and non-phosphorylation protein expression levels of two MAPK pathways including p38 and JNK were detected by Western blot. Rat VSMCs were pre-incubated with p38 inhibitor SB203580 (Sigma) at a final concentration of 10 μmol/L for 2 h, and then treated with β-GP (10 mmol/L) or IL-18 (100 ng/ml) + β-GP (10 mmol/L) for 14 days, respectively. Rat VSMCs were also pre-incubated with JNK inhibitor SP600125 (Sigma) at a final concentration of 10 μmol/L for 30 min, and then treated with β-GP (10 mmol/L) or IL-18 (100 ng/ml) + β-GP (10 mmol/L) for 14 days, respectively.

Serum Analyses

Blood of mice was collected from the caudal vein and serum concentrations of creatinine (Cr), calcium (Ca), phosphate (P), total cholesterol (TC), triglycerides (TG), high-density lipoprotein cholesterol (HDL-C), low-density lipoprotein cholesterol (LDL-C) and high-sensitivity C-reactive protein (hsCRP) were measured by a standardized and certified program with an automatic biochemical analyzer (7170A, HITACHI, Japan).

Measurement of Systolic and Mean Blood Pressures

Systolic blood pressure (SBP) and mean blood pressure (MBP) were obtained by a tail-cuff measurement (BP-98A, Softron, Tokyo, Japan). Conscious rats were placed in a restrainer with an electrical warming pad for 20-min and trained for 1 week before testing. In order to avoid variations of the SBP and MBP, all measurements were carried out between 8 and 11 am. At least three measurements of each rat were taken at 2 min intervals and the mean values of MBP and SBP were calculated.

Alizarin Red S Staining

Alizarin red S staining method was used to determine the calcification of rat aortas and VSMCs (7). The paraffin sections of the rat aortas were deparaffinized twice with xylene. And then the aortic slices were subjected to gradient concentration of ethanol and pure water each time for 5 min. After that, the sections were washed with phosphate buffered saline (PBS, Gibco) and stained with 2% Alizarin (sigma) for 30 min. Finally, the sections were washed with PBS before air-dry, and then sealed with neutral gum. VSMCs were with PBS and then fixed with 4% paraformaldehyde. After that, the cells were washed with PBS and exposed with 2% Alizarin Red S for 10 min, and then observed under the microscope. Positively stained cells displayed a red color.

Von Kossa Staining

The rat aorta and VSMCs slides were fixed with ice acetone at −20°C and washed with PBS. Von Kossa staining was performed as described previously (23). Five percentage silver nitrate solution was added to the slides. Discard the silver nitrate solution and add 1 ml of 5% sodium thiosulfate solution. Back staining with 1% basic fuchsin for 10 s. The slides are dehydrated with anhydrous. Finally, Seal the film with neutral gum and observe the calcium nodules under a light microscope.

Hematoxylin-Eosin Staining of Rat Aorta

Paraffin sections are deparaffinized with xylene, washed with water after gradient ethanol. After hematoxylin staining for 5 min, the sections were washed with water for 1 min. Then, the sections were differentiated with l% hydrochloric acid alcohol and stained with saturated lithium carbonate. Finally, the sections were stained with eosin, then dehydrated and sealed.

Quantification of Calcium Deposition

Quantification of VSMCs and aortic calcium deposition was performed as described previously (24). VSMCs were collected and dissolved in 2 mol/L HNO_3 overnight. Thereafter, VSMCs were re-dissolved with a blank solution (27 nmol/L KCl, 27 μmol/L $LaCl_3$ in de-ionized water). The calcium deposition of VSMCs was measured by an atomic absorption spectrophotometer at 422.7 nm (Hitachi, Z-5000). Calcium deposition of VSMCs was normalized by protein concentration. Take the rat aorta (10–20 mg) and dry it thoroughly at 80°C, and weigh. Add 2 mol/L concentrated nitric acid to digest for 24 h, put the digestion tube into the automatic control electric heating digester to digest until all the acid is volatilized. After cooling, reconstitute it with deionized water containing 27 nmol/L KCl and 27 μmol/L $LaCl_3$ overnight. Then add 1% strontium chloride and measure the optical density value of each tube at 422.7 nm wavelength with an atomic absorption spectrophotometer. Repeat the measurement for each sample three times and take the average value, and then convert it into the calcium content of the tissue (μmol/gdw).

Alkaline Phosphatase Activity Assay

The cells were washed with PBS and treated with 1% Triton X-100 in 0.9% NaCl. After centrifugation at 12,000 rpm at 4°C for 10 min, the supernatants were harvested to detect for alkaline phosphatase (ALP) activity with the use of ALP assay kit (Jiancheng Bioengineering Co., Nanjing, China). ALP activity was measured colorimetrically as thehydrolysis of p-nitrophenyl phosphate and the results were normalized to the levels of total protein.

Immunohistochemistry

For the detection of bone morphogenetic protein-2(BMP-2), immunohistochemical staining was performed. Rat aortas were embedded in paraffin blocks for immunohistochemical staining. Endogenous peroxidase activity was blocked by 3% H_2O_2. Sections were incubated with anti-BMP-2 antibody (dilution 1:250, Santa Cruz, California, US) overnight at 4°C, then washed with PBS. Thereafter, sections were incubated with secondary antibody of anti-horseradish peroxidase (HRP) (dilution 1:50,

Santa Cruz, California, US) at room temperature for 30 min, then washed again three times with PBS prior to staining with 3, 3′-diaminobenzidine (DAB) at room temperature for 4 min. BMP-2 protein expression was visualized as brown deposits using a microscope.

Quantitative Real-Time Polymerase Chain Reaction

Trizol and liquid nitrogen were added to every 1 cm rat aorta. Then the tissue was grinded into powder and centrifuged at 1,2000 g at 4°C for 5 min. And the supernatant was aspirated and transferred into a new EP tube. Total RNA from VSMCs and rat aortas was isolated by the Trizol method (TaKaRa, Japan) and was reverse-transcribed with the PrimeScript RT reagent kit (TaKaRa, Japan) following the manufacturer's recommended protocol (7). Amplification reactions were set up in 20 μl reaction volumes containing amplification primers and SYBR Premix Ex Taq TM II (Takara, Japan). One μl cDNA was used in each amplification reaction. Preliminary experiments were carried out to optimize primer concentrations. The PCR primers were as follows: BMP-2, forward 5′-ACCG TGCTCAGCTTCCATCAC-3′ and reverse5′-CTATTTCCCAAAGCTTCCTGCAT TT-3′; GAPDH, forward 5′-GGCACAGTCAAGGCTGAGAATG-3′ and reverse5′-ATGGTGGTGAAGACGC CAGTA-3′. Each sample was run in triplicates and each experiment was repeated at least once. Amplification data were analyzed using the LightCycler 480 real-time PCR instrument (Roche, Germany). Quantification was performed using the ΔΔCt method. The results were normalized to GAPDH and expressed as percentage of controls.

Western Blot Analysis

The rat aortas were treated with RIPA lysis buffer (Beyotime, Haimen, China) and comminuted with homogenizer on ice. VSMCs were washed twice with cold PBS and treated with RIPA lysis buffer on ice for 30 min. After centrifugation at 12,000 rpm at 4°C for 10 min, the supernatants of the aortic homogenate and VSMCs were harvested to determine the protein expression. The protein samples were mixed with the loading buffer and boiled at 95°C for 5 min. The boiled samples were separated on the SDS–polyacrylamide gels, and the proteins were transferred to the polyvinylidene difluoride (PVDF) membranes. The PVDF membranes were incubated in a blocking buffer containing 5% (w/v) bovine serum albumin (BSA). The blots were then incubated with primary antibodies: anti-total p38 antibody, anti-phospho-p38 antibody, anti-total ERK1/2 antibody, anti-phospho-ERK1/2 antibody, anti-total JNK antibody, anti-phospho-JNK antibody, anti-GAPDH antibody (dilution: 1:1000, Cell signaling technology, Danvers, US), anti-BMP-2 antibody (dilution: 1:300, Santa Cruz, California, US) in TBST containing 5% (w/v) BSA (antibody buffer) overnight at 4°C. The members were then washed and incubated with the horseradish peroxidase-linked secondary antibody (dilution: 1:1000, Cell signaling technology, Danvers, US) and then visualized with the enhanced chemiluminescence (Thermo Fisher Scientific, Waltham, US). The bands were analyzed semi-quantitatively.

TABLE 1 | Comparison of body weight and serum biochemical indexes of rats in each group.

	Sham-operated	CRF	CRF + HF
Weight (g)	360 ± 10	334 ± 37.2	401 ± 40.8$^{\#*}$
Ca (mmol/L)	2.52 ± 0.40	1.92 ± 0.14$^{\#}$	1.92 ± 0.22$^{\#}$
P (mmol/L)	1.07 ± 0.01	1.72 ± 0.21$^{\#}$	1.75 ± 0.26$^{\#}$
Cr (μmol/L)	56.67 ± 4.73	104.31 ± 14.44$^{\#}$	110.47 ± 19.01$^{\#}$
HsCRP (mg/L)	4.45 ± 0.62	8.29 ± 1.25$^{\#}$	9.91 ± 1.81$^{\#*}$
CHOL (mmol/L)	2.10 ± 0.34	2.09 ± 0.35	2.38 ± 0.51
TG (mmol/L)	0.64 ± 0.10	0.58 ± 0.13	1.41 ± 0.45$^{\#*}$
LDL-C (mmol/L)	0.39 ± 0.06	0.34 ± 0.10	0.49 ± 0.17$^{\#*}$
HDL-C (mmol/L)	1.00 ± 0.20	0.94 ± 0.16	0.91 ± 0.18

*$p < 0.05$ vs. CRF group; $^{\#}p < 0.05$ vs. sham-operated group.

Statistical Analysis

Each experiment was repeated three times independently. Data were expressed as means ± SD. The results were compared with one-way ANOVA followed by Student-Newman-Keuls test for *post-hoc* comparison among more than two groups. Pearson's correlation analysis was used to analyze the relationship between serum IL-18 levels and aortic calcium content. All statistical analyses were performed using the software SPSS 17.0. For all statistical tests, two-tailed P-value < 0.05 indicated the statistical significance of the results.

RESULTS

Comparison of Weight and Serum Biochemical Indexes Among CRF, CRF + HFD and Sham-Operated Rats

The weight and biochemical indexes of rats in three groups are shown in **Table 1**. Compared with sham-operated rats, CRF and CRF + HFD rats had higher serum levels of Cr, P and hsCRP ($p < 0.05$) and lower level of Ca ($p < 0.05$). And the weight, serum levels of TG and LDL-C in CRF + HFD rats were significantly higher than sham-operated and CRF rats ($p < 0.05$). Furthermore, the serum level of hsCRP in CRF + HFD rats significantly higher than CRF rats ($p < 0.05$).

Comparison of the Blood Pressure of Rats in Each Group

The blood pressure of the rat tail was measured before the operation and 1, 4, 7, 10, and 13 weeks after the operation. The results showed (**Figures 1A,B**) that the systolic blood pressure (SBP) and mean arterial pressure (MAP) in the CRF and CRF + HFD groups showed an upward trend after surgery, but the SBP and MAP in the sham-operated group did not change significantly. From the first week after surgery, the SBP and MAP in CRF and CRF + HFD group were significantly higher than those in the sham-operated group ($p < 0.05$). From the first week after surgery, the MAP in the CRF + HFD group was significantly higher than that of the CRF group ($p < 0.05$), while the SBP in the CRF + HFD group was not significantly different from that of the CRF group ($p > 0.05$).

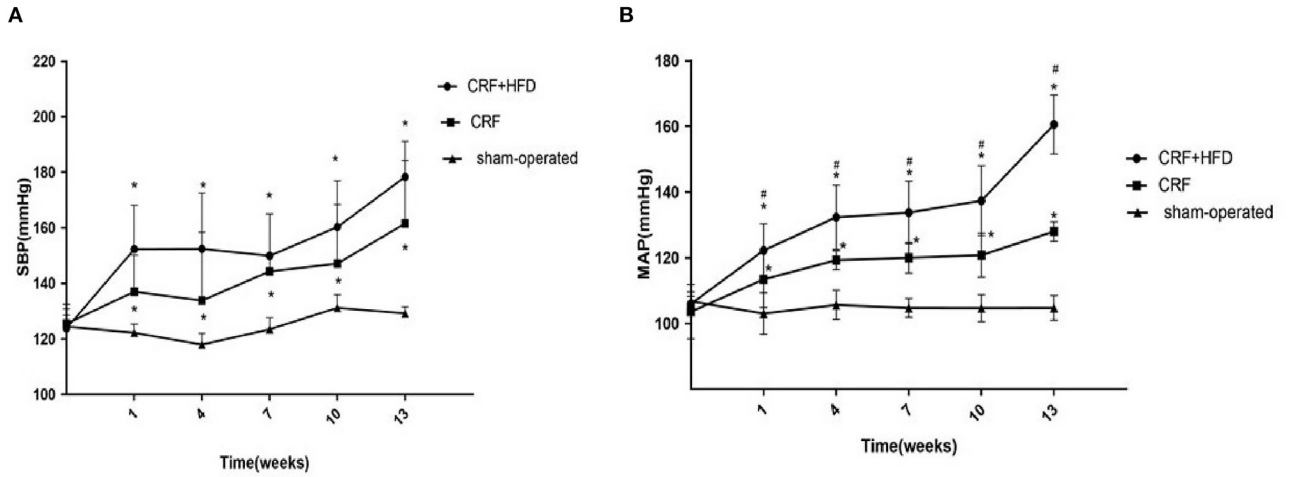

FIGURE 1 | Comparison of systolic blood pressure **(A)** and mean arterial pressure **(B)** of rats in each group. Six rats were included in each group. $^{*}P < 0.05$ vs. sham-operated group; $^{\#}P < 0.05$ vs. CRF group. CRF, chronic renal failure; HFD, high fat diet; MAP, mean arterial pressure; SBP, systolic blood pressure.

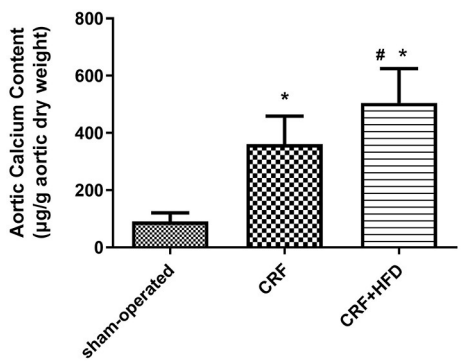

FIGURE 2 | Comparison of calcium content in the aorta of rats in each group. Six rats were included in each group. $^{*}P < 0.05$ vs. sham-operated group; $^{\#}P < 0.05$ vs. CRF group. CRF, chronic renal failure; HFD, high fat diet.

Comparison of Calcium Content in the Aorta of Rats in Each Group

Take the aorta of rats in each group 6 months after operation for the detection of calcium content. The results are shown in **Figure 2**. Compared with the sham-operated group, the calcium content of the aorta in the CRF and CRF + HFD groups were significantly increased (360.68 ± 98.48, 504.82 ± 120.30 vs. 91.17 ± 29.63, $p < 0.05$). Moreover, the calcium content of aorta in the CRF + HFD group was significantly higher than that in the CRF group (504.82 ± 120.30 vs. 360.68 ± 98.48, $p < 0.05$).

HE and Calcification Staining of Rat Aortas in Each Group

The aortic sections of rats in each group were stained with Alizarin Red, Von Kossa and HE staining at 6 months after operation to observe the aortic calcification. As shown in **Figure 3A**, the Alizarin Red staining revealed that there were no obvious calcium nodules in the aorta of the rats in sham-operated group, while the aorta of the rats in CRF and CRF + HFD groups showed scattered orange-red staining. The calcium nodules in the aorta of rats in CRF + HFD group were more obvious than those in CRF group. Von Kossa staining (**Figure 3B**) showed that there was a large amount of black granular calcium deposits between the elastic fibers of the aorta of the rats in CRF and CRF + HFD groups, and the calcium deposits in the aorta of the rats in CRF + HFD group were more significant than those in CRF group. But there was no obvious calcium deposition among the elastic fibers of the aorta in the sham-operated group. The HE staining showed that the aortic intima of rats in CRF and CRF + HFD groups was shrunken and broken and the nuclear arrangement was disordered, while the aortic intima of the sham-operated group was flat. The nuclei are arranged neatly (**Figure 3C**).

Comparison of BMP-2 mRNA and Protein Expression in the Aorta of Rats in Each Group

The rat aortas of each group were taken 6 months after the operation to detect the expression of BMP-2 mRNA and protein. The results showed that compared with the sham-operated group, the BMP-2 mRNA and protein expression of the aortas in the CRF and CRF + HFD groups were significantly increased ($p < 0.05$, **Figure 4A**). Moreover, the expression of BMP-2 mRNA and protein in the aortas of the CRF + HFD group was significantly higher than that of the CRF group ($p < 0.05$, **Figure 4B**).

Immunohistochemical Staining of BMP-2 Protein Expression in Aortas of Rats in Each Group

The aortas of each group were separated 6 months after operation, and routine paraffin sections were used to observe the expression of BMP-2 protein in the aortic wall by

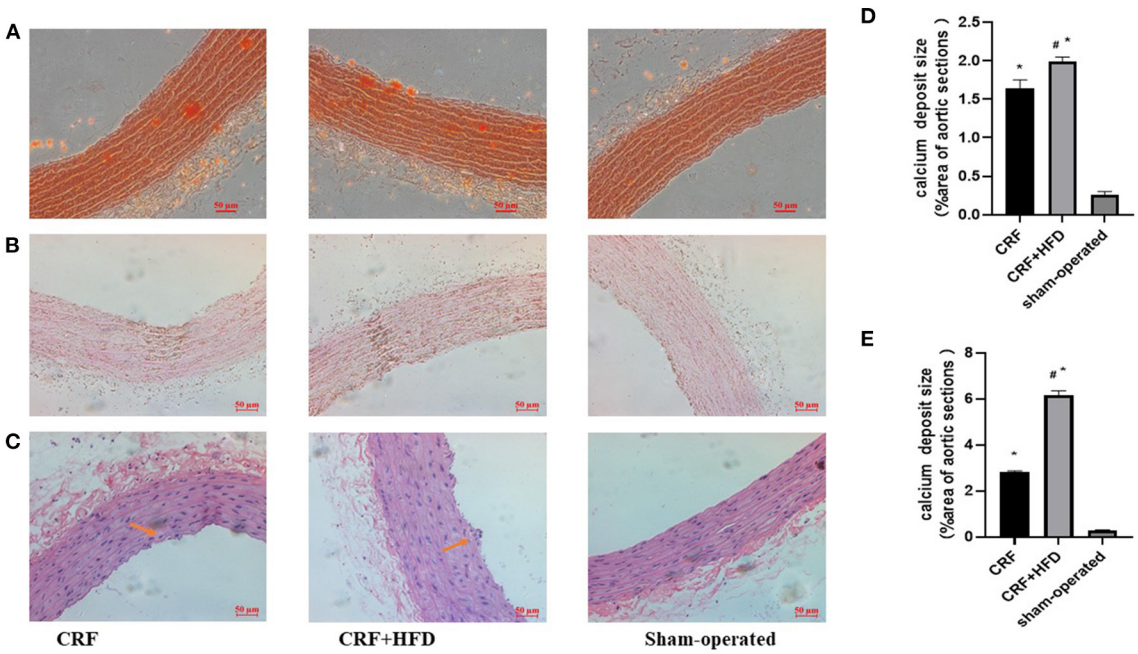

FIGURE 3 | Staining of rat aorta in each group. **(A)** Alizarin red staining of rat aorta in each group. **(B)** Von Kossa staining of rat aorta in each group. **(C)** staining of rat aorta in each group. **(D)** Quantification of calcium deposits in rat aortas stained with Alizarin Red. **(E)** Quantification of calcium deposits in rat aortas stained with Von Kossa. Six rats were included in each group. $^{*}P < 0.05$ vs. sham-operated group; $^{\#}P < 0.05$ vs. CRF group. CRF, chronic renal failure; HFD, high fat diet.

immunohistochemical staining (**Figure 5**). The results revealed that the BMP-2 protein staining of the aortic wall in the CRF and CRF + HFD groups was light brown fine granular, and the BMP-2 protein expression in the aorta of the CRF + HFD group was more obvious than that of the CRF group. While there was no obvious BMP-2 protein expression in the aortic wall of the sham-operated group.

Trend of Serum IL-18 in Rats of Each Group

The venous blood of each group was collected before operation and the second, fourth, and 6th month after the operation, and the serum IL-18 expression level was detected by ELISA (**Figure 6**). The results suggested that the postoperative serum IL-18 level of rats in the CRF and CRF + HFD groups gradually increased with time, while the postoperative serum IL-18 level of rats in the sham-operated group did not change significantly. Moreover, the postoperative serum IL-18 levels of rats in the CRF and CRF + HFD groups were significantly higher than those in the sham-operated group ($p < 0.05$). In addition, the serum IL-18 level in the CRF + HFD group was significantly higher than that in the CRF group ($p < 0.05$).

Correlation Analysis of Rat Serum IL-18 Level and Aortic Calcification Content

Correlation analysis between serum IL-18 level and aortic calcium content of all the rats in three groups at the 6th month after surgery (**Figure 7**) showed that serum IL-18 level was positively correlated with aortic calcium content ($r = 0.934$, $p < 0.001$), indicating that with the increase of serum IL-18 level, the degree of aortic calcification in rats became serious.

The Activation of IL-18 on MAPK Pathways

As shown in **Figure 8**, when IL-18 intervened for 2 min, the expression of phosphorylated p38 (p-p38) protein in VSMCs began to increase. The expression of p-p38 was the most significant when IL-18 intervened for 5 min. After 10 min of IL-18 intervention, the expression of p-p38 began to show a downward trend. Moreover, 2 min after IL-18 treatment, p-JNK protein significantly increased. After IL-18 acted for 5 min, the protein expression of p-JNK showed a gradually decreasing trend.

Effect of p38 Pathway on IL-18-Induced Calcification and Osteogenic Phenotypic Transformation of Rat VSMCs

We found that SB203580 decreased IL-18-enhanced calcium content (35.21 ± 3.46 vs. 81.83 ± 4.05, $p < 0.01$) and ALP activity (74.99 ± 1.63 vs. 141.75 ± 3.32, $p < 0.01$)in the IL-18 + β-GP group (**Figure 9**). Furthermore, SB203580 decreased IL-18-enhanced the expression of BMP-2 mRNA and protein in the IL-18 + β-GP intervention group ($p < 0.01$, **Figure 10**). But SB203580 pre-incubation had no significant effect on the calcium content (31.42 ± l.50 vs. 33.38 ± 2.91, $p > 0.05$) and ALP activity (71.32 ± l.53 vs. 74.06 ± 2.29, $p > 0.05$) of the β-GP group (**Figure 9**). SB203580 pre-incubation had no significant effect on the expression of

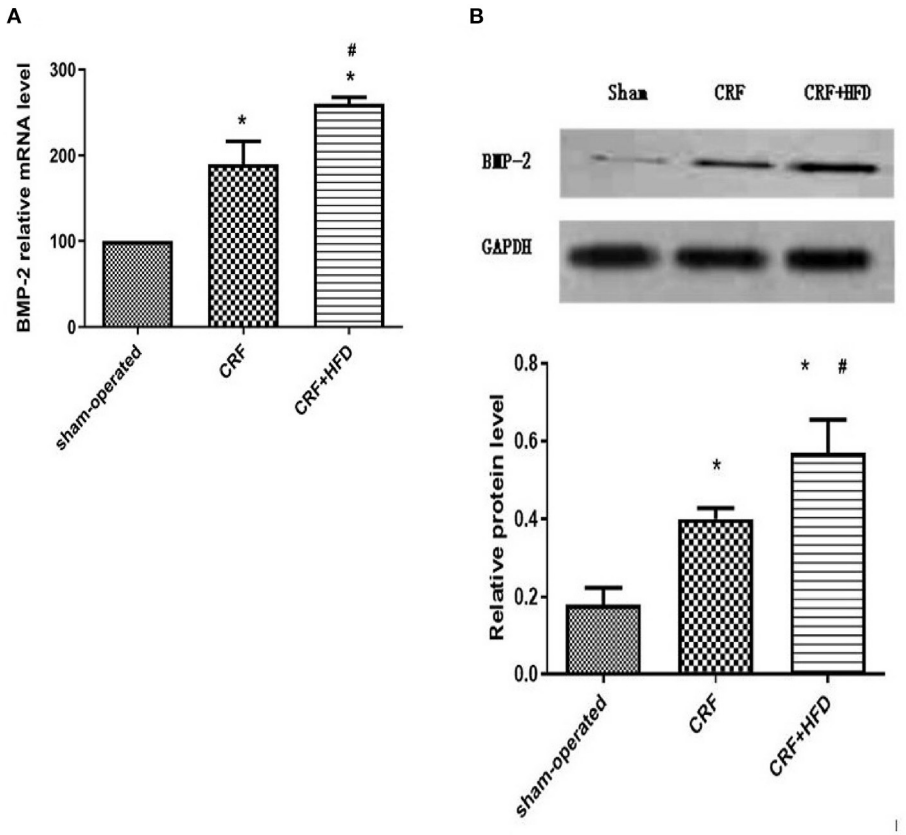

FIGURE 4 | Comparison of BMP-2 mRNA **(A)** and protein **(B)** expression in the aortas of rats in each group. Six rats were included in each group. *$P < 0.05$ vs. sham-operated group; #$P < 0.05$ vs. CRF group. BMP-2, bone morphogenetic protein-2; CRF, chronic renal failure; HFD, high fat diet.

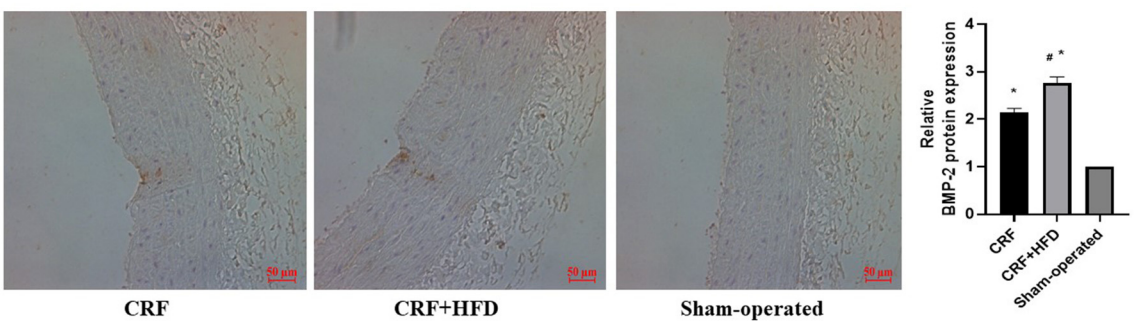

FIGURE 5 | Immunohistochemical staining of BMP-2 protein expression in aortas of rats in each group. Six rats were included in each group. The BMP-2 protein staining of the aortic wall was light brown fine granular. *$P < 0.05$ vs. sham-operated group; #$P < 0.05$ vs. CRF group. CRF, chronic renal failure; HFD, high fat diet.

BMP-2 mRNA and protein in the β-GP group ($p > 0.05$, **Figure 10**). Alizarin Red staining showed that SB203580 pre-incubation can significantly reduce the calcium deposition of IL-18 + β-GP group. The β-GP group pre-incubated with SB203580 and the β-GP group not pre-incubated with SB203580 showed no significant changes in cellular calcium deposition (**Figure 11**).

Effect of JNK Pathway on IL-18-Induced Calcification and Osteogenic Phenotypic Transformation of Rat VSMCs

The results indicated (**Figure 12**) that SP600125 had no significant effect on IL-18-enhanced calcium content (76.42 ± 4.86 vs. 81.83 ± 4.05, $p > 0.05$) and ALP activity (136.36 ± 3.50 vs. 141.75 ± 3.32, $p > 0.05$) in the IL-18 + β-GP group.

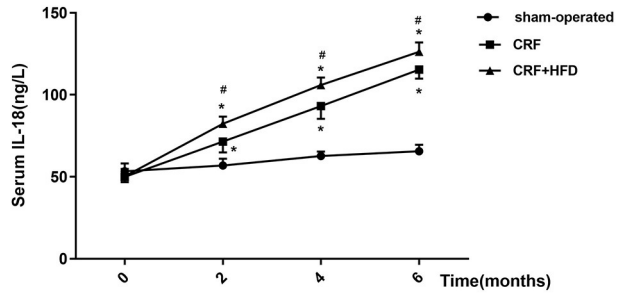

FIGURE 6 | Trend of serum IL-18 in rats of each group after operation. Six rats were included in each group. $^{*}P < 0.05$ vs. sham-operated group; $^{\#}P < 0.05$ vs. CRF group. CRF, chronic renal failure; HFD, high fat diet.

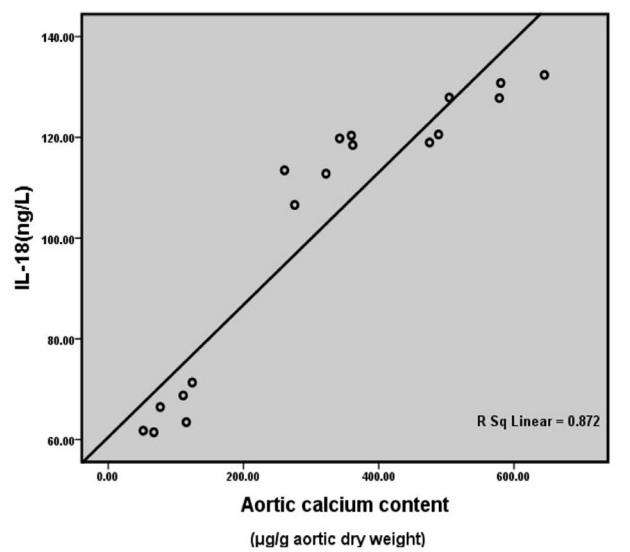

FIGURE 7 | Correlation analysis of rat serum IL-18 level and aortic calcification content. Six rats were included in each group.

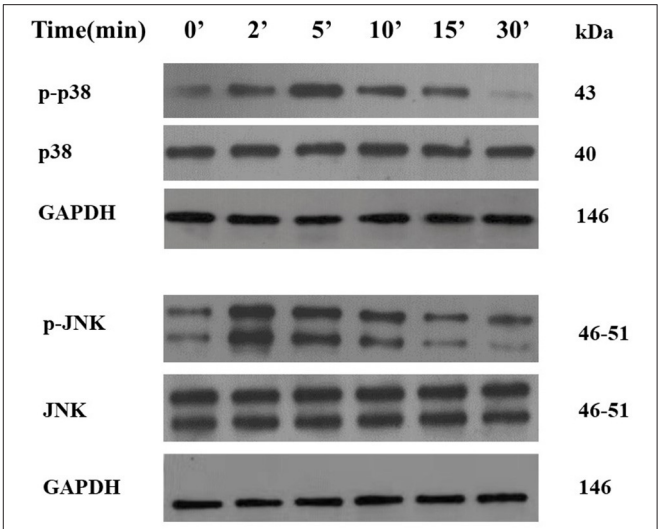

FIGURE 8 | Activation of p38 and JNK pathways by IL-18 in rat VSMCs. After using IL-18 to interfere with rat VSMCs for 2, 5, 10, 15, and 30, the phosphorylation and non-phosphorylation protein expression levels of two MAPK pathways including p38 and JNK were detected by Western blot. The experiment was repeated 3 times independently.

And SP600125 also had no significant effect on IL-18-enhanced expression of BMP-2 mRNA and protein in the IL-18 + β-GP group ($p > 0.05$, **Figure 13**). Furthermore, SP600125 pre-incubation had no significant effect on the calcium content (32.0 ± 3.32 vs. 33.38 ± 2.91, $p > 0.05$) and ALP activity (69.48 ± 3.96 vs. 74.06 ± 2.29, $p > 0.05$) of the β-GP group (**Figure 12**). SP600125 pre-incubation had no significant effect on the expression of BMP-2mRNA and protein in the β-GP group ($p > 0.05$, **Figure 13**). SP600125 pre-intervention has no significant effect on calcium deposition in IL-18 + β-GP and β-GP groups ($p > 0.05$, **Figure 14**).

DISCUSSION

VC is a preventable, reversible and highly adjustable process similar to bone and cartilage formation, and the key mechanism of VC is the osteogenic differentiation of VSMCs (25). Inflammation is currently considered to be one of the important factors regulating the development of VC (7). Our previous research results suggested that in subjects without CRF, obesity-related inflammation might be involved in regulating the formation of VC (15). Obesity conferred greater cardiovascular risk when combined with metabolic syndrome in CRF patients (26). VC is a common vascular complication of CRF and an important indicator of poor prognosis. Nowadays, the relationship between obesity-related inflammation and VC in CRF patients is still controversial. Krasniak et al. had proved that the coronary artery calcification score is positively correlated with BMI in maintenance haemodialysis patients (27). But the study by Kim et al. concluded that there was no significant correlation between obesity and aortic calcification in dialysis patients (28). Therefore, this study explored the effect of obesity caused by high-fat diet on VC in a rat model of CRF.

The results of the study showed that the calcium content and BMP-2 expression of the aorta in the CRF rats fed with high-fat diet were significantly higher than the CRF rats fed with conventional diet. This study confirms for the first time that in a rat model of CRF, feeding with high-fat diet can further induce the osteogenic phenotype transformation and deteriorate VC.

Indeed, it is now widely agreed that obesity is a state of low-grade chronic inflammation (29, 30). Increased circulating levels of inflammatory cytokines have been reported in overweight and obese adults, and this event has been linked to the increased cardiovascular risk seen in obesity (31). Our study also showed that the body weight, blood lipids and hsCRP level of CRF rats fed with high-fat diet were significantly higher than those of CRF rats fed with conventional diet. HsCRP is one of the important inflammatory factors, suggesting that in CRF rats, a high-fat diet may cause obesity-related inflammation.

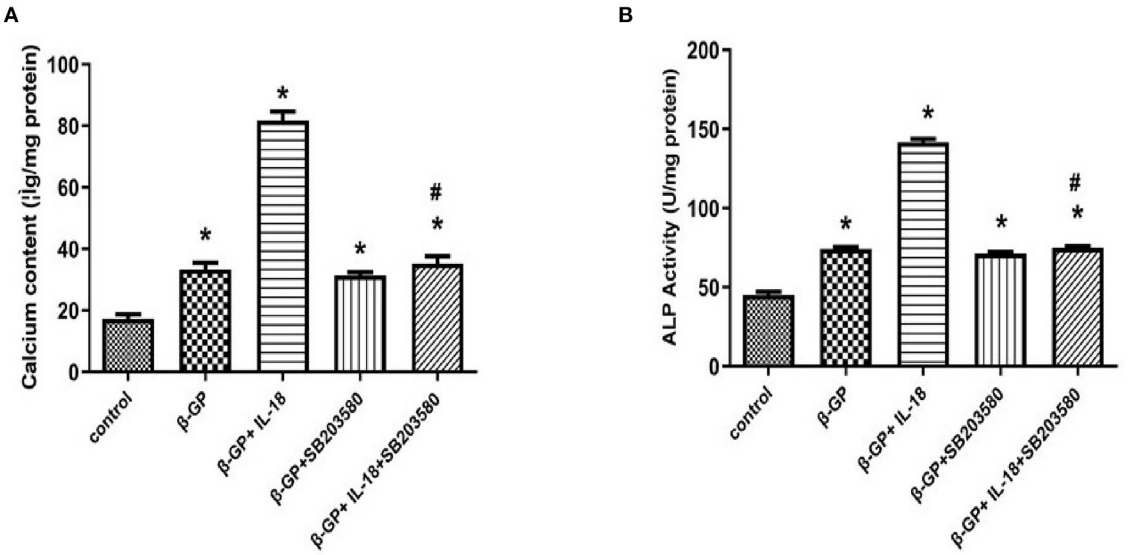

FIGURE 9 | Effect of p38 pathway on IL-18-induced calcification of rat VSMCs. **(A)** Effect of p38 pathway on calcium content of rat VSMCs after IL-18 intervention. **(B)** Effect of p38 pathway on ALP activity of rat VSMCs after IL-18 intervention. Rat VSMCs were pre-incubated with p38 inhibitor SB203580 (10 μmol/L) for 2 h, and then treated with β-GP (10 mmol/L) or IL-18 (100 ng/ml) + β-GP (10 mmol/L) for 14 days, respectively. The experiment was repeated 3 times independently. $^{*}P < 0.01$ vs. control group; $^{\#}P < 0.01$ vs. IL-18 + β-GP group. ALP, alkaline phosphatase; BMP-2, bone morphogenetic protein-2; β-GP, β-glycerol phosphate.

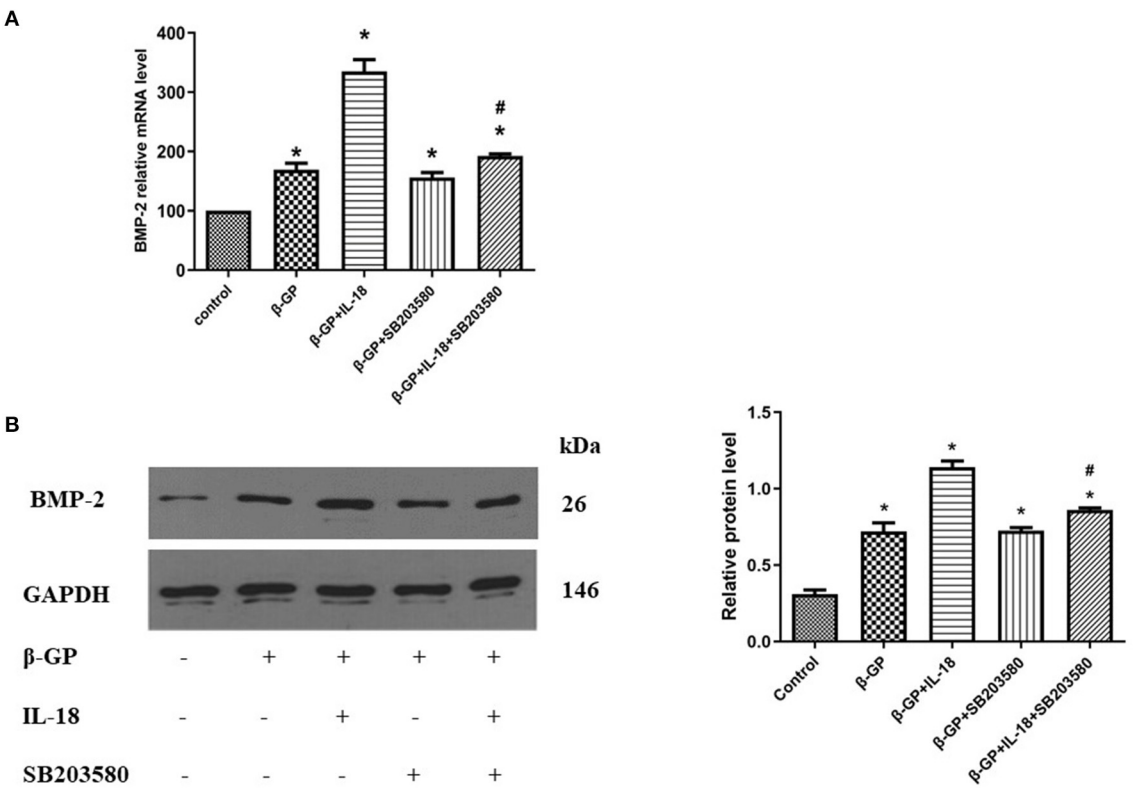

FIGURE 10 | Effect of p38 pathway on IL-18-induced osteogenic phenotypic transformation of rat VSMCs. **(A)** Effect of p38 pathway on the BMP-2 mRNA expression of rat VSMCs after IL-18 intervention. **(B)** Effect of p38 signal pathway on the BMP-2 protein expression of rat VSMCs after IL-18 intervention. Rat VSMCs were pre-incubated with p38 inhibitor SB203580 (10 μmol/L) for 2 h, and then treated with β-GP (10 mmol/L) or IL-18 (100 ng/ml) + β-GP (10 mmol/L) for 14 days, respectively. The experiment was repeated 3 times independently. $^{*}P < 0.01$ vs. control group; $^{\#}P < 0.01$ vs. IL-18 + β-GP group. BMP-2, bone morphogenetic protein-2; β-GP, β-glycerol phosphate.

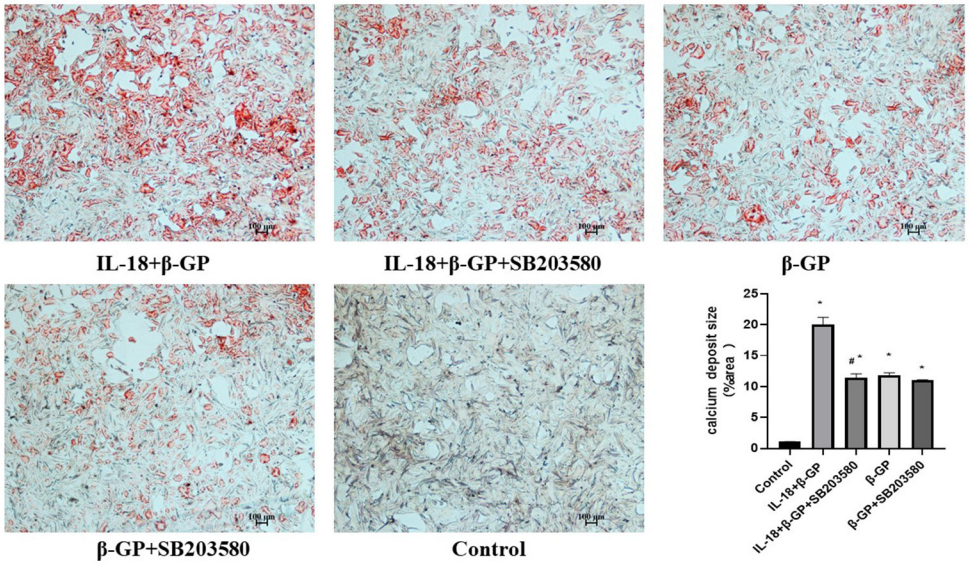

FIGURE 11 | Alizarin red staining of VSMCs. Effect of p38 pathway on IL-18-induced calcium deposition of rat VSMCs. Rat VSMCs were pre-incubated with p38 inhibitor SB203580 (10 μmol/L) for 2 h, and then treated with β-GP (10 mmol/L) or IL-18 (100 ng/ml) + β-GP (10 mmol/L) for 14 days, respectively. The experiment was repeated 3 times independently. $^{*}P < 0.01$ vs. control group; $^{\#}P < 0.01$ vs. IL-18 + β-GP group. β-GP, β-glycerol phosphate.

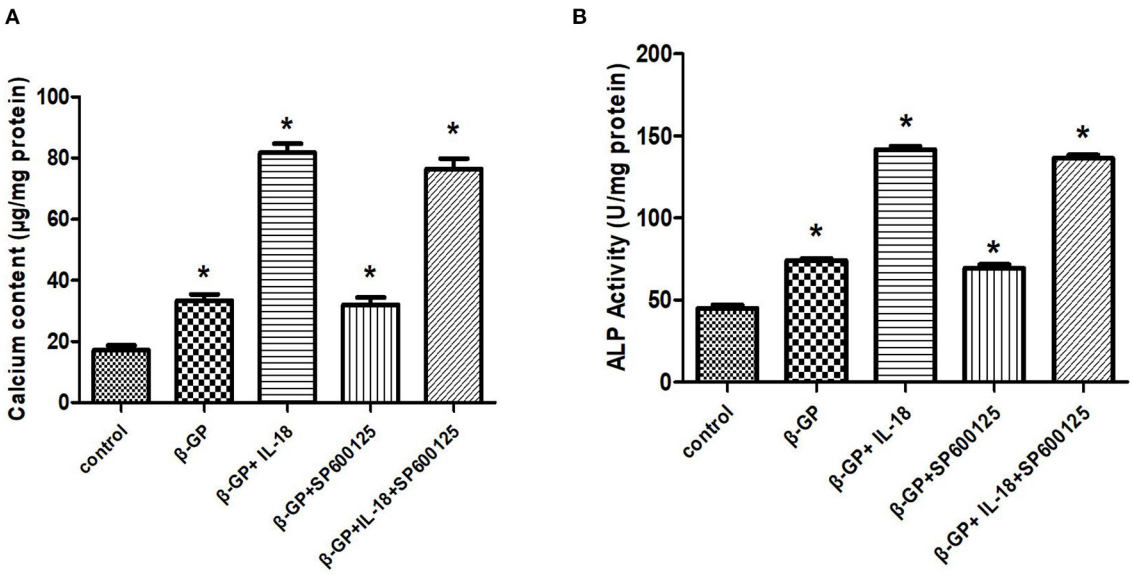

FIGURE 12 | Effect of JNK pathway on IL-18-induced calcification of rat VSMCs. **(A)** Effect of JNK pathway on calcium content of rat VSMCs after IL-18 intervention. **(B)** Effect of JNK pathway on ALP activity of rat VSMCs after IL-18 intervention. Rat VSMCs were pre-incubated with JNK inhibitor SP600125 (10 μmol/L) for 30 min, and then treated with β-GP (10 mmol/L) or IL-18 (100 ng/ml) + β-GP (10 mmol/L) for 14 days, respectively. The experiment was repeated 3 times independently. $^{*}P <$ 0.01 vs. control group. ALP, alkaline phosphatase; BMP-2, bone morphogenetic protein-2; β-GP, β-glycerol phosphate.

Some studies have confirmed that IL-18 is an important inflammatory marker of MetS, which is involved in regulating the development of MetS. In addition, studies have also shown that IL-18 is closely related to obesity and is one of the important regulators of obesity-related inflammation (32, 33). Bruun and Jung et al. all proved that the IL-18 levels in adipose tissue and serum of obese subjects were significantly higher than those of control subjects (34, 35). Our previous study found that IL-18 can induce calcification of VSMCs (7). However, whether IL-18 is involved in the regulation of VC in CRF patients with obesity has not been reported yet. This study indicated that the serum IL-18 levels of CRF rats fed with high-fat diet and a regular diet

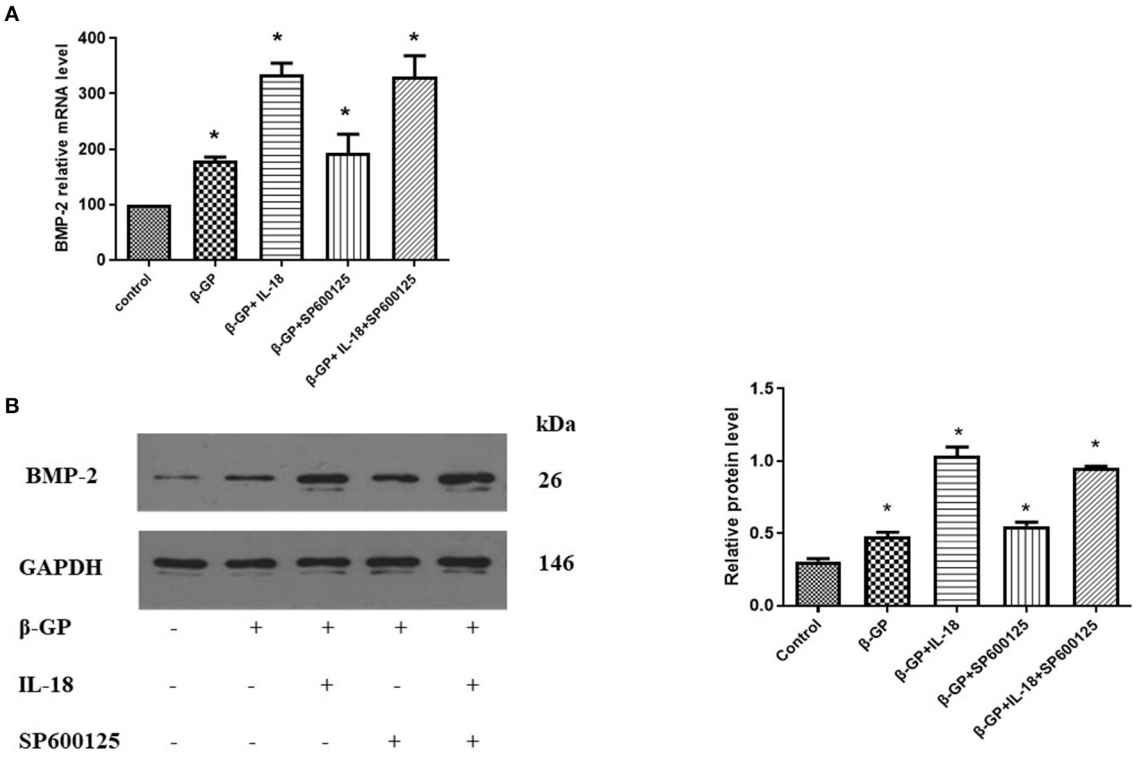

FIGURE 13 | Effect of JNK pathway on IL-18-induced osteogenic phenotypic transformation of rat VSMCs. **(A)** Effect of JNK pathway on the expression of BMP-2 mRNA of rat VSMCs after IL-18 intervention. **(B)** Effect of JNK pathway on the expression of BMP-2 protein of rat VSMCs after IL-18 intervention. Rat VSMCs were pre-incubated with JNK inhibitor SP600125 (10 μmol/L) for 30 min, and then treated with β-GP (10 mmol/L) or IL-18 (100 ng/ml) + β-GP (10 mmol/L) for 14 days, respectively. The experiment was repeated 3 times independently. *$P < 0.01$ vs. control group. BMP-2, bone morphogenetic protein-2; β-GP, β-glycerol phosphate.

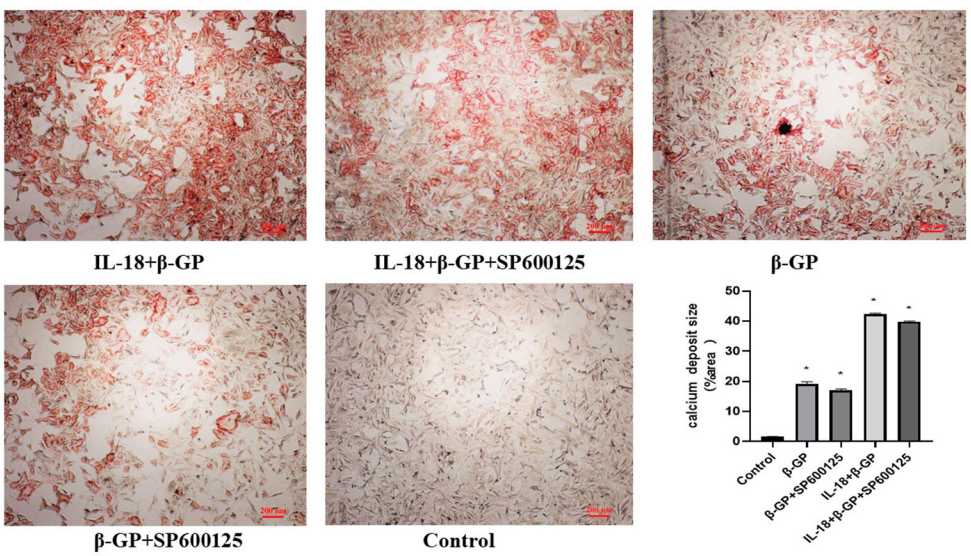

FIGURE 14 | Alizarin red staining of VSMCs. Effect of JNK pathway on IL-18-induced calcium deposition of rat VSMCs. Rat VSMCs were pre-incubated with JNK inhibitor SP600125 (10 μmol/L) for 30 min, and then treated with β-GP (10 mmol/L) or IL-18 (100 ng/ml) + β-GP (10 mmol/L) for 14 days, respectively. And then the VSMCs were stained with Alizarin red. The experiment was repeated 3 times independently. *$P < 0.01$ vs. control group. β-GP, β-glycerol phosphate.

both showed an increasing trend with time, and the serum IL-18 levels of these two groups were significantly higher than the sham-operated group. Moreover, the postoperative serum IL-18 level of CRF rats fed with high-fat diet was significantly higher than that of CRF rats fed with conventional diet, which indicated that obesity caused by high-fat diet can further upregulate serum IL-18 levels in CRF rats. We further analyzed the correlation between serum IL-18 level and VC. The results suggest that the serum IL-18 level of rats is positively correlated with the aortic calcium content, indicating that as the serum IL-18 level increases, the degree of aortic calcification is aggravated. However, the mechanism by which IL-18 regulates the formation of VC is not yet clear and needs to be further explored.

Previous studies have proved that in patients with CRF, the levels of serum CRP, IL-6 and other inflammatory factors are positively correlated with the degree of coronary artery calcification (27, 36). In addition, a large number of *in vivo* and *in vitro* studies have also shown that inflammatory factors can induce the transformation of VSMCs into osteoblast phenotypes, and then promote VSMCs calcification (37, 38). Therefore, inflammation is considered to be an important regulator of VC. In our study, it was proved that the up-regulation of inflammatory factor levels in CRF rats fed with high-fat diet had a close correlation with the development of VC. And this results further indicated that obesity-related inflammation induced by high-fat diet might be an important regulator of VC in CRF rats.

The MAPK signaling pathway is a type of serine/threonine protein kinase that exists widely in mammals, which can be activated by a series of extracellular signals or stimuli. The JNK and p38 pathways are two main members of the MAPK signaling pathway. Previous studies had proved that IL-18 could cause different biological effects by activating the JNK and p38 signaling pathways (21, 22, 39), suggesting that the MAPK pathways might be the important downstream pathways for IL-18. Our research also showed that IL-18 could promote the expression of JNK and P38 pathway phosphorylated proteins in rat VSMCs, indicating that IL-18 could induce biological effects by activating the MAPK pathways in rat VSMCs. The results of Takahisa et al. showed that advanced glycation end products could promote VSMCs calcification by activating the p38 pathway (40). Our research also found that the p38 signaling pathway blocker SB203580 can significantly reduce the calcium content, ALP activity and BMP-2 expression of rat VSMCs induced by IL-18. The P38 signaling pathway is not only involved in the regulation of cell proliferation and survival (41), but also plays a key role in immune and inflammatory responses (42). The above results indicated that the p38 signal transduction pathway is also involved in the regulation of IL-18 to promote the process of osteoblast differentiation and calcification of VSMCs. OPG is one of the osteoblast transcription factors closely related to VC. The study by McCarthy et al. found that the effect of PDGF on osteoblast cell lines to produce OPG is regulated by p38 signaling pathways, but not affected by the JNK signaling pathway (43). Although the results of this study found that IL-18 can also activate the JNK signaling pathway, blocking the JNK pathway has no significant effect on VSMCs calcification induced by IL-18, which suggested that the JNK signaling pathway might not be involved in regulation the process of IL-18-induced VC. Although different MAPK pathways of have similar cascade reactions, the biological effects produced by different extracellular activation signals are not completely the same.

In summary, it was demonstrated that obesity-related inflammation induced by high-fat diet could elevate serum IL-18 levels and exacerbate VC in CRF rats. Furthermore, serum IL-18 level had a positive correlation with the degree of VC. It is also found that IL-18 promoted osteogenic differentiation and calcification of rat VSMCs via p38 pathway activation.

DATA AVAILABILITY STATEMENT

The raw data supporting the conclusions of this article will be made available by the authors, without undue reservation.

ETHICS STATEMENT

The animal study was reviewed and approved by Committee on Ethics of Animal Experiments of Sun Yat-sen University.

AUTHOR CONTRIBUTIONS

YiZ is mainly responsible for experimental design and article writing. HH and JW are responsible for guiding the implementation of the research and the revision of the article. KZ and LZ is responsible for the implementation of animal experiments. YuZ is responsible for data statistical analysis and article revision. All authors contributed to the article and approved the submitted version.

FUNDING

This work was supported by National Natural Science Foundation of China (81900443), Fund for Basic and Applied Basic Research of Guangdong Province (2018A030313749) and PhD Natural Sciences Startup Foundation of Guangdong (2017A030310230) to YiZ.

REFERENCES

1. Goodman WG, Goldin J, Kuizon BD, Yoon C, Gales B, Sider D, et al. Coronary-artery calcification in young adults with end-stage renal disease who are undergoing dialysis. *N Engl J Med.* (2000) 342:1478–83. doi: 10.1056/NEJM200005183422003
2. Fadini GP, Albiero M, Menegazzo L, Boscaro E, Vigili de Kreutzenberg S, Agostini C, et al. Widespread increase in myeloid calcifying cells contributes to ectopic vascular calcification in type 2 diabetes. *Circ Res.* (2011) 108:1112–21. doi: 10.1161/CIRCRESAHA.110.234088
3. Shanahan CM, Crouthamel MH, Kapustin A, Giachelli CM. Arterial calcification in chronic kidney disease: key roles for calcium and phosphate. *Circ Res.* (2011) 109:697–711. doi: 10.1161/CIRCRESAHA.110.234914

4. Duhn V, D'Orsi ET, Johnson S, D'Orsi CJ, Adams AL, O'Neill WC. Breast arterial calcification: a marker of medial vascular calcification in chronic kidney disease. *Clin J Am Soc Nephrol.* (2011) 6:377–82. doi: 10.2215/CJN.07190810
5. Orita Y, Yamamoto H, Kohno N, Sugihara M, Honda H, Kawamata S, et al. Role of osteoprotegerin in arterial calcification: development of new animal model. *Arterioscler Thromb Vasc Biol.* (2007) 27:2058–64. doi: 10.1161/ATVBAHA.107.147868
6. Li JJ, Zhu CG, Yu B, Liu YX, Yu MY. The role of inflammation in coronary artery calcification. *Ageing Res Rev.* (2007) 6:263–70. doi: 10.1016/j.arr.2007.09.001
7. Zhang K, Zhang Y, Feng W, Chen R, Chen J, Touyz RM, et al. Interleukin-18 enhances vascular calcification and osteogenic differentiation of vascular smooth muscle cells through TRPM7 activation. *Arterioscler Thromb Vasc Biol.* (2017) 37:1933–43. doi: 10.1161/ATVBAHA.117.309161
8. Gracie JA, Robertson SE, McInnes IB. Interleukin-18. *J Leukoc Biol.* (2003) 73:213–24. doi: 10.1189/jlb.0602313
9. Chiang CK, Hsu SP, Pai MF, Peng YS, Ho TI, Liu SH, et al. Plasma interleukin-18 levels in chronic renal failure and continuous ambulatory peritoneal dialysis. *Blood Purif.* (2005) 23:144–8. doi: 10.1159/000083620
10. Lonnemann G, Novick D, Rubinstein M, Dinarello CA. Interleukin-18, interleukin-18 binding protein and impaired production of interferon-gamma in chronic renal failure. *Clin Nephrol.* (2003) 60:327–34. doi: 10.5414/CNP60327
11. Wang YC, McPherson K, Marsh T, Gortmaker SL, Brown M. Health and economic burden of the projected obesity trends in the USA and the UK. *Lancet.* (2011) 378:815–25. doi: 10.1016/S0140-6736(11)60814-3
12. Chen J, Muntner P, Hamm LL, Jones DW, Batuman V, Fonseca V, et al. The metabolic syndrome and chronic kidney disease in U.S. adults. *Ann Intern Med.* (2004) 140:167–74. doi: 10.7326/0003-4819-140-3-200402030-00007
13. Chen J, Gu D, Chen CS, Wu X, Hamm LL, Muntner P, et al. Association between the metabolic syndrome and chronic kidney disease in Chinese adults. *Nephrol Dial Transplant.* (2007) 22:1100–6. doi: 10.1093/ndt/gfl759
14. Cao H. Adipocytokines in obesity and metabolic disease. *J Endocrinol.* (2014) 220:T47–59. doi: 10.1530/JOE-13-0339
15. Zhang Y, Chen J, Zhang K, Kong M, Wang T, Chen R, et al. Inflammation and oxidative stress are associated with the prevalence of high aankle-brachial index in metabolic syndrome patients without chronic renal failure. *Int J Med Sci.* (2013) 10:183–90. doi: 10.7150/ijms.5308
16. Zhang Y, Chen J, Zhang K, Wang T, Kong M, Chen R, et al. Combination of high ankle-brachial index and hard coronary heart disease framingham risk score in predicting the risk of ischemic stroke in general population. *PLoS ONE.* (2014) 9:e106251. doi: 10.1371/journal.pone.0106251
17. Arend WP, Palmer G, Gabay C. IL-1, IL-18, and IL-33 families of cytokines. *Immunol Rev.* (2008) 223:20–38. doi: 10.1111/j.1600-065X.2008.00624.x
18. Ge C, Xiao G, Jiang D, Franceschi RT. Critical role of the extracellular signal-regulated kinase-MAPK pathway in osteoblast differentiation and skeletal development. *J Cell Biol.* (2007) 176:709–18. doi: 10.1083/jcb.200610046
19. Gu X, Masters KS. Role of the MAPK/ERK pathway in valvular interstitial cell calcification. *Am J Physiol Heart Circ Physiol.* (2009) 296:H1748–57. doi: 10.1152/ajpheart.00099.2009
20. Ding HT, Wang CG, Zhang TL, Wang K. Fibronectin enhances *in vitro* vascular calcification by promoting osteoblastic differentiation of vascular smooth muscle cells via ERK pathway. *J Cell Biochem.* (2006) 99:1343–52. doi: 10.1002/jcb.20999
21. Amin MA, Rabquer BJ, Mansfield PJ, Ruth JH, Marotte H, Haas CS, et al. Interleukin 18 induces angiogenesis *in vitro* and *in vivo* via Src and Jnk kinases. *Ann Rheum Dis.* (2010) 69:2204–12. doi: 10.1136/ard.2009.127241
22. Koutoulaki A, Langley M, Sloan AJ, Aeschlimann D, Wei XQ. TNFalpha and TGF-beta1 influence IL-18-induced IFNgamma production through regulation of IL-18 receptor and T-bet expression. *Cytokine.* (2010) 49:177–84. doi: 10.1016/j.cyto.2009.09.015
23. Suga T, Iso T, Shimizu T, Tanaka T, Yamagishi S, Takeuchi M, et al. Activation of receptor for advanced glycation end products induces osteogenic differentiation of vascular smooth muscle cells. *J Atheroscler Thromb.* (2011) 18:670–83. doi: 10.5551/jat.7120
24. Li GZ, Jiang W, Zhao J, Pan CS, Cao J, Tang CS, et al. Ghrelin blunted vascular calcification *in vivo* and *in vitro* in rats. *Regul Pept.* (2005) 129:167–76. doi: 10.1016/j.regpep.2005.02.015
25. Johnson RC, Leopold JA, Loscalzo J. Vascular calcification: pathobiological mechanisms and clinical implications. *Circ Res.* (2006) 99:1044–59. doi: 10.1161/01.RES.0000249379.55535.21
26. Barbieri D, Goicoechea M, Garcia-Prieto A, Delgado A, Verde E, Verdalles U, et al. Obesity related risk for chronic kidney disease progression and cardiovascular disease after propensity score matching. *Hipertens Riesgo Vasc.* (2021) 38:63–71. doi: 10.1016/j.hipert.2020.09.004
27. Krasniak A, Drozdz M, Pasowicz M, Chmiel G, Michalek M, Szumilak D, et al. Factors involved in vascular calcification and atherosclerosis in maintenance haemodialysis patients. *Nephrol Dial Transplant.* (2007) 22:515–21. doi: 10.1093/ndt/gfl564
28. Kim HG, Song SW, Kim TY, Kim YO. Risk factors for progression of aortic arch calcification in patients on maintenance hemodialysis and peritoneal dialysis. *Hemodial Int.* (2011) 15:460–7. doi: 10.1111/j.1542-4758.2011.00571.x
29. Kim J, Bhattacharjee R, Kheirandish-Gozal L, Khalyfa A, Sans Capdevila O, Tauman R, et al. Insulin sensitivity, serum lipids, and systemic inflammatory markers in school-aged obese and nonobese children. *Int J Pediatr.* (2010) 2010:846098. doi: 10.1155/2010/846098
30. Das UN. Is obesity an inflammatory condition? *Nutrition.* (2001) 17:953–66. doi: 10.1016/S0899-9007(01)00672-4
31. Antuna-Puente B, Feve B, Fellahi S, Bastard JP. Adipokines: the missing link between insulin resistance and obesity. *Diabetes Metab.* (2008) 34:2–11. doi: 10.1016/j.diabet.2007.09.004
32. Weiss TW, Arnesen H, Troseid M, Kaun C, Hjerkinn EM, Huber K, et al. Adipose tissue expression of interleukin-18 mRNA is elevated in subjects with metabolic syndrome and independently associated with fasting glucose. *Wien Klin Wochenschr.* (2011) 123:650–4. doi: 10.1007/s00508-011-0028-6
33. Yamaoka-Tojo M, Tojo T, Wakaume K, Kameda R, Nemoto S, Takahira N, et al. Circulating interleukin-18: a specific biomarker for atherosclerosis-prone patients with metabolic syndrome. *Nutr Metab.* (2011) 8:3. doi: 10.1186/1743-7075-8-3
34. Jung C, Gerdes N, Fritzenwanger M, Figulla HR. Circulating levels of interleukin-1 family cytokines in overweight adolescents. *Med Inflamm.* (2010) 2010:958403. doi: 10.1155/2010/958403
35. Bruun JM, Stallknecht B, Helge JW, Richelsen B. Interleukin-18 in plasma and adipose tissue: effects of obesity, insulin resistance, and weight loss. *Eur J Endocrinol.* (2007) 157:465–71. doi: 10.1530/EJE-07-0206
36. Stompor T, Pasowicz M, Sullowicz W, Dembinska-Kiec A, Janda K, Wojcik K, et al. An association between coronary artery calcification score, lipid profile, and selected markers of chronic inflammation in ESRD patients treated with peritoneal dialysis. *Am J Kidney Dis.* (2003) 41:203–11. doi: 10.1053/ajkd.2003.50005
37. Al-Aly Z, Shao JS, Lai CF, Huang E, Cai J, Behrmann A, et al. Aortic Msx2-Wnt calcification cascade is regulated by TNF-alpha-dependent signals in diabetic Ldlr-/- mice. *Arterioscler Thromb Vasc Biol.* (2007) 27:2589–96. doi: 10.1161/ATVBAHA.107.153668
38. Bostrom K. Proinflammatory vascular calcification. *Circ Res.* (2005) 96:1219–20. doi: 10.1161/01.RES.0000172407.20974.e5
39. Reddy VS, Prabhu SD, Mummidi S, Valente AJ, Venkatesan B, Shanmugam P, et al. Interleukin-18 induces EMMPRIN expression in primary cardiomyocytes via JNK/Sp1 signaling and MMP-9 in part via EMMPRIN and through AP-1 and NF-kappaB activation. *Am J Physiol Heart Circ Physiol.* (2010) 299:H1242–54. doi: 10.1152/ajpheart.00451.2010
40. Tanikawa T, Okada Y, Tanikawa R, Tanaka Y. Advanced glycation end products induce calcification of vascular smooth muscle cells through RAGE/p38 MAPK. *J Vasc Res.* (2009) 46:572–80. doi: 10.1159/000226225
41. Thornton TM, Rincon M. Non-classical p38 map kinase functions: cell cycle checkpoints and survival. *Int J Biol Sci.* (2009) 5:44–51. doi: 10.7150/ijbs.5.44
42. Cuadrado A, Nebreda AR. Mechanisms and functions of p38 MAPK signalling. *Biochem J.* (2010) 429:403–17. doi: 10.1042/BJ20100323

43. McCarthy HS, Williams JH, Davie MW, Marshall MJ. Platelet-derived growth factor stimulates osteoprotegerin production in osteoblastic cells. *J Cell Physiol.* (2009) 218:350–4. doi: 10.1002/jcp.21600

Conflict of Interest: The authors declare that the research was conducted in the absence of any commercial or financial relationships that could be construed as a potential conflict of interest.

Publisher's Note: All claims expressed in this article are solely those of the authors and do not necessarily represent those of their affiliated organizations, or those of the publisher, the editors and the reviewers. Any product that may be evaluated in this article, or claim that may be made by its manufacturer, is not guaranteed or endorsed by the publisher.

Copyright © 2021 Zhang, Zhang, Zhang, Zhou, Huang and Wang. This is an open-access article distributed under the terms of the Creative Commons Attribution License (CC BY). The use, distribution or reproduction in other forums is permitted, provided the original author(s) and the copyright owner(s) are credited and that the original publication in this journal is cited, in accordance with accepted academic practice. No use, distribution or reproduction is permitted which does not comply with these terms.

frontiers in Cardiovascular Medicine

ORIGINAL RESEARCH
published: 30 November 2021
doi: 10.3389/fcvm.2021.768662

17β-Estradiol Inhibits Proliferation and Oxidative Stress in Vascular Smooth Muscle Cells by Upregulating BHLHE40 Expression

Dan-dan Feng[1], Bin Zheng[1], Jing Yu[1,2], Man-li Zhang[1,3], Ying Ma[1,4], Xiao Hao[1], Jin-kun Wen[1] and Xin-hua Zhang[1]**

[1] Ministry of Education of China, The Key Laboratory of Neural and Vascular Biology, Department of Biochemistry and Molecular Biology, Hebei Medical University, Shijiazhuang, China, [2] The Second Department of Respiratory and Critical Care Medicine, The Second Hospital of Hebei Medical University, Shijiazhuang, China, [3] Department of Critical Care Medicine, The Second Hospital of Hebei Medical University, Shijiazhuang, China, [4] Department of Biochemistry and Molecular Biology, Binzhou Medical University, Yantai, China

Background: Intimal hyperplasia is a major complication of restenosis after angioplasty. The abnormal proliferation and oxidative stress of vascular smooth muscle cells (VSMCs) are the basic pathological feature of neointimal hyperplasia. 17β-Estradiol can inhibit VSMCs proliferation and inflammation. However, it is still unclear whether and how 17β-Estradiol affects intimal hyperplasia.

Methods: The neointima hyperplasia was observed by hematoxylin/eosin staining. The expression of PCNA, cyclin D1, NOX1, NOX4 and $p47^{phox}$ in neointima hyperplasia tissues and VSMCs was determined by qRT-PCR and Western blotting. MTS assay, cell counting and EdU staining were performed to detect cells proliferation. The oxidative stress was assessed by ROS staining.

Results: 17β-Estradiol suppressed carotid artery ligation-induced intimal hyperplasia, which is accompanied by an increase of BHLHE40 level. Furthermore, loss- and gain-of-function experiments revealed that BHLHE40 knockdown promotes, whereas BHLHE40 overexpression inhibits TNF-α-induced VSMC proliferation and oxidative stress. 17β-Estradiol inhibited TNF-α-induced VSMC proliferation and oxidative stress by promoting BHLHE40 expression, thereby suppressing MAPK signaling pathways. In addition, enforcing the expression of BHLHE40 leads to amelioration of intimal hyperplasia.

Conclusions: Our study demonstrates that 17β-Estradiol inhibits proliferation and oxidative stress *in vivo* and *in vitro* by promotion of BHLHE40 expression.

Keywords: 17β-Estradiol, VSMCs, BHLHE40, proliferation, oxidative stress

OPEN ACCESS

Edited by:
Zhen Yang,
The First Affiliated Hospital of Sun Yat-sen University, China

Reviewed by:
Jianyun Yan,
Southern Medical University, China
Kun Wang,
Qingdao University, China

***Correspondence:**
Jin-kun Wen
wjk@hebmu.edu.cn
Xin-hua Zhang
xiaomifeng800815@126.com

Specialty section:
This article was submitted to General Cardiovascular Medicine, a section of the journal Frontiers in Cardiovascular Medicine

Received: *01 September 2021*
Accepted: *01 November 2021*
Published: *30 November 2021*

Citation:
Feng D-d, Zheng B, Yu J, Zhang M-l, Ma Y, Hao X, Wen J-k and Zhang X-h (2021) 17β-Estradiol Inhibits Proliferation and Oxidative Stress in Vascular Smooth Muscle Cells by Upregulating BHLHE40 Expression. Front. Cardiovasc. Med. 8:768662. doi: 10.3389/fcvm.2021.768662

INTRODUCTION

Vascular smooth muscle cell (VSMC), which plays a crucial role in maintaining vascular structure and function, is mainly subsistence in the medial layer of the blood vessel wall (1). Nevertheless, abnormal VSMC proliferation, migration, inflammation or oxidative stress could lead to vascular remodeling, which contributes to the development of a series of vascular diseases, such as

atherosclerosis, hypertension and post-angioplasty restenosis (2, 3). Tumor Necrosis Factor-α (TNF-α) is one of the cytokines which are involved in systemic inflammation. It is reported that TNF-α greatly induces VSMC proliferation and takes part in the formation of neointimal in response to vascular injury (4, 5). Therefore, inhibiting TNF-α signaling may be a useful method for preventing cardiovascular diseases.

Class E basic helix-loop-helix protein 40 (BHLHE40) has been proposed as a transcriptional repressor, which negatively regulates the activity of the clock genes (6). The BHLHE40 protein is widely expressed in a variety of human tissues. Researchers demonstrate that BHLHE40 is closely involved in many kinds of biological processes like cell proliferation, senescence, inflammation and oxidative stress (7–10). A previous study showed that BHLHE40 inhibits high glucose–induced calcification/senescence by directly binding to the promoter region of lncRNA-ES3 in HA-VSMC (11). In addition, multiple reports provide strong support for the association between BHLHE40 and oxidative stress (12). In myogenic cells, downregulation of BHLHE40 significantly reduces mitochondrial efficiency, resulting in the burst of ROS (13). Increased ROS production is integral to hypertension and atherosclerosis burden in mouse, rat and human arteries (14–16). However, whether BHLHE40 participates in the regulation of vascular remodeling is largely unknown. Here we explored the function of BHLHE40 in ligation injury-induced intimal hyperplasia, providing causative evidence that proliferation and oxidative stress were negatively regulated by BHLHE40 protein in VSMC.

17β-Estradiol (E2), an endogenous estrogen secreted by the ovaries of women, plays a vasoprotective role through regulating injury-induced chemokine expression and leukocyte infiltration (17). Previous studies have shown that E2 prevents the formation of atherosclerosis by inhibiting the proliferation and inflammation of VSMC (18). Besides, E2 contributes to reducing in-stent restenosis in porcine coronary injury models via suppressing smooth muscle cells proliferation and improving vascular re-endothelialization (19). Furthermore, it has been known that estrogen treatment can effectively increase the interaction of ERα with NF-κB p50, and reduce the interaction of KLF5 with NF-κB p50 induced by high glucose, thereby inhibiting inflammatory response in VSMC (20). It is therefore significant to gain mechanistic insights into how E2 and VSMC proliferation/oxidative stress are involved in vascular remodeling.

In this study, we identify that E2 exerts a protective effect on carotid artery ligation by regulating BHLHE40 expression. Additionally, we find that the up-expression of BHLHE40 in VSMC results in the suppression of MAPK signaling pathway. Taken together, our findings provide potential therapeutic targets for restenosis.

MATERIALS AND METHODS

Animal Model and Treatment

Animal experiments were approved by the Institutional Animal Care and Use Committee of Hebei Medical University (approval ID: HebMU 20080026). Eight-week-old C57BL/6N male mice were purchased from Vital River Laboratory Animal Technology Co., Ltd., (Beijing, China). Animals were housed in a climatically controlled environment, on a 12 h light/dark cycle, with free access to water and standard food *ad libitum*.

The mice carotid artery ligation model applied has been described previously (21). Briefly, C57BL/6N male mice were anesthetized with 1.5% isoflurane. The left common carotid arteries were exposed and completely ligated with a 6–0 silk suture under the left carotid artery bifurcation to induce intima formation. The silk suture was passed below the exposed left carotid artery but not tightened as the control ($n = 10$). E2 (Sigma, 50-28-2, Purity ≥98%) (0.02 $mg{\cdot}kg^{-1}{\cdot}day^{-1}$) was infused through subcutaneous osmotic minipump (Alzet, Model 2004, USA) implantation 7 days before ligation injury and continuing for 14 days thereafter ($n = 10$). Ligated animals without E2 treatment received DMSO and corn oil at an equivalent amount ($n = 10$). The pcDNA3.1-BHLHE40 plasmids ($n = 10$) or pcDNA3.1-vehicle plasmids ($n = 10$) were diluted with Entranster^{TM} solution (Engreen Biosystem, Beijing, China) and 10% glucose mixture (1:1 v/v) to 0.5 μg/μL *in vivo*. Then, added 10 μL aforesaid mixture into the 90 μL of 20% F-127 pluronic gel (Sigma, 9003-11-6) at 4°C for 2 h. Immediately after ligation, the exposed carotid artery adventitial surface was treated with 100 μL pluronic gel containing plasmids. At 14 days after surgery, all animals were anesthetized and perfused with cold PBS, and tissues were harvested for follow-up experiments.

Hematoxylin and Eosin (HE) Staining

For morphometric analyses, the arteries were fixed with 4% paraformaldehyde and embedded in paraffin. Four μm cross-sections were cut from the proximal carotid ligation site and prepared for hematoxylin and eosin (HE) staining. For each section, six random non-contiguous microscopic fields were analyzed. The neointimal area and intima-to-media ratio were calculated using Image-Pro Plus Analyzer (version 5.1) software (Media Cybernetics, Silver Spring, MD) in a blinded manner.

Cell Culture and Treatment

Mouse aortic vascular smooth muscle cell (mVSMC) (ATCC, No. CRL-2797^{TM}) were cultured in low-glucose Dulbecco's modified Eagle's medium (DMEM, Gibco Life Technologies, Rockville, MD) supplemented with 10% fetal bovine serum (GEMINI, USA) and 1 × Penicillin-Streptomycin-Glutamine (Gbico, USA), containing 100 units/mL of penicillin and 100 μg/mL of streptomycin, cultured at 37°C with 5% CO_2 atmosphere. VSMCs were blocked by incubation in serum-deprived DMEM at 80–90% confluence or 24 h before stimulated with TNF-α or E2.

Cell Transfection

siRNAs targeting mouse BHLHE40 (si-BHLHE40) and negative control (si-Ctrl) were designed and synthesized by GenePharma

(Shanghai, China). The siRNA sequences used in our studies were as follows:

Name	Sequences 5′to 3′
BHLHE40	Sense: GGAGAACGUGUCAGCACAATT
	Antisense:UUGUGCUGACACGUUCUCCTT
Control	Sense: UUCUCCGAACGUGUCACGUTT
	Antisense:ACGUGACACGUUCGGAGAATT

The expression plasmids of BHLHE40 (pcDNA3.1-BHLHE40) were created by the placement of mouse BHLHE40 CDS region of mRNA into the pcDNA3.1 vector. The siRNAs or plasmids were transiently transfected into VSMC with Lipofectamine 2000 (*Invitrogen*) according to the manufacturer's protocols.

Cell Counting

The cell number was determined by Countess^{TM} Automated Cell Counter (*Invitrogen*). After different treatment, VSMCs were digested, resuspended and blown into its individual tube. Ten μL of the cell suspension was mixed with 10 μL of Trypan blue, and counted by an *Invitrogen* Countess. Untreated cells were used for the baseline count. Each sample was counted three times, and the average value from triplicate experiments was measured.

MTS Assay

Cell viability was determined using the MTS assay, as previously described (22). In brief, 1×10^{4} cells/well were seeded into 96-well plates with 5 replicates for each group, The next day, the cells were pretreated in 100 μL serum-free medium for 24 h and then incubated with appropriate treatment. The cells were incubated with CellTiter 96 AQueous One Solution (Promega, G3582) for 3 h, and the absorbance at 490 nm was measured using a Multiskan Spectrum (Thermo).

Isolation of RNA and Real-Time PCR

Total RNA was extracted from VSMC or mouse aortic tissues using Trizol (*Invitrogen*^{TM}) according to the manufacturer's instruction. The concentration and purity of the extracted RNA were detected by NanoDrop ND-2000 spectrophotometer (Thermo Fisher, Waltham, USA).cDNA was synthesized using an M-MLV First Strand Kit (Life Technologies) and real-time PCR analysis was done with the BIO-RAD CFX96^{TM} Real-Time System, using the Platinum SYBR Green qPCR SuperMix UDG Kit (*Invitrogen*). Relative mRNA expression levels were normalized to 18S. All PCRs were performed in triplicate. Relative amount of transcripts was calculated using the $2^{-\Delta\Delta Ct}$ formula.

The primer sequences were as follows:

Name	Sequences 5′to 3′
18s	Forward: CGCCGCTAGAGGTGAAATTC
	Reverse: CCAGTCGGCATCGTTTATGG
PCNA	Forward: GGAGAGCTTGGCAATGGGAA
	Reverse: TAGGAGACAGTGGAGTGGC
cyclin D1	Forward: TGCCATCCATGCGGAAA
	Reverse: AGCGGGAAGAACTCCTCTTC
NOX1	Forward: GTGCCTTTGCCTGGTTCAACAAC
	Reverse: AGCCAGTGAGGAAGAGACGGTAG
NOX4	Forward: CTGGAAGAACCCAAGTTCCA
	Reverse: CTGATGCATCGGTAAAGTCT
$p47^{phox}$	Forward: ATTCACCGAGATCTACGAGTTC
	Reverse: TGAAGTATTCAGTGAGAGTGCC
KLF4	Forward: CTAACCGTTGGCGTGAGGAACTC
	Reverse: TCTAGGTCCAGGAGGTCGTTGAAC
BHLHE40	Forward: GGAGAGGCGAGGTTACAGTG
	Reverse: AATGCCAGGCACATGACAAG

Immunofluorescence Staining

Immunofluorescence staining was performed on 4 μm paraffin cross-sections from mouse artery samples. The sections were deparaffinized with xylene and rehydrated, and then were permeabilized by incubation with 0.5% Triton X-100 in phosphate-buffered saline (PBS). Non-specific sites were blocked by incubation in 10% normal goat serum (710027, KPL, USA) for 30 min. Then the sections were incubated with primary antibodies at 4°C overnight. The primary antibodies were mouse anti-SMα-actin (sc-130617, Santa Cruz) and rabbit anti-BHLHE40 (NB100-1800, Novus). Secondary antibodies were rhodamine-labeled antibody to rabbit IgG (031506, KPL, USA) and fluorescein-labeled antibody to mouse IgG (021815, KPL, USA). Nuclei were stained with DAPI (0100-20, SouthernBiotech) in each experiment. Images were captured by confocal microscopy (DM6000 CFS, Leica) and processed by LAS AF software.

Immunohistochemistry

Immunohistochemical staining was visualized by use of an SPN-9001 Histostain^{TM}-SP kit (Zhongshan Goldenbridge Biotechnology, Beijing, China) according to the manufacturer's instruction. Paraffin cross-sections were deparaffinized with xylene and rehydrated in a graded ethanol series, and endogenous peroxidase activity was inhibited by incubation with 3% H_2O_2 for 30 min. Sections were blocked with 10% normal goat serum for 10 min and incubated overnight at 4°C with anti-BHLHE40 antibody (1:100 dilution, NOVUS, NB100-1800). After a PBS wash, sections were incubated with secondary antibody at 37°C for 30 min. Drops of horseradish enzyme labeled streptomycin were added for 15 min, washed with PBS for 5 min and three times and then DAB staining was performed under the ordinary light microscope. Sections were counterstained with hematoxylin to visualize nuclei.

ROS Assay

The intracellular ROS levels were measured following the instruction of Reactive Oxygen Species Assay Kit (Beyotime Biotechnology, China). Briefly, the cells were seeded in 12-well plates with microscope cover glasses and exposed to various treatments. The treated cells were loaded with 10 μM/L DCFH-DA at 37°C for 20 min. Subsequently, cells were washed with PBS three times and then observed using fluorescence microscopy (Olympus).

Western Blot Analysis

Protein was isolated from VSMC or aortic tissues as the manufacturer's instruction of RIPA Lysis Buffer (Solarbio, Beijing, China). Equal amounts of protein were electrophoresed on 10% SDS-PAGE and transferred onto a PVDF membrane (Millipore). Membranes were blocked with 5% milk in TBS-Tween-20 (TBST) for 1.5 h at 37°C and incubated overnight at 4°C with the following primary antibodies: anti-PCNA (1:1000, ab92552, Abcam), anti-cyclin D1 (1:1000, 60186-1-Ig, Proteintech), anti-NOX1 (1:500, DF8684, Affinity Biotech), anti-NOX4 (1:500, 14347-1-AP, Proteintech), anti-$p47^{phox}$ (1:1000, 4312, Cell Signaling Technology), anti-KLF4 (1:1000, GTX101509, GeneTex), anti-BHLHE40 (1:500, 17895-1-AP, Proteintech), anti-p44/42 MAPK (ERK1/2) (1:1000, 9102, Cell Signaling Technology), anti-phospho-p44/42 MAPK (ERK1/2) (Thr202/Tyr204) (1:1000, 4370, Cell Signaling Technology), anti-JNK (1:500, 9252, Cell Signaling Technology), anti-phospho-SAPK/JNK (Thr183/Tyr185) (1:500, 4668, Cell Signaling Technology), anti-p38 MAPK (1:500, 9212, Cell Signaling Technology), anti-phospho-p38 MAPK (Thr180/Tyr182) (1:500, 4511, Cell Signaling Technology) and anti-β-actin antibody (1:2000, ab6276, Abcam). Membranes were then incubated with secondary antibody (1:10000, Rockland) for 1.5 h at room temperature. At last, protein blots were treated with the Immobilon^{TM} western chemiluminescent HRP substrate (Millipore) and detected by ECL (enhanced chemiluminescence) Fusion Fx (Vilber Lourmat). Images were captured and processed by FusionCapt Advance Fx5 software (Vilber Lourmat).

EdU Incorporation Assay

The EdU incorporation assay was carried out according to the manufacturer's instruction (RiboBio, China). The representative images acquired by fluorescence microscope (Olympus). The cell proliferative rate was calculated as the proportion of Hoechst 33342-staining cells that incorporated EdU in 10 high-power fields per well.

Statistical Analysis

Data are expressed as the means ± S.E.M. of at least three independent experiments. All analyses were performed using GraphPad Prism 5.0 software (GraphPad Software, La Jolla, CA). Differences between two groups were analyzed by Student's *t*-test. For multiple comparisons or repeated measurements, ANOVA or repeated ANOVA followed by a Tukey's *post-hoc* test was used. A value of $p < 0.05$ was considered statistically significant.

RESULTS

E2 Significantly Decreases Neointimal Formation, Proliferation and Oxidative Stress Induced by Carotid Artery Ligation

HE staining showed that carotid arterial intima thickness was significantly increased in ligation injury-induced intimal hyperplasia mice models at 14 days post-operation. Compared with the ligated group, the degree of neointimal formation was obviously reduced in E2-treated group (**Figure 1A**). The ratio of intima to media (I/M ratio) and intimal area were dramatically lower in E2-treated group than that in the ligated group (**Figures 1B,C**). These results indicate that E2 can effectively inhibit neointimal formation induced by carotid artery ligation. Since it is known that ligation injury-induced intimal hyperplasia is closely related to VSMC proliferation and oxidative stress, we next investigate the effects of E2 on proliferation and oxidative stress-related genes expression in carotid arteries. Western blotting analysis revealed that vascular injury increased the expression of PCNA, cyclin D1, NOX1, NOX4 and $p47^{phox}$, whereas KLF4 expression was remarkably downregulated. Notably, carotid artery ligation-induced these changes were reversed by E2 ($10\,mg\cdot kg^{-1}\cdot day^{-1}$) treatment (**Figure 1D**). qRT-PCR analysis of PCNA, cyclin D1, NOX1, NOX4, $p47^{phox}$ and KLF4 expression was consistent with their expression of protein level (**Figure 1E**). Overall, these studies demonstrated E2 could alleviate vascular remodeling in intimal hyperplasia mice partly through limiting the proliferation and oxidative stress of VSMC.

E2 Inhibits TNF-α-Induced VSMC Proliferation and Oxidative Stress

Because it is known that TNF-α stimulates VSMC proliferation and oxidative stress, we sought to determine whether E2 suppressed neointimal hyperplasia through restraining TNF-α-induced VSMC proliferation and oxidative stress. As shown in **Figures 2A–D**, TNF-α treatment markedly increased VSMC viability and number in a dose and time-dependent manner by MTS assay and cell counting. Simultaneously, exposure of VSMC to TNF-α dose and time-dependently enhanced mRNA and protein expression of PCNA, cyclin D1, NOX1, NOX4 and $p47^{phox}$ (**Figures 2E–H**). Next, we detected the effects of E2 treatment on VSMC proliferation and oxidative stress induced by TNF-α. As shown by MTS assay and cell counting, treating VSMC with TNF-α (10 ng/mL) promoted cell proliferation in a time-dependent manner, whereas pretreatment of VSMC with 25, 50 and 100 nM of E2 for 6 h dose-dependently abrogated the inducing effects of TNF-α on VSMC viability and number (**Figures 2I,J**). Western blotting and qRT-PCR assay displayed that E2 offsets the up-regulation of PCNA, cyclinD1, NOX1, NOX4 and $p47^{phox}$ expression induced by TNF-α (**Figures 2K,L**). In addition, EdU staining proved that E2 reversed TNF-α-induced VSMC proliferation (**Figures 2M,N**). In **Figure 2O**, E2 also visibly blocked TNF-α-induced ROS

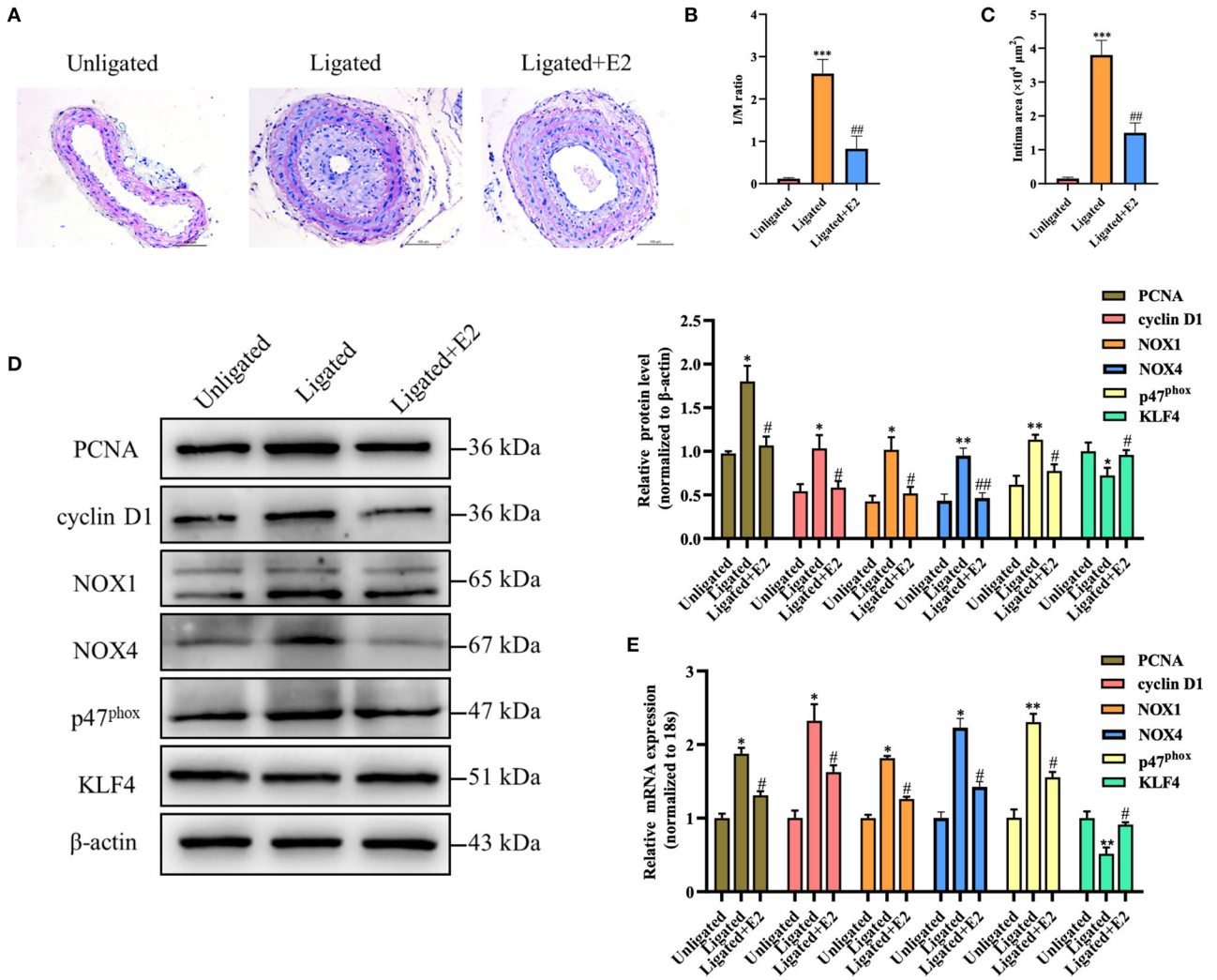

FIGURE 1 | E2 attenuates neointimal formation, proliferation and oxidative stress induced by carotid artery ligation. **(A)** Representative photomicrographs of the HE-stained sections of carotid arteries from unligated vessels, ligated vessels, and ligated vessels treated with E2 ($n = 4$). Scale bars = 100 μm. **(B,C)** Morphometric quantification of I/M ratio and the intima area in the different groups. $^{***}p < 0.001$ vs. Unligated group, $^{\#\#}p < 0.01$ vs. Ligated group. **(D)** PCNA, cyclin D1, NOX1, NOX4, p47^{phox} and KLF4 expression in unligated, ligated and ligated + E2-treated carotid arteries was detected by Western blotting. Statistic of band intensities is shown on the right ($n = 3$). $^{*}p < 0.05$ and $^{**}p < 0.01$ vs. Unligated group, $^{\#}p < 0.05$ and $^{\#\#}p < 0.01$ vs. Ligated group. **(E)** PCNA, cyclin D1, NOX1, NOX4, p47^{phox} and KLF4 expression in unligated, ligated and ligated + E2-treated carotid arteries was detected by qRT-PCR ($n = 3$). $^{*}p < 0.05$ and $^{**}p < 0.01$ vs. Unligated group, $^{\#}p < 0.05$ vs. Ligated group.

production in VSMC. In general, these results indicate that E2 inhibits TNF-α-induced VSMC proliferation and oxidative stress.

E2 Promotes the Expression of BHLHE40 Both *in vivo* and *in vitro*

In order to obtain which genes have been changed during neointimal hyperplasia, we downloaded an expression dataset (GSE56143) from the Gene Expression Omnibus (GEO), and found that the rhythm gene BHLHE40 was down-regulated in the ligated vascular tissue (**Figure 3A**). It has been reported that BHLHE40 can participate in the occurrence and development of cancer (23), but its role in the regulation of proliferation and oxidative stress in VSMC is still unclear. Therefore, we focused our research on BHLHE40. Western blotting and qRT-PCR assay showed that compared with unligated tissues, protein and mRNA expression levels of BHLHE40 were down-regulated by more than 0.5 times at 14 days after carotid artery ligation (**Figures 3B,C**). Furthermore, both immunofluorescence staining and immunochemistry staining of BHLHE40 were markedly reduced in injured arteries compared to sham-operation. Noticeably, carotid artery ligation-induced downregulation of BHLHE40 was reversed by E2 (**Figures 3D,E**). Western blotting (**Figure 3F**) and qRT-PCR assay (**Figure 3G**) revealed that TNF-α treatment lessened protein and mRNA expression of BHLHE40 compared with

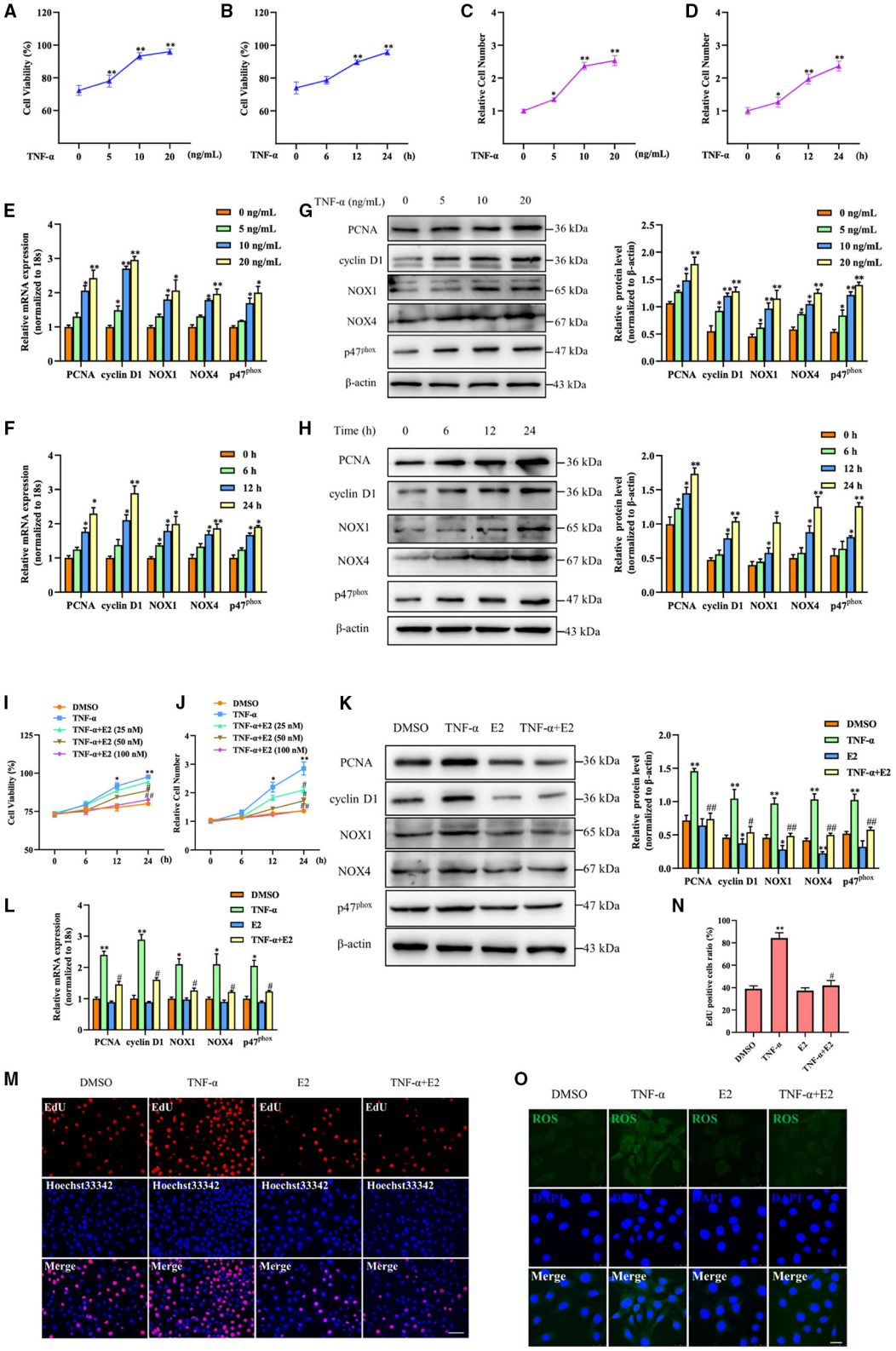

FIGURE 2 | E2 inhibits TNF-α-induced proliferation and oxidative stress in VSMC. **(A–H)** VSMCs were stimulated with TNF-α for indicated doses and times. The cell viability was determined by MTS assay **(A,B)**. *$p < 0.05$ and **$p < 0.01$ vs. untreated group, respectively. Cell counting was carried out using a Countess automated

(Continued)

FIGURE 2 | counter **(C,D)**. *$p < 0.05$ and **$p < 0.01$ vs. untreated group, respectively. qRT-PCR detected the mRNA expression of PCNA, cyclin D1, NOX1, NOX4 and p47^{phox} **(E,F)**. *$p < 0.05$ and **$p < 0.01$ vs. untreated group, respectively. Western blotting detected PCNA, cyclin D1, NOX1, NOX4 and p47^{phox} protein expression **(G,H)**. Statistic of band intensities is shown on the right. *$p < 0.05$ and **$p<0.01$ vs. untreated group, respectively. **(I,J)** VSMCs were pretreated with 25, 50 and 100 nM of E2 for 6 h and then were stimulated with TNF-α (10 ng/mL) for the indicated times. The cell viability was determined by MTS assay **(I)**, and cell counting was carried out using a Countess automated counter **(J)**. *$p < 0.05$ and **$p < 0.01$ vs. DMSO group, $^{\#}p < 0.05$ and $^{\#\#}p < 0.01$ vs. TNF-α group. **(K–O)** VSMCs were pretreated with E2 (100 nM) for 6 h and then were stimulated with TNF-α (10 ng/mL) for 24 h. PCNA, cyclin D1, NOX1, NOX4 and p47^{phox} expression was determined by Western blotting **(K)** and qRT-PCR **(L)**. Statistic of band intensities is shown on the right. *$p < 0.05$ and **$p < 0.01$ vs. DMSO group, $^{\#}p < 0.05$ and $^{\#\#}p < 0.01$ vs. TNF-α group. Cell proliferation was detected by EdU staining **(M)**. Scale bar = 100 μm. Analysis of the percentage of EdU positive cells **(N)**. **$p < 0.01$ vs. DMSO group, $^{\#}p < 0.05$ vs. TNF-α group. ROS levels were detected by DCFH-DA staining **(O)**. Scale bar = 25 μm.

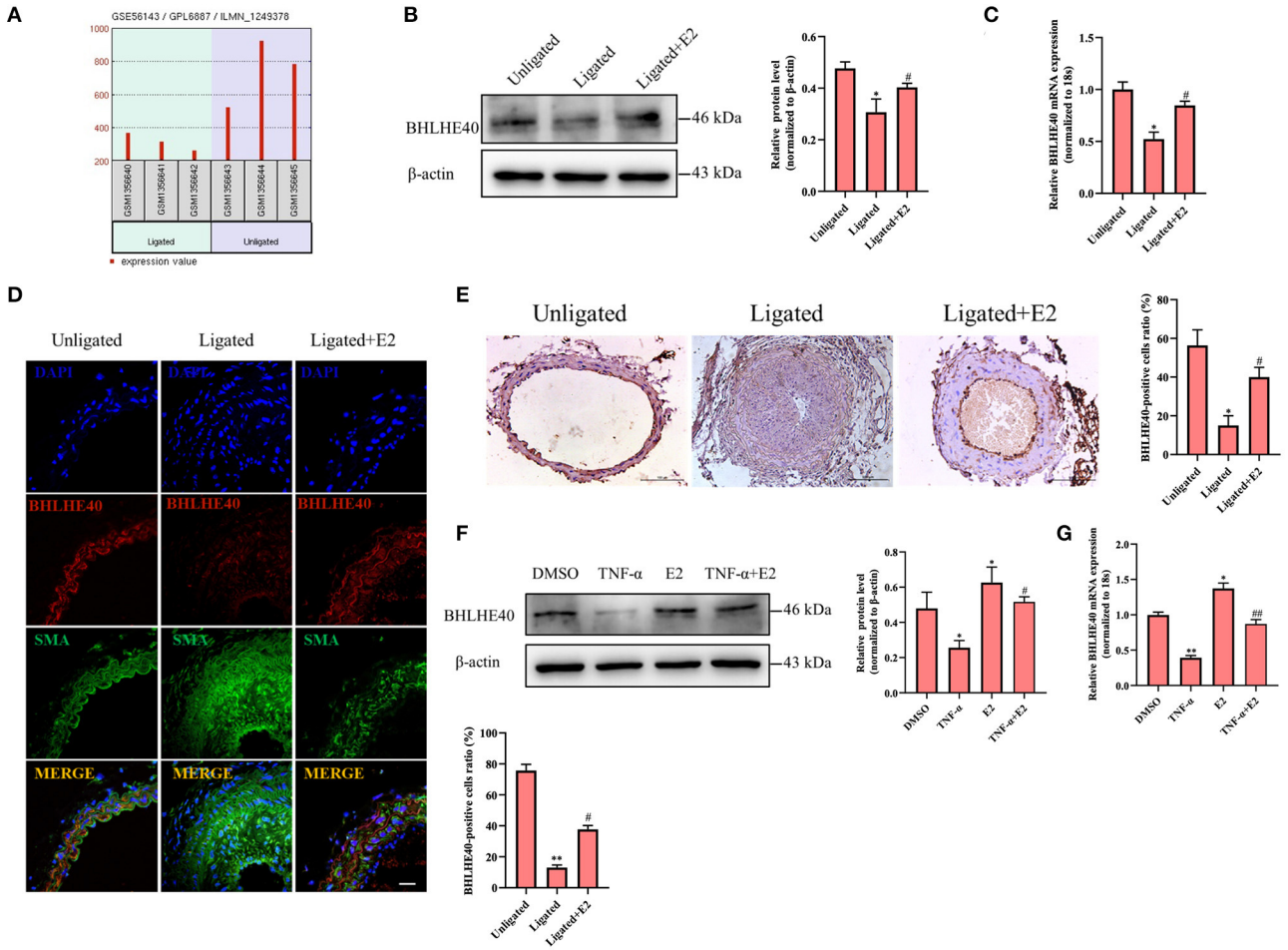

FIGURE 3 | E2 promotes the expression of BHLHE40 both *in vivo* and *in vitro*. **(A)** The data of BHLHE40 expression was downloaded from the GEO databases (GSE56143). **(B,C)** BHLHE40 expression in unligated, ligated and ligated + E2-treated carotid arteries was detected by Western blotting **(B)** and qRT-PCR **(C)**. Statistic of band intensities is shown on the right. *$p < 0.05$ vs. Unligated group, $^{\#}p < 0.05$ vs. Ligated group. **(D)** Immunofluorescence staining of a-SMA (SMA; green), BHLHE40 (red) and the nucleus (DAPI; blue) in unligated, ligated and ligated + E2-treated carotid arteries. Scale bars = 25 μm. Statistics of BHLHE40-positive cells unligated, ligated and ligated + E2-treated carotid arteries is shown on the right. **$p < 0.01$ vs. Unligated group, $^{\#}p < 0.05$ vs. Ligated group. **(E)** Immunochemistry staining of BHLHE40 in unligated, ligated and ligated + E2-treated carotid arteries. Scale bars = 100 μm. Statistics of BHLHE40-positive cells unligated, ligated and ligated + E2-treated carotid arteries is shown on the right. *$p < 0.05$ vs. Unligated group, $^{\#}p < 0.05$ vs. Ligated group. **(F,G)** VSMCs were pretreated with 100 nM of E2 for 6 h and then were stimulated with TNF-α (10 ng/mL) for 24 h, the expression of BHLHE40 was determined by Western blotting **(F)** and qRT-PCR **(G)**. Statistic of band intensities is shown on the right. *$p < 0.05$ and **$p < 0.01$ vs. DMSO group, $^{\#}p < 0.05$ and $^{\#\#}p < 0.01$ vs. TNF-α group.

the control group, whereas pretreatment with E2 (100 nM) largely counteracted the inhibitory effects of TNF-α on BHLHE40 expression. Taken together, these findings suggest that E2 promotes the expression of BHLHE40 both *in vivo* and *in vitro*.

Knockdown of BHLHE40 Promoted TNF-α-Induced VSMC Proliferation and Oxidative Stress

To further illustrate the role of BHLHE40 in ligation injury-induced intimal hyperplasia, we assayed the effects of BHLHE40

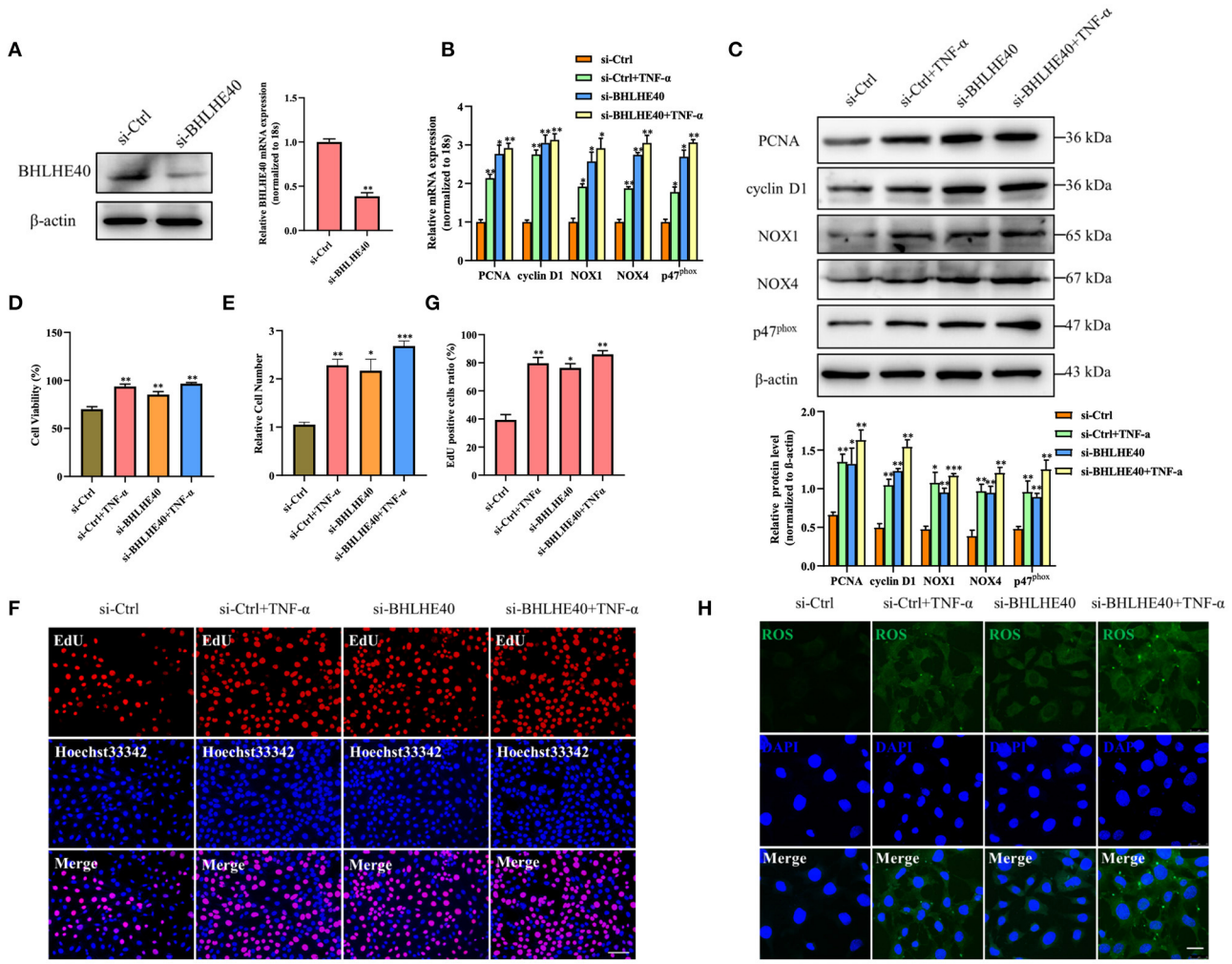

FIGURE 4 | Downregulation of BHLHE40 promotes TNF-α-induced proliferation and oxidative stress in VSMC. **(A)** VSMCs were transfected with si-BHLHE40, and the expression of BHLHE40 was detected by Western blotting and qRT-PCR. $^{**}p < 0.01$ vs. si-Ctrl group. **(B–H)** VSMCs were transfected with si-BHLHE40 and then treated or not with TNF-α for 24 h. The expression of PCNA, cyclin D1, NOX1, NOX4 and p47^{phox} was determined by qRT-PCR **(B)** and Western blotting **(C)**. Statistic of band intensities is shown on the bottom. $^{*}p < 0.05$, $^{**}p < 0.01$ and $^{***}p < 0.001$ vs. si-Ctrl group. The cell viability was determined by MTS assay **(D)**, and cell counting was carried out using a Countess automated counter **(E)**. $^{*}p < 0.05$, $^{**}p < 0.01$ and $^{***}p < 0.001$ vs. si-Ctrl group. Cell proliferation was detected by EdU staining **(F)**. Scale bar = 100 μm. Analysis of the percentage of EdU positive cells **(G)**. $^{*}p < 0.05$, and $^{**}p < 0.01$ vs. si-Ctrl group. ROS levels were detected by DCFH-DA staining **(H)**. Scale bar = 25 μm.

down-regulation on cellular proliferation and oxidative stress in VSMC. Firstly, we confirmed that the expression of BHLHE40 at the protein and mRNA levels was silenced by about 70% in si-BHLHE40 transfected VSMC (**Figure 4A**). Subsequently, we examined the effects of si-BHLHE40 on the expression of proliferation and oxidative stress-related genes, and found that treating VSMC with TNF-α clearly increased the expression of PCNA, cyclinD1, NOX1, NOX4 and p47^{phox}, which was enforced by si-BHLHE40 transfection (**Figures 4B,C**). In follow-up experiments, we found that BHLHE40 knockdown increased TNF-α-induced proliferation in VSMC, as shown by MTS analysis and cell counting (**Figures 4D,E**). Meanwhile, EdU staining evidenced that depletion of BHLHE40 by its siRNA increased TNF-α-induced VSMC proliferation (**Figures 4F,G**). In **Figure 4H**, ROS staining showed that si-BHLHE40 and TNF-α co-treatment further enhanced TNF-α-induced ROS production in VSMC. All in all, these data suggested that knockdown of BHLHE40 contributes to TNF-α-induced VSMC proliferation and oxidative stress.

Overexpression of BHLHE40 in VSMC Inhibits Cell Proliferation and Oxidative Stress

Next, we successfully overexpressed the BHLHE40 at both mRNA and protein level in VSMC (**Figure 5A**). To further explore whether BHLHE40 participates in the induction of proliferation and oxidative stress in TNF-α-treated VSMC,

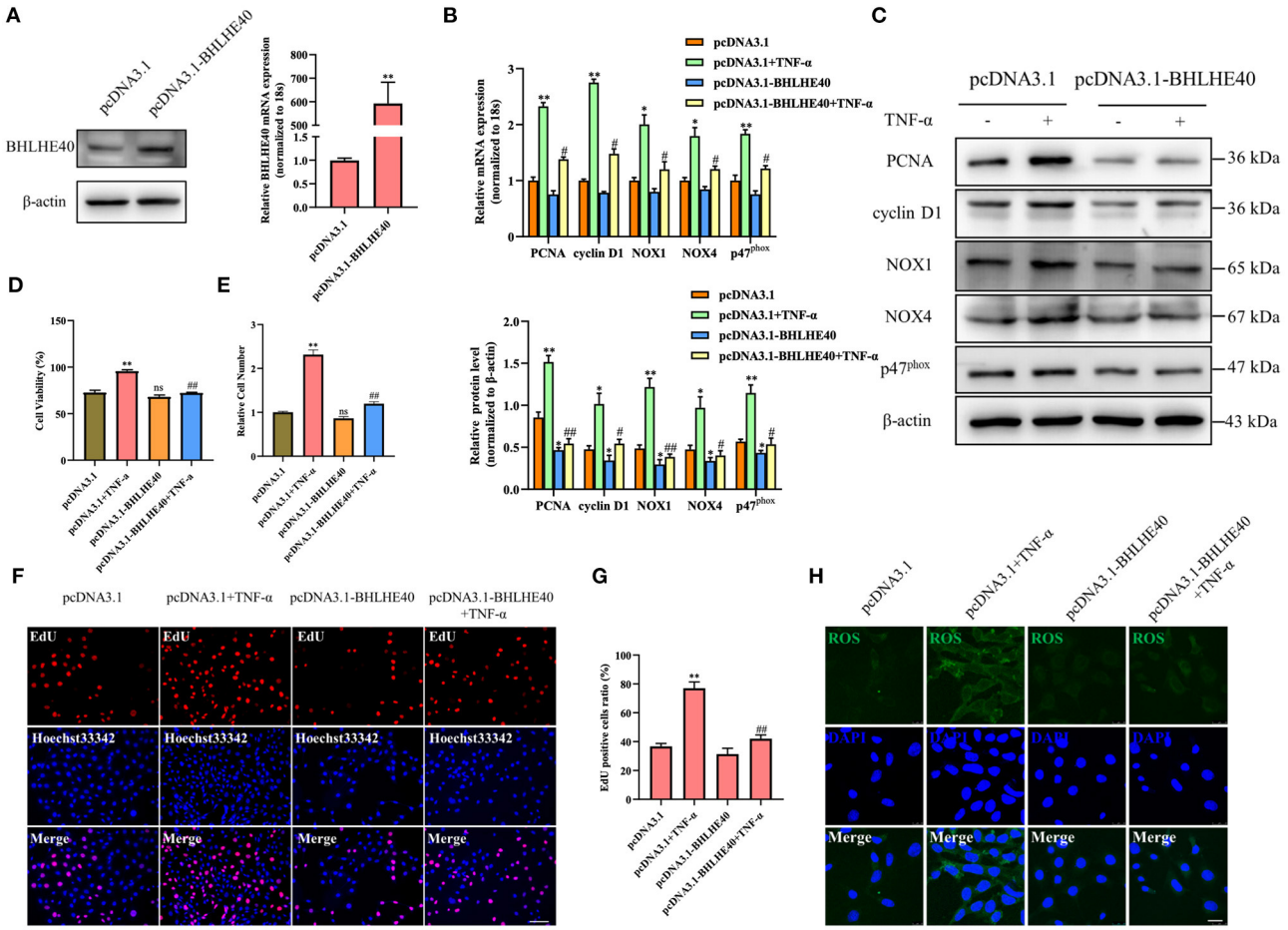

FIGURE 5 | Overexpression of BHLHE40 inhibits TNF-α-induced proliferation and oxidative stress in VSMC. **(A)** VSMCs were transfected with pcDNA3.1-BHLHE40, and the expression of BHLHE40 was detected by Western blotting and qRT-PCR. $^{**}p < 0.01$ vs. pcDNA3.1 group. **(B–H)** VSMCs were transfected with pcDNA3.1-BHLHE40 and then treated or not with TNF-α for 24 h. The expression of PCNA, cyclin D1, NOX1, NOX4 and $p47^{phox}$ was determined by qRT-PCR **(B)** and Western blotting **(C)**. Statistic of band intensities is shown on the left. $^{*}p < 0.05$ and $^{**}p < 0.01$ vs. pcDNA3.1 group, $^{\#}p < 0.05$ and $^{\#\#}p < 0.01$ vs. pcDNA3.1 + TNF-α group. The cell viability was determined by MTS assay **(D)**, and cell counting was carried out using a Countess automated counter **(E)**. $^{**}p < 0.01$ vs. pcDNA3.1 group, $^{\#\#}p < 0.01$ vs. pcDNA3.1 + TNF-α group. Cell proliferation was detected by EdU staining **(F)**. Scale bar = 100 μm. Analysis of the percentage of EdU positive cells **(G)**. $^{**}p < 0.01$ vs. pcDNA3.1 group, $^{\#\#}p < 0.01$ vs. pcDNA3.1 + TNF-α group. ROS levels were detected by DCFH-DA staining **(H)**. Scale bar = 25 μm.

we forcedly expressed BHLHE40 and found that BHLHE40 overexpression distinctly reduced the expression of PCNA, cyclinD1, NOX1, NOX4 and $p47^{phox}$ induced by TNF-α at both mRNA and protein levels (**Figures 5B,C**). As presented by MTS assay and cell counting, overexpression of BHLHE40 efficaciously counteracted the stimulatory effect of TNF-α on VSMC proliferation (**Figures 5D,E**). Similarly, EdU staining showed that the enforced expression of BHLHE40 in VSMC had opposite effects on TNF-α-induced proliferation (**Figures 5F,G**). Up-regulation of BHLHE40 led to a decrease in the production of TNF-α-induced ROS (**Figure 5H**). Altogether, these results indicate that BHLHE40 negatively regulates the proliferation and oxidative stress of VSMC by affecting the expression of PCNA, cyclinD1, NOX1, NOX4 and $p47^{phox}$.

BHLHE40 Suppressed Proliferation and Oxidative Stress Responses Through Inhibiting MAPK Signaling Pathway

Next, we performed BHLHE40 knockdown experiment to investigate whether BHLHE40 mediates the inhibitory role of E2 in the proliferation and oxidative stress of VSMCs. As shown in **Figure 6A**, down-regulation of BHLHE40 can reverse the inhibitory effects of E2 on the proliferation and oxidative stress. It is known that MAPK cascade activation is the center of multiple signaling pathways, and plays a key role in cell proliferation, inflammation and oxidative stress. Western blotting analysis revealed that TNF-α treatment markedly increased phosphorylation of ERK, JNK and P38 in VSMC, but the effects of TNF-α on MAPK signaling pathways were normalized by E2 treatment (**Figure 6B**). In order to clarify

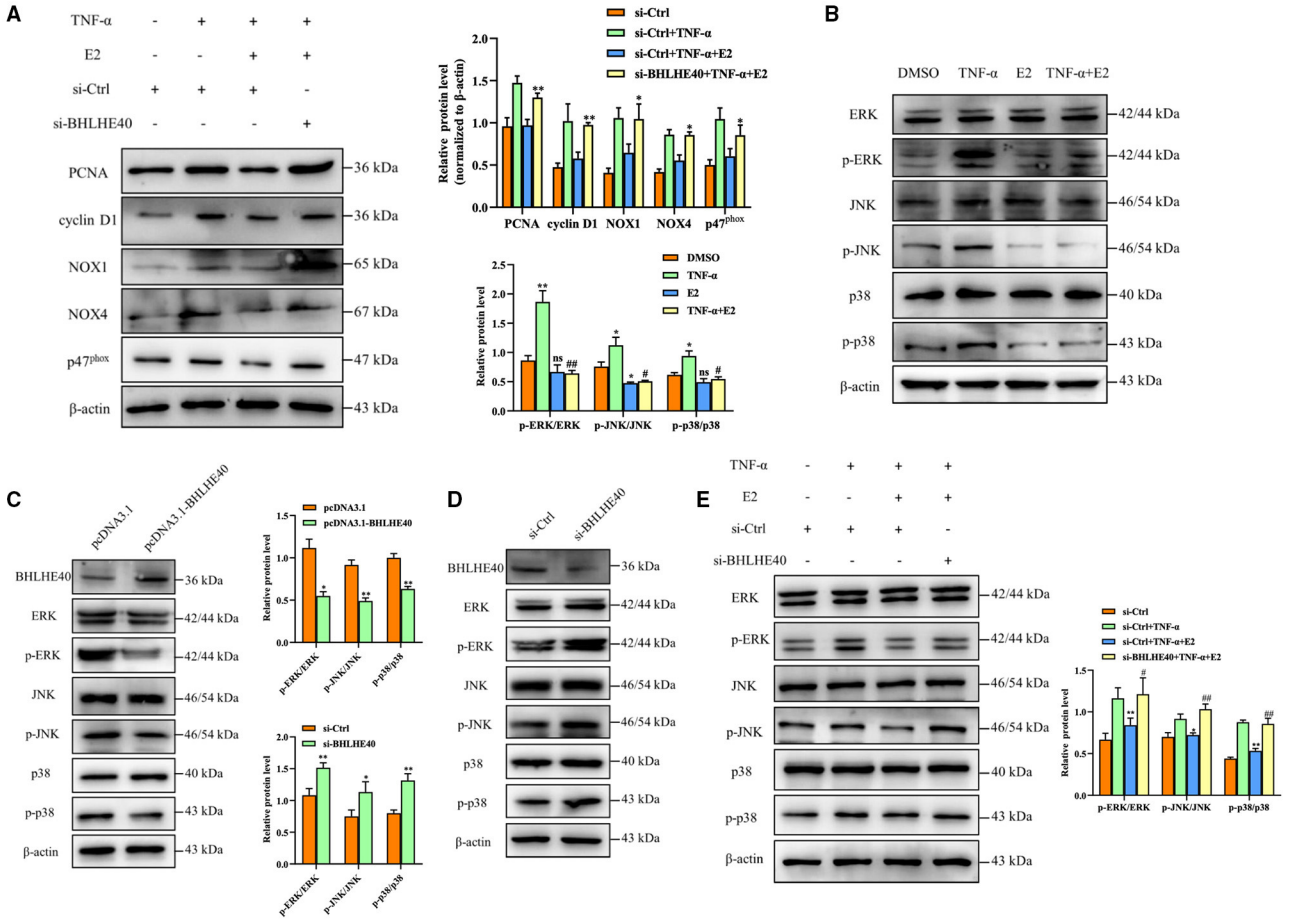

FIGURE 6 | BHLHE40 suppresses proliferation and oxidative stress responses through suppressing MAPK signaling pathways. **(A)** VSMCs were transfected with si-BHLHE40 or si-Ctrl and then treated with the indicated treatments. The expression of PCNA, cyclin D1, NOX1, NOX4 and $p47^{phox}$ was determined by Western blotting. Statistic of band intensities is shown on the right. $^{*}p < 0.05$ and $^{**}p < 0.01$ vs. si-Ctrl + TNF-α + E2 group. **(B)** VSMCs were pretreated with E2 (100 nM) for 6 h and then were stimulated with TNF-α (10 ng/mL) for 24 h. Western blotting was performed for total and phosphorylated ERK, JNK and p38. Statistic of band intensities is shown on the left. $^{*}p < 0.05$ and $^{**}p < 0.01$ vs. DMSO group, $^{\#}p < 0.05$ and $^{\#\#}p < 0.01$ vs. TNF-α group. **(C)** VSMCs were transfected with pcDNA3.1- BHLHE40 for 24 h, and Western blotting analysis was performed for total and phosphorylated ERK1/2, JNK and p38. Statistic of band intensities is shown on the right. $^{*}p < 0.05$ and $^{**}p < 0.01$ vs. pcDNA3.1 group. **(D)** VSMCs were transfected with si-BHLHE40 for 24 h, and Western blotting analysis was performed for total and phosphorylated ERK, JNK and p38. Statistic of band intensities is shown on the left. $^{*}p < 0.05$ and $^{**}p < 0.01$ vs. si-Ctrl group. **(E)** VSMCs were transfected with si-BHLHE40 or si-Ctrl and then treated with the indicated treatments. Total protein lysates were collected and the expression of ERK, JNK and p38 and their phosphorylated forms were examined by Western blotting. Statistic of band intensities is shown on the right. $^{*}p < 0.05$ and $^{**}p < 0.01$ vs. si-Ctrl + TNF-α, $^{\#}p < 0.05$ and $^{\#\#}p < 0.01$ vs. si-Ctrl + TNF-α + E2 group.

the mechanism by which BHLHE40 regulates proliferation and oxidative stress, we up-regulated or down-regulated the expression of BHLHE40 in VSMC, and monitored the expression of related genes in the MAPK signaling pathway. As shown in **Figure 6C**, up-regulation of BHLHE40 can lead to decreased ERK, JNK and p38 phosphorylation. On the contrary, down-regulating the expression of BHLHE40 can usefully increase ERK, JNK and p38 phosphorylation (**Figure 6D**). In order to confirm whether E2 regulates the MAPK signaling pathway by affecting the expression of BHLHE40, we conducted rescue experiments. As demonstrated in **Figure 6E**, TNF-α-induced phosphorylation of ERK, JNK and P38 were partly inhibited after E2 preincubation (**Figure 6E,** lane 3 vs. lane 2). Knockdown of BHLHE40 restrained this inhibitory effect of E2 (**Figure 6E,** lane 4 vs. lane 3). In addition, we examined the effect of E2 and BHLHE40 on AKT phosphorylation, as shown in **Supplementary Figure S1**, E2 treatment can lead to decreased AKT phosphorylation, but down-regulated BHLHE40 have no influence on the inhibitory effect of E2. On balance, the above results confirmed that 100 μM E2 displays suppressive effects on TNF-α-induced pathologic changes through deactivating MAPK signal pathways.

BHLHE40 Overexpression Alleviated Neointimal Formation Induced by Carotid Artery Ligation Through Repressing Proliferation and Oxidative Stress in Arterial Walls

To examine whether BHLHE40 is a key mediator in vascular remodeling, Pluronic F-127 gel solution containing pcDNA3.1

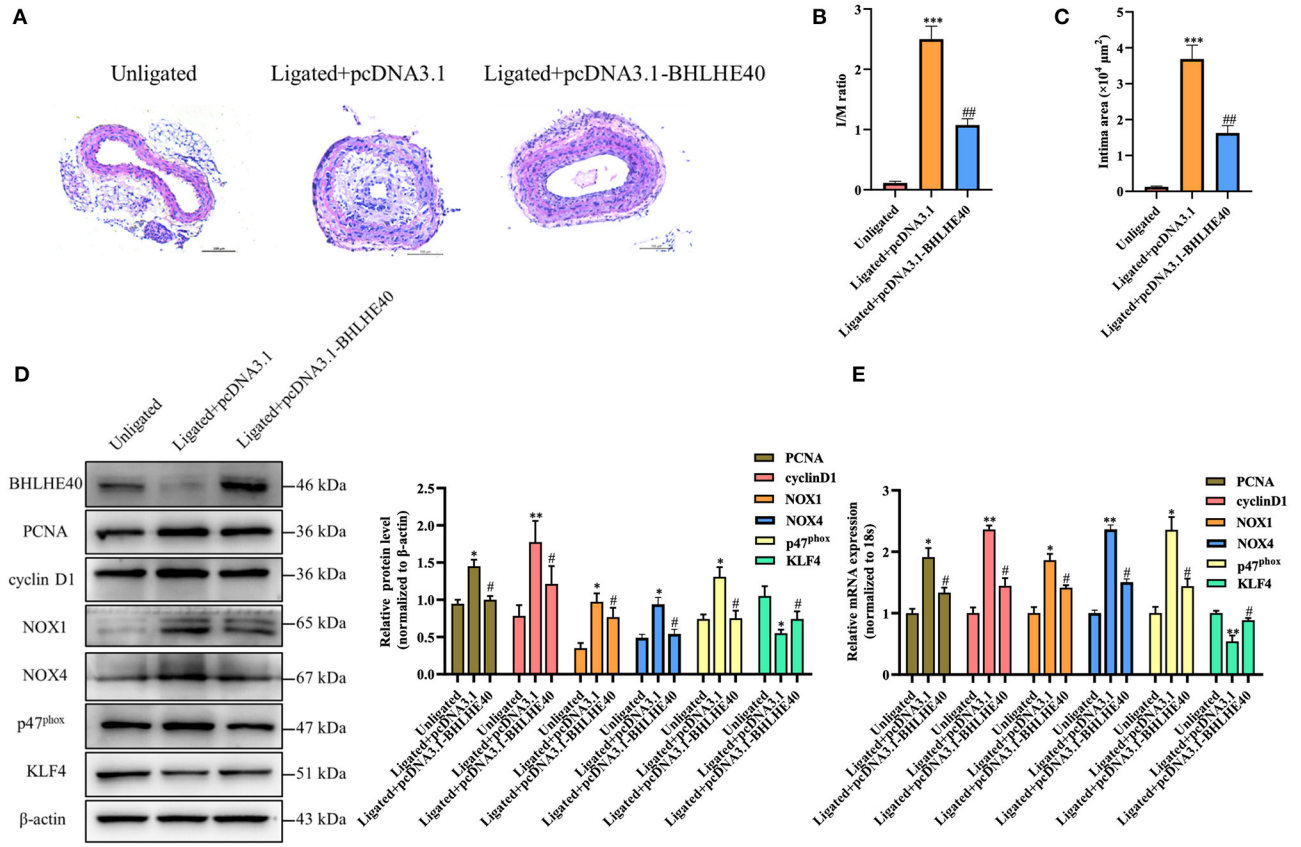

FIGURE 7 | BHLHE40 overexpression alleviates neointimal formation, proliferation and oxidative stress induced by carotid artery ligation. **(A)** Representative photomicrographs of the HE-stained sections of carotid arteries from unligated vessels, ligated + pcDNA3.1 vessels, and ligated + pcDNA3.1-BHLHE40 vessels ($n = 4$). Scale bars = 100 μm. **(B,C)** Morphometric quantification of I/M ratio and the intima area in the different groups. $^{***}p < 0.001$ vs. Unligated group, $^{\#\#}p < 0.01$ vs. Ligated + pcDNA3.1 group. **(D)** BHLHE40, PCNA, cyclin D1, NOX1, NOX4, $p47^{phox}$ and KLF4 expression in unligated, ligated + pcDNA3.1 and ligated + pcDNA3.1-BHLHE40 carotid arteries was detected by Western blotting. Statistic of band intensities is shown on the right ($n = 3$). $^{*}p < 0.05$ and $^{**}p < 0.01$ vs. Unligated group, $^{\#}p < 0.05$ vs. Ligated + pcDNA3.1 group. **(E)** PCNA, cyclin D1, NOX1, NOX4, $p47^{phox}$ and KLF4 expression in unligated, ligated + pcDNA3.1 and ligated + pcDNA3.1-BHLHE40 carotid arteries was detected by qRT-PCR ($n = 3$). $^{*}p < 0.05$ and $^{**}p < 0.01$ vs. Unligated group, $^{\#}p < 0.05$ vs. Ligated + pcDNA3.1 group.

plasmids or pcDNA3.1-BHLHE40 plasmids were applied to the exposed adventitial surface of an ∼5 mm segment of the ligated carotid artery. The intimal thickness of the ligated artery was determined 14 days after the surgery. As expected, carotid arterial ligation increased vascular wall thickness in control-plasmids transfected mice, and this expansion was strongly reduced in BHLHE40-plasmids transfected mice (**Figure 7A**). Consistent with these results, BHLHE40-overexpressed mice showed an important decrease in the ratio of intimal/medial area (I/M ratio) and neointimal area compared with control-plasmids transfected mice (**Figures 7B,C**). Next, we examined the expression of PCNA, cyclinD1, NOX1, NOX4 and $p47^{phox}$ and KLF4 in the injured carotid artery of pcDNA3.1 plasmids or pcDNA3.1-BHLHE40 plasmids transfected mice. Notably, western blotting and qRT-PCR analysis data showed that carotid artery ligation-induced above gene changes were normalized by BHLHE40 overexpression (**Figures 7D,E**). To sum up, these data support the pathophysiological role of BHLHE40 depletion in vascular hypertrophy.

DISCUSSION

Vascular remodeling is the pathological basis of many cardiovascular diseases such as hypertension and atherosclerosis. The abnormal proliferation and oxidative stress of VSMC play an important role in the occurrence and development of vascular remodeling (24, 25). Evidence is also emerging to suggest that treatment of proliferation and oxidative stress of VSMC causes a reduction or prevents the progression of the carotid intima-media thickness, paralleled by a decrease in cardiovascular risk and events (26, 27). Therefore, exploring an effective treatment strategy to block the proliferation of VSMC and the occurrence of oxidative stress is essential for the treatment of cardiovascular diseases.

In this study, we showed that (1) E2 inhibited carotid artery ligation-induced intimal hyperplasia *in vivo* and TNF-α-induced VSMC proliferation and oxidative stress *in vitro*. (2) E2 inhibited TNF-α-induced VSMC proliferation

and oxidative stress by increasing BHLHE40 expression, (3) Overexpression of BHLHE40 abolished TNF-α-induced VSMC proliferation and oxidative stress, (4) BHLHE40 mediated E2-induced suppression of MAPK signaling pathway expression, and (5) BHLHE40 overexpression protected against neointimal hyperplasia induced by carotid artery ligation.

17β-estrogen is a powerful steroid hormone, high in women from puberty to menopause and low in men. Anecdotal evidence suggested that the incidence of atherosclerosis in pre-menopausal women is much lower than that of age-matched males, but the discrepancy narrowed after post-menopausal in women, suggesting the preventive effect of estrogen on cardiovascular diseases (28, 29). Previous studies have indicated that 17β-estradiol treatment reduces neointimal hyperplasia and ameliorates re-endothelialization in injured carotid arteries (19, 30). It is well-known that a key mechanism for inhibiting intimal thickening is the repression of cell proliferation and oxidative stress (31, 32).In line with previous results, and our animal experiment data showing E2 can effectively improve neointimal hyperplasia in ligated carotid arteries by diminution of proliferation-related genes expression and attenuation of NADPH oxidase activity in VSMC. It has long been known that increased PCNA and cyclin D1 expression and enhanced ROS levels in VSMC exposed to TNF-α (33, 34). Our data showing E2 markedly inhibited the TNF-α-induced expression of PCNA, cyclin D1, NOX1, NOX4 and $p47^{phox}$.

It is well-established that the MAPK signaling pathway regulates cellular proliferation, calcification, inflammation and oxidative stress (35, 36). Recently reports showed that increased phosphorylation of ERK1/2 expression contributes to the proliferation of VSMC (37, 38), Beyond cell proliferation, ERK 1/2 phosphorylation modulates VSMC phenotypic switch in Abdominal Aortic Aneurysms (39). In addition, p38 MAPK kinase promotes vascular calcification by inducing the expression of RUNX2 in VSMC (40). In primary mouse VSMC, p38 kinase is key to TGF-β-mediated growth inhibition (41). Previous studies showed that corylin treatment effectively attenuated atherosclerotic lesions by suppressing ROS production, VSMC proliferation and JNK phosphorylation in ApoE-deficient mice (42). Similarly, Ox-LDL induced oxidative stress promoted VSMC transformation from contraction to secretion via the JNK and ERK signaling pathways (43). Our recent study indicated that the activation of MAPK family members, such as ERK1/2, JNK and p38, was largely significantly abolished by E2 in TNF-α-induced VSMC.

Recently, an increasing number of reports have clarified the regulatory mechanisms mediated by BHLHE40 and its associations with the etiopathogenesis of various diseases (44, 45). For example, BHLHE40 directly interacts with estrogen receptor α to suppress the proliferation of ER-positive breast cancer cells (46). According to the newest reports, BHLHE40 deficiency resulted in accelerated osteopenia through attenuated PI3KCA/Akt/GSK3β signaling (47). In addition, the high expression of BHLHE40 in gastric epithelial cells increased the production of CXCL12 by interacting with p-STAT3 in Helicobacter pylori-associated gastritis, which further aggravated the development of gastritis (9). However, only a few studies have been reported on the function of BHLHE40 in vascular remodeling for now. As demonstrated in our study, TNFα-induced ROS levels and NADPH oxidase activation were attenuated and cell proliferation was reduced in BHLHE40-overexpressed VSMC. In the followed experiments, we found that BHLHE40 blocks VSMC proliferation and oxidative stress by inhibiting TNF-α-induced activation of MAPK signaling pathways.

In line with previous results using E2-treated ligated mice, and our *in vivo* data showed that up-expressed BHLHE40 could significantly reduce carotid artery ligation-induced neointimal formation. Because VSMC proliferation requires the activation of the transcription of several cell cycle promoting genes, we examined the expression of PCNA and cyclin D1 in pcDNA3.1-BHLHE40-transfected injured carotid arteries, beyond that, we also measured the expression of the NADPH oxidase catalytic subunits-NOX1, NOX4, and $p47^{phox}$. Consistent with previous results *in vitro*, and our *in vivo* data showing decreased neointimal thickness via reducing ROS production and VSMC proliferation with localized overexpression of BHLHE40 in injured carotid arteries.

Our results demonstrated for the first time that in TNF-α-stimulated mouse VSMC, E2 diminished VSMC proliferation and oxidative stress via restoring TNF-α-decreased BHLHE40 expression. Furthermore, we explore the possibility that E2 may suppress TNF-α-induced MAPK activity by regulating BHLHE40. In conclusion, our results along with previous studies indicate that E2 exerts the cardiovascular protective effect via-multiple molecular mechanisms, but the accurate mechanism needs further study. This research offers a new molecular explanation for the vasoprotective effect of 17β-estrogen.

DATA AVAILABILITY STATEMENT

The raw data supporting the conclusions of this article will be made available by the authors, without undue reservation.

ETHICS STATEMENT

The animal study was reviewed and approved by Institutional Animal Care and Use Committee of Hebei Medical University.

AUTHOR CONTRIBUTIONS

D-dF and X-hZ conceived and designed the experiments, and wrote the manuscript. D-dF, M-lZ, YM, and XH performed all the experiments. BZ analyzed the data. X-hZ and J-kW engaged in material support for obtained funding and

supervised the study. All authors have read and approved the final manuscript.

FUNDING

This research was supported by grants from the National Natural Science Foundation of China (Nos. 31871152, 81770285, and 81971328), the Natural Science Foundation of Hebei Province of China (No. H2021206459), and the Postgraduates Innovation Funding Program of Hebei Province (CXZZBS2019122).

SUPPLEMENTARY MATERIAL

The Supplementary Material for this article can be found online at: https://www.frontiersin.org/articles/10.3389/fcvm.2021.768662/full#supplementary-material

REFERENCES

1. Lacolley P, Regnault V, Segers P, Laurent S. Vascular smooth muscle cells and arterial stiffening: relevance in development, aging, and disease. *Physiol Rev.* (2017) 97:1555–617. doi: 10.1152/physrev.00003.2017
2. Doran AC, Meller N, McNamara CA. Role of smooth muscle cells in the initiation and early progression of atherosclerosis. *Arterioscler Thromb Vasc Biol.* (2008) 28:812–9. doi: 10.1161/ATVBAHA.107.159327
3. Izzo C, Vitillo P, Di Pietro P, Visco V, Strianese A, Virtuoso N, et al. The role of oxidative stress in cardiovascular aging and cardiovascular diseases. *Life (Basel).* (2021) 11:60. doi: 10.3390/life11010060
4. Qin Y, Zheng B, Yang GS, Zhou J, Yang HJ, Nie ZY, et al. Tanshinone A inhibits VSMC inflammation and proliferation *in vivo* and *in vitro* by downregulating miR-712-5p expression. *Eur J Pharmacol.* (2020) 880:173140. doi: 10.1016/j.ejphar.2020.173140
5. Zhang RN, Zheng B, Li LM, Zhang J, Zhang XH, Wen JK. Tongxinluo inhibits vascular inflammation and neointimal hyperplasia through blockade of the positive feedback loop between miR-155 and TNF-alpha. *Am J Physiol Heart Circ Physiol.* (2014) 307:H552–62. doi: 10.1152/ajpheart.00936.2013
6. Honma S, Kawamoto T, Takagi Y, Fujimoto K, Sato F, Noshiro M, et al. Dec1 and Dec2 are regulators of the mammalian molecular clock. *Nature.* (2002) 419:841–4. doi: 10.1038/nature01123
7. Bi H, Li S, Qu X, Wang M, Bai X, Xu Z, et al. DEC1 regulates breast cancer cell proliferation by stabilizing cyclin E protein and delays the progression of cell cycle S phase. *Cell Death Dis.* (2015) 6:e1891. doi: 10.1038/cddis.2015.247
8. Kotolloshi R, Mirzakhani K, Ahlburg J, Kraft F, Pungsrinont T, Baniahmad A. Thyroid hormone induces cellular senescence in prostate cancer cells through induction of DEC1. *J Steroid Biochem Mol Biol.* (2020) 201:105689. doi: 10.1016/j.jsbmb.2020.105689
9. Teng YS, Zhao YL Li MS, Liu YG, Cheng P, Lv YP, et al. Upexpression of BHLHE40 in gastric epithelial cells increases CXCL12 production through interaction with p-STAT3 in Helicobacter pylori-associated gastritis. *FASEB J.* (2020) 34:1169–81. doi: 10.1096/fj.201900464RR
10. Chung SY, Kao CH, Villarroya F, Chang HY, Chang HC, Hsiao SP, et al. Bhlhe40 represses PGC-1alpha activity on metabolic gene promoters in myogenic cells. *Mol Cell Biol.* (2015) 35:2518–29. doi: 10.1128/MCB.00387-15
11. Zhong JY, Cui XJ, Zhan JK, Wang YJ Li S, Lin X, et al. LncRNA-ES3 inhibition by Bhlhe40 is involved in high glucose-induced calcification/senescence of vascular smooth muscle cells. *Ann N Y Acad Sci.* (2020) 1474:61–72. doi: 10.1111/nyas.14381
12. Vercherat C, Chung TK, Yalcin S, Gulbagci N, Gopinadhan S, Ghaffari S, et al. Stra13 regulates oxidative stress mediated skeletal muscle degeneration. *Hum Mol Genet.* (2009) 18:4304–16. doi: 10.1093/hmg/ddp383
13. Chang HC, Kao CH, Chung SY, Chen WC, Aninda LP, Chen YH, et al. Bhlhe40 differentially regulates the function and number of peroxisomes and mitochondria in myogenic cells. *Redox Biol.* (2019) 20:321–33. doi: 10.1016/j.redox.2018.10.009
14. Madamanchi NR, Runge MS. Redox signaling in cardiovascular health and disease. *Free Radical Bio Med.* (2013) 61:473–501. doi: 10.1016/j.freeradbiomed.2013.04.001
15. Jia Z, Aoyagi T, Yang T. mPGES-1 protects against DOCA-salt hypertension via inhibition of oxidative stress or stimulation of NO/cGMP. *Hypertension.* (2010) 55:539–46. doi: 10.1161/HYPERTENSIONAHA.109.144840
16. Dhalla NS, Temsah RM, Netticadan T. Role of oxidative stress in cardiovascular diseases. *J Hypertens.* (2000) 18:655–73. doi: 10.1097/00004872-200018060-00002
17. Xing DQ, Nozell S, Chen YF, Hage F, Oparil S. Estrogen and mechanisms of vascular protection. *Arterioscl Throm Vas.* (2009) 29:289–95. doi: 10.1161/ATVBAHA.108.182279
18. Freudenberger T, Rock K, Dai G, Dorn S, Mayer P, Heim HK, et al. Estradiol inhibits hyaluronic acid synthase 1 expression in human vascular smooth muscle cells. *Basic Res Cardiol.* (2011) 106:1099–109. doi: 10.1007/s00395-011-0217-5
19. Chandrasekar B, Sirois MG, Geoffroy P, Lauzier D, Nattel S, Tanguay JF. Local delivery of 17beta-estradiol improves reendothelialization and decreases inflammation after coronary stenting in a porcine model. *Thromb Haemost.* (2005) 94:1042–7. doi: 10.1160/TH04-12-0823
20. Zhang ML, Zheng B, Tong F, Yang Z, Wang ZB, Yang BM, et al. iNOS-derived peroxynitrite mediates high glucose-induced inflammatory gene expression in vascular smooth muscle cells through promoting KLF5 expression and nitration. *Biochim Biophys Acta Mol Basis Dis.* (2017) 1863:2821–34. doi: 10.1016/j.bbadis.2017.07.004
21. Yang GS, Zheng B, Qin Y, Zhou J, Yang Z, Zhang XH, et al. Salvia miltiorrhiza-derived miRNAs suppress vascular remodeling through regulating OTUD7B/KLF4/NMHC IIA axis. *Theranostics.* (2020) 10:7787–811. doi: 10.7150/thno.46911
22. Straszewski-Chavez SL, Visintin IP, Karassina N, Los G, Liston P, Halaban R, et al. XAF1 mediates tumor necrosis factor-alpha-induced apoptosis and X-linked inhibitor of apoptosis cleavage by acting through the mitochondrial pathway. *J Biol Chem.* (2007) 282:13059–72. doi: 10.1074/jbc.M609038200
23. Kiss Z, Mudryj M, Ghosh PM. Non-circadian aspects of BHLHE40 cellular function in cancer. *Genes Cancer.* (2020) 11:1–19. doi: 10.18632/genesandcancer.201
24. Wang YC, Cui XB, Chuang YH, Chen SY. Janus Kinase 3, a Novel regulator for smooth muscle proliferation and vascular remodeling. *Arterioscl Throm Vas.* (2017) 37:1352. doi: 10.1161/ATVBAHA.116.308895
25. Burtenshaw D, Kitching M, Redmond EM, Megson IL, Cahill PA. Reactive Oxygen Species (ROS), intimal thickening, and subclinical atherosclerotic disease. *Front Cardiovasc Med.* (2019) 6:89. doi: 10.3389/fcvm.2019.00089
26. Cheng KS, Mikhailidis DP, Hamilton G, Seifalian AM, A. review of the carotid and femoral intima-media thickness as an indicator of the presence of peripheral vascular disease and cardiovascular risk factors. *Cardiovasc Res.* (2002) 54:528–38. doi: 10.1016/S0008-6363(01)00551-X
27. He M, Wang C, Sun JH, Liu Y, Wang H, Zhao JS, et al. Roscovitine attenuates intimal hyperplasia via inhibiting NF-kappa B and STAT3 activation induced by TNF-alpha in vascular smooth muscle cells. *Biochem Pharmacol.* (2017) 137:51–60. doi: 10.1016/j.bcp.2017.04.018
28. Gersh FL. Benefits of estrogen in cardiovascular diseases. *Prog Cardiovasc Dis.* (2020) 63:392. doi: 10.1016/j.pcad.2020.03.008
29. Montalcini T, Gorgone G, Gazzaruso C, Sesti G, Perticone F, Pujia A. Role of endogenous androgens on carotid atherosclerosis in non-obese postmenopausal women. *Nutr Metab Cardiovasc Dis.* (2007) 17:705–11. doi: 10.1016/j.numecd.2006.09.007
30. Kyriakides ZS, Lymberopoulos E, Papalois A, Kyrzopoulos S, Dafnomili V, Sbarouni E, et al. Estrogen decreases neointimal hyperplasia and improves re-endothelialization in pigs. *Int J Cardiol.* (2006) 113:48–53. doi: 10.1016/j.ijcard.2005.10.030

31. Ostriker AC, Xie Y, Chakraborty R, Sizer AJ, Bai Y, Ding M, et al. TET2 protects against vascular smooth muscle cell apoptosis and intimal thickening in transplant vasculopathy. *Circulation.* (2021) 144:455–70. doi: 10.1161/CIRCULATIONAHA.120.050553
32. Szocs K, Lassegue B, Sorescu D, Hilenski LL, Valppu L, Couse TL, et al. Upregulation of Nox-based NAD(P)H oxidases in restenosis after carotid injury. *Arterioscler Thromb Vasc Biol.* (2002) 22:21–7. doi: 10.1161/hq0102.102189
33. Chou CC, Wang CP, Chen JH, Lin HH. Anti-atherosclerotic effect of hibiscus leaf polyphenols against tumor necrosis factor-alpha-induced abnormal vascular smooth muscle cell migration and proliferation. *Antioxidants (Basel).* (2019) 8:620. doi: 10.3390/antiox8120620
34. Karki R, Ho OM, Kim DW. Magnolol attenuates neointima formation by inducing cell cycle arrest via inhibition of ERK1/2 and NF-kappaB activation in vascular smooth muscle cells. *Biochim Biophys Acta.* (2013) 1830:2619–28. doi: 10.1016/j.bbagen.2012.12.015
35. Luo XQ, Xiao YJ, Song FL, Yang Y, Xia M, Ling WH. Increased plasma S-adenosyl-homocysteine levels induce the proliferation and migration of VSMCs through an oxidative stress-ERK1/2 pathway in apoE(/) mice. *Cardiovasc Res.* (2012) 95:241–50. doi: 10.1093/cvr/cvs130
36. Li J, Wang C, Wang W, Liu L, Zhang Q, Zhang J, et al. PRDX2 Protects against atherosclerosis by regulating the phenotype and function of the vascular smooth muscle cell. *Front Cardiovasc Med.* (2021) 8:624796. doi: 10.3389/fcvm.2021.624796
37. Zhao Y, Lv M, Lin H, Cui Y, Wei X, Qin Y, et al. Rho-associated protein kinase isoforms stimulate proliferation of vascular smooth muscle cells through ERK and induction of cyclin D1 and PCNA. *Biochem Biophys Res Commun.* (2013) 432:488–93. doi: 10.1016/j.bbrc.2013.02.009
38. Sun HJ, Liu TY, Zhang F, Xiong XQ, Wang JJ, Chen Q, et al. Salusin-beta contributes to vascular remodeling associated with hypertension via promoting vascular smooth muscle cell proliferation and vascular fibrosis. *Bba-Mol Basis Dis.* (2015) 1852:1709–18. doi: 10.1016/j.bbadis.2015.05.008
39. Peng H, Zhang K, Liu Z, Xu Q, You B, Li C, et al. VPO1 Modulates vascular smooth muscle cell phenotypic switch by activating extracellular signal-regulated kinase 1/2 (ERK 1/2) in abdominal aortic aneurysms. *J Am Heart Assoc.* (2018) 7:e010069. doi: 10.1161/JAHA.118.010069
40. Yang Y, Sun Y, Chen J, Bradley WE. Dell'Italia LJ, Wu H, et al. AKT-independent activation of p38 MAP kinase promotes vascular calcification. *Redox Biol.* (2018) 16:97–103. doi: 10.1016/j.redox.2018.02.009
41. Seay U, Sedding D, Krick S, Hecker M, Seeger W, Eickelberg O. Transforming growth factor-beta-dependent growth inhibition in primary vascular smooth muscle cells is p38-dependent. *J Pharmacol Exp Ther.* (2005) 315:1005–12. doi: 10.1124/jpet.105.091249
42. Chen CC Li HY, Leu YL, Chen YJ, Wang CJ, Wang SH. Corylin inhibits vascular cell inflammation, proliferation and migration and reduces atherosclerosis in ApoE-deficient mice. *Antioxidants (Basel).* (2020) 9:275. doi: 10.3390/antiox9040275
43. Wang XQ Li H, Zhang YT, Liu Q, Sun XL, He XM, et al. Suppression of miR-4463 promotes phenotypic switching in VSMCs treated with Ox-LDL. *Cell Tissue Res.* (2021) 383:1155–65. doi: 10.1007/s00441-020-03338-y
44. Cook ME, Jarjour NN, Lin CC, Edelson BT. Transcription factor Bhlhe40 in immunity and autoimmunity. *Trends Immunol.* (2020) 41:1023–36. doi: 10.1016/j.it.2020.09.002
45. Sato F, Bhawal UK, Yoshimura T, Muragaki Y. DEC1 and DEC2 crosstalk between circadian rhythm and tumor progression. *J Cancer.* (2016) 7:153–9. doi: 10.7150/jca.13748
46. Xue J, Dai Y, Li G, Lang W, Li P, Liu Y, et al. DEC1 directly interacts with estrogen receptor (ER) alpha to suppress proliferation of ER-positive breast cancer cells. *Biochem Biophys Res Commun.* (2020) 528:740–5. doi: 10.1016/j.bbrc.2020.05.123
47. He SC, Guan Y, Wu YC, Zhu L, Yan BF, Honda H, et al. DEC1 deficiency results in accelerated osteopenia through enhanced DKK1 activity and attenuated PI3KCA/Akt/GSK3 beta signaling. *Metabolism.* (2021) 118:154730. doi: 10.1016/j.metabol.2021.154730

Conflict of Interest: The authors declare that the research was conducted in the absence of any commercial or financial relationships that could be construed as a potential conflict of interest.

Publisher's Note: All claims expressed in this article are solely those of the authors and do not necessarily represent those of their affiliated organizations, or those of the publisher, the editors and the reviewers. Any product that may be evaluated in this article, or claim that may be made by its manufacturer, is not guaranteed or endorsed by the publisher.

Copyright © 2021 Feng, Zheng, Yu, Zhang, Ma, Hao, Wen and Zhang. This is an open-access article distributed under the terms of the Creative Commons Attribution License (CC BY). The use, distribution or reproduction in other forums is permitted, provided the original author(s) and the copyright owner(s) are credited and that the original publication in this journal is cited, in accordance with accepted academic practice. No use, distribution or reproduction is permitted which does not comply with these terms.

frontiers in Cardiovascular Medicine

ORIGINAL RESEARCH
published: 01 December 2021
doi: 10.3389/fcvm.2021.774755

Identification of CALU and PALLD as Potential Biomarkers Associated With Immune Infiltration in Heart Failure

Xing Liu[1†], Shiyue Xu[2†], Ying Li[3†], Qian Chen[1], Yuanyuan Zhang[1] and Long Peng[1*]*

[1] *Department of Cardiovascular Medicine, The Third Affiliated Hospital, Sun Yat-sen University, Guangzhou, China,*
[2] *Department of Hypertension and Vascular Disease, The First Affiliated Hospital, Sun Yat-sen University, Guangzhou, China,*
[3] *Department of Dermatology, Guangzhou Eighth People's Hospital, Guangzhou Medical University, Guangzhou, China*

OPEN ACCESS

Edited by:
Ji Bihl,
Marshall University, United States

Reviewed by:
Jyotsna Joshi,
Mayo Clinic Arizona, United States
Owais Bhat,
Virginia Commonwealth University, United States
Zijian Xiao,
University of South China, China

****Correspondence:***
Yuanyuan Zhang
zhangyy67@mail.sysu.edu.cn
Long Peng
pengl5@mail.sysu.edu.cn

[†]These authors have contributed equally to this work

Specialty section:
This article was submitted to General Cardiovascular Medicine, a section of the journal Frontiers in Cardiovascular Medicine

Received: *13 September 2021*
Accepted: *08 November 2021*
Published: *01 December 2021*

Citation:
Liu X, Xu S, Li Y, Chen Q, Zhang Y and Peng L (2021) Identification of CALU and PALLD as Potential Biomarkers Associated With Immune Infiltration in Heart Failure. Front. Cardiovasc. Med. 8:774755. doi: 10.3389/fcvm.2021.774755

Background: Inflammatory activation and immune infiltration play important roles in the pathologic process of heart failure (HF). The current study is designed to investigate the immune infiltration and identify related biomarkers in heart failure patients due to ischemic cardiomyopathy.

Methods: Expression data of HF due to ischemic cardiomyopathy (CM) samples and non-heart failure (NF) samples were downloaded from gene expression omnibus (GEO) database. Differentially expressed genes (DEGs) between CM and NF samples were identified. Single sample gene set enrichment analysis (ssGSEA) was performed to explore the landscape of immune infiltration. Weighted gene co-expression network analysis (WGCNA) was applied to screen the most relevant module associated with immune infiltration. The diagnostic values of candidate genes were evaluated by receiver operating curves (ROC) curves. The mRNA levels of potential biomarkers in the peripheral blood mononuclear cells (PBMCs) isolated from 10 CM patients and 10 NF patients were analyzed to further assess their diagnostic values.

Results: A total of 224 DEGs were identified between CM and NF samples in GSE5406, which are mainly enriched in the protein processing and extracellular matrix related biological processes and pathways. The result of ssGSEA showed that the abundance of dendritic cells (DC), mast cells, natural killer (NK) CD56dim cells, T cells, T follicular helper cells (Tfh), gammadelta T cells (Tgd) and T helper 2 (Th2) cells were significantly higher, while the infiltration of eosinophils and central memory T cells (Tcm) were lower in CM samples compared to NF ones. Correlation analysis revealed that Calumenin (CALU) and palladin (PALLD) were negatively correlated with the abundance of DC, NK CD56dim cells, T cells, Tfh, Tgd and Th2 cells, but positively correlated with the level of Tcm. More importantly, CALU and PALLD were significantly lower in PBMCs from CM patients compared to NF ones.

Conclusion: Our study revealed that CALU and PALLD are potential biomarkers associated with immune infiltration in heart failure due to ischemic cardiomyopathy.

Keywords: heart failure, ischemic cardiomyopathy, inflammatory activation, biomarker, diagnosis

INTRODUCTION

Heart failure refers to the complex clinical syndrome and the end-stage manifestations of cardiovascular disease (1, 2). Large-scale epidemiological analysis shows that the global prevalence of HF is on the rise due to the aging of the population and the progress in the diagnosis and treatment of cardiovascular diseases. In developed countries, the prevalence of HF is 1.5–2.2% (3). The latest report in China shows that the prevalence of HF among residents ≥35 years old is 1.3%, that is, there are ∼13.7 million patients (3).Therefore, HF has always been a hot spot in the field of cardiovascular research.

HF is caused by the complicated interaction of myocardial damage, neurohormonal activation, inflammatory response, and renal dysfunction (4–6). During the process, the cytoskeletal and membrane associated proteins are increased and disorganized, while the contractile myofilaments and sarcomeric proteins are decreased in the heart (7). In addition, cardiomyocytes in the failing heart display impaired excitation-contraction coupling due to the decreased calcium transients, enhanced diastolic sarcoplasmic reticulum (SR) calcium leak and diminished SR calcium sequestration (8). Although the pathogenesis of HF is still perplexing, the persistent inflammation and immune abnormalities are believed to participate in the pathogenesis across the spectrum of HF (9). Elevated and long-lasting leukocyte recruitment mediated by G protein-coupled receptor kinase 5 (GRK5) in the injured heart is reported to be associated with chronic cardiac inflammation and heart failure (10). Moreover, evidence indicates that transcriptome changes in immune cells could affect the prognosis of HF. DNA methyltransferase 3 alpha (DNMT3A) mutations in monocytes significantly increase the expression of inflammatory genes and are correlated with the aggravation of chronic HF (11). Metabolically active genes such as fatty acid binding protein 5 (FABP5) are highly enriched in classical monocytes from heart failure patients, whereas b-catenin expression was significantly higher in another functionally distinct monocyte subset ($CD14^{++}CD16^{+}$ intermediate monocytes) (12). These studies suggest that further understanding of the inflammatory response and immune cell infiltration in HF is of great significance for optimizing the diagnosis and treatment of heart failure.

In recent years, microarray technology and integrated bioinformatics analyses have been performed to identify novel genes related to various diseases that might act as diagnostic and prognostic biomarkers (13–15). However, the diagnostic value of genes associated with immune infiltration in heart failure remains unclear. Thus, in the current study, we downloaded two microarray datasets of HF from the GEO database and used bioinformatic methods to screen for immune infiltration related biomarkers in heart failure, and to provide a theoretical basis for the diagnosis and treatment of HF patients.

MATERIALS AND METHODS

Ethics Statement

This study was approved by the institutional review board of the Third Affiliated Hospital, Sun Yat-sen University (IRB: 202102-201-01).

Data Source

In the current study, gene expression profiles of 16 non-failure controls (NF) and 108 heart failure samples caused by ischemic cardiomyopathy (CM) in GSE5406 dataset and 14 NF and 13 CM samples in GSE116250 dataset were downloaded from GEO database.

Identification and Functional Enrichment Analysis of DEGs

Limma R package was used to identify DEGs between NF and CM samples with $|\log2FC| > 0.5$ and adjusted $p < 0.05$ in GSE5406 datasets. ClusterProfiler R package was applied for GO and KEGG pathway enrichment analyses of DEGs. Biological process (BP), molecular function (MF) and cellular component (CC) were included in the GO analysis.

ssGSEA

ssGSEA was performed by Gene Set Variation Analysis (GSVA) R package to analyze the infiltraion of 24 immune cells in NF and CM samples (16). The 24 immune cells were TFH, Th2 cells, B cells, T cells, Tgd, NK CD56dim cells, Tem, macrophages, neutrophils, Th1 cells, mast cells, cytotoxic cells, DC, iDC, eosinophils, T helper cells, aDC, TReg, pDC, NK CD56bright cells, NK cells, Th17 cells, CD8 T cells, and Tcm.

WGCNA Analysis

A sample clustering tree map was first constructed to detect and eliminate outliers. Then, WGCNA was performed based on the gene expression profiles from GSE5406 dataset and sample traits (differentially infiltrated immune cells between NF and CM samples). The pick Soft Threshold function of WGCNA was used to calculate β from 1 to 20 in order to select the best soft threshold. Based on the selected soft threshold, the adjacency matrix was converted to topological overlap matrix to construct the network, and the gene dendrogram and module color were established by using the degree of dissimilarity. We further divided the initial module by dynamic tree cutting and merged similar modules. The Pearson correlation coefficient between the module eigengenes and sample traits were calculated

to find out the most relevant module (hub module) associated with sample traits.

Identification of Biomarkers in CM

First, DEGs were intersected with genes from the hub module in WGCNA analysis to obtain immune infiltration related candidate genes. Next, gene signature was selected by least absolute shrinkage and selection operator (LASSO) algorithm using glmnet R package (17) and support vector machine-recursive feature elimination (SVM-RFE) method using e1071 package (18), respectively. Robust gene signature was identified by overlapping gene signature obtained from LASSO and SVM-RFE. The diagnostic values of gene signature were evaluated by receiver operating curves (ROC) curves. Then, the external validation dataset GSE116250 was used to verify the expressions and diagnostic values of gene signature identified in GSE5406. Validated gene signature was identified as robust diagnostic biomarkers in heart failure.

Functional Analysis of Biomarkers in CM

To investigate the potential mechanisms of diagnostic biomarkers in regulating heart failure, 108 patients in GSE5406 were divided into high- and low-expression groups based on the median expression of each diagnostic biomarker. Moreover, to explore the relationship between diagnostic biomarkers and immune infiltration, the correlations between the expressions of diagnostic biomarkers and the abundance of differentially infiltrated immune cells were calculated.

Subject Characteristics and Realtime-PCR

Patients aged 18 and older, diagnosed with CHD by coronary computed tomography angiography or coronary angiography, with ejection fraction of 40% or less were enrolled into CM group. Age-matched CHD patients without heart failure (ejection fraction of 50% or above) were enrolled into NF control group. Patients with a history of malignancy, acute coronary syndrome, pulmonary embolism, renal failure [Glomerular filtration rate <60 ml/(min·1.73 m^2)] were excluded. The characteristics of CM and NF patients were shown in **Supplementary Table 3**.

RNA of PBMCs from CM ($n = 10$, 7 male and 3 female) and NF ($n = 10$, 8 male and 2 female) patients were extracted using Nuclezol LS RNA Isolation Reagent (ABP Biosciences Inc.) according to manufacturer's instructions. Collected RNA was diluted using nuclease-free water and electrophoresed on a denaturing formaldehyde agarose gel to visualize rRNA and ensure overall sample quality. RNA concentrations and purity were detected on ultraviolet spectrophotometer (Jinghua, Shanghai, China). Reverse transcription was performed on 1 μg total RNA from each sample using the SureScript-First-strand-cDNA-synthesis-kit (GeneCopoeia) according to manufacturer's instructions, and a CFX96 Real-time PCR System (Bio-Rad) was utilized to conduct the real time quantitative PCR (qPCR) reactions. BlazeTaq™ SYBR® Green qPCR Mix 2.0 (GeneCopoeia) was used for qPCR reactions, using 4 μL cDNA and appropriate volumes of specific primers in a final 10 μL volume. Triplicate reactions were performed to ensure accuracy. Glyceraldehyde-3-phosphate dehydrogenase (GAPDH) was used as the reference gene, and the relative gene expression was quantified by the $2^{-\Delta\Delta CT}$ method (19). The primer sequences were given in **Table 1**.

TABLE 1 | Primers sequence.

Genes	Forward	Reverse
CALU	GTTTCTTATGTGCCTGTCCCT	TTCCTTGCTCTCTTCTGGTGT
PALLD	GCCTACTTTCCTCCTGTTTTT	AGTGGTCATTGTTGGATTCTC
GAPDH	CGCTGAGTACGTCGTGGAGTC	GCTGATGATCTTGAGGCTGTTGTC

Statistical Analysis

All data were analyzed by R software (version 4.0.0). Wilcoxon test was used to compare the data between two groups, and significant difference was considered as $p < 0.05$ unless specified.

RESULTS

Transcriptome Profile Analyses of NF and CM Samples

A total of 224 DEGs were identified in GSE5406, including 93 up-regulated and 131 down-regulated genes in CM group compared to NF group (**Figure 1A**). The expression profile of top 50 up-regulated DEGs and top 50 down-regulated DEGs were shown in the heatmap (**Figure 1B**). To investigate the biological function of DEGs, we performed GO and KEGG pathway analysis. A total of 217 BP, 42 CC, 37 MF, and 16 KEGG pathways were significantly enriched (**Supplementary Tables 1**, **2**). As shown in **Figure 1C**, DEGs were mainly enriched into protein processing and extracellular matrix (ECM) related BPs, including response to topologically incorrect protein, response to unfolded protein (UPR), "*de novo*" protein folding, protein folding, chaperone-mediated protein folding, extracellular matrix organization, extracellular structure organization, "*de novo*" posttranslational protein folding, chaperone cofactor-dependent protein refolding, response to mechanical stimulus. Consistent with the results of GO analysis, protein processing and ECM related pathways were significantly enriched, including protein processing in endoplasmic reticulum, ECM-receptor interaction, and focal adhesion. In addition, estrogen signaling and MAPK signaling pathways showed to have close relationship with heart failure (**Figure 1D**).

Identification of Immune Infiltration Pattern in CM

Mounting evidence suggest that immune cells play important roles in heart failure (14–16). Thus, we explored the profile of immune cell infiltration in CM and NF samples by ssGSEA. Twenty-four subpopulations of infiltrated immune cells in CM and NF samples were identified and presented in the heatmap (**Figure 2A**). Interestingly, we found that the abundance of DC, mast cells, NK CD56dim cells, T cells, Tfh, Tgd, and Th2 cells were significantly higher, while the infiltration of eosinophils and Tcm were significantly

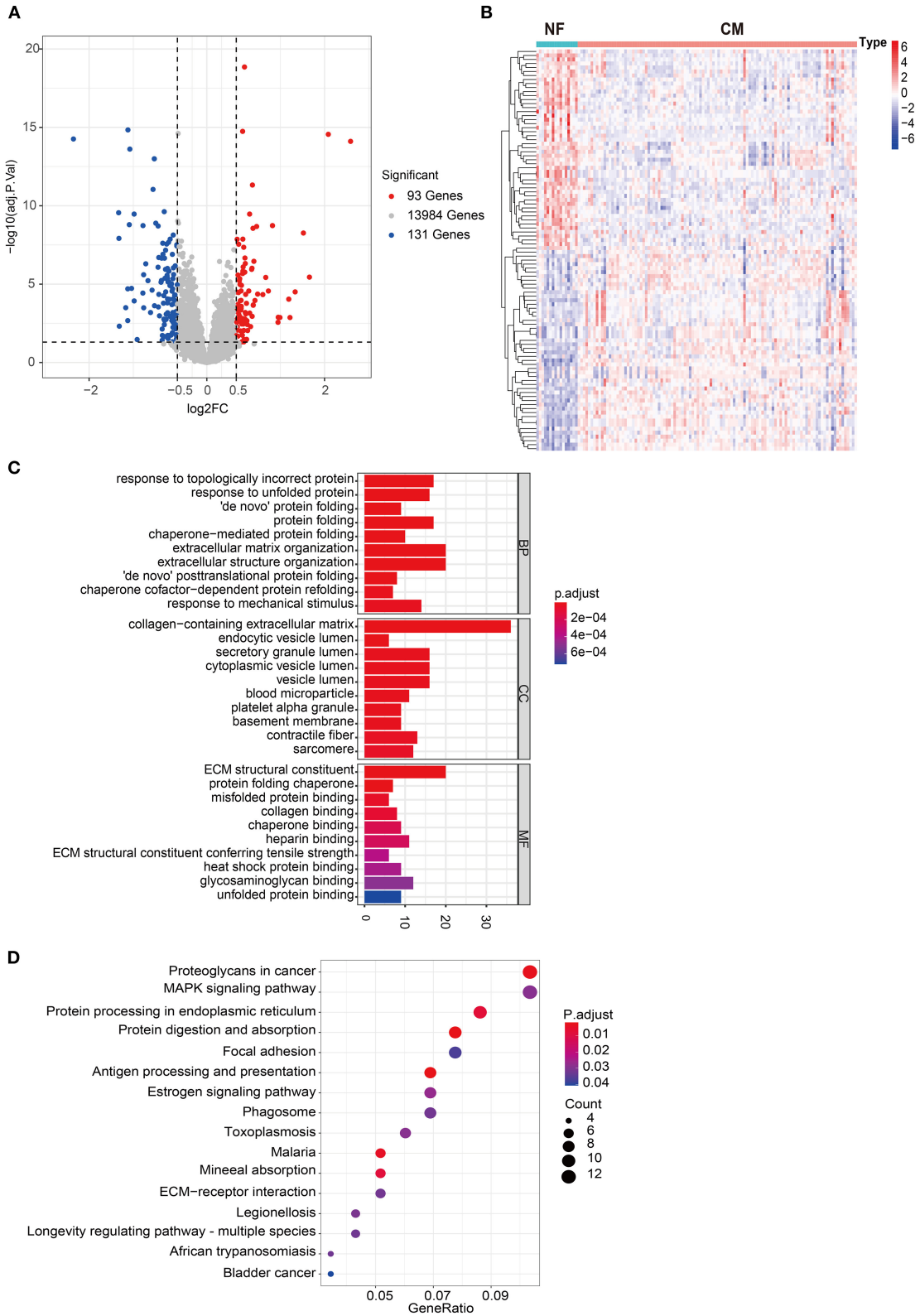

FIGURE 1 | Comprehensive analyses of the transcriptome profiles of NF and CM samples. **(A)** Volcano plot of significant DEGs between NF and CM samples. **(B)** A heatmap of the top 50 significantly upregulated or downregulated DEGs. **(C)** Bar plot of top 10 enriched GO terms of DEGs in each category. BP, biological process; CC, cellular components; MF, molecular functions. **(D)** Bubble plot of significantly enriched KEGG pathways of DEGs.

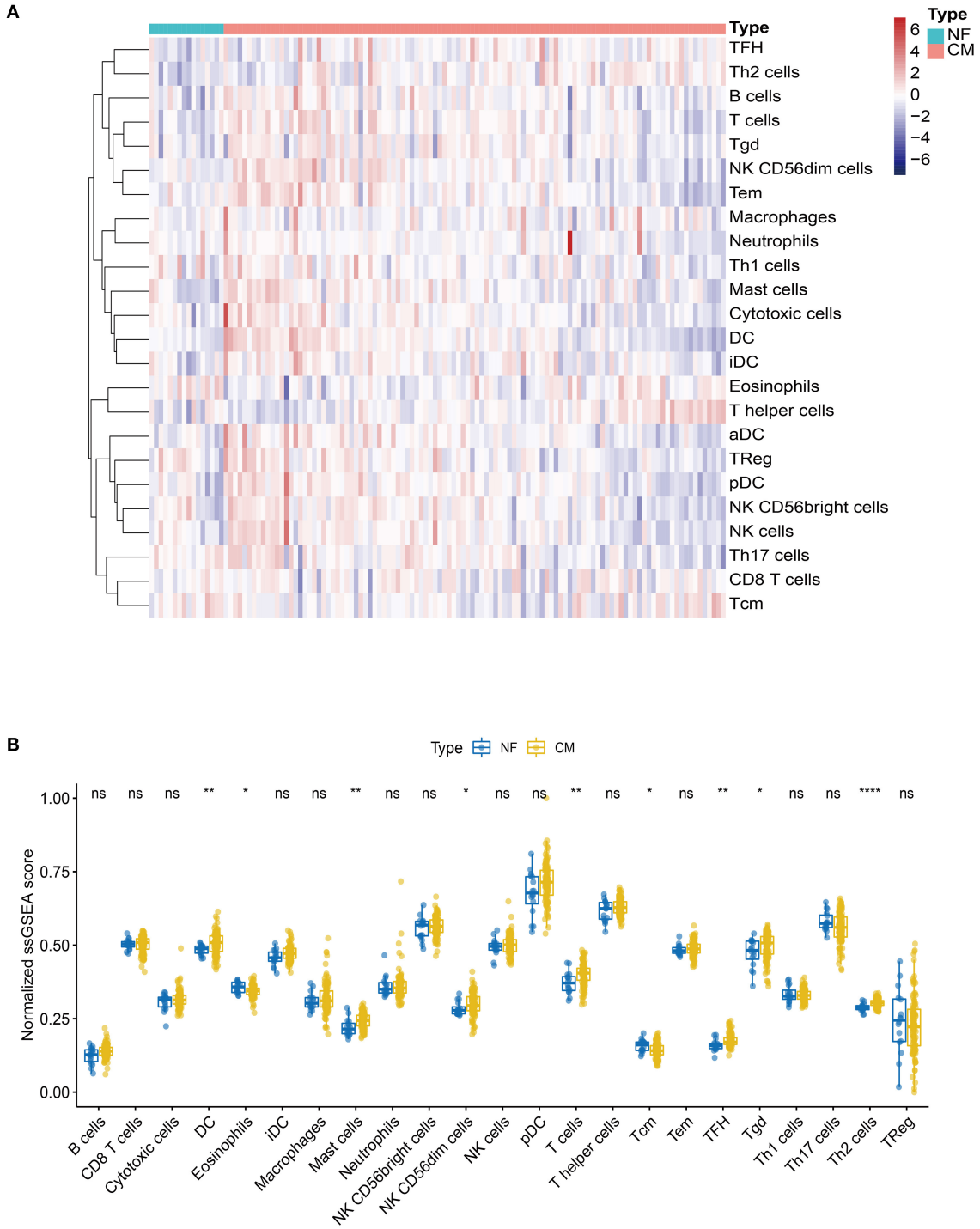

FIGURE 2 | Landscape of the immune infiltration in NF and CM samples. **(A)** Heatmap of the immune infiltration profiles of NF and CM samples analyzed by ssGSEA score-based method. **(B)** Comparison of immune cell infiltration between NF and CM samples. *$p < 0.05$, **$p < 0.01$, ****$p < 0.001$.

lower in CM samples compared to NF ones (**Figure 2B**). These results indicate that the inflammatory response of these immune cells may be critical for the etiology of heart failure.

Screening for Gene Signature of Immune Infiltration in CM

To further explore the genes mostly correlated with the inflammatory response in CM, we performed WGCNA

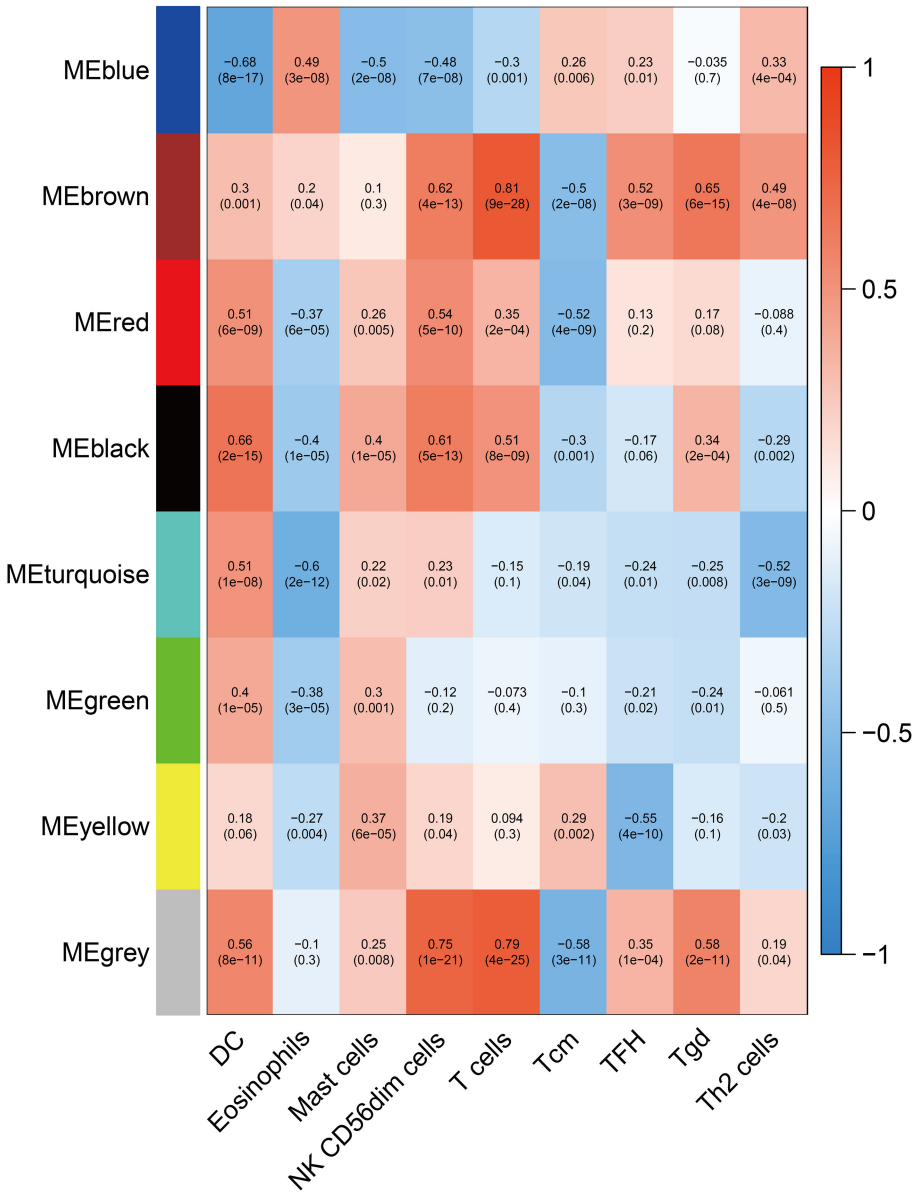

FIGURE 3 | Screening of the hub module associated with immune infiltration in CM. Heatmap of the correlation between module eigengene and differentially infiltrated immune cells. Each row represents a color-coded module eigengene, each column represents a type of infiltrated immune cells. The number in each cell means the correlation coefficient and *p*-value.

to screen for the hub module associated with above infiltrated immune cells. After eliminating the outlier samples (**Supplementary Figure 1**), we built the sample dendrogram and trait heatmap (**Supplementary Figure 2**). By using the pick Soft Threshold function of WGCNA, we found the optimal soft threshold power was 9, in which R^2 was 0.85 (**Supplementary Figure 3A**). After merging similar modules, eight modules from the co-expression network were identified (**Supplementary Figure 3B**). According to the module-trait relationships in **Figure 3**, we found that the MEbrown module was the most relevant module associated with DC (Cor = 0.3, $p < 0.01$), NK CD56dim cells (Cor = 0.62, $p < 0.01$), T cells (Cor = 0.81, $p < 0.01$), Tcm (Cor = −0.5, $p < 0.01$), TFH (Cor = 0.52, $p < 0.01$), Tgd (Cor = 0.65, $p < 0.01$) and Th2 cells (Cor =0.49, $p < 0.01$). Thus, MEbrown module was selected for downstream analysis.

Next, we overlapped DEGs with genes in the MEbrown module and obtained 10 candidate genes (**Figure 4A**). Ten

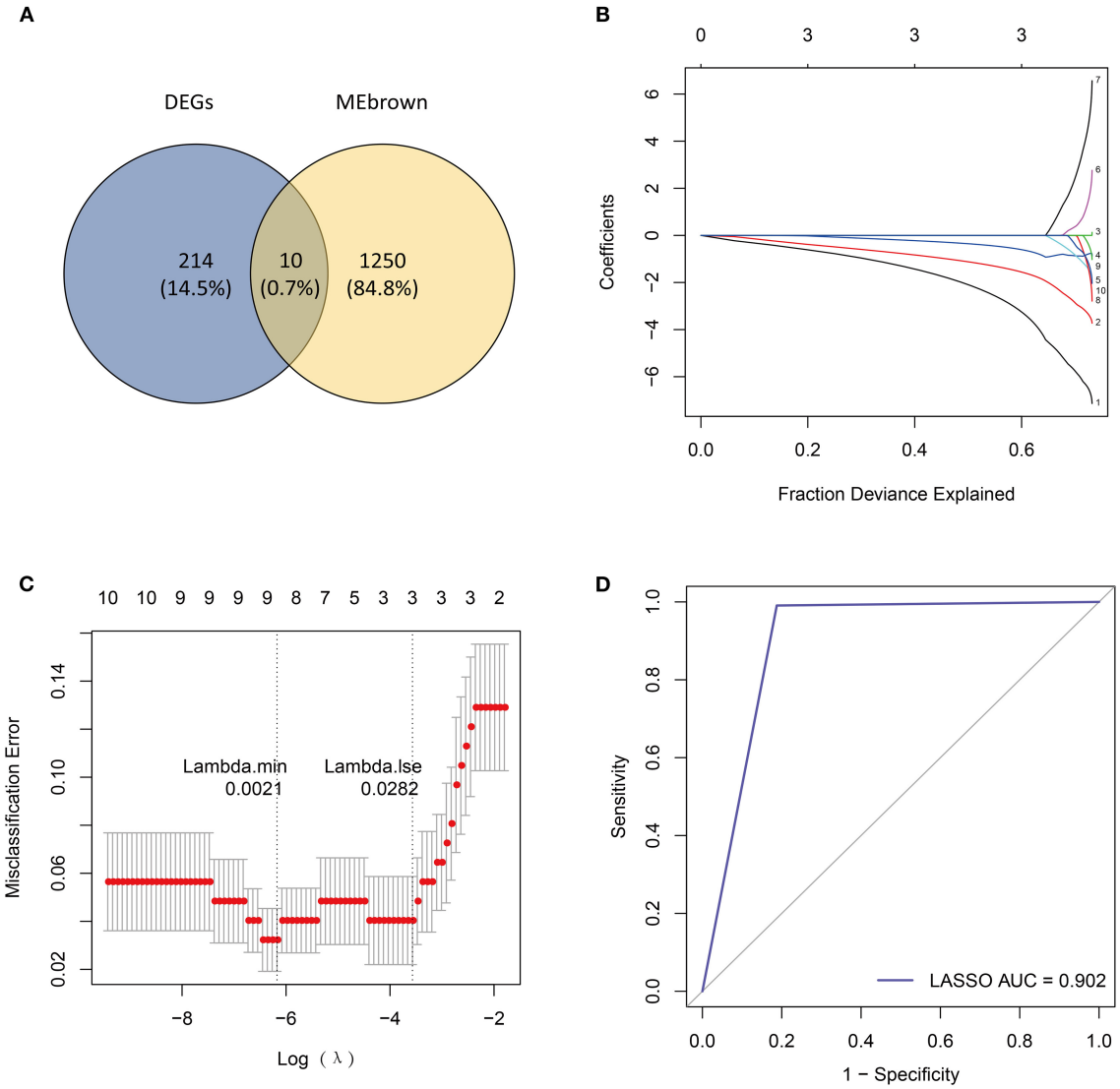

FIGURE 4 | Identification of candidate genes by LASSO regression model. **(A)** Venn diagram of 10 overlapped candidate genes shared by DEGs and MEbrown module. **(B)** LASSO coefficient profiles of candidate genes. **(C)** Cross-validation to select the optimal tuning parameter log (Lambda) in LASSO regression analysis. **(D)** ROC curve evaluation of LASSO regression analysis.

candidate genes were input into LASSO and SVM-RFE to identify gene signature, respectively. LASSO identified nine gene signatures under lambda.min = 0.0021, including PALLD, DexD-box helicase 39A (DDX39A), stress induced phosphoprotein 1 (STIP1), solute carrier family 38 member 2 (SLC38A2), CALU, CD164 molecule (CD164), selenoprotein T (SELT), four and a half LIM domain 1 (FHL1) and claudin domain containing 1 (CLDND1) (**Figures 4B,C**). The accuracy of LASSO was evaluated by ROC curve that the area under the ROC curve (AUC) was 0.902 (**Figure 4D**). Meanwhile, we identified 7 gene signatures by SVM-RFE, including PALLD, DDX39A, CD164, CLDND1, SLC38A2, CALU, and heat shock protein family D member 1 (HSPD1) with the accuracy of 0.962 (**Figures 5A,B**). To get the robust gene signature in heart failure, we overlapped genes from LASSO and SVM-RFE and got six gene signatures (**Figure 5C**), including PALLD, DDX39A, CD164, CLDND1, SLC38A2, and CALU. The expression levels of PALLD, DDX39A, CD164, CLDND1, SLC38A2, and CALU were all significantly higher in NF samples compared to CM ones in GSE5406 (**Figure 5D**).

Verification of the Potential Biomarkers for CM

We further evaluated the diagnostic values of PALLD, DDX39A, CD164, CLDND1, SLC38A2, and CALU in GSE5406 by ROC curves. We found that they all had high accuracy with AUC >0.7 (**Figure 6A**). To verify the diagnostic values of the

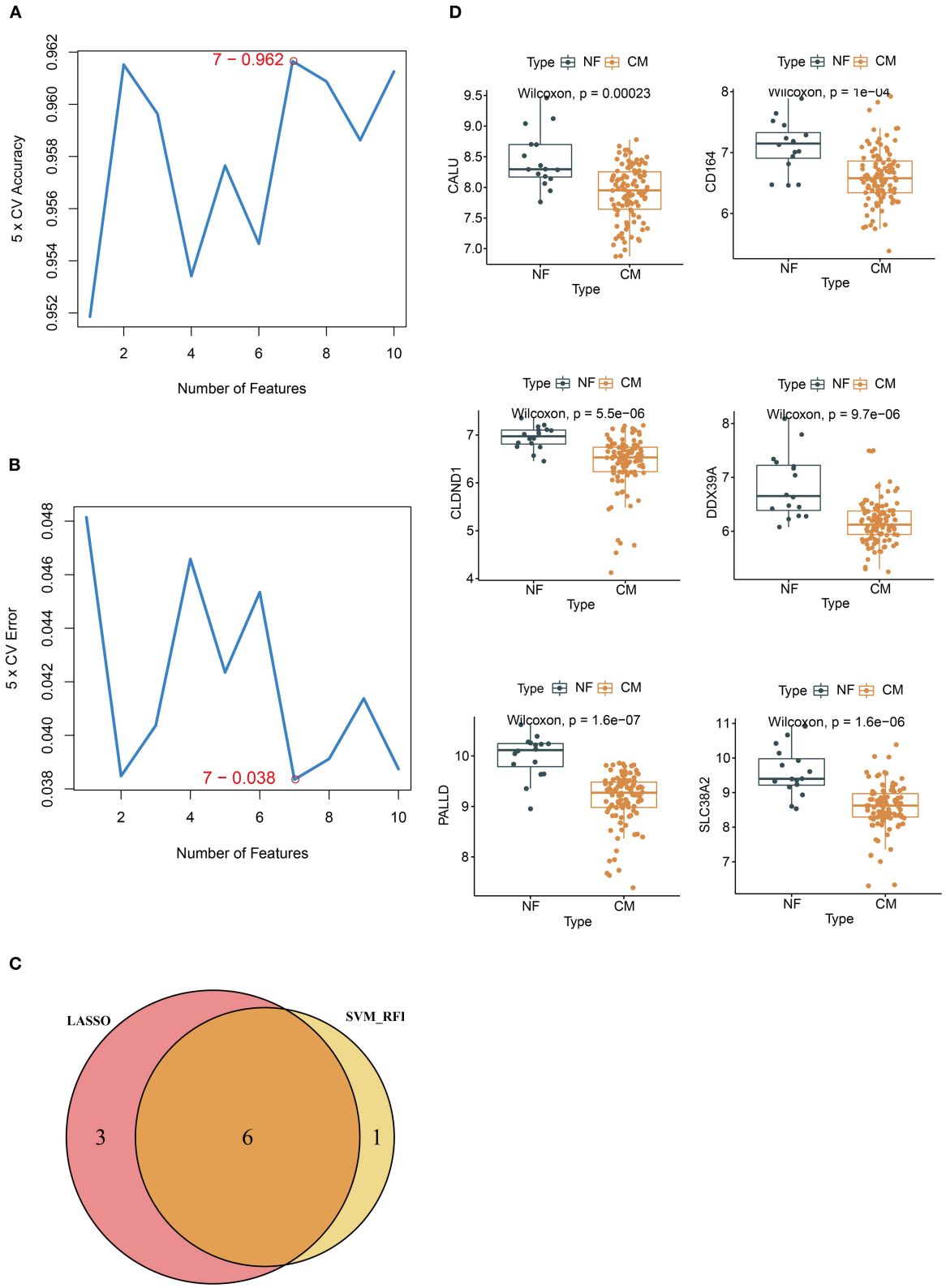

FIGURE 5 | Identification of candidate genes by SVM-RFE. **(A)** 7 gene signatures are identified by SVM-RFE analysis with the accuracy of 0.962 and **(B)** error of 0.038. **(C)** Venn diagram of six overlapped candidate genes shared by the LASSO and SVM-RFE algorithms. **(D)** The expressions of candidate diagnostic biomarkers in the NF and CM samples from GSE5406 dataset.

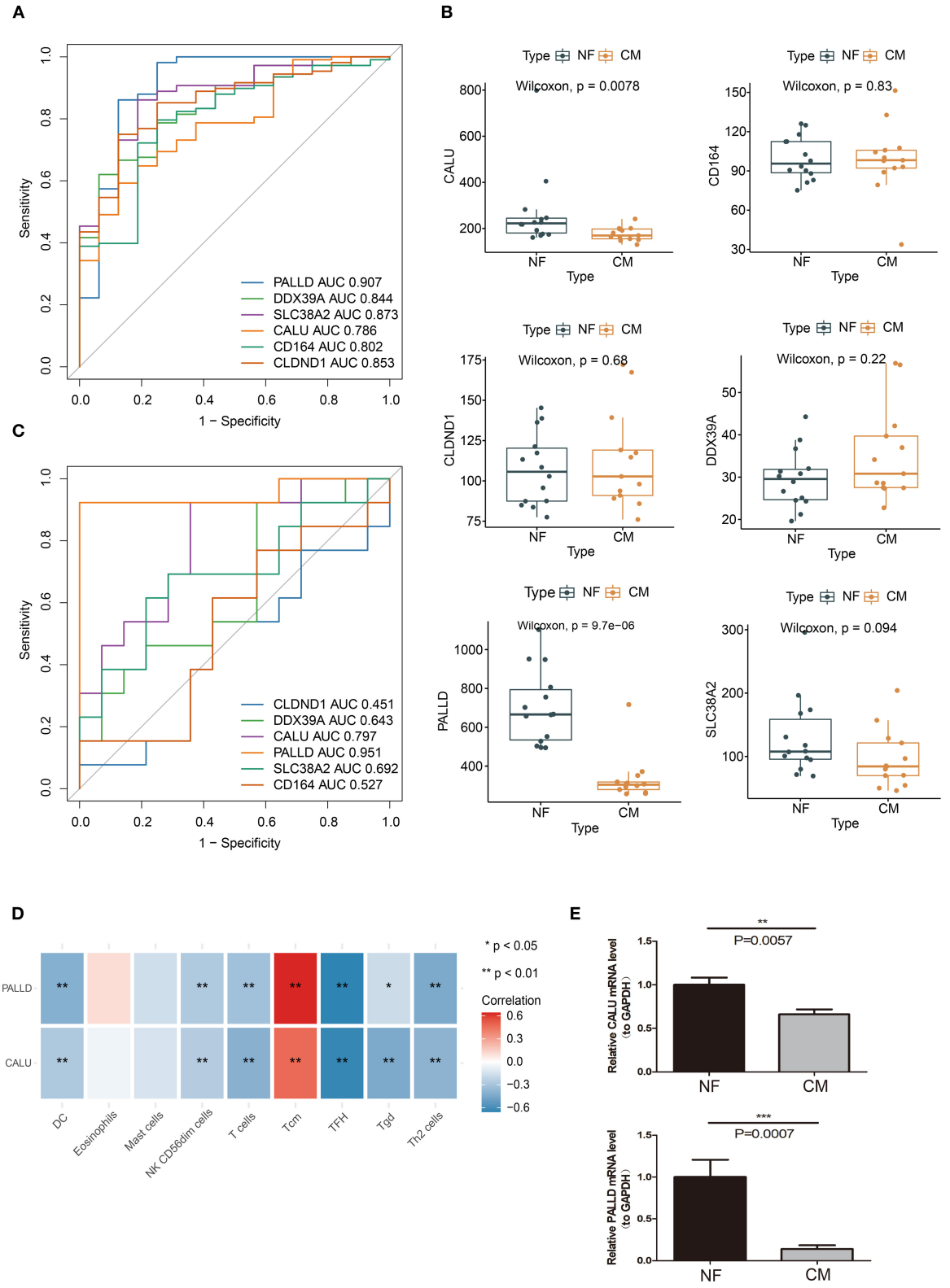

FIGURE 6 | Verification of biomarkers for CM. **(A)** ROC curve evaluation of the diagnostic effectiveness of candidate biomarkers using GSE5406 dataset. **(B)** The expressions of candidate diagnostic biomarkers in the GSE116250 dataset. **(C)** ROC curve evaluation of the diagnostic effectiveness of candidate biomarkers using GSE116250 dataset. **(D)** Heatmap of correlations between PALLD, CALU and differentially infiltrated immune cells. **(E)** Real-time PCR analyses of the expression levels of PALLD and CALU in PBMCs isolated from CM and NF patients $^{*}p < 0.05$, $^{**}p < 0.01$, $^{***}p < 0.001$

candidate biomarkers, we examined their expressions in an external validation dataset GSE116250 to get robust diagnostic biomarkers. We found that the expression trends of CALU and PALLD in GSE116250 were consistent with those in GSE5406 (**Figure 6B**), and that CALU and PALLD also had high accuracy in classifying heart failure samples, as evidenced by AUC >0.7 (**Figure 6C**). Moreover, we found that the expressions of CALU and PALLD were significantly negative correlated with DC, NK CD56dim cells, T cells, Tfh, Tgd, and Th2 cells, and positive correlated with Tcm (**Figure 6D**).

To further evaluate the value of CALU and PALLD as biomarkers, the levels of CALU and PALLD were assessed in PBMCs isolated from CM and NF patients. In agreement with the results in GSE116250 and GSE5406, the levels of CALU and PALLD were also significantly lower in PBMCs collected from CM patients compared to NF ones (**Figure 6E**) Collectively, these results suggest that CALU and PALLD may be potential diagnostic biomarkers for heart failure due to ischemic cardiomyopathy.

DISCUSSION

The prevalence of HF is increasing worldwide and has reached epidemic proportions. Although significant progress has been made in the medications and interventions for HF, the mortality and hospitalization rates remain high (20). Recently, immune cell infiltration has been confirmed to play a vital role in the occurrence and development of cardiovascular diseases (10, 13). Cardiac inflammation and subsequent tissue damage are orchestrated by the infiltration and activation of various immune cells in the myocardium which result in heart failure eventually (20). Thus, it is essential to comprehensively investigate the contributions of infiltrated immune cells in HF. In this study, we analyzed the immune infiltration profiles of CM and NF samples, and identified CALU and PALLD as potential diagnostic biomarkers for heart failure due to ischemic cardiomyopathy by using integrated bioinformatics analyses.

Consistent with a previous report (21), we found that DEGs between NF and CM were mainly enriched into biological processes and pathways related to protein processing and ECM. Structural changes occur in the level of ER and UPR components in cardiomyocytes of patients with HF (22). When maladaptive UPR fails to restore ER homeostasis, it might induce risk factors for HF including increased reactive oxygen species (ROS) production, inflammation and apoptosis which further aggravate HF (22). In addition, numerous studies have explored the relationship between ECM and heart diseases (23, 24). Alterations in the architecture, composition, and distribution of interstitial ECM play a major role in pathological myocardial structural remodeling and left ventricular diastolic dysfunction (25, 26). Myocardial fibrosis is characterized by accumulation of collagen-rich ECM, such as collagen type I and III fibers, results from the predominance of fiber formation and deposition over its degradation and removal (27). ECM dyshomeostasis is also postulated to occur during the development and progression of HF, including changes in the synthesis, processing, degradation, and turnover of proteins such as fibrillar collagen (28). Therefore, those DEGs we found may regulate HF through protein processing and ECM.

Increasing evidence show that immune cell infiltration in the myocardium has adverse effect on heart function (29–31). Single-cell sequencing analyses reveal that the immune cell profiles are remarkably different in healthy and diseased hearts (15, 32, 33). In this study, we found that the abundance of DC, mast cells, NK CD56dim cells, T cells, Tfh, Tgd, and Th2 cells were higher, while the infiltration of eosinophils and Tcm were lower in HF samples, indicating their important roles in the etiology of HF. Consistent with our findings, Patella V et al. and Abdolmaleki F et al. found an increase in numbers of mast cells and T cells in HF, respectively (34, 35). Mast cells initiate adverse myocardial remodeling by activating matrix metalloproteinase (MMP) and fibrosis in the heart (36). Moreover, the profibrotic and antiangiogenic functions of Th17, Th2, and dysfunctional Treg cells are indispensable for the progression to ischemic heart failure (37, 38). On the contrary, inducible depletion of eosinophils exacerbates cardiac dysfunction, cell death, and fibrosis, by producing IL-4 and cationic protein mEar1, fibroblast activation, and neutrophil adhesion (39). Studies from our and other groups suggest a critical role of immune infiltration in the development of heart failure, and further understandings of the effect of each type of infiltrated immune cells may provide us clues for developing novel therapeutic strategies for heart failure.

PALLD encodes a cytoskeleton protein involved in actin reorganization (40), which plays an important role in heart development (41). PALLD was reported to be related to vein graft stenosis after coronary artery bypass grafting. A single-nucleotide polymorphism (SNP) in the PALLD has been reported to be associated with coronary heart disease (CHD) (42). CALU produces a Ca^{2+}-binding protein that is localized in the endoplasmic reticulum (ER) (43). During the excitation-contraction coupling process, CALU regulates Ca^{2+} uptake and plays an important role in maintaining normal heart function (44). Our analyses show that the expressions of CALU and PALLD were significantly negative correlated with the abundances of DC, NK CD56dim cells, T cells, Tfh, Tgd and Th2 cells, and Tcm, suggesting that CALU and PALLD may regulate HF via immune-related pathways mediated by the infiltration of these immune cells. More importantly, we confirmed that the expression levels of CALU and PALLD were markedly lower in PBMCs from CM patients compared with NF ones. Collectively, these findings indicate that CALU and PALLD are potential biomarkers for the diagnosis of HF.

Several limitations of the present study should be noted. Firstly, the study was retrospective, further prospective studies are needed to assess the diagnostic and prognostic value of CALU and PALLD in HF. Secondly, the relationships between the biomarkers and immune regulation in heart failure were only verified by assessing their levels in PBMCs from CM and NF patients. Further *in vitro* and *in vivo* experiments are required to explore the detailed mechanisms through which CALU and PALLD regulate inflammatory responses in HF. Taken together, our analyses delineate the potential etiology of HF due to CM and identified immune infiltration related biomarkers in HF, which

may provide guidance for diagnosis and treatment of patients with HF.

DATA AVAILABILITY STATEMENT

The datasets presented in this study can be found in online repositories. The names of the repository/repositories and accession number(s) can be found in the article/**Supplementary Material**.

ETHICS STATEMENT

The studies involving human participants were reviewed and approved by the Institutional Review Board of the Third Affiliated Hospital, Sun Yat-sen University (IRB: 202102-201-01). The patients/participants provided their written informed consent to participate in this study.

AUTHOR CONTRIBUTIONS

YZ and LP contributed to the study concepts and study design and helped in revising the manuscript. XL, SX, and YL drafted the manuscript, performed data management, and bioinformatics analysis. QC were responsible for clinical sample collection. All authors were involved in reporting the results of this study and approved the final version of the submitted manuscript.

FUNDING

This work was supported by the National Natural Science Foundation of China (82000466), the Medical Science and Technology Research Project of Guangzhou (Grant No. 202002020030), and the cultivation project of National Natural Science Foundation of the Third Affiliated Hospital, Sun Yat-sen University (Grant No. 2021G2RPYQN11).

SUPPLEMENTARY MATERIAL

The Supplementary Material for this article can be found online at: https://www.frontiersin.org/articles/10.3389/fcvm.2021.774755/full#supplementary-material

REFERENCES

1. Ponikowski P, Voors AA, Anker SD, Bueno H, Cleland JGF, Coats AJS, et al. 2016 ESC Guidelines for the diagnosis treatment of acute chronic heart failure: The Task Force for the diagnosis treatment of acute chronic heart failure of the European Society of Cardiology (ESC)Developed with the special contribution of the Heart Failure Association (HFA) of the ESC. *Eur Heart J.* (2016) 37:2129–200. doi: 10.1093/eurheartj/ehw128
2. Yancy CW, Jessup M, Bozkurt B, Butler J, Casey DE, Colvin MM, et al. 2017 ACC/AHA/HFSA Focused Update of the 2013 ACCF/AHA guideline for the management of heart failure: a report of the American College of Cardiology/American heart association task force on clinical practice guidelines and the heart failure society of America. *Circulation.* (2017) 136:e137–61. doi: 10.1161/CIR.0000000000000509
3. Cunningham JW, Claggett BL, O'Meara E, Prescott MF, Pfeffer MA, Shah SJ, et al. Effect of sacubitril/valsartan on biomarkers of extracellular matrix regulation in patients with HFpEF. *J Am Coll Cardiol.* (2020) 76:503–14. doi: 10.1016/j.jacc.2020.05.072
4. Mann DL. Inflammatory mediators and the failing heart: past, present, and the foreseeable future. *Circ Res.* (2002) 91:988–98. doi: 10.1161/01.RES.0000043825.01705.1B
5. Zimmet JM, Hare JM. Nitroso-redox interactions in the cardiovascular system. *Circulation.* (2006) 114:1531–44. doi: 10.1161/CIRCULATIONAHA.105.605519
6. Braunwald E. Biomarkers in heart failure. *N Engl J Med.* (2008) 358:2148–59. doi: 10.1056/NEJMra0800239
7. Hein S, Kostin S, Heling A, Maeno Y, Schaper J. The role of the cytoskeleton in heart failure. *Cardiovasc Res.* (2000) 45:273–8. doi: 10.1016/S0008-6363(99)00268-0
8. Luo M, Anderson ME. Mechanisms of altered Ca(2)(+) handling in heart failure. *Circ Res.* (2013) 113:690–708. doi: 10.1161/CIRCRESAHA.113.301651
9. Dick SA, Epelman S. Chronic heart failure and inflammation what do we really know? *Circul Res.* (2016) 119:159–76. doi: 10.1161/CIRCRESAHA.116.308030
10. de Lucia C, Grisanti LA, Borghetti G, Piedepalumbo M, Ibetti J, Maria Lucchese A, et al. GRK5 contributes to impaired cardiac function and immune cell recruitment in post-ischemic heart failure. *Cardiovasc Res.* (2021) 9:cvab044. doi: 10.1093/cvr/cvab044
11. Abplanalp WT, Cremer S, John D, Hoffmann J, Schuhmacher B, Merten M, et al. Clonal hematopoiesis-driver DNMT3A mutations alter immune cells in heart failure. *Circ Res.* (2021) 128:216–28. doi: 10.1161/CIRCRESAHA.120.317104
12. Abplanalp WT, John D, Cremer S, Assmus B, Dorsheimer L, Hoffmann J, et al. Single-cell RNA-sequencing reveals profound changes in circulating immune cells in patients with heart failure. *Cardiovasc Res.* (2021) 117:484–94. doi: 10.1093/cvr/cvaa101
13. Zhao E, Xie H, Zhang Y. Predicting diagnostic gene biomarkers associated with immune infiltration in patients with acute myocardial infarction. *Front Cardiovasc Med.* (2020) 7:586871. doi: 10.3389/fcvm.2020.586871
14. Cao Y, Tang W, Tang W. Immune cell infiltration characteristics and related core genes in lupus nephritis: results from bioinformatic analysis. *BMC Immunol.* (2019) 20:37. doi: 10.1186/s12865-019-0316-x
15. Martini E, Kunderfranco P, Peano C, Carullo P, Cremonesi M, Schorn T, et al. Single-cell sequencing of mouse heart immune infiltrate in pressure overload-driven heart failure reveals extent of immune activation. *Circulation.* (2019) 140:2089–107. doi: 10.1161/CIRCULATIONAHA.119.041694
16. Hanzelmann S, Castelo R, Guinney J. GSVA: gene set variation analysis for microarray and RNA-seq data. *BMC Bioinformatics.* (2013) 14:7. doi: 10.1186/1471-2105-14-7
17. Vasquez MM, Hu CC, Roe DJ, Chen Z, Halonen M, Guerra S. Least absolute shrinkage and selection operator type methods for the identification of serum biomarkers of overweight and obesity: simulation and application. *Bmc Med Res Methodol.* (2016) 16:254. doi: 10.1186/s12874-016-0254-8
18. Noble WS. What is a support vector machine? *Nat Biotechnol.* (2006) 24:1565–7. doi: 10.1038/nbt1206-1565
19. Schmittgen TD, Livak KJ. Analyzing real-time PCR data by the comparative C-T method. *Nat Protoc.* (2008) 3:1101–8. doi: 10.1038/nprot.2008.73
20. Strassheim D, Dempsey EC, Gerasimovskaya E, Stenmark K, Karoor V. Role of inflammatory cell subtypes in heart failure. *J Immunol Res.* (2019) 2019:2164017. doi: 10.1155/2019/2164017
21. Ren J, Bi YG, Sowers JR, Hetz C, Zhang YM. Endoplasmic reticulum stress and unfolded protein response in cardiovascular diseases. *Nat Rev Cardiol.* (2021) 18:499–521. doi: 10.1038/s41569-021-00511-w
22. Glembotski CC. Endoplasmic reticulum stress in the heart. *Circ Res.* (2007) 101:975–84. doi: 10.1161/CIRCRESAHA.107.161273

23. Frangogiannis NG. The extracellular matrix in ischemic and nonischemic heart failure. *Circul Res.* (2019) 125:117–46. doi: 10.1161/CIRCRESAHA.119.311148
24. Guo Y, Gupte M, Umbarkar P, Singh AP, Sui JY, Force T, et al. Entanglement of GSK-3beta, beta-catenin and TGF-beta1 signaling network to regulate myocardial fibrosis. *J Mol Cell Cardiol.* (2017) 110:109–20. doi: 10.1016/j.yjmcc.2017.07.011
25. Kasner M, Westermann D, Lopez B, Gaub R, Escher F, Kuhl U, et al. Diastolic tissue Doppler indexes correlate with the degree of collagen expression and cross-linking in heart failure and normal ejection fraction. *J Am Coll Cardiol.* (2011) 57:977–85. doi: 10.1016/j.jacc.2010.10.024
26. Zile MR, Baicu CF, Ikonomidis JS, Stroud RE, Nietert PJ, Bradshaw AD, et al. Myocardial stiffness in patients with heart failure and a preserved ejection fraction: contributions of collagen and titin. *Circulation.* (2015) 131:1247–59. doi: 10.1161/CIRCULATIONAHA.114.013215
27. Lopez B, Ravassa S, Gonzalez A, Zubillaga E, Bonavila C, Berges M, et al. Myocardial collagen cross-linking is associated with heart failure hospitalization in patients with hypertensive heart failure. *J Am College Cardiol.* (2016) 67:251–60. doi: 10.1016/j.jacc.2015.10.063
28. Gonzalez A, Schelbert EB, Diez J, Butler J. Myocardial interstitial fibrosis in heart failure: biological and translational perspectives. *J Am Coll Cardiol.* (2018) 71:1696–706. doi: 10.1016/j.jacc.2018.02.021
29. Carrillo-Salinas FJ, Ngwenyama N, Anastasiou M, Kaur K, Alcaide P. Heart inflammation immune cell roles and roads to the heart. *Am J Pathol.* (2019) 189:1482–94. doi: 10.1016/j.ajpath.2019.04.009
30. Lafuse WP, Wozniak DJ, Rajaram MVS. Role of cardiac macrophages on cardiac inflammation, fibrosis and tissue repair. *Cells.* (2020) 10:51. doi: 10.3390/cells10010051
31. Kawada J, Takeuchi S, Imai H, Okumura T, Horiba K, Suzuki T, et al. Immune cell infiltration landscapes in pediatric acute myocarditis analyzed by CIBERSORT. *J Cardiol.* (2021) 77:174–8. doi: 10.1016/j.jjcc.2020.08.004
32. Farbehi N, Patrick R, Dorison A, Xaymardan M, Janbandhu V, Wystub-Lis K, et al. Single-cell expression profiling reveals dynamic flux of cardiac stromal, vascular and immune cells in health and injury. *Elife.* (2019) 8:43882. doi: 10.7554/eLife.43882
33. Suryawanshi H, Clancy R, Morozov P, Halushka MK, Buyon JP, Tuschl T. Cell atlas of the foetal human heart and implications for autoimmune-mediated congenital heart block. *Cardiovasc Res.* (2020) 116:1446–57. doi: 10.1093/cvr/cvz257
34. Patella V, Marino I, Arbustini E, Lamparter-Schummert B, Verga L, Adt M, et al. Stem cell factor in mast cells and increased mast cell density in idiopathic and ischemic cardiomyopathy. *Circulation.* (1998) 97:971–8. doi: 10.1161/01.CIR.97.10.971
35. Abdolmaleki F, Gheibi Hayat SM, Bianconi V, Johnston TP, Sahebkar A. Atherosclerosis and immunity: A perspective. *Trends Cardiovasc Med.* (2019) 29:363–71. doi: 10.1016/j.tcm.2018.09.017
36. Ngkelo A, Richart A, Kirk JA, Bonnin P, Vilar J, Lemitre M, et al. Mast cells regulate myofilament calcium sensitization and heart function after myocardial infarction. *J Exp Med.* (2016) 213:1353–74. doi: 10.1084/jem.20160081
37. Bansal SS, Ismahil MA, Goel M, Patel B, Hamid T, Rokosh G, et al. Activated T lymphocytes are essential drivers of pathological remodeling in ischemic heart failure. *Circ-Heart Fail.* (2017) 10:3688. doi: 10.1161/CIRCHEARTFAILURE.116.003688
38. Bansal SS, Ismahil MA, Goel M, Zhou GH, Rokosh G, Hamid T, et al. Dysfunctional and proinflammatory regulatory T-lymphocytes are essential for adverse cardiac remodeling in ischemic cardiomyopathy. *Circulation.* (2019) 139:206–21. doi: 10.1161/CIRCULATIONAHA.118.036065
39. Liu J, Yang CZ, Liu TX, Deng ZY, Fang WQ, Zhang X, et al. Eosinophils improve cardiac function after myocardial infarction. *Nat Commun.* (2020) 11:5. doi: 10.1038/s41467-020-19297-5
40. Mykkanen OM, Gronholm M, Ronty M, Lalowski M, Salmikangas P, Suila H, et al. Characterization of human palladin, a microfilament-associated protein. *Mol Biol Cell.* (2001) 12:3060–73. doi: 10.1091/mbc.12.10.3060
41. Mori M, Nakagami H, Koibuchi N, Miura K, Takami Y, Koriyama H, et al. Zyxin mediates actin fiber reorganization in epithelial-mesenchymal transition and contributes to endocardial morphogenesis. *Mol Biol Cell.* (2009) 20:3115–24. doi: 10.1091/mbc.e09-01-0046
42. Bare LA, Morrison AC, Rowland CM, Shiffman D, Luke MM, Iakoubova OA, et al. Five common gene variants identify elevated genetic risk for coronary heart disease. *Genet Med.* (2007) 9:682–9. doi: 10.1097/GIM.0b013e318156fb62
43. Sahoo SK, Kim DH. Characterization of calumenin in mouse heart. *BMB Rep.* (2010) 43:158–63. doi: 10.5483/BMBRep.2010.43.3.158
44. Sahoo SK, Kim DH. Calumenin interacts with SERCA2 in rat cardiac sarcoplasmic reticulum. *Mol Cells.* (2008) 26:265–9. doi: 10.1186/1476-4598-7-74

Conflict of Interest: The authors declare that the research was conducted in the absence of any commercial or financial relationships that could be construed as a potential conflict of interest.

Publisher's Note: All claims expressed in this article are solely those of the authors and do not necessarily represent those of their affiliated organizations, or those of the publisher, the editors and the reviewers. Any product that may be evaluated in this article, or claim that may be made by its manufacturer, is not guaranteed or endorsed by the publisher.

Copyright © 2021 Liu, Xu, Li, Chen, Zhang and Peng. This is an open-access article distributed under the terms of the Creative Commons Attribution License (CC BY). The use, distribution or reproduction in other forums is permitted, provided the original author(s) and the copyright owner(s) are credited and that the original publication in this journal is cited, in accordance with accepted academic practice. No use, distribution or reproduction is permitted which does not comply with these terms.

frontiers in Cardiovascular Medicine

ORIGINAL RESEARCH
published: 02 December 2021
doi: 10.3389/fcvm.2021.765591

Spermidine Affects Cardiac Function in Heart Failure Mice by Influencing the Gut Microbiota and Cardiac Galectin-3

Yufeng Chen[1†], *Zhiqin Guo*[1†], *Shaonan Li*[1,2], *Zhen Liu*[1,2] *and Pingan Chen*[1*]

[1] *Department of Cardiology, The Second Affiliated Hospital, School of Medicine, South China University of Technology, Guangzhou, China,* [2] *Department of Cardiology, Guangzhou First People's Hospital, Guangzhou, China*

Spermidine, which can be synthesized by the gut microbiota, can prevent cardiac hypertrophy and delay the progression to heart failure (HF). However, it is not clear whether the effect of spermidine on cardiac function is mediated by modulating the gut microbiota when HF occurs. Female HF Kunming mice induced by transverse aortic constriction were administered spermidine (HF+S group) or its antagonist (HF+SR group). Echocardiography, messenger ribonucleic acid (RNA) and protein expression of galectin-3 in the heart, cardiomyocyte apoptosis assays and gut microbiota analysis were detected. Left ventricular end-diastolic volume and diameter (LVVd and LVDd), and left ventricular end-systolic volume and diameter in the HF+SR group were significantly enlarged compared with those in the HF group (all $P < 0.05$). The HF+S group had a smaller LVDd and LVVd than the HF+SR group (5.01 ± 0.67 vs. 6.13 ± 0.45 mm, $P = 0.033$; 121.44 ± 38.74 vs. 189.94 ± 31.42 μL, $P = 0.033$). The messenger RNA and protein expression of galectin-3 and the number of apoptotic cardiomyocytes increased significantly in the HF+SR group compared to the HF group. Gut microbiota analysis showed that spermidine antagonists reduced the *Firmicutes/Bacteroidetes* ratio and changed the microbial community richness and diversity. In conclusion, spermidine can improve cardiac function in HF, and the regulation of gut microbiota and cardiac fibrosis may be a factor in the effect of spermidine on the improvement of cardiac function.

Keywords: heart failure, spermidine, microbiota, cardiac fibrosis, galectin-3

OPEN ACCESS

Edited by:
Yuli Huang,
Southern Medical University, China

Reviewed by:
Zuheng Liu,
First Affiliated Hospital of Xiamen University, China
Jin-Jer Chen,
National Taiwan University, Taiwan

***Correspondence:**
Pingan Chen
cpadejxyx@gzhmu.edu.cn

[†]These authors have contributed equally to this work

Specialty section:
This article was submitted to General Cardiovascular Medicine, a section of the journal Frontiers in Cardiovascular Medicine

Received: *27 August 2021*
Accepted: *08 November 2021*
Published: *02 December 2021*

Citation:
Chen Y, Guo Z, Li S, Liu Z and Chen P (2021) Spermidine Affects Cardiac Function in Heart Failure Mice by Influencing the Gut Microbiota and Cardiac Galectin-3. Front. Cardiovasc. Med. 8:765591. doi: 10.3389/fcvm.2021.765591

INTRODUCTION

Cardiac function and gut microbiota can affect each other. Reduced cardiac output causes intestinal wall ischemia, edema and structural disruption of the intestinal epithelial barrier function in heart failure (HF), leading to increased intestinal permeability, which in turn, contributes to the progression of HF (1). Furthermore, the impairment of intestinal barrier function leads to the translocation of gut bacterial deoxyribonucleic acid (DNA) and/or endotoxins into the bloodstream (2) and contributes to the deterioration of cardiac function (3). Studies have shown that in chronic HF, the gut microbiota is characterized by large compositional shifts with low bacterial richness and depletion of the core microbiota (4, 5). Therefore, the intestinal microbiota plays an important role in the development and progression of HF (6–8).

Spermidine is a natural polyamine present in all living organisms at levels from micromolar to millimolar that is critically involved in the maintenance of cellular homeostasis (9, 10), usually with endogenous spermidine concentrations decreasing during the natural process of organismal aging (11, 12). Some studies have shown that dietary spermidine protects against cardiovascular aging (13), prevents cardiac hypertrophy and delayed the progression to HF (14), suggesting a beneficial effect on HF. One possible mechanism is that spermidine can enhance cardiac autophagy, mitophagy and mitochondrial respiration (14, 15). Moreover, the gut microbiota is significantly related to the synthesis of spermidine (16) and some gut microorganisms contain spermidine synthase (17). Spermidine can also enhance the gut barrier integrity and alter the gut microbiota in diet-induced obese mice (18). Although spermidine and the gut microbiota are both associated with HF, it is not clear whether cardiac function can be affected by spermidine through modulating the gut microbiota when HF occurs. We speculated that regulation of the gut microbiota might be a contributing factor to the effect of spermidine on the improvement of cardiac function. A close relationship may exist among spermidine, HF and the gut microbiota, and the cardioprotective role of spermidine, especially to HF, may be mediated by optimizing the gut microbiota composition.

In this study, we investigated the effect of spermidine on HF by altering its levels and assessed the association between spermidine and gut microbiota in an HF model induced by transverse aortic constriction (TAC) to explore whether spermidine can affect cardiac function by modulating the gut microbiota.

MATERIALS AND METHODS

Aortic Constriction

TAC was performed as described previously (19). Briefly, female Kunming mice, weighing 45–52 g, 11 weeks old, after anesthetization with pentobarbital sodium (40 mg/kg, intraperitoneally injected), were intubated and ventilated with a small animal respirator, at a rate of 130 breaths/min and a tidal volume of 0.4 ml. Aortic constriction was applied by tying a 7.0 silk string ligature around a 27-gauge needle and then removing the needle. Sham-operated mice served as controls and were subjected to the same surgeries except for the ligation of the aorta. These experiments conformed to the Guide for the Care and Use of Laboratory Animals published by the US National Institutes of Health (NIH publication No. 85-23, revised 2011). The protocol was approved by the institutional ethics committee of Guangzhou First People's Hospital.

The HF mice were then randomly divided into three groups at 70 days post-operation: the HF group ($n = 5$), treated with saline; the HF+S group ($n = 8$), administered with spermidine by intraperitoneal injection of 10 mg/kg/d (Sigma-Aldrich, USA, diluted with saline solution) for 7 days (20); and the HF+SR group ($n = 8$), treated with trans-4-methylcycloh exylamine (4-MCHA), an antagonist of spermidine, by intraperitoneal injection of 100 mg/kg/d (Sigma-Aldrich, USA, diluted with saline solution) for 7 days (21). All animals had free access to common food and water. At 70 days after administration, the mice were sacrificed by pentobarbital sodium overdose (150 mg/kg), and then fecal samples and left ventricular tissues were harvested for the analysis (**Figure 1**).

Quantitative Real-Time Polymerase Chain Reaction

Total ribonucleic acid (RNA) was isolated from left ventricular biopsies using TRIzol reagent (Invitrogen) according to the manufacturer's protocol. Primers were designed to detect galectin-3 gene expression (forward: GAGTACTAGAAGCGGCCGAG, reverse: CTGTGCCGCTCACCTGATTA) based on the sequences available in NCBI database (at http://ncbi.nlm.nih.gov) using Primer software. After measuring RNA concentration, 1.5 μg RNA was treated with DNase I (Invitrogen) and used for cDNA synthesis by reverse transcriptase M-MLV (Takara, Japan). The galectin-3 messenger RNA (mRNA) levels were measured with CFX96 quantitative real-time polymerase chain reaction (QT-PCR) system (Bio-Rad). The relative amounts of mRNA were determined based on 2-ΔΔCt calculations.

Echocardiography

Transthoracic echocardiography was performed using a Vevo 2100 imaging system equipped with a 15–30 MHz linear array transducer (VisualSonics, Inc., Canada) by a single blinded observer as described previously (14). The following parameters were measured and averaged from 3 cardiac cycles: stroke volume, left ventricular end-diastolic volume and diameter (LVVd and LVDd), and left ventricular end-systolic volume and diameter (LVVs and LVDs), left ventricular anterior and posterior wall thickness in systole and diastole (LVAWs, LVAWd, LVPWs, and LVPWd). The left ventricular mass was calculated following the previously described method of Gao et al.: left ventricular mass $= [(\text{LVDd} + \text{LVAWd} + \text{LVPWd})^3 - \text{LVDd}^3] \times 1.055$, where 1.055 is the gravity of the myocardium (22). Fractional shortening (FS, %) was calculated using the equation: $100 \times [(\text{LVDd} - \text{LVDs})/\text{LVDd}]$. Left ventricular ejection fraction (LVEF, %) was calculated as $100 \times (\text{LVVd} - \text{LVVs})/\text{LVVd}$.

Western Blot Analysis

Left ventricular tissues were homogenized in RIPA buffer (Beyotime Biotechnology, China) to obtain whole cell lysates and centrifuged to isolate the protein. Fifty micrograms of protein was subjected to SDS-polyacrylamide gel electrophoresis and blotted onto a PVDF membrane. After blocking with 5% non-fat milk, the membranes were incubated with the following primary antibodies: galectin-3 (Abcam, Shanghai, China), spermidine (Abcam, Shanghai, China) or β-actin (Proteintech, Wuhan, China). Then, after incubation with anti-rabbit HRP-conjugated IgG (1:2,500, Boster, China) or anti-mouse HRP-conjugated IgG (1:2,500, Boster, China) for 1 h at room temperature, the immunoreactive bands were visualized by chemiluminescence reagents (ECL; KeyGEN BioTECH, Nanjing, China). The band intensity was quantified using ImageJ analysis software in a blinded manner, and all bands were normalized to the corresponding β-actin bands.

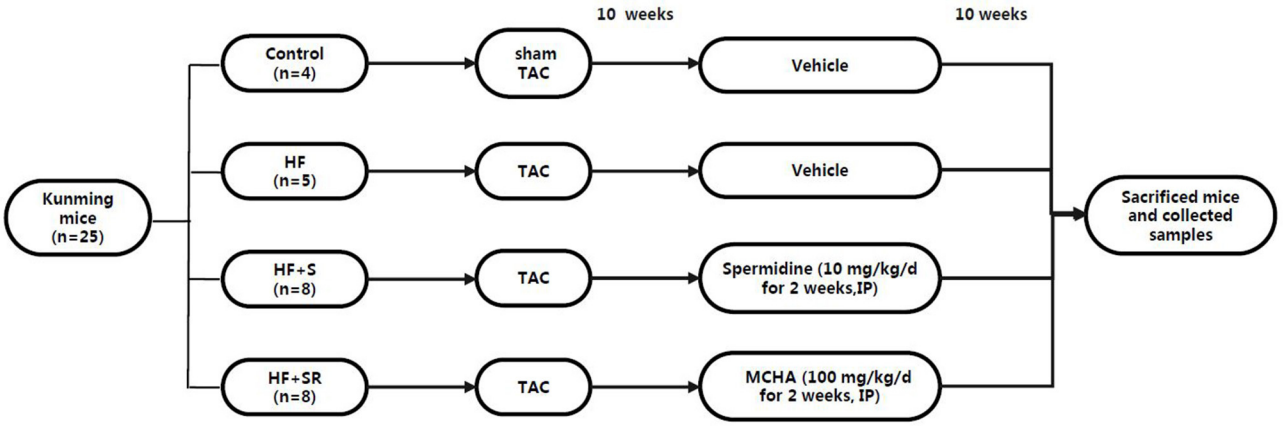

FIGURE 1 | The animal grouping and time line of the experimental protocol.

Immunohistochemistry

For galectin-3 and spermidine immunohistochemistry, formalin-fixed left ventricular tissues were embedded in paraffin and sectioned into 5-μm-thick sections. After deparaffinization, rehydration and pre-treatment with hydrogen peroxide, the sections were incubated with primary antibodies against galectin-3 (Abcam, Shanghai, China) and spermidine (Abcam, Shanghai, China) overnight at 4°C before being incubated with a secondary antibody for 1 h at room temperature. The sections were stained with DAB (Servicebio, China) followed by counterstaining with hematoxylin. Three entire sections per heart were examined by skilled observers blinded to the treatment group.

Terminal Deoxynucleotidyl Transferase–Mediated dUTP Nick-End Labeling Staining

TUNEL assays were performed to detect apoptotic cells in the heart tissue sections according to the manufacturer's protocols (Roche, China). Briefly, the left ventricular tissues were deparaffinized and rehydrated with serial changes in xylene and five different concentrations of ethanol. After proteinase K and endogenous peroxidase treatment, the heart tissue sections were stained with DAB (Servicebio, China). The TUNEL-positive cells were quantified using Image-Pro Plus analysis software.

Microbiome Sequencing and Analysis

Mouse fecal samples were collected under sterile conditions by pressing on the outer wall of the colon to push its contents into sterile tubes, at which time they were snap frozen in liquid nitrogen and then stored at −80°C until analysis. Total genomic DNA from the samples was extracted using the CTAB/SDS method by Novogene (Tianjin, China). The DNA concentrations and purity were analyzed on 1% agarose gels. The diluted DNA was used as the template to amplify the 16S rRNA (16S V4: 515F-806R) with specific barcoded primers. All polymerase chain reaction (PCR) reactions were carried out with Phusion® High-Fidelity PCR Master Mix (New England Biolabs). The PCR products were purified with the GeneJET Gel Extraction Kit (Thermo Scientific). The sequencing libraries were generated using the NEB Next® UltraTM DNA Library Prep Kit for Illumina (NEB, USA) and index codes were added. The library quality was assessed on the Qubit@ 2.0 Fluorometer (Thermo Scientific) and the Agilent Bioanalyzer 2100 system. Then the qualified library was sequenced on the Illumina MiSeq platform, and 250 bp paired-end reads were generated. The paired-end reads were combined using FLASH (V1.2.7) and assigned to the samples according to their barcodes.

Sequence analysis was conducted by Uparse software (V7.0.1001) and sequences with ≥ 97% similarity were assigned to the same operational taxonomic units (OTUs). Alpha diversity was analyzed through 3 parameters, including Chao 1, abundance coverage estimator (ACE), observed- species and phylogenetic diversity (PD)-whole tree. The linear discriminant analysis (LDA) effect size (LEfSe) was selected for the quantitative analysis of the microbial biomarkers within the different groups. The differences between the groups were assessed according to the LDA scores [OTUs with (log10)]. Cluster assessment was preceded by principal component analysis (PCA) using QIIME software (V1.7.0).

Statistical Analyses

Continuous variables were expressed as the mean ± standard deviation. Differences among the means were evaluated with a two-independent-sample *t*-test or one-way ANOVA test with S-N-K analysis, as appropriate. *P*-values were two-sided and considered significant when < 0.05. Statistical analyses were carried out using the SPSS version 17.0 software package (SPSS Inc., Chicago, USA).

RESULTS

Assessment of the HF Model Induced by Aortic Constriction and Grouping

During the observation period after the operation, three mice died, while all sham-operated animals (controls, $n = 4$) survived.

The TAC mice showed some signs of congestive HF such as anorexia, dyspnea and lethargy at 70 days post-operation, indicating the appearance of HF. Echocardiography showed that LVDs, LVDd, LVVs, LVVd, left ventricular mass average weight (LV Mass AW), and LV Mass AW (corrected) were significantly increased, and LVEF and FS were significantly decreased in the HF mice compared to the sham-operated mice (all $P < 0.05$, **Table 1**).

Variation in Echocardiographic Parameters After the Administration of Spermidine or Its Antagonist

After administration of spermidine or 4-MCHA, the HF mice were examined by Doppler echocardiography. **Figure 2** shows that the echocardiographic parameters, including LVDs, LVDd, LVVs, LVVd, FS, LVEF, LV mass AW, and LV mass AW (corrected) were not significantly different at 14 days after administration among the three groups: the HF, HF+S, and HF+SR groups. However, statistically significant differences were noted 56 days after administration. The LVDs, LVDd, LVVs, and LVVd in the HF+SR group were greatly enlarged (5.51 ± 0.69 vs. 4.14 ± 0.47 mm, $P = 0.033$; 6.13 ± 0.45 vs. 5.02 ± 0.40 mm, $P = 0.019$; 150.44 ± 41.68 vs. 76.92 ± 21.08 μL, $P = 0.040$; 189.94 ± 31.42 vs. 119.83 ± 22.31 μL, $P = 0.022$) compared with those in the HF group. Furthermore, LVDd and LVVd were significantly smaller (5.01 ± 0.67 vs. 6.13 ± 0.45 mm, $P = 0.033$; 121.44 ± 38.74 vs. 189.94 ± 31.42 μL, $P = 0.033$) in the HF+S group than in the HF+SR group (**Figure 3**).

The mRNA Expression of Galectin-3 in the Heart

Relative gene expression of galectin-3 in the left ventricular tissues was analyzed using QT-PCR at 70 days after administration. The results showed that galectin-3 expression was significantly increased in the two treated groups. The galectin-3 mRNA levels increased 3.5-fold in the HF+S group and 3.1-fold in the HF+SR group compared to the HF group (both $P < 0.05$). However, there was no difference between the HF+S and HF+SR groups (**Figure 4A**).

The Protein Expression of Galectin-3 in the Heart

To investigate the protein expression of galectin-3 in the heart, western blotting was conducted. The results showed that the expression levels of spermidine were elevated in the HF+S group, and the relative protein expression levels of galectin-3 were higher in the HF+SR group than in the HF and HF+S groups (∼2.1-fold, all $P < 0.05$). However, no difference was observed in the protein expression of galectin-3 between the HF and HF+S groups (**Figures 4B,C**).

Immunohistochemistry of Galectin-3 in the Heart Tissue

The protein expression of galectin-3 in the heart was also confirmed by immunohistochemistry and semiquantitative analysis, indicated as the values of the average optical density (AOD) measured by Image-Pro Plus 6.0. Immunohistochemistry staining showed that the protein expression of galectin-3 was significantly increased in the HF+SR group compared with the control and HF groups (AOD, 0.051 ± 0.005 vs. 0.040 ± 0.005 and 0.043 ± 0.005, both $P < 0.05$). There was also no difference in the expression of galectin-3 between the HF and HF+S groups (AOD, 0.043 ± 0.005 vs. 0.043 ± 0.010, $P = 0.976$) (**Figure 5**).

Effect of Spermidine on Cardiomyocyte Apoptosis

To assess the effect of spermidine on cardiomyocyte apoptosis, a TUNEL assay was used. Brown-stained cells accompanied by condensed or fragmented nuclei were considered TUNEL-positive cells. The number of apoptotic cardiomyocytes was significantly increased in the HF, HF+S and HF+SR groups compared with the controls. There was a modest 0.5-fold increase in the number of apoptotic cells in the HF+SR group compared to the HF group, but no difference was observed between the HF and HF+S groups (**Figure 6**).

Compositional Alteration of Gut Microbiota in Mice With Different Treatment Schemes

The compositions of the microbial community richness or diversity were assessed by ACE, observed-species and PD-whole

TABLE 1 | Comparisons of echocardiographic parameters between sham-operated and heart failure groups at 10 weeks post-operation and before administration.

	Heart rate (bpm)	LVDs (mm)	LVDd (mm)	LVVs (uL)	LVVd (uL)	FS (%)	LVEF (%)	LV mass AW (mg)	LV mass AW corrected (mg)
Sham ($n = 4$)	438 ± 35	2.54 ± 0.56	4.12 ± 0.54	24.69 ± 13.71	76.63 ± 24.48	38.79 ± 5.32	69.29 ± 7.12	138.03 ± 29.41	110.42 ± 23.53
HF ($n = 21$)	499 ± 40	3.53 ± 0.47	4.89 ± 0.42	53.45 ± 17.04	113.38 ± 23.67	27.89 ± 5.98	53.39 ± 9.12	218.56 ± 46.25	174.84 ± 37.00
P	0.008	0.004	0.011	0.012	0.023	0.008	0.010	0.010	0.010

Values presented as mean ± SD. bpm, beats per minute; LVDs, left ventricular end-systolic diameter; LVDd, left ventricular end-diastolic diameter; LVVs, left ventricular end-systolic volume; LVVd, left ventricular end-diastolic volume; FS, fractional shortening; LVEF, left ventricular ejection fraction; LV Mass AW, left ventricular mass average weight.

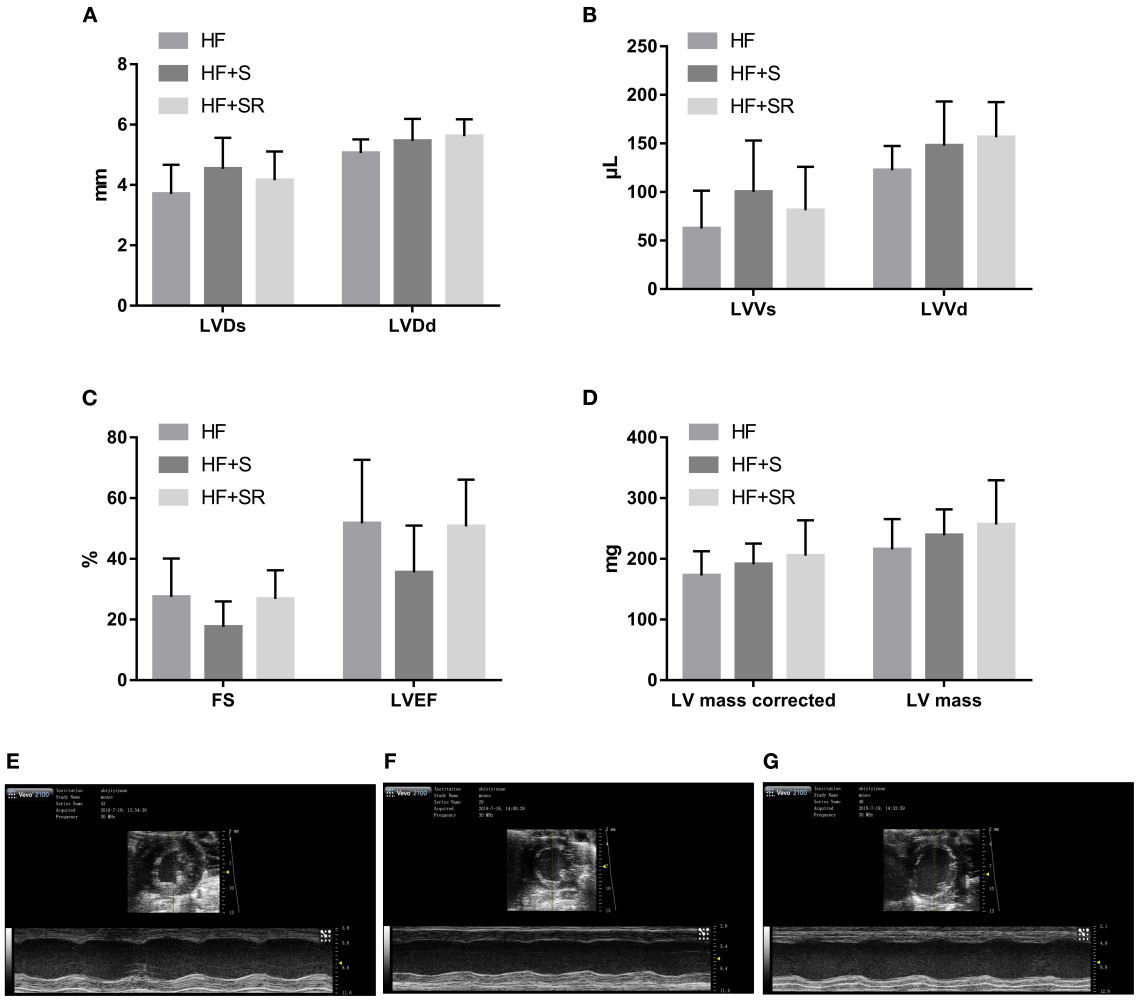

FIGURE 2 | Difference in the echocardiographic parameters among the HF ($n = 5$), HF+S ($n = 8$) and HF+SR ($n = 8$) mice at 14 days after administration. There were no differences in LVDs, LVDd **(A)**, LVVs, LVVd **(B)**, FS, LVEF **(C)**, LV mass or LV mass corrected **(D)** among the three groups. Representative echocardiographic images showing cardiac function and dimensions in the HF **(E)**, HF+S **(F),** and HF+SR **(G)** mice.

tree. The ACE and observed-species index were significantly higher in the controls than in the HF, HF+S or HF+SR groups (**Figures 7A,B**, all $P < 0.05$). The PD-whole tree index was lower only in the HF+S group than in the controls (**Figure 7C**, $P = 0.023$). Moreover, a significant difference in unweighted UniFrac distances was observed between these two groups ($P = 0.038$; **Figure 7D**).

LefSe analysis showed that at the family and genus levels, the HF+S mice had an increased abundance of *Muribaculaceae*, whereas increased abundances of *Tannerellaceae*, *Beijerinckiaceae*, *Bacteroidaceae*, *Parabacteroides* and *Bacteroides* were found in the HF mice (**Figure 7E**). When compared to the HF mice, the HF+SR mice possessed more *Muribaculaceae*, but no other difference was found between the two groups.

MetaStat analysis showed that the spermidine antagonist reduced the relative abundance of *Millionella massiliensis* and other unidentified bacteria (both $P < 0.05$, **Figure 8A**).

By comparison with the top 35 most frequent bacterial genera, the HF mice had 5 abundant genera (red color) within *Bacteroidetes* and 4 rare genera (blue color) within *Firmicutes*, and the HF+S mice possessed 3 abundant genera within *Firmicutes* and 4 rare genera within *Bacteroidetes*, whereas the HF+SR mice had 2 abundant genera within *Bacteroidetes* and 4 rare genera within *Firmicutes* (**Figure 8B**).

As shown in **Figure 8C**, all tested mice dominated two major microbiota among the top 10 phyla: *Bacteroidetes* (54–74%) and *Firmicutes* (19–40%). However, the *Firmicutes*/*Bacteroidetes* ratio was different. The HF+SR mice had more *Bacteroidetes* and less *Firmicutes*.

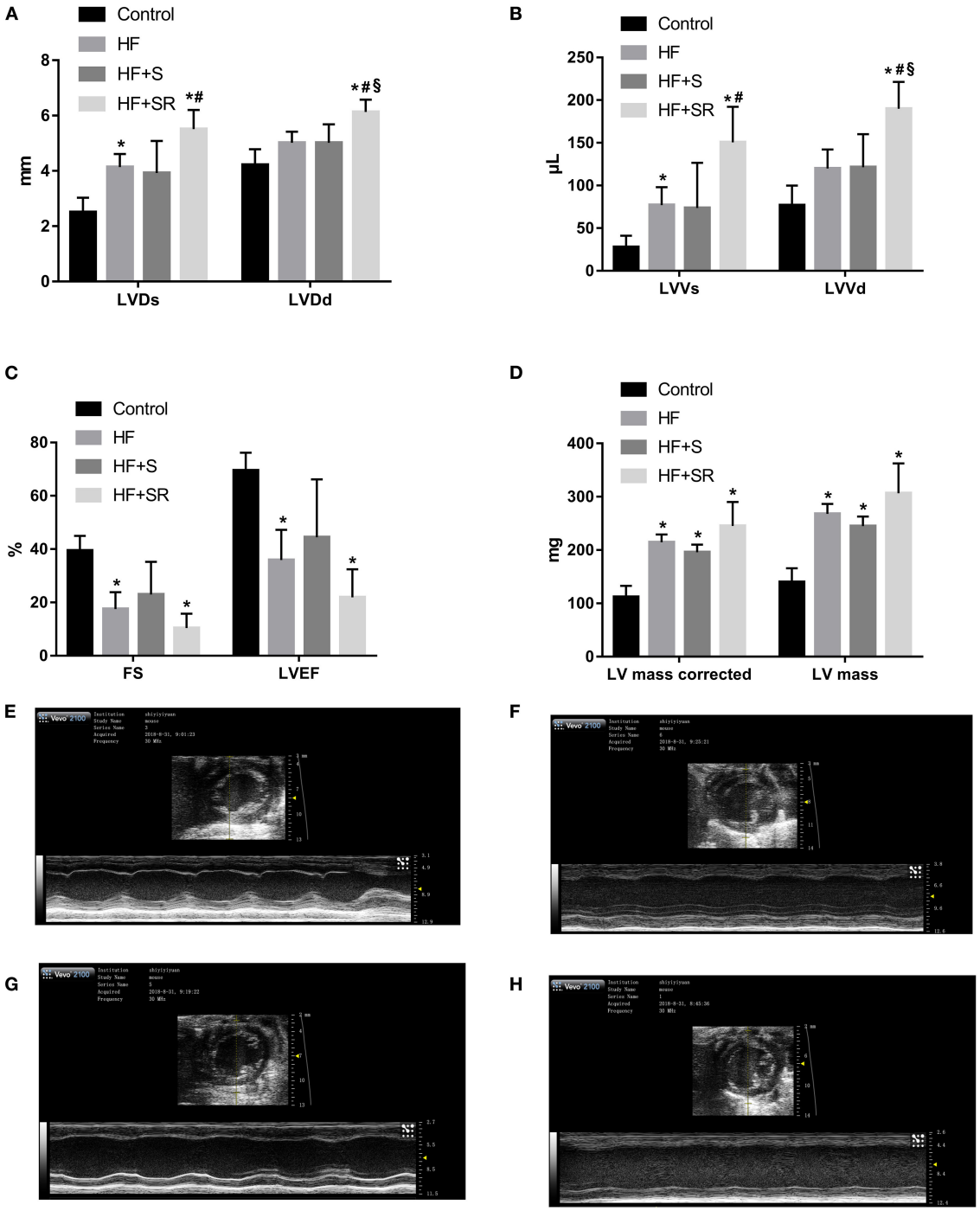

FIGURE 3 | Comparison of echocardiographic parameters among the different groups at 56 days after administration. Comparisons of LVDs, LVDd **(A)**, LVVs, LVVd **(B)**, FS, LVEF **(C)**, LV mass and LV mass corrected **(D)** among the control ($n = 4$), HF ($n = 5$), HF+S ($n = 8$), and HF+SR ($n = 8$) mice. Representative echocardiographic images in the control **(E)**, HF **(F)**, HF+S **(G)**, and HF+SR **(H)** mice. $^{*}P < 0.05$ vs. controls, $^{\#}P < 0.05$ vs. HF group, and $^{\S}P < 0.05$ vs. HF+S group.

DISCUSSION

In the present study, the HF+SR mice presented worsening echocardiographic parameters including LVDs, LVDd, LVVs, and LVVd compared with the HF mice. LVDd and LVVd were better in the HF+S mice than in the HF+SR mice. The mRNA and protein expression levels of galectin-3 in the heart were significantly higher in the HF+SR mice than in the

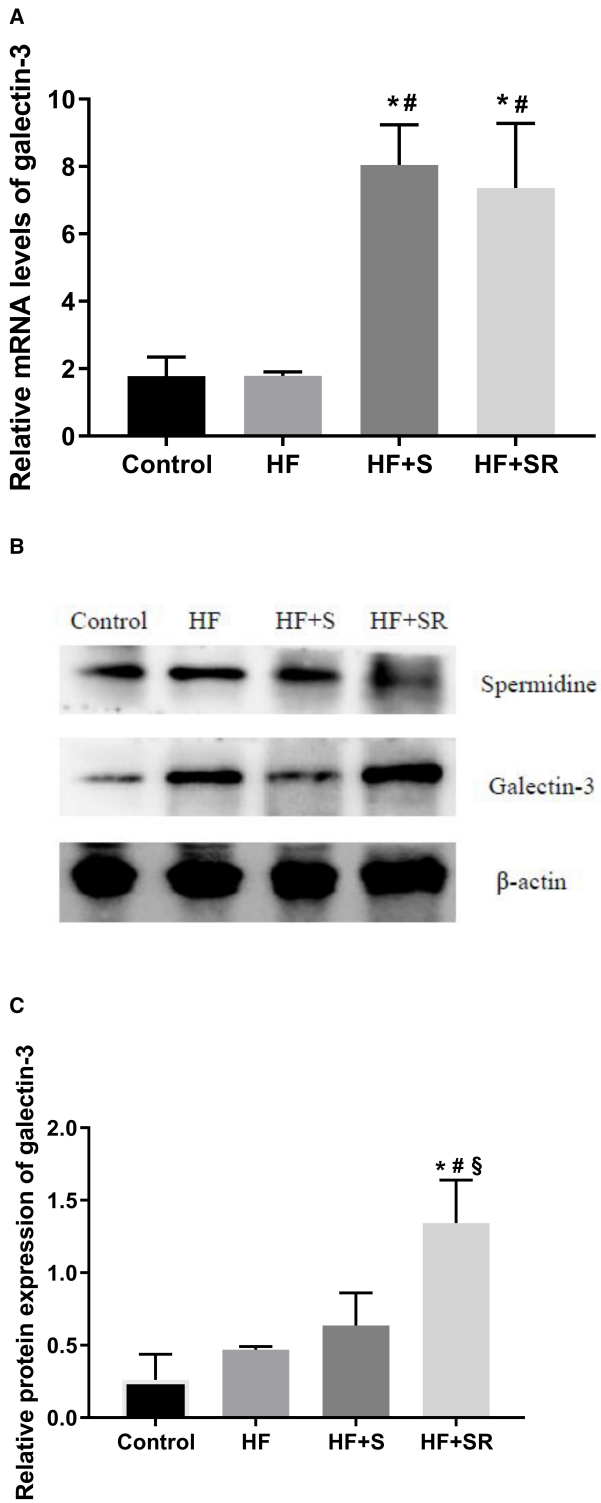

FIGURE 4 | The mRNA and protein expression of galectin-3 in the heart in different groups. Relative mRNA levels of galectin-3 in the heart **(A)**. Representative immunoblots for galectin-3 in the heart **(B)**. Quantitation of galectin-3 protein levels in the heart **(C)**. $^{*}P < 0.05$ vs. controls ($n = 4$), $^{\#}P < 0.05$ vs. HF group ($n = 5$) and $^{\S}P < 0.05$ vs. HF+S group ($n = 8$).

HF mice. In addition, the amount of cardiomyocyte apoptosis was the highest in the mice treated with an antagonist of spermidine. Analysis of the gut microbiota showed that the alpha diversity was significantly higher in the controls than in the HF, HF+S, or HF+SR groups. Moreover, the microbial community diversity decreased significantly and the microbial composition changed considerably after administration of the spermidine antagonist, especially decrease of *Millionella massiliensis*, the *Firmicutes*/*Bacteroidetes* ratio and the increase of *Muribaculaceae*. These findings showed that inhibiting spermidine deteriorated cardiac function and that increasing spermidine was beneficial to cardiac function in HF, and the regulation of the gut microbiota might be a contributing factor to the effect of spermidine on cardiac function.

Dietary spermidine protects against cardiovascular aging (23). In rats with hypertension-induced congestive heart failure, spermidine feeding decreased their systolic blood pressure and prevented cardiac hypertrophy, thus delaying the progression to HF. In humans, high levels of dietary spermidine increase survival and are inversely related to the incidence of cardiovascular disease (13, 14). These results implied that supplementation with spermidine might prevent the occurrence of cardiovascular diseases including HF. However, how was HF affected when changing the levels of spermidine? Our results showed that in HF, reducing spermidine levels by administrating its antagonist led to worsening of the echocardiographic parameters and an increase of galectin-3, a marker of cardiac fibrosis (24), suggesting that decreasing spermidine levels can aggravate cardiac fibrosis and deteriorate cardiac function. Thus, spermidine may be helpful in alleviating cardiac fibrosis during the process of HF and may be beneficial for the recovery of cardiac function. Similar to other potential novel biomarkers for myocardial fibrosis such as secreted frizzled-related protein (25, 26), spermidine may have potential preventive or therapeutic value in myocardial fibrosis and HF.

Spermidine plays many important roles in many aspects of cardiovascular pathophysiology. It can reverse arterial stiffness and restore arterial endothelial function in old mice (27). It reduces lipid accumulation and the formation of atherosclerotic plaques (28, 29). These results show that spermidine has a protective role to arteries and is beneficial for supplying cardiocytes with oxygen and nutrients and maintaining cardiac function. Therefore, maintenance of the appropriate spermidine levels may be important for maintaining cardiac function.

Our results showed that a decrease in spermidine reduced cardiac function, and supplementation with spermidine had a beneficial effect on cardiac function. Although the galectin-3 mRNA levels increased after spermidine supplementation, an increase in protein levels was not observed. Post-transcriptional regulation and translation of mRNA proteins may be responsible for the discrepancy in mRNA and protein levels in galectin-3. The method and duration of spermidine supplementation may be one cause of the small beneficial effect of spermidine supplementation in this study, because the absorption rate may be different when spermidine is administered by injection

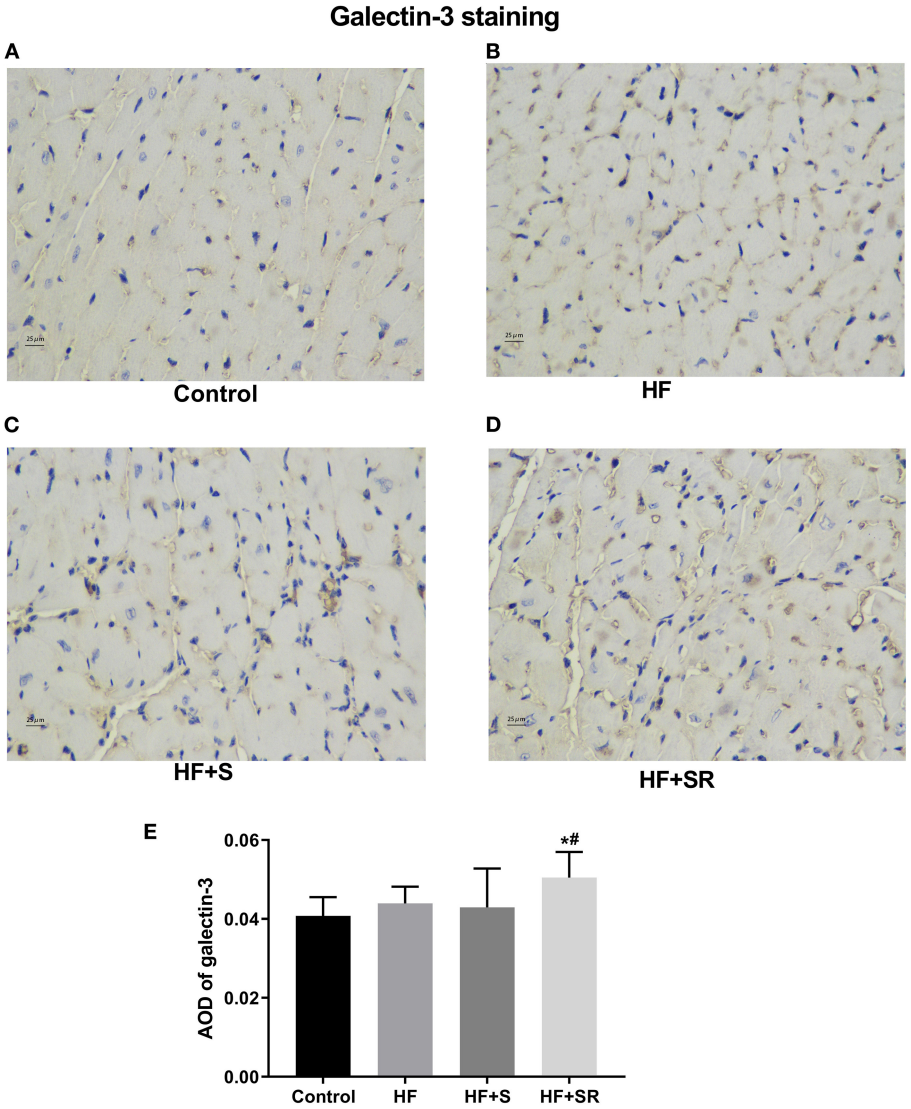

FIGURE 5 | Immunohistochemistry of galectin-3 in heart tissues from different groups. The controls had almost no galectin-3 expression **(A)**. The HF ($n = 5$) and HF+S ($n = 8$) mice had some galectin-3 expression **(B,C)**. The HF+SR mice ($n = 8$) showed significantly stronger staining for galectin-3 **(D)**. Semiquantitative analysis of galectin-3 levels by measuring AOD **(E)**. $^{*}P < 0.05$ vs. controls, $^{\#}P < 0.05$ vs. HF group.

or orally. In addition, spermidine is a two-edged sword, and only appropriate concentrations can improve cardiac function because inappropriate spermidine levels damage tissue and organs. In rats, spermidine had a potential antipsychotic effect at a low dose (10 mg/kg), but adverse effects appeared at a higher dose (20 mg/kg) (30). It has been reported that excessive intake of spermidine is not without risk. Spermidine showed dose-dependent cytotoxicity in the cultured cells via necrosis and was found to be toxic when its concentrations were above the maximum at which they have been found in food (31). Cancer patients with higher levels of spermidine have a worsed prognosis suggesting that abundant spermidine likely contributes to enhanced growth rates of cancer cells because it is indispensable for cell growth and tumor progression (7, 32).

Moreover, spermidine is not associated with a protective role in cardiovascular disease. It also has an adverse effect on the cardiovascular system. Patients with higher metabolic scores calculated according to the metabolic profile including spermidine levels had worse New York Heart Association functional classes and an adverse prognosis (33). In addition, because cardiac dysfunction is often accompanied by microcirculation disorders (34), a sufficient supply of the myocardium with oxygen and energy by the microcirculation plays very important roles in maintaining normal cardiac function (35, 36). However, Wierich et al. thought that spermidine had no effect on the quantitative characteristics of capillaries or arterioles, including the capillary volume, surface area and length as well as vascular endothelial growth factor-A

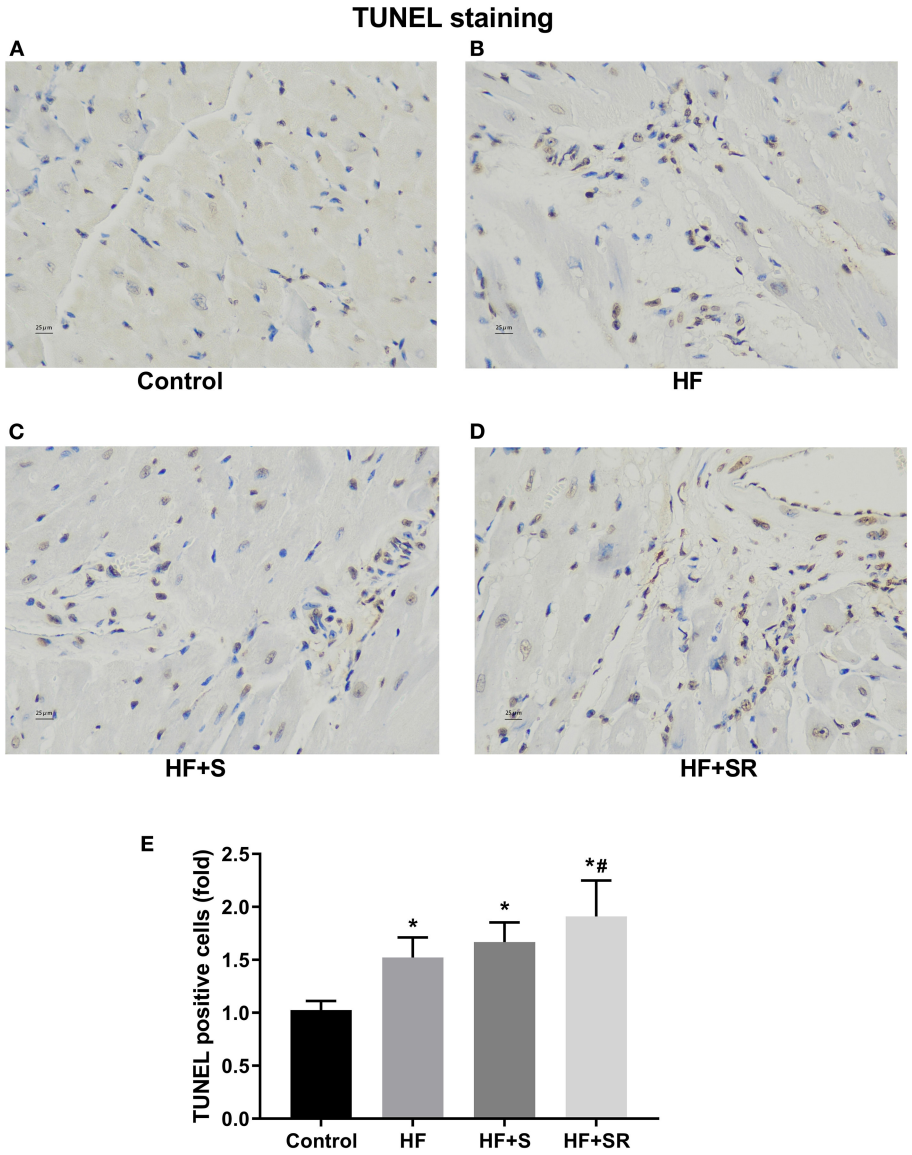

FIGURE 6 | Differences in the number of apoptotic cardiomyocytes among the four groups. Representative photomicrographs of ventricular tissue stained for TUNEL. The controls had very few TUNEL-positive cells **(A)**. Many TUNEL-positive cells appeared in the HF ($n = 5$) and HF+S ($n = 8$) mice **(B,C)**. The percentage of TUNEL-positive cells was significantly increased in the HF+SR mice ($n = 8$) **(D)**. Quantitative analysis of TUNEL-positive cells in the heart sections **(E)**. $^{*}P < 0.05$ vs. controls, $^{\#}P < 0.05$ vs. the HF group.

expression, suggesting that spermidine has no effect on the quantitative structural characteristics of the microcirculation in the aging heart (37). Therefore, the therapeutic role of spermidine may be dose-dependent and identifying a suitable concentration for the improvement of heart failure is very important.

For gut microbiota analysis, consistent with previous observations (3, 4), our results showed that the bacterial richness decreased when HF occurred, regardless of whether spermidine or its antagonist was administered. Furthermore, spermidine increased the abundance of *Muribaculaceae* and its antagonist significantly decreased the *Firmicutes*/*Bacteroidetes* ratio, a widely used marker of gut dysbiosis, meaning that reduced *Firmicutes*/*Bacteroidetes* ratio was related to deteriorated cardiac function. *Firmicutes* and *Bacteroidetes* are the two dominant phyla in the murine and human intestinal microbiota (38), and the *Firmicutes*/*Bacteroidetes* ratio was associated with many disorders. Elderly individuals have a lower *Firmicutes*/*Bacteroidetes* ratio than adults (39), and the *Firmicutes*/*Bacteroidetes* ratio decreased in isoproterenol-induced acute myocardial ischemia rats and chronic intermittent hypoxia exposed pigs (40, 41).

However, different results were also observed in other studies. Lataro et al. thought that the *Firmicutes*/*Bacteroidetes* ratio was not altered in HF model rats subjected to myocardial

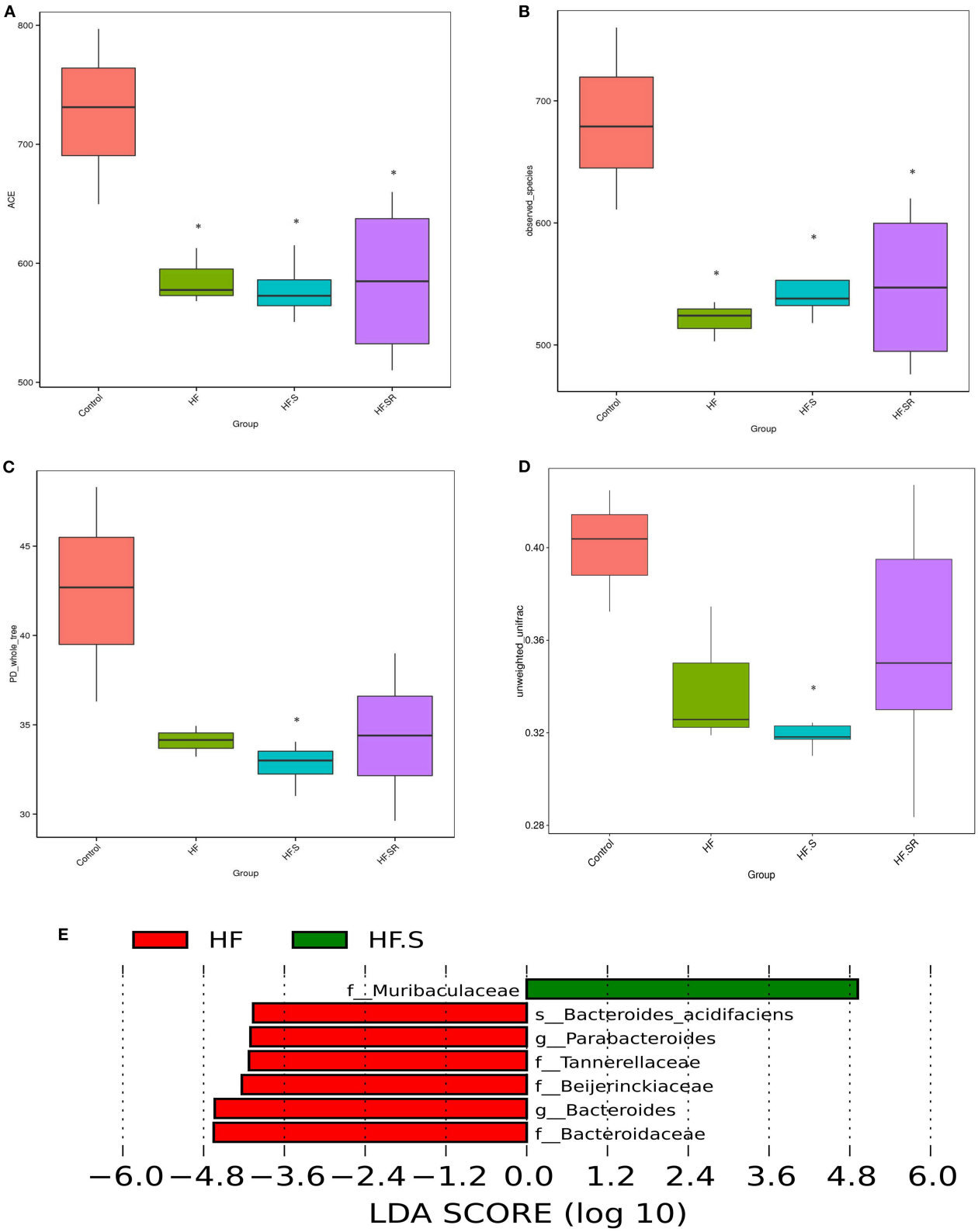

FIGURE 7 | The compositions of the microbial community richness or diversity in the different groups. The community richness was estimated by ACE **(A)** and the observed-species **(B)**. The community diversity is represented by the PD-whole tree **(C)**. Unweighted UniFrac distances revealed significant differences between the controls ($n = 4$) and HF+S mice ($n = 8$) **(D)**. The relative abundance of 6 taxa decreased, while only one increased in the HF+S mice compared with the HF mice ($n = 5$) **(E)**. *$P < 0.05$ vs. controls.

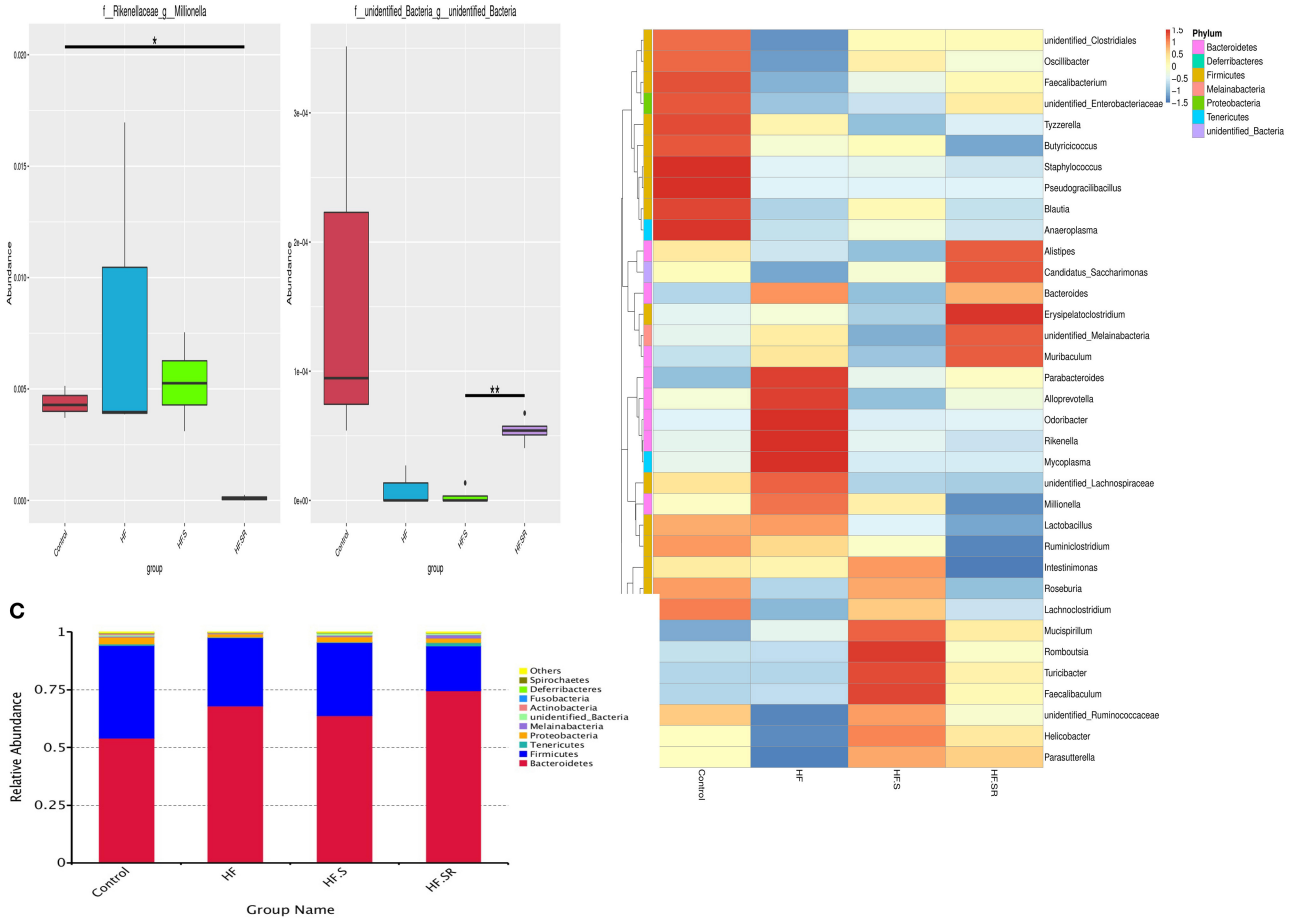

FIGURE 8 | Distribution of bacterial abundance. MetaStat analysis showing the bacterial abundance at the genus level among the control ($n = 4$), HF ($n = 5$), HF+S ($n = 8$) and HF+SR ($n = 8$) mice **(A)**. Top 35 most frequent bacterial genera in the four different groups **(B)**. Relative abundance of the major phyla among the gut microbiota in the four groups. *Bacteroidetes* and *Firmicutes* were the two most abundant bacteria **(C)**. $^{*}P < 0.05$ vs. controls. $^{**}P < 0.05$ vs. HF.S group.

infarction (42). However, Marques et al. found that a high fiber diet led to a decrease in the *Firmicutes*/*Bacteroidetes* ratio and prevented the development of hypertension and heart failure in hypertensive mice (43). An increased *Firmicutes*/*Bacteroidetes* ratio was also observed in hypertensive patients and rats (44). Perhaps the age of the host, the type of disease, the dietary composition, the environment and other factors can all affect the abundance and composition of gut microbiota (45, 46). The gut microbiota is significantly associated with some polyamines including spermidine. In addition to synthesizing spermidine (14), some gut microorganisms, including *Firmicute* species, also contain spermidine synthase and some accumulate spermidine as the sole polyamine (15). Therefore, the levels and function of spermidine and the microbial community richness or diversity can affect each other. Moreover, decreasing spermidine resulted in the deterioration of HF and a reduction in the *Firmicutes*/*Bacteroidetes* ratio. Thus, spermidine may also play beneficial roles by optimizing the gut microbiota composition.

Several limitations should be discussed. First, in this study, the timing of the administration of spermidine or its antagonist was only 1 week, which was shorter than other reports in which spermidine was administered for 6–12 weeks or longer (13, 14). It is possible that a significant beneficial effect of spermidine in improving cardiac function might be seen if it was administered for a longer period of time. Second, to avoid the effects of sex differences on the roles of spermidine, only female mice were used in this study. The roles of spermidine in cardiac function in male mice need to be investigated further. Third, we did not investigate the appropriate concentrations of spermidine for improving cardiac function and did not measure the variation of spermidine in the blood. Last, our results showed that the abundance of *Millionella massiliensis* decreased significantly in HF mice treated with 4-MCHA, a spermidine synthase inhibitor. However, spermidine can be synthesized by some gut microorganisms. We did not investigate whether *Millionella massiliensis* possessed much greater spermidine

synthesis ability than other microbiota and 4-MCHA acted as a spermidine synthase inhibitor by decreasing the abundance of *Millionella massiliensis*.

In summary, these findings showed that inhibiting spermidine by inhibiting its synthesis deteriorated cardiac function, while increasing spermidine improved cardiac function, and the regulation of gut microbiota and cardiac fibrosis might be a factor in the effects of spermidine on the modulation of cardiac function.

DATA AVAILABILITY STATEMENT

The original contributions presented in the study are included in the article/**Supplementary Material**, further inquiries can be directed to the corresponding author.

ETHICS STATEMENT

The animal study was reviewed and approved by Institutional Ethics Committee of Guangzhou First People's Hospital.

AUTHOR CONTRIBUTIONS

PC designed the study. Material preparation and data collection were performed by ZG, YC, ZL, and SL. ZG and YC conducted the statistical analyses. PC, ZG, and YC drafted the paper, which was reviewed by all authors. All authors read and approved the final manuscript.

FUNDING

This work was supported by Natural Science Foundation of Guangdong Province (Grant Number 2020A1515010384), the Science and Technology Planning Project Foundation of Guangzhou (Grant Number 201804010463), and National Natural Science Foundation of China (Grant Number 81770398).

SUPPLEMENTARY MATERIAL

The Supplementary Material for this article can be found online at: https://www.frontiersin.org/articles/10.3389/fcvm.2021.765591/full#supplementary-material

REFERENCES

1. Sandek A, Bjarnason I, Volk HD, Crane R, Meddings JB, Niebauer J, et al. Studies on bacterial endotoxin and intestinal absorption function in patients with chronic heart failure. *Int J Cardiol.* (2012) 157:80–5. doi: 10.1016/j.ijcard.2010.12.016
2. Morris NL, Hammer AM, Cannon AR, Gagnon RC, Li X, Choudhry MA. Dysregulation of microRNA biogenesis in the small intestine after ethanol and burn injury. *Biochim Biophys Acta Mol Basis Dis.* (2017) 1863:2645–53. doi: 10.1016/j.bbadis.2017.03.025
3. Sandek A, Swidsinski A, Schroedl W, Watson A, Valentova M, Herrmann R, et al. Intestinal blood flow in patients with chronic heart failure: a link with bacterial growth, gastrointestinal symptoms, and cachexia. *J Am Coll Cardiol.* (2014) 64:1092–102. doi: 10.1016/j.jacc.2014.06.1179
4. Kummen M, Mayerhofer CCK, Vestad B, Broch K, Awoyemi A, Storm-Larsen C, et al. Gut microbiota signature in heart failure defined from profiling of 2 independent cohorts. *J Am Coll Cardiol.* (2018) 71:1184–86. doi: 10.1016/j.jacc.2017.12.057
5. Luedde M, Winkler T, Heinsen FA, Ruhlemann MC, Spehlmann ME, Bajrovic A, et al. Heart failure is associated with depletion of core intestinal microbiota. *Esc Heart Fail.* (2017) 4:282–90. doi: 10.1002/ehf2.12155
6. Tang WH, Wang Z, Levison BS, Koeth RA, Britt EB, Fu X, et al. Intestinal microbial metabolism of phosphatidylcholine and cardiovascular risk. *N Engl J Med.* (2013) 368:1575–84. doi: 10.1056/NEJMoa1109400
7. Wang Z, Klipfell E, Bennett BJ, Koeth R, Levison BS, Dugar B, et al. Gut flora metabolism of phosphatidylcholine promotes cardiovascular disease. *Nature.* (2011) 472:57–63. doi: 10.1038/nature09922
8. Li W, Huang A, Zhu H, Liu X, Huang X, Huang Y, et al. Gut microbiota-derived trimethylamine N-oxide is associated with poor prognosis in patients with heart failure. *Med J Aust.* (2020) 213:374–9. doi: 10.5694/mja2.50781
9. Soda K. The mechanisms by which polyamines accelerate tumor spread. *J Exp Clin Cancer Res.* (2011) 30:95. doi: 10.1186/1756-9966-30-95
10. Madeo F, Bauer MA, Carmona-Gutierrez D, Kroemer G. Spermidine: a physiological autophagy inducer acting as an anti-aging vitamin in humans? *Autophagy.* (2019) 15:165–68. doi: 10.1080/15548627.2018.1530929
11. Minois N, Carmona-Gutierrez D, Madeo F. Polyamines in aging and disease. *Aging (Albany NY).* (2011) 3:716–32. doi: 10.18632/aging.100361
12. de Cabo R, Carmona-Gutierrez D, Bernier M, Hall MN, Madeo F. The search for antiaging interventions: from elixirs to fasting regimens. *Cell.* (2014) 157:1515–26. doi: 10.1016/j.cell.2014.05.031
13. Kiechl S, Pechlaner R, Willeit P, Notdurfter M, Paulweber B, Willeit K, et al. Higher spermidine intake is linked to lower mortality: a prospective population-based study. *Am J Clin Nutr.* (2018) 108:371–80. doi: 10.1093/ajcn/nqy102
14. Eisenberg T, Abdellatif M, Schroeder S, Primessnig U, Stekovic S, Pendl T, et al. Cardioprotection and lifespan extension by the natural polyamine spermidine. *Nat Med.* (2016) 22:1428–38. doi: 10.1038/nm.4222
15. Yan J, Yan JY, Wang YX, Ling YN, Song XD, Wang SY, et al. Spermidine-enhanced autophagic flux improves cardiac dysfunction following myocardial infarction by targeting the AMPK/mTOR signalling pathway. *Br J Pharmacol.* (2019) 176:3126–42. doi: 10.1111/bph.14706
16. Noack J, Dongowski G, Hartmann L, Blaut M. The human gut bacteria Bacteroides thetaiotaomicron and Fusobacterium varium produce putrescine and spermidine in cecum of pectin-fed gnotobiotic rats. *J Nutr.* (2000) 130:1225–31. doi: 10.1093/jn/130.5.1225
17. Hanfrey CC, Pearson BM, Hazeldine S, Lee J, Gaskin DJ, Woster PM, et al. Alternative spermidine biosynthetic route is critical for growth of Campylobacter jejuni and is the dominant polyamine pathway in human gut microbiota. *J Biol Chem.* (2011) 286:43301–12. doi: 10.1074/jbc.M111.307835
18. Ma L, Ni Y, Wang Z, Tu W, Ni L, Zhuge F, et al. Spermidine improves gut barrier integrity and gut microbiota function in diet-induced obese mice. *Gut Microbes.* (2020) 12:1–19. doi: 10.1080/19490976.2020.1832857
19. Date MO, Morita T, Yamashita N, Nishida K, Yamaguchi O, Higuchi Y, et al. The antioxidant N-2-mercaptopropionyl glycine attenuates left ventricular hypertrophy in in vivo murine pressure-overload model. *J Am Coll Cardiol.* (2002) 39:907–12. doi: 10.1016/S0735-1097(01)01826-5
20. Chai N, Zhang H, Li L, Yu X, Liu Y, Lin Y, et al. Spermidine prevents heart injury in neonatal rats exposed to intrauterine hypoxia by inhibiting oxidative stress and mitochondrial fragmentation. *Oxid Med Cell Longev.* (2019) 2019:5406468. doi: 10.1155/2019/5406468
21. Kobayashi M, Watanabe T, Xu YJ, Tatemori M, Goda H, Niitsu M, et al. Control of spermidine and spermine levels in rat tissues by trans-4-methylcyclohexylamine, a spermidine-synthase inhibitor. *Biol Pharm Bull.* (2005) 28:569–73. doi: 10.1248/bpb.28.569
22. Gao XM, Dart AM, Dewar E, Jennings G, Du XJ. Serial echocardiographic assessment of left ventricular dimensions and

function after myocardial infarction in mice. *Cardiovasc Res.* (2000) 45:330–8. doi: 10.1016/S0008-6363(99)00274-6
23. Madeo F, Eisenberg T, Pietrocola F, Kroemer G. Spermidine in health and disease. *Science*. (2018) 359:eaan2788. doi: 10.1126/science.aan2788
24. Ho JE, Liu C, Lyass A, Courchesne P, Pencina MJ, Vasan RS, et al. Galectin-3, a marker of cardiac fibrosis, predicts incident heart failure in the community. *J Am Coll Cardiol.* (2012) 60:1249–56. doi: 10.1016/j.jacc.2012.04.053
25. Wu J, Zheng H, Liu X, Chen P, Zhang Y, Luo J, et al. Prognostic value of secreted frizzled-related protein 5 in heart failure patients with and without type 2 diabetes mellitus. *Circ Heart Fail.* (2020) 13:e007054. doi: 10.1161/CIRCHEARTFAILURE.120.007054
26. Yang S, Chen H, Tan K, Cai F, Du Y, Lv W, et al. Secreted frizzled-related protein 2 and extracellular volume fraction in patients with heart failure. *Oxid Med Cell Longev.* (2020) 2020:2563508. doi: 10.1155/2020/2563508
27. LaRocca TJ, Gioscia-Ryan RA, Hearon CM, Jr., Seals DR. The autophagy enhancer spermidine reverses arterial aging. *Mech Ageing Dev.* (2013) 134:314–20. doi: 10.1016/j.mad.2013.04.004
28. Michiels CF, Kurdi A, Timmermans JP, De Meyer GRY, Martinet W. Spermidine reduces lipid accumulation and necrotic core formation in atherosclerotic plaques via induction of autophagy. *Atherosclerosis*. (2016) 251:319–27. doi: 10.1016/j.atherosclerosis.2016.07.899
29. de la Pena NC, Sosa-Melgarejo JA, Ramos RR, Mendez JD. Inhibition of platelet aggregation by putrescine, spermidine, and spermine in hypercholesterolemic rabbits. *Arch Med Res.* (2000) 31:546–50. doi: 10.1016/S0188-4409(00)00238-1
30. Yadav M, Parle M, Jindal DK, Sharma N. Potential effect of spermidine on GABA, dopamine, acetylcholinesterase, oxidative stress and proinflammatory cytokines to diminish ketamine-induced psychotic symptoms in rats. *Biomed Pharmacother.* (2018) 98:207–13. doi: 10.1016/j.biopha.2017.12.016
31. Del Rio B, Redruello B, Linares DM, Ladero V, Ruas-Madiedo P, Fernandez M, et al. Spermine and spermidine are cytotoxic towards intestinal cell cultures, but are they a health hazard at concentrations found in foods? *Food Chem.* (2018) 269:321–26. doi: 10.1016/j.foodchem.2018.06.148
32. Weiss TS, Bernhardt G, Buschauer A, Thasler WE, Dolgner D, Zirngibl H, et al. Polyamine levels of human colorectal adenocarcinomas are correlated with tumor stage and grade. *Int J Colorectal Dis.* (2002) 17:381–7. doi: 10.1007/s00384-002-0394-7
33. Wang CH, Cheng ML, Liu MH, Kuo LT, Shiao MS. Metabolic profile provides prognostic value better than galectin-3 in patients with heart failure. *J Cardiol.* (2017) 70:92–8. doi: 10.1016/j.jjcc.2016.10.005
34. Chen J, Yaniz-Galende E, Kagan HJ, Liang L, Hekmaty S, Giannarelli C, et al. Abnormalities of capillary microarchitecture in a rat model of coronary ischemic congestive heart failure. *Am J Physiol Heart Circ Physiol.* (2015) 308:H830–40. doi: 10.1152/ajpheart.00583.2014
35. Cai X, Liu X, Sun L, He Y, Zheng S, Zhang Y, et al. Prediabetes and the risk of heart failure: a meta-analysis. *Diabetes Obes Metab.* (2021) 23:1746–53. doi: 10.1111/dom.14388
36. Zheng H, Zhu H, Liu X, Huang X, Huang A, Huang Y. Mitophagy in diabetic cardiomyopathy: roles and mechanisms. *Front Cell Dev Biol.* (2021) 9:750382. doi: 10.3389/fcell.2021.750382
37. Wierich MC, Schipke J, Brandenberger C, Abdellatif M, Eisenberg T, Madeo F, et al. Cardioprotection by spermidine does not depend on structural characteristics of the myocardial microcirculation in aged mice. *Exp Gerontol.* (2019) 119:82–8. doi: 10.1016/j.exger.2019.01.026
38. Clavel T, Lagkouvardos I, Blaut M, Stecher B. The mouse gut microbiome revisited: from complex diversity to model ecosystems. *Int J Med Microbiol.* (2016) 306:316–27. doi: 10.1016/j.ijmm.2016.03.002
39. Mariat D, Firmesse O, Levenez F, Guimaraes V, Sokol H, Dore J, et al. The Firmicutes/Bacteroidetes ratio of the human microbiota changes with age. *BMC Microbiol.* (2009) 9:123. doi: 10.1186/1471-2180-9-123
40. Sun L, Jia H, Li J, Yu M, Yang Y, Tian D, et al. Cecal gut microbiota and metabolites might contribute to the severity of acute myocardial ischemia by impacting the intestinal permeability, oxidative stress, and energy metabolism. *Front Microbiol.* (2019) 10:1745. doi: 10.3389/fmicb.2019.01745
41. Lucking EF, O'Connor KM, Strain CR, Fouhy F, Bastiaanssen TFS, Burns DP, et al. Chronic intermittent hypoxia disrupts cardiorespiratory homeostasis and gut microbiota composition in adult male guinea-pigs. *Ebiomedicine.* (2018) 38:191–205. doi: 10.1016/j.ebiom.2018.11.010
42. Lataro RM, Imori PFM, Santos ES, Silva LEV, Duarte RTD, Silva CAA, et al. Heart failure developed after myocardial infarction does not affect gut microbiota composition in the rat. *Am J Physiol Gastrointest Liver Physiol.* (2019) 317:G342–G48. doi: 10.1152/ajpgi.00018.2019
43. Marques FZ, Nelson E, Chu PY, Horlock D, Fiedler A, Ziemann M, et al. High-fiber diet and acetate supplementation change the gut microbiota and prevent the development of hypertension and heart failure in hypertensive mice. *Circulation.* (2017) 135:964–77. doi: 10.1161/CIRCULATIONAHA.116.024545
44. Yang T, Santisteban MM, Rodriguez V, Li E, Ahmari N, Carvajal JM, et al. Gut dysbiosis is linked to hypertension. *Hypertension.* (2015) 65:1331–40. doi: 10.1161/HYPERTENSIONAHA.115.05315
45. Turnbaugh PJ, Hamady M, Yatsunenko T, Cantarel BL, Duncan A, Ley RE, et al. A core gut microbiome in obese and lean twins. *Nature.* (2009) 457:480–4. doi: 10.1038/nature07540
46. Hill JE, Hemmingsen SM, Goldade BG, Dumonceaux TJ, Klassen J, Zijlstra RT, et al. Comparison of ileum microflora of pigs fed corn-, wheat-, or barley-based diets by chaperonin-60 sequencing and quantitative PCR. *Appl Environ Microbiol.* (2005) 71:867–75. doi: 10.1128/AEM.71.2.867-875.2005

Conflict of Interest: The authors declare that the research was conducted in the absence of any commercial or financial relationships that could be construed as a potential conflict of interest.

Publisher's Note: All claims expressed in this article are solely those of the authors and do not necessarily represent those of their affiliated organizations, or those of the publisher, the editors and the reviewers. Any product that may be evaluated in this article, or claim that may be made by its manufacturer, is not guaranteed or endorsed by the publisher.

Copyright © 2021 Chen, Guo, Li, Liu and Chen. This is an open-access article distributed under the terms of the Creative Commons Attribution License (CC BY). The use, distribution or reproduction in other forums is permitted, provided the original author(s) and the copyright owner(s) are credited and that the original publication in this journal is cited, in accordance with accepted academic practice. No use, distribution or reproduction is permitted which does not comply with these terms.

frontiers in Cardiovascular Medicine

ORIGINAL RESEARCH
published: 06 December 2021
doi: 10.3389/fcvm.2021.766613

Inflammatory Cells Accelerated Carotid Artery Calcification *via* MMP9: Evidences From Single-Cell Analysis

*Xiaobing Liang[1], Wanbing He[2], Hua Zhang[1], Dongling Luo[1], Zhengzhipeng Zhang[1], Aiting Liu[1], Jinkai Wang[3] and Hui Huang[1,2]**

[1] Department of Cardiology, The Eighth Affiliated Hospital, Sun Yat-sen University, Guangdong, China, [2] Department of Cardiology, Sun Yat-sen Memorial Hospital, Sun Yat-sen University, Guangdong, China, [3] Department of Medical Informatics, ZhongShan School of Medicine, Sun Yat-sen University, Guangdong, China

Background: Vascular calcification (VC) is an important predictor of prognosis in atherosclerosis, the phenotypic transformation of vascular smooth muscle cells (VSMCs) is thought to be a process of VC. However, the implications and potential mechanisms for VSMCs phenotypic transition remain unknown.

Methods: To study the transformation of vascular smooth muscle cells (VSMCs) in the calcification early period, we analyzed single-cell sequencing data from carotid artery calcified core and paracellular tissue, based on the results of enrichment analysis and protein-protein interaction analysis. Upstream transcription factors were tracked and finally the results were validated using the MESA database.

Results: We successfully identified a subpopulation of inflammatory macrophage-like VSMCs and determined that MMP9 is an important factor in the phenotypic transformation of VSMCs. We found that RELA regulates MMP9 expression and that knockdown of RELA attenuated MMP9 expression and reduced the expression of BMP2 and the macrophage marker LGALS3 in vascular smooth muscle in inflammatory states, while serum levels of MMP9 correlated significantly with the inflammatory response.

Conclusion: This study reveals that the phenotypic transformation of VSMCs can be regulated by modulating MMP9, providing a new idea for the early treatment of VC.

Keywords: single cell sequencing, vascular calcification, vascular smooth muscle cells, phenotypic modulation, MMP9, atherosclerosis, inflammation

OPEN ACCESS

Edited by:
Yuli Huang,
Southern Medical University, China

Reviewed by:
Qi Guo,
Hebei Medical University, China
Danyan Xu,
Central South University, China

***Correspondence:**
Hui Huang
huangh8@mail.sysu.edu.cn

Specialty section:
This article was submitted to General Cardiovascular Medicine, a section of the journal Frontiers in Cardiovascular Medicine

Received: *29 August 2021*
Accepted: *08 November 2021*
Published: *06 December 2021*

Citation:
Liang X, He W, Zhang H, Luo D, Zhang Z, Liu A, Wang J and Huang H (2021) Inflammatory Cells Accelerated Carotid Artery Calcification via MMP9: Evidences From Single-Cell Analysis. Front. Cardiovasc. Med. 8:766613. doi: 10.3389/fcvm.2021.766613

INTRODUCTION

Vascular calcification (VC) is an independent predictor for the prognosis in atherosclerotic patients. Despite the current advances in various treatments for atherosclerosis, including drug therapy and surgical resection, VC is still associated with increased mortality in patients (1). Various pharmacological treatments have been administered for arterial VC, including calcium channel blockers, inhibitors of the renin-angiotensin-aldosterone system, statins, vitamin K and others (2), but the results are unsatisfactory. vascular smooth muscle cells (VSMCs) play an important role in the process of arterial VC (3). It has been previously shown that VSMCs

phenotypic transdifferentiation from contractile to osteogenic is a prerequisite for VC (4, 5) in the atherosclerotic setting, VSMCs undergo phenotypic modulation can develop into inflammatory macrophage-like cells with upregulated expression of LGALS3, or become 'synthetic' VSMCs (6). However, the specific regulatory processes involved in the regulation of VSMCs phenotypes have not been clarified. Since VC is irreversible and when it occurs, the vascular condition will not fully recover (7), prediction and prevention of VC is essential. Recent advances in single-cell transcriptomic sequencing have made comprehensive analysis of transcriptome expression of individual cells possible, providing the opportunity to identify cells into different states of transition (8). The use of single-cell sequencing to study the phenotypic transition of VSMCs in the calcification process has not been reported. Seurat is an algorithm that can integrate multiple single cell sequencing datasets to enable the classification of different cells based on their characteristics (9). By using Seurat and enrichment analysis, we can sort out subclasses of cells in samples from different sampling sites and explore the role of this class of cells in arterial VC.

In this study, we used a single-cell transcriptome sequencing database of entire calcified atherosclerotic core (AC) plaques and patient-matched proximal adjacent (PA) portions of carotid artery tissue from patients undergoing carotid endarterectomy. Macrophage-like cell subpopulations were identified by the t-distributed stochastic neighbor embedding (tSNE) algorithm (10), which revealed that the proportion of macrophage-like cells was most variable in the comparison between AC and PA. We further explored the biological functions of macrophage-like cells using enrichment analysis and found that they were associated with neutrophil activation. Protein interaction analysis was used to obtain that MMP9 was central to the overall protein regulatory network. Then, based on the differentially expressed genes in this subpopulation, we traced the common upstream of these genes and found that the expression of most differential genes was regulated by NFκB1 and RELA. Finally, we selected a high-throughput sequencing database associated with VSMCs with knockout of RELA genes and calculated the expression of related genes based on the inflammatory state. Induction of the inflammatory state in VSMCs with TNFα resulted in a decrease in the rise of MMP9, BMP2 and the macrophage marker LGALS3 following knockout of RELA. We determined that knockout of RELA reduces the expression of MMP9, which can affect phenotypic transition and calcification progression in VSMCs. The Multi-Ethnic Study of Atherosclerosis (MESA) examines disease characteristics in patients with cardiovascular disease across multiple regions and uses these risk factors to predict the progression of cardiovascular disease. The baseline examination 1 collected demographics, laboratory data and coronary computed tomography scans. To further define our results, we analyzed the relationship between serum MMP9 levels and clinicopathophysiological characteristics by using the MESA database. Significant associations were found between MMP9 and BMI, Agatston calcium score, C-reactive protein, and TNF-R1. This study could provide new ideas for the prevention and early intervention of arterial VC.

MATERIALS AND METHODS

Data Collection

ScRNA-seq data from human carotid endarterectomy tissues and multiple high-throughput sequencing data were used for analysis in this study. ScRNA-seq data for a total of 51,721 cells from three human atherosclerotic calcified core plaques and their collateral tissues were obtained from Gene Expression Omnibus (GEO, http://www.ncbi.nlm.nih.gov/geo), registration number GSE159677 database, which contains 39,244 cells from the calcified core and 12,477 cells from the paratissue, based on Illumina NextSeq 500 with a read depth of 10x genomics. A total of 8 data from vascular smooth muscle cell samples with registration numbers GSM3175352, GSM3175352, GSM3175354, GSM3175355, GSM3175360, GSM3175361, GSM3175362, GSM3175363, from human embryonic stem cells with CRISPR / Cas9-mediated Gene edited human embryonic stem cells (hESCs) that differentiate into VSMCs.

Processing of scRNA-Seq Data

A total of 51,721 cells from the calcified core and its paracrine tissue were included in this analysis. The Seurat software package in R with version number 3.2.0 was used for quality control, statistical analysis and exploration of the scRNA-seq data.

Supplementary Figure 1 lists gene expression before exclusions.

We excluded 6,711 low quality cells based on quality control criteria.

1. Exclusion of genes detected in <3 cells;
2. Excluded cells with <200 total genes detected;
3. Excluded cells with more than 6,000 total genes detected;
4. Cells with $\geq 10\%$ of mitochondria-expressed genes were excluded.

Gene expression of the remaining 45,010 cells was normalized by using a linear regression model. Integrating data points were found for 6 samples and integrated (11). PCA was performed on the integrated results to identify usable data with a $p < 0.05$. Twenty initial PCs were used and the t-distributed stochastic neighbor embedding (tSNE) algorithm was applied for dimensionality reduction. A final cluster classification analysis was performed on all cells to obtain 20 clusters. Differential expression analysis was performed between genes with LogFC ≥ 0.5 within cell clusters using the limma package in R with version number 3.44.3 to identify marker genes for each cluster, adjusted for a $P < 0.05$. Subsequently, the marker genes were manually validated and corrected according to their compositional patterns by using the CellMarker database and existing experimentally proven cellular marker genes.

The corresponding genes used to annotate cell surface markers for cell clusters are listed in **Supplementary Table 1**.

Enrichment Analysis and Protein-Protein Interactions Analysis

The external-gene-name was converted to entrezgeneid by using the biomaRt package (12) in R, version 2.44.1. The clusterProfiler package (13), version 3.16.1 in R, which automates the process

of biomaRt classification and gene cluster enrichment analysis, was used to perform KEGG differential analysis (14) and GO differential analysis (15) of differential genes in cluster 7. The differential genes screened from cluster 7 are fed into PPI (https://string-db.org/) for analysis, which is used to construct protein-protein interaction networks and to analyse the molecular mechanisms of disease from multiple perspectives such as physical interactions or functional correlations. The PPI-derived data were subjected to statistical analysis using RStudio.

Tracing Upstream Transcription Factors

Using TRRUST version 2 (https://www.grnpedia.org/trrust/), which contains data on human and murine transcriptional regulatory networks, the differential genes screened by cluster 7 were imported for analysis to obtain the transcription factors regulating the differential genes. Transcription factors and differential genes were counted and linked using Cytoscape software.

High-Throughput Sequencing Data Processing and Statistics

All subgroups were divided into mainly WT and KO types, control and TNFα addition groups. The number of read counts of sequencing data was normalized using the DESeq2 package (16) with version number 1.28.1 in R. The gene expressions of RELA, MMP9, BMP2 and LGALS3 were extracted and analyzed using ANOVA as well as ordinary ANOVA test to assess whether the differences between gene expressions were statistically significant. And compare the mean on each column with the mean of every other column, with a confidence interval of 95%.

Meta data for 8 samples of VSMCs are presented in **Supplementary Table 2**.

MESA Data Statistics and Analysis

MESA is a multi-ethnic observational cohort study that includes Caucasians, African, Americans, Chinese and Hispanics. A test from MESA in 2012 was used for this study, which included a test for serum MMP9 level. Institutional Review Board approval and informed consent of participants were obtained prior to the review (17). Blood pressure was classified according to "Hypertension by JNC VI (1997) criteria" and medical history. Body mass index (BMI) is calculated by dividing body weight (kg) by the square of height (m). The Agatston calcium score is used to determine the progression of coronary artery calcification (CAC) and is classified according to the presence or absence of CAC: no CAC (Agatston $= 0$) and CAC (Agatston > 0). C-reactive protein (CRP) rises in response to infection or tissue damage and can be classified according to the amount of level: normal (CRP $\leq$10), abnormal (CRP $>$10). Ankle-brachial index (ABI) is used to reveal vasoconstrictor function and can be divided into two types: normal (ABI $\geq$ 0.97) and abnormal (ABI $<$ 0.97). The level of TNF-R1 was divided into two groups based on the median 1,223.

Statistical analysis was performed using IBM SPSS Statistics 25, and whether serum MMP9 level were associated with the clinicopathological characteristics was calculated using the Mann Whitney test or the Unpaired *t*-test. Subgroup analysis of the association between MMP9 levels and CAC progression using binary logistic analysis. Graphing was performed using GraphPad Prism 9.

RESULTS

Analysis of scRNA-Seq Data Reveals High Cell Heterogeneity in Carotid Artery Calcification Core Tissues

Single-cell sequencing data from six carotid artery calcification core tissues were normalized according to quality control criteria, excluding cells with selection criteria, and the total number of cells in the six samples was reduced from 51,721 to 45,010, and the six samples were then combined. The number of genes detected correlated significantly with the depth of sequencing (**Figure 1A**). Principal component analysis (PCA) was performed on the tissue cells to identify available principal components (PCs) that were subsequently used to screen for relevant genes. There was some separation between tissue cells in the PCA results (**Figure 1B**). The differential genes in the heat map of the first four PCs were not identical (**Figure 1C**). Based on the results of the analysis, 20 PCs were selected for subsequent analysis (**Figure 1D**). Subsequently, using the t-distributed stochastic neighbor embedding (tSNE) algorithm, the carotid artery calcified core tissue was divided into 20 cell clusters (**Figure 2A**) and differential analysis was performed to obtain marker genes with logFC $>$0.5 in the 20 clusters (**Figure 1E**). These tissue cells could be divided into two groups, carotid artery calcified core (AC) and proximal adjacent to carotid artery (PA), based on different sampling locations.

The Calcified Core and Paracellular Tissues Can Be Classified Into 20 Clusters

Based on the summary annotation of CellMarker and the currently known expression patterns of marker genes for each type of cell (**Figure 2B**), we have classified the 20 clusters as follows. Clusters 0, 2, 5 and 15 were labeled as T cells, contain a total of 14,981 cells; clusters 1, 12 were labeled as endothelial cells, containing a total of 5,964 cells; cluster 3 was labeled as fibroblasts, contained a total of 4,292 cells; cluster 4 was labeled as VSMCs, contained a total of 3,625 cells; clusters 6 were labeled as M2 Macrophage, contained a total of 3,499 cells; cluster 7 was labeled as macrophage-like VSMCs, contained a total of 2,722 cells; clusters 8 were labeled as M1 Macrophage, contained a total of 2,568 cells; cluster 9 was labeled as B-cells, contained a total of 1,602 cells; clusters 10 and 13 were labeled as NK cells, contained a total of 2,231 cells; cluster 11 was labeled as mesenchymal cells, contained a total of 1,287 cells; clusters 16 were labeled as M2 Monocyte, contained a total of 581 cells; cluster 17 was labeled as mast cells, contained a total of 509 cells.

In both groups, the proportion of different cell types varied (**Figure 2C**). In the AC group, the higher proportion were T

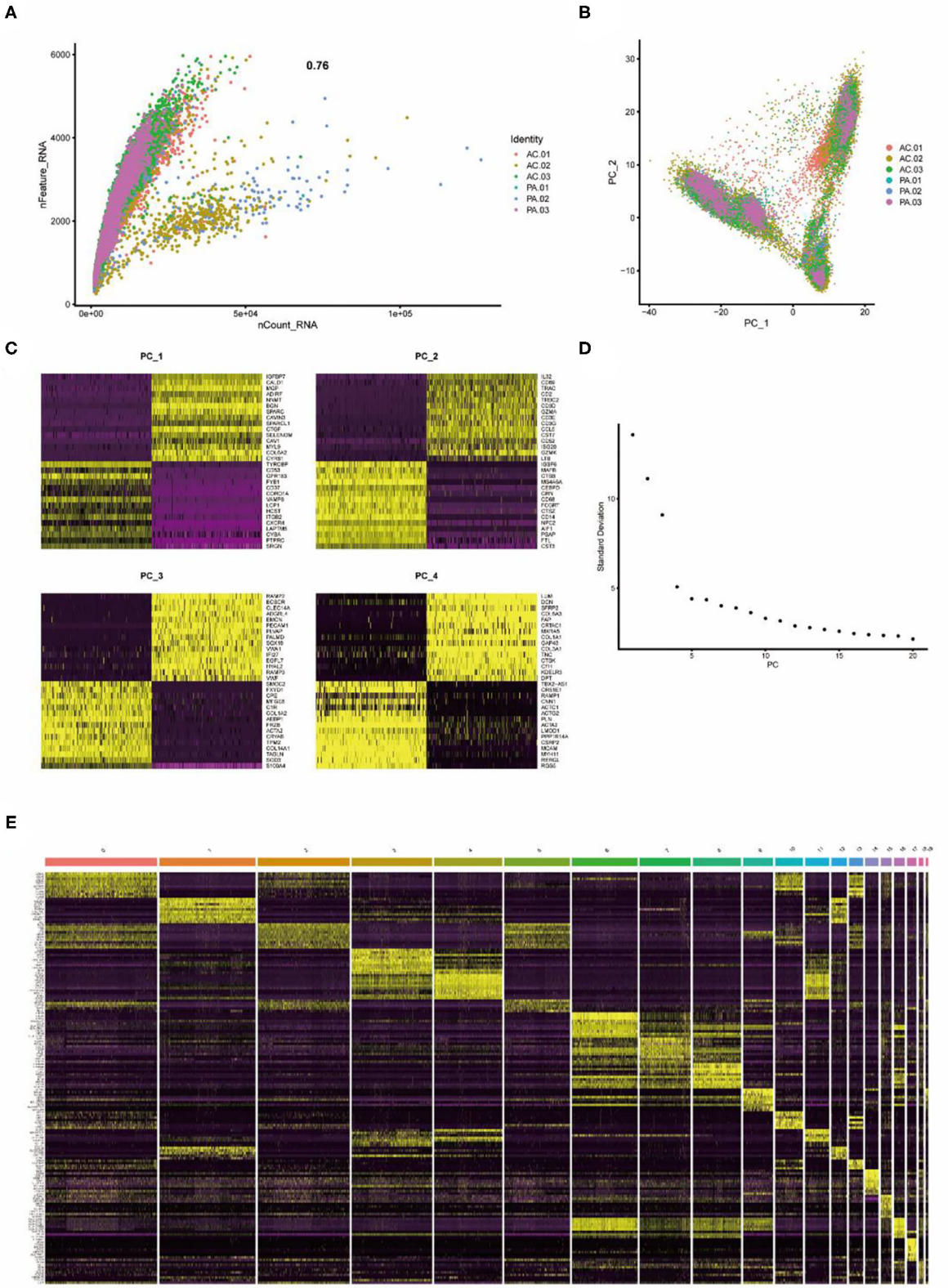

FIGURE 1 | Twenty clusters identified based on single-cell RNA-Seq data reveal multiple cell subpopulations in calcified plaques. **(A)** The number of genes detected correlates significantly with the depth of sequencing. **(B)** PCA showing separation of cells in calcified plaques. **(C)** Differential genes in the first 4 PCs. **(D)** PCA identifies 20 PCs. **(E)** Differential analysis identifying the top 10 marker genes for each cell cluster is shown in the heat map. From yellow to purple indicates gene expression levels from high to low.

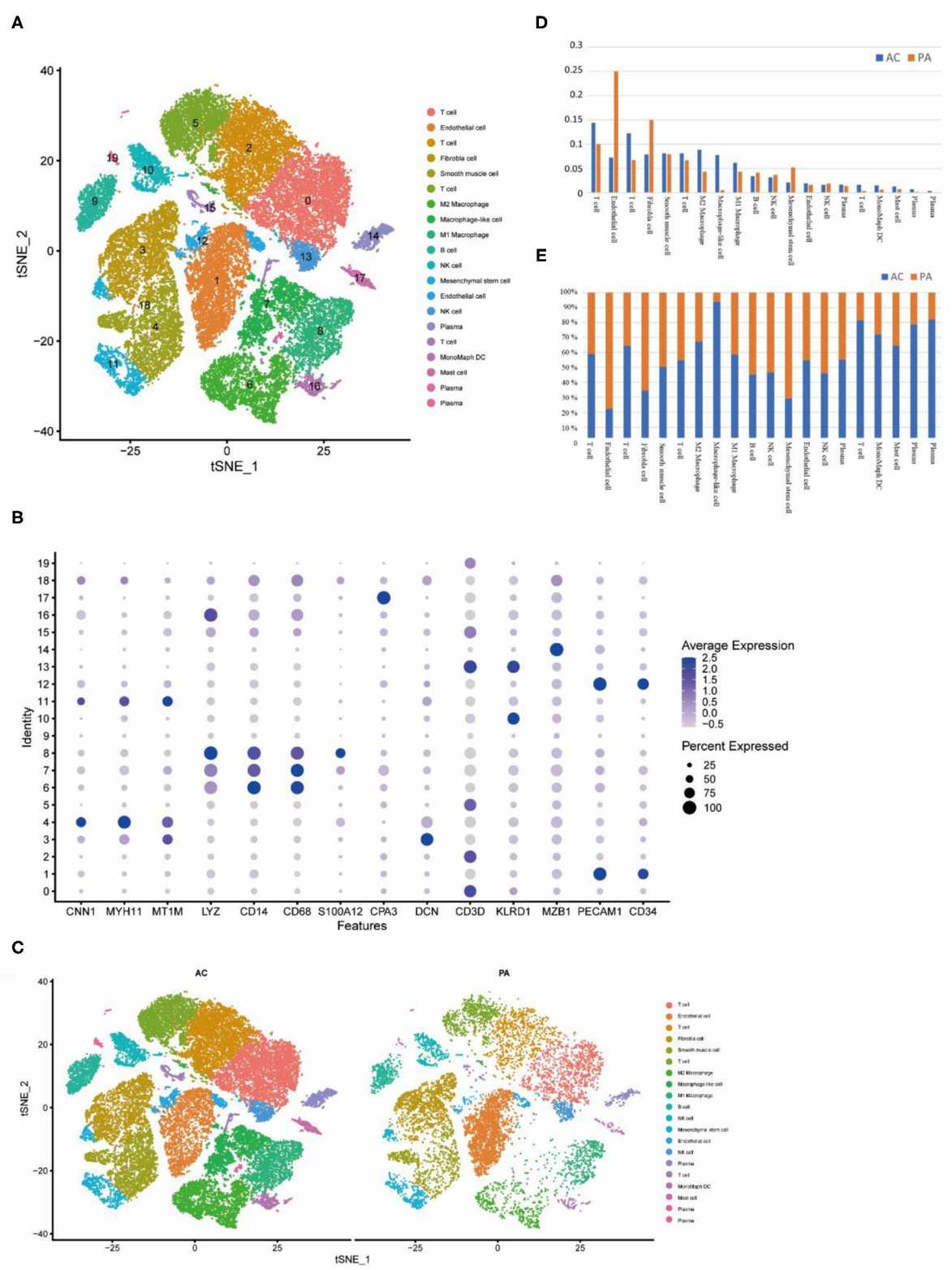

FIGURE 2 | Cellular annotation of subpopulations of calcified core cells, grouped and shown in varying proportions. **(A)** The tSNE algorithm was applied to downscale the 20 PCs and divide the cells into 20 cell clusters. **(B)** Identification of markers for different cell clusters. **(C)** Different cell clusters have different proportions in AC and PA respectively. **(D)** Proportions of each of the 20 cell clusters in AC and PA respectively. **(E)** Variation in the proportion of the 20 cell clusters in AC and PA, with closer to 50% representing less variation.

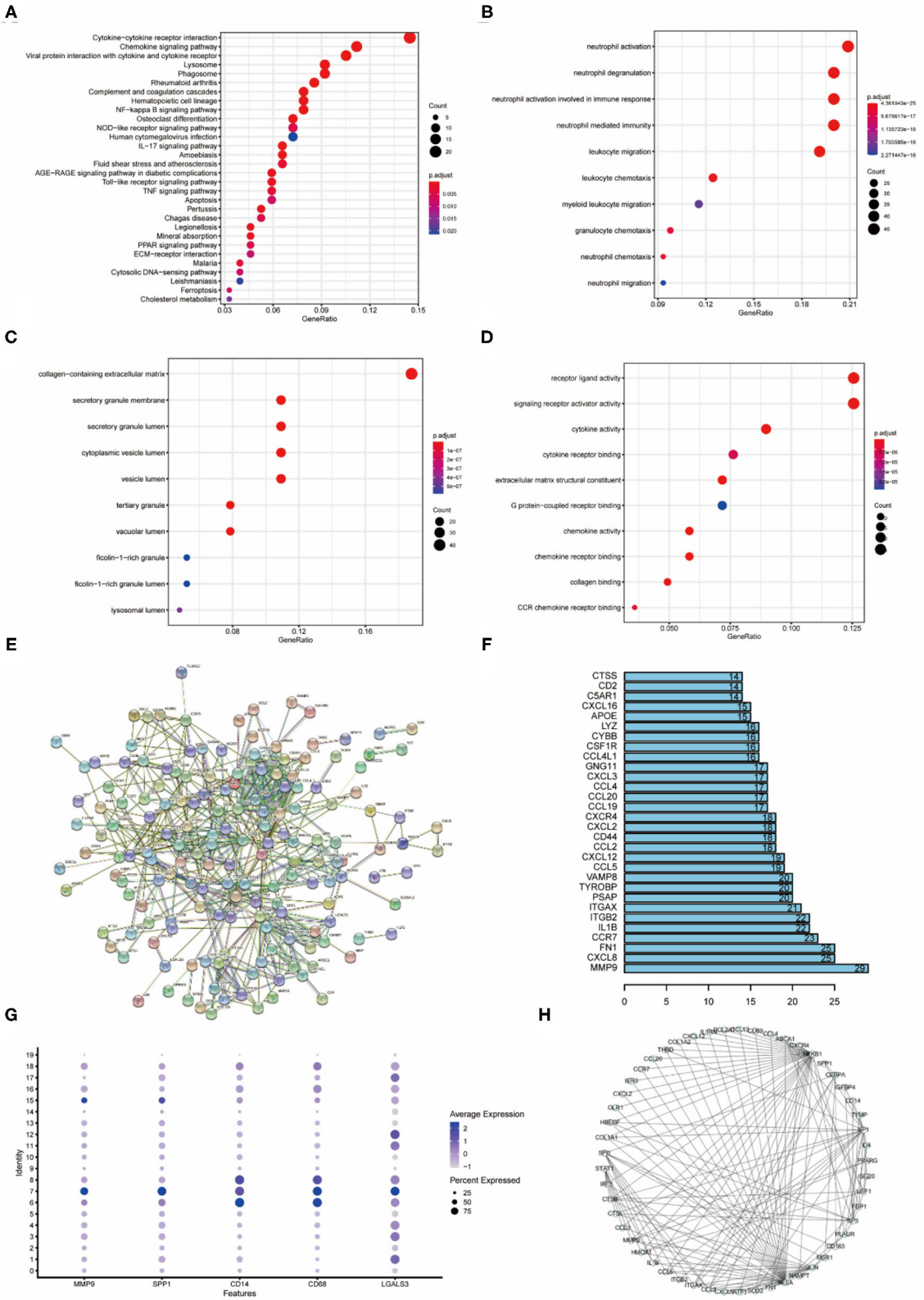

FIGURE 3 | Enrichment analysis of cluster7, protein interactions, upstream transcription factors **(A)** KEGG enrichment analysis of cluster 7. **(B)** Biological process enrichment analysis of cluster 7. **(C)** Enrichment analysis of cellular component of cluster 7. **(D)** Enrichment analysis of molecular function of cluster 7. **(E)** Protein interaction network of cluster 7 differential genes. **(F)** Statistics of cluster 7 protein-interaction pairs. **(G)** Specific expression of cluster 7 genes. **(H)** Upstream transcription factor relationship map of cluster 7 differential genes.

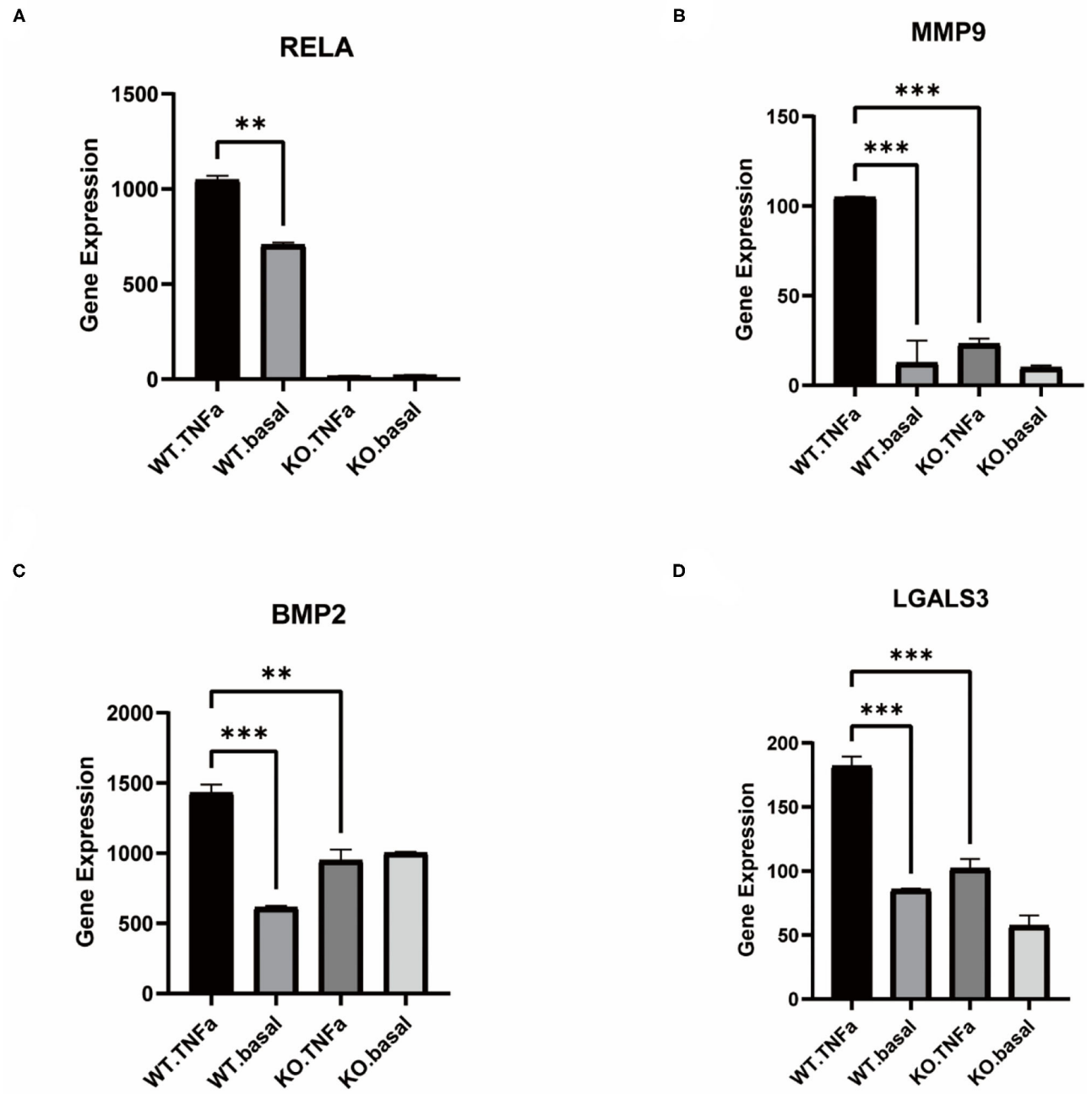

FIGURE 4 | Comparison of gene expression in VSMCs before knockdown of RELA and after knockdown. **(A–D)** Expression of RELA, MMP9, BMP2 and LGALS3 in control and TNFα-added groups after knockdown vs. before knockdown, respectively. $^{**}P<0.01$, $^{***}P<0.001$.

cells, monocytes. In the PA group, the higher proportions were endothelial cells, fibroblasts (**Figure 2D**). In the comparison of the proportions of cells in the two groups, the largest percentage rise in the AC group was in cluster 7, which is macrophage-like smooth muscle cells, while inflammation-related cells such as T cells and monocytes all rose to varying degrees. In contrast, endothelial cells, fibroblasts and mesenchymal cells decreased substantially (**Figure 2E**).

Enrichment Analysis Reveals That Cluster 7 Is Highly Correlated With Inflammatory Activity

Gene enrichment analysis (KEGG, BP, CC, MF) was performed on cluster 7 for the identification of relevant pathways, biological processes, cellular components, and molecular functions of macrophage-like VSMCs. The results showed that the

cellular pathways of cluster 7 were mainly associated with cytokine receptor interactions and chemokine signaling (p < 0.001) (**Figure 3A**). The biological processes of cluster 7 were mainly associated with neutrophil activation, degranulation, migration, and immune response ($p < 0.001$) (**Figure 3B**). The main active cellular components of cluster 7 are the extracellular matrix and the granule membrane associated with secretion, and the granule lumen ($p < 0.001$) (**Figure 3C**). Cluster 7 active cellular functions are mainly for receptor ligands and signaling receptor activators ($p < 0.001$) (**Figure 3D**).

Protein interaction analysis of the differential genes of cluster 7 contained physical interactions and functional correlations between proteins (**Figure 3E**). In the protein-protein interaction network, there are 629 relational pairs, of which MMP9 is involved in 29 pairs, and other proteins that are more involved are CXCL8, FN1 and CCR7 (**Figure 3F**). MMP9, SPP1 (OPN), and LGALS3 were specifically expressed in cluster 7 (**Figure 3G**). The upstream transcription factors regulating differentially expressed genes in cluster 7 were identified based on the regulatory information of the genes, and the results showed that NFκB1 and RELA regulated the highest number of downstream (**Figure 3H**). Other transcription factors that regulated many downstream were SP1, JUN and SPI.

Knockout of RELA Affects the Cellular Phenotypic Transition of VSMCs

TNFα induced an inflammatory response in the cells, and the addition of TNFα to WT-type VSMCs resulted in a rise in RELA expression, whereas it was not expressed in the KO-type VSMCs with RELA knocked out (**Figure 4A**). MMP9 expression was significantly higher in the inflammatory response, whereas knockdown of RELA resulted in a significantly lower rise in MMP9 than the WT-type (**Figure 4B**). Similarly, BMP2 expression rose in the inflammatory response but did not change significantly in the KO-type (**Figure 4C**). In contrast, the macrophage phenotype marker gene LGALS3, which was significantly elevated in the WT type stimulated with TNFα, had a reduced rise after knockdown of RELA compared to the WT-type (**Figure 4D**).

Association Between Baseline Characteristics of MESA Participants and MMP9

A total of 999 participants were tested for serum MMP9 levels and 57.0% of the population were female with a mean age of all was 59.35 years at baseline (**Table 1**). Of the study population, 408 (40.8%) participants had hypertension and 716 (71.6%) had a BMI at overweight levels. Of these, 554 (55.4%) had no CAC (Agatston=0),445 (44.5%) had at least moderate CAC. In contrast, 927 (92.7%) had an ABI at or above 0.97 and only 0.72% had <0.97. In the serum level test, 97 (0.97%) people had CRP >10mg/L and 50% had TNF-R1 levels over 1223pg/mL. There was no significant difference in the effect of age, hypertension and ABI on MMP9 levels.

TABLE 1 | Association between serum MMP9 level and the clinicopathological characteristics.

	N	Mean ± SD	*P*-value
Age (years)			
≤60	579	242.98 ± 5.65	0.54
>60	420	248.58 ±7.38	
Gender			
Female	570	255.07 ± 6.32	0.035
Male	429	232.40 ± 6.25	
Hypertension			
No	591	240.87 ± 5.65	0.238
Yes	408	251.80 ± 7.40	
BMI (kg/m²)			
<25	282	232.29 ± 8.20	0.024
≥25	716	250.02 ± 5.37	
Agatston calcium score			
0	554	236.46 ± 5.59	0.031
>0	445	256.37 ± 7.33	
C-reactive protein (mg/L)			
≤10	901	236.68 ± 4.48	<0.0001
>10	97	322.40 ±18.60	
Ankle-brachial index			
<0.97	72	280.47 ± 20.57	0.086
≥0.97	927	242.6 ± 4.58	
TNF-R1 (pg/mL)			
<1,223	499	214.31 ± 4.99	<0.0001
≥1,223	500	276.3 ± 7.25	

MMP9 levels were higher in overweight than normal individuals (**Figure 5A**) and higher in those with CAC than in those without CAC (**Figure 5B**). CRP associated with infection and injury in the organism had a significant effect on serum MMP9 levels (**Figure 5C**). TNF-R1 plays a role in cellular inflammation and there was a significant difference in serum MMP9 levels between the two groups divided by a median of 1,223 pg/mL, with higher serum MMP9 levels in those with high TNF-R1 levels (**Figure 5D**).

To explore the specific populations at increased risk of CAC progression due to altered MMP9 levels, we conducted subgroup analyses based on traditional risk factors (**Table 2**). We found that the positive association between MMP9 levels and CAC progression was significant in females (OR 1.002; 95%CI 1.001–1.003; $P < 0.0001$).

DISCUSSION

Our study shows that macrophage-like cells transformed from VSMCs are involved in VC progression and that these cells are mainly associated with inflammatory responses. MMP9 plays an important role in the phenotypic transition of VSMCs and is regulated by RELA.

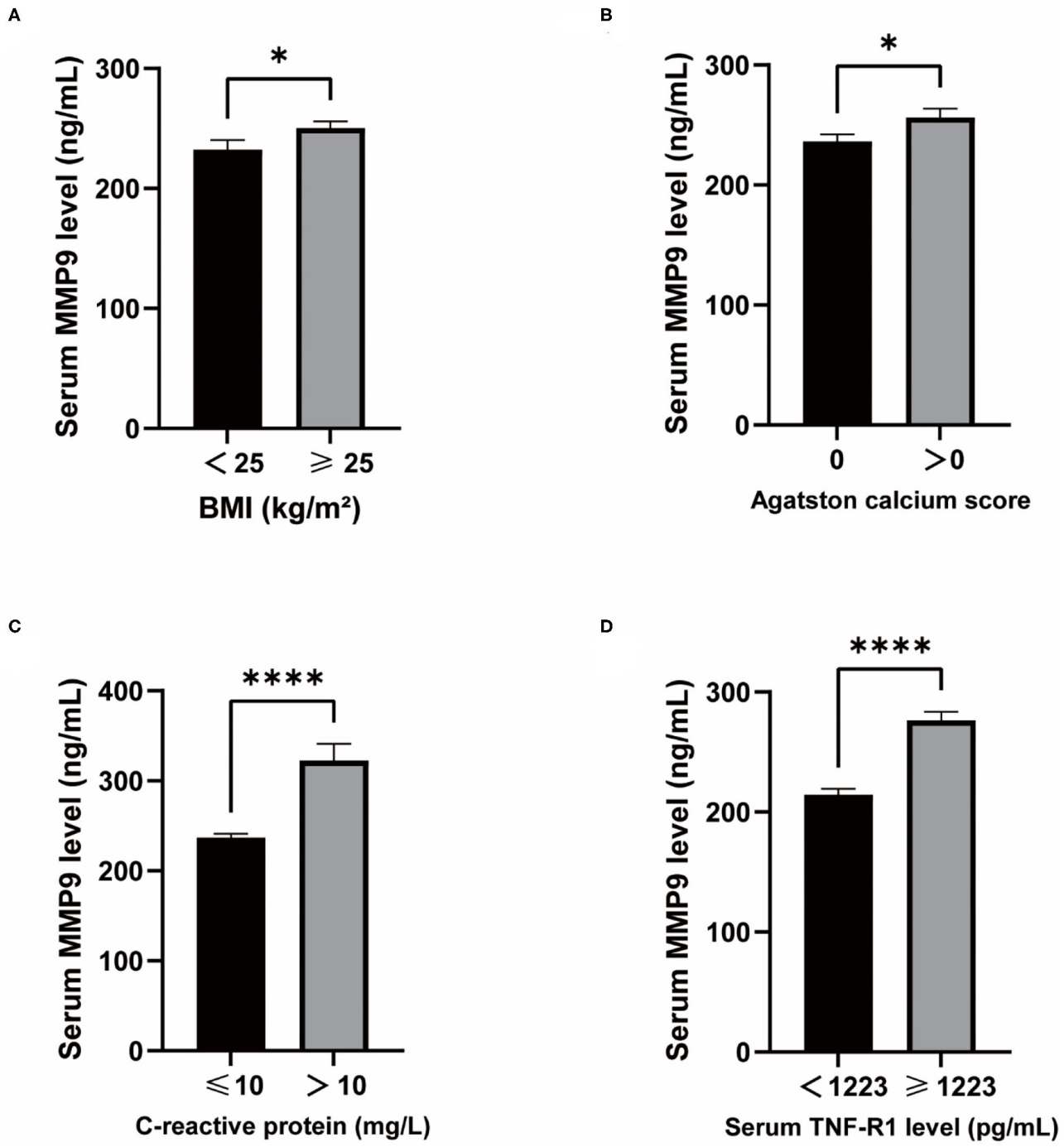

FIGURE 5 | Differences in serum MMP9 levels and clinical physiopathological characteristics. **(A)** MMP9 levels in BMI ≥25 vs. BMI <25. **(B)** MMP9 levels in Agatston calcium score = 0 vs. Agatston calcium score > 0. **(C)** MMP9 levels in CRP ≤10 vs. CRP >10. **(D)** MMP9 levels in TNF-R1 < 1,223 vs. TNF-R1 ≥1,223. *P<0.05, ****P<0.0001.

The phenotypic changes in VSMCs during the calcification process were often investigated using various chemicals or growth factors for experiments. A number of *in vitro* studies have found increased or decreased expression of smooth muscle cell markers, including upregulation of the macrophage marker LGALS3 (6), and the resulting differentiation of VSMCs into multiple subpopulations. In an *in vivo* study, Wirka et al. (18) proposed that VSMCs regulated by phenotypic alterations would change from contractile VSMCs to fibroblast-like cells along a continuous trajectory.

TABLE 2 | Subgroup analysis of the association between MMP9 level and CAC progression.

Subgroups	OR	95%CI	*P*-value
Age, years(%)			
≤64 (69.6)	1.002	1.000–1.003	0.008
>64 (30.4)	1.001	1.000–1.003	0.02
Sex(%)			
Female (57.1)	1.002	1.001–1.003	<0.0001
Male (42.9)	1	0.999–1.002	0.569
BMI, kg/m² (%)			
≤25 (28.2)	1.001	1.000–1.003	0.031
>25 (71.8)	1.001	1.000–1.002	0.043
Hypertension (%)			
No (59.2)	1.001	1.000–1.003	0.042
Yes (40.8)	1.001	1.000–1.002	0.063

In this study, we found that macrophage-like cells were highly variable in calcified core plaques and were associated with inflammatory responses. These findings were based on a single cell transcriptome sequencing database and we validated the results using data from VSMCs with knockout RELA. As there are multiple cells in the calcified core plaques, we classified all cells into 20 cell clusters. In addition to the macrophage-like cells studied in this experiment, there were T cells, endothelial cells, fibroblasts, VSMCs, monocytes, B cells, NK cells, mesenchymal cells, and mast cells, all of which are consistent with the composition of the vasculature. In addition to the upregulation of LGALS3 expression in macrophage-like cells, the macrophage markers CD14 and CD68 were also upregulated, as were bone bridging protein (OPN) and bone morphogenetic protein 2 (BMP2), which are associated with calcification.

The results of the enrichment analysis showed that macrophage-like cells are involved in neutrophil activation and migration mainly through cytokine receptor interactions. To further explore the biological processes of macrophage-like cells, we analyzed the protein-protein interaction network and found that MMP9 was associated with the action of numerous proteins. The matrix metalloproteinase (MMP) family is involved in the breakdown of the extracellular matrix in numerous physiopathological processes and plays an important role in leukocyte migration. NFκB and RELA are transcriptional regulators that modulate the intracellular expression of MMP9 (19), and their inappropriate activation can lead to various inflammatory conditions. Previous experiments have demonstrated that TNFα action activates NFκB to promote the osteogenic transformation of VSMCs (20), however the exact process is not yet known.

By analyzing high-throughput sequencing data, we found that the expression of MMP9 in VSMCs could be reduced by knocking out RELA. In contrast, VSMCs induced by the addition of TNFα could transdifferentiate into macrophage-like cells, and the macrophage marker LGALS3 decreased dramatically after knockout of RELA. BMP2 induces cartilage and bone formation and plays an important role in the calcification process of VSMCs, and BMP2 expression rises in the inflammatory response and promotes calcification of VSMCs, while BMP2 expression after knockout of RELA did not change significantly.

This suggests that RELA may regulate the phenotypic transition and calcification process of VSMCs in the inflammatory response through MMP9. MMP9 increases the density of inflammatory infiltration, accelerates vascular injury and regulates the entry of monocytes and T cells into the vessel wall (21), and inhibition of MMP9 expression protects the vascular intima and reduces the inflammatory response.

In our derived results, inhibition of MMP9 inhibited the conversion of VSMCs into macrophage-like cells, delayed bone and cartilage differentiation and affected the formation of atherosclerotic calcified core plaques. The results of the MESA data analysis also demonstrate that MMP9 in plasma is associated with an inflammatory response, and that MMP9 levels are elevated to varying degrees in people with overweight and CAC.

A potential limitation of our study is that an animal model of arterial vascular calcification has not been used to further validate the specific effects of MMP9 on the transdifferentiation of VSMCs. Although an association between MMP9 and some of the clinical physiopathological features was clearly established, a causal relationship could not be demonstrated.

CONCLUSIONS

Using scRNA-seq and high-throughput RNA-seq data, we found that inflammation can affect the transdifferentiation of VSMCs into macrophage-like cells, and that MMP9 is an important factor in this process. The role of MMP9 in promoting atherosclerotic plaque calcification was validated based on the MESA database. This study highlights the impact of MMP9 in early vascular calcification, as well as providing new ideas for improving prognosis in patients with atherosclerosis.

DATA AVAILABILITY STATEMENT

The datasets presented in this study can be found in online repositories. The names of the repository/repositories and accession number(s) can be found in the article/**Supplementary Material**.

AUTHOR CONTRIBUTIONS

XL is responsible for data collection and analysis, as well as article writing. HZ and DL are responsible for data collection. WH, ZZ, JW, and AL are responsible for the revision of the article.

HH is financial support and revision of the article. All authors contributed to the article and approved the submitted version.

FUNDING

This work was supported by National Natural Science Foundation of China (8201101103, 82073408, 81870506, 81670676, and 81422011), project of Traditional Chinese Medicine in Guangdong province (20201062), Basic Research Project of Shenzhen Science and Technology Innovation Committee (JCYJ20180306174648342 and JCYJ20190808102005602), Shenzhen Futian District Public Health Research Project (FTWS2019003), and Shenzhen Key Medical Discipline Construction Fund (SZXK002).

ACKNOWLEDGMENTS

We thank to Dr. Dong Wei for his support in data analysis.

SUPPLEMENTARY MATERIAL

The Supplementary Material for this article can be found online at: https://www.frontiersin.org/articles/10.3389/fcvm.2021.766613/full#supplementary-material

REFERENCES

1. Rocha-Singh KJ, Zeller T, Jaff MR. Peripheral arterial calcification: prevalence, mechanism, detection, and clinical implications. *Catheter Cardiovasc Interv.* (2014) 83:212–20. doi: 10.1002/ccd.25387
2. Vossen LM, Kroon AA, Schurgers LJ, de Leeuw PW. Pharmacological and nutritional modulation of vascular calcification. *Nutrients.* (2019) 12:100. doi: 10.3390/nu12010100
3. Durham AL, Speer MY, Scatena M, Giachelli CM, Shanahan CM. Role of smooth muscle cells in vascular calcification: implications in atherosclerosis and arterial stiffness. *Cardiovasc Res.* (2018) 114:590–600. doi: 10.1093/cvr/cvy010
4. Zhang K, Zhang Y, Feng W, Chen R, Chen J, Touyz RM, et al. Interleukin-18 enhances vascular calcification and osteogenic differentiation of vascular smooth muscle cells through TRPM7 activation. *Arterioscler Thromb Vasc Biol.* (2017) 37:1933–43. doi: 10.1161/ATVBAHA.117.309161
5. Giachelli CM. Vascular calcification: in vitro evidence for the role of inorganic phosphate. *J Am Soc Nephrol.* (2003) 14(9 Suppl. 4):S300–4. doi: 10.1097/01.ASN.0000081663.52165.66
6. Shankman LS, Gomez D, Cherepanova OA, Salmon M, Alencar GF, Haskins RM, et al. KLF4-dependent phenotypic modulation of smooth muscle cells has a key role in atherosclerotic plaque pathogenesis. *Nat Med.* (2015) 21:628–37. doi: 10.1038/nm.3866
7. Alappan HR, Vasanth P, Manzoor S, O'Neill WC. Vascular calcification slows but does not regress after kidney transplantation. *Kidney Int Rep.* (2020) 5:2212–7. doi: 10.1016/j.ekir.2020.09.039
8. Wagner A, Regev A, Yosef N. Revealing the vectors of cellular identity with single-cell genomics. *Nat Biotechnol.* (2016) 34:1145–60. doi: 10.1038/nbt.3711
9. Butler A, Hoffman P, Smibert P, Papalexi E, Satija R. Integrating single-cell transcriptomic data across different conditions, technologies, and species. *Nat Biotechnol.* (2018) 36:411–20. doi: 10.1038/nbt.4096
10. Cieslak MC, Castelfranco AM, Roncalli V, Lenz PH, Hartline DK. t-Distributed stochastic neighbor embedding (t-SNE): a tool for eco-physiological transcriptomic analysis. *Mar Genomics.* (2020) 51:100723. doi: 10.1016/j.margen.2019.100723
11. Stuart T, Butler A, Hoffman P, Hafemeister C, Papalexi E, Mauck WM, 3rd, et al. Comprehensive integration of single-cell data. *Cell.* (2019) 177:1888–902.e21. doi: 10.1016/j.cell.2019.05.031
12. Durinck S, Spellman PT, Birney E, Huber W. Mapping identifiers for the integration of genomic datasets with the R/Bioconductor package biomaRt. *Nat Protoc.* (2009) 4:1184–91. doi: 10.1038/nprot.2009.97
13. Yu G, Wang LG, Han Y, He QY. ClusterProfiler: an R package for comparing biological themes among gene clusters. *OMICS.* (2012) 16:284–7. doi: 10.1089/omi.2011.0118
14. Kanehisa M, Furumichi M, Tanabe M, Sato Y, Morishima K. KEGG: new perspectives on genomes, pathways, diseases and drugs. *Nucleic Acids Res.* (2017) 45:353–61. doi: 10.1093/nar/gkw1092
15. Kramarz B, Lovering RC. Gene Ontology: A Resource for Analysis and Interpretation of Alzheimer's Disease Data. In: Wisniewski T, editor. *Alzheimer's Disease*. Brisbane, AU: Codon Publications (2019). doi: 10.15586/alzheimersdisease.2019.ch2
16. Love MI, Huber W, Anders S. Moderated estimation of fold change and dispersion for RNA-seq data with DESeq2. *Genome Biol.* (2014) 15:550. doi: 10.1186/s13059-014-0550-8
17. Bild DE, Bluemke DA, Burke GL, Detrano R, Diez Roux AV, Folsom AR, et al. Multi-ethnic study of atherosclerosis: objectives and design. *Am J Epidemiol.* (2002) 156:871–81. doi: 10.1093/aje/kwf113
18. Wirka RC, Wagh D, Paik DT, Pjanic M, Nguyen T, Miller CL, et al. Atheroprotective roles of smooth muscle cell phenotypic modulation and the TCF21 disease gene as revealed by single-cell analysis. *Nat Med.* (2019) 25:1280–9. doi: 10.1038/s41591-019-0512-5
19. Wang C, Li Q, Yang H, Gao C, Du Q, Zhang C, et al. MMP9, CXCR1, TLR6, and MPO participant in the progression of coronary artery disease. *J Cell Physiol.* (2020) 235:8283–92. doi: 10.1002/jcp.29485
20. Zhao G, Xu MJ, Zhao MM Dai XY, Kong W, Wilson GM, et al. Activation of nuclear factor-kappa B accelerates vascular calcification by inhibiting ankylosis protein homolog expression. *Kidney Int.* (2012) 82:34–44. doi: 10.1038/ki.2012.40
21. Watanabe R, Maeda T, Zhang H, Berry GJ, Zeisbrich M, Brockett R, et al. MMP (Matrix Metalloprotease)-9-producing monocytes enable T cells to invade the vessel wall and cause vasculitis. *Circ Res.* (2018) 123:700–15. doi: 10.1161/CIRCRESAHA.118.313206

Conflict of Interest: The authors declare that the research was conducted in the absence of any commercial or financial relationships that could be construed as a potential conflict of interest.

Publisher's Note: All claims expressed in this article are solely those of the authors and do not necessarily represent those of their affiliated organizations, or those of the publisher, the editors and the reviewers. Any product that may be evaluated in this article, or claim that may be made by its manufacturer, is not guaranteed or endorsed by the publisher.

Copyright © 2021 Liang, He, Zhang, Luo, Zhang, Liu, Wang and Huang. This is an open-access article distributed under the terms of the Creative Commons Attribution License (CC BY). The use, distribution or reproduction in other forums is permitted, provided the original author(s) and the copyright owner(s) are credited and that the original publication in this journal is cited, in accordance with accepted academic practice. No use, distribution or reproduction is permitted which does not comply with these terms.

frontiers in Cardiovascular Medicine

ORIGINAL RESEARCH
published: 23 December 2021
doi: 10.3389/fcvm.2021.777757

Aortic Dissection Auxiliary Diagnosis Model and Applied Research Based on Ensemble Learning

Jingmin Luo[1], Wei Zhang[1], Shiyang Tan[2], Lijue Liu[2], Yongping Bai[1]* and Guogang Zhang[3]**

[1] Xiangya Hospital of Central South University, Changsha, China, [2] Information Science and Engineering School of Central South University, Changsha, China, [3] Third Xiangya Hospital of Central South University, Changsha, China

Aortic dissection (AD), a dangerous disease threatening to human beings, has a hidden onset and rapid progression and has few effective methods in its early diagnosis. At present, although CT angiography acts as the gold standard on AD diagnosis, it is so expensive and time-consuming that it can hardly offer practical help to patients. Meanwhile, the artificial intelligence technology may provide a cheap but effective approach to building an auxiliary diagnosis model for improving the early AD diagnosis rate by taking advantage of the data of the general conditions of AD patients, such as the data about the basic inspection information. Therefore, this study proposes to hybrid five types of machine learning operators into an integrated diagnosis model, as an auxiliary diagnostic approach, to cooperate with the AD-clinical analysis. To improve the diagnose accuracy, the participating rate of each operator in the proposed model may adjust adaptively according to the result of the data learning. After a set of experimental evaluations, the proposed model, acting as the preliminary AD-discriminant, has reached an accuracy of over 80%, which provides a promising instance for medical colleagues.

Keywords: aortic dissection, early detection, artificial intelligence, diagnosis model, RS-easy ensemble

OPEN ACCESS

Edited by:
Yuli Huang,
Southern Medical University, China

Reviewed by:
Longhou Fang,
Houston Methodist Research Institute, United States
Yanfang Chen,
Wright State University, United States

****Correspondence:***
Guogang Zhang
zhangguogang@csu.ehu.cn
Lijue Liu
ljliu@csu.edu.cn
Yongping Bai
baiyongping@csu.edu.cn

Specialty section:
This article was submitted to General Cardiovascular Medicine, a section of the journal Frontiers in Cardiovascular Medicine

Received: *15 September 2021*
Accepted: *15 November 2021*
Published: *23 December 2021*

Citation:
Luo J, Zhang W, Tan S, Liu L, Bai Y and Zhang G (2021) Aortic Dissection Auxiliary Diagnosis Model and Applied Research Based on Ensemble Learning. Front. Cardiovasc. Med. 8:777757. doi: 10.3389/fcvm.2021.777757

INTRODUCTION

Aortic dissection (AD) is a dangerous cardiovascular disease with complex pathogenesis. AD cause damage in the aortic intima and tunica media membrane structure, blood in the aortic lumen flows into the tunica media from the tear of aortic intimal film, causing membrane separation along the aorta extending along the long axis of cavities and false cavities of the aortic wall separating state, and cause the corresponding symptoms like chest pain. Incidences of AD each year are about 5–10 cases per million population and peak ages are 50–70 years old, with the ratio of male to female about 2–3: 1.65–70%, all have a hidden onset and rapid progression (1). AD prognosis is poor without timely treatment, patients shall receive a quick death because of the acute complications such as cardiac tamponade and arrhythmia (2).

At present, acknowledged etiology of AD is relatively limited and known risk factors associated with AD include vascular endothelial damage and high blood pressure (1). Due to the hidden onset and rapid progression of AD in the early phase leading to higher mortality, many primary medical institutions, without appropriate equipment such as CT, have serious difficulty providing early diagnosis and prognosis of AD. Most doctors of these basic level medical institutions diagnose AD based on their experience instead of with CT angiography because tests are expensive and take a long time due to their complexity. Since only a handful of large hospitals are equipped with the

necessary equipment, many AD patients who first come to a basic level hospital are not accurately diagnosed and treated, which means they lose the best chance of getting effective treatment or referral (3). Therefore, establishing an early auxiliary diagnosis model of AD recognition that uses routine medical data that can be gained by basic level medical staff is an urgent and important task.

Using an auxiliary diagnosis model based on artificial intelligence is a hot topic in the field of biomedical engineering, and it is a very good example of combining multiple technologies, such as computer science, big data technology, cognitive science, and logic, with the practice of medicine. There has been great progress in using artificial intelligence assisted diagnostic technology in diagnosis of AD, such as using machine learning model to classify aortic dissection patients. Da Huo et al. used Weka toolkit to employ four common classifiers on dataset including Bayesian Network, Naïve Bayes, J48 and SMO, and found Bayes Net model has the best performance among four classifiers (4). Lijue Liu et al. used multiple machine learning models, include AdaBoost, SmoteBagging, EasyEnsemble and CalibratedAdaMEC, to study aortic dissection screening method, and found that the screening performance of the models had a misdiagnosis rate lower than 25% except AdaBoost (5). These research showed that artificial intelligence technology can help clinicians build a new early screening approach for AD.

Although machine learning methods are helpful for the diagnosis of AD, the high death rate of AD requires higher accuracy and single modeling and analysis method is not enough. Ensemble learning strategies have demonstrated impressive capacities to improve the prediction accuracy of base learning algorithms. Zhenya Qi et al. used *t*-test to investigate if the performance of an ensemble for heart disease prediction, which contains five heterogeneous classifiers: random forest, logistic regression, support vector machine, extreme learning machine and k-nearest neighbor, was better than individual classifiers and the contribution of Relief algorithm (6). The best performance was achieved by the proposed method according to 10-fold cross validation. The statistical tests demonstrated that the performance of the proposed ensemble was significantly superior to individual classifiers, and the efficiency of classification was distinctively improved by Relief algorithm (6). Therefore, establishing an auxiliary diagnosis model by using artificial intelligence technology and applying it to the early diagnosis of AD should increase the positive diagnostic rate of AD greatly. At the same time, the establishment of a model may improve the survival rate and prognosis of AD patients.

METHODS

Case Information Collection

After signing all relevant documents, including the confidentiality agreements and ethical review document, patient's information are retrieved from the Xiangya hospital's electronic medical record system and statistics from 2006 to 2016. A total number of 3,249 AD patients' and another 95,711 cases of non-AD patients' clinical data had been collected. All these data were divided into three categories: (1) patients' basic information: gender, age, height, weight, family history, past medical history, personal habits; (2) text messages about symptoms and complaints: presence of chest pain, heart palpitations, dizziness or headache symptoms, frequency and extent, presence of abnormal blood vessel pulsing, aortic valve area signs such as noise; (3) quantitative index of tests and examinations: Blood routine, coagulation routine, hepatorenal function, etc.

Indexes Screening

The indexes chosen for this research come mainly from the following tests and examinations: blood routine (BR), coagulation routine (CR), hepatorenal function and serum lipid, myocardial enzymology, and serum electrolyte. These indexes are commonly used in basic level medical institutions. Furthermore, results can be quickly obtained after sampling, meaning it takes less time to judge the situation of a patient compared to some examinations that require special equipment, such as coronary CTA and CT angiographic. If these indexes, which used to have little significance in AD diagnosis, can actually play an important role in some way, they may be irreplaceable to AD patients because of their cheap price and accessibility.

BR is one of the most commonly used laboratory tests in clinical laboratories and the basic principle is using electrical impedance and spectrophotometric colorimetry to detect if the blood's composition, composed of red blood cells, white blood cells and platelets, is in the normal range. The number and normal of size of cells, can be used to identify if the cells are normal. BR can also figure average density and conversion of various types of cells in the blood by formula, such as hematocrit, mean corpuscular volume, or mean corpuscular hemoglobin. Using BR to assess the patient's blood type and quantity of cells may help detect significant hemodynamic changes in the early phase of AD. Existing studies have shown that 43% of AD patients have different degrees of BR abnormalities (7). Therefore, 22 indexes of BR are taken from Xiangya hospital into further analysis (**Table 1**).

CR is an activity to detect various coagulation factors with solidification method, hair color substrate method and immune turbidity method by using photoelectric principle. CR can assess a patient's blood coagulation function and bleeding risk from the activity of coagulation factors such as PT, APTT, TT and FBG in the blood. Research shows that a considerable number of preoperative AD patients have lower levels of coagulation factor than normal and the MAp MAf is in a state of relative hyperthyroidism. This may be because the blood contact with the endothelium of the false lumen height of thrombin activation in the early phase of AD. Because acute AD patients' onset time is very short, blood coagulation function is still in the stage of high activation of high condensation, and under the action of thrombin, the expression of platelet fibrinogen are increased. The indexes od CR, D—dimer especially have been proven to have guiding function in the process of AD diagnosis (8). Thus, 10 indexes of CR are taken from Xiangya hospital into further analysis (**Table 2**).

Hepatorenal function and myocardial enzymology are commonly used tests to detect several important organs'

TABLE 1 | Twenty two indexes of blood routine (BR) from Xiangya hospital.

Index name	Unit	Reference range
White blood cells count	10'9/L	3.5–9.5
Red blood cells count	10'12/L	3.85–5.1
Hemoglobin	g/L	115–150
Thrombocyte	10'9/L	125–350
Hematocrit	%	35.0–45.0
Neutrophil granulocyte count	10'9/L	1.8–6.3
Lymphocyte count	10'9/L	1.1–3.2
Eosnophils granulocyte count	10'9/L	0.02–0.52
Basophilic granulocyte count	10'9/L	0.00–0.6
Monocyte count	10'9/L	0.1–0.6
Neutrophil percentage	%	40.0–75.0
Lymphocyte percentage	%	20.0–50.0
Eosnophils percentage	%	0.1–1.0
Basophilic percentage	%	0.4–8.0
Monocyte percentage	%	3.0–10.0
Mean corpuscular volume	fl	82.0–100.0
Mean corpuscular hemoglobin	PG	27.0–34.0
Mean corpuscular hemoglobin concentration	g/L	316–354
Red blood cells distribution width	%	<15
Thrombocytocrit	%	0.18–0.22
Mean platelet volume	fl	7.6–13.2
Platelet distribution width	%	<17.2

TABLE 2 | Ten indexes of coagulation routine (CR) from Xiangya hospital.

Index name	Unit	Reference range
Prothrombin time (PT)	sec	10.0–16.0
Prothrombin percentage (PP)	%	70–140
International normalized ratio (INR)	–	0.8–1.2
Activated partial thromboplastin time (APTT)	sec	25.0–43.0
Thrombin time	sec	14.0–21.0
Fibrinogen	g/L	2.0–4.0
Plasma fibrinogen degradation products	mg/L	0–5
D - dimer	mg/L	0–0.5
Plasma plasminogen antigen	mg/L	230–386
Plasma antithrombin III antigen	mg/L	180–392

function, like heart, liver and kidney, and whole body metabolic function in clinical way. These tests mainly use the enzyme circulation method, enzyme coupling method, continuous monitoring method, Reitman colorimetric method and fluorescent method to complete the systematic analysis of indicators related to the metabolism of an organ. The tests can reflect the basic situation of important organs and whole body metabolic function. In the early phase of AD, the effects of hemodynamic changes on metabolism may be subtle, but they do exist. Due to the organizational microenvironment disorder and myocardial damage caused by hemodynamic changes, some abnormal results may be reflected in the results of such tests

TABLE 3 | Eighteen indexes of hepatorenal function and myocardial enzymology from Xiangya hospital.

Index name	Unit	Reference range
Total protein	g/L	65.0–85.0
Albumin	g/L	40.0–50.0
Globulin	g/L	20.0–40.0
A/G	–	1.2–2.4
Total bilirubin	μ mol/L	1.7–17.1
Direct bilirubin	μ mol/L	0.0~6.8
Total bile acid	μ mol/L	0.0–12.0
Glutamic-pyruvic transaminase	U/L	7.0–40.0
Glutamic oxalacetic transaminase	U/L	13.0–15.0
Glycated serum protein	mmol/L	1.18–2.20
Urea nitrogen	mmol/L	3.10–8.80
Creatinine	mmol/L	41.0–111.0
Trioxypurine	μ mol/L	155.0–357.0
Glucose	μ mol/L	3.90–6.10
Lactic dehydrogenase	U/L	120.0–250.0
Creatine kinase	U/L	40.0–200.0
Creatine kinase isoenzymes	U/L	<24.0
Myohemoglobin	μ g/L	<70.0

TABLE 4 | Five indexes of serum lipid from Xiangya hospital.

Index name	Unit	Reference range
Total triglyceride (TG)	mmol/L	<1.70
Total cholesterol (TC)	mmol/L	<5.18
High-density lipoprotein (HDL)	mmol/L	1.04–1.55
Low-density lipoprotein (LDL)	mmol/L	1.55–3.19
HDL/TC	-	0.17–0.45

(9, 10). Thus, 18 indexes of hepatorenal function and myocardial enzymology are taken into further analysis (**Table 3**).

Serum lipid is a routine test given to patients with cardiovascular diseases since abnormal lipids metabolism is believed to have an important relationship with angiocardiopathy. The purpose of this test is to analyze blood lipid levels and species of patients through the Cholesterol oxidase-peroxidase-anti-peroxidase method (COD—PAP method) and super centrifugal plasma combined with selective precipitation. As one of the most common risk factors for coronary heart disease, blood lipid results can also be an indirect risk factor for AD patients. Lipid metabolism may allow us to assess AD patients' vascular stability and risk of sudden death by indirect methods (11). Therefore, five indexes of serum lipid are also taken into further analysis (**Table 4**).

Serum electrolyte is the test that detects specific ion concentrations in serum. The concentration of several important ions that maintain balance of osmotic pressure between blood and interstitial fluid, such as sodium, chloride, and calcium, are measured by the ion selective electrode method. It is not surprising to find that hemodynamic changes of AD patients

affect their level of serum electrolytes in blood and tissue fluid microenvironment (12, 13). Therefore, 8 indexes of serum electrolyte are taken from Xiangya hospital into further analysis (**Table 5**).

Modeling Method and Data Mining

Research adopts the following main modeling methods: linear discriminant analysis (LDA), artificial neural networks (ANNs), decision tree (DT), support vector machine (SVM) and EasyEnsemble learning. LDA is one of the most classic analyses to classify statistical models of simple discriminant function. In the feature space, LDA can be used to compare different categories of discriminant function value size and classify them by analyzing different categories (14). ANNs is a method to calculate by simulating the way of people thinking. It is a non-linear dynamic system and has the characteristics of distributed storage and parallel collaborative information processing. Back Propagation (BP) neural network algorithm, which is also known as the error Back Propagation algorithm, and it is an artificial neural network supervised learning algorithm. In theory, the BP algorithm can approximate arbitrary functions because its basic structure is composed of a non-linear change unit and it has a strong non-linear mapping ability. Furthermore, due to parameters such as number of the middle layer, processing units of each layer and network coefficient of learning can be set according to the concrete situation; BP has great flexibility (15). DT is an algorithm to calculate the net present value of the probability of expectation, which is greater than or equal to zero based on the probability of known situations. Using a decision tree, the project risk and feasibility evaluation can be easily done with a graphic method. To be specific, DT is a prediction model with tree structure, and it represents the object properties and a mapping relationship between object values, where each internal node is a test on an attribute; each branch represents a test output; each leaf node represents one kind of category (16). SVM is a kind of supervised learning model related to the relevant learning algorithm and mainly used to analyze data and recognize patterns in classification and regression analysis. The statistical learning theories that SVM is based on, like Vapnik-Chervonenkis (VC) dimension theory and structure risk minimum principle, enable SVM to get the best generalization ability and seek the best compromise between the complexity of the model (i.e., on a particular learning accuracy of training samples) and learning ability (i.e., the ability to identify random sample correctly) according to the sample of limited information (17).

All modeling data mining is given operation with nGram function of a decision tree model and session texts are segmented in pairs and get the keyword combination table (**Figure 1**). Each word combination contains two words and the high frequency word combinations will be picked out after statistic analysis. Then the words that already exist in the table are filtered out and the possible keywords combinations (**Figure 2**) are obtained.

TABLE 5 | Eight indexes of serum lipid from Xiangya hospital.

Index name	Unit	Reference range
Potassium	mmol/L	3.50–5.30
Sodium	mmol/L	137.0–147.0
Chlorine	mmol/L	99.0–110.0
Calcium	mmol/L	2.00–2.60
Phosphorus	mmol/L	0.86–1.78
Magnesium	mmol/L	0.66–1.07
Carbon dioxide (CO_2)	mmol/L	19.0–33.0
Anion gap (AG)	mmol/L	8.0–16.0

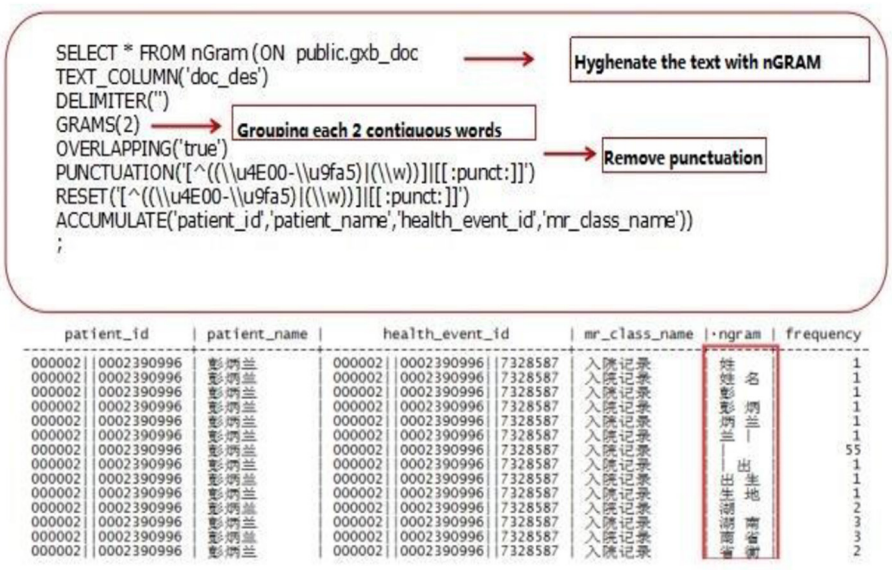

FIGURE 1 | Preliminary discrimination of keywords.

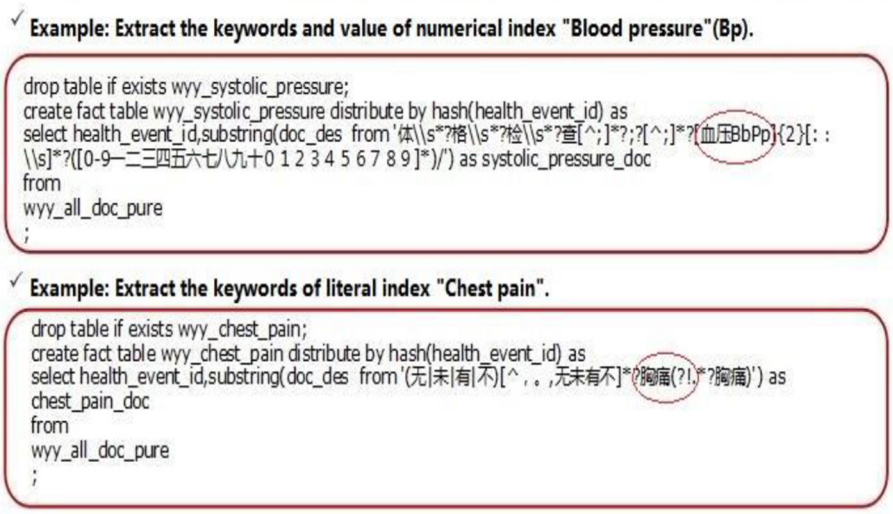

FIGURE 2 | Secondary screening of keywords.

Finally, there is human intervention for keyword selection and confirming official keyword combinations (**Table 6**).

Modeling Parameters and the Training Process

Because of the uncertainty of the AD on each patients, the majority of data that patients provide to doctors are fuzzy and inaccurate. Inevitably, one must try a variety of modeling methods in the process of creating an AD auxiliary diagnosis aneurysm model. According to analysis of the actual AD diagnosis process and knowledge of artificial intelligence and medical statistics, a variety of methods are built to analyze the data and compare the effect of different models (**Figure 3**). The goal of this research is not only to gain an auxiliary diagnosis aneurysm model that simulate the diagnosis of AD, but also adaptively adjust diagnosis model parameters and improve the accuracy of the auxiliary diagnosis with the accumulation of cases. After eliminating imbalances of each modeling method, the final ensemble learning model is established (**Figure 4**). All clinic data are organized by the Excel files and numbering (**Supplementary Materials 1**, **2**). Finally 80 features are used and obtained corresponding data from the electronic medical record and number all features as 1–80. These features were input into the machine learning model as feature vectors.

Linear Discriminant Analysis Model

For the *i*th feature vector $X_i = (x_{i1}, x_{i2} \ldots, x_{i80})$, LDA calculate the discriminant functions $g_c(X_i) = X_i W_c^{\mathrm{T}}$, where $c \in \{1, 2\}$ is the number of categories, X_i is the feature vector of the *i*th sample, $W_c = (W_{c1}\ W_{c2} \ldots, W_{c80})$ is the weight vector of class *c*. The final decision result depends on which category of decision function has a larger value.

BP Neural Network Model

BP neural network is an ANNs algorithm and its basic idea is a kind of gradient descent method. BP creates the minimum actual output value of the network and the minimum desired output error of the mean square error by using gradient search technology. The function of one neuron is to seek the inner product of input vectors and weight vectors, and obtain a scalar result via a non-linear transfer function. The individual neurons split an n-dimensional vector space into two parts with a hyperplane and make a judgment that the vector belong to which side of the hyperplane by given an input vector. The BP network applied in these paper was a 2 layer network with 80 input unit, 1 hidden layer and 1 output unit.

Decision Tree Model

DT establishes the model of decision-making based on data attribute tree structure, and it is often used to solve classification and regression problems. Common algorithms of DT include Classification and Regression Tree (CART), ID3, C4.5, and Random Forests (RF). DT classification can be used as a prediction model and it represents a mapping between object and object attribute values. From the root node, each minor node can express attributes of object judgment conditions, while the branch is representative of the object that meets the requirements and the leaves nodes are the object's prediction results.

Support Vector Machine Model

SVM modeling depends on different Kernel functions, such as the kernel function including Linear Kernel (LK), Polynomial Kernel (PK) and Radial Basis Kernel Function (RBF). RBF is also known as the Gaussian Kernel (GK), The operation results of SVM default parameters are satisfactory, so some adjustments are made in the penalty coefficient and kernel functions. The final parameters are penalty coefficient C = 0.125; kernel = "rbf;" degree = 3; gamma = 0.0078125.

TABLE 6 | Text indexes of basic information and complaint.

Indexes	Type	Value/unit	Notes
Main complaint			
Thoracalgia	Text	① Yes ②No	Yes = 1, No = 0 (below)
Stomachache	Text	①Yes ②No	
Palpitation	Text	①Yes ②No	
Dizziness or Headache	Text	①Yes ②No	
Abnormal pulse	Text	①Yes ②No	
Aortic area murmur	Text	①Yes ②No	
Family history			
Hypertension	Text	①Yes ②No	
Diabetes	Text	①Yes ②No	
Marfan syndrome	Text	①Yes ②No	
Aortic dissection	Text	①Yes ②No	
Medical history			
Chest trauma	Text	①Yes ②No	
Marfan syndrome	Text	①Yes ②No	
Time of Marfan syndrome	Numerical	Year	
Hypertension	Text	①Yes ②No	
Time of Hypertension	Numerical	Year	
Diabetes	Text	①Yes ②No	
Time of Diabetes	Numerical	Year	
Basic information			
Age	Numerical	Year	
Gender	Text	①Male ②Female	Male = 1, Female = 0
Heart rate	Numerical	Beats/min	
Systolic pressure	Numerical	mmhg	
Diastolic pressure	Numerical	mmhg	
Smoking status	Text	①Yes ②No③Quit	Yes = 1, N0 = 0, Quit = 2
Time of Smoking	Numerical	Year	
Time of Quitting Smoking	Numerical	Year	
Drinking status	Text	①Yes ②No③Quit	Yes = 1, N0 = 0, Quit = 2
Time of Drinking	Numerical	Year	
Time of Quitting Drinking	Numerical	Year	
Aortic dissection	text	①Yes ②No	Target variable

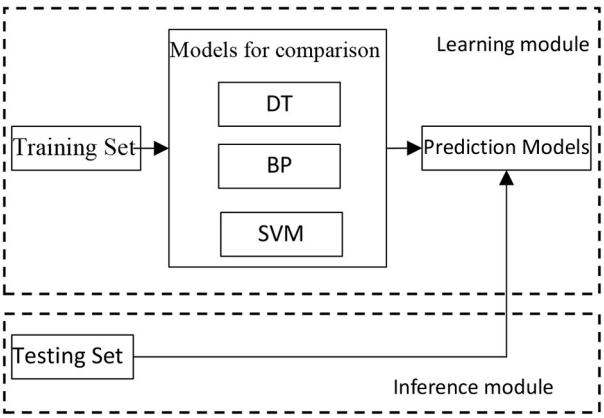

FIGURE 3 | Comparison of modeling method algorithms.

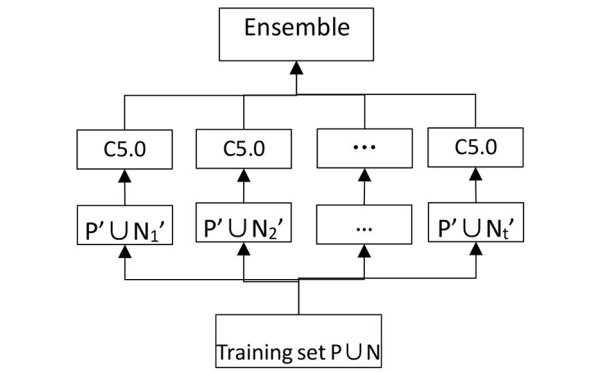

FIGURE 4 | Eliminate imbalances of modeling method.

EasyEnsemble Model

EasyEnsemble is a kind of integrated learning which deals with big categories of data by using the down-sampling method with Adaboost as a weak classifier, and it is an efficient path to dealing with unbalanced data. Data ratio is severely unbalanced due to the rarity of AD; the amount of data from AD patients is very small compared with non-AD patients, and the two kinds of data have an ∼1: 65 ratio imbalance. Therefore, EasyEnsemble is the best choice to build an effective model. The specific practices are as follows: Assuming P as the dataset of the minority class, and N as the dataset of the majority class, |P| and |N| as the cardinal number meet the condition that $|N| >> |P|$. The dataset of the majority class is divided into several subdatasets like class N1, N2 and N3...NT, for any dataset Ni ($1 < I < T$), give $|Ni| = |P|$. Each Ni dataset will be trained to be a classifier Hi by combining with P as training set. AdaBoost is used to train Hi in this algorithm and make up the final model through the combination of classifier with number T.

RESULTS

Data Preliminary Processing and Screening

All relevant data are exported from the electronic medical records of Xiangya hospital and obtained a total of 3,249 AD patients' medical records and 95,711 cases of non-AD patients' medical records from 2006 to 2016. After preliminary statistical analysis and exclusion of patients with undetermined diagnoses or incomplete data, a total of 53,213 cases are taken as the modeling cases, including 802 AD patients and 52,411 non-AD patients and finally 43 indexes, which $P \leq 0.001$, are designated as model analysis indexes (**Table 7**).

TABLE 7 | Forty-three indexes of modeling analysis.

Indexes	AD patients (*N* = 802)	Non-AD patients (*N* = 52,411)	t/Chi	*p*
Age (Mean ± SD)	55.57 ± 12.90	62.56 ± 13.06	15.03	<0.001
Gender (Male, %)	574 (71.57)	29,994 (57.23)	66.47	<0.001
Thoracalgia	206 (25.79)	9,460 (18.05)	30.99	<0.001
Palpitation	63 (7.86)	6,106 (11.65)	11.10	0.001
Dizziness or headache	62 (7.73)	7,803 (14.89)	32.13	<0.001
Aortic area murmur	23 (2.87)	377 (0.72)	48.88	<0.001
Chest trauma	11 (1.37)	206 (0.39)	18.62	<0.001
Smoking status			85.79	<0.001
Never smoking	296 (36.91)	12,293 (23.46)		
Smoking	485 (60.47)	37,121 (70.83)		
Quit smoking	21 (2.62)	2,997 (5.71)		
Time of smoking	10.22 ± 14.39	7.34 ± 13.88	−5.63	<0.001
Hypertension	530 (66.08)	31,571 (60.24)	11.29	0.001
Diabetes	88 (10.97)	11,910 (22.72)	62.47	<0.001
Time of diabetes	0.85 ± 2.87	1.82 ± 3.83	9.40	<0.001
Heart rate	81.74 ± 13.87	78.73 ± 14.20	−6.10	<0.001
Systolic pressure	142.41 ± 26.71	136.86 ± 21.90	−5.85	<0.001
Diastolic pressure	83.20 ± 16.59	80.46 ± 13.01	−4.66	<0.001
Neutrophil granulocyte count	7.16 ± 4.08	4.79 ± 3.47	−16.35	<0.001
Neutrophil percentage	72.83 ± 10.79	65.30 ± 12.09	−19.59	<0.001
Lymphocyte percentage	16.94 ± 9.10	24.22 ± 10.44	22.43	<0.001
Lymphocyte count	1.36 ± 0.60	1.57 ± 2.03	9.07	<0.001
Mean platelet volume	8.93 ± 1.39	9.36 ± 1.58	8.60	<0.001
Total protein	64.58 ± 7.06	65.43 ± 8.04	3.41	0.001
Albumin	37.08 ± 5.67	38.61 ± 6.26	7.60	<0.001
Globulin	27.57 ± 5.19	26.94 ± 5.32	−3.39	0.001
A/G	1.40 ± 0.36	1.49 ± 0.37	6.77	<0.001
Total bilirubin	16.19 ± 21.62	13.20 ± 26.81	−3.86	<0.001
Glutamic-pyruvic transaminase	66.50 ± 296.27	32.47 ± 108.73	−3.25	0.001
Glycated serum protein	2.25 ± 0.62	2.03 ± 0.73	−9.79	<0.001
Lactic dehydrogenase	322.03 ± 684.10	236.51 ± 283.48	−3.54	<0.001
Myohemoglobin	72.69 ± 84.95	57.60 ± 59.02	−5.01	<0.001
Potassium	3.83 ± 0.56	3.97 ± 0.52	7.52	<0.001
Sodium	139.37 ± 4.28	140.71 ± 3.79	8.77	<0.001
Chlorine	101.08 ± 4.95	102.59 ± 4.62	8.56	<0.001
Calcium	2.16 ± 0.16	2.21 ± 0.18	8.88	<0.001
PP	99.83 ± 18.59	106.62 ± 17.36	10.28	<0.001
INR	1.06 ± 0.39	1.01 ± 0.28	−3.91	<0.001
APTT	37.66 ± 11.29	35.54 ± 9.68	−5.29	<0.001
Fibrinogen	4.44 ± 1.81	3.77 ± 1.22	−10.45	<0.001
D – dimer	1.37 ± 1.94	0.97 ± 1.27	−5.49	<0.001
Plasma plasminogen antigen	252.01 ± 24.57	255.86 ± 27.68	4.40	<0.001
PT	13.57 ± 4.39	13.02 ± 3.06	−3.58	<0.001

Classification of Model Operation Results

Since thoracalgia is the most important symptom in diagnosing AD, and because it is very difficult to distinguish AD patients with thoracalgia from other patients with ailments such as hypertension or CAD in time, collected research data are divided into three parts: (1) AD patients confirmed by coronary CTA or observed in surgical, (2) non-AD patients with thoracalgia confirmed by coronary CTA or coronary angiogram, (3) non-AD patients without thoracalgia confirmed by coronary CTA or coronary angiogram. Model are built with five methods according to the data sets, namely LDA, BP, DT, SVM and EasyEnsemble. First, all data are divided into four categories:

True Positive (TP): predicting outcome and actual outcome are both AD; True Negative (TN): predicting outcome and actual outcome are both non-AD; False Positive (FP): predicting outcome is AD but actual outcome is non-AD; False Negative (FN): predicting outcome is non-AD but actual outcome is AD. The main evaluation indexes are used to assess the model are as follows.

Accuracy

Accuracy (A) is the correct identification of all kinds of patients, and it is one of the most important indexes that assesses model prediction efficiency in this research. Specifically, the proportion of each model diagnosing correct real results of the total number of AD patients and non-AD patients are taken as the accuracy of the model. The formula is:

$$A = \frac{TP + TN}{TP + TN + FP + FN} * 100\% \quad (1)$$

Error Rate

Error rate (ER) is the index that represents how many non-AD patients are mispredicted as AD patients. Because of the importance of thoracalgia in AD diagnosis, ER of non-AD patients with thoracalgia and non-AD patients without thoracalgia are calculated separately. The non-AD patients with thoracalgia are expressed as TN_t or FP_t, the non-AD patients without thoracalgia are expressed as TN_{nt} or FP_{nt}, Similarly there are ER_t and ER_{nt}. The formulas:

$$ER_t = \frac{FP_t}{TN_t + FP_t} * 100\% \quad (2)$$

$$ER_{nt} = \frac{FP_{nt}}{TN_{nt} + FP_{nt}} * 100\% \quad (3)$$

Recall

Recall® can tell how many positive examples are predicted correctly according to the original sample. Due to the low incidence of AD, A and ER are not precise enough to assess the model prediction efficiency, so Recall are added to ensure model soundness. The proportion of AD patients that are correctly predicted by each model out of the total number of AD patients is taken as the recall. The formula is:

$$R = \frac{TP}{TP + FN} * 100\% \quad (4)$$

Comparison of Prediction Results

The final results of the five models have obvious differences (**Table 8**). Based on the results, EasyEnsemble is chosen as the main modeling method for the AD auxiliary diagnosis model. It is not the model with the highest accuracy or lowest ER, but its highest recall enables it to discover the most AD patients. After some adjustments and verified model stability through multiple tests, the official algorithm code are finalized. Under the premise of maintaining the EasyEnsemble basic algorithm, number M EasyEnsemble model is constructed for Hi ($1 <= I <= M$) and took half training characteristics, which were randomly selected from the whole data set, as the new training characteristics of the training set. The final model was acquired when the simple average of number M/2 selected from number M EasyEnsemble complete training finished. The upgrade algorithm called RS - EasyEnsemble and pseudo code of the algorithm are shown. The final model has basically achieved expected goals, and it is ready to put into formal application in clinical work after software development work.

RS-EasyEnsemble algorithm code

1. Load in t subsets of set N, for each subset T_i, $|T_i|=|P|$, $T_i \cap T_j = \Phi(i \neq j)$, let $TS_i = T_i \bigcup P$, TS_i is the training set of the ith base classifier of ensemble model, P is the set of minority class, N is the set of majority class, where $|P|<<|N|$. Initial the number of base classifiers M.
2. i=1
3. while i<=M repeat
   3.1: Randomly sample some features to create a subspace S_i.
   3.2 Map the samples to feature subspace S_i to create a new sample set P' and N', where P' and N' are the set P and N in feature subspace S_i.
   3.3 Using each T_i to train the base classifier H_i.
   3.4 i=i+1
3 : Select a half of best model from the M models.
4 : Output an Ensemble model $H(x)$
$H(x) = Round(\frac{2}{M} \sum_{i=1}^{\frac{M}{2}} H_i)$

DISCUSSION

From the trend of medical science development, the combination of artificial intelligence technology and clinical medical analysis is increasingly tight and plays an important role in early warning and auxiliary diagnosis of many diseases (18, 19). Models built by various algorithms can replicate the process of diagnosing diseases which used to depend on the subjective judgment of a clinician with objective data and can provide a better basis for decision-making by clinical doctors by collecting and analyzing new disease information to update the diagnosis methods. As there is uncertainty in the diagnosis of AD based on medical records that are collected in a hurry, using the auxiliary diagnosis model to help in the diagnosis is a good choice. This research has searched for the appropriate algorithm to build an AD auxiliary diagnosis model with the highest accuracy by trying a variety of algorithms.

LDA is a classical method used to figure out a vector a which make the new ubspace that has both the largest and minimum class distance in same time and construct the prediction model (20). Accuracy of LDA was 78.4% and ERs of thoracalgia and non-thoracalgia patients were 4 and 5.77%. This could indicate the LDA model is overall good and rarely misdiagnoses non-AD patients as AD patients. However, the recall was only 4.35% and this did not meet the level to identify as many AD patients as possible. So LDA was not taken into the final model's building.

TABLE 8 | Prediction efficiency results of modeling five algorithms.

Model	LDA	BP	DT	SVM	RS-EasyEnsemble
Accuracy	78.40%	77.60%	71.79%	83.20%	80.09%
Recall	4.35%	34.78%	20.48%	73.91%	81.11%
Error rate (t)	4.00%	16.00%	0%	20.00%	19.20%
Error rate (nt)	5.77%	9.62%	0%	9.62%	11.80%

The BP neural network basic algorithm includes signal forward-propagating and error back-propagation in two parts (21). The direction of calculation error output is from input to output and changes to output to input when weight and threshold values are adjusted. The accuracy of the BP model was 77.6%, which is lower than the LDA model, and two ERs were higher than the LDA model, too. Though accuracy and ERs of the BP model were not as good as the LDA model, it had better recall with 34.78%. This may not be good enough to be used in practical applications, but the BP model can be consider as a more advantageous than the LDA model in identifying AD patients.

The main method of the DT model is random forests, and it is a classifier that contains multiple decision trees; the output category is decided by the mode of the individual tree output category. Samples can be trained and provide better prediction by using multiple decision trees (22). Two of DT model ERs were reduced to 0%, which means the DT model can identify all non-AD patients. However, the DT model is still not the first choice since 20.48% of recall and 71.79% of accuracy did not enable us to find enough AD patients.

SVM has the advantages of dimension reduction ability, small sample training, and quick sort. The SVM model aims to find a hyperplane as demarcation of two types of training sample segmentation so that it could ensure minimum classification ERs. Furthermore, the linear inseparable samples are raised from a low dimension feature space to higher one so it became linear separable by using kernel function RBF (23). Under the premise of maintaining accuracy at 83.2%, the recall of the SVM model rose to 73.91% from 8.7% in default parameters. Although the ERs of thoracalgia and non-thoracalgia patients were up to 20 and 9.62%, respectively, the SVM model was really close to experimental objective.

RS-EasyEnsemble is the improved method based on EasyEnsemble, and its main principle is random subspace (RS). Since the key of integrated learning is diversity of base classifiers integration, decision forests are made with RS to increase diversity. Specifically, different parts of characteristics are randomly selected when constructing each decision tree, then all of the map samples are putted into a feature subspace and built new decision trees by using samples after mapping (24). Random feature subspace enables the model to effectively avoid dimension disaster or reduce the redundancy feature space when it meet the dimension disaster (25). The random proportion of the feature space is set to 0.5 because it is close to the optimal combination of precision after experiments on several data sets. RS-EasyEnsemble had the highest recall at 81.11%, which means it is the best model to identify AD patients. Though accuracy of 80.09% is a little lower than the SVM model and two ERs of 19.2 and 11.8%, are not ideal, RS-EasyEnsemble is still the last choice of the main modeling algorithm since the goal of this research is to build an auxiliary diagnostic model that discovers the maximum number of AD patients in the early stage, and it is acceptable to have a few more false AD patients in order to reduce AD mortality caused by missing the diagnosis. From this point of view, this AD auxiliary diagnosis model based on RS-EasyEnsemble achieves experimental objective.

According to the analysis of the actual diagnosis process of AD, an auxiliary diagnosis model had been built whose core algorithm is an integrated learning algorithm and tested the prediction efficiency of the model. From the results, in which the accuracy and recall were both over 80%, this auxiliary diagnosis model is proven to do well in simulating AD diagnosis, and it can improve the diagnosis accuracy with the adaptively adjusted diagnosis model parameters with new data. Though there were some disadvantages in this research, such as positive sample sizes being too small, partial information collection not being complete, and raw data text messages being incomplete digital transformation. This AD auxiliary diagnosis model is a positive attempt in solving clinical problems by using artificial intelligence technology and opening some new research directions and ideas in AD diagnosis. After further improvement and software development work, the AD auxiliary diagnosis model may provide good help for basic level medical staff and save more lives of AD patients.

DATA AVAILABILITY STATEMENT

The raw data supporting the conclusions of this article will be made available by the authors, without undue reservation.

ETHICS STATEMENT

Written informed consent was obtained from the individual(s) for the publication of any potentially identifiable images or data included in this article.

AUTHOR CONTRIBUTIONS

JL: complete clinical data collection, data analysis, diagnosis model testing improvement, and article writing. WZ: complete

clinical data analysis and diagnosis model building. ST: complete diagnosis model building and testing. GZ: guide clinical data collection. LL: guide diagnosis model building and testing. YB: guide data analysis and article writing. All authors contributed to the article and approved the submitted version.

ACKNOWLEDGMENTS

We acknowledge the data set supported by the Xiangya Hospital of Central South University in China and the students of Central South University for their help and support — Xueting Qiu, Lingfang He, Yamei Liu, Ningbo Zhou, and Caiwang Zhang who collect the data used in this study.

SUPPLEMENTARY MATERIAL

The Supplementary Material for this article can be found online at: https://www.frontiersin.org/articles/10.3389/fcvm.2021.777757/full#supplementary-material

REFERENCES

1. Erbel R, Aboyans V, Boileau C, Bossone E, Di Bartolomeo R, Eggebrecht H, et al. Corrigendum to: 2014 ESC guidelines on the diagnosis and treatment of aortic diseases. *Eur Heart J.* (2015) 36:2779. doi: 10.1093/eurheartj/ehv178
2. Zhang L, Zhou J, Jing Z. Serum uric acid might be associated with aortic dissection in Chinesemen. *Int J Cardiol.* (2016) 203:420–1. doi: 10.1016/j.ijcard.2015.10.185
3. Li X, Zhang W, Liu J, Gonzalez L, Liu D, Zhang L, et al. Contrast-induced kidney nephropathy in thoracic endovascular aortic repair: a 2-year retrospective study in 470 patients. *Angiology.* (2020) 71:242–8. doi: 10.1177/0003319719893578
4. Huo D, Kou B, Zhou Z, Lv M. A machine learning model to classify aortic dissection patients in the early diagnosis phase. *Sci Rep.* (2019) 9:2701. doi: 10.1038/s41598-019-39066-9
5. Cheng B, Liu M, Shen D, Li Z, Zhang D. Multi-domain transfer learning for early diagnosis of Alzheimer's disease. *Neuroinformatics.* (2017) 15:115–32. doi: 10.1007/s12021-016-9318-5
6. Zhenya Q, Zhang Z. A hybrid cost-sensitive ensemble for heart disease prediction. *BMC Med Inform Decis Mak.* (2021) 21:73. doi: 10.1186/s12911-021-01436-7
7. Markus HS, Hayter E, Levi C, Feldman A, Venables G, Norris J. Antiplatelet treatment compared with anticoagulation treatment for cervical artery dissection (CADISS): a randomised trial. *Lancet Neurol.* (2015) 14:361–7. doi: 10.1016/S1474-4422(15)70018-9
8. Gottfried S, Hans D, Martin S, Marek PE, Georg E, Harald H, et al. D-dimer in ruling out acute aortic dissection: a systematic review and prospective cohort study. *Eur Heart J.* (2007) 28:3067–75. doi: 10.1093/eurheartj/ehm484
9. Ren Y, Tang Q, Liu W, Tang Y, Zhu R, Li B. Serum biomarker identification by mass spectrometry in acute aortic dissection. *Cell Physiol Biochem.* (2017) 44:2147–57. doi: 10.1159/000485954
10. Suzuki T, Katoh H, Tsuchio Y, Hasegawa A, Kurabayashi M, Ohira A, et al. Diagnostic implications of elevated levels of smooth-muscle myosin heavy-chain protein in acute aortic dissection: the smooth muscle myosin heavy chain study. *Ann Intern Med.* (2000) 133:537–41. doi: 10.7326/0003-4819-133-7-200010030-00013
11. Chen X, Tang L, Jiang J, Jiang J, Hu XY, Yu WF, et al. Increased levels of lipoprotein(a) in non-smoking aortic dissection patients. *Clin Exper Med.* (2008) 8:123–7. doi: 10.1007/s10238-008-0167-x
12. Ayrik C, Cece H, Aslan O, Karcioglu O, Yilmaz E. Seeing the invisible: painless aortic dissection in the emergency setting. *Emerg Med J.* (2006) 23:e24. doi: 10.1136/emj.2004.021790
13. Chen Z, Huang B, Lu H, Zhao Z, Hui R, Zhang S, et al. The effect of admission serum potassium levels on in-hospital and long-term mortality in type a acute aortic dissection. *Clin Biochem.* (2017) 50:843–50. doi: 10.1016/j.clinbiochem.2017.05.008
14. Yuan S, Zhou W, Chen L. Epileptic seizure prediction using diffusion distance and bayesian linear discriminate analysis on intracranial EEG. *Int J Neural Syst.* (2018) 28:0129-657. doi: 10.1142/S0129065717500435
15. Wu D, Kim K, El Fakhri G, Li Q. Iterative low-dose CT reconstruction with priors trained by artificial neural network. *IEEE Trans Med Imag.* (2017) 36:2479–86. doi: 10.1109/TMI.2017.2753138
16. Moon M, Lee SK. Applying of decision tree analysis to risk factors associated with pressure ulcers in long-term care facilities. *Healthc Inform Res.* (2017) 23:43–52. doi: 10.4258/hir.2017.23.1.43
17. Kumar R, Kumari B, Kumar M. Prediction of endoplasmic reticulum resident proteins using fragmented amino acid composition and support vector machine. *PeerJ.* (2017) 5:e3561. doi: 10.7717/peerj.3561
18. Feng F, Wu Y, Wu Y, Nie G, Ni R. The effect of artificial neural network model combined with six tumor markers in auxiliarydiagnosis of lung cancer. *J Med Syst.* (2012) 36:2973–80. doi: 10.1007/s10916-011-9775-1
19. Shi Y, Liu X, Kok SY, Rajarethinam J, Liang S, Yap G, et al. Three-month real-time dengue forecast models: an early warning system for outbreak alerts and policy decision support in Singapore. *Environ Health Perspect.* (2016) 124:1369–75. doi: 10.1289/ehp.1509981
20. Raeisi Shahraki H, Bemani P, Jalali M. Classification of bladder cancer patients via penalized linear discriminant analysis. *Asian Pac J Cancer Prev.* (2017) 18:1453–7. doi: 10.22034/APJCP.2017.18.5.1453
21. Disse E, Ledoux S, Bétry C, Caussy C, Maitrepierre C, Coupaye M, et al. An artificial neural network to predict resting energy expenditure in obesity. *Clin Nutr.* (2018) 37:1661–69. doi: 10.1016/j.clnu.2017.07.017
22. Kleinhans S, Herrmann E, Kohnen T, Bühren J. Comparison of discriminant analysis and decision trees for the detection of subclinical keratoconus. *Klin Monbl Augenheilkd.* (2019) 236:798–805. doi: 10.1055/s-0043-112859
23. He Y, Ma J, Ye X. A support vector machine classifier for the prediction of osteosarcoma metastasis with high accuracy. *Int J Mol Med.* (2017) 40:1357–64. doi: 10.3892/ijmm.2017.3126
24. Fawcett TF. *ROC graphs: Notes and practical considerations for data mining researchers.* Technical report HPL-2003-4. Palo Alto, CA: HPLaboratories (2004). Available online at: http://www.purl.org/NET/tfawcett/papers/ROC101.pdf.C
25. Xu-Ying L, Jianxin W, Zhi-Hua Z. Exploratory undersampling for class-imbalance learning. *IEEE Trans Syst Man Cybern B Cybern.* (2009) 39:539–50. doi: 10.1109/TSMCB.2008.2007853

Conflict of Interest: The authors declare that the research was conducted in the absence of any commercial or financial relationships that could be construed as a potential conflict of interest.

Publisher's Note: All claims expressed in this article are solely those of the authors and do not necessarily represent those of their affiliated organizations, or those of the publisher, the editors and the reviewers. Any product that may be evaluated in this article, or claim that may be made by its manufacturer, is not guaranteed or endorsed by the publisher.

Copyright © 2021 Luo, Zhang, Tan, Liu, Bai and Zhang. This is an open-access article distributed under the terms of the Creative Commons Attribution License (CC BY). The use, distribution or reproduction in other forums is permitted, provided the original author(s) and the copyright owner(s) are credited and that the original publication in this journal is cited, in accordance with accepted academic practice. No use, distribution or reproduction is permitted which does not comply with these terms.

frontiers in Cardiovascular Medicine

ORIGINAL RESEARCH
published: 20 January 2022
doi: 10.3389/fcvm.2021.783872

Andrographolide Promotes Interaction Between Endothelin-Dependent EDNRA/EDNRB and Myocardin-SRF to Regulate Pathological Vascular Remodeling

*Wangming Hu[1†], Xiao Wu[1†], Zhong Jin[1†], Zheng Wang[1], Qiru Guo[1], Zixian Chen[2], Song Zhu[3], Haidi Zhang[3], Jian Huo[4], Lingling Zhang[1], Xin Zhou[1], Lan Yang[1], Huan Xu[1], Liangqing Shi[1] and Yong Wang[1]**

[1] College of Basic Medicine, Chengdu University of Traditional Chinese Medicine, Chengdu, China, [2] School of Ethnic Medicine, Chengdu University of Traditional Chinese Medicine, Chengdu, China, [3] Hospital of Chengdu University of Traditional Chinese Medicine, Chengdu University of Traditional Chinese Medicine, Chengdu, China, [4] Chengdu Women's and Children's Central Hospital, School of Medicine, University of Electronic Science and Technology of China, Chengdu, China

OPEN ACCESS

Edited by:
Yuli Huang,
Southern Medical University, China

Reviewed by:
Ning Zhu,
Third Affiliated Hospital of Wenzhou Medical University, China
Xinyu Weng,
Fudan University, China

***Correspondence:**
Yong Wang
yongwang1008@hotmail.com;
wangyong@cdutcm.edu.cn

[†] These authors have contributed equally to this work and share first authorship

Specialty section:
This article was submitted to General Cardiovascular Medicine, a section of the journal Frontiers in Cardiovascular Medicine

Received: 27 September 2021
Accepted: 15 December 2021
Published: 20 January 2022

Citation:
Hu W, Wu X, Jin Z, Wang Z, Guo Q, Chen Z, Zhu S, Zhang H, Huo J, Zhang L, Zhou X, Yang L, Xu H, Shi L and Wang Y (2022) Andrographolide Promotes Interaction Between Endothelin-Dependent EDNRA/EDNRB and Myocardin-SRF to Regulate Pathological Vascular Remodeling. Front. Cardiovasc. Med. 8:783872. doi: 10.3389/fcvm.2021.783872

Introduction: Pathological vascular remodeling is a hallmark of various vascular diseases. Smooth muscle cell (SMC) phenotypic switching plays a pivotal role during pathological vascular remodeling. The mechanism of how to regulate SMC phenotypic switching still needs to be defined. This study aims to investigate the effect of Andrographolide, a key principle isolated from Andrographis paniculate, on pathological vascular remodeling and its underlying mechanism.

Methods: A C57/BL6 mouse left carotid artery complete ligation model and rat SMCs were used to determine whether Andrographolide is critical in regulating SMC phenotypic switching. Quantitative real-time PCR, a CCK8 cell proliferation assay, BRDU incorporation assay, Boyden chamber migration assay, and spheroid sprouting assay were performed to evaluate whether Andrographolide suppresses SMC proliferation and migration. Immunohistochemistry staining, immunofluorescence staining, and protein co-immunoprecipitation were used to observe the interaction between EDNRA, EDNRB, and Myocardin-SRF.

Results: Andrographolide inhibits neointimal hyperplasia in the left carotid artery complete ligation model. Andrographolide regulates SMC phenotypic switching characterized by suppressing proliferation and migration. Andrographolide activates the endothelin signaling pathway exhibited by dramatically inducing EDNRA and EDNRB expression. The interaction between EDNRA/EDNRB and Myocardin-SRF resulted in promoting SMC differentiation marker gene expression.

Conclusion: Andrographolide plays a critical role in regulating pathological vascular remodeling.

Keywords: Andrographolide, EDNRA, EDNRB, Myocardin-SRF, CArG box, pathological vascular remodeling

INTRODUCTION

Pathological vascular remodeling exhibits smooth muscle cell (SMC) phenotypic switching (1). SMCs have remarkable plasticity, and can undergo phenotypic switching in response to vascular endothelium damage (2), altered blood flow (3), inflammatory stimulation (4), or various disease conditions. Typical SMC phenotypic switching from the differentiation stage to the dedifferentiation stage is characterized by enhanced proliferation and decreased expression of SMC contractile-specific marker genes, including smooth muscle (SM) α-actin, smooth muscle myosin heavy chains (SM MHCs), smooth muscle myosin light chains, h1-calponin, and smooth muscle α-tropomyosin (1). SMC phenotypic switching is critical in initiation of vascular diseases, including atherosclerosis, post angioplasty restenosis, aneurysm, pulmonary hypertension, diabetic-related retinal vasculopathy, allograft vasculopathy, and transplantation associated vasculopathy (5, 6).

SMCs express differentiated marker genes. Tremendous progress has been made in serum response factor (SRF) homodimers with conserved CArG boxes and promoter-enhancer regions of several SMC differentiated marker genes to regulate SMC differentiated marker gene expression (1, 7, 8). The CArG box-dependent SMC differentiation marker genes include smooth muscle a-actin, Calponin, SM22a, and MHC. Whereas CArG box-independent SMC differentiation marker genes include FRNK, Smoothelin, and a1-integrin (1). Myocardin dramatically promotes the interaction between SRF and CArG boxes (9). Additional coactivators have been reported to enhance Myocardin and SRF-CArG boxes interaction, such as Prx1, stat3, Klf4, GATA4, Nkx3.2, and MRTFA/B (10–13).

The endothelin/sarafotoxin family comprises three isoforms, including ET-1, ET-2, and ET-3, which comprise similar structures with 21 amino acids (14, 15). Endothelins are produced primarily in the vascular endothelium, and the most potent vasoconstrictors through activation of two G protein-coupled receptors are endothelinA (EDNRA) and endothelinB (EDNRB) (16). Endothelins play critical roles in regulating vascular homeostasis, such as atherosclerosis and pulmonary hypertension (17). Endothelins are also implicated vascular diseases of several organ systems, including the heart, lungs, kidneys, and brain (18). Endothelin 1 has been reported to promote SMC migration and is critical for neointima hyperplasia in giant-cell arteritis (19). Endothelin 1 also contributes to regulate vascular remodeling (20). However, the underlying mechanism of endothelin 1 in regulating pathological vascular remodeling is not well defined.

Traditional Chinese Medicine is used in the treatment of cardiovascular diseases. Numerous studies indicated that Andrographolide (21) suppresses vascular angiogenesis through p300, VEGF, and Mir-21-5p/TIMP3 signaling pathways (22–25). Andrographolide inhibits neointimal hyperplasia in arterial restenosis (26). Our previous studies demonstrated that Andrographolide is critical in gastric vascular homeostasis regulation (27). However, the role of Andrographolide in regulating pathological vascular remodeling through SMC phenotypic switching has not been reported. We found that Andrographolide promoted SMC contractile-specific marker gene expression in different culture conditions, as well as *in vivo* vascular injury studies. We observed that Andrographolide significantly promotes the expression of EDNRA, EDNRB, SRF, and Myocardin *in vivo* and *in vitro*. However, whether and how Andrographolide can regulate pathological vascular remodeling still need to be illustrated. In this study, we tried to determine whether Andrographolide suppresses pathological vascular remodeling by enhancing the interaction between EDNRA, EDNRB, and Myocardin-SRF to regulate smooth muscle cell differentiated marker gene expression.

MATERIALS AND METHODS

Animal Ethical Approval

The use of mice in this study was approved by the Experimental Animal Ethics Committee of Chengdu University of Traditional Chinese Medicine. Ethical approval number: 2019-04.

Mouse Common Carotid Artery Complete Ligation Model

The mouse left common carotid artery complete ligation model that induces vascular remodeling is based on the previously described method (28). Briefly, mice were pretreated with Andrographolide (10 mg/kg) for 5 consecutive days, and anesthetized with ketamine (80 mg/kg) and xylazine (5 mg/kg) by intraperitoneal injection. We exposed the left common carotid arteries and completely ligated them at the bifurcation site with 6-0 silk. The right carotid artery was exposed, but not ligated. After continuous consecutive treatment with Andrographolide for 14 or 21 days, sections (5 μm) were collected between 100 and 1,000 μM away from the ligation site. Morphological analysis based on H&E staining was conducted. The quantification of neointima areas and media layer area was completed using Image J software (29).

Rat Aortic SMC Culture

SMC culture from the thoracic artery of Sprague-Dawley rats was separated as previously reported (30, 31). Briefly, we harvested thoracic aorta after the rats were anesthetized, removed periadventitial tissues, and denuded the endothelium under a microscope. We digested the aorta with a Blend enzyme III solution (Roche, 0.5 U/ml) for 10 min at 37°C, and removed the adventitial layer. Then, we minced the medial layer into small pieces, and following a second digestion with Blend enzyme III for 2 h at 37°C, we suspended cells in 10% FBS DMEM medium.

CCK8 Cell Proliferation Assay

A total of 3×10^3 rat SMCs (each well) were seeded in a 96-well culture plate, and treated with Andrographolide (5 μM) for 24 h. Absorbance at 450 nm was evaluated using a CCK8 kit.

BRDU Incorporation Assay

Rat SMCs were suspended in culture media contained Andrographolide (5 μM), followed by BRDU reagent labeling for 24 h. Immunofluorescence staining was performed to determine BRDU-incorporated SMCs.

Scratch Wound Healing Assay

The rat SMCs were seeded into a 6-well culture dish. Scratch wounds were made with a 10 μl pipette tip, and scratch gaps were monitored at different time points based on crystal violet staining.

Boyden Chamber Migration Assay

A total of 1×10^6 rat SMCs were suspended in 100 ul of FBS free culture media and seeded in a Boyden chamber (353097, FALCON). We set up the Boyden chamber with a 24-well culture plate which contained 500 μl of complete culture medium (10% FBS) and 5 μM Andrographolide. We fixed the cells after incubation for 12–24 h, and manually counted cells numbers in five random microscopic fields after crystal violet staining (32).

Spheroid Sprouting Assay

The spheroid sprouting assay was performed as described previously (33). The methylcellulose solution was prepared by dissolving 6 g of methylcellulose (sigma) into 250 ml of prewarmed serum free medium, and 250 ml of DMEM containing 10% serum was added. Suspended cells were added to the dissolved methylcellulose solution which was prepared by 10 ml of methylcellulose solution and 40 ml of culture medium to form the spheres. We added the neutralized collagen solution to a 24-well culture plate and incubated it at 37°C until the collagen solidified. We mixed the spheres with dissolved collagen solution and transferred it to a collagen-solidified culture plate. We solidified the culture plate for 30 min at 37°C, added 200 ul of complete medium containing Andrographolide, and cultured overnight. Spheroid sprouting was visualized after calcein AM staining. Images were captured using a confocal microscope (Leica Microsystem CMS GmbH). The number of sprouts and the sprout length of each sphere were analyzed by Image J software.

Co-immunoprecipitation Assay

Total protein from rat SMCs was extracted using RIPA buffer. We precleared the cell lysate using anti-species-specific IgG beads. We incubated the precleared cell lysate with EDNRB (abcam), EDNRA (abcam), Myocardin (Santa Cruz), and SRF (abcam) for 1 h at 4°C. Next, we incubated the lysate with pre-equilibrated protein A/G agarose beads on a rocking platform overnight at 4°C. The co-immunoprecipitated targets were evaluated by western blotting.

SiRNA Transfection

Scrambled siRNA and siRNA targeting rat SRF and EDNRA were synthesized from GenePharma. The siRNAs were transfected into rat SMCs by using Lipofectamin 2000 reagent following the manufacturer's protocol.

Quantitative Real Time PCR Analysis

Total RNA from rat SMCs was extracted using Trizol reagent. Quantification of RNA was monitored by a spectrophotometer (Denovix, USA). A total of 600 ng of RNA was used as the template, random hexamer primers were used for the reverse transcription reaction to obtain cDNA using an iScript cDNA synthesis kit. Real-time PCR was performed twice for each

TABLE 1 | List of primer sequences used for real time PCR in the study.

Gene name	Species	Sequence
RPLPO	Rat	F: 5′-GGACCCGAGAAGACCTCCTT-3 ′
	Rat	R: 5′-TGCTGCCGTTGTCAAACACC-3′
SRF	Rat	F: 5′-GATGGAGTTCATCGACAACAAGCTG-3′
	Rat	R: 5′-CCCTGTCAGCGTGGACAGCTCATA-3′
SM α-actin	Rat	F: 5′-ATGCTCCCAGGGCTGTTTTCCCAT-3′
	Rat	R: 5′-GTGGTGCCAGATCTTTTCCATGTCG-3′
Calponin	Rat	F: 5′-AACTGGCACCAGCTGGAGAACATAG-3′
	Rat	R: 5′-GAGTAGACTGAACTTGTGTATGATTGG-3′
SM MHC	Rat	F: 5′-CAGTTGGACACTATGTCAGGGAAA-3′
	Rat	R: 5′-ATGGAGACAAATGCTAATCAGCC-3′
Myocardin	Rat	F: 5′-GTTCAGCTACCCTGGGATGCACCAA-3′
	Rat	R: 5′-GGCCTGGTTTGAGAGAAGAAACACC-3′
KLF4	Rat	F: 5′-CGGGAAGGGAGAAGACACTGC-3′
	Rat	R: 5′-GCTAGCTGGGGAAGACGAGGA-3′
SM22α	Rat	F: 5′-TGACATGTTCCAGACTGTTGACCTCT-3′
	Rat	R: 5′-CTTCATAAACCAGTTGGGATCTCCAC-3′
MRTFA	Rat	F: 5′-CAGAGAGATCAGAGCTGGTCAG−3′
	Rat	R: 5′-CATCGCTGCTGTCCTCGTCAAA-3′
FGF9	Rat	F: 5′-GACTTGCCGATTTGCTCTGCACTT-3′
	Rat	R: 5′-AGCCTCTCTCCCTGCTTTCACAAT-3′
SIRT1	Rat	F: 5′-TAGCCTTGTCAGATAAGGAAGGA-3′
	Rat	R: 5′-ACAGCTTCACAGTCAACTTTGT-3′
Gata6	Rat	F: 5′-GCCCCTCATCAAGCCACA−3′
	Rat	R: 5′-CATAGCAAGTGGTCGAGGCA−3′
TBX2	Rat	F: 5′-CATCCTGAACTCCATGCACAAG−3′
	Rat	R: 5′-ACAGTGCTCCTCATACAAACGG−3′
TBX3	Rat	F: 5′-TTATAGCTGCTGATGACTGTCG−3′
	Rat	R: 5′-GCTGGTACTTGTGCATGGAGTT−3′
TBX18	Rat	F: 5′-CGAGTGCACATCATCCGTAAAG−3′
	Rat	R: 5′-GCATATGACTCCACCAGAGCTT−3′
EDN1	Rat	F: 5′-GACCAGCGTCCTTGTTCCAA-3′
	Rat	R: 5′-TTGCTACCAGCGGATGCAA-3′
EDN2	Rat	F: 5′-GGCTTGACAAGGAATGTGTGTACT-3′
	Rat	R: 5′-CACGTCTTGCTAGTCTCTAACACA-3′
EDN3	Rat	F: 5′-CGTGCTTCACTTATAAGGACAAGG-3′
	Rat	R: 5′-CAACGTAAGCGTGTCTGTGGAGAA-3′
EDNRA	Rat	F: 5′-CTCAACGCCACGACCAAGTT-3′
	Rat	R: 5′-GCAAGCTCCCATTCCTTCTG-3′
EDNRB	Rat	F: 5′-TGGCCATTTGGAGCTGAGAT-3′
	Rat	R: 5′-TCCAAGAAGCAACAGCTCGAT-3′
CCND1	Rat	F: 5′-AATGGAACTGCTTCTGGTGAACA-3′
	Rat	R: 5′-CGGATGATCTGCTTGTTCTCATC-3′
c-Myc	Rat	F: 5′-CCCCTCAGTGGTCTTCCCCTAC-3′
	Rat	R: 5′-TGTTCTCGCCGTTTCCTCAGTA-3′
ADK	Rat	F: 5′-TGGCTTCTTTCTCAGCGTCT-3′
	Rat	R: 5′-ACTCCACAGCCTGAGTTGCT-3′
CDKN1A	Rat	F: 5′-ATGACTGAGTATAAACTTGTGG-3′
	Rat	R: 5′-TCAVATGACTATACACCTTGTC-3′
CDKN1B	Rat	F: 5′-GTCTCAGGCAAACTCTGAG-3′
	Rat	R: 5′-GTTTACGTCTGGCGTCGAAG-3′
p53	Rat	F: 5′-GACTTCTTGTAGATGGCCATGG-3′

(Continued)

TABLE 1 | Continued

Gene name	Species	Sequence
	Rat	R: 5′-ATGGAGGATTCACAGTCGGATA-3′
GADD45	Rat	F: 5′-ATGACTTTGGAGGAATTCTCGG-3′
	Rat	R: 5′-TCACCGTTCGGGGAGATTAATC-3′
PTEN	Rat	F: 5′-GCACAAGAGGCCCTGGATT-3′
	Rat	R: 5′-TGAAACAACAGTGCCACTGG-3′
c-Fos	Rat	F: 5′-GGGACAGCCTTTCCTACTACC-3′
	Rat	R: 5′-AGATCTGCGCAAAAGTCCTG-3′
IL-15	Rat	F: 5′-ACTACCTGTGTTTCCTTCTCAAC-3′
	Rat	R: 5′-TTGGCCTCTGTTTTAGGG-3′
IL-18	Rat	F: 5′-TCCTTTGAGGAAATGAATCC-3′
	Rat	R: 5′-GCTAGAAAGTGTCCTTCATAC-3′
PDCD4	Rat	F: 5′-AACTATGATGATGACCAGGAGAAC-3′
	Rat	R: 5′-GCTAAGGACACTGCCAACAC-3′
CCN3	Rat	F: 5′-GGAAGTGCATTCGTTGAGGC-3′
	Rat	R: 5′-AAGCAAGTCACCCCTAAGCC-3′
MyD88	Rat	F: 5′-GATCCCACTCGCAGTTTGTT-3′
	Rat	R: 5′-GATGCGGTCCTTCAGTTCAT-3′
Thbs-1	Rat	F: 5′-CGGTTTGATCAGAGTGGTGA-3′
	Rat	R: 5′-CGGCACTCGTATTTCATGTC-3′
Cdh13	Rat	F: 5′-AACCCACAGACCAACGAG-3′
	Rat	R: 5′-TGATCAGCAGGGTGTGAA-3′
Hif1α	Rat	F: 5′-ACAGGATTCCAGCAGACCC-3′
	Rat	R: 5′-GCTGATGCCTTAGCAGTGGTC−3′
IGFBP5	Rat	F: 5′-ATGAAGCTGCCGGGC-3′
	Rat	R: 5′-TCAACGTTACTGCTGTCGAAG-3′
IGF1	Rat	F: 5′-GGCACTCTGCTTGCTCACCTTT-3′
	Rat	R: 5′-CACGAATTGAAGAGCGTCCACC-3′
GSK3β	Rat	F: 5′-GGGCACCAGAGCTGATCTTT-3′
	Rat	R: 5′-GCCGAAAGACCTTCGTCCA-3′
Cav1	Rat	F: 5′-GACGAGGTGAATGAGAAGCAAG-3′
	Rat	R: 5′-GAGAGGATGGCAAAGTAGATGC-3′
Ddx39b	Rat	F: 5′-CAACTATGACATGCCAGAGGAC-3′
	Rat	R: 5′-GATTCCTCTACCGTGTCTGTTC-3′

sample on the Bio-Rad real-time PCR system. The primer sequences used in this study are exhibited in **Table 1**. The relative gene expression level was analyzed using the $2^{-\Delta\Delta ct}$ method against RPLP0.

Protein Extraction and Western Blotting

Protein from rat SMCs was extracted using RIPA lysis buffer. Protein concentration was determined by a BCA kit (Biosharp). The protein was denatured at 98°C, separated by sodium dodecyl sulfate-polyacrylamide gel electrophoresis (SDS-PAGE), and transferred onto polyvinylidene fluoride (PVDF) membranes. Next, we blocked the protein with 5% fat free milk, and incubated it with specific antibodies at 4°C overnight. Images were captured using an ImageQuant LAS 4000 Imager Station and we quantified densities of protein bands using ImageQuant TL software.

Hematoxylin and Eosin Staining, Immunohistochemistry, and Immunofluorescence Staining (IF)

We harvested carotid arteries and fixed them with 4% paraformaldehyde overnight at 4°C. Slides of 5 μm thickness were collected after being paraffin-embedded. H&E staining was performed as per our previous study (34). For IHC staining, the slides were deparaffinized, antigen retrieval was performed by citric acid treatment at 98°C for 5 to 10 min. After antigenic unmasking, the slides were incubated with EDNRB (abcam), EDNRA (abcam), Myocardin (Santa Cruz), and SRF (abcam) overnight at 4°C, followed by incubation with biotinylated secondary antibody at room temperature for 1 h (Vector Laboratories), and then incubated with ABC solution (Vector Laboratories) for 30 min at room temperature. The targets were visualized after the DAB solution was added. For IF staining, the deparaffinized slides were permeabilized with PBS contained 0.25% Triton-X-100, blocked with 10 % goat serum, incubated with primary antibodies overnight at 4°C, washed with PBST, and incubated with Alexa 594-conjugated or Alexa 488-conjugated secondary antibody at room temperature for 1 h. Nuclei were visualized with 4′, 6′-diamidino-2-phenylindole (DAPI) staining. For BRDU staining, DNA was denaturized using 2N HCl, followed by antibodies incubation. Images were captured using confocal microscopy (LS510, Zeiss).

Statistics

Quantitative data are presented as mean±SEM. The statistical analysis was performed by GraphPad prism software. Normal distribution was determined by the Kolmogorov-Smirnov test. Statistical comparisons between two groups were analyzed using two-tailed unpaired Student's *t* test or one- or two-way analysis of variance (ANOVA) followed by Bonferroni's *post hoc* tests when appropriate. Two-sided *P* values were quantified. * $P < 0.05$ was considered statistically significant.

RESULTS

Andrographolide Attenuates Neointima Hyperplasia Induced by Vascular Ligation Injury

To evaluate whether Andrographolide had an inhibitory effect on neointimal hyperplasia, we created a vascular injury model using C57BL/6 mice and complete ligation of the left common carotid artery, followed by consecutive Andrographolide treatment (10 mg/kg) (21, 27). The arteries were harvested and paraffin-embedded. Slides of 5 μm thickness at different locations from the ligation site were collected. We performed H&E staining to visualize vascular morphological changes. After 14 consecutive days of treatment, Andrographolide significantly attenuated neointimal hyperplasia (**Figure 1A**). We analyzed the neointima areas at different locations from the ligation site using Image J software. Our data showed that the neointimal areas from 100 to 700 μm distance significantly decreased after Andrographolide treatment (**Figure 1B**). We compared the ratio

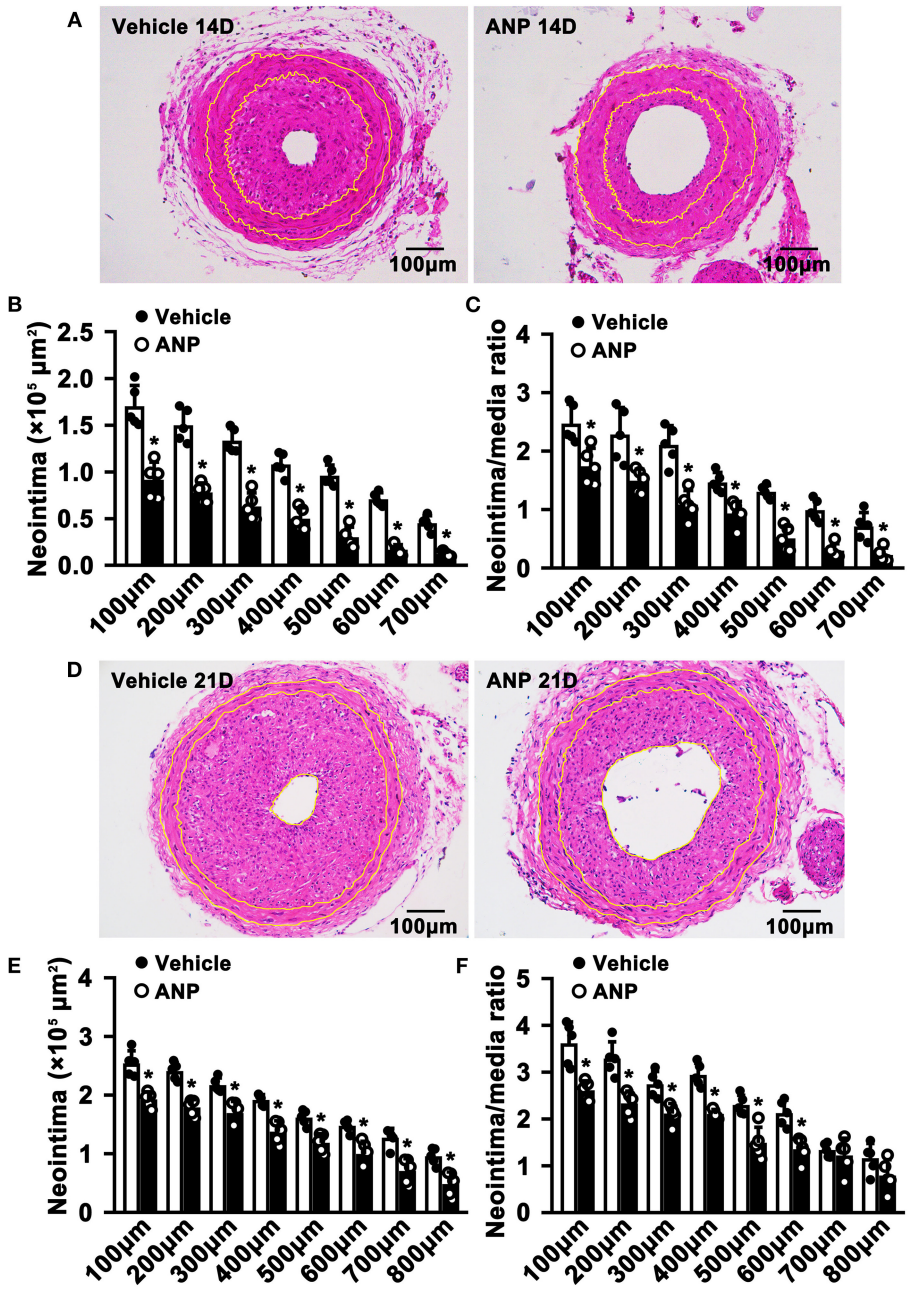

FIGURE 1 | Andrographolide attenuates neointima hyperplasia induced by vascular ligation injury. **(A)** Complete ligation of the left common carotid artery in C57BL/6 mice, and following Andrographolide treatment (10 mg/kg) by intraperitoneal injection for 14 consecutive days. The arteries were harvested and paraffin-embedded. Slides of 5 μm thickness at different locations from the ligation site were collected. H&E staining was performed to visualize vascular morphological changes. **(B,C)** Analysis areas of the neointimal hyperplasia and ratio of the neointimal areas to the medium layer area ($n = 5$). **(D)** Andrographolide (10 mg/kg) was administered by intraperitoneal injection for 21 consecutive days, the representative image of H&E staining. **(E,F)** Analysis areas of the neointimal hyperplasia and ratio of the neointimal areas to the medium layer area ($n = 5$). Data are expressed as mean ± SEM. $^*P < 0.05$.

of neointima area to media smooth muscle layer area, and found the ratio significantly deceased after Andrographolide treatment (**Figure 1C**). The areas of the media smooth muscle cells layer were determined, however, no significance was found (**Supplementary Figure 1A**). We also observed the vascular morphological changes after 21 consecutive days of treatment with Andrographolide, our data demonstrated that Andrographolide treatment significantly inhibited neointimal hyperplasia (**Figure 1D**), decreased both neointima areas and the ratio of neointima area to media smooth muscle layer area

(**Figures 1E,F**), whereas no statistical changes were observed on the media smooth muscle cell layer (**Supplementary Figure 1B**). The data indicated that Andrographolide significantly attenuated the formation of vascular neointimal hyperplasia.

Andrographolide Is Critical in Regulating Smooth Muscle Cell Phenotypic Switching

The phenotypic switching of SMCs plays a critical role during the process of pathological vascular remodeling. However, whether Andrographolide is critical in regulating SMC phenotypic switching is not well defined. We cultured primary rat aortic SMCs and treated them with Andrographolide (5 μM). After treatment for 30 h, quantitative real-time PCR was performed to determine the transcription level of SMC differentiated genes and cell growth positive regulated genes. The data indicated that SMC differentiated genes, including Myocardin, SRF, MRTFA, klf4, and smooth muscle α-actin were dramatically increased, and genes inhibiting cell proliferation, such as CDKN1A and CDKN1B, were upregulated (**Figure 2A**). Some other signaling pathways involved in SMC differentiation regulation were also enhanced (**Supplementary Figure 2A**). The characteristics of phenotypic switching for matured SMCs exhibited enhanced proliferation, whereas differentiation was decreased. We sought to determine whether Andrographolide is critical in regulating SMC phenotypic switching. First, we mimicked a condition that promotes cell growth by PDGF-BB treatment (**Supplementary Figure 2B**). With presence of PDGF-BB, Andrographolide treatment could inhibit the expression of PCNA, c-Myc, and ADK, whereas it enhanced CDKN1A, CDKN1B, and PTEN expression (**Figure 2B**). We next induced SMC differentiation by Rapamycin treatment (**Supplementary Figure 2C**). After Rapamycin incubation, following Andrographolide treatment, SMC differentiated specific marker genes, including Myocardin, SRF, KLF4, Calponin, SM22a, and MHC markedly induced differentiation (**Figure 2C**). We further induced SMC differentiation by starvation treatment (**Supplementary Figure 2D**). Andrographolide treatment also promoted the expression of Myocardin, SRF, KLF4, Calponin, and smooth muscle a-actin (**Figure 2D**). Our data demonstrated that Andrographolide is critical in regulating SMC phenotypic switching.

Andrographolide Inhibits Proliferation of Vascular Smooth Muscle Cells

The hallmark of SMC phenotypic switching is characterized by enhanced proliferation. We sought to determine whether Andrographolide can inhibit SMC proliferation. We treated rat aortic SMCs with Andrographolide (5 μM) and the cell

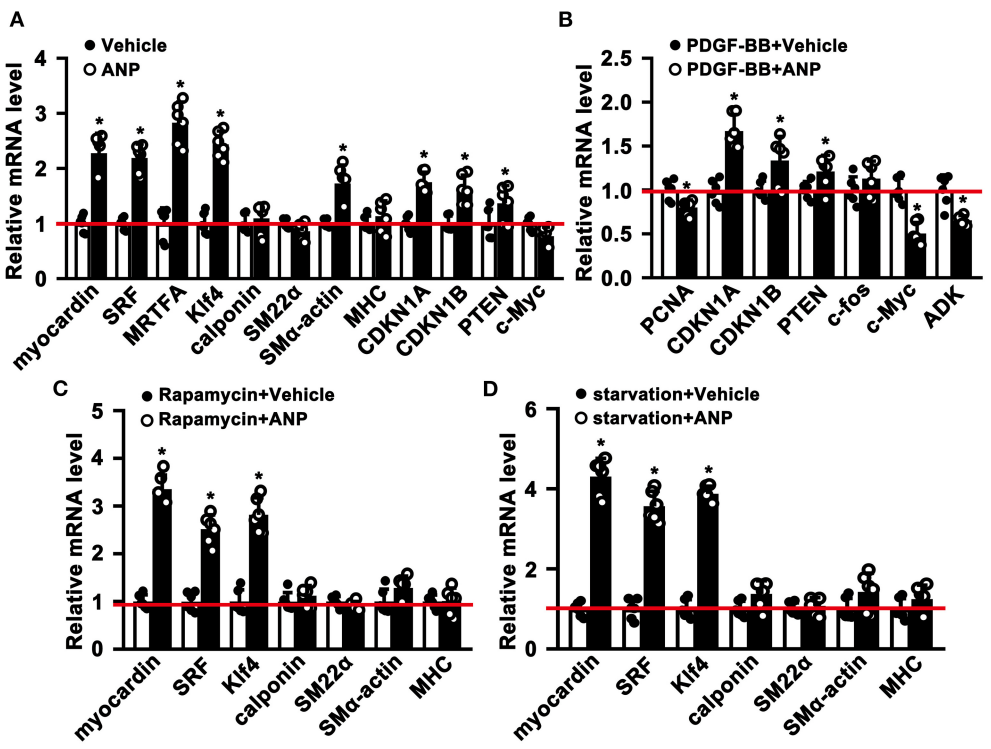

FIGURE 2 | Andrographolide is critical in regulating smooth muscle cells phenotypic switching. **(A)** Rat SMCs were treated with Andrographolide (5 μM) for 30 h, the mRNA levels of SMC-specific marker genes, including myocardin, SRF, klf4, calponin, SM22α, SM α-actin, MHC, MRTFA, and proliferation-related genes including CDKN1A, CDKN1B, PTEN, and c-Myc were detected by real-time PCR (n = 6). **(B)** Proliferation of rat SMCs induced by PDGF-BB (25 ng/ml) incubation, following Andrographolide (5 μM) treatment. Proliferation-related genes were evaluated by real-time PCR ($n = 6$). **(C)** Differentiation of rat SMCs was induced by rapamycin (100 nM/L), following Andrographolide (5 μM) treatment. Real-time PCR was performed to determine SMC-specific marker gene expression ($n = 6$). **(D)** Differentiation of rat SMCs was mimicked by starvation (0.2% FBS), following Andrographolide (5 μM) treatment. Real-time PCR was performed to determine SMC-specific marker gene expression ($n = 6$). Data are expressed as mean ± SEM. $^*P < 0.05$.

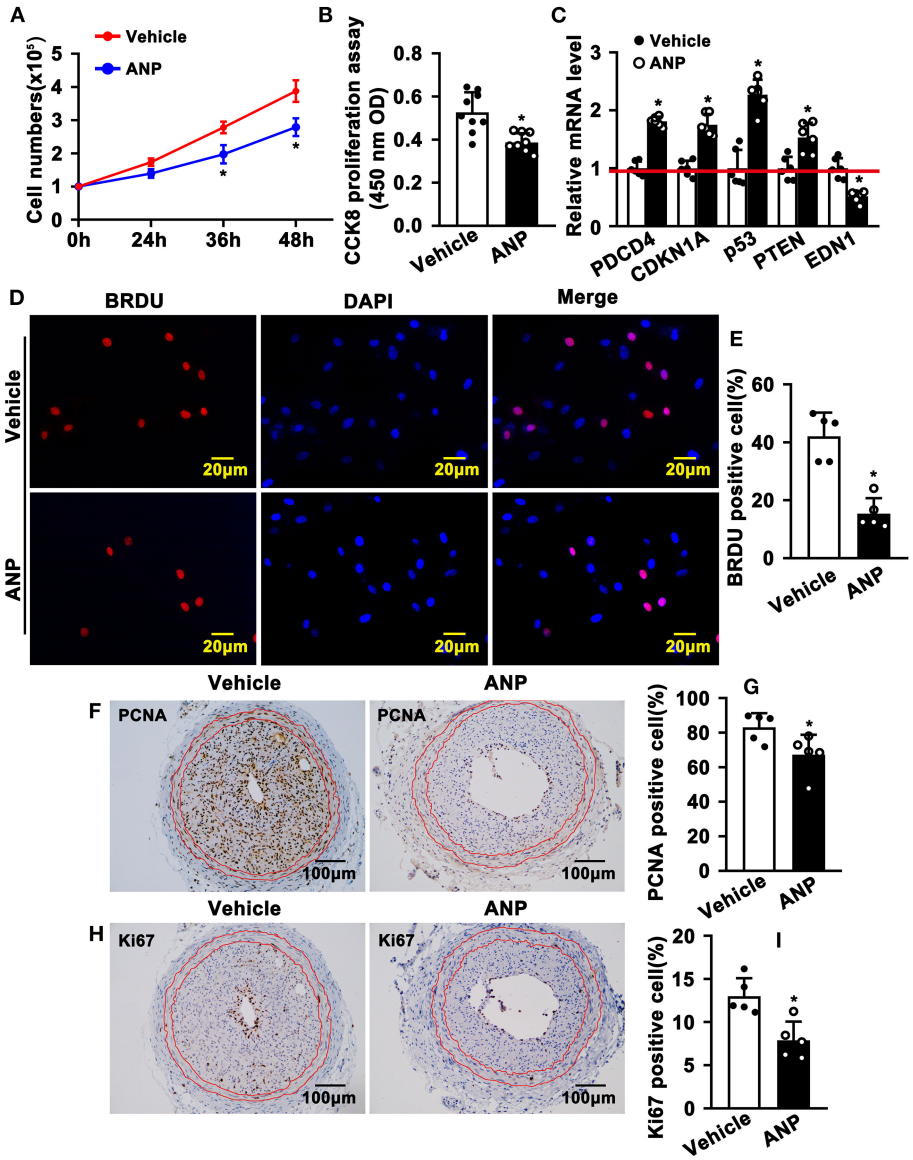

FIGURE 3 | Andrographolide inhibits proliferation of vascular smooth muscle cells. **(A)** Rat SMCs were treated with Andrographolide (5 μM), and the cell numbers were counted at different time points ($n = 6$). **(B)** Cell viability was detected by a CCK8 cell proliferation assay ($n = 8$). **(C)** The mRNA levels of proliferation-related genes were detected by real-time PCR ($n = 6$). **(D)** Rat SMCs were incubated with BRDU labeling buffer for 20 h, following Andrographolide treatment overnight. Immunofluorescence staining was performed to evaluate BRDU incorporation and BRDU-positive cells shown in **(E)**. **(F,H)** Immunohistochemical staining was performed against proliferation marker genes PCNA and Ki67 on the left common carotid artery complete ligation model. PCNA and Ki67-positive SMCs in neointimal areas are shown in **(G,I)** ($n = 5$). The analysis data are expressed as means ± SEM. *$P < 0.05$.

numbers were counted. Andrographolide treatment significantly decreased cell numbers at 36 h and 48 h following treatment (**Figure 3A**). Andrographolide treatment decreased SMCs viability which was measured by CCK8 (**Figure 3B**). Cell growth-related genes were determined by real-time PCR. Andrographolide treatment promoted expression of cell cycle negative-related genes, including PDCD4, CDKN1A, P53, and PTEN (**Figure 3C**). The BRDU incorporation assay was also performed to evaluate whether Andrographolide could suppress SMC proliferation. With the addition of Andrographolide, the BRDU-positive cells—which were detected by immunofluorescence staining—were dramatically decreased (**Figures 3D,E**). That Andrographolide suppressed SMC proliferation was validated *in vivo*. We performed immunohistochemistry staining on slides from injured animals. Andrographolide treatment dramatically decreased the number of both PCNA and Ki67 positive numbers within the neointimal area (**Figures 3F–I**). However, no statistical difference of PCNA or Ki67 positive numbers within the media smooth muscle layer between the

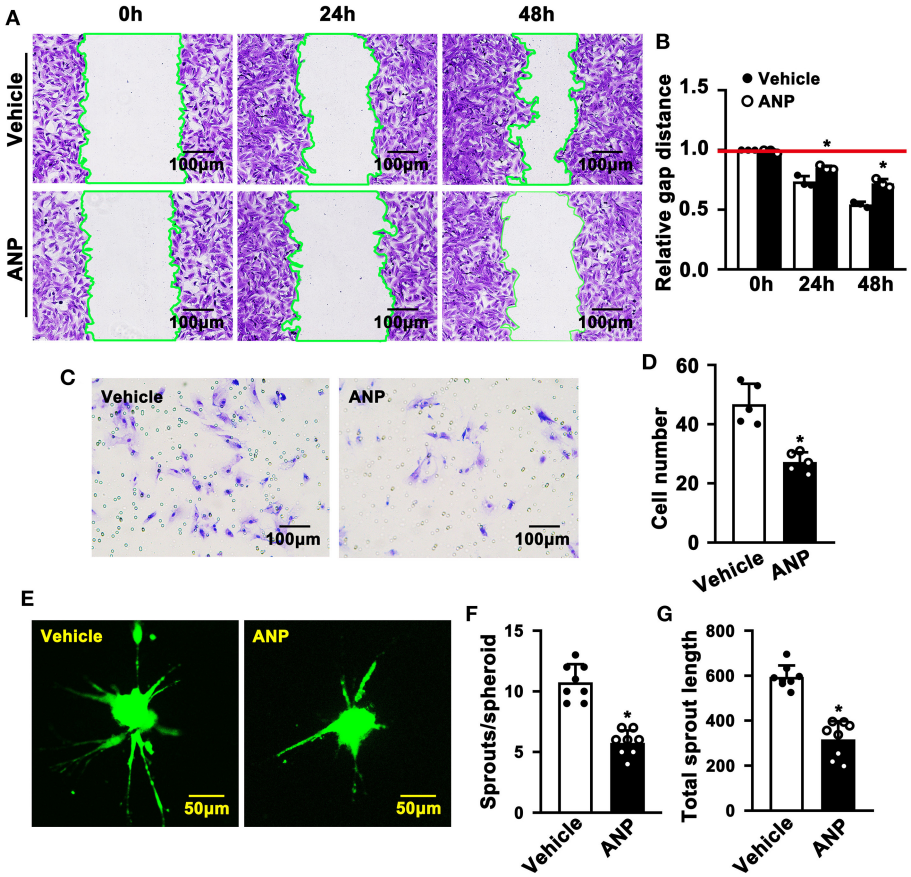

FIGURE 4 | Andrographolide inhibits migration of rat smooth muscle cells. **(A)** A wound scratching assay was performed to determine whether Andrographolide treatment (5 μM) suppressed SMC migration. The number of scratch gaps at 24 h and 48 h is exhibited in **(B)** ($n = 5$). **(C)** A Boyden chamber cell migration assay was performed in the presence of Andrographolide (5 μM), the migrated cells were visualized by crystal violet staining, and cell numbers are exhibited in **(D)** ($n = 5$). **(E)** A spheroid sprouting assay was performed in the presence of Andrographolide (5 μM), the sprouting of SMCs was visualized by calcein AM staining. Quantification of sprouts and sprout length is exhibited in **(F,G)** ($n = 8$). The analysis data are expressed as means ± SEM. $^*P < 0.05$.

Andrographolide treatment group and vehicle treatment group was exhibited (**Supplementary Figures 3A,B**). The data demonstrated that Andrographolide suppressed SMC proliferation.

Andrographolide Inhibits Migration of Rat Smooth Muscle Cells

Enhanced migration of smooth muscle cells is evident during SMC phenotypic switching. To explore whether Andrographolide plays a critical role in regulating the migration of SMC, we performed a scratch wound healing assay following crystal violet staining to visualize the scratch gap at different time points. Much bigger scratch gaps were seen after Andrographolide treatment (**Figures 4A,B**). We next performed a Boyden chamber migration assay to evaluate the effect of Andrographolide on regulating the migration of SMCs. The data indicated that Andrographolide treatment observably reduced rat SMCs passing through the Boyden chamber (**Figures 4C,D**). Furthermore, we performed a spheroid sprouting assay, and found that Andrographolide remarkably suppressed both sprouts and sprout length (**Figures 4E–G**). The data indicated that Andrographolide could significantly inhibit the migration of rat SMCs.

Andrographolide Activates Endothelin Family Response to Vascular Injury Stress

Andrographolide plays a critical role in maintaining the differentiated stage of SMCs which is characterized by inhibiting proliferation and migration of vascular SMCs. However, the underlying mechanism is not well defined. We performed real-time PCR to evaluate different signaling pathways that are associated with SMC phenotypic switching regulation. The data indicated that expression of Myd88, P53, IGFBP5, GS3Kβ, EDNRA, and EDNRB was dramatically enhanced after Andrographolide treatment. The most obvious change in expression level occurred in EDNRA and EDNRB (**Supplementary Figure 4**). Both EDNRA and EDNRB are receptors for the endothelin/sarafotoxin family which is critical in regulating vasoconstriction. We first

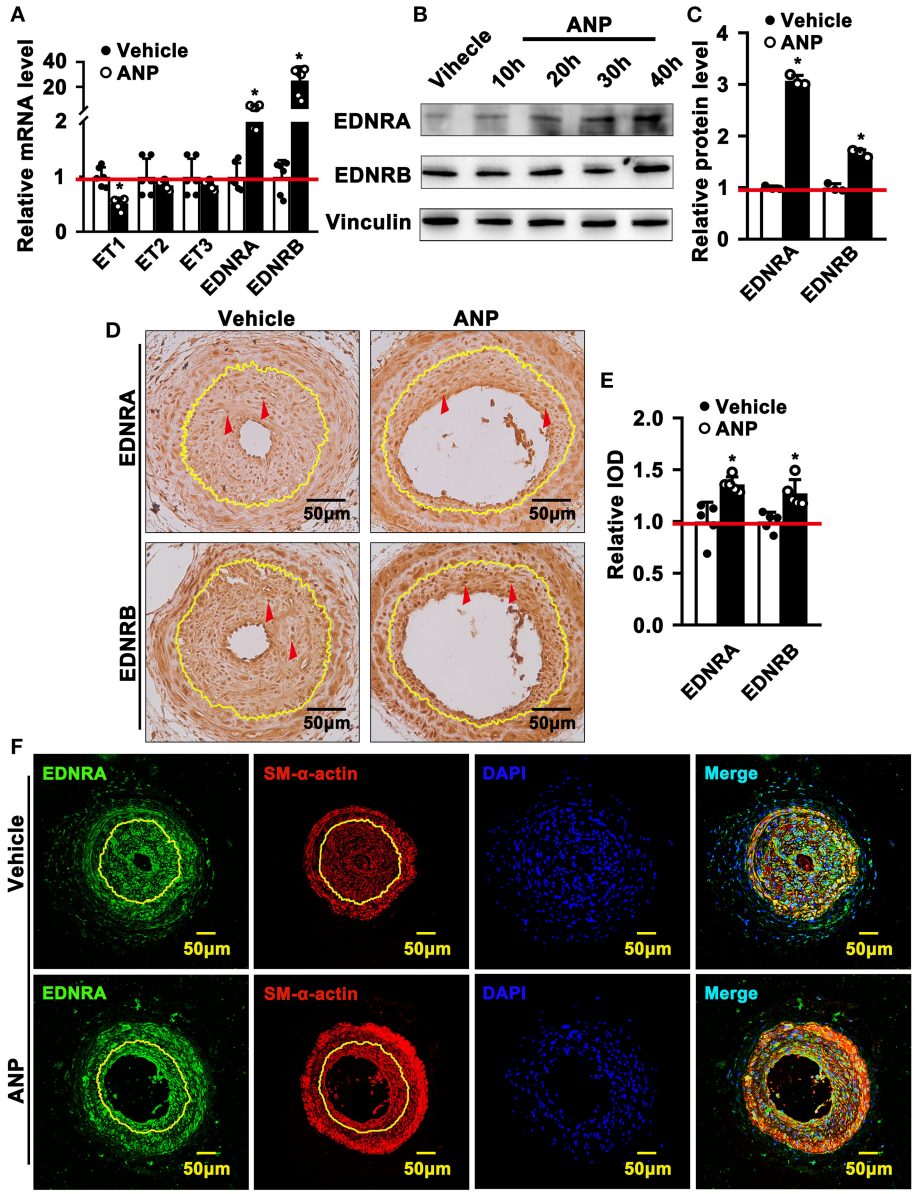

FIGURE 5 | Andrographolide activates endothelin family response to vascular injury stress. **(A)** Rat SMCs were treated with Andrographolide (5 μM) for 30 h. Real-time PCR was performed to detect the mRNA level of the endothelin family ($n = 6$). **(B)** Western blot was performed to determine the expression of EDNRA and EDNRB in SMCs after Andrographolide (5 μM) treatment for different time points, and the quantification data are shown **(C)** ($n = 3$). **(D)** Immunohistochemistry staining was performed to detect the expression of EDNRA and EDNRB in the completely ligated carotid arteries. **(E)** The relative protein levels were quantified by Average Optical Density (Integrated option density/Area) using Image J software ($n = 5$). **(F)** Immunofluorescence staining was used to evaluate the expression of EDNRA ligated left carotid arteries. The analysis data are expressed as means ± SEM. *$P < 0.05$.

evaluated the expression of ET1, ET2, and ET3 in SMCs. We observed the highest expression level in ET1 under normal culture conditions (**Supplementary Figure 5A**). The expression of EDNA was much higher than that of EDNB (**Supplementary Figure 5B**). In order to confirm the potential targets for Andrographolide, we further treated rat SMCs with different doses of Andrographolide, and performed real-time PCR to determine the expression of the endothelin family and its receptors. Treatment with 1 μM Andrographolide did not change the expression of ET1, ET2, and ET3 in rat SMCs, whereas it significantly induced EDNRA and EDNRB expression (**Supplementary Figures 6A,B**). The treatment with 5 μM Andrographolide dramatically suppressed the transcription levels of ET1, ET2, and ET3 in rat SMC, whereas it observably induced EDNRA and EDNRB transcription levels (**Figure 5A**). The protein levels

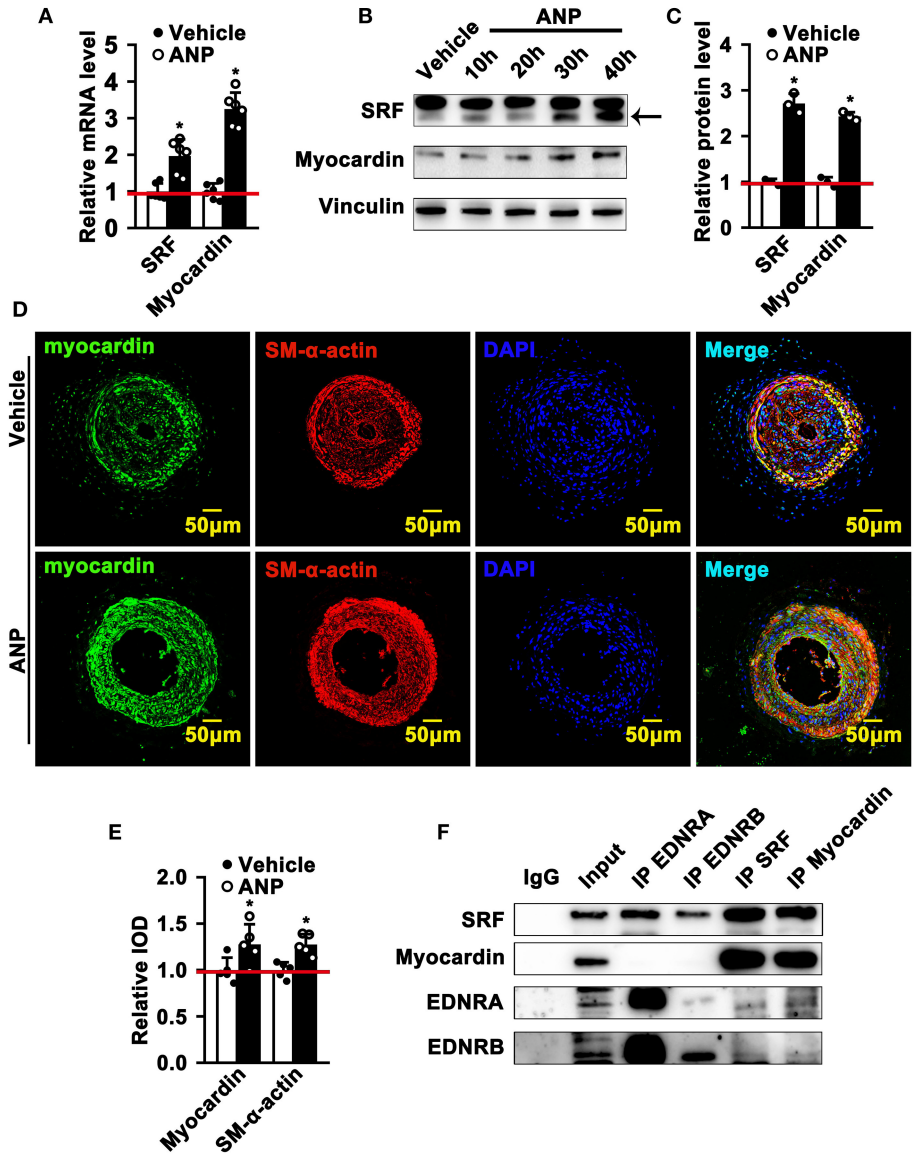

FIGURE 6 | Andrographolide promotes the interaction of EDNRA and EDNRB with the Myocardin-SRF complex. **(A)** Real-time PCR was performed to determine SRF and Myocardin mRNA levels in SMCs after 5 μM Andrographolide treatment ($n = 6$). **(B)** Rat SMCs were treated with Andrographolide (5 μM) over different time points. A western blot assay was performed to evaluate the protein level of SRF and Myocardin, quantified densities of protein were bound by Integral Optical Density (IOD) using ImageQuant TL software **(C)** ($n = 3$). **(D,E)** Immunofluorescence staining was performed to evaluate the expression of Myocardin in ligated left carotid arteries. **(F)** Co-immunoprecipitation was performed to determine the interaction of EDNRA/EDNRB and Myocardin-SRF. Total protein from rat SMCs was extracted using RIPA buffer. The cell lysate was precleared using anti-species-specific IgG beads. The precleared cell lysate was incubated with EDNRB (abcam), EDNRA (abcam), Myocardin (Santa Cruz), and SRF (abcam) for 1 h at 4°C. Following incubation with pre-equilibrated protein A/G agarose beads on a rocking platform overnight at 4°C, the co-immunoprecipitated targets were evaluated by western blotting. *$P < 0.05$.

of EDNRA and EDNRB were also enhanced after 5 μM Andrographolide treatment in SMCs (**Figures 5B,C**). We induced proliferation of rat SMCs by PDGF-BB treatment, and similar results were exhibited (**Supplementary Figures 6C,D**). To validate whether Andrographolide could regulate the endothelin/sarafotoxin family *in vivo*, we performed immunohistochemistry against EDNRA and EDRNB antibodies on pathological sections of complete ligation of the left common carotid artery. The results showed that the expressions of EDNRA and EDRNB were remarkably increased after Andrographolide treatment (**Figures 5D,E**). That Andrographolide treatment enhanced the expression of EDNRA was also validated by immunofluorescence staining (**Figure 5F**). The data demonstrated that Andrographolide activates the endothelin/sarafotoxin family by increasing both EDNRA and EDRNB in vascular SMCs.

Andrographolide Promotes the Interaction of EDNRA and EDNRB and the Myocardin-SRF Complex Resulting in Inducing the Expression of SMC Differentiated-Specific Genes

The most exciting and significant advance in SMC phenotypic switching is the discovery of SRF and Myocardin, which can bind to the CArGA box to regulate the expression of SMC differentiated genes (1). Andrographolide promotes the expression of both EDNRA and EDNRB in SMCs. However, whether enhanced EDNRA and EDNRB expression can regulate the expression of SRF and Myocardin is not fully defined. We first determined whether Andrographolide treatment could regulate the expression of SRF and Myocardin. We found that different doses (1 μM and 5 μM) of Andrographolide treatment dramatically enhanced SRF and Myocardin transcription levels (**Supplementary Figure 7A**; **Figure 6A**). Similar results were found with PDGF-BB (**Supplementary Figure 7B**). Different time points of Andrographolide (5 μM) treatment significantly induced the protein levels of SRF and Myocardin (**Figures 6B,C**). We next evaluated the expression of Myocardin *in vivo*; immunofluorescence staining showed that Andrographolide treatment obviously increased the expression of Myocardin in the completely ligated left common carotid artery (**Figures 6D,E**). To further explore whether EDNRA and EDNRB could interact with SRF and Myocardin, a co-immunoprecipitation experiment was performed. Pooled protein from rat SMCs was used. After being precleared using anti-species-specific IgG beads, incubated with EDNRB (abcam), EDNRA (abcam), Myocardin (Santa Cruz), and SRF (abcam) antibodies, and following incubation with pre-equilibrated protein A/G agarose beads, the co-immunoprecipitated proteins were evaluated by western blotting. We observed that EDNRA can bind to EDNRB to form a complex; SRF and Myocardin can also interact with each other (**Figure 6F**). The data indicated that EDNRA binds to EDNRB to form a complex which interacts with Myocardin-SRF complexes.

Inhibition of Endothelin Receptors and SRF Attenuates Andrographolide-Promoted SMC Dedifferentiation

EDNRA and EDNRB can bind to SRF. However, whether this binding is critical in regulating SMC phenotypic switching is not well defined. We treated SMC with Macitentan, a non-specific inhibitor for EDNRA and EDNRB, and detected whether Macitentan regulated SMC proliferation and migration. The BRDU incorporation assay and CCK8 cell proliferation assay indicated that Macitentan alone can promote SMC proliferation (**Supplementary Figures 8A–C**). Macitentan treatment also promoted SMC migration, which was evident in our spheroid cell migration assay (**Supplementary Figures 9A–C**). Following Andrographolide treatment, the BRDU incorporation assay indicated that Andrographolide suppressing SMC proliferation was obviously attenuated in the presence of Macitentan (**Figures 7A,B**). Similar results were exhibited in the CCK8 cell proliferation assay (**Supplementary Figure 10**). Macitentan dramatically attenuated the suppressed migration of SMCs induced by Andrographolide treatment (**Figures 7C–E**). We further used siRNA to delete EDNRA and SRF in rat SMCs. After transfection, real-time PCR was performed to evaluate deletion efficiency (**Supplementary Figures 11A,B, 12A,B**). The siRNA targeted deletion of EDNRA and SRF was chosen from three difference sequences, and the sequences are exhibited in **Table 2**. After transfection of si-EDNRA, Andrographolide treatment significantly suppressed the expression of MHC, calponin, SM22α, and smooth muscle α-actin (**Supplementary Figure 13**). After transfection of si-SRF, no difference in the expression of smooth muscle marker genes was found between si-SRF and Andrographolide treatment alone (**Supplementary Figure 14**). However, after transfection with both si-EDNRA and si-SRF, following Andrographolide treatment, the smooth muscle marker genes were dramatically inhibited, including MHC, calponin, SM22α, smooth muscle α-actin, and klf4 (**Figure 7F**) and which resulting the increase of cell viability (**Figure 7G**). The data demonstrated that Andrographolide promotes the interaction between endothelin-dependent EDNRA/EDNRB and Myocardin-SRF to regulate pathological vascular remodeling.

In summary, vascular injury suppresses the expression of SRF and Myocardin, resulting in decreased expression of SMC-specific marker genes, which is characterized by enhanced proliferation and migration, and eventually leads to vascular hyperplasia. The treatment of SMC with Andrographolide activates the endothelin signaling pathway and promotes the interaction of EDNA and EDNB with the Myocardin-SRF complex to induce SMC-specific marker gene expression (**Figure 7H**).

DISCUSSION

This study provides evidence that Andrographolide regulates pathological vascular remodeling. The treatment of rat SMCs with Andrographolide activates the endothelin signaling pathway and promotes interaction of EDNA and EDNB with the Myocardin-SRF complex to induce SMC-specific marker gene expression, resulting in restrained pathological vascular remodeling. We provide first evidence that Traditional Chinese Medicine Andrographolide regulates pathological vascular remodeling through interaction between endothelin receptors with the Myocardin-SRF complex.

Endothelin was first identified from bovine endothelial cell in 1985 (35). The endothelin/sarafotoxin family consists of three isoforms, including ET-1, ET-2, and ET-3 (14). The expression of ET-1 is much higher than ET-2 and ET-3 (**Supplementary Figure 5A**). The transcription level of ET-1 was obviously changed after Andrographolide treatment. We focused on ET-1 in this study and evaluated whether and how Andrographolide regulates pathological vascular remodeling. However, as a secreted peptide, it is difficult to evaluate the concentration and activation of ET in tissues and organs. We monitored the transcription level of ET-1 in SMCs by real-time PCR following Andrographolide treatment.

ET-1 interacts with cognate receptors to regulate vasoconstriction. Three types of G protein-coupled endothelin/sarafotoxin family receptors have been identified, including EDNRA, EDNRB, and $EDNRB_2$ (36). Both ET-1

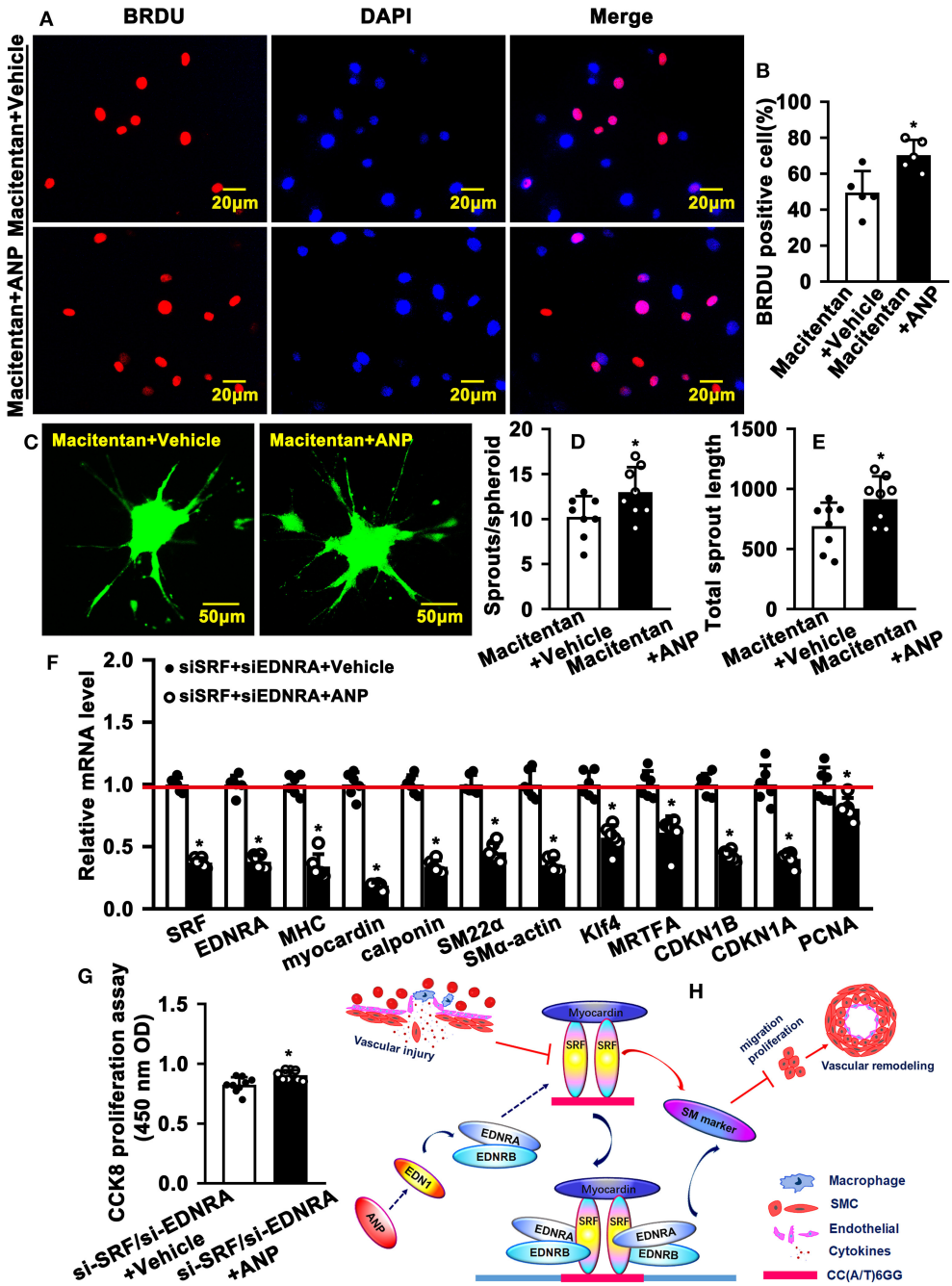

FIGURE 7 | Inhibition of endothelin receptors and SRF attenuates Andrographolide-promoted SMC dedifferentiation. **(A)** Rat SMCs were treated with Macitentan (1 μM) and Andrographolide (5 μM), followed by incubation with BRDU labeling buffer for 20 h. Immunofluorescence staining was performed to observe BRDU incorporation, and BRDU-positive cells were quantified, as shown in **(B)** ($n = 5$). **(C)** A spheroid sprouting assay was performed in the presence of Macitentan (1 μM) and Andrographolide (5 μM). The sprouting was visualized by calcein AM staining, and sprouts and sprouting length are quantified in **(D,E)** ($n = 8$). **(F)** Rat SMCs were transfected with small interfering RNA si-SRF and si-EDNRA for 4-6 h, and then treated with Andrographolide (5 μM) for 30 h, the mRNA levels of SMC-specific marker genes, including SRF, Myocardin, MHC, calponin, SM22α, SMα-actin, KLF4, and MRTFA, and proliferation-related genes including CDKN1A, CDKN1B, and PCNA were detected by real-time PCR ($n = 6$). **(G)** Rat SMCs were transfected with small interfering RNA si-SRF and si-EDNRA for 4–6 h, and then treated with Andrographolide (5 μM) for 24 h, the cell viability was detected by CCK8 ($n = 9$). Data are presented as mean ± SEM. $^*P < 0.05$. **(H)** The schematic diagram indicates that vascular injury suppresses the expression of SRF and Myocardin, resulting in decreased expression of SMC-specific marker genes, which is characterized by enhanced proliferation and migration, eventually leading to vascular hyperplasia. Treatment of SMCs with Andrographolide activates the endothelin signaling pathway and promotes the interaction of EDNA and EDNB with the Myocardin-SRF complex to induce SMC-specific marker gene expression.

TABLE 2 | The sequences of siRNA.

Gene name	Species	Sequence
Si-control	Rat	S: 5′-UUCUCCGAACGUGUCACGUTT-3′
	Rat	AS: 5′-ACGUGACACGUUCGGAGAATT-3′
Si-SRF	Rat	S: 5′-CACCUCCACAAUCCAAACATT-3′
	Rat	AS: 5′-UGUUUGGAUUGUGGAGGUGTT-3′
Si-EDNRA	Rat	S: 5′-CACGACGGCUUUCAAAUAUTT-3′
	Rat	AS: 5′-AUAUUUGAAAGCCGUCGUGTT-3′

and ET-2 can activate these three kinds of receptors, whereas ET-3 only activates EDNRB and $EDNRB_2$. EDNRB is a major receptor that is expressed in SMCs (**Supplementary Figure 5B**). However, Andrographolide treatment dramatically enhanced the expression of EDNRA and EDNRB. In this study, we determined whether Andrographolide treatment regulates pathological vascular remodeling by the interaction between ET-1 and EDNRA or EDNRB.

In this study, we identified a novel mechanism where Andrographolide activates the endothelin signaling pathway and promotes the interaction of receptors EDNA and EDNB with the Myocardin-SRF complex to induce SMC-specific marker gene expression. Previous studies demonstrated that ET-1 promotes proliferation and migration of vascular smooth muscle cells. Although the majority of ET-1 is generated by endothelial cells, ET-1 can also be released by vascular SMCs (37, 38). However, whether and how Andrographolide regulates SMC differentiation is not well defined. Identification of SRF and Myocardin represents tremendous progress in defining SMC phenotypic switching. SRF dimerism binds to the CArG element that exists in the promoter regions of multiple SMC marker genes. Myocardin induces multiple SMC marker gene expression by binding to SRF. In this study, we demonstrated that Andrographolide promoted the interaction of EDNA and EDNB with Myocardin-SRF, and induced CArG boxes containing SMC-specific marker gene expression (**Figure 7G**).

Pathological vascular remodeling involves SMC proliferation, endothelial cell inflammation, collagen synthesis (39), and macrophages, etc. We performed a CCK8 cell proliferation assay and BRDU cell incorporation assay to evaluate whether Andrographolide suppresses SMC proliferation. We also performed a Boyden chamber migration assay and spheroid sprouting assay to determine whether Andrographolide inhibits SMC migration. Furthermore, we defined that Andrographolide activates the endothelin signaling pathway and promotes the interaction of receptor EDNA and EDNB with Myocardin-SRF to induce CArG boxes containing SMC-specific marker gene expression. The data are very interesting. However, these data cannot account for every detail that happens during pathological vascular remodeling. More studies need to focus on how Andrographolide regulates endothelial cell behaviors during pathological vascular remodeling.

Although we provide evidence that Andrographolide regulates pathological vascular remodeling by inducing the interaction of EDNRA and EDNRB with the Myocardin-SRF complex, resulting in enhanced expression of CArG boxes containing SMC-specific marker genes. Some other signaling pathways may also be involved during pathological vascular remodeling. Our real-time PCR data exhibited that IL-15, IL-18, IGF1, and Hif1a were also regulated in SMCs after Andrographolide treatment (**Supplementary Figure 4**).

Extra matric deposition, degradation, and rearrangement are critical for development of the vascular system and aging of tissue and organs. Our real-time PCR data indicated that expression of versicon, collagen I, collagen II, and fibronectin were decreased in SMCs following Andrographolide treatment (**Supplementary Figure 10**).

In summary, this study not only demonstrates the critical role of Andrographolide on regulating pathological vascular remodeling, but also identifies a novel mechanism where Andrographolide activates the endothelin signaling pathway and promotes the interaction of EDNA and EDNB with Myocardin-SRF to induce CArG boxes containing SMC-specific marker gene expression.

DATA AVAILABILITY STATEMENT

The original contributions presented in the study are included in the article/**Supplementary Material**, further inquiries can be directed to the corresponding author/s.

ETHICS STATEMENT

The animal study was reviewed and approved by Experimental Animal Ethics Committee of Chengdu University of Traditional Chinese Medicine.

AUTHOR CONTRIBUTIONS

YW, LY, HX, and LS designed the research. WH, XW, ZJ, ZW, QG, ZC, SZ, HZ, and LZ performed the experiments. JH, LZ, XZ, and WH analyzed the data. YW and WH wrote and revised the manuscript. All authors contributed to the article and approved the submitted version.

FUNDING

This study was supported by Grants (81870363 and 81741007) from the National Natural Science Foundation of China, Grant (2020JDTD0025) from the Science and Technology Departments of Sichuan Province, and Grants (008066, 030038199, 030041023, 030041224, 0300500092, 0300510026, 030055180, 319020056, 242030016, and MPRC2021038) from Cheng Du University of Traditional Chinese Medicine.

SUPPLEMENTARY MATERIAL

The Supplementary Material for this article can be found online at: https://www.frontiersin.org/articles/10.3389/fcvm.2021.783872/full#supplementary-material

REFERENCES

1. Alexander MR, Owens GK. Epigenetic control of smooth muscle cell differentiation and phenotypic switching in vascular development and disease. *Annu Rev Physiol.* (2012) 74:13–40. doi: 10.1146/annurev-physiol-012110-142315
2. Harika S, Arti V, Sandeep A, Daniel A, Oge A, Fang L, et al. Pharmacological inhibition of β-catenin prevents EndMT *in vitro* and vascular remodeling *in vivo* resulting from endothelial Akt1 suppression. *Biochem Pharmacol.* (2019) 164:205–15. doi: 10.1016/j.bcp.2019.04.016
3. Chiang HY, Korshunov VA, Serour A, Shi F, Sottile J. Fibronectin is an important regulator of flow-induced vascular remodeling. *Arterioscler Thromb Vasc Biol.* (2009) 29:1074–9. doi: 10.1161/ATVBAHA.108.181081
4. Penn DL, Witte SR, Komotar RJ, Sander Connolly E Jr. The role of vascular remodeling and inflammation in the pathogenesis of intracranial aneurysms. *J Clin Neurosci.* (2014) 21:28–32. doi: 10.1016/j.jocn.2013.07.004
5. Chan S, Yan C. PDE1 isozymes, key regulators of pathological vascular remodeling. *Curr Opin Pharmacol.* (2011) 11:720–4. doi: 10.1016/j.coph.2011.09.002
6. Cai Y, Knight WE, Guo S, Li JD, Knight PA, Yan, C. Vinpocetine suppresses pathological vascular remodeling by inhibiting vascular smooth muscle cell proliferation and migration. *J Pharmacol Exp Ther.* (2012) 343:479–88. doi: 10.1124/jpet.112.195446
7. Nagao M, Lyu Q, Zhao Q, Wirka RC, Bagga J, Nguyen T, et al. Coronary disease-associated gene TCF21 inhibits smooth muscle cell differentiation by blocking the myocardin-serum response factor pathway. *Circ Res.* (2020) 126:517–29. doi: 10.1161/CIRCRESAHA.119.315968
8. McDonald OG, Wamhoff BR, Hoofnagle MH, Owens GK. Control of SRF binding to CArG box chromatin regulates smooth muscle gene expression *in vivo*. *J Clin Invest.* (2006) 116:36–48. doi: 10.1172/JCI26505
9. Wang Z, Wang DZ, Hockemeyer D, McAnally J, Nordheim A, Olson EN. Myocardin and ternary complex factors compete for SRF to control smooth muscle gene expression. *Nature.* (2004) 428:185–9. doi: 10.1038/nature02382
10. Yoshida T, Hoofnagle MH, Owens GK. Myocardin and Prx1 contribute to angiotensin II-induced expression of smooth muscle α-actin. *Circul Res.* 94:1075–82. doi: 10.1161/01.RES.0000125622.46280.95
11. Liao XH, Wang N, Zhao DW, Zheng DL, Zheng L, Xing WJ, et al. STAT3 protein regulates vascular smooth muscle cell phenotypic switch by interaction with myocardin. *J Biol Chem.* (2015) 290:19641–52. doi: 10.1074/jbc.M114.630111
12. Davis-Dusenbery BN, Chan MC, Reno KE, Weisman AS, Layne MD, Lagna G, et al. A down-regulation of Krüppel-like factor-4 (KLF4) by microRNA-143/145 is critical for modulation of vascular smooth muscle cell phenotype by transforming growth factor-β and bone morphogenetic protein 4. *J Biol Chem.* (2011) 286:28097–110. doi: 10.1074/jbc.M111.236950
13. Rahman NT, Schulz VP, Wang L, Gallagher PG, Denisenko O, Gualdrini F, et al. augments megakaryocyte maturation by enhancing the SRF regulatory axis. *Blood Adv.* (2018) 2:2691–703. doi: 10.1182/bloodadvances.2018019448
14. Dhaun N, Webb DJ. Endothelins in cardiovascular biology and therapeutics. *Nat Rev Cardiol.* (2019) 16:491–502. doi: 10.1038/s41569-019-0176-3
15. Luscher TF, Barton, M. Endothelins and endothelin receptor antagonists: therapeutic considerations for a novel class of cardiovascular drugs. *Circulation.* (2000) 102:2434–40. doi: 10.1161/01.cir.102.19.2434
16. Kawanabe Y, Nauli SM. Endothelin. *Cell Mol Life Sci.* (2011) 2:195–203. doi: 10.1007/s00018-010-0518-0
17. Miyauchi T, Sakai, S. Endothelin and the heart in health and diseases. *Peptides.* (2019) 111:77–88. doi: 10.1016/j.peptides.2018.10.002
18. Agapitov AV, Haynes WG. Role of endothelin in cardiovascular disease. *J Renin Angiotensin Aldosterone Syst.* (2002) 3:1–15. doi: 10.3317/jraas.2002.001
19. Planas-Rigol E, Terrades-Garcia N, Corbera-Bellalta M, Lozano E, Alba MA, Segarra M, et al. Endothelin-1 promotes vascular smooth muscle cell migration across the artery wall: a mechanism contributing to vascular remodelling and intimal hyperplasia in giant-cell arteritis. *Ann Rheum Dis.* (2017) 9:1624–34. doi: 10.1136/annrheumdis-2016-210792
20. Takahashi M. The role of endothelin-1 in vascular remodeling *in vivo*. *Cardiovasc Res.* (2006) 1:4–5. doi: 10.1016/j.cardiores.2006.05.006
21. Wu Z, Xu H, Xu Y, Fan W, Yao H, Wang Y, et al. Andrographolide promotes skeletal muscle regeneration after acute injury through epigenetic modulation. *Eur J Pharmacol.* (2020) 888:173470. doi: 10.1016/j.ejphar.2020.173470
22. Peng YL, Wang Y, Tang N, Sun DD, Lan YL, Yu ZL, Zhao XY, et al. Andrographolide inhibits breast cancer through suppressing COX-2 expression and angiogenesis via inactivation of p300 signaling and VEGF pathway. *J Exp Clin Canc Res.* (2018) 37:1–14. doi: 10.1186/s13046-018-0926-9
23. Shen KK Ji LL, Lu B, Xu C, Gong CY, Morahan G, Wang ZT. Andrographolide inhibits tumor angiogenesis via blocking VEGFA/VEGFR2-MAPKs signaling cascade. *Chem-Biol Interact.* (2014) 218:99–106. doi: 10.1016/j.cbi.2014.04.020
24. Kajal K, Panda AK, Bhat J, Chakraborty D, Bose S, Bhattacharjee P, et al. Andrographolide binds to ATP-binding pocket of VEGFR2 to impede VEGFA-mediated tumor-angiogenesis. *Sci Rep.* (2019) 9:1–10. doi: 10.1038/s41598-019-40626-2
25. Dai JW, Lin YY, Duan YF Li ZX, Zhou DL, Chen WS, et al. Andrographolide inhibits angiogenesis by inhibiting the Mir-21-5p/TIMP3 signaling pathway. *Int J Biol Sci.* (2017) 5:660–8. doi: 10.7150/ijbs.19194
26. Wang YJ, Wang JT, Fan QX, Geng JG. Andrographolide inhibits NF-kappaBeta activation and attenuates neointimal hyperplasia in arterial restenosis. *Cell Res.* (2007) 17:933–41. doi: 10.1038/cr.2007.89
27. Yao H, Wu ZQ, Xu YM, Xu H, Lou GH, Jiang Q, et al. Andrographolide attenuates imbalance of gastric vascular homeostasis induced by ethanol through glycolysis pathway. *Sci Rep.* (2019) 9:1–10. doi: 10.1038/s41598-019-41417-5
28. Kumar A, Lindner V. Remodeling with neointima formation in the mouse carotid artery after cessation of blood flow. *Arterioscler Thromb Vasc Biol.* (1997) 10:2238–44. doi: 10.1161/01.atv.17.10.2238
29. Wang Y, Xu YM, Yan SY, Cao KX, Zeng XQ, Zhou YQ, et al. Adenosine kinase is critical for neointima formation after vascular injury by inducing aberrant DNA hypermethylation. *Cardiovasc Res.* (2021) 117:561–75. doi: 10.1093/cvr/cvaa040
30. Wang XB, Hu GQ, Gao XW, Wang Y, Zhang W, Harmon EY, et al. The induction of yes-associated protein expression after arterial injury is crucial for smooth muscle phenotypic modulation and neointima formation. *Arterioscl Throm Vasc.* (2012) 32:2662–9. doi: 10.1161/Atvbaha.112.254730
31. Xu S, Fu J, Chen J, Xiao P, Lan T, Le K, et al. Development of an optimized protocol for primary culture of smooth muscle cells from rat thoracic aortas. *Cytotechnology.* (2009) 61:65–72. doi: 10.1007/s10616-009-9236-6
32. Zhu N, Xiang YJ, Zhao XY, Cai CH, Chen H, Jiang WB, et al. Thymoquinone suppresses platelet-derived growth factor-BB-induced vascular smooth muscle cell proliferation, migration and neointimal formation. *J Cell Mol Med.* (2019) 12:8482–92. doi: 10.1111/jcmm.14738
33. Schmitt BM, Boewe AS, Becker V, Nalbach L, Gu Y, Gotz C, et al. Protein kinase CK2 regulates nerve/glial antigen (NG)2-mediated angiogenic activity of human pericytes. *Cells.* (2020) 9:9061546. doi: 10.3390/cells9061546
34. Wang Y, Hu GQ, Liu F, Wang XB, Wu MF, Schwarz JJ, et al. Deletion of yes-associated protein (YAP) specifically in cardiac and vascular smooth muscle cells reveals a crucial role for YAP in mouse cardiovascular development. *Circul Res.* (2014) 114:957–65. doi: 10.1161/Circresaha.114.303411
35. Hickey KA, Rubanyi G, Paul RJ, Highsmith RF. Characterization of a coronary vasoconstrictor produced by cultured endothelial cells. *Am J Physiol.* (1985) 248:C550–6. doi: 10.1152/ajpcell.1985.248.5.C550
36. Rodriguez-Pascual F, Busnadiego O, Lagares D, Lamas S. Role of endothelin in the cardiovascular system. *Pharmacol Res.* (2011) 63:463–72. doi: 10.1016/j.phrs.2011.01.014
37. Tian XY, Zhang QY, Huang YQ, Chen SL, Tang CS, Sun Y, et al. Endothelin-1 downregulates sulfur dioxide/aspartate aminotransferase pathway via reactive oxygen species to promote the proliferation and migration of vascular smooth muscle cells. *Oxid Med Cell Longev.* (2020) 2020:9367673. doi: 10.1155/2020/9367673
38. Wort SJ, Woods M, Warner TD, Evans TW, Mitchell JA. Endogenously released endothelin-1 from human pulmonary artery smooth muscle promotes cellular proliferation: relevance to pathogenesis of pulmonary hypertension and vascular remodeling. *Am J Respir Cell Mol Biol.* (2001) 25:104–10. doi: 10.1165/ajrcmb.25.1.4331
39. Liu X, Zhang S, Wang X, Wang Y, Song J, Sun C. Endothelial cell-derived SO(2) controls endothelial cell inflammation, smooth muscle cell proliferation, and collagen synthesis to inhibit hypoxic pulmonary vascular

remodelling. *Oxid Med Cell Longev.* (2021) 2021:5577634. doi: 10.1155/2021/5577634

Conflict of Interest: The authors declare that the research was conducted in the absence of any commercial or financial relationships that could be construed as a potential conflict of interest.

Publisher's Note: All claims expressed in this article are solely those of the authors and do not necessarily represent those of their affiliated organizations, or those of the publisher, the editors and the reviewers. Any product that may be evaluated in this article, or claim that may be made by its manufacturer, is not guaranteed or endorsed by the publisher.

Copyright © 2022 Hu, Wu, Jin, Wang, Guo, Chen, Zhu, Zhang, Huo, Zhang, Zhou, Yang, Xu, Shi and Wang. This is an open-access article distributed under the terms of the Creative Commons Attribution License (CC BY). The use, distribution or reproduction in other forums is permitted, provided the original author(s) and the copyright owner(s) are credited and that the original publication in this journal is cited, in accordance with accepted academic practice. No use, distribution or reproduction is permitted which does not comply with these terms.

frontiers in Cardiovascular Medicine

ORIGINAL RESEARCH
published: 07 February 2022
doi: 10.3389/fcvm.2022.818162

Association Between Serum Galectin-3 Levels and Coronary Stenosis Severity in Patients With Coronary Artery Disease

*Mingxing Li[1,2], Kai Guo[2], Xuansheng Huang[2], Li Feng[2], Yong Yuan[2], Jiewen Li[2], Yi Lao[2] and Zhigang Guo[1]**

[1] Division of Cardiology, Huiqiao Medical Centre, Nanfang Hospital, Southern Medical University, Guangzhou, China,
[2] Department of Cardiology, Zhongshan People's Hospital, Zhongshan, China

Background: The relationship between galectin-3 (Gal-3) and coronary artery disease (CAD) has not been fully elucidated.

Aim: This study aimed to determine the relationship between the presence and severity of CAD and serum Gal-3 levels.

Patients and Methods: Three-hundred thirty-one consecutive CAD patients were enrolled as the study group. An additional 62 patients without CAD were enrolled as the control group. Serum Gal-3 levels were separately compared between the non-CAD and CAD groups, among the stable CAD and Acute coronary syndrome (ACS) groups, and between CAD patients with low and high SYNTAX scores (SSs). The 1-year cumulative rate of major adverse cardiac events (MACEs) was also compared among ACS patients by Gal-3 levels.

Results: Serum Gal-3 was significantly higher in the CAD group than in the non-CAD group 3.89 (0.16–63.67) vs. 2.07 (0.23–9.38) ng/ml, $P < 0.001$. Furthermore, serum Gal-3 was significantly higher in the non-ST-segment elevation ACS (NSTE-ACS) group than that in the stable CAD group, 4.72 (1.0–16.14) vs. 2.23 (0.65–23.8) ng/ml, $P = 0.04$ and higher in the ST-segment elevation myocardial infarction (STEMI) group than that in the stable CAD group 7.87 (0.59–63.67) vs. 2.23 (0.65–23.8) ng/ml, $P < 0.001$. Serum Gal-3 level was an independent predictor of ACS compared with stable CAD group (OR = 1.131, 95% CI: 1.051–1.217, $P = 0.001$) as well as high SS (OR = 1.030, 95% CI: 1.021–1.047, $P = 0.038$) after adjust other confounding risk factors. Acute coronary syndrome patients with Gal-3 levels above the median (gal-3 = 4.78 ng/ml) showed a higher cumulative MACE rate than those with Gal-3 levels below the median. After adjusting other confounding risk factors, Gal-3 remained an independent risk factor for the cumulative rate of MACEs in ACS patients (6% higher rate of MACEs incidence per 1 ng/ml increment of Gal-3).

Conclusion: Galectin-3 correlated with the presence of CAD as well as coronary stability and complexity. Galectin-3 may be valuable in predicting mid-term prognosis in ACS patients.

Keywords: coronary artery disease, galectin-3, syntax score, prognosis, acute coronary syndrome

OPEN ACCESS

Edited by:
Yuli Huang,
Southern Medical University, China

Reviewed by:
Pingan Chen,
Guangzhou First People's Hospital, China
Tianyi Ma,
Central South University, China

***Correspondence:**
Zhigang Guo
guozhigang126@126.com

Specialty section:
This article was submitted to General Cardiovascular Medicine, a section of the journal Frontiers in Cardiovascular Medicine

Received: *19 November 2021*
Accepted: *10 January 2022*
Published: *07 February 2022*

Citation:
Li M, Guo K, Huang X, Feng L, Yuan Y, Li J, Lao Y and Guo Z (2022) Association Between Serum Galectin-3 Levels and Coronary Stenosis Severity in Patients With Coronary Artery Disease. Front. Cardiovasc. Med. 9:818162. doi: 10.3389/fcvm.2022.818162

INTRODUCTION

Cardiovascular diseases (CVDs) remain the leading cause of death worldwide (1). Atherosclerosis is a major cause of stroke and CVDs (2) and is characterized by the excessive accumulation of lipoprotein in macrophages, monocyte chemo-attraction in vascular lesions, and the infiltration of vascular smooth muscle cells (VSMCs) into the sub-endothelial space (3). Inflammation mediated by macrophages plays an important role in the initiation and progression of atherosclerosis (3, 4).

Galectin-3 (Gal-3) is a pro-inflammatory cytokine that is mainly secreted by activated macrophages (5). It is a circulating 35 kDa β-galactosidase-binding lectin and the unique chimera-like galectin member of the vertebrate family (6). It has one C-terminal carbohydrate recognition domain connected to a long N-terminal domain, and in the human genome, it is encoded solely by LGALS3, located on chromosome 14, locus q21-22 (5, 6). Galectin-3 has several biological functions, including intracellular and short-distance signaling, regulation of gene expression, cell-to-cell interaction, and exchanges between cells and the extracellular matrix (ECM) (7, 8). Over-expression of Gal-3 has been observed in patients with decompensated congestive heart failure (CHF). In addition, Gal-3 may play an important role in the inflammatory response, fibrosis and scar formation, cardiac remodeling, and heart failure in the clinical setting of acute myocardial infarction (AMI) (9).

Recently, clinical data have suggested that Gal-3 is closely correlated with coronary atherosclerosis (9–13). However, the precise role of Gal-3 in coronary artery disease (CAD) has not yet been fully elucidated, and more data are needed to systemically explore the association between serum Gal-3 levels and atherosclerotic plaque burden and stability. We therefore performed a retrospective cohort clinical study to explore the relationship between peripheral Gal-3 levels and the presence of CAD as well as plaque burden and stability. The value of Gal-3 in predicting mid-term prognosis in acute coronary syndrome (ACS) patients was also evaluated.

PATIENTS AND METHODS

Study Population

This is a single-center, retrospective cohort study. From January 1 to December 1, 2018, we continuously enrolled 393 consecutive patients who underwent coronary angiography due to suspected coronary heart disease. Patients who met one of the following criteria were excluded: (1) patients with acute or chronic infectious diseases or autoimmune diseases or recently used drugs that affect the immune response; (2) patients with severe heart failure, liver or kidney dysfunction; (3) patients complicated with any kind of tumor; and (4) patients who refused to sign the informed consent form and did not want to participate in this research.

Methods

First, the enrolled patients were divided into the control (non-CAD group, $n = 62$) and CAD groups ($n = 331$). Serum Gal-3 levels were compared between the two groups. Then, we did subgroup analysis and all the enrolled CAD patients were further divided into the stable CAD, non-ST-segment elevation ACS (NSTE-ACS) group and ST-segment elevation myocardial infarction (STEMI) group. Serum Gal-3 levels were compared among the three groups. The SYNTAX score (SS) was then calculated for all CAD patients, and the serum Gal-3 level was also compared between the low SS (<22) group and the high SS (≥22) group. We performed multivariate logistic regression analysis to explore the correlation between serum Gal-3 and ACS compared with stable CAD and high SS compared with low SS.

Clinical Data Collection

The patient's medical history, sex, age, body mass index (BMI), and laboratory test results such as white blood cell (WBC) count, the serum creatinine (CR), fasting glucose (FG) level, glycosylated hemoglobin level, hs-CRP, left atrial diameter, and left ventricular ejection fraction (LVEF) according to echocardiography, Killip grades, medication treatment during hospitalization were obtained and collected from the hospital medical record system.

Definitions

Coronary artery disease was defined as ≥50% luminal diameter stenosis of at least one major epicardial coronary artery. ST-segment elevation myocardial infarction was defined as follows: (i) There is evidence of myocardial injury which is defined as an elevation of cardiac troponin values with at least one value above the 99th percentile upper reference limit. (ii) Patients with persistent chest discomfort or other symptoms suggestive of ischemia. (iii) ST-segment elevation in at least two contiguous leads (14). Non-ST-segment elevation ACS was defined according to 2020 European Society of Cardiology (ESC) Guidelines (15) and was stated as follows: patients with acute chest discomfort but no persistent ST-segment elevation. ECG changes may include transient ST-segment elevation, persistent or transient ST-segment depression, T-wave inversion, flat T waves, or pseudonormalization of T waves; or the ECG may be normal.

Stable CAD was defined according to the 2013 ESC guidelines recommended (16).

Galectin-3 Detection

The blood sample was collected from the cubital vein in an ethylene diaminetetraacetic acid (EDTA) vacuum tube, placed in a 4°C refrigerator, allowed to stand for 4 h, and centrifuged at 1,000 × g for 15 min. Then, the supernatant was collected and placed in a −80°C refrigerator for later inspection. The assay was performed and calibrated according to the manufacturer's protocol using an enzyme-linked immunosorbent assay. Measurements were performed in duplicate, and the results were averaged. The standard curve ranged between 0.47 and 30.0 ng/ml. The limit of detection was 0.29 ng/ml, and the intra- and inter-assay reproducibility coefficients of variation were 7.5 and 5.4%, respectively.

TABLE 1 | The baseline clinical and biochemical characteristics of the study with CAD or no-CAD.

Variable	no-CAD, $n = 62$	CAD, $n = 331$	*P*
Age, years	60.35 ± 10.36	60.81 ± 11.78	0.601
Gender male sex, % (*n*)	49 (79.0)	268 (80.9)	0.833
BMI, kg/m^2	24.51 ± 2.22	24.10 ± 2.58	0.248
Hypertension, % (*n*)	26 (41.9)	195 (58.9)	0.013*
DM, % (*n*)	8 (12.9)	65 (19.6)	0.285
History of hyperlipidemia, % (*n*)	1 (1.6)	12 (3.6)	0.701
Smoking, % (*n*)	23 (37.1)	136 (41.1)	0.330
Family history of CAD, % (*n*)	0 (0)	9 (2.7)	0.365
Systolic blood pressure, mm Hg	134.87 ± 22.83	142.32 ± 23.33	0.420
WBC, 10^9/L	7.33 ± 1.74	9.51 ± 4.91	<0.001*
Hb, g/L	139.27 ± 15.48	140.31 ± 21.89	0.704
Fasting blood glucose, mmol/L	5.53 ± 1.18	6.55 ± 2.29	<0.001*
Hb A1c, %	6.11 ± 1.51	6.35 ± 1.41	0.026*
Creatinine, μmol/l	71 (43–131)	85 (33–187)	<0.001*
hs-CRP, mg/L	5.16 ± 1.72	8.22 ± 1.13	0.029*
Total cholesterol, mmol/L	4.26 ± 0.94	4.52 ± 1.23	0.119
HDL cholesterol, mmol/L	0.68–1.99	0.27–4.62	0.829
LDL cholesterol, mmol/L	2.45 ± 0.74	2.81 ± 1.08	0.028*
Triglycerides, mmol/L	1.7 (0.56–5.82)	1.52 (0.49–7.93)	0.176
ApoA1, mg/dl	1.09 ± 0.17	1.11 ± 0.25	0.747
ApoB100, mg/dl	0.84 ± 0.22	1.02 ± 0.39	0.001*
Lpa, mg/dl	176 (0–885)	168 (0–3,440)	0.334
LV diameter, mm	45.5 (31–59)	46.5 (28–69)	0.082
LVEF,%	65 (50–75)	59 (22–80)	0.016*
Serum Gal-3, ng/ml	2.07 (0.23–9.38)	3.89 (0.16–63.67)	<0.001*

CAD, coronary artery disease; BMI, body mass index; DM, diabetic mellitus; WBC, white blood cell; Hb, hemoglobin; HbA1C, hemoglobin A1C; CRP, C-reactive protein; TC, total cholesterol; HDL-C, high density lipoprotein cholesterol; LDL-C, low-density lipoprotein cholesterol; TG, triglyceride; ApoA1, apolipoprotein A1; ApoB, apolipoprotein B; LP(a), Lipoprotein(a); LVEF, left venticular ejection fraction.
**P< 0.05.*

TABLE 2 | Association between serum Gal-3 and presence of CAD.

Gal-3	Incident rate	Model 1		Model 2		Model 3	
		OR (95%CI)	*P*-value	OR (95%CI)	*P*-value	OR (95%CI)	*P*-value
Per ng/ml	331/393	1.30 (1.13, 1.50)	<0.001	1.21 (1.07, 1.37)	0.002	1.21 (1.07, 1.38)	0.003

Model 1, adjusted for age, gender; Model 2, further adjusted for SBP, WBC, Cr, LDL-c, apoB 100; Model 3, further adjusted for fasting glucose, ejection fraction.

Coronary Angiography and SYNTAX Score

All patients underwent coronary angiography in the catheter lab of the Department of Cardiology in our hospital. Coronary arteriography was conducted using the standard Judkins technique (17). The results of the angiography were judged by two experienced specialists. The SS of each of the selected patients in this study was calculated by the online SS calculator version 2.1 (www.syntaxscore.com).

Follow-Up

All enrolled ACS patients were followed up for 12 months. Major adverse cardiac events (MACEs) are defined as re-infarction, worsening heart failure, or recurrent angina. The survival time without a MACE is the time before the first MACE during follow-up. Data were obtained through outpatient or telephone interviews.

Statistical Analysis

Statistical analysis was performed using the SPSS package, version 17.0 (Chicago, Illinois, USA). To test differences between the groups, the Student's *t*-test was used for numerical variables with a regular distribution, and the Mann–Whitney *U*-test was employed if there was an irregular distribution. Categorical variables were analyzed with the chi-squared and Fisher's exact tests. Logistic regressions were used to assess the relationship between serum gal-3 and ACS, high SS. The initial model adjusted

TABLE 3 | The baseline clinical and biochemical characteristics of STEMI vs NSTE-ACS vs Stable CAD vs. non-CAD in the study.

	No CAD *n* = 62	Stable CAD *n* = 95	NSTE-ACS *n* = 97	STEMI *n* = 139	*P*-value
Age, years	60.35 ± 10.36	61.00 ± 10.61	61.95 ± 10.17	58.49 ± 13.19	0.058
Gender male sex, % (*n*)	39 (62.9)	57 (60)	82 (84.5)	120 (89.4)	<0.001
BMI, kg/m^2	24.51 ± 2.22	24.18 ± 2.53	24.17 ± 2.50	24.00 ± 2.67	0.483
Hypertension, % (*n*)	26 (41.9)	59 (62.1)	60 (75.9)	76 (54.6)	0.026
DM, % (*n*)	8 (12.9)	21 (21.1)	22 (22.7)	22 (15.8)	0.292
History of hyperlipidemia, % (*n*)	1 (1.6)	6 (6.3)	3 (3.1)	3 (2.2)	0.096
Smoking, % (*n*)	23 (37.1)	29 (30.5)	37 (38.1)	70 (50.4)	0.014
Family history of CAD, % (*n*)	0 (0)	3 (3.1)	4 (4.1)	2 (1.4)	0.507
Systolic blood pressure, mm Hg	142.32 ± 23.33	137.93 ± 20.50	136.06 ± 22.84	131.94 ± 24.12	0.020
Total cholesterol, mmol/L	4.26 ± 0.94	4.23 ± 1.13	4.26 ± 1.09	4.84 ± 1.33	0.042
HDL cholesterol, mmol/L	1.05 (0.68–1.99)	1.12 (0.48–2.89)	1.10 (0.07–4.62)	1.02 (0.26–3.4)	0.692
LDL cholesterol, mmol/L	2.45 ± 0.74	2.48 ± 0.90	2.49 ± 0.91	3.27 ± 1.14	<0.001
Triglycerides, mmol/L	1.7 (0.56–5.82)	1.32 (0.54–6.51)	1.46 (0.56–7.93)	1. 63 (0.49–6.87)	0.140
ApoA1, mg/dl	1.09 ± 0.17	1.04 ± 0.24	1.08 ± 0.27	1.15 ± 0.24	0.026
ApoB100, mg/dl	0.77 (0.51–1.39)	0.82 (0.33–2.58)	0.88 (0.36–2.58)	1.10 (0.26–2.91)	0.031
Lpa, mg/dl	176 (0–885)	128 (4–1,334)	173 (1.5–1,546)	188 (4–3,440)	0.007
WBC, 10^9/L	7.33 ± 1.74	7.02 ± 1.72	8.45 ± 2.39	11.94 ± 6.37	<0.001
Hb, g/L	136 (116–169)	136 (69–172)	144 (75–274)	142 (69–274)	0.005
Fasting blood glucose, mmol/L	5.31 (4.15–10.28)	5.36 (4.02–12.79)	5.91 (4.36–15.9)	6.04 (3.7–18.79)	<0.001
Hemoglobin A1c, %	5.85 (5–11)	5.9 (3.46–11.1)	6.1 (4.4–11.1)	6.0 (5.0–14.5)	0.008
Creatinine, mmol/l	71 (43–131)	75 (43–131)	92 (48–187)	81 (42–401)	<0.001
hs-CRP, mg/l	1 (0–67.6)	0.7 (0–12.4)*	2.1 (0–54.2)	5.8 (0–183.2)	<0.001
Troponin T, ng/L	40 (3–89)	40 (3–48)	40 (3–2000)	108 (40–3,650)	<0.001
Pro-BNP, pg/ml	60 (24–560)	60 (5–892)	165 (17–9000)	514 (24–11,232)	<0.001
LV diameter, mm	45 (31–59)	45 (28–61)	47 (38–64)	46 (35–69)	0.006
LVEF, %	65 (48–75)	65 (42–79)	62 (30–80)	58 (22–74)	<0.001
Number of lesion vessels	–	1 (1–3)	3 (1–3)	3 (1–3)	<0.001
Antiplatelet therapy	6 (9.6)	86 (93.4)	94 (97)	136 (98)	<0.001
Statins use,% (*n*)	10 (16.1)	94 (98.9)	94 (97)	137 (98.6)	0.187
β blocker use,% (*n*)	14 (22.6)	53 (55.8)	81 (83.5)	115 (82.7)	<0.001
ACEI/ARB use,% (*n*)	10 (15.1)	62 (65.3)	71 (73.2)	97 (69.8)	<0.001
Diuretics use,% (*n*)	6 (9.7)	19 (20)	40 (41.2)	57 (41)	<0.001
Gal-3, ng/ml	2.07 (0.23–9.38)	2.23 (0.65–23.8)*	4.47 (0.16–27.1)▲	7.87 (0.59–63.67)※	<0.001

CAD, coronary artery disease; BMI, body mass index; DM, Diabetic mellitus; WBC, white blood cell; HbA1C, hemoglobin A1C; CRP, C-reactive protein; TC, total chelosterol; HDL-C, high density lipoprotenchlesterol; LDL-C, low density lipoprotein cholesterol; TG, triglyceride; ApoA1, apolipoprotein A1; ApoB, apolipoprotein B; LP(a), Lipoprotein (a); LVEF, left venticular ejection fraction; Gal-3, galectin-3.

** means Stable CAD group vs. no CAD group, P = 0.035.*

※ means STEMI group vs. Stable CAD group, P < 0.001.

▲ means NSTE-ACS group vs. Stable CAD group, P = 0.04.

for age and gender. A second model additionally adjusted for SBP, WBC, Cr, LDL-c, apoB 100, FG, and LVEF. Kaplan-Meier analysis was used to compare the cumulative rate of MACEs. We used the median Gal-3 level as the cut-off value to divide the ACS patients into a high Gal-3 (>4.78 ng/ml, $n = 118$) and low Gal-3 (≤4.78 ng/ml, $n = 118$) group. The 1-year cumulative rate of MACEs was compared between ACS patients whose Gal-3 level was above and below the median level. Multivariate logistic regression analysis was performed to explore the correlation between Gal-3 and 1 year of MACEs in ACS patients in this study. A p-value of < 0.05 was regarded as statistically significant.

RESULTS

Serum Galectin-3 Expression in Patients With CAD vs. No CAD

The baseline characteristics of the patients in CAD and control groups are shown in **Table 1**. Compared with that in the no-CAD group, a higher proportion of the patients in the CAD group had a history of hypertension. The biochemical results showed that the WBC count and fasting blood glucose, glycosylated hemoglobin, CR, and hs-CRP levels were higher in the CAD group than in the non-CAD group. The levels of low-density

TABLE 4 | Logistic regression analysis for risk factors attributing to ACS presence in the study.

Variable	Univariate analysis		Multivariate analysis	
	OR (95% CI)	*P*-value	OR (95% CI)	*P*-value
Gender male sex, % (*n*)	3.784 (2.379–6.018)	<0.001	1.648 (0.599–4.532)	0.333
Smoking, % (*n*)	1.688 (1.109–2.569)	0.015	0.991 (0.455–2.154)	0.981
Systolic blood pressure, mm Hg	0.989 (0.980–0.997)	0.012	0.979 (0.962–0.996)	0.015 *
WBC, 10^9/L	1.630 (1.448–1.835)	<0.001	1.523 (1.286–1.803)	<0.001*
Hb, g/L	1.012 (1.002–1.023)	0.022	1.019 (0.999–1.038)	0.056
Fasting blood glucose, mmol/L	1.338 (1.168–1.532)	0.001	1.313 (1.062–1.623)	0.012 *
Creatinine, μmol/L	1.023 (1.013–1.033)	<0.001	1.017 (0.999–1.035)	0.057
hs-CRP, mg/L	1.082 (1.041–1.124)	<0.001	1.009 (0.976–1.043)	0.602
Totalcholesterol, mmol/L	1.124 (1.047–1.487)	0.013	0.983 (0.515–1.873)	0.957
HDL cholesterol, mmol/L	0.802 (0.487–1.320)	0.386		
LDLcholesterol, mmol/L	1.631 (1.305–2.391)	<0.001	0.959 (0.439–2.096)	0.916
Triglycerides, mmol/L	1.139 (0.944–1.373)	0.174		
ApoA1, mg/dl	3.027 (1.226–7.472)	0.016	4.321 (0.713–26.086)	0.112
ApoB100, mg/dl	7.062 (3.363–14.831)	<0.001	1.907 (0.555–6.549)	0.733
Lpa, mg/dl	1.001 (1.000–1.002)	0.001	1.001 (0.999–1.002)	0.380
LVEF, %	0.000 (0.000–0.004)	<0.001	0.851 (0.804–0.902)	0.006 *
Gal-3, ng/ml	1.141 (1.081–1.204)	<0.001	1.131 (1.051–1.217)	0.001*

*CAD, coronary artery disease; BMI, body mass index; DM, Diabetic mellitus; WBC, white blood cell; Hb, hemoglobin; HbA1C, hemoglobin A1C; CRP, C-reactive protein; TC, total chelosterol; HDL-C, high density lipoprotein cholesterol; LDL-C, low density lipoprotein cholesterol; TG, triglyceride; ApoA1, apolipoprotein A1; ApoB, apolipoprotein B; LP(a), Lipoprotein(a); LVEF, leftventicular ejection fraction; Gal-3, galectin-3; *P<0.05.*

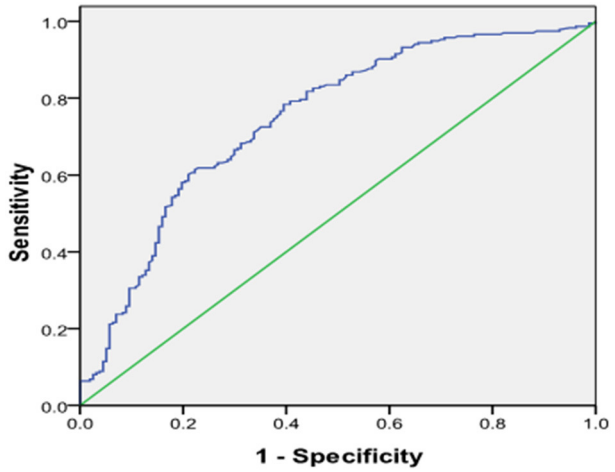

FIGURE 1 | Receiver operating characteristic (ROC) plot of serum level of galetcin-3 predicting presence of ACS. Area under the curve was 0.746, 95% CI (0.696–0.797), $P < 0.001$. When the cut-off value of galectin-3 was 3.93 ng/ml, the sensitivity was 60% with specificity 79% for predicting the presence of ACS.

lipoprotein cholesterol (LDL-C) and ApoB100 were also higher in the CAD group. The level of serum Gal-3 in the CAD group was significantly higher than that in the non-CAD group, 3.89 (0.16–63.67) vs. 2.07 (0.23–9.38) ng/ml, $P < 0.001$. To further clarify the relationship, we subsequently adjusted confounding risk factors such as age, gender, SBP, WBC, Cr, LDL-c, apoB 100, FG, and LVEF. Serum Gal-3 remained an independent risk factor for CAD with an increase of 1 ng/ml in Gal-3 associated with a 21% higher rate of presence of CAD (OR = 1.21, 95% CI: 1.07–1.38, $P = 0.003$, **Table 2**).

Serum Galectin-3 Expression in Patients With STEMI vs. NSTE-ACS vs. Stable CAD

We further divided the CAD patients into the stable coronary heart disease group (stable-CAD, $n = 95$), Non-ST segment elevation myocardial infarction (NSTE-ACS, $n = 97$) and STEMI ($n = 139$). The serum Gal-3 level in the NSTE-ACS group was higher than those in the stable CAD group, 4.72 (1.0–16.14) vs. 2.23 (0.65–23.8) ng/ml, $P = 0.04$. The same trend was found in the STEMI group compared with the stable-CAD group 7.87 (0.59–63.67) vs. 2.23 (0.65–23.8) ng/ml, $P < 0.001$ see in **Table 3**. Univariate and multivariate logistic regression analysis showed that after adjusting for other risk factors, Gal-3 was an independent risk factor for ACS, with an OR = 1.131 (95% CI: 1.051–1.217, $P = 0.001$) (**Table 4**). Receiver operator characteristic (ROC) analysis showed that the area under the curve for serum Gal-3 level predicting ACS was 0.746 (95% CI: 0.696–0.797) and the best cut-off value was 3.93 ng/ml, with a specificity of 79% and a sensitivity of 60% (**Figure 1**).

Serum Galectin-3 Expression in Patients With High vs. Low SYNTAX Scores

To explore the correlation between the level of serum Gal-3 and the plaque burden of CAD, we calculated the coronary SS of each CAD patient and divided the patients into a low SS (<22, $n = 248$) and a high SS group (≥22, $n = 83$). The serum Gal-3 expression of the high SS group was significantly higher than that

TABLE 5 | The baseline clinical and biochemical characteristics of the low SS group and High SS group.

Variable	SS < 22, *n* = 280	SS ≥ 22, *n* = 51	*P*-value
Age, years	60.49 ± 11.88	62.49 ± 11.20	0.198
Gender male sex, % (*n*)	222 (79.3)	46 (90.2)	0.048
BMI, kg/m^2	24.16 ± 2.51	23.81 ± 2.93	0.137
Hypertension, % (*n*)	164 (58.6)	31 (60.7)	0.887
DM, % (*n*)	56 (20)	9 (17.6)	0.848
History of hyperlipidemia, % (*n*)	12 (4.28)	0 (0)	0.225
Smoking, % (*n*)	117 (41.8)	18 (35.3)	0.389
Systolic blood pressure, mm Hg	135.36 ± 22.65	132.19 ± 23.89	0.364
WBC, 109/L	10.03 (4.01–28.7)	11.25 (6.39–21.25)	0.752
Hb, g/L	141 (69–274)	140 (84–223)	0.482
Creatinine, μmol/l	84.72 ± 24.70	90.62 ± 25.70	0.152
hs-CRP, mg/l	2.3 (0–183)	2.25 (0–50)	0.384
Fasting blood glucose, mmol/L	5.8 (3.70–15.24)	6.0 (4.03–18.79)	0.697
Hemoglobin A1c, %	6 (4.6–14.5)	6.0 (4.5–13)	0.325
Total cholesterol, mmol/L	4.52 ± 1.21	4.49 ± 1.35	0.872
HDL cholesterol, mmol/L	1.029 (0.07–4.62)	1.05 (0.17–2.46)	0.159
LDL cholesterol, mmol/L	2.82 ± 1.06	2.80 ± 1.19	0.923
Triglycerides, mmol/L	1.54 (0.49–7.93)	1.38 (0.54–6.87)	0.591
ApoA1, mg/dl	1.07 (0.46–1.99)	1.06 (0.74–1.74)	0.683
ApoB100, mg/dl	0.96 (0.26–2.91)	0.95 (0.41–2.21)	0.864
Lpa, mg/dl	175 (0–3,440)	253 (0–1,961)	0.116
LA diameter, mm	33.28 ± 4.31	33.03 ± 3.06	0.705
LV diameter, mm	46 (35–69)	46 (40–58)	0.592
LVEF,%	57 (31–87)	62 (35–85)	0.595
Gal-3, ng/ml	3.48 (0.16–63.67)	5.62 (1.64–60.15)	0.037

CAD, coronary artery disease; WBC, white blood cell; Hb, hemoglobin; HbA1C, hemoglobin A1C; CRP, C-reactive protein; TC, total chelosterol; HDL-C, high density lipoprotein cholesterol; LDL-C, low density lipoprotein cholesterol; TG, triglyceride; ApoA1, apolipoprotein A1; ApoB, apolipoprotein B; LP(a), Lipoprotein (a); LVEF, left venticular ejection fraction; Gal-3, galectin-3.
**P < 0.05.*

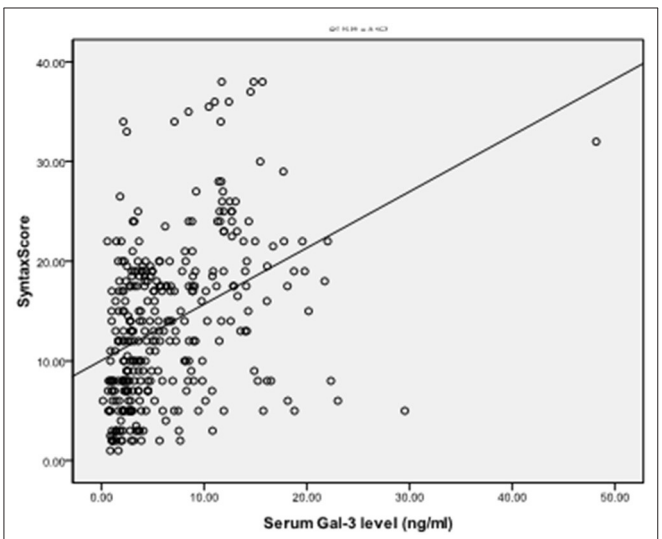

FIGURE 2 | Positive correlation of serum Gal-3 with Syntax Score (SS), $r = 0.397$, $P < 0.001$.

of the low SS group 5.62 (1.64–60.15) vs. 3.48 (0.16–63.67) ng/ml, $P = 0.037$, see in **Table 5**. Spearman correlation analysis showed that the serum Gal-3 levels were positively correlated with SS ($r = 0.397$, $P < 0.001$) (**Figure 2**). Multivariate logistic regression analysis showed that after adjusting for other risk factors, serum Gal-3 level remained a risk factor for high SS (OR = 1.030, 95% CI: 1.021–1.047, $P = 0.038$) (**Table 6**).

The Value of Serum Gal-3 Level in Predicting 1-Year MACEs in ACS Patients

Four patients were lost during follow-up, three of which were in the Gal-3 >4.78 ng/ml group while the other one was in the Gal-3 ≤ 4.78 ng/ml. Kaplan-Meier analysis showed that 1-year MACEs were significantly higher in the high Gal-3 group (Gal-3 >4.78 ng/ml) than in the low Gal-3 group (Gal-3 ≤ 4.78 ng/ml), $P = 0.036$ (**Figure 3**). Logistic regressions showed that after adjusting other confounding risk factors, Gal-3 remained an independent risk factor for the cumulative rate of MACEs in ACS patients. A 6% higher rate of presence of MACEs per 1 ng/ml increment in Gal-3 level (**Table 7**).

TABLE 6 | Univariate and multivaiate logistic regression analysis for risk factors attributing to high SS (SS>22) in the CAD patient.

Variable	Univariate analysis		Multivariateanalysis	
	OR (95% CI)	*P*	OR (95% CI)	*P*
Gender male sex, % (*n*)	2.146 (1.055–4.367)	0.035	2.418 (1.013–5.773)	0.047*
WBC, 10^9/L	1.071 (1.001–1.146)	0.048	1.040 (0.957–1.130)	0.355
Fasting blood glucose, mmol/L	1.145 (1.031–1.271)	0.011	1.088 (0.951–1.245)	0.220
hs-CRP, mg/l	1.015 (1.001–1.030)	0.039	1.006 (0.991–1.021)	0.462
Total cholesterol, mmol/L	1.071 (0.861–1.333)	0.536		
HDL cholesterol, mmol/L	0.588 (0.271–1.276)	0.179		
LDL cholesterol, mmol/L	1.154 (0.903–1.475)	0.251		
Triglycerides, mmol/L	0.927 (0.723–1.188)	0.548		
ApoA1, mg/dl	0.914 (0.302–2.768)	0.874		
ApoB100, mg/dl	1.641 (0.839–3.207)	0.148		
Lpa, mg/dl	1.00 (1.000–1.001)	0.206		
LV diameter, mm	1.063 (1.006–1.123)	0.030	1.027 (0.955–1.105)	0.470
LVEF,%	0.058 (0.006–0.604)	0.017	0.724 (0.026–20.300)	0.849
Gal-3, ng/ml	1.047 (1.020–1.076)	0.001	1.031 (1.021–1.047)	0.038*

CAD, coronary artery disease; WBC, white blood cell; Hb, hemoglobin; HbA1C, hemoglobin A1C; CRP, C-reactive protein; TC, total chelosterol; HDL-C, high density lipoprotein cholesterol; LDL-C, low density lipoprotein cholesterol; TG, triglyceride; ApoA1, apolipoprotein A1; ApoB, apolipoprotein B; LP(a), lipoprotein(a); LVEF, left venticular ejection fraction; Gal-3, galectin-3.

*$P < 0.05$.

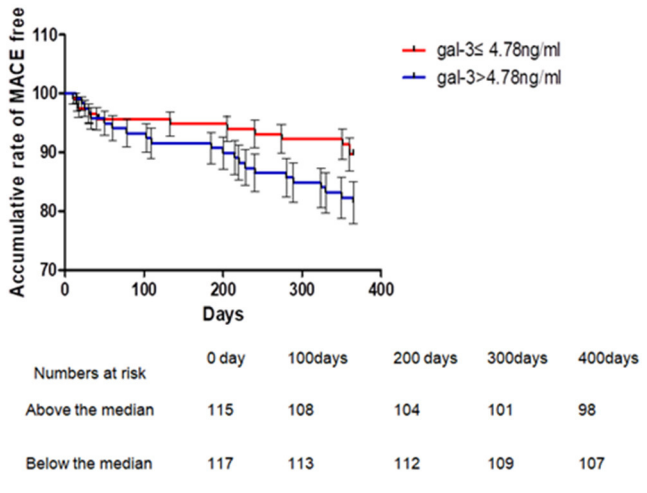

FIGURE 3 | Kaplan-Meier's curves for 1 year MACE according to levels above or below median of serum Gal-3 in patients with ACS. One-year MACE events were significantly higher in Gal-3 >4.78 ng/ml group than that in the Gal-3 = 4.78 ng/ml group, $P = 0.036$ (Breslow). ACS, acute coronary syndrome.

DISCUSSION

The main findings of the present study were as follows. (1) Serum Gal-3 was significantly higher in CAD patients than in non-CAD patients and was higher in ACS patients than in stable CAD patients. (2) Galectin-3 was an independent predictor of the presence of CAD as well as the presence of non-stable CAD (ACS). (3) Galectin-3 positively correlated with the complexity of CAD and was an independent risk factor for a high SS. (4) A high level of serum Gal-3 was associated with a higher rate of MACEs in ACS patients over the 1 year of follow up.

Inflammation and oxidative stress play a key role in all stages of atherosclerosis, from initiation to progression of atheromatous plaque, finally leading to ACS (18). In recent years, the role of many new inflammatory-related markers in CVD has been explored, including secret frizzled related proteins (19, 20), gut microbiota produced trimethylamine N-oxide (TMAO) (21), Gal-3 (22), etc. Galectin-3 is a macrophage- and endothelium-derived mediator actively involved in the regulation of many aspects of inflammatory cell behavior (12). It has been found to be involved in proliferation, macrophage chemotaxis, phagocytosis, neutrophil extravasation, and deposition of type-1 collagen in the ECM, resulting in adverse matrix remodeling (23). Clinically, limited data have shown that plasma Gal-3 is significantly higher in CAD patients than in non-CAD patients. However, the precise role of Gal-3 in CAD remains unclear; more data are needed to determine the association between circulating Gal-3 and atherosclerosis. Abayomi Oyenuga et al. showed that higher levels of Gal-3 were associated with greater carotid atherosclerosis (24). In the present study, we found that serum Gal-3 was significantly higher in CAD patients than in non-CAD patients and that Gal-3 was an independent predictor of the presence of CAD. Our data are consistent with previous results (11). Furthermore, we found that Gal-3 levels were positively correlated with WBC count and hs-CRP levels. Although this correlation was weak, these data support the hypothesis that Gal-3 is involved in inflammation and contributes to the formation of atherosclerosis.

Galectin-3 is not only involved in the formation of atherosclerotic plaques but may also contribute to plaque destabilization. To date, it hasn't reached an agreement on the role of Gal-3 on plaque stability, and clinical study and experimental study showed conflicting results (12, 18, 25–29). Current evidence has shown that Gal-3 may play a dual role in plaque instability (22). Our study showed that serum Gal-3 was

TABLE 7 | Association between serum Gal-3 and incident rate of MACEs.

Gal-3	Incident rate	Model 1		Model 2		Model 3		Model 4	
		OR (95%CI)	*P*-value	OR (95%CI)	*P*-value	OR (95%CI)	*P*-value	OR (95%CI)	*P*-value
Per ng/ml	26/236	1.051 (1.010, 1.094)	0.014	1.065 (1.018, 1.114)	0.007	1.058 (1.011,1.108)	0.015	1.060 (1.010, 1.112)	0.017

Model 1, adjusted for age, gender; Model 2, further adjusted for Cr, apoB 100; Model 3, further adjusted for fasting glucose, number of lesion vessels; Model 4, further adjusted for N-Terminal Pro-Brain Natriuretic Peptide, Troponin T.

higher in ACS patients than in stable CAD and non-CAD patients and was an independent predictor of the presence of ACS with a specificity of 79% and a sensitivity of 60% for a cut-off value of 3.93 ng/ml. Our data was in favor of the conception that gal-3 was positively correlated with plaque destabilization. To date, no firm conclusions about the action of Gal-3 (pro-inflammatory vs. anti-inflammatory) during atherosclerosis evolution in rodents have been drawn. More data are needed to clarify the relationship between coronary plaque destabilization and plasma levels of Gal-3.

The SS was developed as a tool to assess the complexity of coronary lesions in the SYNTAX (Synergy between Percutaneous Coronary Intervention with TAXUS and Cardiac Surgery) study. This score adds many characteristics to the simple definition of the number of diseased vessels related to the severity of CAD and has also been indicated to have the prognostic ability (30). To date, few studies have explored the correlation between Gal-3 and SS (18, 31). Aksan et al. found that the plasma concentration of Gal-3 was higher in high SS CAD patients but was not an independent risk factor for high SS after adjusting for other confounding risk factors (19). Turan et al. found that Gal-3 was independently associated with SS (31). In this study, we found that Gal-3 levels were positively correlated with SS. The serum Gal-3 level was shown to be a risk factor for high SS, even after adjusting for other risk factors. The different number of samples and high cut-off SS values may have contributed to the differences in the results. Our data indicated that Gal-3 could be used as a valuable biomarker for the assessment of the severity of CAD.

In our study, we found that serum Gal-3 was positively correlated with LDL-C and ApoB100. It is well known that the interaction between dyslipidemia and inflammation is the basis of atherosclerosis, and many inflammatory factors are involved in the regulation of lipid metabolism disorders (3, 32). This may be evidence that Gal-3 directly regulates cholesterol metabolism, which is an interesting topic that deserves further exploration.

LIMITATIONS

This study has several limitations. First, it is a single center retrospective cohort study and investigated only a relatively small number of patients, further prospective studies with larger sample sizes should be conducted to explore the relationship between Gal-3 and CAD. Second, as it was an observational study, we could not exclude residual confounding factors, despite we had adjusted for potential covariates as much as possible. Thirdly, timing of interventional treatment for ACS was an important confounding risk factor that has an impact on the prognosis. However, data were lacking in our study, which was one of the limitations of the study. Finally, we did not assess serial changes in circulating levels of Gal-3 among STEMI patients and there was evidence that showed that Gal-3 was in dynamic changes during acute phage.

CONCLUSION

Galectin-3 correlated with the presence of CAD as well as coronary stability and complexity. Galectin-3 may be valuable in predicting mid-term prognosis in ACS patients.

DATA AVAILABILITY STATEMENT

The original contributions presented in the study are included in the article/**Supplementary Material**, further inquiries can be directed to the corresponding author/s.

ETHICS STATEMENT

The studies involving human participants were reviewed and approved by Ethics Committee on Clinical Scientific Research and Laboratory Animal of Zhongshan People's Hospital approved the study. The patients/participants provided their written informed consent to participate in this study.

AUTHOR CONTRIBUTIONS

ML wrote and edited the manuscript. KG, XH, LF, YY, JL, and YL collected the research data for the article. ZG reviewed the manuscript and approved the final manuscript. All authors contributed to the article and approved the submitted version.

ACKNOWLEDGMENTS

We thank JL for his great help in follow-up information collection.

SUPPLEMENTARY MATERIAL

The Supplementary Material for this article can be found online at: https://www.frontiersin.org/articles/10.3389/fcvm.2022.818162/full#supplementary-material

REFERENCES

1. Roth GA, Johnson C, Abajobir A, Abd-Allah F, Ferede AS, Murray C, et al. Global, regional, and national burden of cardiovascular diseases for 10 causes, 1990 to 2015. *J Am Coll Cardiol.* (2017) 70:1–25. doi: 10.1016/j.jacc.2017.04.052
2. Bonow RO, Smaha LA, Smith Jr SC, Mensah GA, Lenfant C. World Heart Day 2002: the international burden of cardiovascular disease: responding to the emerging global epidemic. *Circulation.* (2002) 106:1602–5. doi: 10.1161/01.CIR.0000035036.22612.2B
3. Lusis AJ. Atherosclerosis. *Nature.* (2000) 407:233–41. doi: 10.1038/35025203
4. Yongsakulchai P, Settasatian C, Settasatian N. Senthong V. Association of combined genetic variations in PPARγ, PGC-1α, and LXRα with coronary artery disease and severity in Thai population. *Atherosclerosis.* (2016) 248:140–8. doi: 10.1016/j.atherosclerosis.2016.03.005
5. Suthahar N, Meijers WC, Sillje HH, Ho JE, Liu FT, de Boer RA. Galectin-3 activation and inhibition in heart failure and cardiovascular disease: an update. *Theranostics.* (2018) 8:593–609. doi: 10.7150/thno.22196
6. Dumic J, Dabelic S, Flögel M. Galectin-3: an open-ended story. *Biochim Biophys Acta.* (2006) 1760:616–35. doi: 10.1016/j.bbagen.2005.12.020
7. Ruvolo PP. Galectin 3 as a guardian of the tumor microenvironment. *Biochim Biophys Acta.* (2016) 1863:427–37. doi: 10.1016/j.bbamcr.2015.08.008
8. Di Lella S, Sundblad V, Cerliani JP, Guardia CM, Estrin DA, Vasta GR, et al. When galectins recognize glycans: from biochemistry to physiology and back again. *Biochemistry.* (2011) 50:7842–57. doi: 10.1021/bi201121m
9. Li M, Yuan Y, Guo K, Huang XS, Lao Y, Feng L. Value of galectin-3 in acute myocardial infarction. *Am J Cardiovasc Drugs.* (2019) 20:333–42. doi: 10.1007/s40256-019-00387-9
10. Madrigal-Matute J, Lindholt JS, Fernandez-Garcia CE, BenitoMartin A, Burillo E, Zalba G, et al. Galectin-3, a biomarker linking oxidative stress and infammation with the clinical outcomes of patients with atherothrombosis. *J Am Heart Assoc.* (2014) 3:e000785. doi: 10.1161/JAHA.114.000785
11. Kusaka H, Yamamoto E, Hirata Y, Fujisue K, Tokitsu T, Sugamura K, et al. Clinical significance of plasma galectin-3 in patients with coronary artery disease. *Int J Cardiol.* (2015) 201:532–4. doi: 10.1016/j.ijcard.2015.08.099
12. Falcone C, Lucibello S, Mazzucchelli I, Bozzini S, D'Angelo A, Schirinzi S, et al. Galectin-3 plasma levels and coronary artery disease: a new possible biomarker of acute coronary syndrome. *Int J Immunopathol Pharmacol.* (2011) 24:905–13. doi: 10.1177/039463201102400409
13. Ghorbani A, Bhambhani V, Christenson RH, Meijers WC, de Boer RA, Levy D, et al. Longitudinal change in galectin-3 and incident cardiovascular outcomes. *J Am Coll Cardiol.* (2018) 72:3246–54. doi: 10.1016/j.jacc.2018.09.076
14. Ibanez B, James S, Agewall S, Antunes MJ, Bucciarelli-Ducci C, Buen H, et al. 2017 ESC Guidelines for the management of acute myocardial infarction in patients presenting with ST-segment elevation: The Task Force for the management of acute myocardial infarction in patients presenting with ST-segment elevation of the European Society of Cardiology (ESC). *Eur Heart J.* (2018). 39:119–77. doi: 10.1093/eurheartj/ehx393
15. Roffi M, Patrono C, Collet JP, Mueller C, Valgimigli M, Andreotti F, et al. 2015 ESC guidelines for the management of acute coronary syndromes in patients presenting without persistent ST-segment elevation: Task Force for the Management of Acute Coronary Syndromes in Patients Presenting without Persistent ST-Segment Elevation of the European Society of Cardiology (ESC). *Eur Heart J.* (2016). 37:267–315. doi: 10.1093/eurheartj/ehv320
16. Task Force Members, Montalescot G, Sechtem U, Achenbach S, Andreotti F, Arden C. et al. 2013 ESC guidelines on the management of stable coronary artery disease: the Task Force on the management of stable coronary artery disease of the European Society of Cardiology. *Eur Heart J.* (2013). 34:2949–3003. doi: 10.1093/eurheartj/eht296
17. Ludman PF, Stephens NG, Harcombe A, Lowe MD, Shapiro LM, Schofield PM, et al. Radial versus femoral approach for diagnostic coronary angiography. *Am J Cardiol.* (1997) 9:1239–41. doi: 10.1016/S0002-9149(97)00089-1
18. Tsai TH, Sung PH, Chang LT, Sun CK, Yeh KH, Chung SY, Chua S, et al. Value and level of galectin-3 in acute myocardial infarction patients undergoing primary percutaneous coronary intervention. *J Atheroscler Thromb.* (2012) 19:1073–82. doi: 10.5551/jat.12856
19. Wu J, Zheng H, Liu X, Chen P, Zhang Y, Luo J, et al. Prognostic value of secreted frizzled-related protein 5 in heart failure patients with and without type 2 diabetes mellitus. *Circ Heart Fail.* (2020) 13:e007054. doi: 10.1161/CIRCHEARTFAILURE.120.007054
20. Huang A, Huang Y. Role of Sfrps in cardiovascular disease. *Ther Adv Chronic Dis.* (2020) 11:2040622320901990. doi: 10.1177/2040622320901990
21. Li W, Huang A, Zhu H, Liu X, Huang X, Huang Y, et al. Gut microbiota-derived trimethylamine N-oxide is associated with poor prognosis in patients with heart failure. *Med J Aust.* (2020) 213:374–9. doi: 10.5694/mja2.50781
22. Gao Z, Liu Z, Wang R, Yang, L. Galectin-3 is a potential mediator for atherosclerosis. *J Immunol Res.* (2020) 2020:5284728. doi: 10.1155/2020/5284728
23. Aksan G, Gedikli Ö, Keskin K, Nar G, Inci S, Yildiz SS, et al. Is galectin-3 a biomarker, a player-or both-in the presence of coronary atherosclerosis? *J Investig Med.* (2016) 64:764–70. doi: 10.1136/jim-2015-000041
24. Oyenuga A, Folsom AR, Fashanu O, Aguilar D, Ballantyne CM, et al. Plasma galectin-3 and sonographic measures of carotid atherosclerosis in the atherosclerosis risk in communities study. *Angiology.* (2019) 70:47–55. doi: 10.1177/0003319718780772
25. Menini S, Iacobini C, Ricci C, Blasetti Fantauzzi C, Salvi L, Pesce CM, et al. The galectin-3/RAGE dyad modulates vascular osteogenesis in atherosclerosis. *Cardiovasc Res.* (2013) 100:472–80. doi: 10.1093/cvr/cvt206
26. Lin YH, Lin LY, Wu YW, Chien KL, Lee CM, Hsu RB, et al. The relationship between serum galectin-3 and serum markers of cardiac extracellular matrix turnover in heart failure patients. *Clin Chim Acta.* (2009) 409:96–9. doi: 10.1016/j.cca.2009.09.001
27. Papaspyridonos M, McNeill E, de Bono J, Smith A, Burnand KG, Channon KM, et al. Galectin-3 is an amplifer of infammation in atherosclerotic plaque progression through macrophage activation and monocyte chemoattraction. *Arterioscler Thromb Vasc Biol.* (2008) 28:433–40. doi: 10.1161/ATVBAHA.107.159160
28. Iacobini C, Menini S, Ricci C, Scipioni A, Sansoni V, Cordone S, et al. Accelerated lipid-induced atherogenesis in galectin-3-deficient mice: role of lipoxidation via receptor-mediated mechanisms. *Arterioscler Thromb Vasc Biol.* (2009) 29:831–6. doi: 10.1161/ATVBAHA.109.186791
29. Kadoglou NP, Sfyroeras GS, Spathis A, Gkekas C, Gastounioti A, Mantas G, et al. Galectin-3, carotid plaque vulnerability, and potential effects of statin therapy. *Eur J Vasc Endovasc Surg.* (2015) 49:4–9. doi: 10.1016/j.ejvs.2014.10.009
30. Sianos G, Morel M-A, Kappetein AP, Morice M-C, Colombo A, Dawkins K, et al. The SYNTAX Score: an angiographic tool grading the complexity of coronary artery disease. *EuroIntervention.* (2005) 1:219–27.
31. Turan Y, Demir V. The relation of endocan and galectin-3 with ST-segment resolution in patients with ST-segment elevation myocardial infarction. *Adv Clin Exp Med.* (2020) 29:453–8. doi: 10.17219/acem/118126
32. Steinberg, D. Atherogenesis in perspective: hypercholesterolemia and inflammation as partners in crime. *Nat Med.* (2002). 8:1211–7. doi: 10.1038/nm1102-1211

Conflict of Interest: The authors declare that the research was conducted in the absence of any commercial or financial relationships that could be construed as a potential conflict of interest.

Publisher's Note: All claims expressed in this article are solely those of the authors and do not necessarily represent those of their affiliated organizations, or those of the publisher, the editors and the reviewers. Any product that may be evaluated in this article, or claim that may be made by its manufacturer, is not guaranteed or endorsed by the publisher.

Copyright © 2022 Li, Guo, Huang, Feng, Yuan, Li, Lao and Guo. This is an open-access article distributed under the terms of the Creative Commons Attribution License (CC BY). The use, distribution or reproduction in other forums is permitted, provided the original author(s) and the copyright owner(s) are credited and that the original publication in this journal is cited, in accordance with accepted academic practice. No use, distribution or reproduction is permitted which does not comply with these terms.

frontiers in Cardiovascular Medicine

ORIGINAL RESEARCH
published: 10 February 2022
doi: 10.3389/fcvm.2022.821553

Prognostic Value of β1 Adrenergic Receptor Autoantibody and Soluble Suppression of Tumorigenicity-2 in Patients With Acutely Decompensated Heart Failure

Yanxiang Sun, Li Feng, Bing Hu, Jianting Dong, Liting Zhang, Xuansheng Huang and Yong Yuan**

Department of Cardiology, Zhongshan People's Hospital, Sun Yat-sen University, Zhongshan, China

OPEN ACCESS

Edited by:
Yuli Huang,
Southern Medical University, China

Reviewed by:
Jiandi Wu,
Foshan Second People's Hospital, China
Chen Yequn,
Shantou University, China

***Correspondence:**
Xuansheng Huang
peanuthuang@163.com
Yong Yuan
2637240556@qq.com

Specialty section:
This article was submitted to General Cardiovascular Medicine, a section of the journal Frontiers in Cardiovascular Medicine

Received: *24 November 2021*
Accepted: *10 January 2022*
Published: *10 February 2022*

Citation:
Sun Y, Feng L, Hu B, Dong J, Zhang L, Huang X and Yuan Y (2022) Prognostic Value of β1 Adrenergic Receptor Autoantibody and Soluble Suppression of Tumorigenicity-2 in Patients With Acutely Decompensated Heart Failure. Front. Cardiovasc. Med. 9:821553. doi: 10.3389/fcvm.2022.821553

Background: Both β1 adrenergic receptor autoantibody (β1-AA) and soluble suppression of tumorigenicity-2 (sST2) take a role in the pathological remodeling of heart failure. However, limited studies investigated the correlation between the expression of β1-AA and sST2 in patients with acutely decompensated heart failure (ADHF).

Objective: To explore the correlation between β1-AA and sST2, and evaluate their prognostic value in patients with ADHF.

Methods: Patients who were admitted for ADHF were included. The N-terminal pro-brain natriuretic peptide (NT-proBNP), sST2, and β1-AA in blood samples were tested at hospital admission and then followed up for assessing the outcomes. Pearson correlation analysis was used to explore the correlation between β1-AA and sST2. The effects of β1-AA, sST2, or the combination of them on the all-cause mortality of patients with ADHF were assessed by Multivariate Cox regression analysis.

Results: There were 96 patients with ADHF and 96 control populations enrolled. The β1-AA was significantly higher in ADHF than in the control group (0.321 ± 0.06 vs. 0.229 ± 0.04, $P = 0.000$). Pearson correlation analysis showed that β1-AA was positively correlated with sST2 ($r = 0.593$), NT-proBNP ($r = 0.557$), Procalcitonin ($r = 0.176$), and left ventricular end-diastolic diameter ($r = 0.315$), but negatively correlated with triglycerides ($r = -0.323$), and left ventricular ejection fraction ($r = -0.430$) (all $P < 0.05$) in ADHF. Patients with ADHF, complicated with both high β1-AA and sST2, showed the highest all-cause mortality during an average of 25.5 months of follow-up. Multivariate Cox regression showed the combination of both high β1-AA and sST2 independently correlated with the all-cause mortality after adjustment for other risk factors (hazard ratio 3.348, 95% CI 1.440 to 7.784, $P = 0.005$). After adding with β1-AA and sST2, the area under the curves for the prognostic all-cause mortality could increase from 0.642 to 0.748 ($P = 0.011$).

Conclusion: The β1-AA is positively correlated with sST2 in patients with ADHF. Elevated plasma β1-AA and sST2 level in patients with ADHF are associated with poorer prognoses.

Keywords: β1 adrenergic receptor (β1-AR), autoantibodies, heart failure, soluble suppression of tumorigenicity-2 (sST2), mortality

INTRODUCTION

Heart failure (HF) is a terminal stage of heart disease characterized by high mortality, which becomes more and more prevalent and brings a huge burden to health care (1). Acutely decompensated HF (ADHF) may have a higher in-hospital mortality risk (2). On the other hand, HF is associated with various pathophysiological and biochemical disorders. No single biomarker can display all these characteristics. Therefore, earlier identification of patients with ADHF, with high mortality risk and more sensitive assessing prognosis by the combination of cardiac multi markers that implement effective cardiovascular preventive measures, can improve the survival of those patients.

The β1 adrenergic receptor (β1-AR) is a G protein-coupled receptor that triggers physiological or pathological responses *via* activating the signaling cascade of adenylate cyclase, cyclic adenosine 3',5'-monophosphate, and protein kinase A. This signaling pathway regulates intracellular calcium concentration and determines cardiomyocyte contractility (3). The β1 adrenergic receptor autoantibody (β 1-AA) is a kind of autoantibody existing in the serum of patients with heart failure (4), which binds to the second extracellular loop of the β1-AR. The β1-AA is found in 30–75% of patients with dilated cardiomyopathy (DCM) (5, 6), which appear to be functionally active and are associated with a markedly worse prognosis in DCM (7). The β 1-AA is characterized by continuous activation without desensitization in HF, which result in intracellular calcium overload and myocardial apoptosis, promoting cardiac remodeling, prolonging QT dispersion to malignant arrhythmias, and cardiac sudden death (5, 8). Studies on clinical heart failure found that the β 1-AA can be antagonized by β-blockers and can be eliminated through immunoadsorption, which reverses the pathological remodeling and improves cardiac function (9, 10).

Soluble suppression of tumorigenicity-2 (sST2) has been implicated in the pathogenesis of myocardial fibrosis and remodeling in HF (11). The sST2 concentration is not influenced by age, kidney function, or body mass index, unlike the natriuretic peptides (12). So, the sST2 provides additional prognostic value over N-terminal pro-brain natriuretic peptide (NT-proBNP) in the prediction of death in patients with ADHF (13). At present, the sST2 assay has been tested for diagnosis and prediction in either acute or chronic HF populations (13, 14).

The involvement of both β1-AA and sST2 in the pathological remodeling of HF suggests a relationship between them. However, few studies investigated the correlation between the expression of β1-AA and sST2 in patients with ADHF. The current study aimed to analyze the correlation between the β1-AA and sST2. Furthermore, we also investigated whether the combination of β1-AA and sST2 was more accurate than β1-AA or sST2 alone in predicting the short-term survival in patients with ADHF.

MATERIALS AND METHODS

Study Population

The study was approved by the Medical Ethics Committee of the Zhongshan People's Hospital, Guandong Province, China. All the participants in this study had signed written informed consents.

According to the 2021 European Society of Cardiology (ESC) Guidelines for the diagnosis and treatment of acute and chronic heart failure (2), the patients included in the study should have the signs and symptoms which indicated they had an attack of new-onset HF or acutely decompensated chronic HF (e.g., dyspnea, edema, weight gain). Also, they should be observed with elevated levels of NT-proBNP and the impaired systolic or diastolic function of the heart by echocardiography. The control populations without heart failure were from the physical examination center or outpatient clinic of Zhongshan People's Hospital. The exclusion criteria were age <18 years, acute coronary syndrome, unstable hemodynamics, cardiac surgery, malignant tumor, serious hepatic dysfunction (ALT ≥3ULN), kidney insufficiency (eGFR<60 ml/min·1.73m^2 or Scr ≥ 265 umol/L), and cerebrovascular diseases. Between November 2018 and October 2019, 228 patients with ADHF were enrolled prospectively. At last, 96 patients with ADHF were enrolled because of deaths during hospitalization, loss to follow-up, and missing data. Ninety-six control populations without heart failure were selected for baseline comparison.

Baseline Data Collection

Clinical data of each patient would be collected including age, gender, hypertension and diabetes history, and smoking. Furthermore, the results of laboratory examination such as Serum Creatinine (Scr), Total cholesterol (TC), Low-Density Lipoprotein Cholesterol (LDL-c), triglycerides (TG), C-reactive protein (CRP), and Procalcitonin (PCT) would be recorded. Left ventricular ejection fraction (LVEF) and left ventricular end-diastolic diameter (LVEDd) were tested with Simpson's method. Blood samples for the tests were obtained from each participant within the first 24 h after admission. We centrifuged blood samples at 18,000 g for 10 min and stored the serum samples at −80°C.

Follow-Up

The follow-up period would start from the first day when the participants were discharged. The subjects would be investigated by the cardiologists. All the patients with ADHF were treated with standard HF management according to the current

clinical practice guidelines, the control group were treated with antihypertensive or antidiabetic drugs if needed. Data of an all-cause mortality was collected with the means of regular telephone interviews, administrative databases, and medical records monthly.

Biochemical Measurement

The serum sample of β1-AA was sent to the Laboratory of Cardiovascular Immunology, Union Hospital, Tongji Medical College of Huazhong University of Science and Technology. The level of β1-AA was measured by the enzyme linked immunosorbent assay (ELISA) as previously described (15). The optical density (OD) was determined using an ELISA plate reader at 450 nm. Serum sST2 was measured with a human ST2 Quantikine ELISA Kit (R&D Systems, Inc., Minneapolis, Minnesota, United States). Serum NT-proBNP was tested by electrochemiluminescence immunoassay (Roche, Basel, Switzerland).

Statistical Analysis

Data were expressed as mean ± SEM or median (interquartile range, IQR). Comparison of continuous variables between two groups was performed by analysis of variance with the independent-sample student's *t*-test. Otherwise, the rank-sum test was used. Categorical data such as the incidence of disease were analyzed by chi-square test. Pearson correlation analysis was used for correlation analysis between β1-AA and sST2. Kaplan-Meier assessed the effect of different levels of β1-AA and sST2 (above or below mean) on the survival rate of patients with heart failure by Log-rank test. Cox regression analysis and LR Forward ($P < 0.05$ in, >0.1 out) was performed to identify the risk factors for an all-cause mortality. To evaluate the improvement in predictive accuracy, we built the receiver operating characteristic (ROC) curves of the risk prognostic models and calculated the area under the curves (AUC), respectively. The comparisons between models by a pair-wise method were performed with the method of Hanley JA and McNeil BJ (16). The IBM SPSS Statistics 26.0 software was used for statistical analysis (IBM SPSS Inc., Chicago, USA). Values of $P < 0.05$ were considered to denote statistical significance.

RESULTS

Patient Characteristics

The baseline characteristics of patients with ADHF and the control population enrolled were shown in **Table 1**. There was no significant difference in age, gender, LDL level, hypertension, and smoking history between the two groups, but the incidence of diabetes ($P = 0.018$) and median follow-up of an all-cause death ($P < 0.01$) were significantly higher in the ADHF group than in the control group. The TC and TG in the ADHF group (4.11 ± 1.14 mmol/L and 1.16 ± 0.53 mmol/L) were lower than the control group (4.58 ± 0.98 mmol/L and 1.70±0.62 mmol/L), but the mean concentration of NT-proBNP and sST2 is 5543 (IQR, 2,889.75, 10,667.25) pg/ml and 21.21 (IQR, 12.89, 41.26) ng/ml in the ADHF group, which were significantly higher than those in the control group. Left ventricular ejection fraction (LVEF) in the ADHF group (46.15%±10.43%) was lower than that in the control group (65.53%±6.11%), while LVEDD was significantly higher in the ADHF group (53.85 ± 10.49 mm) than that in the control group (46.02 ± 4.83 mm). The OD value of β 1-AA in the ADHF group (0.321±0.06) was also significantly higher than that in the control group (0.229±0.04). The levels of PCT, serum creatinine, and C-reactive protein in the ADHF group were higher than those in the control group (all *P*-values <0.01).

TABLE 1 | Baseline characteristics of patients.

	ADHF (*N* = 96)	Control (*N* = 96)	*P*
Male, *n* (%)	54 (56.5%)	53 (55.2%)	0.500
Age (years)	71.53 ± 14.24	70.69 ± 12.57	0.668
Hypertension, *n* (%)	59 (61.6%)	54 (56.3%)	0.279
Diabetes, *n* (%)	23 (23.9%)	11 (11.5%)	0.018
Mortality, *n* (%)	39 (40.6%)	0 (0)	0.000
Smoking, *n* (%)	39 (40.6%)	31 (32.3%)	0.147
NT-proBNP (pg/mL) $^{\Delta}$	5,543 (2,889.75, 10,667.25)	93.80 (27.25,187.50)	0.000
sST2 (ng/mL) $^{\Delta}$	21.21 (12.89,41.26)	8.49 (4.79, 13.81)	0.000
β1-AA OD	0.321 ± 0.06	0.229 ± 0.04	0.000
LVEF%	46.15 ± 10.43	65.53 ± 6.11	0.000
LVEDd (mm)	53.85 ± 10.49	46.02 ± 4.83	0.000
TC (mmol/L)	4.11 ± 1.14	4.58 ± 0.98	0.000
TG (mmol/L)	1.16 ± 0.53	1.7 ± 0.62	0.000
LDL-c (mmol/L)	2.53 ± 0.97	2.55 ± 0.74	0.872
PCT (ng/mL) $^{\Delta}$	0.064 (0.035, 0.133)	0.035 (0.022,0.049)	0.000
SCr (umol/L) $^{\Delta}$	107.00 (83.25, 125.75)	74.00 (62.00,90.25)	0.000
CRP (mg/L) $^{\Delta}$	10.80 (2.84, 20.30)	1.50 (0.70,3.50)	0.000

Data are presented as the x± SD, the median ($^{\Delta}$); sST2, soluble suppression of tumorigenicity-2; β1-AA, β1-adrenoceptor autoantibody; TC, Total cholesterol; TG, triglycerides; LDL-c, low-density lipoprotein cholesterol; LVEF, left ventricular ejection fraction; LVEDd, left ventricular end-diastolic diameter; NT-proBNP, N-terminal proB-type natriuretic peptide; PCT, procalcitonin; and SCr, serum creatinine.
P values are comparison between ADHF and Control groups.

Correlation Analysis Between β 1-AA and Other Indicators of Heart Failure

Age, sST2, NT-proBNP, CRP, PCT, CR, TC, TG, LVEF, and LVEDD values were included in the Pearson correlation analysis for all data. Results showed that sST2 ($r = 0.525$, $P < 0.01$) and TG ($r = -0.305$, $P < 0.01$) were correlated with the value of β1-AA in all population. In the ADHF group, sST2 ($r = 0.593$, $P < 0.01$), NT-proBNP ($r = 0.557$, P < 0.01), PCT ($r = 0.176$, $P = 0.026$), LVEDd ($r = 0.315$, $P < 0.01$), TG ($\beta = -0.323$, $P < 0.01$), and LVEF ($\beta = -0.430$, $P < 0.01$) were correlated with the β1-AA level (**Table 2**).

Effects of Different Levels of the β1-AA and SST2 on the All-Cause Mortality in Patients With ADHF

Groups were divided according to the mean of β1-AA and the median of sST2 in the patients with ADHF: the high-value group and the low-value group. Cumulative all-cause mortality was higher in the high β1-AA or sST2 groups than in the low β1-AA or sST2 groups (respectively, 25 vs.15.63%, $P = 0.017$; 26.04 vs.

TABLE 2 | Correlation between the β1-AA and indexes by Pearson correlation analysis in all population and patients with ADHF.

	All population		ADHF	
	r	*P*	*r*	*P*
sST2	0.525	0.000	0.593	0.000
NT-proBNP	0.189	0.066	0.557	0.000
TG	−0.305	0.005	−0.323	0.000
PCT	0.105	0.329	0.176	0.026
LVEDd	0.088	0.392	0.315	0.000
LVEF	−0.183	0.074	−0.430	0.000

2Log transformations were made for the sST2, NT-proBNP, and PCT in the analysis because of their skewed distribution.

TABLE 3 | The relationship between levels of the β1-AA, sST2 and the all-cause mortality in patients with ADHF by Chi-square analysis.

	All-cause mortality % (n)		*chi-square value*	*df*	*P-value*
	High	Low			
β1-AA (*N* = 96)	25% (24)	15.63% (15)	5.671	1	0.017
sST2 (*N* = 96)	26.04% (25)	14.58% (14)	6.028	1	0.014
β1-AA+sST2 (*N* = 70)	27.14% (19)	12.85% (9)	8.037	1	0.018

High: the level of β1-AA was above the mean in β1-AA line, the level of sST2 was above the median in sST2 line, the level of β1-AA and sST2 was both above their mean or median in β1-AA+ sST2 line.

Low: the level of β1-AA was below the mean in β1-AA line, the level of sST2 was below the median in sST2 line, the level of β1-AA and sST2 was both below their mean or median in β1-AA+ sST2 line.

Compared with the low value group, the all-cause mortality in the high value group was significantly increased, and P < 0.05.

14.58%, $P = 0.014$). After the combination of β1-AA and sST2, the cumulative all-cause mortality of both high-value groups was significantly higher than that of the low-value groups (27.14 vs. 12.85%, $P = 0.018$) by chi-square test (**Table 3**).

The β1-AA and SST2 Are Independent Risk Factors for an All-Cause Death in Patients With ADHF

A total of 228 patients were discharged, except for 32 deaths during hospitalization. Thirty-six other cases were lost with follow-up information and 64 data were lacking during an average of 25.5 ± 1.47 months of follow-up. There was no incidence of death in the control group during follow-up, we, thus, analyzed the effect of the β1-AA and sST2 on the prognosis only in patients with ADHF. We group according to the mean levels of β1-AA and median levels of sST2. Kaplan-Meier analysis showed that patients with high β1-AA, high sST2, and both high β1-AA and sST2 showed a higher cumulative rate of an all-cause mortality than those with low β1-AA, low sST2 and both low β1-AA and sST2 (*P* for log-rank test =0.046,0.027, and.014, respectively, **Figures 1A–C**). Multivariate Cox regression analysis showed the high β1-AA (*HR* 2.199; 95% *CI* 1.106–4.373, $P = 0.025$), high sST2(*HR* 2.333; 95% *CI* 1.173–4.638, $P = 0.016$), and the combination of both high β1-AA and sST2 (*HR* 3.348; 95% *CI* 1.440–7.784, $P = 0.005$) were independent risk factors for all-cause mortality after adjusting other risk factors (**Table 4**).

The Combination of β1-AA and SST2 Provides Incremental Prognostic Value in the Survival of Patients With ADHF

Model 1 consisted of age, diabetes, NT-proBNP, and PCT. Model 2 was made up of Model 1 and β1-AA. Model 3 was constructed by Model 1 with Log2 sST2. Model 4 was built by combining Model 1 with β1-AA and Log2 sST2. **Table 5** showed the ROC curves of models for predicting the all-cause mortality of patients with ADHF, in which the AUC of Models 1, 2, 3, and 4 were 0.642 (95% CI.519–0.765),0.714 (95% CI.599–0.830), 0.735 (95% CI.625–0.846), and.748 (95% CI.638–0.858), respectively (all $P < 0.05$). Among them, the area under the curves (AUC) of Model 2, 3 and 4 performed better than that of Model 1 (respectively, ΔAUC.072, $P = 0.041$; ΔAUC 0.093, $P = 0.018$; ΔAUC 0.106, $P = 0.011$), but the prognosis of all-cause mortality had no significant difference among Models 2, 3, and 4 (AUC4-AUC2 = 0.034, AUC4-AUC3 = 0.013, both $P > 0.05$). More details about the different ROC curves of models were shown in **Table 5**. The result showed that the risk stratification value of β1-AA and sST2 was additive in patients with ADHF.

DISCUSSION

A number of studies have suggested that the β1-AA has an important role in pathophysiological processes of heart failure (6, 9, 10, 17) The current study found that the β1-AA was positively correlated with sST2 and NT-proBNP in ADHF. Therefore, this study demonstrates for the first time the internal relationship between the expression of β1-AA and sST2. It has been suggested that the inflammatory factors, including interleukine-6 (IL-6), various viral and microbial candidate proteins can promote β1AR-directed autoimmune cardiomyopathy through enhancing the β1-AA production (15, 18, 19). The sST2 is also involved in inflammatory diseases. The sST2 is increased in conditions of cardiac and vascular stress, particularly in HF. (14, 20) Interestingly, sST2 induces the secretion of IL-6, a pro-inflammatory cytokine that stimulates β1-AA production, leading to a cardiac damage by promoting oxidative stress and inflammation (21). Therefore, we speculate that the high-level sST2 in patients with ADHF promotes the secretion of IL-6, which increases the production of β1-AA and exaggerates myocardial injury. This provides a possible explanation for the positive correlation between the β1-AA and the sST2. Similar to the effect of sST2, the β1-AA can also induce an IL-6 secretion through mediating T lymphocyte disorder, aggravating cardiac remodeling (17). In addition, β1-AA and the sST2 activate a similar intracellular signal pathway that induces myocardial fibrosis. Studies showed that the β1-AA promotes proliferation in cardiac fibroblasts through activating p38 mitogen-activated protein kinase (p38MAPK) through specifically binding to the

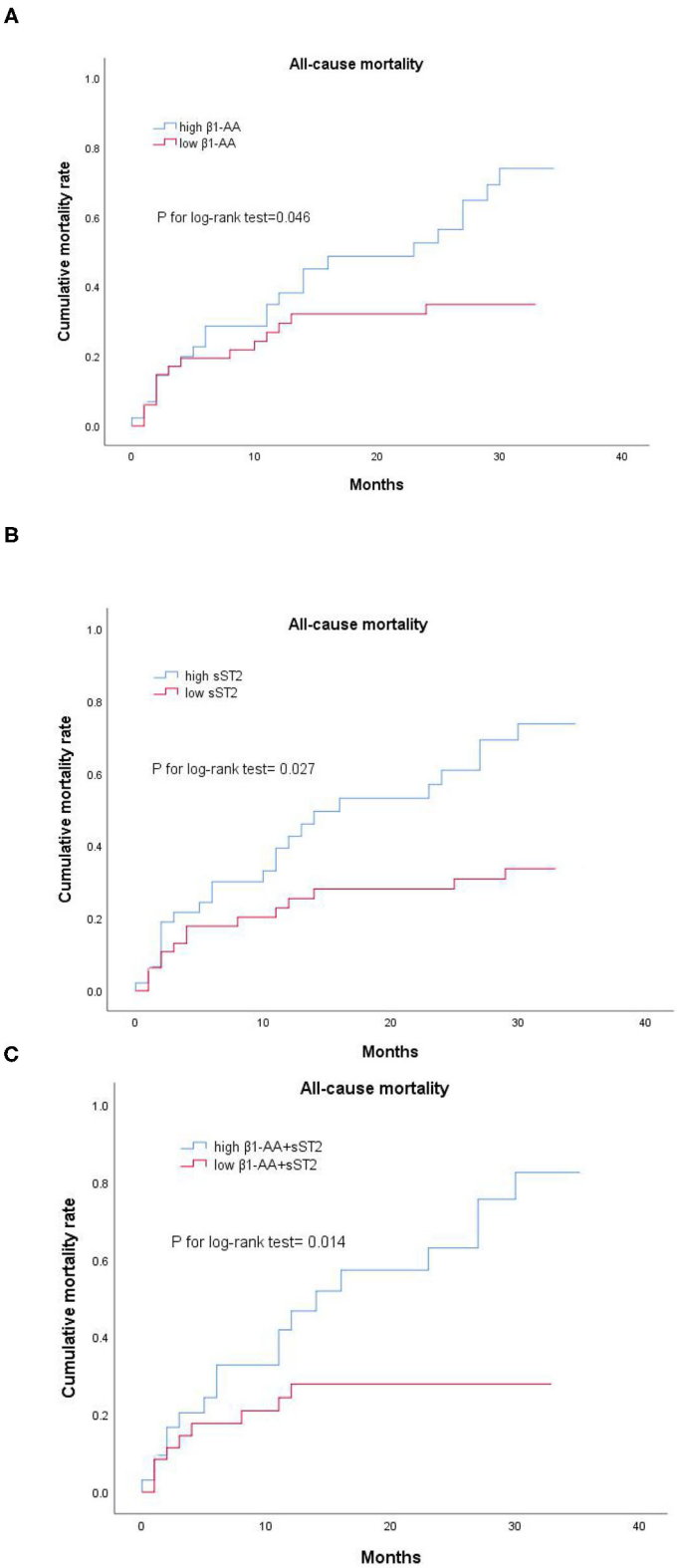

FIGURE 1 | (A–C) Survival analysis of β1-AA and sST2 baseline levels in patients with ADHF. Kaplan-Meier analysis showed that patients with high β1-AA and sST2 had obviously higher cumulative rates of the all-cause mortality than those with low β1-AA and sST2. High β1-AA and high sST2, the level of β1-AA and sST2 was above their mean or median; low β1-AA and low sST2, the level of β1-AA and sST2 was below their mean or median. High β1-AA+ sST2, the level of β1-AA and sST2 was both above their mean or median; low β1-AA+ sST2, the level of β1-AA and sST2 was both below their mean or median.

TABLE 4 | Association between level of β1-AA/sST2 and all-cause mortality by Multivariate Cox regression.

	B	S.E.	W value	HR	95 % CI	P
β1-AA[#]	0.788	0.351	5.05	2.199	1.106–4.373	0.025
sST2[*]	0.847	0.351	5.381	2.333	1.173–4.638	0.016
β1-AA+ sST2[§]	1.208	0.430	7.880	3.348	1.440–7.784	0.005

β1-AA, sST2 and combination of β1-AA and sST2 were independent risk factors for an all-cause mortality in ADHF by multivariate cox regression, all P < 0.05. B, regression coefficient; S.E., standard error; W value, Wald chi-square value; HR, hazard ratio; CI, confidence interval.

[#] *adjust for age, diabetes, sST2, NT-proBNP,and PCT.*

[*] *adjust for age, diabetes, β1-AA, NT-proBNP, and PCT.*

[§] *adjust for age,diabetes, NT-proBNP, and PCT.*

TABLE 5 | The AUC and Δ AUC of the ROC curves from different models and the comparisons.

	AUC	95% CI	P	ΔAUC	P^{Δ}
Model 1	0.642	0.519–0.765	0.024		
Model 2	0.714	0.599–0.830	0.001	0.072[#]	0.041
Model 3	0.735	0.625–0.846	0.000	0.093[*]	0.018
Model 4	0.748	0.638–0.858	0.000	0.106[§]	0.011

Model 1: age, diabetes, NT-proBNP and PCT; Model 2: Mode l +β1-AA; Model 3: Mode l + Log 2 sST2; Model 4: Mode l +β1-AA+ Log 2 sST2.

[#] *ΔAUC, Model 2-Model1;* [*] *ΔAUC, Model 3-Model1;* [§] *ΔAUC, Model 4-Model1.*

AUC, the area under the curves. ΔAUC, the difference of two AUC. P, the significance of the probability for ROC curves of models for predicting the all-cause mortality of patients with ADHF. P^{Δ}, the significance of the probability for difference of ΔAUC. CI, confidence interval.

β1-AR (7), leading to a myocardial fibrosis. The sST2 can also activate p38MAPK and nuclear factor-κB (NF-κB) signaling pathways, inducing ventricular remodeling, and fibrosis (11, 22). Of note, both β1-AA and the sST2 in promoting intracellular p38MAPK phosphorylation can be antagonized by β blockers (10, 11). Studies have shown that the dose of β-blockers in patients with HF may affect the concentration of sST2, and the combination of sST2 value and the dose of beta-blockers can be used for risk stratification on the prognosis of patients with HF (23). Therefore, the positive correlation between β1-AA and sST2 may be that sST2 promote the secretion of β1-AA on the one hand, and on the other hand, both of them share a common intracellular signaling pathway that causes myocardial fibrosis and is antagonized by β blockers, so, they are both interrelated and synergistic in inducing myocardial fibrosis. Consequently, we speculated that the degree of myocardial fibrosis may be more obvious when the β1-AA and sST2 are elevated simultaneously in patients with heart failure. So far, there is no relevant report and the next study of synergistic effect of β1-AA and sST2 on promoting cardiac fibrosis will be testified by cardiac MRI in our future study.

Another important finding in this study is that the β1-AA and sST2 were, respectively, independent risk factors for a short-term all-cause death in patients with ADHF, and higher levels of these biomarkers were associated with a higher risk of an all-cause death. Of particular significance, the combination of β1-AA and sST2 could improve risk stratification in predicting short-term survival among patients with ADHF. An animal study confirmed that the NT-proBNP was increased and the left ventricular shortening rate was decreased in rats immunized with β1-AA (18). Meanwhile, the β1-AA level is an independent predictor of myocardial reverse remodeling (24). The β1-AA reduces cardiac function, enhances arrhythmia, and sudden cardiac death, (5, 8, 25) so it can be used as a predictor for death risk in patients with heart failure (8, 26). Consistent with previous findings, this study showed that the β1-AA was positively correlated with NT-proBNP and negatively correlated with the EF value in ADHF. The current results indicated that β1-AA could accelerate myocardial remodeling and was an independent risk factor for a short-term all-cause death in patients with ADHF.

Many novel biomarkers had been explored in the prognosis of HF, such as Secreted frizzled-related proteins (Sfrps) (27–29) and Trimethylamine N-oxide (TMAO) (30). In addition, our previous study demonstrated the biomarkers of myocardial fibrosis, such as sST2 and Procollagen Type III N-Terminal Peptide (PIIINP), are independent prognostic factors for all-cause mortality in patients with ADHF (31), and the combination of biomarkers could be more sensitive to predict an all-cause death in patients with ADHF. Our finding showed that the β1-AA and sST2 were, respectively, independent predictors for short-term all-cause death in patients with ADHF after adjustment for other risk factors. Importantly, the combination of β1-AA and sST2 is a stronger predictive for an all-cause mortality in patients with ADHF.

LIMITATIONS

Limitations of the presented study include that this study was performed on a single center with small sample size and many confounders cannot be adjusted, the conclusion of which still warrants confirmation in multiple centers with larger sample sizes. In addition, the current study only analyzed the levels of the β1-AA and sST2 in patients when they were admitted to the hospital. We should take the blood sample after the HF guideline-directed management at different periods. It is more helpful to elucidate the relationship between the expression of the biomarkers and the prognosis of ADHF.

Further studies should establish the optimal timing of β1-AA and sST2 sampling, and more importantly, assess whether specific action in response to the prognostic information conveyed by β1-AA and sST2 indeed improves patient status and outcomes.

CONCLUSIONS

The current study confirmed that the β1-AA was positively correlated with sST2 in patients with HF. Furthermore, elevated plasma β1-AA and sST2 level in patients with patients is associated with poorer prognoses.

DATA AVAILABILITY STATEMENT

The raw data supporting the conclusions of this article will be made available by the authors, without undue reservation.

ETHICS STATEMENT

Written informed consent was obtained from the individual(s) for the publication of any potentially identifiable images or data included in this article.

AUTHOR CONTRIBUTIONS

YS wrote and edited the manuscript. YS, BH, LF, JD, and LZ collected the research data for the article. XH and YY reviewed the manuscript and approved the final manuscript. All authors contributed to the article and approved the submitted version.

FUNDING

This work was supported by Medical Scientific Research Foundation of Guangdong Province, China (No. A2013864).

ACKNOWLEDGMENTS

The authors thank Yan Wang, MD, Min Wang, MD, and Feng Zhu, MD, from Laboratory of Cardiovascular Immunology, Union Hospital, Tongji Medical College of Huazhong University of Science and Technology for the β1-AA detection.

REFERENCES

1. Heidenreich PA, Albert NM, Allen LA, Bluemke DA, Butler J, Fonarow GC, et al. Forecasting the impact of heart failure in the United States: a policy statement from the American Heart Association. *Circ Heart Fail.* (2013) 6: 606–19. doi: 10.1161/HHF.0b013e318291329a
2. McDonagh TA, Metra M, Adamo M, Gardner RS, BaumbachA, Böhm M, et al. 2021 ESC Guidelines for the diagnosis and treatment of acute and chronic heart failure. *Eur Heart J.* (2021) 42:3599–726. doi: 10.1093/eurheartj/ehab368
3. Engelhardt S. Alternative signaling: cardiomyocyte beta1-adrenergic receptors signal through EGFRs. *J Clin Invest.* (2007) 117:2396–8. doi: 10.1172/JCI33135
4. Jahns R, Boivin V, Siegmund C, Inselmann G, Lohse MJ, Boege F. Autoantibodies activating human beta1-adrenergic receptors are associated with reduced cardiac function in chronic heart failure. *Circulation.* (1999) 99:649–54. doi: 10.1161/01.CIR.99.5.649
5. Holthoff HP, Zeibig S, Jahns-Boivin V. Bauer J, Lohse MJ, Kääb S, et al. Detection of anti-β1-AR autoantibodies in heart failure by a cell-based competition. *ELISA Circ Res.* (2012) 111:675–84. doi: 10.1161/CIRCRESAHA.112.272682
6. Wallukat G, MüllerJ, Podlowski S, Nissen E, Morwinski R, Hetzer R. Agonist-like beta-adrenoceptor antibodies in heart failure. *Am J Cardiol.* (1999) 83:75H−9H. doi: 10.1016/S0002-9149(99)00265-9
7. Lv T, Du Y, Cao N, Zhang S, Gong Y, Bai Y, et al. Proliferation in cardiac fibroblasts induced by β1-adrenoceptor autoantibody and the underlying mechanisms. *Sci Rep.* (2016) 6:32430. doi: 10.1038/srep32430
8. Pei J, Li N, Chen J, Li X, Zhang Y, Wang Z, et al. The predictive values of beta1-adrenergic and M2 muscarinic receptor autoantibodies for sudden cardiac death in patients with chronic heart failure. *Eur J Heart Fail.* (2012) 14:887–94. doi: 10.1093/eurjhf/hfs082
9. Wallukat G, Haberland A, Berg S. Schulz A, Freyse EJ, Dahmen C, et al. The first aptamer-apheresis column specifically for clearing blood of beta1-receptor autoantibodies. *Circ J.* (2012) 76:2449–55. doi: 10.1253/circj.CJ-12-0212
10. Nagatomo Y, Yoshikawa T, Kohno T, Yoshizawa A, Baba A, Anzai T, et al. A Pilot study on the role of autoantibody targeting the β1-adrenergic receptor in the response to beta-blocker therapy for congestive heart failure. *J Card Fail.* (2009) 15:224–32. doi: 10.1016/j.cardfail.2008.10.027
11. Mccarthy CP, Januzzi JL. Soluble ST2 in heart failure. *Heart Fail Clin.* (2018) 14:41–8. doi: 10.1016/j.hfc.2017.08.005
12. Defilippi CR, Herzog CA. Interpreting cardiac biomarkers in the setting of chronic kidney disease. *Clin Chem.* (2017) 63:59–65. doi: 10.1373/clinchem.2016.254748
13. Emdin M, Aimo A,Vergaro G, Bayes-Genis A, Lupón J, Latini R, et al. sST2 Predicts outcome in chronic heart failure beyond NT-proBNP and high-sensitivity troponin T. *J Am Coll Cardiol.* (2018) 72:2309–20. doi: 10.1016/j.jacc.2018.08.2165
14. Aimo A, Januzzi JL, Bayes-Genis A, Vergaro G, Sciarrone P, Passino C, et al. Clinical and prognostic significance of sST2 in heart failure: JACC review topic of the week. *J Am Coll Cardiol.* (2019) 74:2193–203. doi: 10.1016/j.jacc.2019.08.1039
15. Bornholz B, Roggenbuck D, Jahns R, Boege F. Diagnostic and therapeutic aspects of β1-adrenergic receptor autoantibodies in human heart disease. *Autoimmun Rev.* (2014) 13:954–62. doi: 10.1016/j.autrev.2014.08.021
16. Hanley JA, McNeil BJ. The meaning and use of the area under a receiver operating characteristic (ROC) curve. *Radiology.* (1982) 143: 29–36. doi: 10.1148/radiology.143.1.7063747
17. Du Y, Li X, Yu H. Yan L, Lau WB, Zhang S, et al. Activation of T Lymphocytes as a novel mechanism in beta1-adrenergic receptor autoantibody-induced cardiac remodeling. *Cardiovasc Drugs Ther.* (2019) 33: 149–61. doi: 10.1007/s10557-019-06856-2
18. Ma LP, Premaratne G, Bollano E, Lindholm C, Fu M. Interleukin-6-deficient mice resist development of experimental autoimmune cardiomyopathy induced by immunization of beta1-adrenergic receptor. *Int J Cardiol.* (2012) 155:20–5. doi: 10.1016/j.ijcard.2011.01.085
19. Levin MJ, Hoebeke J. Cross-talk between anti-beta1-adrenoceptor antibodies in dilated cardiomyopathy and Chagas' heart disease. *Autoimmunity.* (2008) 41: 429–33. doi: 10.1080/08916930802031702
20. Vianello E, Dozio E, Tacchini L, Frati L, Corsi Romanelli MM. ST2/IL-33 signaling in cardiac fibrosis. *Int J Biochem Cell Biol.* (2019) 116:105619. doi: 10.1016/j.biocel.2019.105619
21. Matilla L. Ibarrola J, Arrieta V, Garcia-Peña A, Martinez-Martinez E, Sádaba R, et al. Soluble ST2 promotes oxidative stress and inflammation in cardiac fibroblasts: an *in vitro* and *in vivo* study in aortic stenosis. *Clin Sci (Lond).* (2019) 133:1537–48. doi: 10.1042/CS20190475
22. Yin H, Li P, Hu F. Wang Y, Chai X, Zhang Y. IL-33 attenuates cardiac remodeling following myocardial infarction via inhibition of the p38MAPK and NF-kB pathway. *Mol Med Rep.* (2014) 9: 1834–38. doi: 10.3892/mmr.2014.2051
23. Gaggin HK, Motiwala S, Bhardwaj A, Parks KA, Januzzi JL. Soluble concentrations of the interleukin receptor family member ST2 and β-blocker therapy in chronic heart failure. *Circ Heart Fail.* (2013) 6:1206–13. doi: 10.1161/CIRCHEARTFAILURE.113.000457
24. NagatomoY, Yoshikawa T, Okamoto H, Kitabatake A, Hori M. Presence of autoantibody directed against β1-adrenergic receptors is associated with amelioration of cardiac function in response to carvedilol: Japanese Chronic Heart Failure (J-CHF) study. *J Card Fail.* (2015) 21:198–207. doi: 10.1016/j.cardfail.2014.12.005
25. Dandel M, Wallukat G, Potapov E, Hetzer R. Role of β1-adrenoceptor autoantibodies in the pathogenesis of dilated cardiomyopathy. *Immunobiology.* (2012) 217:511–20. doi: 10.1016/j.imbio.2011.07.012
26. Düngen HD, Dordevic A. Felix SB, Pieske B, Voors AA, McMurray, JJV, et al. β1-adrenoreceptor autoantibodies in heart failure:

physiology and therapeutic implications. *Circ Heart Fail.* (2020) 13:e006155. doi: 10.1161/CIRCHEARTFAILURE.119.006155
27. Wu J, Zheng H, Liu X, Chen P, Zhang Y, Zhang Y. et al. Prognostic value of secreted frizzled-related protein 5 in heart failure patients with and without type 2 diabetes. *MellitusCirc Heart Fail.* (2020) 13:e007054. doi: 10.1161/CIRCHEARTFAILURE.120.007054
28. Ma T, Huang X, Zheng H, Huang G, Li W, Liu X, et al. SFRP2 improves mitochondrial dynamics and mitochondrial biogenesis, oxidative stress, and apoptosis in diabetic cardiomyopathy. *Oxid Med Cell Longev*. (2021) 2021:9265016. doi: 10.1155/2021/9265016
29. Yang S, Chen H, Tan K, Cai F, Du Y, Lv W, et al. Secreted frizzled-related protein 2 and extracellular volume fraction in patients with heart failure. *Oxid Med Cell Longev*. (2020) 2020:2563508. doi: 10.1155/2020/2563508
30. Li W, Huang A, Zhu H, Liu X, Huang X, Huang Y, et al. Gut microbiota-derived trimethylamine N-oxide is associated with poor prognosis in patients with heart failure. *Med J Aust.* (2020) 213: 374–9. doi: 10.5694/mja2.50781
31. Yao Y, Feng L, Sun Y, Wang S, Sun J, Hu B. Myocardial fibrosis combined with NT-proBNP improves the accuracy of survival prediction in ADHF patients. *BMC Cardiovasc Disord.* (2021) 21: 264. doi: 10.1186/s12872-021-02083-6

Conflict of Interest: The authors declare that the research was conducted in the absence of any commercial or financial relationships that could be construed as a potential conflict of interest.

Publisher's Note: All claims expressed in this article are solely those of the authors and do not necessarily represent those of their affiliated organizations, or those of the publisher, the editors and the reviewers. Any product that may be evaluated in this article, or claim that may be made by its manufacturer, is not guaranteed or endorsed by the publisher.

Copyright © 2022 Sun, Feng, Hu, Dong, Zhang, Huang and Yuan. This is an open-access article distributed under the terms of the Creative Commons Attribution License (CC BY). The use, distribution or reproduction in other forums is permitted, provided the original author(s) and the copyright owner(s) are credited and that the original publication in this journal is cited, in accordance with accepted academic practice. No use, distribution or reproduction is permitted which does not comply with these terms.

frontiers in Cardiovascular Medicine

ORIGINAL RESEARCH
published: 17 February 2022
doi: 10.3389/fcvm.2022.803695

The Impact of Occupational Noise on Hypertension Risk: A Case-Control Study in Automobile Factory Personnel

Xiaomei Wu[1†], *Chaoxiu Li*[1†], *Xiaohong Zhang*[2], *Yumeng Song*[1], *Dan Zhao*[1], *YueYan Lan*[1] *and Bo Zhou*[1*]

[1] *Department of Clinical Epidemiology and Center of Evidence Based Medicine, The First Hospital of China Medical University, Shenyang, China,* [2] *Department of Clinical Epidemiology, The Fourth Affiliated Hospital of China Medical University, Shenyang, China*

Background: Many epidemiological studies have investigated the relationship between occupational noise and hypertension, but with conflicting findings. This study aimed to assess the relationship between occupational noise exposure and the risk of hypertension.

Methods: A case-control study was conducted to explore hypertension predictors, and then sensitivity analysis was performed based on propensity score matching (PSM). Data were collected from participants' annual physical examinations and occupational noise exposure measurements. Odds ratios (ORs) and 95% confidence intervals (CIs) were estimated using logistic regression analysis. A restricted cubic spline (RCS) function was used to fit the dose-effect relationship.

Results: 500 cases and 4,356 controls were included in the study. Multivariate logistic regression showed that an increase in the level of occupational noise [range 68–102 dB(A)] of 1 dB(A), corresponded to an increase in hypertension risk of 8.3% (OR: 1.083, 95% CI: 1.058–1.109). Compared to the first quartile, the risk of hypertension in the fourth quartile was 1.742 (95% CI: 1.313–2.310). After applying PSM to minimize bias, we obtained a population of 500 cases and 1,000 controls. Noise level was significantly associated with the risk of hypertension. In addition, the RCS curve showed the risk of hypertension was relatively stable until a predicted noise level of around 80 dB(A) and then started to increase rapidly afterward ($P_{nonlinear} = 0.002$).

Conclusions: Occupational noise exposure was significantly associated with hypertension risk and there was a positively correlated dose-response relationship.

Keywords: hypertension, noise, dose effect relationship, epidemiology, risk factors

OPEN ACCESS

Edited by:
Yuli Huang,
Southern Medical University, China

Reviewed by:
Denis Vinnikov,
Al-Farabi Kazakh National University, Kazakhstan
Javier Varas,
Novartis, Spain

***Correspondence:**
Bo Zhou
zhoubo@cmu.edu.cn

†These authors have contributed equally to this work and share first authorship

Specialty section:
This article was submitted to General Cardiovascular Medicine, a section of the journal Frontiers in Cardiovascular Medicine

Received: *03 November 2021*
Accepted: *25 January 2022*
Published: *17 February 2022*

Citation:
Wu X, Li C, Zhang X, Song Y, Zhao D, Lan Y and Zhou B (2022) The Impact of Occupational Noise on Hypertension Risk: A Case-Control Study in Automobile Factory Personnel. Front. Cardiovasc. Med. 9:803695. doi: 10.3389/fcvm.2022.803695

INTRODUCTION

Noise exposure is a common occupational hazard. Noise exposure not only adversely affects health, but also increases the risk of diseases such as hearing loss (1), ischemic heart disease (2), mental distress, and sleep disturbance (3). To protect workers, an occupational exposure limit has been set for the workplace (standard GBZ2.2-2007) of 85 dB(A) (4). However, even if occupational noise

exposure does not exceed this limit, increased incidences of chronic diseases such as hypertension have been shown among workers as revealed by annual physical examinations (5). Hypertension is a serious medical condition associated with increased disease risk to the heart, brain, kidneys, and other organ systems. The burden of hypertension disproportionately affects workers in low and middle-income countries, with two-thirds of cases being found there, largely due to recent increases in risk factors in these populations (6). Previous studies have focused on the typical risk factors for hypertension, such as salt intake (7), smoking (8), and obesity (9), with some studies also addressing the impact of noise exposure on the incidence and development of hypertension (10–15).

Evidence from animal and human studies has suggested hyperactivity of the sympathetic nervous system to be a possible mechanism for the association between noise exposure and hypertension (16). The sympathetic nervous system plays an important role in long-term blood pressure regulation in both normotension and hypertension (17). Noise exposure increases sympathetic activity triggering the release of stress hormones, such as epinephrine and norepinephrine, which act on the corresponding vascular receptors to enhance the contractility of resistance arterioles and increase blood pressure (18, 19). In addition, elevated stress hormone levels trigger the inflammatory and oxidative stress pathways by activating the nicotinamide adenine dinucleotide phosphate oxidase uncoupling of endothelial/neuronal nitric oxide synthase, thereby inducing endothelial and neuronal dysfunction (20).

Some epidemiological studies have suggested associations between traffic noise and hypertension, with one study relating aircraft noise and road traffic noise to an increased risk of hypertension (10, 11). However, epidemiological investigations conducted in the working population have not yet reached a consistent conclusion (12–15). Differences in findings have been attributed to differences in study design, sample sizes and baseline characteristics, and the influence of confounding factors. Meta-analyses have been used to summarize the relationship between occupational noise exposure and the risk of hypertension. However, their conclusions have been limited. Meta-analyses conducted by Wang et al. (21) and Yang et al. (22) included only Chinese literature and Chinese workers. Different study designs (cross-sectional studies, cohort studies, and case-control studies) were included in the three meta-analyses (23–25), which may indirectly explain the results. Recent meta-analyses have been limited by the overall low methodological quality of the included epidemiological studies, with only three of the 24 studies having a low risk of bias (26).

The purpose of this study was to explore the relationship between occupational noise exposure and hypertension risk, to provide a theoretical basis for improving conditions for factory workers and promoting workplace protection.

METHODS

This was a case-control study. It was conducted according to the Strengthening the Reporting of Observational Studies in Epidemiology (STROBE) reporting guidelines (27) (**Supplementary Table S1**).

Study Design and Population

Male workers were recruited from a modern automobile manufacturing facility in Shenyang. Participants underwent occupational health examinations between July and October 2013. The inclusion criteria of participants were as follows: (1) Those working in places where occupational noise may exist; (2) Those with a cumulative duration of noise exposure of $\geq$1 year; (3) Those who were physically healthy. Participants were excluded if they were new employees, worked in an office space free of occupational noise (e.g., finance department, management department, etc.), or those who suffered from coronary heart disease, liver disease, kidney disease, or any endocrine disease. Hypertension was defined as a systolic blood pressure of $\geq$140 mmHg and or a diastolic blood pressure of $\geq$90 mmHg (2018 ESC/ESH Practice Guidelines) (28). Participants who met the criteria for hypertension were assigned to the case group, otherwise, they were placed in the control group.

This study was approved by the medical scientific research ethics committee of the First Affiliated Hospital of China Medical University (No. AF-SOP-07-1.0-01). All procedures performed in the study complied with the ethical standards of the institution, the National Research Committee, and the 1964 Helsinki Declaration and its subsequent amendments, or similar ethical standards.

Data Collection

The patients and the public were not involved in the design and analysis of this study. Demographic and clinical examination data were extracted from the management system of the medical examination center. Occupational noise exposure was measured in the workplace where the members of factory personnel were located, and measurements were undertaken by an occupational health assessment institution with the relevant safety assessment qualification.

Basic participant information was collected by two trained interviewers using a questionnaire survey that included their age, family history of hypertension (yes/no), smoking status (yes/no), job role, and duration in post. Smoking was defined as at least 1 cigarette per day for a year or more.

Clinical examination and blood sample collection were conducted by a healthcare professional. The clinical examination included height (m), weight (kg), body mass index (BMI), blood pressure (mmHg), listening test (normal/abnormal), and pulmonary function (normal/abnormal). Normal pulmonary function was defined using the ratio of forced expiratory volume in 1 s (FEV1) to forced vital capacity (FVC) taking a value of $>$80 %. Height and weight were measured using an automatic measuring instrument, and body mass index (BMI) was calculated as weight/height^2 (kg/m^2). Blood pressure was measured in the upper left arm after 5–10 m of rest in a seated position using an automated device (HEM-746C, Omron, Japan). Each of the above was measured twice, and the mean of the two measurements was used in the analysis. Blood tests were conducted using an automatic biochemical instrument

operated by trained technicians, including total cholesterol (TC), triglyceride (TG), high-density lipoprotein (HDL), and low-density lipoprotein (LDL) levels.

Occupational noise exposure was measured by occupational safety inspection professionals, using a statistical noise analyzer (AWA6218; Beijing Xihua Instrument Technology Co., Ltd.). Actual noise levels were recorded according to the normalization of the equivalent continuous A-weighted sound pressure level to a nominal 8-hour working day (LEX, 8h).

Statistical Analysis

In the presence of any missing data, multiple imputation was used to complete the dataset. Continuous variables were shown as median and inter-quartile ranges (25, 75%), and categorical variables were shown as frequencies (%). Mann-Whitney U-tests and chi-square tests, respectively, were used to compare the distributions of continuous and categorical variables between the two groups.

The odds ratio (OR) and 95% confidence interval (CI) of each variable were calculated using logistic regression. A univariate model was used to describe the linear effects of continuous variables. The continuous variables that were included in the corresponding risk models were transformed into categorical variables by selecting the corresponding critical values to ensure the clinically relevant balance between the groups (29). For occupational noise, the critical value was <85 dB(A), and ≥85 dB(A). For age, thresholds of <24, 24–25, 26–29 and ≥30 years were used. For BMI, the critical value was <18.55, 18.55-23.98, and ≥23.99 kg/m^2. For heart rate, the critical value was <60, 60–100, and ≥100 beats per minute. For TG, the critical value was <1.70, 1.70–2.25, and ≥2.26 mmol/L. For TC, the critical value was <5.18, 5.18-6.21, and ≥6.22 mmol/L. For LDL, the critical value was <3.37, 3.37–4.13, and ≥4.14 mmol/L. For HDL, the critical value was <1.04, 1.04–1.54, and ≥1.55 mmol/L (30). Years of working at the facility were included as a continuous variable. Smoking status (reference: none), family history (reference: none), pulmonary function (reference: normal), and hearing (reference: normal) were also included in the risk model.

To explore the accuracy of using occupational noise as a predictor of hypertension, the association was explored according to the inter-quartile range of occupational noise levels [≤76.4 dB(A), 76.41–78.8 dB(A), 78.81–80.90 dB(A), and >80.90 dB(A)]. Finally, Restricted cubic splines (RCS) with knots at the 25, 50, and 75th percentiles of the distribution were used to assess the dose-effect relationship between them, with 80 dB(A) as the reference group. A Spearman correlation test was performed to evaluate the association between occupational noise level and hypertension.

As participants were not randomly assigned to case and control groups, therefore, we used propensity score matching (PSM) to minimize the impact of confounds on the sensitivity analysis (31, 32). We then calculated the propensity score of each participant using multivariate logistic regression modeling. A nearest-neighbor matching method was then used, making the ratio between the case group and control group 1:2, that is, each 1 participant from the case group was matched to 2 participants in the control group with similar propensity scores. The balance of the matched model was assessed using the standardized mean differences between the two groups (33). Finally, the corresponding OR and 95% CI of noise exposure on the risk of hypertension were calculated using univariate logistic regression.

Statistical analyses were conducted using SPSS version 25 (Armonk, NY: IBM Corp.) (34), except for spline fitting, which was performed using SAS version 9.4 (SAS Institute, Cary, NC). A two-sided P-value < 0.05 was considered statistically significant.

RESULT

Demographic Characteristics

Table 1 shows the participant characteristics of the case and control groups across the entire study cohort. There were 500 cases and 4,356 controls. Noise exposure level, age, TG, TC, LDL, BMI, heart rate, years working at the facility, and pulmonary function were higher in the case group than in the control group ($P < 0.05$). HDL was lower in the case group than in the control group ($P < 0.05$). Smoking, family history of hypertension, and hearing level did not significantly differ between the two groups ($P > 0.05$).

Identify Predictors of Hypertension

Independent predictors of hypertension in the entire participant cohort were identified using logistic regression models with the original value for each variable (**Supplementary Table S2**). In the multivariate logistic regression, an increase in occupational noise exposure level of 1 dB(A) was associated with an increased hypertension risk of 8.3% (OR: 1.083, 95% CI: 1.058–1.109). Age, heart rate, and BMI were independent predictors of the risk of hypertension.

Table 2 shows the independent predictors of hypertension in the entire cohort identified by analyzing the nonlinear effects of the continuous variables. Multivariate logistic regression showed that exposure to occupational noise ≥85 dB(A) was significantly associated with the risk of hypertension (OR: 4.917, 95%CI: 2.920–8.279). When occupational noise level was analyzed as a categorical variable, the risk of having hypertension in the fourth quartile was 1.742 (95% CI: 1.313–2.310), compared to the first quartile. In addition, age, heart rate, BMI, TG, and TC were independent predictors of hypertension.

Sensitivity Analysis

PSM was used for sensitivity analysis to minimize the effects of confounding factors. The baseline characteristics of participants after PSM are shown in **Table 3**. When occupational noise was analyzed as either a continuous or categorical variable, it was significantly associated with the risk of hypertension, consistent with the results of the other analyses performed (**Table 4**).

Dose Effect Relationship Between Noise and Hypertension

The Spearman correlation test showed that the correlation between occupational noise exposure and hypertension was significant at the 0.01 level (2-tailed). Subsequently, the RCS curve showed a positively correlated nonlinear dose-response

TABLE 1 | Baseline characteristics of the groups in all participants.

	Total = 4,856	Case (n = 500)	Control (n = 4,356)	P-value
Noise [dB(A)]	78.8(76.4–80.9)	78.8(78.8–81.1)	78.8(75.9–80.6)	<0.001*
Demographics				
Age (year)	26(24–30)	28.5(25.5–32)	26(24–29)	<0.001*
Years of working (year)	2(1–3)	2(1–6)	2(1–3)	<0.001*
Smoking				0.57
No	2,020(41.6%)	202(40.4%)	1,818(41.7%)	
Yes	2,836(58.4%)	298(59.6%)	2,538(58.3%)	
Family history of hypertension				0.90
No	84(1.7%)	9(1.8%)	75(1.7%)	
Yes	4,772(98.3%)	491(98.2%)	4,281(98.3%)	
Clinical examination				
Heart rate (beats per minute)	79(72–87)	83.5(77–94)	78.5(72–86)	<0.001*
BMI (kg/m^2)	23.95(21.3–26.81)	27.68(24.79–29.48)	23.66(21.11–26.23)	<0.001*
Hearing				0.89
Normal	4,629(95.3%)	476(95.2%)	4,153(95.3%)	
Abnormal	227(4.7%)	24(4.8%)	203(4.7%)	
Pulmonary function				0.001*
Normal	4,651(95.8%)	465(93.0%)	4,186(96.1%)	
Abnormal	205(4.2%)	35(7.0%)	170(3.9%)	
Blood biochemistry				
TG (mmol/L)	1.27(0.84–1.9)	1.76(1.22–2.73)	1.2(0.81–1.83)	<0.001*
TC (mmol/L)	4.4(3.9–5)	4.9(4.2–5.5)	4.4(3.8–5.0)	<0.001*
LDL (mmol/L)	2.51(2.08–2.94)	2.78(2.35–3.24)	2.47(2.06–2.91)	<0.001*
HDL (mmol/L)	1.07(0.94–1.21)	1.02(0.91–1.15)	1.07(0.95–1.22)	<0.001*

TG, triglyceride; HDL, high-density lipoprotein; LDL, low-density lipoprotein; TC, total cholesterol; BMI, body mass index. The differences in the distribution of noise, age, heart rate, TG, HDL, LDL, TC, BMI, and years of working between the two groups by Mann-Whitney U tests. The differences in the distribution of smoke, family history of hypertension, hearing, pulmonary function between the two groups by Chi square test.
**P < 0.05.*

relationship between noise exposure and hypertension ($P_{\text{nonlinear}} = 0.002$; **Figure 1**). The risk of hypertension was relatively stable until a predicted occupational noise level of around 80 dB(A) and then started to increase rapidly afterward.

DISCUSSION

Main Results and Description

We used a case-control study design to explore predictors of hypertension. Independent of whether occupational noise was analyzed as a continuous or categorical variable, there was a nonlinear dose-response relationship between it and hypertension.

Literature Review

We found that occupational noise exposure was associated with an increased risk of hypertension. Previous studies have reported that occupational noise exposure increases the risk of hypertension. A cross-sectional study reported this in steelworkers (OR: 2.03, 95% CI: 1.15–3.58) (12), Bolm et al. (26) conducted a meta-analysis of 24 studies and concluded that the risk of hypertension increased 1.77-fold (95% CI 1.36–2.29) for employees exposed to occupational noise levels of 80–85 dB(A), and increased 3.50-fold (95% CI 1.56–7.86) for employees exposed at 85–90 dB(A). However, Tessier et al. (13) and Stokholm et al. (14) reported an absence of any such association. The inconsistency of these findings may be attributed to the noise exposures reported in their studies not being high enough to detect an effect. In addition, the present results show a nonlinear dose-response relationship between occupational noise and the risk of hypertension. For occupational noise exposures in the range 68–80 dB(A), the risk of hypertension was relatively stable. Exposures above 80 dB(A) were associated with a risk of hypertension that increased rapidly with noise exposure level. Lin et al. (15) also reported a curved exposure-response pattern between occupational noise and hypertension, whereby the risk of hypertension increased for exposures between 82 and 106 dB(A), and then sharply decreased for exposures over 107 dB(A). This may be related to the extensive use of personal protective equipment in people exposed to high levels of occupational noise, thereby reducing the incidence of hypertension.

Study Strengths and Limitations

Hypertension is a consequence of many factors working together. The influence of potential confounding factors on research

TABLE 2 | The OR and 95% CI of the relationship between classified variables and hypertension in all participants.

	Univariate model		Multivariate model [a]	
	OR (95%CI)	**P value**	**OR (95%CI)**	**P value**
Noise [dB(A)]				
Reference: <85	3.953 (2.491–6.274)	<0.001*	4.917 (2.920–8.279)	<0.001*
Noise [dB(A)]				
Reference: ≤76.40	1	0.004*	1	<0.001*
76.41–78.80	1.096 (0.850–1.413)	0.48	0.955 (0.730–1.250)	0.739
78.81–80.90	1.208 (0.894–1.632)	0.22	1.073 (0.781–1.475)	0.66
>80.90	1.570 (1.206–2.046)	0.001*	1.742 (1.313–2.310)	<0.001*
Demographics				
Age(year)				
Reference: <24	1	<0.001*	1	<0.001*
24–25	1.440 (1.041–1.994)	0.03*	1.402 (0.998–1.969)	0.05
26–29	1.421 (1.038–1.945)	0.03*	1.098 (0.787–1.530)	0.58
≥30	3.292 (2.468–4.390)	<0.001*	2.094 (1.503–2.917)	<0.001*
Years of working (year)	1.068 (1.039–1.098)	<0.001*	1.001 (0.968–1.035)	0.954
Smoking				
Reference: No	1.057 (0.875–1.276)	0.57	1.038 (0.847–1.272)	0.72
Family history of hypertension				
Reference: No	0.956 (0.476–1.920)	0.9	0.802 (0.376–1.714)	0.57
Clinical examination				
Heart rate (beats per minute)				
Reference: 60–99	1	<0.001*	1	<0.001*
<60	0.492 (0.179–1.351)	0.17	0.631 (0.223–1.786)	0.39
≥100	3.679 (2.739–4.941)	<0.001*	4.018 (2.889–5.586)	<0.001*
BMI (kg/m^2)				
Reference: 18.55– 23.89	1	<0.001*	1	<0.001*
<18.55	0.406 (0.148–1.116)	0.08	0.443 (0.159–1.234)	0.12
≥23.99	4.879 (3.855–6.221)	<0.001*	3.942 (3.047–5.100)	<0.001*
Hearing				
Reference: Normal	1.032 (0.669–1.591)	0.89	0.897 (0.564–1.427)	0.65
Pulmonary function				
Reference: Normal	1.853 (1.272–2.700)	0.001*	1.457 (0.964–2.204)	0.07
Blood biochemistry				
TG (mmol/L)				
Reference: <1.70	1	<0.001*	1	<0.001*
1.70–2.25	1.896 (1.462–2.460)	<0.001*	1.180 (0.888–1.569)	0.25
≥2.26	3.456 (2.796–4.272)	<0.001*	1.699 (1.302–2.216)	<0.001*
TC (mmol/L)				
Reference: <5.18	1	<0.001*	1	0.02*
5.18–6.21	2.321 (1.872–2.877)	<0.001*	1.365 (1.027–1.815)	0.03*
≥6.22	4.391 (3.159–6.103)	<0.001*	1.923 (1.165–3.174)	0.01*
LDL (mmol/L)				
Reference: <3.37	1	<0.001*	1	0.39
3.37–4.13	2.288 (1.773–2.952)	<0.001*	1.117 (0.789–1.582)	0.53
≥4.14	3.800 (2.301–6.275)	<0.001*	1.606 (0.812–3.175)	0.17
HDL (mmol/L)				
Reference: <1.04	1	<0.001*	1	0.84
1.04–1.54	2.139 (1.076–4.252)	0.03*	0.938 (0.450–1.954)	0.86
≥1.55	1.486 (0.747–2.957)	0.26	1.001 (0.486–2.062)	0.99

OR, odds ratio; CI, confidence interval; TG, triglyceride; HDL, high-density lipoprotein; LDL, low-density lipoprotein; TC, total cholesterol; BMI, body mass index.

[a]*Multivariable models include noise, age, years of working, smoking, family history, heart rate, BMI, hearing, pulmonary function, TG, TC, LDL, HDL.*

**P < 0.05.*

TABLE 3 | Baseline characteristics of the groups in PSM participants.

	Total = 1,500	Case (n = 500)	Control (n = 1,000)	Standardized mean differences		P–value
				Before PSM	After PSM	
Noise [dB(A)]	78.8(78.2–80.9)	78.8(78.8–81.1)	78.8(75.9–80.6)	/	/	<0.001*
Demographics				/	/	
Age (year)[b]		28.5(25–32)	28(25–32)	0.43	0.04	0.96
Years of working (year)	2(1–7)	2(1–6)	2(1–7)	/	/	0.24
Smoking				/	/	0.97
No	607(40.5%)	202(40.4%)	405(40.5%)	/	/	
Yes	893(59.5%)	298(59.6%)	595(59.5%)	/	/	
Family history of hypertension				/	/	0.66
No	24(1.6%)	9(1.8%)	15(1.5%)	/	/	
Yes	1,476(98.4%)	491(98.2%)	985(98.5%)	/	/	
Clinical examination				/	/	
Heart rate (beats per minute) [b]	83(77–92)	83.5(77–94)	83(77–92)	0.48	0.06	0.41
BMI (kg/m^2) [b]	27.1(24.68–29.48)	27.68(24.79–29.48)	27.02(24.5–29.48)	0.93	0.05	0.26
Hearing				/	/	0.19
Normal	1,411(94.1%)	476(95.2%)	935(93.5%)	/	/	
Abnormal	89(5.9%)	24(4.8%)	65(6.5%)	/	/	
Pulmonary function				/	/	0.11
Normal	1,415(94.3%)	465(93%)	950(95%)	/	/	
Abnormal	85(5.7%)	35(7%)	50(5%)	/	/	
Blood biochemistry				/	/	
TG (mmol/L) [b]	1.73(1.2–2.6)	1.76(1.22–2.73)	1.71(1.18–2.51)	0.34	0.05	0.23
TC (mmol/L) [b]	4.9(4.3–5.5)	4.9(4.2–5.5)	4.85(4.3–5.5)	0.5	0.04	0.64
LDL (mmol/L)	2.77(2.35–3.24)	2.78(2.35–3.24)	2.77(2.35–3.23)	/	/	0.80
HDL (mmol/L)	1.02(0.9–1.15)	1.02(0.91–1.15)	1.01(0.9–1.15)	/	/	0.56

PSM, propensity score matching; TG, triglyceride; HDL, high-density lipoprotein; LDL, low-density lipoprotein; TC, total cholesterol; BMI, body mass index. The differences in the distribution of noise, age, heart rate, TG, HDL, LDL, TC, BMI, and years of working between the two groups by Mann–Whitney U tests. The differences in the distribution of smoke, family history of hypertension, hearing, pulmonary function between the two groups by Chi square test.

[b] Those variables (age, heart rate, BMI, TG, TC) that has been identified as independent predictors of hypertension.

**P < 0.05.*

TABLE 4 | The OR and 95% CI of the relationship between noise and hypertension in PSM participants.

	Univariate model	
	OR (95%CI)	*P* value
Noise, per 1 dB(A)	1.068(1.040–1.096)	<0.001*
Noise:		
Reference: <85	3.114(1.698–5.711)	<0.001*
Noise(dB)		
Reference: ≤76.40	1	0.001*
76.41–78.80	1.138(0.851–1.521)	0.384
78.81–80.90	1.054(0.749–1.483)	0.762
>80.90	1.797(1.316–2.454)	<0.001*

OR, odds ratio; CI, confidence interval.

**P < 0.05.*

findings must be considered when analyzing the impact of noise exposure on the risk of hypertension. Multifactor regression analysis is the most commonly used method that adjusts for confounding factors, but collinearity between variables can lead to instabilities in such a model (35). Firstly, we used PSM to balance the distributions of potentially confounding variables between participant groups by matching participants in the case group with those from the control group, thereby reducing the error (36). Secondly, we used RCR regression to flexibly model the association between occupational noise and the risk of hypertension. As such, we obtained a more intuitive dose-effect relationship curve.

Our study also had some limitations. Firstly, we have no information about the use of antihypertensive drugs within the participant cohort, which may provide a confounding factor to determining the association between occupational noise exposure and hypertension. Secondly, we did not set the caliper value for the PSM, potentially leading to a deviation in the results (37). However, the balance achieved between the groups after PSM suggests that the model was stable. In addition, noise exposure and blood pressure measurements were collected at a single time point, so it is not possible to infer any causal relationship between noise exposure and hypertension. Prospective longitudinal studies will be needed

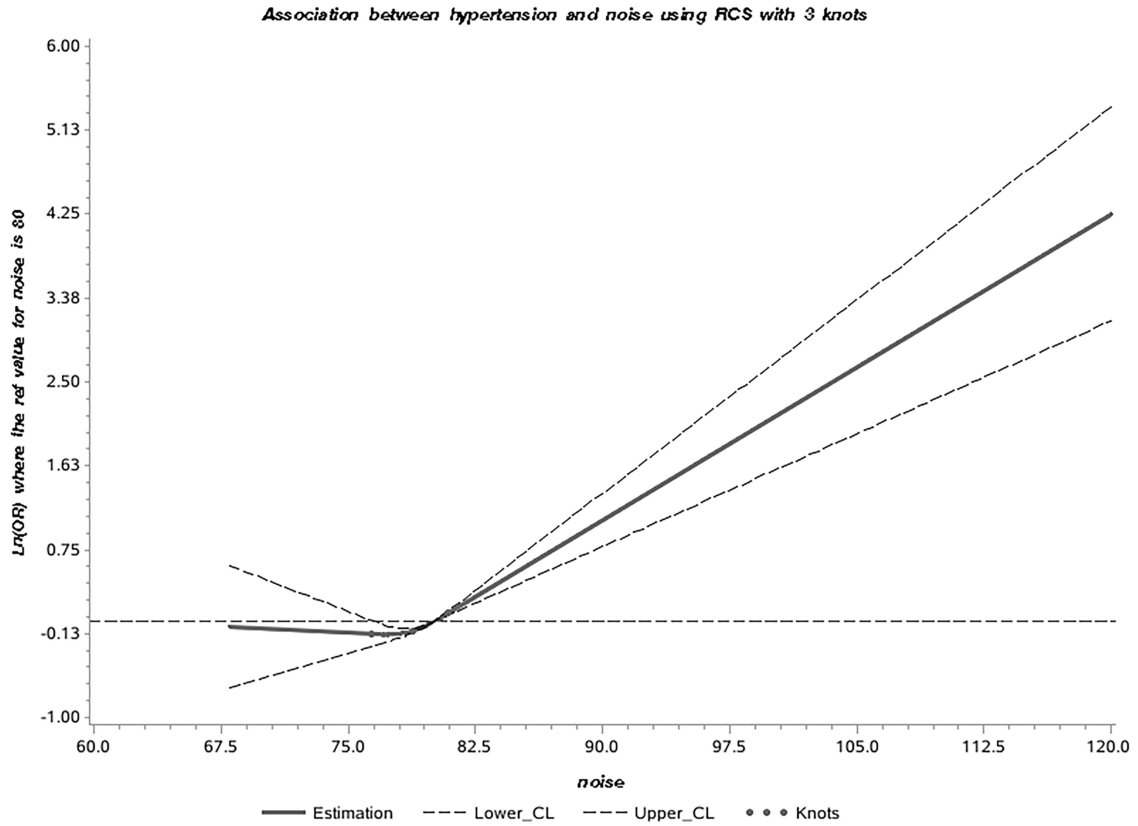

FIGURE 1 | Dose effect relationship between occupational noise and hypertension in entire participants.

to explore the causal relationship between noise exposure and hypertension.

DATA AVAILABILITY STATEMENT

The raw data supporting the conclusions of this article will be made available by the authors, without undue reservation.

ETHICS STATEMENT

This study has been approved by the medical scientific research Ethics Committee of the First Affiliated Hospital of China Medical University (No. AF-SOP-07-1.0-01). Written informed consent for participation was not required for this study in accordance with the national legislation and the institutional requirements.

AUTHOR CONTRIBUTIONS

XW, CL, and BZ contributed to conception and design of the study. XZ and YS organized the database. BZ and XW performed the statistical analysis. CL wrote the first draft of the manuscript. XW, CL, YS, and XZ wrote sections of the manuscript. XW, CL, DZ, and YL revised various parts of the manuscript. All authors contributed to manuscript revision, read, and approved the submitted version.

SUPPLEMENTARY MATERIAL

The Supplementary Material for this article can be found online at: https://www.frontiersin.org/articles/10.3389/fcvm.2022.803695/full#supplementary-material

REFERENCES

1. Zhou J, Shi Z, Zhou L, Hu Y, Zhang M. Occupational noise-induced hearing loss in China: a systematic review and meta-analysis. *BMJ Open.* (2020) 10:e039576. doi: 10.1136/bmjopen-2020-039576
2. Pyko A, Andersson N, Eriksson C, de Faire U, Lind T, Mitkovskaya N, et al. Long-term transportation noise exposure and incidence of ischaemic heart disease and stroke: a cohort study. *Occup Environ Med.* (2019) 76:201–7. doi: 10.1136/oemed-2018-105333
3. Beutel ME, Brahler E, Ernst M, Klein E, Reiner I, Wiltink J, et al. Noise annoyance predicts symptoms of depression, anxiety and sleep disturbance 5 years later. Findings from the Gutenberg Health Study. *Eur J Public Health.* (2020) 30:516–21. doi: 10.1093/eurpub/ckaa015

4. *Occupational Exposure Limits for Hazardous Factors in the Workplace Part 2: Physical Factors*. Beijing: China Science Publishing & Media Ltd. (CSPM) (2007). p. 14p:A4.
5. Zhao S, He D, Zhang H, Hou T, Yang C, Ding W, et al. Health study of 11,800 workers under occupational noise in Xinjiang. *BMC Public Health.* (2021) 21:460. doi: 10.1186/s12889-021-10496-3
6. *Hypertension.* Available at: https://www.who.int/health-topics/hypertension/#tab=tab_1 (accessed on September 1, 2021).
7. Rust P, Ekmekcioglu C. Impact of Salt Intake on the Pathogenesis and Treatment of Hypertension. *Adv Exp Med Biol.* (2017) 956:61–84. doi: 10.1007/5584_2016_147
8. Gloria-Bottini F, Banci M, Neri A, Magrini A, Bottini E. Smoking and hypertension: Effect of adenosine deaminase polymorphism. *Clin Exp Hypertens.* (2019) 41:548–51. doi: 10.1080/10641963.2018.1516776
9. Becton LJ, Shatat IF, Flynn JT. Hypertension and obesity: epidemiology, mechanisms and clinical approach. *Indian J Pediatr.* (2012) 79:1056–61. doi: 10.1007/s12098-012-0777-x
10. Zeeb H, Hegewald J, Schubert M, Wagner M, Droge P, Swart E, et al. Traffic noise and hypertension - results from a large case-control study. *Environ Res.* (2017) 157:110–7. doi: 10.1016/j.envres.2017.05.019
11. Seidler A, Wagner M, Schubert M, Droge P, Romer K, Pons-Kuhnemann J, et al. Aircraft, road and railway traffic noise as risk factors for heart failure and hypertensive heart disease-A case-control study based on secondary data. *Int J Hyg Environ Health.* (2016) 219:749–58. doi: 10.1016/j.ijheh.2016.09.012
12. Zhou F, Shrestha A, Mai S, Tao Z, Li J, Wang Z, et al. Relationship between occupational noise exposure and hypertension: A cross-sectional study in steel factories. *Am J Ind Med.* (2019) 62:961–8. doi: 10.1002/ajim.23034
13. Tessier-Sherman B, Galusha D, Cantley LF, Cullen MR, Rabinowitz PM, Neitzel RL. Occupational noise exposure and risk of hypertension in an industrial workforce. *Am J Ind Med.* (2017) 60:1031–8. doi: 10.1002/ajim.22775
14. Stokholm ZA, Bonde JP, Christensen KL, Hansen AM, Kolstad HA. Occupational noise exposure and the risk of hypertension. *Epidemiology.* (2013) 24:135–42. doi: 10.1097/EDE.0b013e31826b7f76
15. Lin YT, Chen TW, Chang YC, Chen ML, Hwang BF. Relationship between time-varying exposure to occupational noise and incident hypertension: A prospective cohort study. *Int J Hyg Environ Health.* (2020) 226:113487. doi: 10.1016/j.ijheh.2020.113487
16. Said MA, El-Gohary OA. Effect of noise stress on cardiovascular system in adult male albino rat: implication of stress hormones, endothelial dysfunction and oxidative stress. *Gen Physiol Biophys.* (2016) 35:371–7. doi: 10.4149/gpb_2016003
17. Joyner MJ, Charkoudian N, Wallin BG, A. sympathetic view of the sympathetic nervous system and human blood pressure regulation. *Exp Physiol.* (2008) 93:715–24. doi: 10.1113/expphysiol.2007.039545
18. Munzel T, Daiber A, Steven S, Tran LP, Ullmann E, Kossmann S, et al. Effects of noise on vascular function, oxidative stress, and inflammation: mechanistic insight from studies in mice. *Eur Heart J.* (2017) 38:2838–49. doi: 10.1093/eurheartj/ehx081
19. Schmidt FP, Basner M, Kroger G, Weck S, Schnorbus B, Muttray A, et al. Effect of nighttime aircraft noise exposure on endothelial function and stress hormone release in healthy adults. *Eur Heart J.* (2013) 34:3508-14a. doi: 10.1093/eurheartj/eht269
20. Hahad O, Prochaska JH, Daiber A, Muenzel T. Environmental noise-induced effects on stress hormones, oxidative stress, and vascular dysfunction: key factors in the relationship between cerebrocardiovascular and psychological disorders. *Oxid Med Cell Longev.* (2019) 2019:4623109. doi: 10.1155/2019/4623109
21. Wang D, Zhou M, Li W, Kong W, Wang Z, Guo Y, et al. Occupational noise exposure and hypertension: the Dongfeng-Tongji Cohort Study. *J Am Soc Hypertens.* (2018) 12:71–9 e5. doi: 10.1016/j.jash.2017.11.001
22. Yang Y, Zhang E, Zhang J, Chen S, Yu G, Liu X, et al. Relationship between occupational noise exposure and the risk factors of cardiovascular disease in China: A meta-analysis. *Medicine (Baltimore).* (2018) 97:e11720. doi: 10.1097/MD.0000000000011720
23. Rabiei H, Ramezanifar S, Hassanipour S, Gharari N. Investigating the effects of occupational and environmental noise on cardiovascular diseases: a systematic review and meta-analysis. *Environ Sci Pollut Res Int.* (2021) 28:62012–29. doi: 10.1007/s11356-021-16540-4
24. Fu W, Wang C, Zou L, Liu Q, Gan Y, Yan S, et al. Association between exposure to noise and risk of hypertension: a meta-analysis of observational epidemiological studies. *J Hypertens.* (2017) 35:2358–66. doi: 10.1097/HJH.0000000000001504
25. Tomei G, Fioravanti M, Cerratti D, Sancini A, Tomao E, Rosati MV, et al. Occupational exposure to noise and the cardiovascular system: a meta-analysis. *Sci Total Environ.* (2010) 408:681–9. doi: 10.1016/j.scitotenv.2009.10.071
26. Bolm-Audorff U, Hegewald J, Pretzsch A, Freiberg A, Nienhaus A, Seidler A. Occupational Noise and Hypertension Risk: A Systematic Review and Meta-Analysis. *Int J Environ Res Public Health.* (2020) 17:6281. doi: 10.3390/ijerph17176281
27. Vandenbroucke JP, von Elm E, Altman DG, Gotzsche PC, Mulrow CD, Pocock SJ, et al. Strengthening the Reporting of Observational Studies in Epidemiology (STROBE): explanation and elaboration. *PLoS Med.* (2007) 4:e297. doi: 10.1371/journal.pmed.0040297
28. Williams B, Mancia G, Spiering W, Rosei EA, Azizi M, Burnier M, et al. 2018 ESC/ESH Guidelines for the management of arterial hypertension (vol 39, pg 3021, 2018). *Eur Heart J.* (2019) 40:475. doi: 10.1093/eurheartj/ehy686
29. de Francisco ALM, Varas J, Ramos R, Merello JI, Canaud B, Stuard S, et al. Proton Pump Inhibitor Usage and the Risk of Mortality in Hemodialysis Patients. *Kidney Int Rep.* (2018) 3:374–84. doi: 10.1016/j.ekir.2017.11.001
30. Junren Zhu, Runlin Gao, Shuiping Zhao, Guoping Lu, Dong Zhao, Jianjun Li. Guidelines for the prevention and treatment of dyslipidemia in Chinese adults (revised in 2016). *Chin J Health Manage.* (2017) 11:7-28 %@1674-0815%L11-5624/R%WCNKI.
31. Staffa SJ, Zurakowski D. Five Steps to Successfully Implement and Evaluate Propensity Score Matching in Clinical Research Studies. *Anesth Analg.* (2018) 127:1066–73. doi: 10.1213/ANE.0000000000002787
32. Varas J, Perez-Saez MJ, Ramos R, Merello JI, de Francisco ALM, Luno J, et al. Returning to haemodialysis after kidney allograft failure: a survival study with propensity score matching. *Nephrol Dial Transplant.* (2019) 34:667–72. doi: 10.1093/ndt/gfy215
33. Austin PC. Goodness-of-fit diagnostics for the propensity score model when estimating treatment effects using covariate adjustment with the propensity score. *Pharmacoepidemiol Drug Saf.* (2008) 17:1202–17. doi: 10.1002/pds.1673
34. Thoemmes F. *Propensity Score Matching in SPSS*. Available at: http://arxiv.org/abs/1201.6385 (accessed on December 2, 2021).
35. Wilson A, Zigler CM, Patel CJ, Dominici F. Model-averaged confounder adjustment for estimating multivariate exposure effects with linear regression. *Biometrics.* (2018) 74:1034–44. doi: 10.1111/biom.12860
36. Benedetto U, Head SJ, Angelini GD, Blackstone EH. Statistical primer: propensity score matching and its alternatives. *Eur J Cardiothorac Surg.* (2018) 53:1112–7. doi: 10.1093/ejcts/ezy167
37. Lunt M. Selecting an appropriate caliper can be essential for achieving good balance with propensity score matching. *Am J Epidemiol.* (2014) 179:226–35. doi: 10.1093/aje/kwt212

Conflict of Interest: The authors declare that the research was conducted in the absence of any commercial or financial relationships that could be construed as a potential conflict of interest.

Publisher's Note: All claims expressed in this article are solely those of the authors and do not necessarily represent those of their affiliated organizations, or those of the publisher, the editors and the reviewers. Any product that may be evaluated in this article, or claim that may be made by its manufacturer, is not guaranteed or endorsed by the publisher.

Copyright © 2022 Wu, Li, Zhang, Song, Zhao, Lan and Zhou. This is an open-access article distributed under the terms of the Creative Commons Attribution License (CC BY). The use, distribution or reproduction in other forums is permitted, provided the original author(s) and the copyright owner(s) are credited and that the original publication in this journal is cited, in accordance with accepted academic practice. No use, distribution or reproduction is permitted which does not comply with these terms.

frontiers | Frontiers in Cardiovascular Medicine

ORIGINAL RESEARCH
published: 02 May 2022
doi: 10.3389/fcvm.2022.788476

Red Blood Cell Distribution Width: A Prognostic Marker in Patients With Type B Aortic Dissection Undergoing Endovascular Aortic Repair

Cheng Jiang[1†], Anbang Liu[1,2†], Lei Huang[1], Quanjun Liu[1,2], Yuan Liu[1] and Qingshan Geng[1,2*]*

[1] Department of Cardiology, Guangdong Cardiovascular Institute, Guangdong Provincial People's Hospital, Guangdong Academy of Medical Sciences, Guangzhou, China, [2] School of Medicine, South China University of Technology, Guangzhou, China

OPEN ACCESS

Edited by:
Yuli Huang,
Southern Medical University, China

Reviewed by:
Zhihui Dong,
Fudan University, China
Dan Rudic,
Augusta University, United States
Lin Xiao,
Southern Medical University, China

***Correspondence:**
Qingshan Geng
gengqingshan@gdph.org.cn
Yuan Liu
13711652730@139.com

[†]These authors have contributed equally to this work and share first authorship

Specialty section:
This article was submitted to General Cardiovascular Medicine, a section of the journal Frontiers in Cardiovascular Medicine

Received: *02 October 2021*
Accepted: *31 March 2022*
Published: *02 May 2022*

Citation:
Jiang C, Liu A, Huang L, Liu Q, Liu Y and Geng Q (2022) Red Blood Cell Distribution Width: A Prognostic Marker in Patients With Type B Aortic Dissection Undergoing Endovascular Aortic Repair. Front. Cardiovasc. Med. 9:788476. doi: 10.3389/fcvm.2022.788476

Background: Red blood cell distribution width (RDW) is associated with cardiovascular mortality. However, the relationship between preoperative RDW and outcomes after thoracic endovascular aortic repair (TEVAR) in type B aortic dissection (TBAD) remains to be determined.

Methods: We review the records of 678 patients with TBAD and treated with TEVAR in three centers. Patients were divided into two groups according to the admission RDW cut-off by receiver operating characteristic curve analysis [≤13.5% (n = 278) and >13.5% (n = 400)]. The association between RDW and long-term mortality was evaluated using Cox survival analysis. Additionally, we used general additive models (GAM) with restricted cubic splines (RCS) to explore non-linear relationships between RDW and outcomes.

Results: Subjects with a high RDW had significantly higher in-hospital mortality rates (1.4 vs. 4.3%, P = 0.038). A total of 70 subjects died after a median follow-up period of 3.3 years. Kaplan–Meier analysis showed that subjects with an RDW >13.5% had worse survival rates than those with lower RDW values (P < 0.001). Multivariate Cox proportional hazard modeling revealed that an RDW >13.5% was an independent predictor of long-term mortality (adjusted HR = 2.27, P = 0.006). Also, we found that there was a non-linear relationship between RDW and mortality from RCS, and RDW of 13.5% might be an inflection point to distinguish the long-term mortality risk of TBAD patients.

Conclusion: As an inexpensive and routinely measured parameter, RDW holds promise as a novel prognostic marker in patients with TBAD receiving TEVAR. We found that an RDW >13.5% on admission was independently associated with increased long-term mortality.

Keywords: aortic dissection, red blood cell distribution width, thoracic endovascular aortic repair, prognostic marker, in-hospital mortality

INTRODUCTION

Type B aortic dissection (TBAD) is a fatal disease, characterized by acute and subacute forms that present with several complications including a high mortality [(1), p. 2873–926]. Thoracic endovascular aortic repair (TEVAR) is an emerging treatment approach that has rapidly gained acceptance by clinicians for treating acute and sub-acute TBAD [(2, 3); (4), p. 407–16]. Compared to open surgery and medical treatment, TEVAR is considered a superior treatment strategy with lower mortality rates (5). However, postoperative mortality is still high during short- and long-term follow-ups [(3); (6), p. 213–25]. Therefore, early identification of patients at high risk for adverse outcomes is essential for clinicians to make the necessary therapeutic adjustments in a timely manner to improve prognosis.

Red blood cell distribution width (RDW) is a routine laboratory test parameter that reflects variations in the volume of red blood cells (RBC) volume [(7), p. 71–4]. In TBAD patients, blood entering the intima-media space may lead to blood loss. Liu et al. found that RDW was significantly higher in patients with anemia than in those with normal RBC levels [(8), p. 205–9]. In addition, RDW can be influenced by imbalanced physiological conditions, including oxidative stress, tissue hypoxia, neurohumoral hyperactivity, endothelial dysfunction, and chronic inflammation, all of which play an important role in aortic dissection (AD) [(9), p. 72–3]. In several clinical conditions, a high RDW has been associated with adverse outcomes. Therefore, we hypothesized that RDW could be a prognostic marker for patients with TBAD receiving TEVAR. The present study aimed to determine the relationship between RDW and adverse outcomes in patients with TBAD after TEVAR.

MATERIALS AND METHODS

Patient Selection

Included in the study, were patients with consecutive TBAD who underwent TEVAR between January 2010 and July 2015, they were retrospectively identified at the Guangdong Provincial People's Hospital (Guangzhou, China), Nanhai Hospital of Guangdong General Hospital (Foshan, China), and Zhuhai Hospital of Guangdong Provincial People's Hospital (Zhuhai, China). TBAD was diagnosed according to a multi-detector computed tomography scanning, and patients without complications received TEVAR when the true lumen was severely compressed or when the false lumen was >22 mm in diameter [(10), p. 374–81]. The operation was performed in a cardiac catheterization room with a suitable anatomical structure. According to the pathology of the aorta, the aortic stent diameter generally exceeds the standard by 5–10%. In order to eliminate tears at the proximal entrance, all stent grafts were deployed retrogradely through the percutaneous femoral artery approach. The left subclavian artery was covered when necessary to obtain a 1.5–2-cm proximal landing area. The exclusion criteria were as follows: (1) age <18 years; (2) AD caused by trauma, iatrogenic injury, or intramural hematoma; (3) diagnosis of Marfan syndrome; (4) previous TEVAR or surgery for AD; (5) chronic AD (onset >90 days before treatment) (11); (6) no previous TEVAR interventions; (7) history of malignancy or hematological disease, except anemia; and (8) end-stage kidney disease (**Figure 1**). The study protocol was approved by the central ethics committee of the Guangdong Provincial People's Hospital (2017-15), with a waiver for informed consent. This approval by the central ethics committee applied to the other two collaborating hospitals as well.

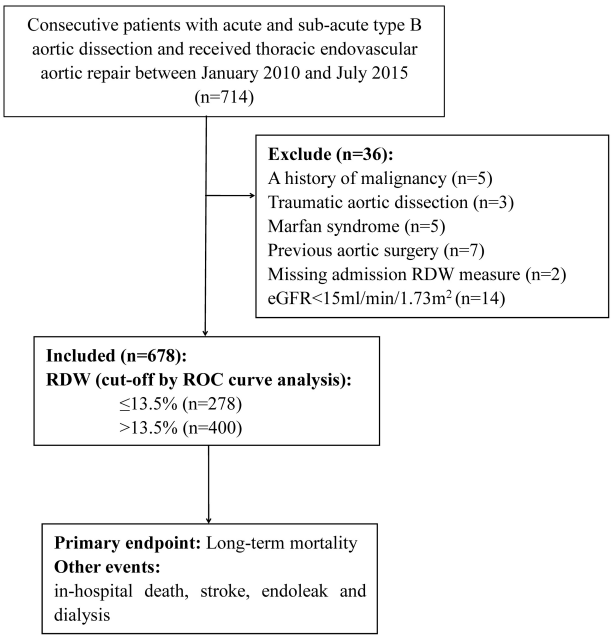

FIGURE 1 | Study population flow chart.

Biochemical Assays and Data Collected

Upon admission of the patients, venous blood was collected to determine specific laboratory parameters. RDW was measured using an automated blood cell counter (LH780, Beckman Coulter, Brea, CA, United States), with a normal range of 11–16%. Clinical data were collected through chart review and electronic case reports entered into EpiData software 3.1 (The EpiData Association, Odense, Denmark) and processed using a consistency check on two copies. The estimated glomerular filtration rate (eGFR) in Chinese patients was evaluated using the 4-variable Modification of Diet in Renal Disease (MDRD) equation [(12), p. 2937–44].

Follow-Up and Endpoints

All patients were followed up by trained researchers *via* telephone interviews or clinic record visits from 9 August 2016 to 30 February 2017. In addition, the full clinical records of readmitted patients and outpatients were reviewed for adverse events. The primary endpoint was long-term mortality, which was defined as death from all causes after being diagnosed with TBAD. In-hospital death, stroke, type I endoleak, and dialysis

events were recorded. Type I endoleak is defined as significant when detected during intraoperative control angiography or primary postoperative CTA control (in-hospital) [(13), p. 1022–33, 1033.e15]. Stroke includes ischemic or hemorrhagic stroke, with the clinical diagnosis supported by brain imaging.

Statistical Analysis

All statistical analyses were performed using SPSS software (version 22.0; SPSS, Inc., Chicago, IL, United States) and R version 3.6.1[1] (the R Foundation). Mean (±SD) or median (quartile range) values were used to describe continuous variables, which were compared using two independent sample *t*-tests or non-parametric tests based on the data. Categorical variables were reported as absolute values with percentages and compared using the Chi-squared test. Receiver operator characteristic (ROC) curve analysis was performed to evaluate the predictive value of RDW for in-hospital and long-term mortality. In addition, the optimal cut-off values were calculated. The optimal cut-off values for the ROC curves were established using the Youden index. Univariate Cox survival analysis was conducted to assess the risk factors for long-term mortality, indicators with *P*-values less than 0.05 were placed in a multivariate Cox proportional hazard model for further analysis. To visually evaluate the functional relationships between continuous variable and outcomes, the way similar with previous studies explored [(14), p. e007054; (15), p. 4322–9], we used general additive models (GAM) with restricted cubic splines (RCS) to assess the non-linear relationships between RDW and outcomes. Statistical significance was set at $P < 0.05$.

RESULTS

After screening, data from 678 patients were included in the final analysis. The mean age of the patients was 55 ± 11 years, 86.6% were men, and 21 (3.1%) died during the initial hospitalization. An ROC curve analysis was conducted to determine the predictive value of RDW at admission for in-hospital mortality. The optimal cut-off value was 13.5%, with relatively high sensitivity and specificity (AUC = 0.646, 95% CI, 0.530–0.763, $P = 0.023$, **Figure 2**).

Patients were classified into two groups according to the threshold value of RDW, with RDW ≤13.5% ($n = 278$) and RDW >13.5% ($n = 400$). At admission, 26.8% of patients developed anemia, with a higher percentage of subjects with a high RDW (33.3 vs. 16.9%, $P < 0.001$). Clinical information was compared between the two groups (**Table 1**). Hemoglobin and eGFR were lower in the group with a RDW >13.5%, while the serum creatinine was higher.

During hospitalization, 51 (7.5%) patients experienced endovascular leaks after the TEVAR procedure, 23 (3.4%) developed stroke, and 14 (2.1%) required dialysis. There was no statistically significant difference between the patients with an RDW above or below 13.5%. However, the in-hospital mortality was higher in patients with an RDW >13.5% (4.3 vs 1.4%, $P = 0.038$, **Table 1**).

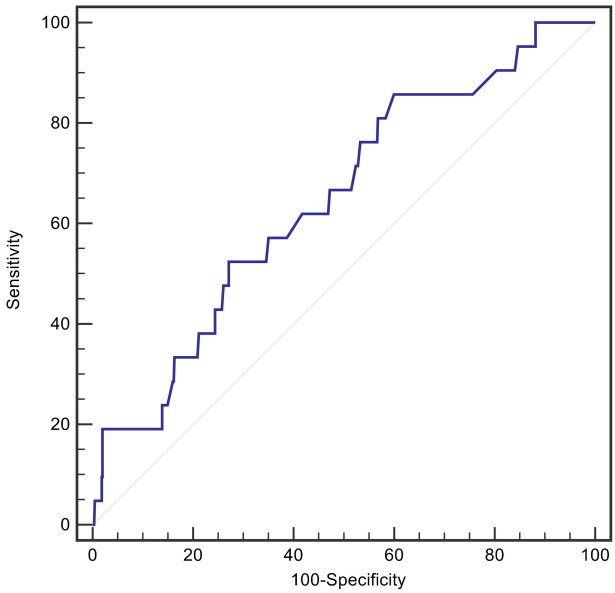

FIGURE 2 | The ROC curves for RDW in predicting in-hospital death.

After a median follow-up of 3.3 years, 70 (10.3%) patients died, and 87 (12.8%) were lost to follow-up. Kaplan–Meier curve analysis showed that patients with an RDW >13.5% had a worse survival than those with a lower RDW (15.9 vs 6.1%, log-rank test = 13.37, $P < 0.001$, **Figure 3**). The results of the Cox proportional hazard modeling analysis are presented in **Table 2**. Univariate survival analysis indicated that RDW >13.5% was associated with long-term mortality (HR = 2.78; 95% CI, 1.57–4.92; $P < 0.001$). After the adjustment for these variables, RDW >13.5% remained an independent predictor of long-term mortality (adjusted HR = 2.27; 95% CI, 1.27–4.07; $P = 0.006$).

The RCS suggested a non-linear association between RDW and mortality, while this significance was not observed in RDW-MACE relationship (**Figure 4**). There were increasing relationships between RDW and outcomes. The difference was that, RDW-mortality relation first showed a plateau phase and then increased, while RDW-MACE relation was the opposite. Notably, for RDW-mortality relation (**Figure 4A**), when RDW (*x*-axis) was 13.5%, the Log RR (relative risk) for mortality (*y*-axis) was approximately 0, suggesting that RR = 1, which implied RDW at this cutoff value had no impact on the probability of mortality. When RDW >13.5%, the Log RR of mortality increased monotonically, reflecting that the increased long-term mortality risk of TBAD patients with the increase of RDW.

DISCUSSION

To the best of our knowledge, this study is the first to investigate the prognostic value of RDW in patients with TBAD receiving TEVAR. The results showed that RDW could be a

[1]http://www.R-project.org

TABLE 1 | Clinical characteristics according to RDW cut-off.

Clinical variables	RDW ≤ 13.5% (*n* = 278)	RDW >13.5% (*n* = 400)	*P*
Age (years)	53.7 ± 10.5	55.4 ± 10.9	0.050
Females, *n* (%)	37 (13.3)	54 (13.5)	0.943
Hypertension, *n* (%)	228 (82.0)	347 (86.8)	0.091
Diabetes mellitus, *n* (%)	14 (5.0)	28 (7.0)	0.297
Type, *n* (%)			
Acute	223 (80.2)	328 (82.0)	0.558
Sub-acute	55 (19.8)	72 (18.0)	
Hemoglobin (g/L)	130.0 ± 14.5	125.1 ± 19.6	<0.001
Anemia, *n* (%)	47 (16.9)	135 (33.8)	<0.001
CRP (mg/L)	74.0 (28.1, 114.5)	77.4 (26.2,126.8)	0.926
lgDDI	3.11 ± 0.54	3.12 ± 0.53	0.751
Serum creatinine (μmol/L)	97.5 ± 43.1	105.7 ± 50.5	0.024
eGFR (mL/min/1.73 m^2)	83.8 ± 29.5	78.7 ± 32.6	0.037
LVEF (%)	64.8 ± 5.8	65.0 ± 7.3	0.689
Artery affected, *n* (%)			
Celiac axis	84 (32.7)	119 (31.7)	0.801
SMA	48 (18.8)	78 (20.9)	0.506
Right renal artery	54 (21.0)	108 (28.6)	0.032
Left renal artery	68 (26.4)	93 (24.9)	0.673
Pleural effusion, *n* (%)	130 (48.0)	188 (47.5)	0.900
Aortic arch bypass, *n* (%)	45 (16.2)	81 (20.3)	0.181
Stent inserted ≥2, *n* (%)	55 (19.8)	72 (18.0)	0.558
Hospital stay, days	13.0 (9.0, 18.0)	13.0 (10.0,18.0)	0.351
In-hospital events, *n* (%)			
Stroke	9 (3.2)	14 (3.5)	0.853
Type I endoleak	20 (7.2)	31 (7.8)	0.787
Dialysis	4 (1.4)	10 (2.5)	0.339
Death	4 (1.4)	17 (4.3)	0.038
Long-term mortality, *n* (%)	15 (6.1)	55 (15.9)	<0.001

CRP, C-reactive protein; DDI, D-dimer; eGFR, estimated glomerular filtration rate; LVEF, left ventricular ejection fraction; SMA, superior mesenteric artery.

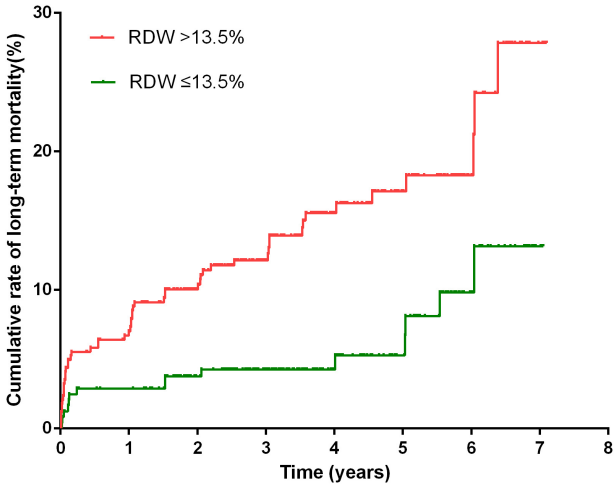

FIGURE 3 | Cumulative rate of long-term mortality in patients with RDW >13.5% and patients with RDW <13.5%.

predictor of in-hospital mortality. In addition, an RDW >13.5% was independently associated with an increased risk of long-term mortality.

Besides, we found a non-linear RDW-mortality relationship by GAM with RCS, suggesting that there was a threshold effect in the trend of mortality with RDW, and the two-piecewise linear regression models on both sides of the inflection point were statistically significant. As can be seen from the **Figure 4A**, the RDW of 13.5% might be the inflection point for distinguishing the mortality risk of TBAD patients, corresponding to the RDW cut-off value determined by the ROC curve.

Type B aortic dissection of the descending aorta or arch of the aorta is a life-threatening disease. Open surgical treatment has a high mortality and significant late complications, which have gradually been replaced by TEVAR [(13, 16), p. 1022–33, 1033.e15]. The epidemiological data indicate that the in-hospital mortality rate is 32% for patients with TBAD and treated with surgery, 7% for those treated with TEVAR, and 10% for those treated with medicine only [(17), p. 800–11]. In our study, the long-term mortality rate was 10.3%, which is similar to previous data [(4), p. 407–16]. Despite the decrease in TEVAR mortality, a significant number of patients still die after this intervention. Therefore, there is an urgent need to identify patients with a high mortality risk.

Red blood cell distribution width quantifies the heterogeneity of circulating RBCs and has been used to differentiate the causes of anemia. Subsequently, RDW is a well-established predictor of short- and long-term outcomes in various clinical conditions, including coronary artery disease and infectious diseases, as well as in the general population [(18), p. 515–23; (19), p. 163–8; (20), 123–7]. However, its potential to provide prognostic information for patients with TBAD remains unclear. In this study, we found that increased RDW was associated with in-hospital and long-term mortality after TEVAR for TBAD.

The following features can explain this effect. First, blood could enter the false lumen through the endovascular tear in patients with TBAD, leading to a decrease in circulating blood volume. This phenomenon can be detected by routine blood tests and may present as anemia. In our analysis, 26.8% of the subjects had anemia on admission. A previous study demonstrated a significant increase in RDW in patients with anemia [(8), p. 205–9]. Anemia is a predictor of adverse outcomes in several cardiovascular diseases [(21), p. 610–20; (22), p. 818–27]. However, this result was not the only explanation, as the RDW significance could not be eliminated by including anemia in our multivariate analysis. Second, increased oxidative stress has been found in patients with AD (23). Oxidative stress can directly damage RBCs and decrease their survival, resulting in increased anisocytosis (24, 25) and increased RDW. Selenium was negatively correlated with RDW as a component of the antioxidant defense system (26). A higher RDW may reflect severe oxidative stress, leading to adverse outcomes. Third, stress on the endoplasmic reticulum might occur, altering the regulation of apoptosis and inflammation. Excessive apoptosis could subsequently promote inflammation and degeneration of the vascular wall, which is an important mechanism for the

TABLE 2 | Univariate and multivariate Cox proportional hazard modeling analysis for long-term mortality.

	Univariate analysis			Multivariate analysis		
Clinical variables	**HR**	**95% CI**	***P***	**HR**	**95% CI**	***P***
Age	1.05	1.02, 1.07	<0.001	1.05	1.02, 1.07	<0.001
Females	1.82	1.01, 3.27	0.046	2.10	1.14, 3.87	0.017
Hypertension	1.55	0.71, 3.39	0.271			
Diabetes	0.86	0.32, 2.37	0.777			
Acute TBAD	0.93	0.51, 1.69	0.804			
RDW >13.5%	2.78	1.57, 4.92	<0.001	2.27	1.27, 4.07	0.006
Anemia	1.90	1.18, 3.06	0.008	1.22	0.73, 2.02	0.452
CRP	1.00	0.99, 1.00	0.549			
lgDDI	1.68	1.07, 2.65	0.025	1.47	0.93, 2.34	0.100
Serum creatinine	1.00	1.00, 1.01	0.028	1.01	1.00, 1.01	0.019
LVEF	0.97	0.94, 1.01	0.109			
Celiac axis affected	1.23	0.72, 2.10	0.440			
SMA affected	1.73	0.99, 3.05	0.056			
Right renal artery affected	1.42	0.82, 2.46	0.217			
Left renal artery affected	1.08	0.61, 1.91	0.799			
Pleural effusion	1.07	0.67, 1.72	0.768			
Aortic arch bypass	1.28	0.74, 2.21	0.381			
Stent inserted ≥2	1.08	0.58, 2.03	0.801			

SBP, systolic blood pressure; DBP, diastolic blood pressure; CRP, C-reactive protein; DDI, D-dimer; eGFR, estimated glomerular filtration rate; LVEF, left ventricular ejection fraction; SMA, superior mesenteric artery.

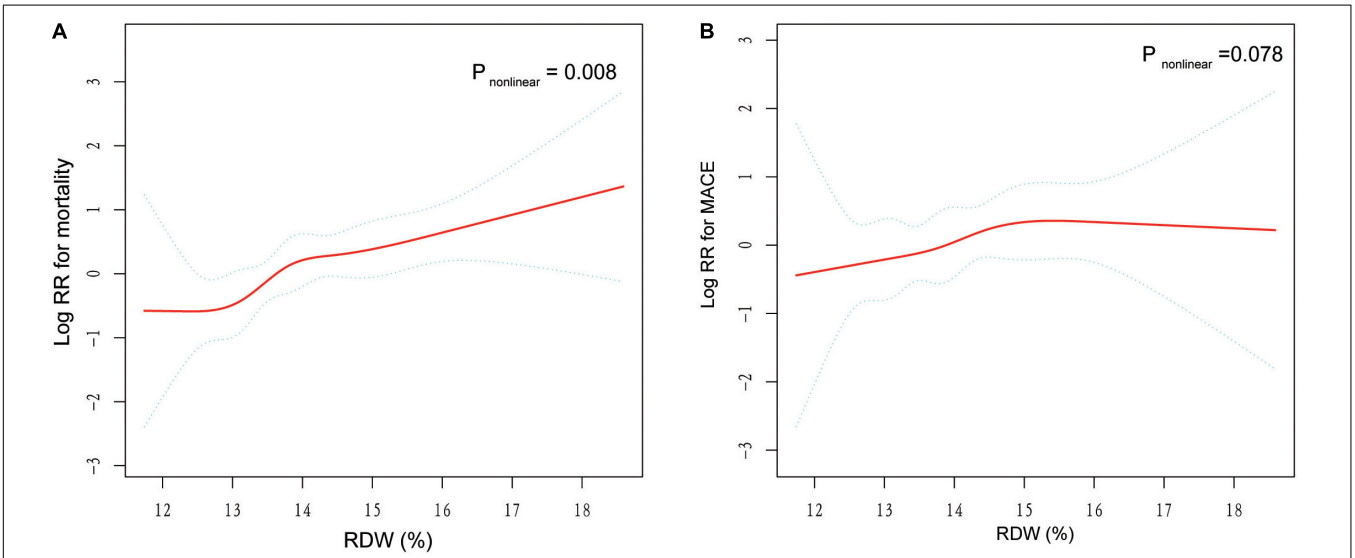

FIGURE 4 | General additive models (GAM) with restricted cubic splines (RCS) demonstrate the relationship between RDW and the risk of mortality and MACE. The resulting figures show the predicted log RR (relative risk) in the *y*-axis and the RDW in the *x*-axis. Log RR can be converted to a relative risk by taking antilog. For example, a log RR of 0 implies the relative risk of 1 (no impact on the probability of prognosis), whereas a log RR of 1 implies the relative risk of 2.71 (i.e., 2.71-fold increase in the probability of MACE or mortality). **(A)** Association between RDW and log RR for mortality. **(B)** Association between RDW and log RR for MACE.The results were adjusted for covariates that statistically significant in multivariate analysis in **Table 2**, including age, gender, and serum creatinine.

formation and progression of AD (27). In response to this inflammatory process, pro-inflammatory cytokines are released, resulting in an increase in RDW [(28), p. 1011–23]. Finally, shear stress may be another factor leading to a high RDW and adverse outcomes. Taguchi et al. found that a high shear stress could induce intimal tears, which can progress to overt AD [(29), p. 78–82]. In addition, increased shear stress was associated with the development of retrograde aortic type A dissection, which is a severe complication of TBAD [(30), p. 324–330]. Shear stress can also impair RBC deformation and precipitate hemolysis, promoting increased RDW [(31), p. 1017–25].

The current study found that an increase in RDW levels upon admission is independently associated with an increase in long-term mortality in patients with TBAD. As an easily available

indicator in routine blood testing, RDW can be used as an important factor in prognostic risk stratification, selecting high-risk patients, guiding treatment strategies, and reducing the risk of all-cause death in patients with TBAD. In view of the common prognostic effect of high RDW in several cardiovascular and infectious diseases, a high RDW is likely to represent secondary damage related to inflammatory responses, and oxidative stress. Monitoring changes in RDW may reflect the effects of controlling cardiovascular risk factors. It may be possible to base future follow-up plans on patients' RDW and improve the long-term survival of AD patients, since many patients with TBAD may not strictly follow the annual follow-up recommendation.

Study Limitation

This study had several limitations. First, due to its retrospective design, confounding factors may have affected the results. However, a multivariate analysis was performed to reduce these. Second, the predictive value of RDW was not compared with that of other inflammatory markers. Third, the RDW was not detected dynamically. Therefore, it is not clear whether a continuous measurement of the dynamic changes in RDW rather than the measurement of the baseline RDW would have a better predictive value for the outcomes of the patient. Finally, the lost to follow-up rate (12.8%) in the present study was relatively high and could lead to selection bias.

CONCLUSION

As an inexpensive and routinely measured RBC parameter, RDW has been proven to be a useful prognostic marker in patients with TBAD receiving TEVAR. Increased RDW was significantly associated with in-hospital and long-term mortality. This relationship should be investigated in prospective studies with larger sample sizes.

DATA AVAILABILITY STATEMENT

The original contributions presented in the study are included in the article/supplementary material, further inquiries can be directed to the corresponding authors.

ETHICS STATEMENT

Ethical review and approval was not required for the study on human participants in accordance with the local legislation and institutional requirements. Written informed consent for participation was not required for this study in accordance with the national legislation and the institutional requirements.

AUTHOR CONTRIBUTIONS

QG, YL, and CJ contributed to the conception and design of the study. CJ, AL, LH, and QL contributed to the acquisition, analysis, and interpretation of data. CJ and AL drafted the manuscript. QG and YL critically revised the manuscript. All authors gave final approval and agreed to be accountable for all aspects of work ensuring integrity and accuracy.

FUNDING

This work was supported by the grants of Natural Science Foundation of Guangdong Province (2019A1515011224) and the High-Level Hospital Construction Project of Guangdong Provincial People's Hospital (DFJH201811, DFJH201922, and DFJH2020003).

REFERENCES

1. Erbel R, Aboyans V, Boileau C, Bossone E, Bartolomeo RD, Eggebrecht H, et al. 2014 ESC Guidelines on the diagnosis and treatment of aortic diseases: document covering acute and chronic aortic diseases of the thoracic and abdominal aorta of the adult. The task force for the diagnosis and treatment of aortic diseases of the European society of cardiology (ESC). *Eur Heart J.* (2014) 35:2873–926. doi: 10.1093/eurheartj/ehu281
2. Brunkwall J, Lammer J, Verhoeven E, Taylor P. ADSORB: a study on the efficacy of endovascular grafting in uncomplicated acute dissection of the descending aorta. *J Vasc Surg.* (2012) 56:31–6. doi: 10.1016/j.ejvs.2012.03.023
3. Fattori R, Montgomery D, Lovato L, Kische S, Di Eusanio M, Ince H, et al. Survival after endovascular therapy in patients with type B aortic dissection: a report from the International registry of acute aortic dissection (IRAD). *JACC Cardiovasc Interv.* (2013) 6:876–82. doi: 10.1016/j.jcin.2013.05.003
4. Nienaber CA, Kische S, Rousseau H, Eggebrecht H, Rehders TC, Kundt G, et al. Endovascular repair of type B aortic dissection: long-term results of the randomized investigation of stent grafts in aortic dissection trial. *Circ Cardiovasc Interv.* (2013) 6:407–16. doi: 10.1161/CIRCINTERVENTIONS.113.000463
5. Fattori R, Tsai TT, Myrmel T, Evangelista A, Cooper JV, Trimarchi S, et al. Complicated acute type B dissection: is surgery still the best option?: a report from the International registry of acute aortic dissection. *JACC Cardiovasc Interv.* (2008) 1:395–402. doi: 10.1016/j.jcin.2008.04.009
6. Heijmen RH, Thompson MM, Fattori R, Goktay Y, Teebken OE, Orend KH. Valiant thoracic stent-graft deployed with the new captivia delivery system: procedural and 30-day results of the valiant captivia registry. *J Endovasc Ther.* (2012) 19:213–25. doi: 10.1583/11-3652MR.1
7. Evans TC, Jehle D. The red blood cell distribution width. *J Emerg Med.* (1991) 9:71–4. doi: 10.1016/0736-4679(91)90592-4
8. Liu Q, Dang AM, Chen BW, Lv NQ, Wang X, Zheng DY. The association of red blood cell distribution width with anemia and inflammation in patients with Takayasu arteritis. *Clin Chim Acta.* (2015) 438:205–9. doi: 10.1016/j.cca.2014.08.025
9. Loprinzi PD. Comparative evaluation of red blood cell distribution width and high sensitivity C-reactive protein in predicting all-cause mortality and coronary heart disease mortality. *Int J Cardiol.* (2016) 223:72–3. doi: 10.1016/j.ijcard.2016.08.156
10. Ding H, Liu Y, Xie N, Fan R, Luo S, Huang W, et al. Outcomes of chimney technique for preservation of the left subclavian artery in type B aortic dissection. *Eur J Vasc Endovasc Surg.* (2019) 57:374–81. doi: 10.1016/j.ejvs.2018.09.005
11. Steuer J, Björck M, Mayer D, Wanhainen A, Pfammatter T, Lachat M. Distinction between acute and chronic type B aortic dissection: is there a sub-acute phase? *J Vasc Surg.* (2013) 57:627–31. doi: 10.1016/j.ejvs.2013.03.013
12. Ma YC, Zuo L, Chen JH, Luo Q, Yu XQ, Li Y, et al. Modified glomerular filtration rate estimating equation for Chinese patients with chronic kidney

disease. *J Am Soc Nephrol.* (2006) 17:2937–44. doi: 10.1681/ASN.2006040368
13. Fillinger MF, Greenberg RK, McKinsey JF, Chaikof EL. Reporting standards for thoracic endovascular aortic repair (TEVAR). *J Vasc Surg.* (2010) 52:1022–33. doi: 10.1016/j.jvs.2010.07.008
14. Wu J, Zheng H, Liu X, Chen P, Zhang Y, Luo J, et al. Prognostic value of secreted frizzled-related protein 5 in heart failure patients with and without type 2 diabetes mellitus. *Circ Heart Fail.* (2020) 13:e007054. doi: 10.1161/CIRCHEARTFAILURE.120.007054
15. Garzotto M, Beer TM, Hudson RG, Peters L, Hsieh YC, Barrera E, et al. Improved detection of prostate cancer using classification and regression tree analysis. *J Clin Oncol.* (2005) 23:4322–9. doi: 10.1200/JCO.2005.11.136
16. Hagan PG, Nienaber CA, Isselbacher EM, Bruckman D, Karavite DJ, Russman PL, et al. The International registry of acute aortic dissection (IRAD): new insights into an old disease. *JAMA.* (2000) 283:897–903. doi: 10.1001/jama.283.7.897
17. Nienaber CA, Clough RE. Management of acute aortic dissection. *Lancet.* (2015) 385:800–11. doi: 10.1016/S0140-6736(14)61005-9
18. Patel KV, Ferrucci L, Ershler WB, Longo DL, Guralnik JM. Red blood cell distribution width and the risk of death in middle-aged and older adults. *Arch Intern Med.* (2009) 169:515–23. doi: 10.1001/archinternmed.2009.11
19. Tonelli M, Sacks F, Arnold M, Moye L, Davis B, Pfeffer M. Relation between red blood cell distribution width and cardiovascular event rate in people with coronary disease. *Circulation.* (2008) 117:163–8. doi: 10.1161/CIRCULATIONAHA.107.727545
20. Ku NS, Kim HW, Oh HJ, Kim YC, Kim MH, Song JE, et al. Red blood cell distribution width is an independent predictor of mortality in patients with gram-negative bacteremia. *Shock.* (2012) 38:123–7. doi: 10.1097/SHK.0b013e31825e2a85
21. Kwok CS, Tiong D, Pradhan A, Andreou AY, Nolan J, Bertrand OF, et al. Meta-analysis of the prognostic impact of anemia in patients undergoing percutaneous coronary intervention. *Am J Cardiol.* (2016) 118:610–20. doi: 10.1016/j.amjcard.2016.05.059
22. Groenveld HF, Januzzi JL, Damman K, van Wijngaarden J, Hillege HL, van Veldhuisen DJ, et al. Anemia and mortality in heart failure patients a systematic review and meta-analysis. *J Am Coll Cardiol.* (2008) 52:818–27. doi: 10.1016/j.jacc.2008.04.061
23. Liao M, Liu Z, Bao J, Zhao Z, Hu J, Feng X, et al. A proteomic study of the aortic media in human thoracic aortic dissection: implication for oxidative stress. *J Thorac Cardiovasc Surg.* (2008) 136:65–72. doi: 10.1016/j.jtcvs.2007.11.017
24. Kiefer CR, Snyder ML. Oxidation and erythrocyte senescence. *Curr Opin Hematol.* (2000) 7:113–6. doi: 10.1097/00062752-200003000-00007
25. Friedman JS, Lopez MF, Fleming MD, Rivera A, Martin FM, Welsh ML, et al. SOD2-deficiency anemia: protein oxidation and altered protein expression reveal targets of damage, stress response, and antioxidant responsiveness. *Blood.* (2004) 104:2565–73. doi: 10.1182/blood-2003-11-3858
26. Semba RD, Patel KV, Ferrucci L, Sun K, Roy CN, Guralnik JM, et al. Serum antioxidants and inflammation predict red cell distribution width in older women: the women's health and aging study I. *Clin Nutr.* (2010) 29:600–4. doi: 10.1016/j.clnu.2010.03.001
27. Jia LX, Zhang WM, Zhang HJ, Li TT, Wang YL, Qin YW, et al. Mechanical stretch-induced endoplasmic reticulum stress, apoptosis and inflammation contribute to thoracic aortic aneurysm and dissection. *J Pathol.* (2015) 236:373–83. doi: 10.1002/path.4534
28. Weiss G, Goodnough LT. Anemia of chronic disease. *N Engl J Med.* (2005) 352:1011–23. doi: 10.1056/NEJMra041809
29. Taguchi E, Nishigami K, Miyamoto S, Sakamotoand T, Nakao K. Impact of shear stress and atherosclerosis on entrance-tear formation in patients with acute aortic syndromes. *Heart Vessels.* (2014) 29:78–82. doi: 10.1007/s00380-013-0328-z
30. Osswald A, Karmonik C, Anderson JR, Rengier F, Karck M, Engelke J, et al. Elevated wall shear stress in aortic type B dissection may relate to retrograde aortic type A dissection: a computational fluid dynamics pilot study. *Eur J Vasc Endovasc Surg.* (2017) 54:324–30. doi: 10.1016/j.ejvs.2017.06.012
31. Horobin JT, Sabapathy S, Simmonds MJ. Repetitive supra-physiological shear stress impairs red blood cell deformability and induces hemolysis. *Artif Organs.* (2017) 41:1017–25. doi: 10.1111/aor.12890

Conflict of Interest: The authors declare that the research was conducted in the absence of any commercial or financial relationships that could be construed as a potential conflict of interest.

Publisher's Note: All claims expressed in this article are solely those of the authors and do not necessarily represent those of their affiliated organizations, or those of the publisher, the editors and the reviewers. Any product that may be evaluated in this article, or claim that may be made by its manufacturer, is not guaranteed or endorsed by the publisher.

Copyright © 2022 Jiang, Liu, Huang, Liu, Liu and Geng. This is an open-access article distributed under the terms of the Creative Commons Attribution License (CC BY). The use, distribution or reproduction in other forums is permitted, provided the original author(s) and the copyright owner(s) are credited and that the original publication in this journal is cited, in accordance with accepted academic practice. No use, distribution or reproduction is permitted which does not comply with these terms.

Advantages of publishing in Frontiers

OPEN ACCESS
Articles are free to read for greatest visibility and readership

FAST PUBLICATION
Around 90 days from submission to decision

HIGH QUALITY PEER-REVIEW
Rigorous, collaborative, and constructive peer-review

TRANSPARENT PEER-REVIEW
Editors and reviewers acknowledged by name on published articles

Frontiers
Avenue du Tribunal-Fédéral 34
1005 Lausanne | Switzerland

Visit us: www.frontiersin.org
Contact us: frontiersin.org/about/contact

REPRODUCIBILITY OF RESEARCH
Support open data and methods to enhance research reproducibility

DIGITAL PUBLISHING
Articles designed for optimal readership across devices

FOLLOW US
@frontiersin

IMPACT METRICS
Advanced article metrics track visibility across digital media

EXTENSIVE PROMOTION
Marketing and promotion of impactful research

LOOP RESEARCH NETWORK
Our network increases your article's readership